NASA Contractor Report 172154

SOME ASPECTS OF WIND TUNNEL MAGNETIC
SUSPENSION SYSTEMS WITH SPECIAL
APPLICATION AT LARGE PHYSICAL SCALES

C. P. Britcher

UNIVERSITY OF SOUTHAMPTON
Southampton, England

NASA

National Aeronautics and
Space Administration

Langley Research Center
Hampton, Virginia 23665

NF02030

CONTENTS   Page

DISCLAIMER

Reference in this thesis to commercial manufacturers, products or trade names thereof is essential to a complete understanding of subject material but in no way implies any endorsement.

UNIVERSITY OF SOUTHAMPTON

ABSTRACT

FACULTY OF ENGINEERING

DEPARTMENT OF AERONAUTICS AND ASTRONAUTICS

SOME ASPECTS OF WIND TUNNEL MAGNETIC SUSPENSION SYSTEMS WITH SPECIAL
APPLICATION AT LARGE PHYSICAL SCALES

by Colin Paul Britcher

Despite over a quarter of a century of development, wind tunnel
magnetic suspension and balance systems (MSBSs) have so far failed to
find application at the large physical scales necessary for the majority
of whole model aerodynamic testing.   Recent developments, such as the
cryogenic operation of wind tunnels and advances in superconducting
electromagnet technology have greatly reduced the apparent cost of a
large, or perhaps more specifically, high Reynolds Number MSBS (LMSBS).
Many difficulties remain, however, and three are addressed in this
thesis.

A powerful method of magnetic roll torque generation is essential for
any LMSBS.   Two variants of the new Spanwise Magnet scheme are studied
herein.   Spanwise Permanent Magnets are shown to be a practical method
and are experimentally demonstrated using the Southampton University
MSBS, though precise evaluation of maximum torque capabilities has not
been possible.

Extensive computations of the performance of the Spanwise Iron
Magnet scheme indicate potentially powerful capability, limited
principally by current electromagnet technology.   Some experimental
verification of the computed performance at low applied field levels
is presented.

Aerodynamic testing at extreme attitudes is shown to be practical
in relatively conventionally configured MSBSs.   Preliminary operation
of the Southampton University MSBS over a wide range of angles of
attack is demonstrated.

The impact of a requirement for highly reliable operation on the
overall architecture of LMSBSs is studied.   It is shown that the
system's cost and complexity need not be unduly increased, provided
certain of its unique characteristics are exploited.

SYMBOLS   (SI units used throughout, except where noted)

a x-wise coordinate of element

A transformation matrix (field components)

A_o wing root chordwise cross sectional area

b y-wise coordinate of element

B transformation matrix (field gradient components)

B_i magnetic flux density (magnitude, in tesla, direction and/or gradient denoted by subscript)

$\underline{B}$ magnetic flux density (vector)

BH_{max} peak energy product for permanent magnet material

c z-wise coordinate of element

C_L lift coefficient

C_{L_β} roll moment due to sideslip coefficient (US notation)

d parameter locating E/M axis

E_i even function (of subscript)

F_i magnetic force (in subscript direction)

$\underline{F}$ magnetic force (vector)

$g(b)$ unknown function of b

H_i magnetic field strength (magnitude, in A/m, direction and/or gradient denoted by subscript)

H_c coercive force (A/m)

H_{ci} intrinsic coercive force (A/m)

H_k effective coercive force (A/m, see Section 4.3)

$\underline{H}$ magnetic field strength (vector)

I_i current (in E/M i)

J current density (in A/cm^2)

J_i magnetic polarization (magnitude, in tesla, direction denoted by subscript)

J_r current density in E/Ms generating through-wing field

J_m current density in E/Ms generating wing magnetizing field

$J_{r,m}$	J_r and J_m
J_r	remanent induction (Section 4 only)
$\underline{J}$	magnetic polarization (vector)
L	roll torque (balance axes)
L_v	roll moment due to sideslip coefficient (UK notation)
M	mach number
M_i	magnetization (magnitude, in tesla, direction denoted by subscript) THIS IS NOT TO SI STANDARD
$\underline{M}$	magnetization (vector)
$\underline{M}^*$	magnetic dipole moment ($\underline{M} \times \delta v$)
$\underline{M}'$	magnetization (traditional, in A/m, see Appendix 4)
n	number of E/Ms in an array
N	yaw torque (balance axes)
O_i	odd function (of subscript)
$\underline{r}$	position vector of element
s	wing semi-span
S	wing area
$\underline{T}$	magnetic torque (vector)
δv	volume of incremental element
V	volume of whole core or non-incremental element thereof
$\underline{V}$	arbitrary vector
x	balance axis or model axis (fixed model or model only)
x'	model axis (model free in balance axes)
y	balance axis or model axis (as above)
y'	model axis (as above)
z	balance axis or model axis (as above)
z'	model axis (as above)
β	angle between magnetic force vector (in xz plane) and x axis
$\delta(i)$	incremental element of i

θ	pitch attitude (Euler angles)
ζ	wing sweepback angle
Θ	pitch transformation matrix (model axes to balance axes)
μ	magnetic permeability (used in Section 5 to represent μ_r)
μ_0	magnetic permeability of free space ($4\pi \times 10^{-7} \, \text{Hm}^{-1}$)
μ_r	relative magnetic permeability
ξ	parameter locating E/M axis
ϕ	roll attitude (Euler angles)
Φ	roll transformation matrix (model axes to balance axes)
χ_m	magnetic susceptibility
ψ	yaw attitude (Euler angles)
Ψ	yaw transformation matrix (model axes to balance axes)
M	pitch torque (balance axes)

SUBSCRIPT NOTATION

x, y, z	component in x, y, z direction
x', y', z'	component in x', y', z' direction
o	at origin of balance axes (field properties only)
t	value at wing tip

Magnetic subscript notation dealt with fully in Appendix 4

SUPERSCRIPT NOTATION

'	in model axes
p	peak value

ABBREVIATIONS

A.C.	alternating or unsteady current
A/D	analogue to digital (converter)
APO	Automatic Power Off
AR	wing aspect ratio
CCD	charge coupled device
CID	charge injection device
D/A	digital to analogue (converter)
D.C.	direct or quasi-steady current
E/M	electromagnet
EPS	Electromagnetic Position Sensor
LHe	liquid helium
LN_2	liquid nitrogen
LMSBS	Large Magnetic Suspension and Balance System
MSBS	Magnetic Suspension and Balance System
N/A	not applicable
PR	Passive Redundancy
PWM	pulse width modulation
ReCo	rare-earth cobalt (permanent magnet)
RSS	Rapid Shutdown Sequence
SIM	Spanwise Iron Magnet(s)
$SmCo_5$	samarium cobalt (permanent magnet)
SPM	Spanwise Permanent Magnet(s)
SUMSBS	Southampton University Magnetic Suspension and Balance System
t/c	wing thickness to chord ratio
+, X, L, V etc.	classical representations of MSBS geometries (see Section 1.2.1)

1. INTRODUCTION

1.1 Magnetic Suspension and Balance Systems (MSBS) with emphasis on Large Systems (LMSBS)

The first MSBS for wind tunnel application was constructed in France by ONERA and first reported by Tournier and Laurenceau in 1957 (1) . This system successfully demonstrated 5 component control of a range of simple models in work such as wake and drag studies up to intermediate supersonic Mach numbers. The potential advantages of wind tunnel testing without mechanical model supports, including the elimination of support interference and more straight-forward dynamic testing, fired the imagination of researchers in numerous institutions and quite soon many systems conceptually similar to the early ONERA system were under construction.

A total of eleven MSBSs of various designs could be considered as constituting this first wave of effort and are tabulated briefly below. All bar one of the institutions involved presented papers at the First International Symposium on MSBSs in 1966 (2) .

Table 1.1   MSBSs pre-1970   (listing in alphabetical order)

Institution	Degrees of freedom controlled	Approx. test section size $\sqrt{cm^2}$	Application
AEDC/NASA Langley	5	30	Wake studies /R&D
Univ. Michigan	1	4.5	Low Re. No. sphere drag
MIT (A)	5	10	Static/dynamic
MIT (B)	5/6	9 - 15	Static/dynamic/ R&D/Magnus
NASA Langley	1	11	R&D
ONERA (A)	5	5.5 - 8.5	Drag/base pressure
ONERA (B)	5	26	Base pressure/heat transfer
Princeton Univ.	3	13	Wake studies
R.A.E. Farnborough	5	18	Sting effect/Magnus
Univ. Southampton	6	13 - 18	Static/dynamic/ R&D/Magnus
Univ. Virginia (A)	3	9	Cone & sphere drag

(data from Ref. 3 and various)

Two further MSBSs were commissioned in the early 1970's, including the first system utilising superconducting electro-magnets. A Second International Symposium was held in 1971 (4).

Table 1.2	MSBSs post-1970		
Oxford Univ.	3	8	Low density sphere drag
Univ. Virginia (B)	3	13.5	Dynamic stability/R&D

Contemporary with these developments there was an increasing recognition in the aerodynamic testing community that the majority of existing wind tunnels were of too low a Reynolds number capability for the test purposes to which they were put. Further, it was clear that the bulk of production testing over the coming years would be at Mach numbers no higher than low supersonic (< 2.5), thus including the regimes where Reynolds number and support interference tend to have their greatest influence. Interest in MSBSs waned, due principally, it is thought, to the realisation that scaling of existing technology MSBSs to the large wind tunnels then known to be necessary, would be impractical for one reason or another, for instance E/M power requirements, with associated high capital and running costs, or lack of adequate roll torque capability. Indeed the modern day resurrection of the cryogenic wind tunnel concept, now universally accepted as the best approach to high Reynolds number testing in the crucial transonic regime, came about as a part of efforts to reduce the size of wind tunnels necessary for a high Reynolds number MSBS.

Relatively recently however, various factors have acted to increase the apparent viability of a LMSBS. Concern over the accuracy and validity of support interference corrections is now widespread, particularly and rather paradoxically in the case of the new breed of high Reynolds number cryogenic wind tunnels, since these tunnels are generally operated at high pressures.

MSBSs of the type considered to date are inherently capable of dynamic testing, which otherwise presents severe difficulties with mechanical model supports, and several small systems have been successfully used for this purpose.

A related capability is that fixed model attitudes may be selected or changed rapidly and with little restriction, potentially manifesting a highly productive system.

Further potential advantages of a LMSBS are thought to lie in
the areas of high angle of attack (extreme attitude) testing, where
support interference can become rather intractable, and as an
alternative solution to the difficulties involved with operation of
complex conventional strain gauge force balances in the low
temperature environment of the cryogenic wind tunnel.

The above factors, coupled with the recent rapid developments
of large scale superconducting E/Ms for power generation and nuclear
physics research indicated that revived effort aimed at developing
a LMSBS would be worthwhile.   This effort was and is principally
directed by NASA Langley Research Center with the intention of
developing a LMSBS at that institution.

1.2 Status of MSBS development circa 1978

Many of the aforementioned small MSBSs were in no way intended to
be representative of large systems, rather being specialised designs
tackling specific and specialised problems.   Only two systems are
known to have been constructed with scaling to larger systems
specifically in mind, namely MIT(B) and UVa(B).   Nevertheless much
existing technology was thought to be applicable to a future LMSBS
and some of the relevant design features will be reviewed here.
The reader must carefully note that the comments below refer only
to the state of developments at the time that this project commenced
(late 1978).   Considerable developments are reported in later
chapters herein and it must be assumed that corresponding or
complementary developments have taken place elsewhere.

1.2.1 E/M configurations

Most current MSBS E/M configurations can be considered as falling
into one of three broad categories as follows (See Fig. 1.1):

    I)   Geometrically orthogonal simple E/Ms
           e.g ONERA (A) & (B), Univ. Southampton

    II) Convoluted E/M e.g MIT(B)

    III) Orthogonal force, isotropic model e.g UVa (A) & (B)

Class I above is characterized by separated E/Ms often of simple
solenoidal form arranged in a relatively straightforward configura-
tion around the test section, generally with the total number of
E/Ms equal to or only marginally greater than the number of degrees
of freedom controlled.

Fig. 1.1(a) Schematic
diagram of a representative
Class I MSBS
(Southampton)

Vertical E/Ms

Lateral
E/Ms

y

Lateral E/Ms

x

Axial E/M

z

Fig. 1.1(b)
Schematic diagram
of a representative
Class III MSBS
(after UVa (A & B))

Lateral and
longitudinal
gradient E/Ms

z

y

x

Magnetizing E/Ms
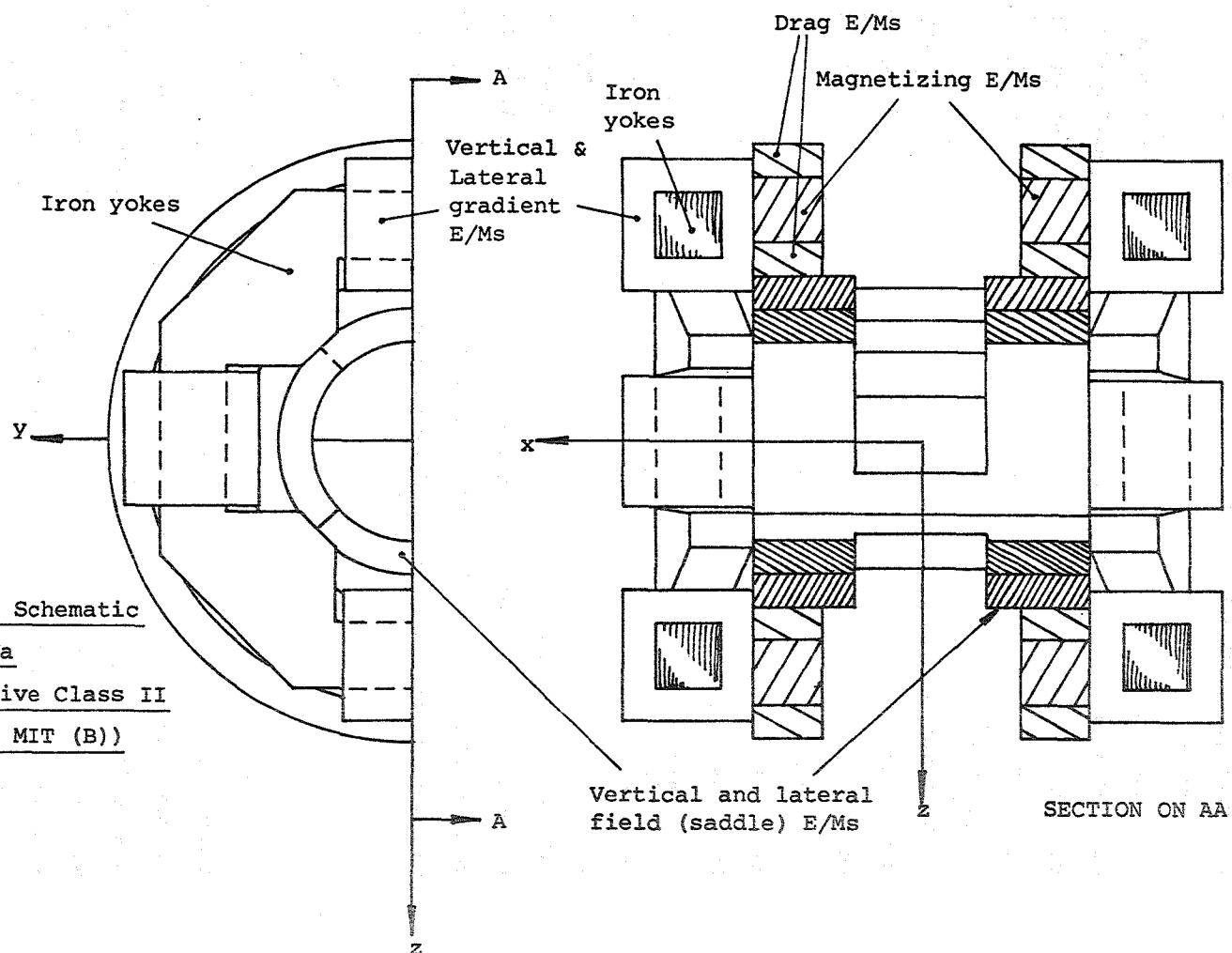
Fig. 1.1(c) Schematic diagram of a representative Class II MSBS (after MIT (B))

Drag E/Ms

Magnetizing E/Ms

Iron yokes

Vertical & Lateral gradient E/Ms

Iron yokes

A

Y

x

z

Vertical and lateral field (saddle) E/Ms

z

SECTION ON AA

A

- 5 -

Class II features E/Ms, other than the axial field E/Ms, usually of non-solenoidal form, arranged in relatively complex ways around the test section with the intention of achieving relatively high uniformity and symmetry of all fields as well as high magnetic efficiency. The number of E/Ms is not strongly influenced by the number of degrees of freedom controlled.

Class III is inherently limited to three degree of freedom control (zero magnetic torques), being originally developed to perform dynamic testing. This class cannot be considered viable for a LMSBS where principally static testing is to be performed since there is no possibility of selecting arbitrary model attitudes.

Numerous subclasses of Class I exist, mainly classified by the E/M disposition in a cross section through the test section, such as "L", "V", etc. It seems certain that any future LMSBS will exhibit considerable E/M symmetry for various reasons, including E/M efficiency and system reliability, so only subclasses such as the classical "+" and "X" need be considered.

Considerable efforts have been expended over many years in attempts to derive "optimum" E/M configurations but early design studies of superconducting E/Ms for a LMSBS have indicated that E/M configuration and geometry is likely to be forced predominantly by technological limits of superconductors and by requirements for roll control (5) . All configurations studied herein fall into Class I above, but further discussion of E/M configurations may be found in Ref. 6.

1.2.2 Power supplies

The class of supply almost universally used to date has been the phase controlled multiphase rectifier, with thyristor switching elements in all but the most venerable units. This type is easily scaled to high powers. One institution is known to have experimented with rotating machinery for primary power supplies (MIT) although it is difficult to achieve high output slewing rates with conventional generator designs.

The high reactive powers that would be experienced in dynamic operation of LMSBSs make some form of energy storage in the supply most attractive, in order to raise the system's overall energy efficiency by regenerating power from the load E/Ms. The only MSBS

operated with superconducting E/Ms to date (UVa(B)), utilised power supplies that were specially constructed but can now be regarded as of relatively conventional design, a notable feature being capacitive load energy storage and regeneration (7) .

Bipolar operation will be essential in at least some of the suspension E/Ms in any realistic LMSBS but relatively few small MSBSs have utilised bipolar supplies, mostly using gravitational or D.C. current biasing to achieve bidirectional control field capability.

No power supply of the required characteristics for LMSBS application is known to have been demonstrated at design power levels remotely approaching the LMSBS requirement.

1.2.3 Position sensors

Optical methods of model position sensing have been employed in the overwhelming majority of cases. In turn, the majority of these methods are detail variants of the simple analogue shadow movement detection systems described in Appendix 1. These systems are inapplicable to LMSBSs because of the lack of immunity to light path degradation. ONERA developed a target scanning/tracking system using vidicon tubes (8) , which is thought to represent a broad class of sensor suitable for LMSBS use, albeit with the magnetic field sensitive vidicons replaced with more modern solid state CCD or CID imaging arrays. Oxford University also used a scanning method (9) more closely approaching conventional T.V. techniques although the system was only used to detect the centroids of small spheres.

The MIT Electromagnetic Position Sensor (EPS) (10) has often been viewed as a first choice for a LMSBS position sensor since the non-optical approach accrues, in principal, considerable flexibility and versatility. At the time of writing that view must be considered still valid since the system has amassed hundreds of hours of operation at small scale, although the problem of electromagnetic noise pickup is severe enough to demand very careful design for a large system. Numerous advanced optical methods have been proposed and some subjected to preliminary evaluation. None has so far been demonstrated on a comprehensive and fully representative basis at any scale.

1.2.4 Control systems

These have almost universally consisted of simple analogue feed-

back networks. Digital controllers have recently been demonstrated with an idealized single degree of freedom system (MIT) but no comprehensive application has been attempted. There does not appear to be serious difficulty with the control hardware for a LMSBS, the technology of reliable high speed digital flight control computers developed for civil, military and space applications appearing adequate.

Existing control algorithms generally do not encompass the aerodynamic characteristics of the model, nor the magnetic or inertial cross-couplings between model degrees of freedom which exist in all MSBSs, rather controlling each degree of freedom separately with aerodynamic loads being small with respect to model mass. This approach is unlikely to yield the best performance from a LMSBS since, firstly, the aerodynamic loads may be large with respect to model mass and, secondly, the aerodynamic and magnetic cross-couplings may be severe, particularly at extreme model attitudes. More sophisticated control algorithms, perhaps including self-adaptation or self-optimisation with changing test conditions, thus seem necessary for effective operation of a LMSBS. No such algorithms yet exist.

1.2.5 Miscellaneous

No MSBS yet exhibits any viable hardware redundancy or utilises any failure tolerant features and, principally for this reason, all systems tend to be relatively unreliable in operation.

Several methods of roll control exist but all are unsatisfactorily weak in torque capability. Thus, whereas the generation of adequate forces and torques in degrees of freedom other than roll appears practical at large scales, the generation of adequate roll torque does not.

1.3 Contents of this thesis

The underlying emphasis is towards the concept of a LMSBS though the majority of contents are unspecific in their application. At the commencement of the current phase of investigations, there appeared to be several specific and fundamental obstacles to be surmounted, or shown to be surmountable, before detail design of a LMSBS could commence. These include (not in any particular order of importance):

1) Generation of adequate roll torque.

2) Provision of adequate overall system
   reliability and integrity.

3) Design of very large capacity power amplifiers
   (loosely referred to in the context of
   MSBSs as power supplies).

4) Design of large multipurpose A.C. capable super-
   conducting E/M arrays.

5) Development of large scale, precise and versatile
   position sensors.

6) Development of advanced control algorithms including
   full magnetic decoupling and some self-adaptive
   features.

Of course only a few of these topics could be addressed within
the scope of a study of this kind.   3) and 4) above are quite
beyond the capability and experience of this University.   It had
been felt initially that 6) above would represent a worthwhile and
significant early advance but this view was quickly modified.
Other problems, such as 1)-5) quoted, were recognised as representing
potential blocks to the development of a LMSBS, whereas advanced
control algorithms need not be made available until quite late in
the construction of such a system.   Since it seems certain that,
for reasons of reliability and versatility, the major part of the
control system of a LMSBS would be implemented with some form of
digital computer, merely realistic estimates of required computer
power would be required in the early stages of design.

Some attention was paid to 5) above but it was eventually
concluded that the technological advances of certain sensing devices,
such as solid state photo-detector arrays, currently occurring for
application in other areas, may alleviate this problem in the
relatively near term.

The bulk of this thesis is therefore directed towards problems
1) and 2) above, also the matter of extreme attitude testing in MSBSs
which, although potentially very advantageous for a LMSBS does not
represent a crucial block to its development.

2. THE SOUTHAMPTON UNIVERSITY MAGNETIC SUSPENSION AND BALANCE SYSTEM (SUMSBS)

2.1 Historical aspect

Studies of magnetic suspension systems began at Southampton in 1959, construction of a system beginning in 1962, with the principal objective of performing dynamic testing in conventional wind tunnels without mechanical model supports. Work was under the direction of Dr. M. Judd, latterly and to date Dr. M.J. Goodyer. It was quickly shown that dynamic testing was indeed feasible although the high frequencies of oscillation required at small scale led to the development of the two-mass "tuned" model (11) . Extensive Magnus force testing was performed on ballistic-type models with reverse Magnus force, absent in corresponding sting supported tests, being discovered (12) . Several winged models (AGARD-G etc.) were tested in 6-component suspension and methods of rapid data acquisition were developed (13) . Studies of scaling of MSBSs (14) revealed difficulties that were also being identified by other groups of researchers, particularly that the power consumption of conventional copper conductor E/Ms in a MSBS scale as a high power of characteristic dimension. It became clear that systems designed for wind tunnels of realistic scale and Reynolds number capability, ambient temperature operation being mandatory at that time, would be quite out of the question, consuming megawatts of steady power.

SUMSBS fell into temporary disuse but was re-commissioned in 1978 and adapted to demonstrate operation with the University's 0.1m low speed cryogenic wind tunnel, the first known operation of a MSBS with such a tunnel (15, 16) .

2.2 Modifications to SUMSBS to achieve current status

2.2.1 E/M configuration

As previously mentioned it seems certain that any future LMSBS will exhibit considerable E/M symmetry. It thus appeared desirable to reconstruct SUMSBS, previously of the unusual " $\perp$ " configuration (11) to a more representative arrangement. Subsequently, it was realised that extensive E/M symmetry would be advantageous to suspension of models at extreme attitudes (Section 7). Further, spanwise magnet rolling moment generation systems (Sections 4, 5, 6) require in general at least a quadrupole field disposed in the

cross-sectional plane of the test section. Thus, in order to demonstrate such roll control systems, suspension at high angles of attack and representative LMSBS configurations, the previous E/M layout of SUMSBS was augmented and modified by the addition of two new "vertical" E/Ms, identical to the six "vertical" and "lateral" E/Ms existing, and provision of twin symmetrical (fore-and-aft) "drag" E/Ms, replacing the single E/M previously used (Fig. 2.1; Ref. 11; Appendix 1).

The system appears to fall into the "+" subclass of Class I as defined earlier but in order to accommodate spanwise magnet roll control, 6-component suspension takes place with the model's axes inclined at 45° to the horizontal, in the roll sense (Fig 2.2), wherein the system falls into the "X" subclass.

2.2.2 Power supplies

In common with the majority of contemporary MSBSs, SUMSBS utilised monopolar three-phase thyristor E/M power supplies. These were satisfactory insofar as they were relatively simple and had operated almost faultlessly for over a decade and a half. The low frequency switching inherent to the mode of operation does introduce considerable ripple in the output current and although this was not unduly troublesome in normal suspension there is an undesirable frequency response cutoff associated with the firing frequency (150Hz with U.K. mains supply). The monopolar operation presents obvious restrictions and the single quadrant capability of the supplies necessitated the installation of ballast resistors in series with each E/M to shorten the time constant of current decay. This also eases control system design, reducing the lag between E/M current and applied voltage, but would be quite unacceptable in a LMSBS due to the enormous power wastage that would result.

Since some bipolar supplies were necessary for SUMSBS effectively to demonstrate suspension at high angles of attack (Section 7) it was decided to take the opportunity to solve many problems simultaneously and incorporate a more sophisticated type of power supply, that is Pulse Width Modulated (PWM) transistor switching supplies, discarding the thyristor types completely. The supplies chosen (Appendix 1) were designed for use with industrial D.C. servomotors and feature the ability to store some regenerated energy from the

Fig. 2.1 Schematic diagram
of modified Southampton
University MSBS (SUMSBS)

New aft axial E/M

Revised forward
axial E/M

New lower E/Ms

+ arrangement

(5 component suspension, model wings for illustration only)

y,y'

z,z'

X arrangement

(6 component suspension, SPM roll control)

y

y'

Gravity vector acts along this axis

z

z'
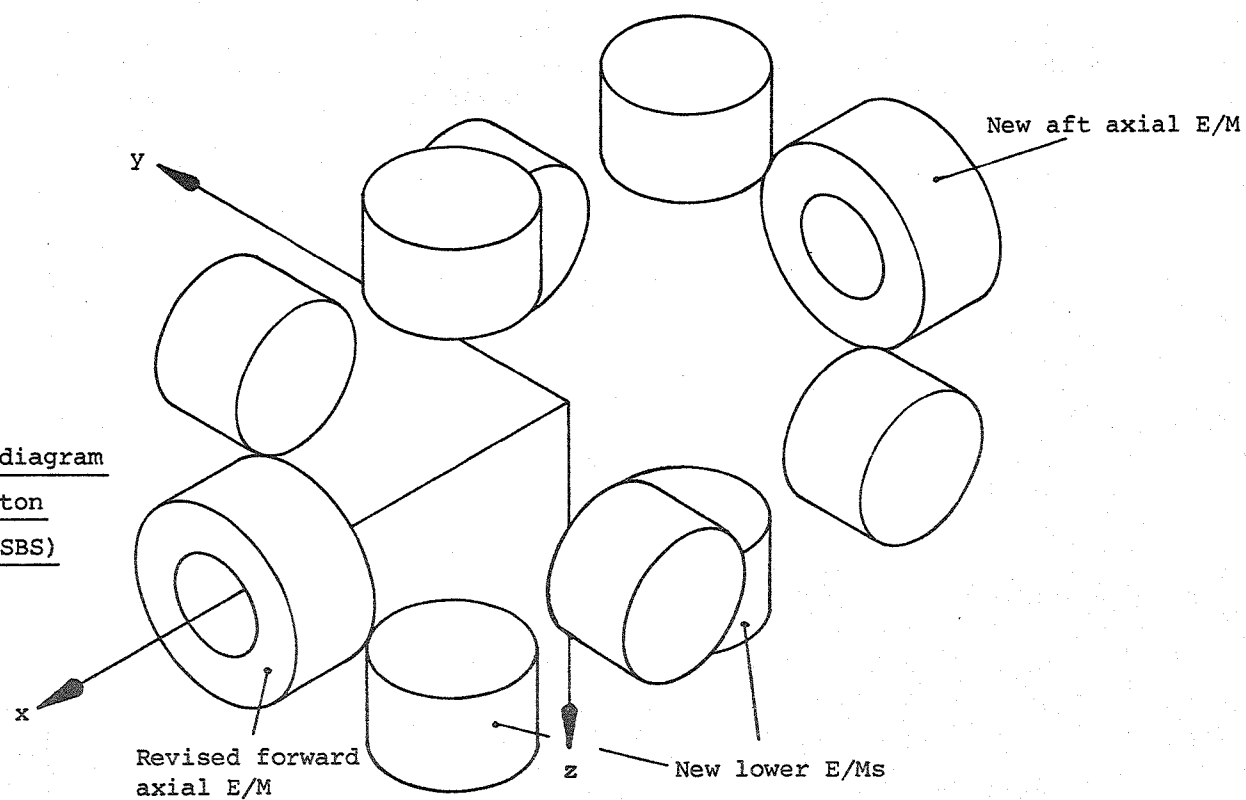
Fig.2.2 Configuration of SUMSBS in + or X E/M arrangement

load. The switching frequency is 5kHz which permits more
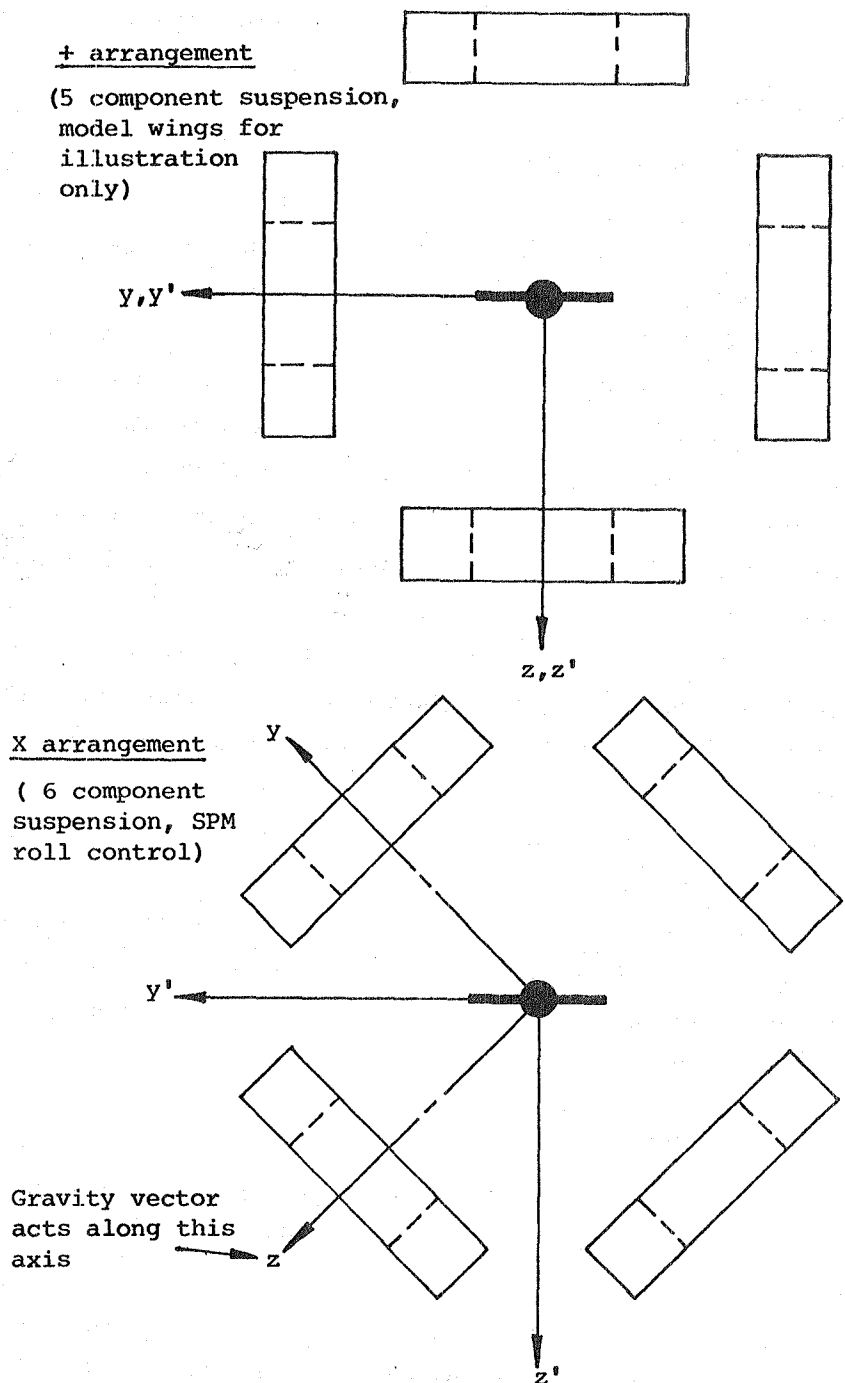effective filtering of high frequency components of load current
than was previously possible and renders the frequency response
of the supplies near infinite as far as the control system is concerned.

2.2.3 Position sensors

The position sensing systems used in SUMSBS since its inception
all fall into the category of simple analogue optical shadow move-
ment detectors and have never been capable of tracking a particularly
wide range of model movement, perhaps $\pm$ 15 degrees pitch/yaw,
without mechanical realignment (11) . Other types of sensor exist,
capable of tracking a wider range, notably the MIT electromagnetic
position sensor (EPS) (10) , and other types are proposed with
promise of still wider capabilities such as photodiode or CID array
target trackers (5, 17) . SUMSBS requires 6-component sensors
capable of tracking ideally 90° of pitch rotation with simple models.
Despite long deliberations and much experimentation it was concluded
that in the context of the current research none of the more advanced
sensors could be incorporated into SUMSBS due to various time and/or
physical space and/or financial constraints. Thus a new set of
traditional sensors has been constructed with widerange pitch
tracking capability effected by arranging that the appropriate sensors
may be rotated about the model's pitch axis, conventional fixed
sensors being used where extreme model attitudes are not required
(Appendix 1). The obvious should be stressed, that is that these
sensors are quite inappropriate for use in a LMSBS and do not
represent current thinking in this area.

2.2.4 Control systems

The simple all analogue control systems previously used with
SUMSBS (11) were not capable of straightforward or realistic
adaption to the requirements for suspension over wide ranges of
attitude or for incorporation of more advanced control algorithms.
The major part of the control system was thus abandoned and
replaced by a mini-computer with local A/D and D/A conversion and
limited analogue pre- and post-processing (Appendix 1).

3. ROLLING MOMENT GENERATION SYSTEMS FOR MSBSs

3.1 Introduction, the need for roll control

Historically, one of the key obstacles to the development of MSBSs for application to large scale wind tunnels was the development of a rolling moment generation system of adequate power. Nevertheless numerous small MSBSs have operated over many years without any active roll control system, indeed to date only two MSBSs have been demonstrated with such control (11, 18, 19). It is pertinent to examine how this can be and why operation at large scales would be impractical without active roll control.

Firstly, much useful testing could be, and has been, performed in small scale systems on bodies of revolution, notably sphere or missile drag measurements and Magnus force investigations, where active roll control was not required. Secondly, a considerable percentage of the research effort expended with MSBSs has been in developing the systems themselves, particularly features such as position sensors, where suspension of models other than bodies of revolution is unnecessary. Where fixed roll attitude was required it frequently proved relatively easy to induce a preferred roll attitude, with slight positive stiffness about that attitude, by arranging the model's magnetic centre to lie above its centre of gravity.

The overwhelming majority of testing in a LMSBS would certainly involve winged aircraft models. Small "tare" roll moments are likely to exist due to slight magnetic, aerodynamic or mass asymmetries but presumably these could be countered by designing in a preferred roll attitude in the classical fashion. In general, however, whenever a winged model is tested with non-zero yaw angle (w.r.t. tunnel axes) significant roll moments will be generated, typically via the L_v aerodynamic derivative. In order to permit testing under these conditions a magnetic torque must be generated to oppose the net aerodynamic torque. Further, at high angles of attack the onset of stall is frequently asymmetric, producing steady roll torque of either sign or perhaps oscillatory torque, such as with asymmetric vortex shedding. Damping of roll oscillations is essential under all the above-mentioned conditions and is best introduced by appropriate manipulation of a method of positive roll control.

It is difficult to estimate the magnitudes of torque that
might be met in a future LMSBS because the aerodynamic character-
istics of the models are of course unknown.   However, Ref. 20
includes the following data for an F-94A :

C_{L_β} (U.S. equivalent notation for L_v) in the range
-0.07 (high speed) to -0.05 (low speed)

Span = 11.37m   Wing area = 22.2m^2

Scaling to a 4-foot span model in an atmospheric
pressure tunnel at M = 0.85 :

$$L \simeq 11 \text{ Nm/degree Yaw}$$

Data from Ref. 21 relating to an arbitrary design resembling a
Hunter gives a somewhat larger result (43 Nm/deg).   It is clear
that considerable roll torques are to be expected from this source.

In the case of asymmetric stall we may take an arbitrary case of
an aircraft with one wing completely stalled and the other com-
pletely unstalled.   A stalled C_L of approximately unity might be
expected with the unstalled perhaps twice this value.   Without
reference to any specific geometry or test conditions it is
immediately seen that in the (worst) case of an untapered uniformly
loaded wing the resultant lift vector will act some one-sixth of
the semi-span outboard of the aircraft centreline along the unstalled
panel.

There thus seems little possibility of realistic operation of
a LMSBS without a powerful method of magnetic roll torque generation.

3.2 Methods of magnetic roll torque generation

3.2.1. Introduction

Various methods of generating roll torque, falling into three
main categories, have been proposed and evaluated over a number of
years.   These include:

D.C. field systems

1)	"Bent" fuselage core	(22)
2)	Shaped fuselage core	(11, 23)
3)	Through wing magnetized wing cores	(11, 18)
4)	Active model mounted coils	(11)
5)	Passive model mounted coils	(11)
6)	Spanwise magnets	(24)

A.C. systems

    7)   Planar conducting loop   (19, 22)

Aerodynamic systems

    8)   Active aileron control   (11)

    9) L_v (C_{L_β}) control   (11)

Types 4, 5, 8, 9 are currently considered unsuitable for LMSBS application and types 1, 2, 3 have shown inadequate torque capability in previous analyses.   Type 7, the A.C. system, promises high torques but significant complication of overall MSBS design seems necessary to accommodate the strong A.C. fields required.

An investigation of the two subclasses of type 6 is presented later.   No studies of the current status of other methods have been undertaken so direct comparison between methods cannot be included.

3.2.2. D.C. methods

3.2.2.1 Theory of D.C. torque production

At any point in a magnetized body, where magnetizations and applied fields are quasi-steady, the forces and torques acting on an incremental element of material can be written as follows :

$$\delta\underline{F} = (\underline{M} \cdot \nabla) \; \underline{H} \; \delta V \qquad \delta\underline{T} = (\underline{M} \times \underline{H}) \; \delta V$$

If $\underline{M}$ represents permanent magnetization (polarization) there is no difficulty and $\underline{H}$ may be taken directly as the external or applied $\underline{H}$ field. Where $\underline{M}$ is composed wholly or partly of induced magnetization there is some ambiguity since $\underline{M}$ will be a function of applied $\underline{H}$. If the total force and torque on an isolated body are required then it is valid to consider the induced magnetization as permanent and the effective $\underline{H}$ field as that field that would exist if the body in question were removed. A body of magnetically soft material will require a low demagnetizing factor in at least one direction for the product ($\underline{M} \times \underline{H}$) to be large.

Resolving using the co-ordinate system of Fig 3.1 :
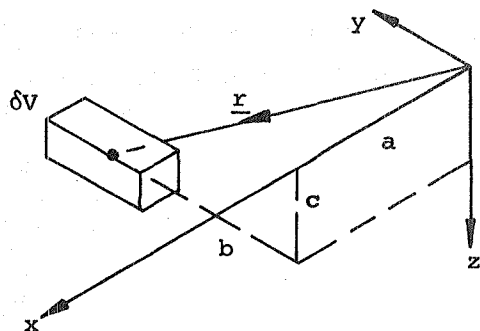
$$\underline{r} = a\underline{i} + b\underline{j} + c\underline{k}$$

Fig. 3.1

Axis system for magnetic calculations

- 17 -

we have :

$$\delta F_x = (M_x H_{xx} + M_y H_{xy} + M_z H_{xz}) \delta V$$

$$\delta F_y = (M_x H_{xy} + M_y H_{yy} + M_z H_{yz}) \delta V$$

$$\delta F_z = (M_x H_{xz} + M_y H_{yz} + M_z H_{zz}) \delta V$$

$$\delta L = (M_y H_z - M_z H_y) \delta V$$

$$\delta M = (M_z H_x - M_x H_z) \delta V \qquad\qquad\qquad - (3.1)$$

$$\delta N = (M_x H_y - M_y H_x) \delta V$$

$$\underline{F} = \sum_V \delta \underline{F}$$

$$\underline{T} = \sum_V \{\delta \underline{T} + (\underline{r} \times \delta \underline{F})\}$$

Integrating roll torque over the volume of the core :

$$L = \sum_V \{\delta T_x + (\underline{r} \times \delta \underline{F})_x\}$$

$$\therefore \quad L = \int_V (M_y H_z - M_z H_y) + (M_x H_{xz} + M_y H_{yz} + M_z H_{zz}) b$$

$$- (M_x H_{xy} + M_y H_{yy} + M_z H_{yz}) c \quad dV$$

$$\qquad\qquad\qquad\qquad - (3.2)$$

3.2.2.2 Review of some existing D.C. methods

Shaped fuselage cores exploit the terms $M_x H_{xy}$ and $M_x H_{xz}$. In normal suspension $\int_V M_x H_{xz} \, dV$ and $\int_V M_x H_{xy} \, dV$ represent the "lift" and "lateral" forces respectively and rolling moment can be generated essentially by redistributions of these forces over the volume of the core such that $\int_V (-M_x H_{xy} c + M_x H_{xz} b) \, dV$ is non-zero. The core cannot be axisymmetric to satisfy this condition. Drawbacks of the method are that either $(H_{xy})_z$ or $(H_{xz})_y$ the vertical and lateral gradients of the conventional "sideforce" or "lift" fields respectively, must be of large magnitude with slender fuselages and that valuable fuselage core volume must normally be omitted to satisfy the condition of non-axisymmetry.

Bent fuselage cores introduce transverse components of magnetization, M_y, M_z. Principal variations of the method proposed to date seek to exploit the terms $M_y H_z$ or $M_z H_y$ by arranging suitable distributions of transverse magnetization and applied fields to make the relevant integrals non-zero, for example the E coil method (22).

Large transverse magnetization components will be required to generate high torques but this can only be achieved in general by severe camber of the core magnetization or by use of more complex multiple reverse camber core geometries which in turn necessitate rather awkward field distributions.

The previous wing mounted magnet scheme used at Southampton University introduces asymmetrically disposed vertical components of magnetization, which, with a suitable applied field distribution, produces roll torque via the $M_z H_y$ term above. Historically, the system was chosen to suit an existing E/M arrangement. The self demagnetizing factors of vertically magnetized wing cores are very high in all conventional aircraft geometries, making iron cores difficult to magnetize and permanent magnet cores susceptible to demagnetization.

3.2.2.3 General comments

Moment generation via integration of fuselage forces (shaped cores) seems intuitively unattractive for conventional geometries due to the rather short moment arms available within a slender fuselage. However, there are at least three cases where this method may at least contribute usefully to an overall torque figure. These are :

(1) Wide body transport.

A wide body transport will exhibit simultaneously a high ratio of fuselage volume to first moment of wing area and a conservative test attitude/speed envelope. It may thus be argued that if sufficient forces and moments (apart from roll torques) can be generated with slender aircraft geometries then some of the fuselage core volume may be sacrificed, in the wide body case , for roll torque production.

(2) F-15 style fighter.

Several modern fighters are now exhibiting partial bifurcation of the rear fuselage to accommodate well separated twin engines. Such peculiarities of aerodynamic design create a non-axisymmetric fuselage of rather high moment of volume to volume ratio . Suitably exploited, therefore, such designs may yield useful roll torque without sacrifice of any core volume.

(3) Underwing stores, engine pods, etc.

These create a similar effect to that described under (2) above.

However, production of torque by exploitation of these character-
istics could not be regarded as generally applicable for obvious
reasons.

Torque generation via transverse components of magnetization
seems appropriate but attempts to introduce transverse magnetization
in soft iron fuselage cores are hampered by the usual requirement
for powerful axial magnetization. Permanent magnet fuselage cores
would need to be carefully configured to avoid strong mutual de-
magnetizing effects between adjacent orthogonal magnetization
components.

It is logical to concentrate the spanwise magnetizations in the
wings of the model, though parts of the fuselage may be used, since
the self-demagnetizing factors of cores of the general proportions
of conventional wings, magnetized along their long axis, are very
low.

Examination of equations 3.1 indicates that cross couplings
between degrees of freedom are likely if transverse components of
magnetization are introduced. Cross couplings exist in all
practical MSBS designs but it has been standard practice to arrange
for each degree of freedom to be controllable by relatively simple
spatial distributions of applied field with cross couplings well
suppressed at the datum model position. It is not thought that
elimination of all significant cross couplings is a realistic goal
for LMSBS design since a wide variation in model geometries,
including magnetization distribution, is expected and a modestly
sophisticated control system should be capable of handling quite
severe cross couplings. There is considerable advantage in E/M
array design, however, if primary forces and moments can be
generated by simple field distributions.

Simple unidirectional transverse magnetization cannot be ruled
out simply on the basis of its severe cross coupling into pitch,
nor because it destroys the mirror symmetry of the model, but it
will exhibit a null torque line unless vertical fields can be
generated relatively independently in the areas of axial (fuselage)
and transverse (wing) magnetizations.
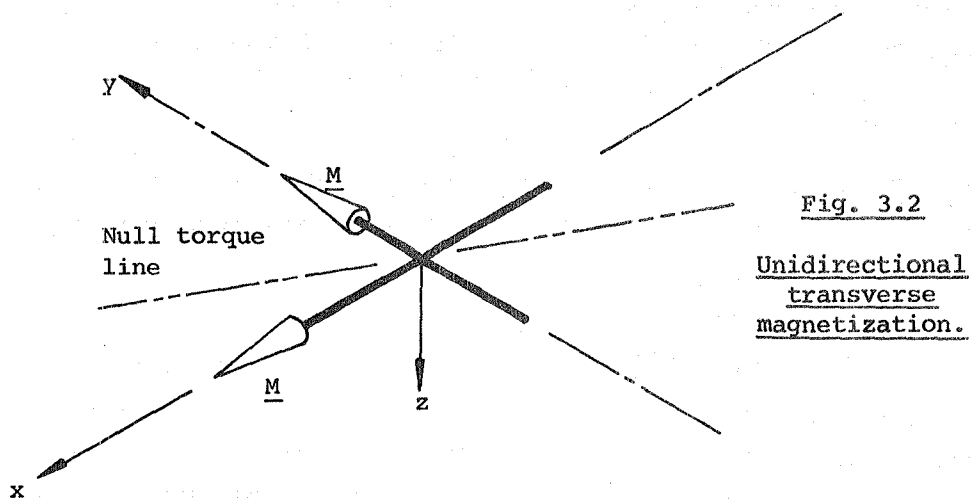
Fig. 3.2

Unidirectional
transverse
magnetization.

Null torque
line

The null torque line exists in uniform
applied field gradients.

Symmetrically disposed transverse magnetization components
will generate roll torque with application of a vertical field
with transverse gradient as Fig. 3.3.
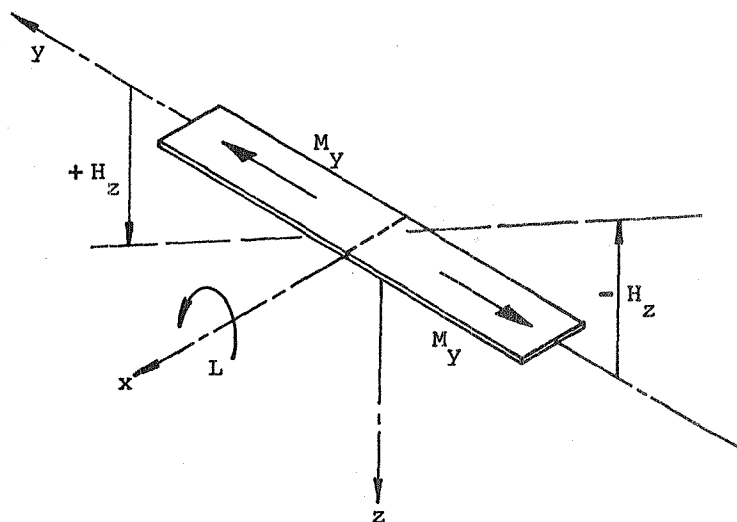
Fig. 3.3

Spanwise magnet
rolling moment
generation.

There are two subclasses of this system which will be dealt with separately and are referred to here as the Spanwise Permanent Magnet (SPM) and the Spanwise Iron Magnet (SIM) schemes.

3.2.3. A.C. Methods

The planar conducting loop method proposed by Stephens and since successfully demonstrated at M.I.T. is an ingenious approach to the problem and does have the advantage of minimal coupling between roll and other degrees of freedom. However, the strong A.C. fields required would be difficult to generate in a large scale system and may not be possible at all with current technology superconducting E/Ms. The predictions of roll torque capability appear promising but it is felt that the practical difficulties of operating an A.C. system at large scales would lead LMSBS designers to choose a D.C. system, if one were available with sufficient torque capability, in preference to the existing A.C. method.

4. SPANWISE PERMANENT MAGNETS (SPMs)

4.1 Introduction

If transverse magnetization components are generated by installation of permanent magnet cores, predominantly in the model's wings, then roll torque is directly generated by application of the appropriate through-wing fields as Fig. 3.3.

In all good permanent magnet materials at low applied fields the polarization (J) is practically independent of applied field strengths and may also be considered uniform over the volume of the core in the case of rare-earth cobalt (ReCo) materials, this class of permanent magnet exhibiting by far the highest known values of energy product and coercive force (25). A serious disadvantage of all known materials suitable for SPM application is poor mechanical properties, particularly high brittleness, that would preclude the use of permanent magnet cores as major load bearing members in the model's structure. Only some fraction of the available wing volume could thus be utilised for the SPM cores.

4.2 Theory

4.2.1 Ideal applied fields and simple spanwise magnetization

Where the transverse magnetizations are entirely in the y direction (spanwise) then equations 3.1 reduce to:

$$F_x = \int_V J_y H_{xy} \, dV$$

$$F_y = \int_V J_y H_{yy} \, dV$$

$$F_z = \int_V J_y H_{yz} \, dV$$

$$L = \int_V J_y H_z + J_y H_{yz} \, b - J_y H_{yy} \, c \, dV \qquad - (4.1)$$

$$M = \int_V J_y H_{xy} \, c - J_y H_{yz} \, a \, dV$$

$$N = \int_V -J_y H_x + J_y H_{yy} \, a - J_y H_{xy} \, b \, dV$$

If it is assumed that the applied field gradients are constant over the volume of the core then since:

$$\int_V J_y \, dV = 0 \qquad \text{(by symmetry about the xz plane)}$$

equations 4.1 collapse to:

$$F_x = F_y = F_z = M = 0$$

$$L = \int_V J_y (H_z + H_{yz}b)\, dV$$

$$N = \int_V -J_y (H_x + H_{xy}b)\, dV$$

further, if it is assumed that applied fields exhibiting large H_x components, (axial, magnetizing, lift) will be symmetrical about the xz plane (Appendix 5), then:

$$\int_V J_y H_x\, dV \simeq 0$$

Thus we have:

$$F_x = F_y = F_z = M = 0$$

$$L = \int_V J_y (H_z + H_{yz}b)\, dV \qquad\qquad - \quad (4.2)$$

$$N \simeq \int_V -J_y H_{xy} b\, dV$$

It is immediately seen that, since H_{xy} is the principal applied field gradient for sideforce generation via conventional axial (fuselage) magnetization, there exists one fundamental cross coupling due to the presence of the spanwise magnetizations, that is coupling into yaw from a sideforce demand. It is not thought that this presents any serious difficulty since the magnitudes of aerodynamic forces and moments in the lateral plane are generally considerably smaller than in the vertical, whereas the magnetic force and moment capability due to the axial magnetization will often be approximately equal in these two planes.

Examining a SPM wing core with ideal applied fields we have (see Fig. 4.1) :

From Eqns. 4.2:

$$L = \int_{b=-s}^{s} J_y A_o g(b) (H_z + H_{yz}b)\, db \qquad\qquad - \quad (4.3)$$

Now H_z may be written as $H_{z_t} \dfrac{b}{s}$ where H_{z_t} is the value of H_z at the tip. Assuming symmetry about the xz plane:

$$L = 2 \int_o^s J_y A_o g(b)\, H_{z_t} \frac{2b}{s}\, db$$

If J_y may be considered constant:

$$L = \frac{2H_{z_t} J_y}{s} \int_0^s 2A_o g(b) b \; db \qquad - \quad (4.4)$$

$$* \; A_b = A_o g(b)$$

$$H_{yz} \simeq \frac{H_{z_t}}{s}$$

$$H_z \simeq H_{z_t} \frac{b}{s}$$
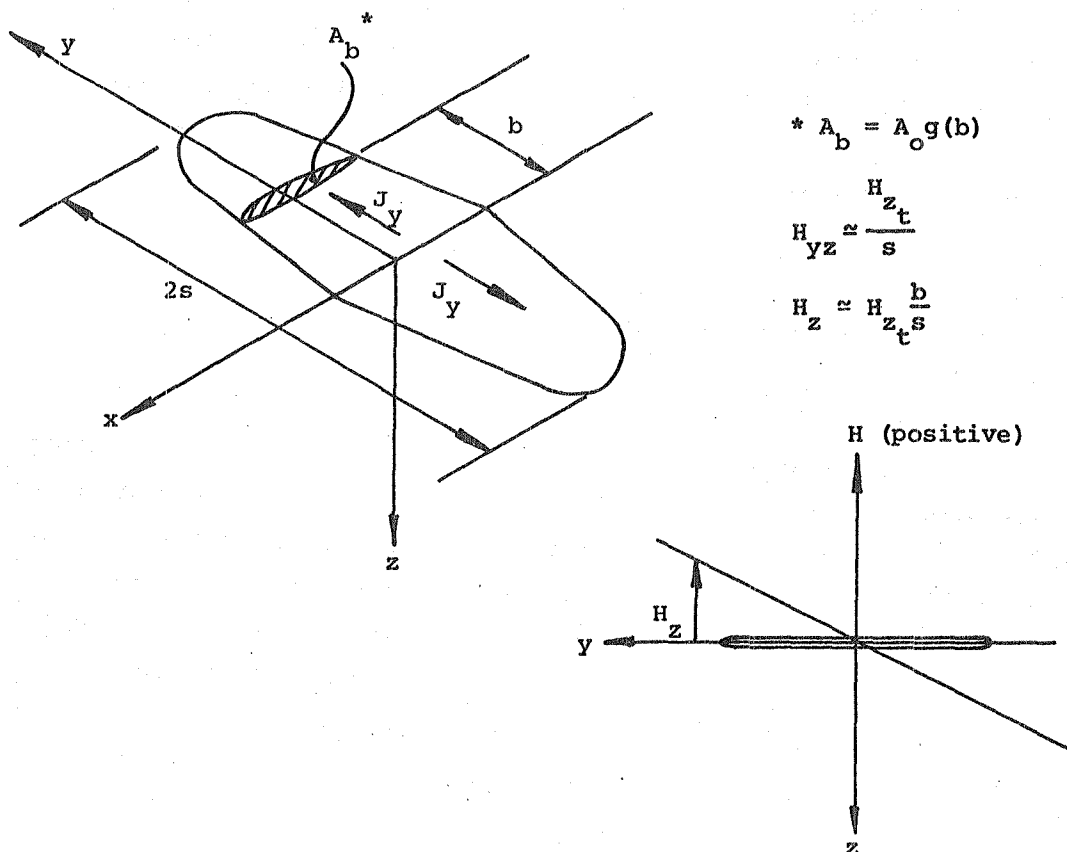
Fig. 4.1   SPM configuration

The integral is the first moment of volume of the core and depends only on its geometry. J_y is material dependent but does not vary dramatically amongst the best permanent magnet materials.   The maximum usable value of H_{z_t} depends on material properties and the internal demagnetizing influences of the core and can vary considerably between different materials and core geometries.

If the cross sectional area of the core is constant with b then $g(b) = 1$ and we have:

$$L = 2H_{z_t} J_y A_o s \qquad - \quad (4.5)$$

4.2.2 Theory. General applied fields and simple spanwise magnetization

In realistic MSBS configurations, uniform applied fields or field gradients cannot be achieved. Some treatment of cross couplings arising due to the interaction between non-uniform applied fields and the transverse magnetizations is important and can be made using Eqns. 4.1. The general approach taken here is to break down the integrals of 4.1 into x, y and z forms and express all integral arguments as odd (O) or even (E) functions of x, y and z. The characteristic geometrical symmetry (Fig. 4.1) immediately yields, writing an odd function of y as O_y etc.:

$$\int_{y(wing)} O_y \, dy = 0 \qquad - \quad (4.6)$$

Where the wing has a symmetrical section, similarly:

$$\int_{z(wing)} O_z \, dz = 0 \qquad - \quad (4.7)$$

Little error in fact occurs in using Eqn. 4.7 in most cases since the wing thickness is typically small with respect to other dimensions.

Applied fields may be represented by their characteristic symmetry in model axes, although this must be recognized as a considerable idealization, valid exactly with the model in the usual datum location, but only approximately so otherwise. The characteristic symmetry of the applied through-wing roll field is as follows:
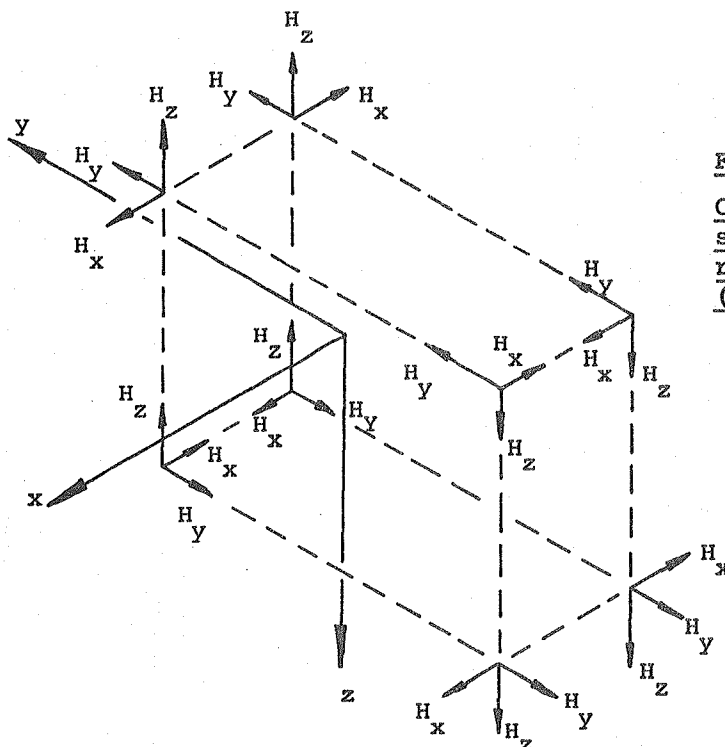

Fig. 4.2

Characteristic symmetry of applied roll field (Appendix 5)

Field null along x axis

-26-

which may be represented by the matrix equation:

$$\begin{pmatrix} H_x \\ H_y \\ H_z \end{pmatrix} = \begin{pmatrix} O & O & O \\ E & E & O \\ E & O & E \end{pmatrix} \begin{pmatrix} x \\ y \\ z \end{pmatrix} \qquad - \ (4.8)$$

Using $\dfrac{\partial}{\partial i}(E_i) = O_i$ and $\dfrac{\partial}{\partial i}(O_i) = E_i$ we have:

$$\begin{pmatrix} H_{xx} \\ H_{xy} \\ H_{xz} \\ H_{yy} \\ H_{yz} \\ H_{zz} \end{pmatrix} = \begin{pmatrix} E & O & O \\ O & E & O \\ O & O & E \\ E & O & O \\ E & E & E \\ E & O & O \end{pmatrix} \begin{pmatrix} x \\ y \\ z \end{pmatrix} \qquad - \ (4.9)$$

Now $J_y = O_y E_x E_z$ and using:

$$E_i E_i = E_i \ ; \quad O_i O_i = E_i \ ; \quad O_i E_i = E_i O_i = O_i \ ;$$

$$b = E_x O_y E_z \ ; \quad c = E_x E_y O_z \ \text{and} \ a = O_x E_y E_z \ ;$$

equations 4.1 become:

$$F_x = \int_x O_x \int_y O_y \int_z O_z \, dz \, dy \, dx = O$$

$$F_y = \int_x E_x \int_y E_y \int_z O_z \, dz \, dy \, dx = O$$

$$F_z = \int_x E_x \int_y O_y \int_z E_z \, dz \, dy \, dx = O$$

$$L = \int_x E_x \int_y E_y \int_z E_z \, dz \, dy \, dx \ (J_y H_z \text{ term}) \qquad \neq O$$

$$+ \int_x E_x \int_y E_y \int_z E_z \, dz \, dy \, dx \ (J_y H_{yz} b \text{ term}) \qquad \neq O$$

$$- \int_x E_x \int_y E_y \int_z E_z \, dz \, dy \, dx \ (J_y H_{yy} c \text{ term}) \qquad \neq O$$

$$M = \int_x O_x \int_y O_y \int_z E_z \, dz \, dy \, dx \ (J_y H_{xy} c \text{ term}) \qquad = O$$

$$- \int_x O_x \int_y O_y \int_z E_z \, dz \, dy \, dx \ (J_y H_{yz} a \text{ term}) \qquad = O$$

$$N = -\int\limits_x O_x \int\limits_y E_y \int\limits_z O_z \, dz \, dy \, dx \quad (J_y H_x \text{ term}) \quad = 0$$

$$+ \int\limits_x O_x \int\limits_y E_y \int\limits_z O_z \, dz \, dy \, dx \quad (J_y H_{yy} a \text{ term}) \quad = 0$$

$$- \int\limits_x O_x \int\limits_y E_y \int\limits_z O_z \, dz \, dy \, dx \quad (J_y H_{xy} b \text{ term}) \quad = 0$$

Thus equations 4.1 collapse to:

$$F_x = F_y = F_z = M = N = 0$$

$$L = \int\limits_v J_y H_z + J_y H_{yz} b - J_y H_{yy} c \, dV \qquad - (4.10)$$

Of course c is small (Fig 4.1), thus equations 4.10 reduce further to:

$$F_x = F_y = F_z = M = N = 0$$

$$L \cong \int\limits_v J_y H_z + J_y H_{yz} b \, dV \qquad - (4.11)$$

It is immediately seen that there exist no primary couplings due to the transverse magnetizations with typical applied roll fields. There may, however, exist couplings due to the applied roll field with the conventional axial (fuselage) magnetization or due to other applied fields and the transverse (wing) magnetizations. Couplings between the applied roll field and conventional axial magnetization will be small with all realistic geometries, since the roll field exhibits a null along the x axis (Fig. 4.2), and will be zero with axisymmetric fuselage cores.

The full calculations as shown above will not be carried through here for all cases but the important results are as follows:

Table 4.1 Characteristic symmetries of applied fields
          (Appendix 5)

Field classification	Primary field or field gradient component	Field component characteristic symmetry matrix (as Eqn. 4.8)		
Magnetizing	H_x	E	E	E
		O	O	E
		O	E	O
Drag	H_{xx}	O	E	E
		E	O	E
		E	E	O

Lift	H_{xz}	$\begin{pmatrix} E & E & O \\ O & O & O \\ O & E & E \end{pmatrix}$		
Pitch	$-H_z$	$\begin{pmatrix} O & E & O \\ E & O & O \\ E & E & E \end{pmatrix}$		
Sideforce	H_{xy}	$\begin{pmatrix} E & O & E \\ O & E & E \\ O & O & O \end{pmatrix}$		
Yaw	H_y	$\begin{pmatrix} O & O & E \\ E & E & E \\ E & O & O \end{pmatrix}$		

From equations 4.1 etc. the following conditions can be identified:

$F_x \neq O$ where $H_{xy} = O_y E_z$

$F_y \neq O$ where $H_{yy} = O_y E_z$

$F_z \neq O$ where $H_{yz} = O_y E_z$

$L \neq O$ where $H_z = O_y E_z$ $(J_y H_z$ term)

or $H_{yz} = E_y E_z$ $(J_y H_{yz} b$ term)

or $H_{yy} = O_y O_z$ $(J_y H_{yy} c$ term)

$M \neq O$ where $H_{xy} = O_y O_z$ $(J_y H_{xy} c$ term)

or $H_{yz} = O_y E_z$ $(J_y H_{yz} a$ term)

$N \neq O$ where $H_x = O_y E_z$ $(J_y H_x$ term)

or $H_{yy} = O_y E_z$ $(J_y H_{yy} a$ term)

or $H_{xy} = E_y E_z$ $(J_y H_{xy} b$ term)

These criteria can be related to the symmetry matrices in
Table 4.1 either directly or by using:

$$H_{ij} = E_k(O_k) \Rightarrow (\text{implies}) \quad H_i = E_k(O_k) \quad \text{and} \quad H_j = E_k(O_k)$$

$$H_{ij} = E_j(O_j) \Rightarrow \quad\quad\quad H_i = O_j(E_j) \quad \text{and} \quad H_j = E_j(O_j)$$

$$H_{ii} = E_i(O_i) \Rightarrow \quad\quad\quad H_i = O_i(E_i)$$

The conditions above become:

$F_x \neq O$ with the applied field symmetry matrix as:
$$\begin{pmatrix} X & E & E \\ X & O & E \\ X & X & X \end{pmatrix}$$
$\quad X \equiv$ don't care

 - Satisfied by magnetizing and drag fields only

$F_y \neq O$ with
$$\begin{pmatrix} X & X & X \\ X & E & E \\ X & X & X \end{pmatrix}$$

 - Satisfied by yaw and sideforce fields only

$F_z \neq O$ with
$$\begin{pmatrix} X & X & X \\ X & O & O \\ X & E & E \end{pmatrix}$$

 - Satisfied by pitch and lift fields only

$L \neq O$ with
$$\begin{pmatrix} X & X & X \\ X & X & X \\ X & O & E \end{pmatrix} \text{or} \begin{pmatrix} X & X & X \\ X & E & O \\ X & O & E \end{pmatrix} \text{or} \begin{pmatrix} X & X & X \\ X & E & O \\ X & X & X \end{pmatrix}$$

 - Satisfied by no fields

$M \neq O$ with
$$\begin{pmatrix} X & E & O \\ X & O & O \\ X & X & X \end{pmatrix} \text{or} \begin{pmatrix} X & X & X \\ X & O & O \\ X & E & E \end{pmatrix}$$

 - Satisfied by pitch and lift fields only

$N \neq O$ with
$$\begin{pmatrix} X & O & E \\ X & X & X \\ X & X & X \end{pmatrix} \text{or} \begin{pmatrix} X & X & X \\ X & E & E \\ X & X & X \end{pmatrix} \text{or} \begin{pmatrix} X & O & E \\ X & E & E \\ X & X & X \end{pmatrix}$$

 - Satisfied by yaw and sideforce fields only

The origin of many of these cross couplings is easily identified as core asymmetry in the yz plane. If this condition is abandoned and a fully symmetric core considered then further couplings disappear, leaving:

$F_x \neq 0$ with magnetizing field

$F_y \neq 0$ with yaw field

$F_z \neq 0$ with pitch field

$L = 0$ with all fields

$M \neq 0$ with lift field

$N \neq 0$ with sideforce field

4.2.3 Theory. General spanwise magnetization
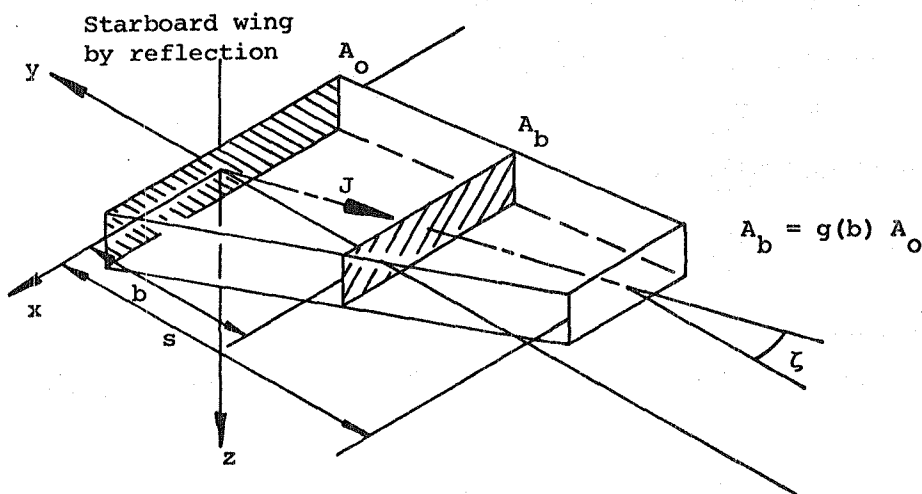
Fig. 4.3 Sweptback SPM core

In the majority of cases of interest the model's wings will be sweptback as shown in Fig. 4.3 above. To preserve low demagnetizing factors for the SPM cores the direction of magnetization must be sweptback also, perhaps to lie along the axis of centroids of core cross-sectional area.

Full analysis of this case becomes complex since both J_x and J_y components exist. However, if the SPM cores are assumed slender, whence applied fields may be considered uniform over any core cross-section, the fundamental effects of the x-wise magnetization components can be identified:

- 31 -

$$J_x = - J A_0 g(b) \sin \zeta$$

$$J_y = J A_0 g(b) \cos \zeta$$

$$J_z = 0$$

From Eqns. 3.1:

$$L = \int_V J_y H_z + (J_x H_{xz} + J_y H_{yz})b - (J_x H_{xy} + J_y H_{yy}) c \, dV$$

$$L = \int_V J_y (H_z + b H_{yz} - c H_{yy}) + J_x (b H_{xz} - c H_{xy}) \, dV$$

The J_x terms may be broken down as before, using Eqns. 4.9:

$$\int_V J_x b H_{xz} \, dV \equiv \int_x X \int_y E_y O_y O_y \int_z E_z E_z E_z \, dz \, dy \, dx \neq 0$$

$$\int_V J_x c H_{xy} \, dV \equiv \int_x X \int_y E_y E_y E_y \int_z E_z O_z O_z \, dz \, dy \, dx \neq 0$$

But since c is typically small, we may write:

$$L \simeq \int_V J_y (H_x + b H_{yz}) + J_x b(H_{xy}) \, dV \qquad - (4.12)$$

The J_x term is identified as the sum of the moments of the "lift" force (F_z) components over the wing volume, the J_y terms being as in Eqn. 4.11.

4.3 Theoretical performance

Direct evaluation of the integrals in Eqns. 4.1 etc. is not generally possible since field and field gradient components can seldom be represented as simple functions of x, y and z. Where the MSBS E/Ms are air cored, the applied field at any point within the model core may be calculated analytically or numerically (Appendix 2), permitting evaluation of the total forces and torques acting on the model, where the magnetization distribution is known, effectively by numerical integration of Eqns. 3.1 over the core volume. The magnetization distribution may be assumed known in the case of ReCo materials below the onset of irreversible de-magnetization, then typically being constant and uniform, otherwise tending to be difficult to compute.

A key requirement for LMSBS application is the identification of the absolute maximum torque capability of a particular core, which in the SPM case will be determined by the onset of irreversible

demagnetization of the core.

The total field within the core is the sum of the applied (E/M) field and the internal self-demagnetizing field of the core. The self-demagnetizing field of cores of arbitrary shape and known magnetization distribution may be calculated numerically and certain idealised forms yield to direct analysis. Where the total field acts parallel to the local direction of magnetization the onset of irreversible demagnetization may be predicted directly from the materials BH (or JH) curve, ReCo materials generally exhibiting near straight-line curves in the 2nd quadrant (Fig. 4.4).

Fig. 4.4 Classical 2nd quadrant

of BH curve for ReCo materials

(idealised)
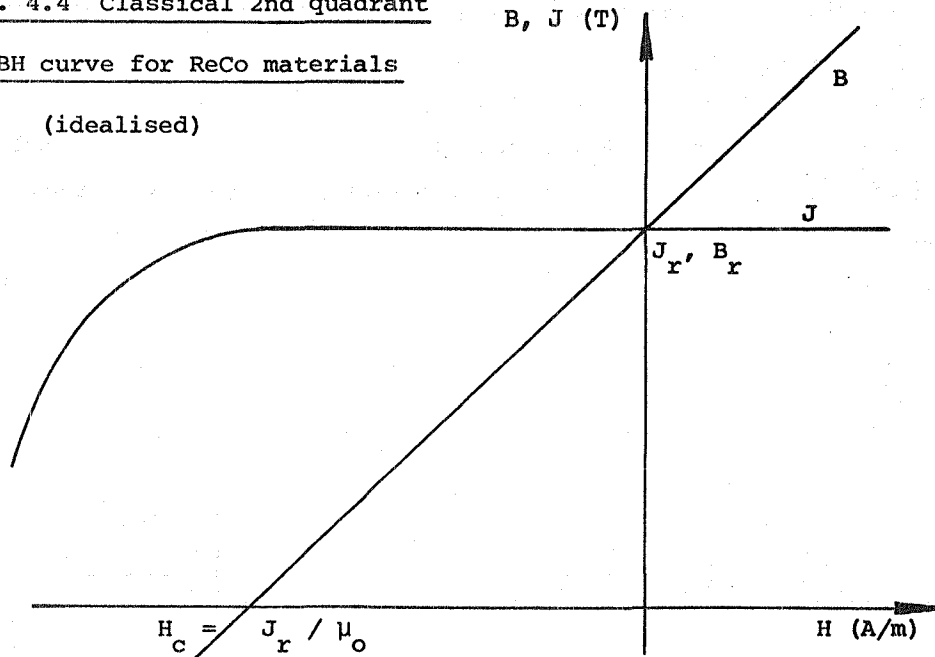
Unfortunately, the total field will seldom act as described above, and whereas some data exists concerning the demagnetization of single crystals of certain materials with total fields not parallel to the direction of magnetization (for instance see Refs. 26, 27, 28), it is not thought that this can be applied to bulk materials, demagnetization then being powerfully affected by processes principally dependent on the material's microstructure, such as domain wall movement (28, 29, 30). No relevant data

concerning bulk ReCo materials has been discovered (see Ref. 31 for treatment of particular ferrites), rendering predictions of maximum torque capability of general SPM systems impossible at present. However, a crude estimate of the order of magnitude of available torque may be made by the following argument.

In slender cores magnetized along their long axis, the internal self-demagnetizing field is small over the majority of the volume and may be neglected here. The effects of the magnetization reversal at the wing root (Fig. 4.1) and of the detail geometry of the cores is beyond the scope of this treatment. The magnetic field strengths internal to the cores may thus be regarded as predominantly due to the applied field. The conventional parameters characterising the performance of permanent magnet materials, such as H_c, H_{ci}, J_r, BH_{max} etc. (25), are insufficient for identification of incipient irreversible demagnetization. Several authors resort to use of the parameter H_k, representing the demagnetizing field strength that reduces the intrinsic polarization to 90% of the remanent value (25, 32, 33), illustrated in Fig. 4.5.
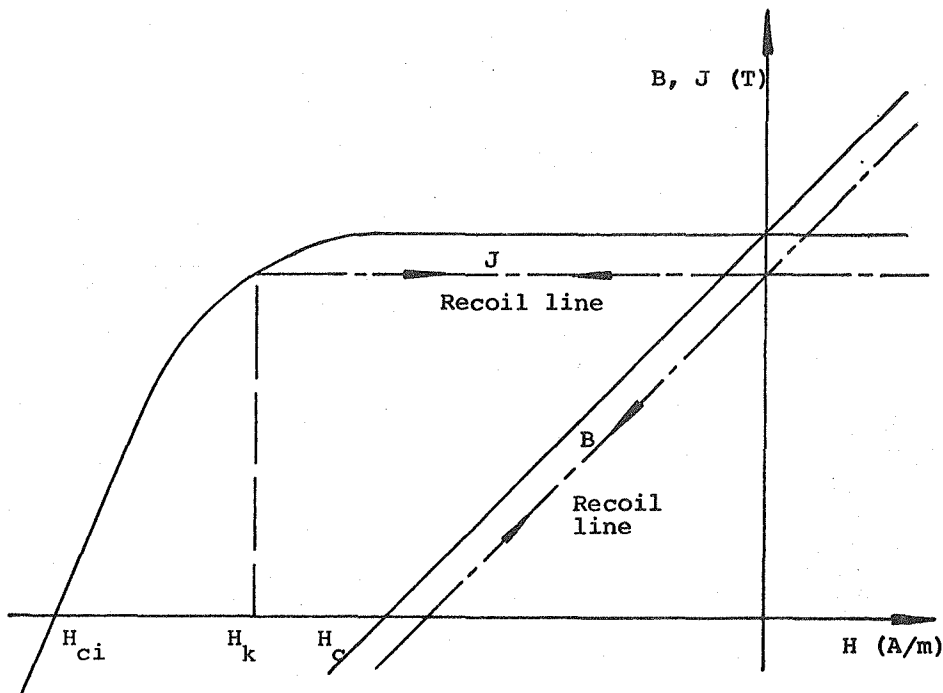

Fig. 4.5 Definition of H_k

Values of H_k for relevant materials are sparsely quoted, reflecting the arbitrariness of the parameter's definition, some available data being reproduced in Table 4.2 below:

Table 4.2 Some properties of bulk ReCo materials

Material	J_r (T)	H_c	H_k (kA/m)	H_{ci}	Reference	
Sintered Sm Co$_5$	0.85	650	900	1200	25	(1977)
"Commercial" Sm Co$_5$	0.84	560	488	800	32	(1971)
Sm Co$_5$ based "RECOMA 20"	0.90	700	1000	1200	33	(1976)

Current material developments are expected to result in improvements in H_c and J_r with H_k tending to comfortably exceed H_c. At this stage it would not appear unreasonable to assume a usable value of H_k of some 800 kA/m ($\mu_o H_k \simeq 1T$) and J_r of 0.85 T. If this value of H_k can be taken to represent the peak total field strength that can be applied to the material before the onset of irreversible demagnetization, with the working polarization taken as 90% of the value of J_r quoted immediately above, then some progress may be made.

The applied field is a sum of many contributory fields ("lift", "drag", etc.), but it should be noted that the two fields (neglecting roll) likely to involve the most powerful fields within the test section need not cause the exposure of the wing core to those high field strengths (Fig. 4.6).

If it can thus be assumed that the principal component of applied field within the wing cores is the applied "roll" field then H_{z_t} in Eqns. 4.4, 4.5, etc. becomes H_k. Taking the values assumed above, we have from Eqn. 4.4:

$$L \simeq \frac{2.4 \times 10^6}{s} \int_o^s A_o \, g(b) \, b \, db \qquad - \quad (4.13)$$

and from Eqn. 4.5 for rectangular slab cores:
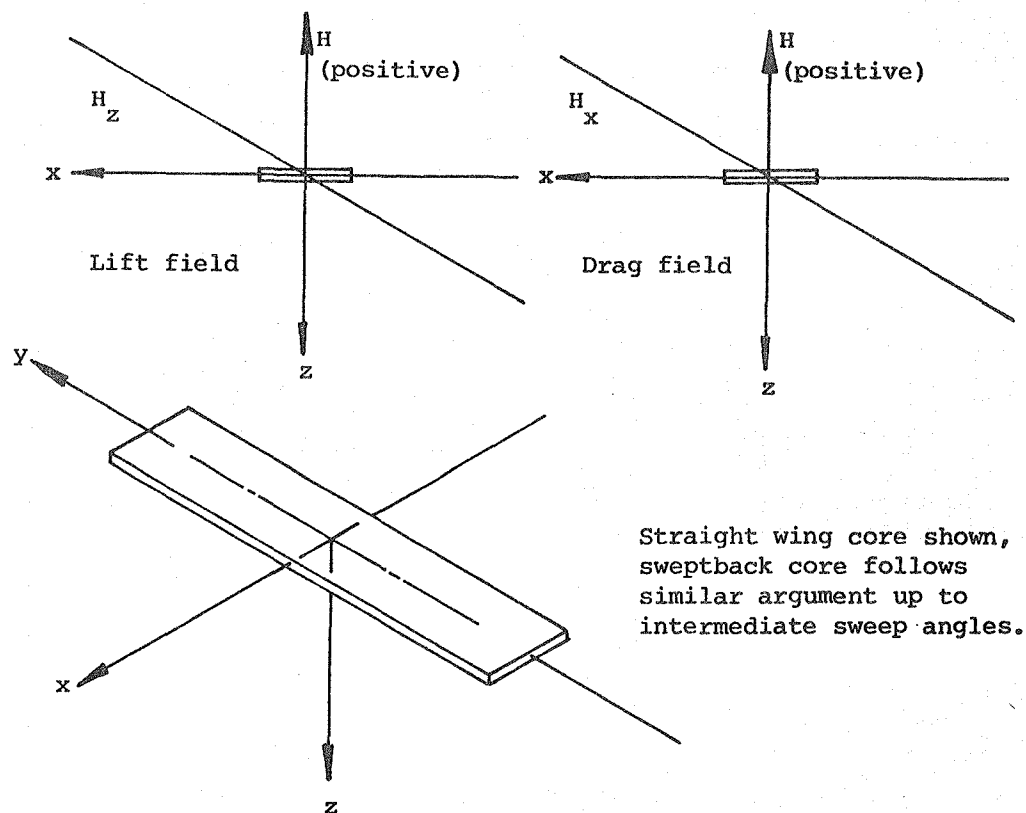
$$L \simeq 1.2 \times 10^6 A_o s \qquad - \quad (4.14)$$

Fig. 4.6 Components of lift and drag fields
at the wing core

Eqn. 4.14 corresponds to 600,000 Nm/m^3 of core. For the represen-
tative SPM core studied in Section 4.3.1 below, this would indicate
a maximum capability of approximately 500 Nm. It may be, however,
that applied fields of sufficient strength to realise this capability
cannot be generated with existing technology E/Ms. In fact, taking
the roll torque calibration calculated below (Section 4.3.1), maximum
torque would occur at around 16,000 A/cm^2 in the specified E/Ms.
This is well beyond current E/M technology (see Section 5.8.2).
Present apparent LMSBS roll torque requirements (5) may be
approachable with more carefully configured E/M arrays.

4.3.1 Performance of representative SPM configurations

Since accurate analytic predictions of performance (below the
onset of demagnetization) are not practical, numerical examination
of representative SPM configurations is appropriate, the computer
program FORCE (Appendix 2) being suitable for such studies. Some
preliminary results are presented here.

The geometry of E/M array and model is chosen so as to be directly comparable to the baseline geometry used in the studies of the SIM system (Section 5) and readers should refer to Section 5.4 for explanation of the evolution of these geometries. The wing core is chosen to occupy one half of the available cross section (Fig. 4.7), the aerodynamic and other loads being assumed as principally carried by the surrounding structure. A quadrupole field elegantly provides the required through-wing field, in turn being supplied by the appropriate quartet of E/Ms from the baseline SIM array (Figs. 4.8, 5.4), though the entire SIM array is used for examination of 360° roll capability.

Confirmation of some of the predicted couplings between axial or spanwise magnetization and the applied roll or other fields is straightforward. Conventionally configured but arbitrarily dimensioned E/Ms are specified to provide lift, pitch, etc. fields (Figs. 4.9, 4.10). It should be noted that the overall E/M array is realistically proportioned although the axial and main E/Ms do (unintentionally) spatially conflict.

The magnetic forces and torques generated on the model and their variation with simple displacements or rotations of the model are shown in Figs. 4.11 - 4.19. Confirmation of the predicted magnetic couplings due to the spanwise magnetizations can now be made. These are (from Section 4.2.2):

Force/torque	Applied field	Figure (zero displacements)
F_x	Magnetizing	4.19
F_y	Yaw	4.18
F_z	Pitch	4.17
L	None	---
M	Lift	4.14
N	Sideforce	4.16

The wing core's symmetry about the yz plane is conveniently destroyed by a displacement in the x direction. Consulting the relevant Figures therefore, the extra predicted couplings for a core lacking symmetry about the yz plane may be confirmed also:

0.0080

0.12 ⌀

1.2

1.2

J

J

J

0.09

A

y

x

z

Dimensions in
metres. All core
polarizations =
1 Tesla

x

z

SIM cores (Section
5) this size

Non-magnetic
envelope (7.2cm^2)

Magnetic core (7.2cm^2)

Detail view on A showing direct comparison
to baseline SIM geometry (Fig.5.5)

x

z

Equivalent airfoil
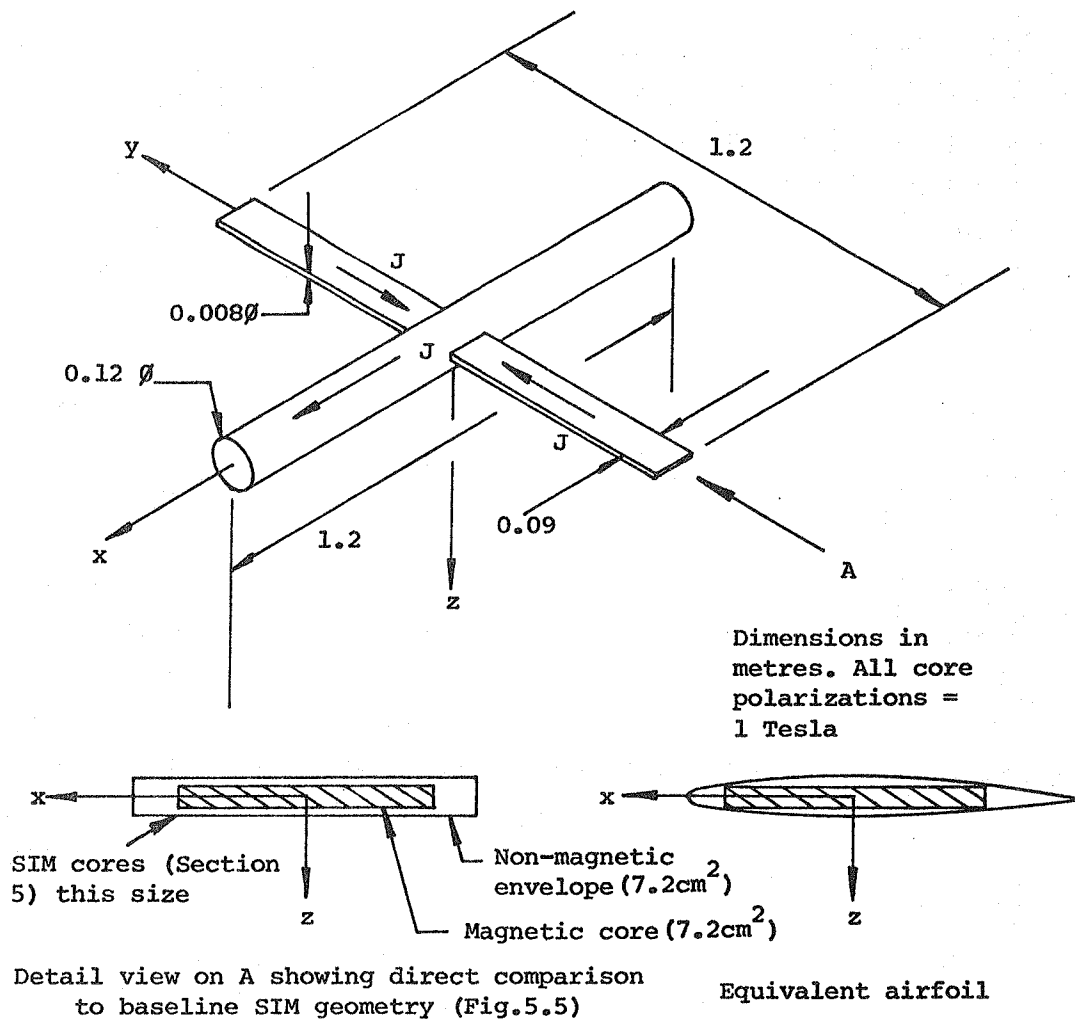
Fig. 4.7   Model magnetic configuration for SPM calculations

0.765 rad

0.383 rad

0.382

y

z

45°

2.245

This array
represents the
appropriate
quartet of E/Ms
from the SIM
array of Section
5 (Fig. 5.4)

This figure
is schematic
only.
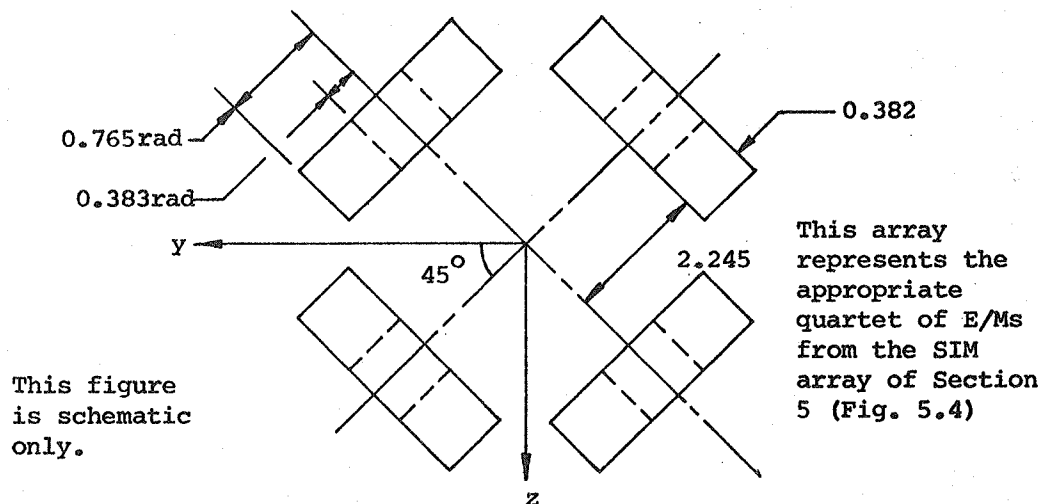
Fig. 4.8   Roll E/M configuration for SPM calculations.

All dimensions in metres

Location of
roll E/Ms
(Fig. 4.8)

1.829

1.829

1.213

1.613

0.4

MAIN
E/Ms

Part section on BB

B

1.765

x

1.213

1.613

B

View on A

Dimensions in metres

AXIAL
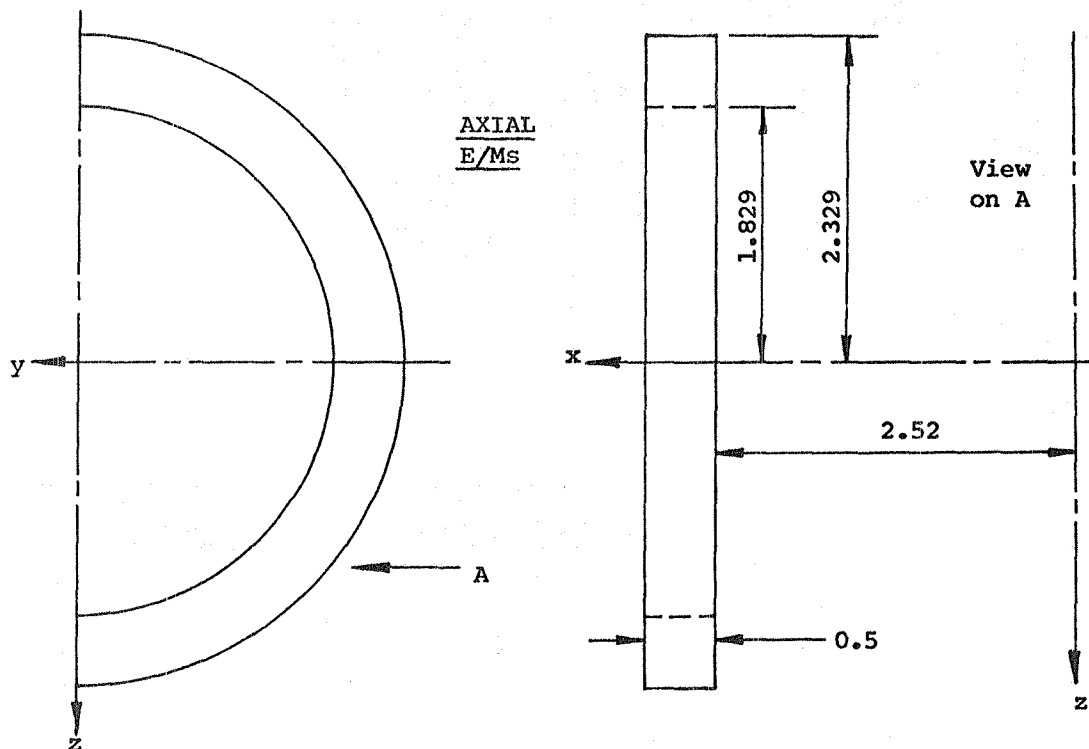E/Ms

y

A

x

1.829

2.329

View
on A

2.52

0.5

z
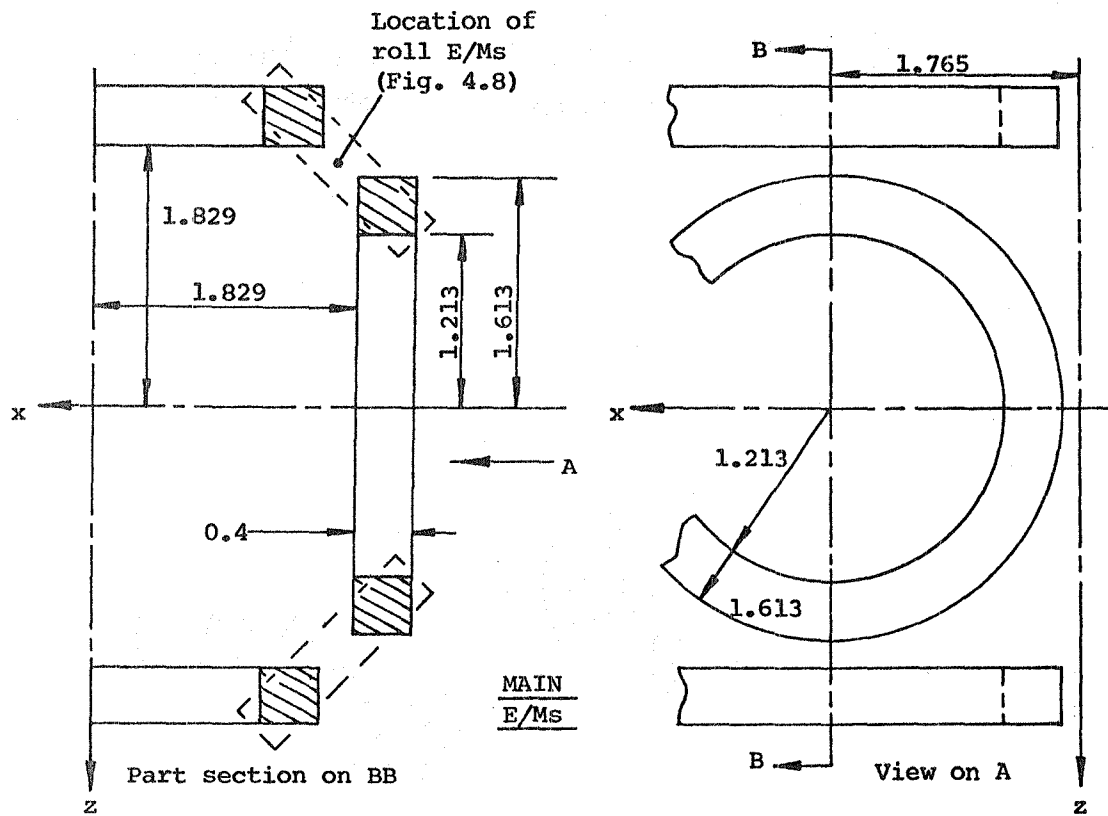
Fig. 4.9 Geometry and dimensions of E/Ms for roll coupling study

- 39 -

Applied fields defined by the following relationships of currents :

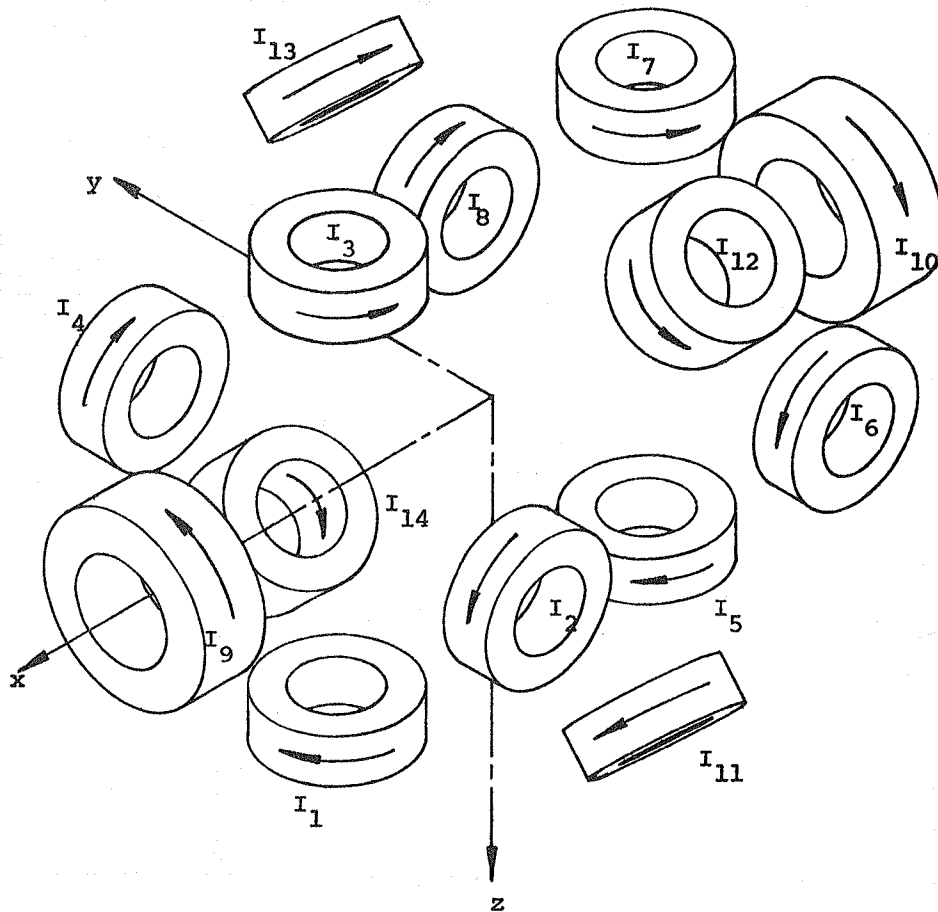|	I_1	I_2	I_3	I_4	I_5	I_6	I_7	I_8	I_9	I_{10}	I_{11}	I_{12}	I_{13}	I_{14}
	currents not specifically shown are zero													
Drag									+	−				
Magnetizing									+	+				
Roll											+	−	+	−
Lift	+		−		−		+							
Pitch	−		+		−		+							
Sideforce		−		+		+		−						
Yaw		−		+		−		+						

Fig. 4.10 Schematic diagram of complete E/M array for roll coupling
studies. All currents directions positive as shown.

Fig. 4.11 Couplings for wing in roll field

E/Ms as Fig. 4.8, 4.10

Model as Fig. 4.7

Roll field defined by :

$$+I_{11} = -I_{12} = +I_{13} = -I_{14} = 1,459,240 \text{ A} \quad (1000 \text{ A/cm}^2)$$

$$I_1 - I_{10} = 0$$

Sense of model rotations

(ϕ, θ, ψ) and torques

(L, M, N)

Torques are expressed
in translated but
unrotated axes

All force and torque components not shown are exactly or
effectively zero.
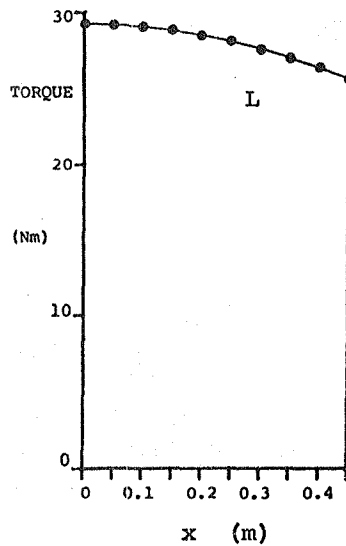
Fig. 4.11a

Fig. 4.11b
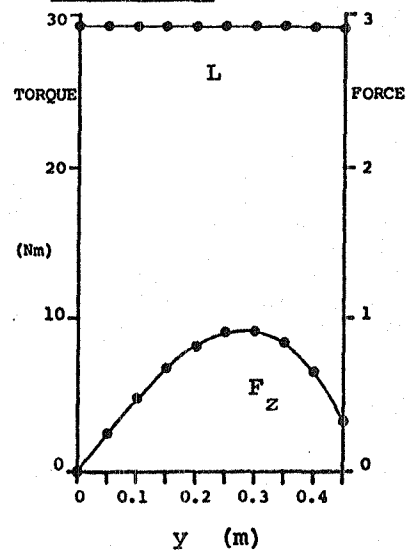
Fig. 4.11c
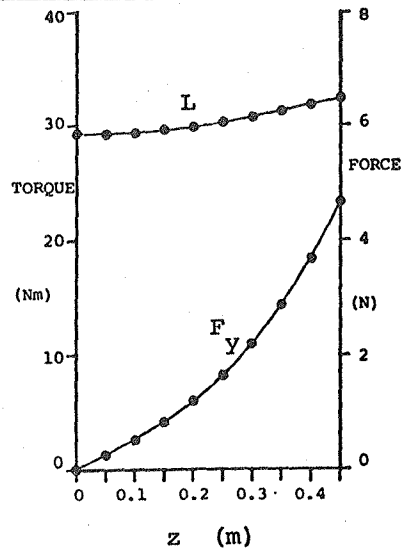
Fig. 4.11d
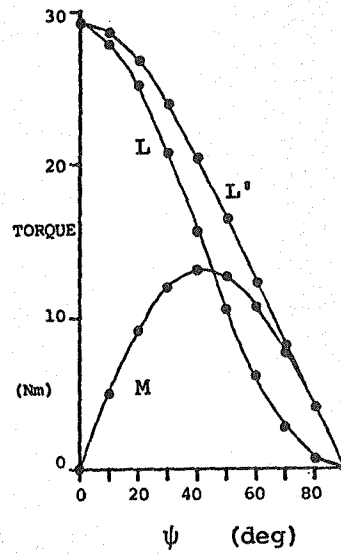
Fig. 4.11e
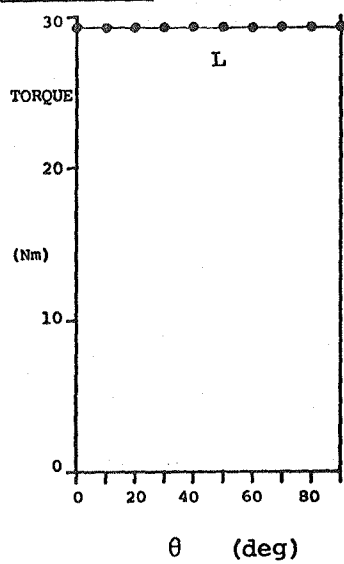
Fig. 4.11f
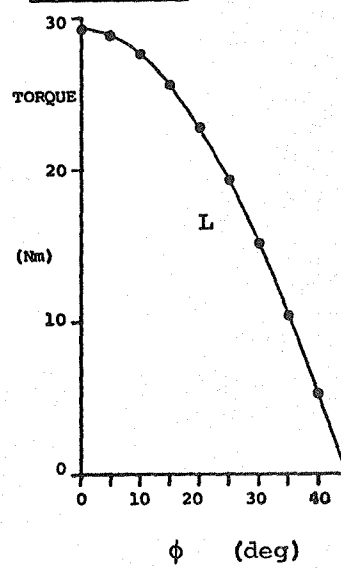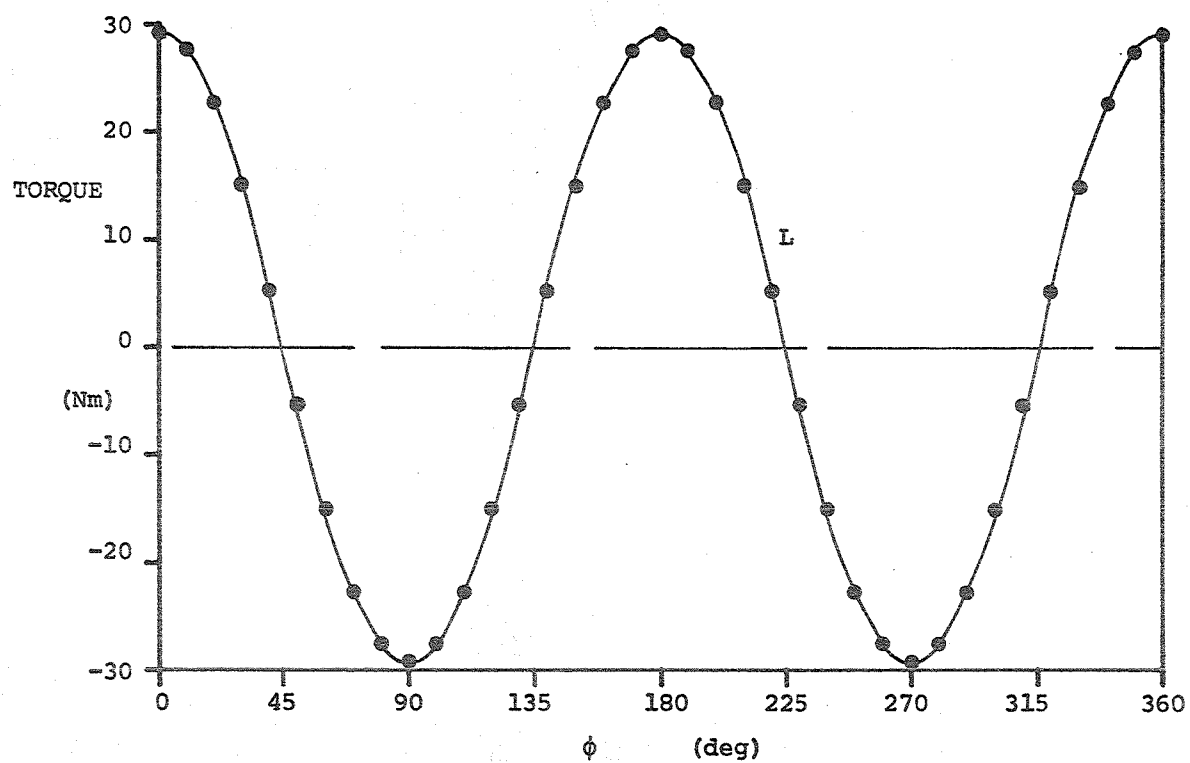
Fig. 4.12 Couplings for
wing in roll field.

E/Ms as Fig. 4.8

Model as Fig. 4.7

E/M currents etc.
   as Fig. 4.11

Fig. 4.13 Couplings for fuselage in roll field
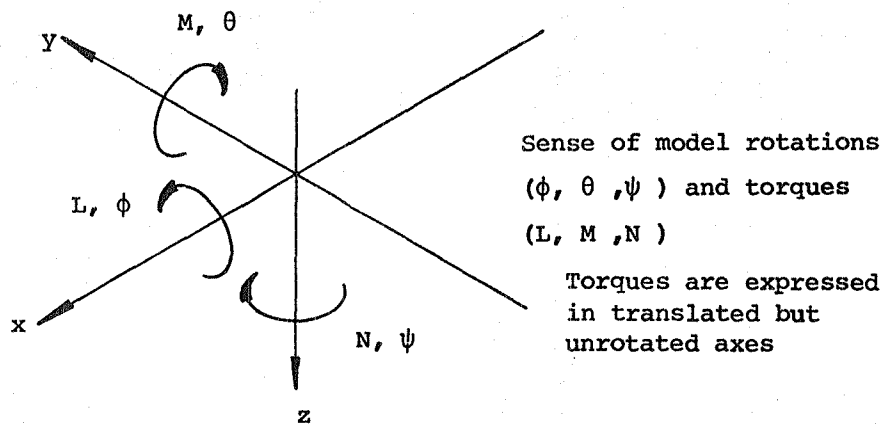
E/Ms as Fig. 4.8, 4.10

Model as Fig. 4.7

Roll field defined by :

$$+I_{11} = -I_{12} = +I_{13} = -I_{14} = 1,459,240 \text{ A}$$

$$I_1 - I_{10} = 0$$

Model rotations and torques as Fig. 4.11

All force and torque components not shown are exactly or effectively zero.

Fig. 4.13a

x   (m)

Fig. 4.13b

y   (m)
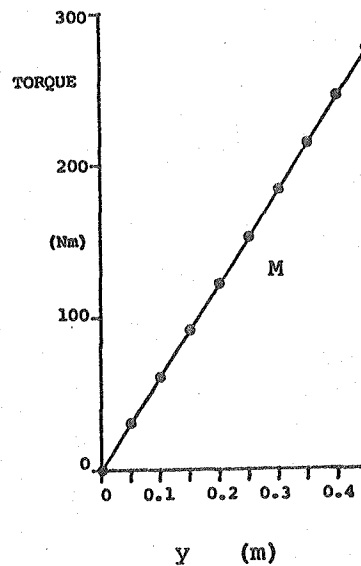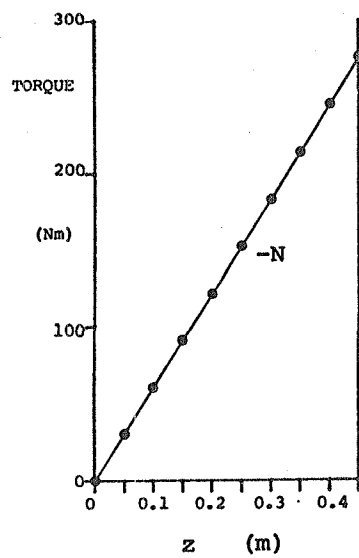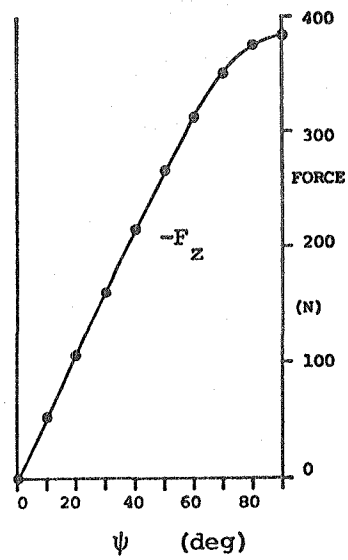
Fig. 4.13c

Fig. 4.13d

Fig. 4.13e
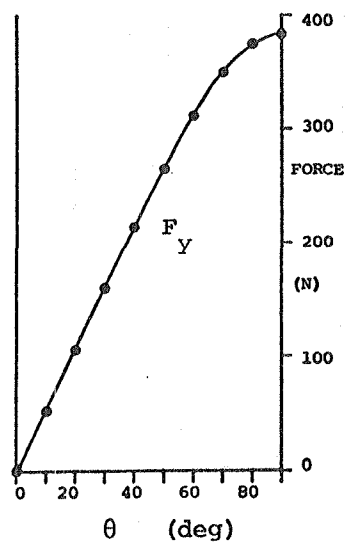
Fig. 4.13f
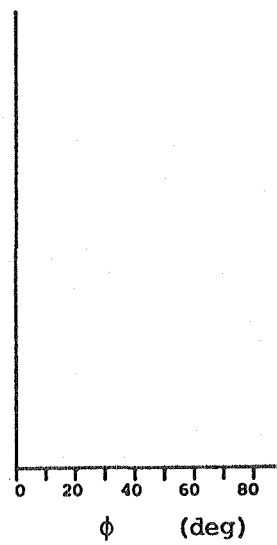
Fig. 4.14 Couplings for wing in lift field
_____

E/Ms as Fig. 4.9, 4.10

Model as Fig. 4.7

Lift field defined by :

$$+I_1 = -I_3 = -I_5 = +I_7 = 1,600,000 \text{ A } (1000 \text{ A/cm}^2)$$

$$I_2, \; I_4, \; I_6 \text{ and } I_8 - I_{14} = 0$$

Model rotations and torques as Fig 4.11

All force and torque components not shown are exactly or effectively zero.

Fig. 4.14a
_____

Fig. 4.14b
_____


x (m)

y (m)

- 46 -
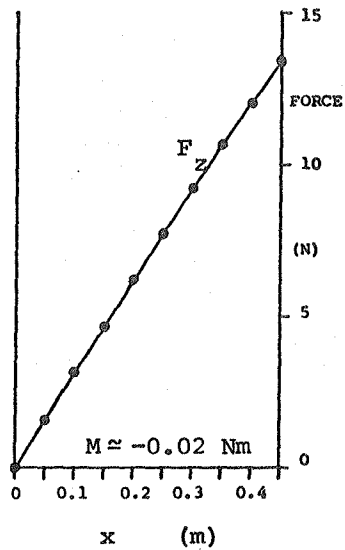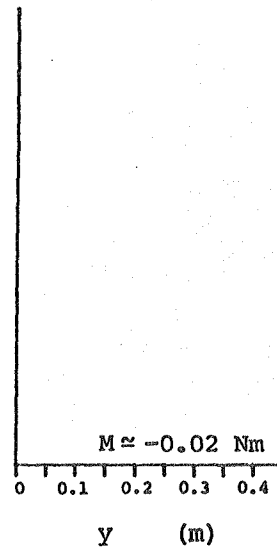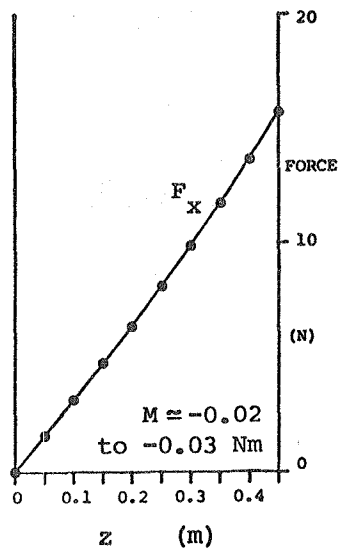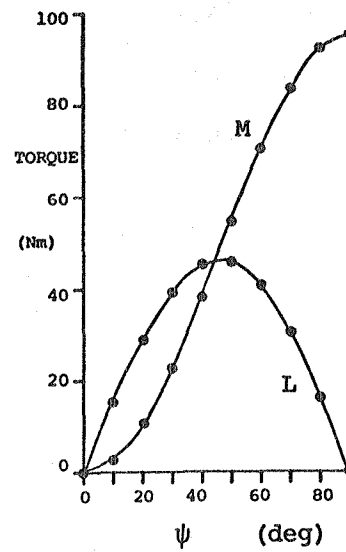
Fig. 4.14c

Fig. 4.14d

Fig. 4.14e
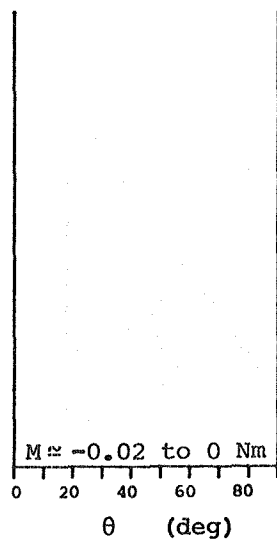
Fig. 4.14f
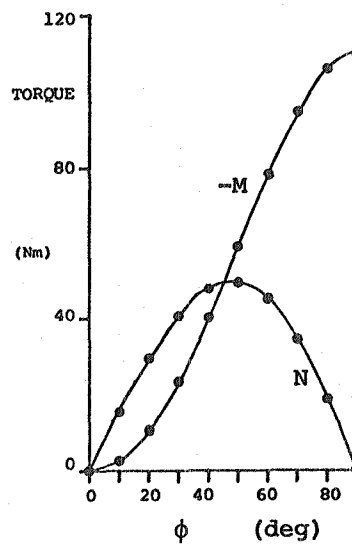
Fig. 4.15 Couplings for wing in drag field

E/Ms as Fig. 4.9, 4.10

Model as Fig. 4.7

Drag field defined by :

$$+I_9 = -I_{10} = \quad 2,500,000 \text{ A } (1000 \text{ A/cm}^2)$$

$$I_1 - I_8 \text{ and } I_{11} - I_{14} = 0$$

Model rotations and torques as Fig. 4.11

All force and torque components not shown are exactly or effectively zero.

Fig. 4.15a

x   (m)

Fig. 4.15b

y   (m)

Fig. 4.15c

FORCE

(N)

−F$_z$

Z (m)

Fig. 4.15d

TORQUE

(Nm)

−N

ψ (deg)

Fig. 4.15e

θ (deg)

Fig. 4.15f

φ (deg)
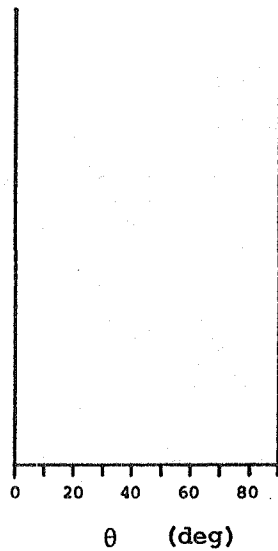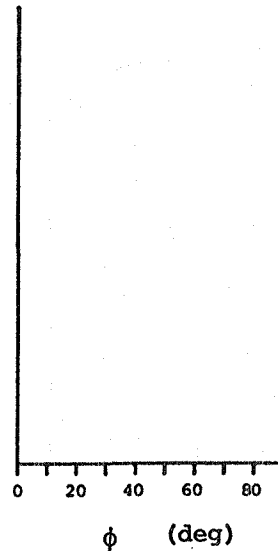
Fig. 4.16   Couplings for wing in sideforce field

E/Ms as Fig. 4.9,4.10

Model as Fig. 4.7

Sideforce field defined by :

$$-I_2 = +I_4 = +I_6 = -I_8 = 1,600,000 \text{ A } (1000 \text{ A/cm}^2)$$

$$I_1, I_3, I_5, I_7, I_9 - I_{14} = 0$$

Model rotations and torques as Fig. 4.11

All force and torque components not shown are exactly or effectively zero.

Fig. 4.16a
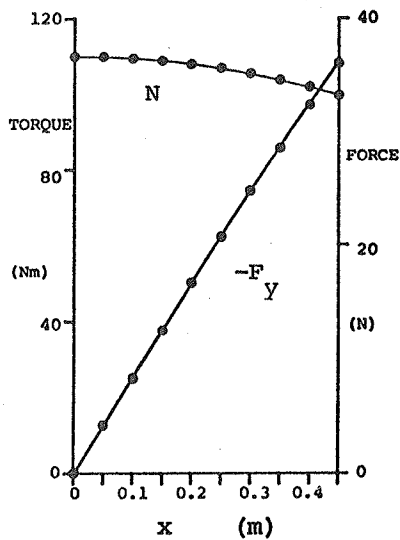
Fig. 4.16b
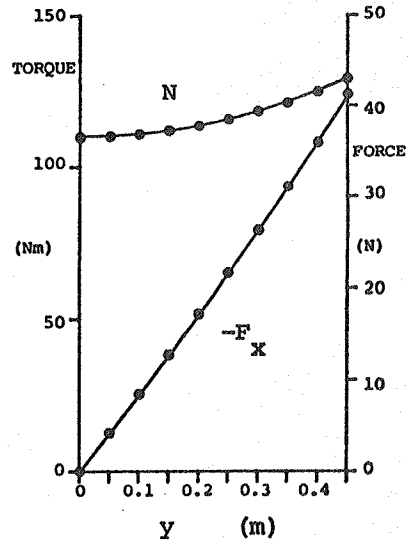
Fig. 4.16c
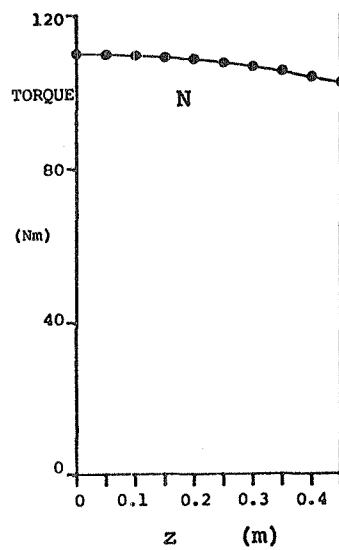
Fig. 4.16d
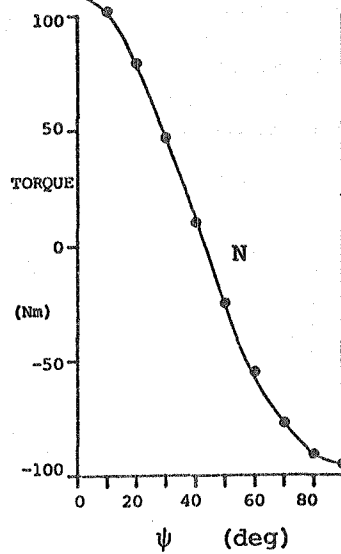
Fig. 4.16e
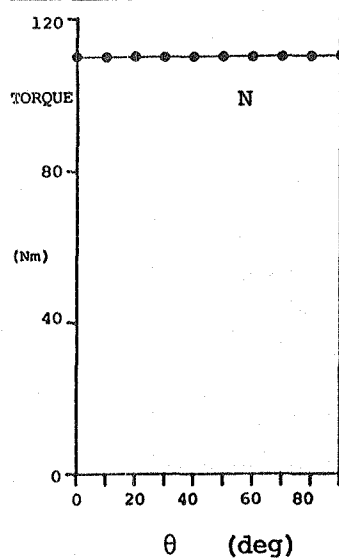
Fig. 4.16f
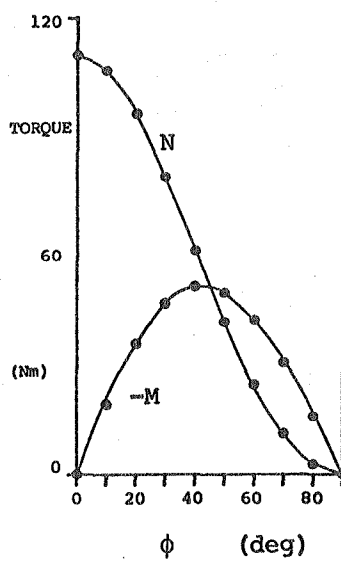
Fig. 4.17 Couplings for wing in pitch field

E/Ms as Fig. 4.9,4.10

Model as Fig. 4.7

Pitch field defined by :

$$-I_1 = +I_3 = -I_5 = +I_7 = 1,600,000 \text{ A } (1000 \text{ A/cm}^2)$$

$$I_2, I_4, I_6, I_8 - I_{14} = 0$$

Model rotations and torques as Fig. 4.11

All force and torque components not specified are exactly or effectively zero.

M is non-zero but less than 0.003 Nm in Figs. 4.17a-f

Fig. 4.17a
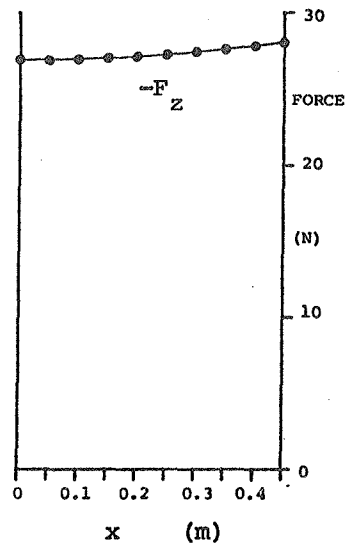
Fig. 4.17b
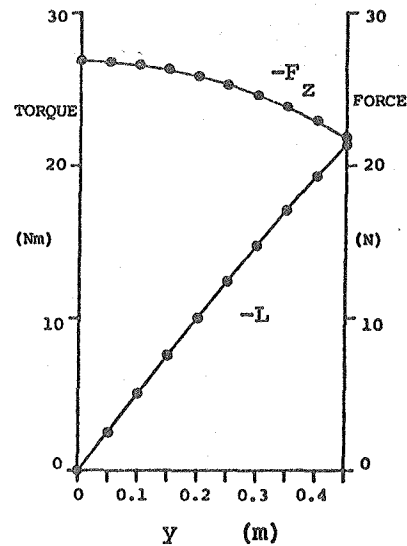
Fig. 4.17c
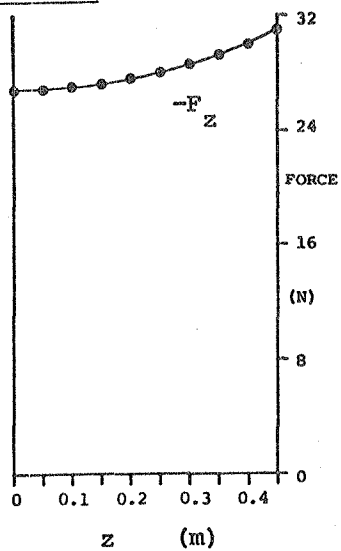
Fig. 4.17d
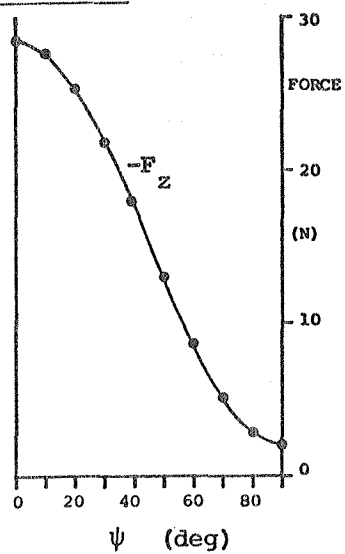
Fig. 4.17e
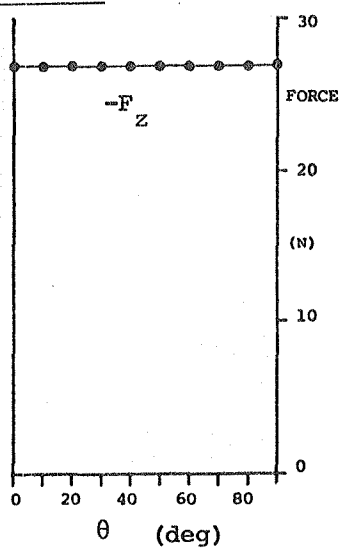
Fig. 4.17f
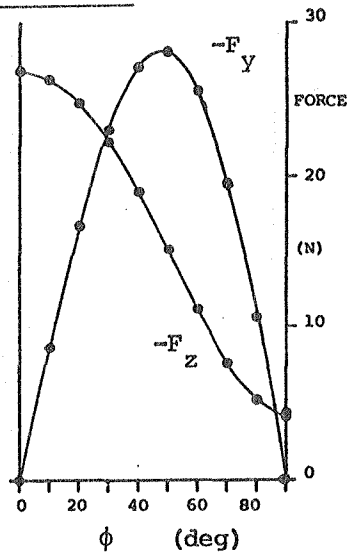
Fig. 4.18   Couplings for wing in yaw field

E/Ms as Fig. 4.9, 4.10

Model as Fig. 4.7

Yaw field specified by :

$$-I_2 = +I_4 = -I_6 = +I_8 = 1,600,000 \text{ A } (1000 \text{ A/cm}^2)$$

$$I_1, \ I_3, \ I_5, \ I_7, \ I_9 - I_{14} = 0$$

Model rotations and torques as Fig. 4.11

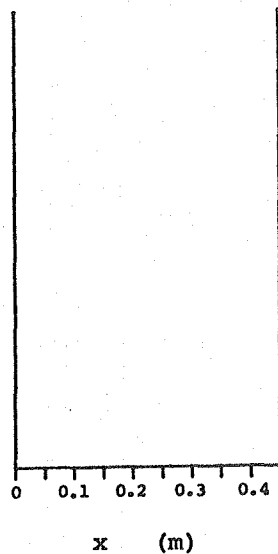All force and torque components not shown are exactly or effectively zero.

Fig. 4.18a

Fig. 4.18b

TORQUE   N   FORCE   F_y

FORCE   F_y

x   (m)   y   (m)
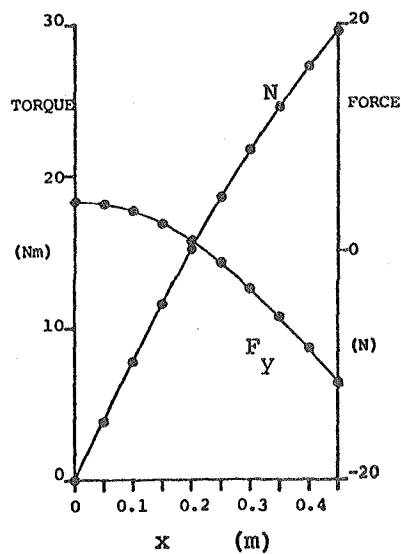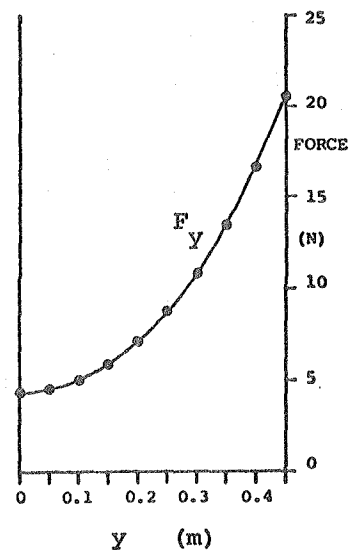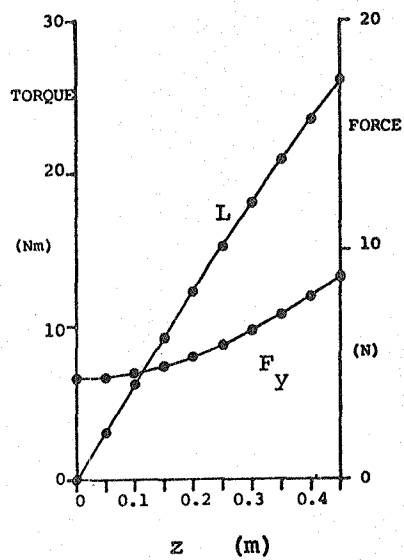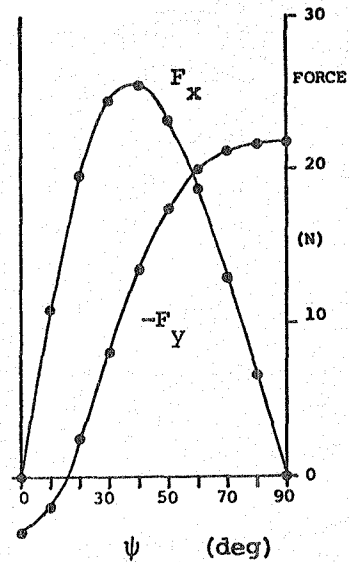
Fig. 4.18c

Fig. 4.18d

Fig. 4.18e
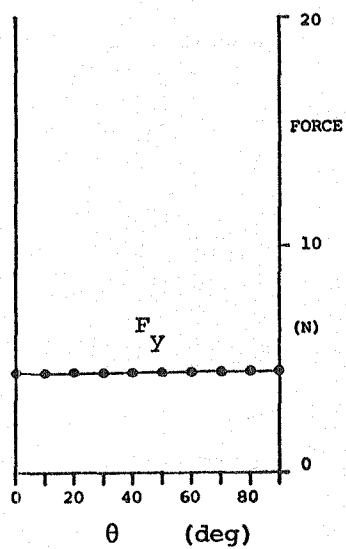
Fig. 4.18f
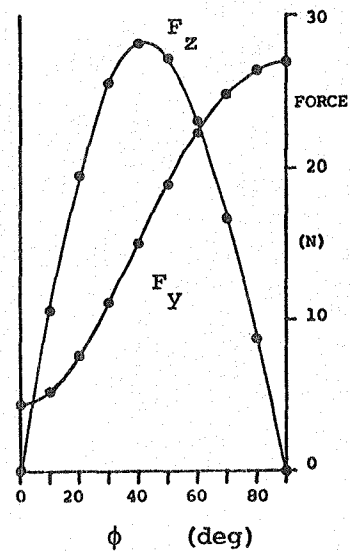
Fig. 4.19   Couplings for wing in magnetizing field

E/Ms as Fig. 4.9,4.10

Model as Fig. 4.7

Magnetizing field defined by :

$$+I_9 =+I_{10} = 2,500,000 \text{ A } (1000 \text{ A/cm}^2)$$

$$I_1 - I_8 \text{ and } I_{11} - I_{14} = 0$$

Model rotations and torques as Fig. 4.11

All force and torque components not shown are exactly or
effectively zero.

Fig. 4.19a

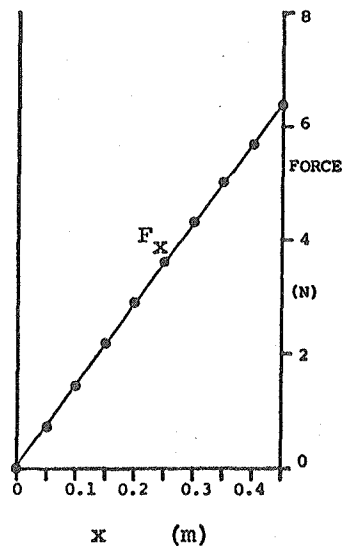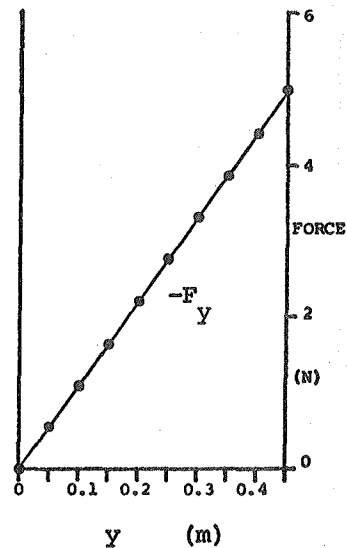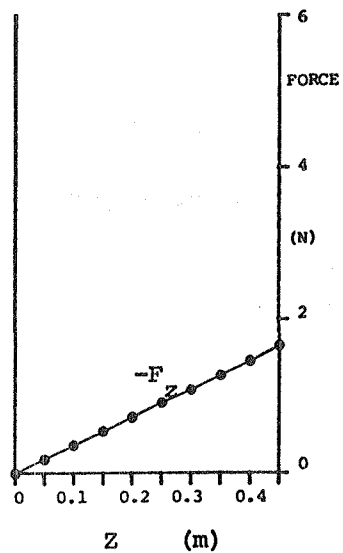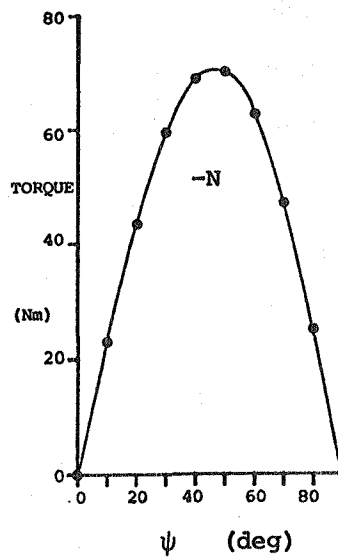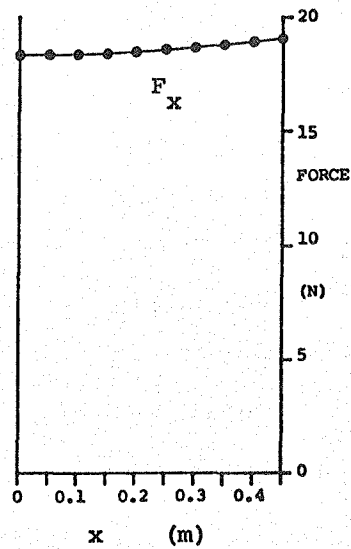Fig. 4.19b
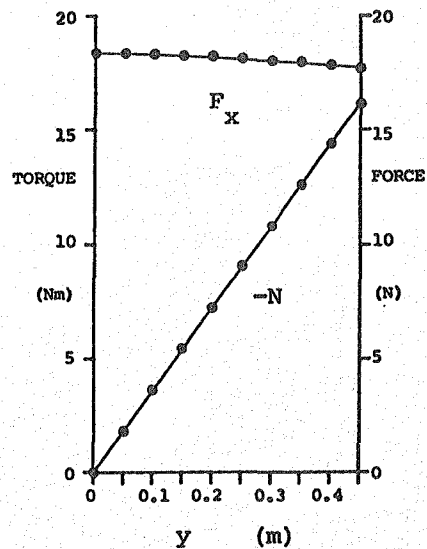
Fig. 4.19c
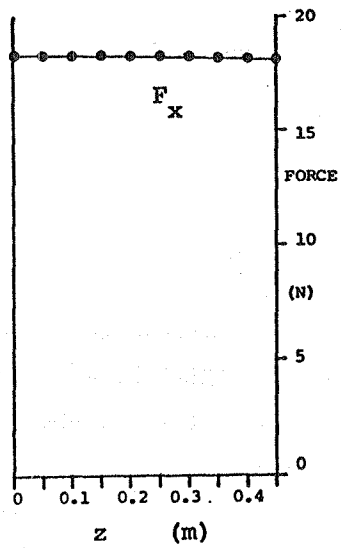
Fig. 4.19d
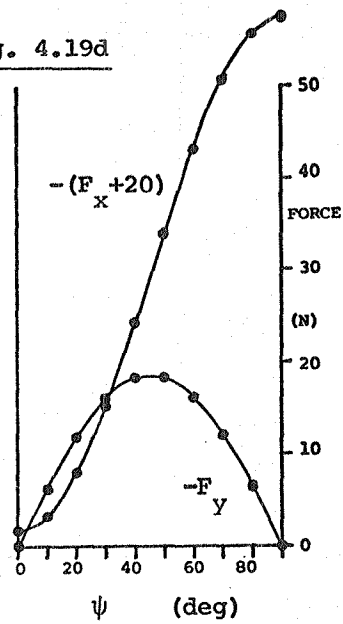
Fig. 4.19e
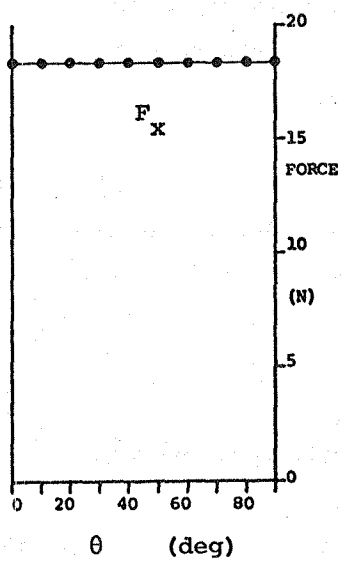
Fig. 4.19f
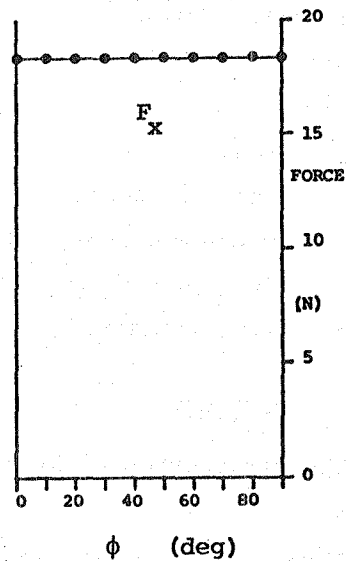
Force/torque	Applied field	Figure (positive x displacement)
F_x	Drag	4.15a
F_y	Sideforce	4.16a
F_z	Lift	4.14a
L	None	---
M	Pitch	4.17a
N	Yaw	4.18a

It should be noted that the two couplings involving generation of pitching moments (from applied lift or pitch fields) are very weak, due to the short moment arms of wing core elements about the y' axis in the chosen configuration.

The full information presented in Figs. 4.11 - 4.19 indicates that further couplings will occur when the model is displaced or rotated from its datum position, for instance a lift field is seen to generate pitch and yaw torques when the wing core is rolled. The principal result of these will be the manifestation of magnetic stiffnesses (positive or negative) in various model degrees of freedom when the classical fields considered are applied. These effects will somehow disturb the magnetic stiffnesses and dampings generated by conventional control algorithms and may require action to counter adverse effects.

However, study of the Figures reveals that these extra couplings occur in a relatively straightforward manner and few are of large magnitude. Whilst further treatment of this topic cannot be presented here, it is felt that modest adjustments to and expansions of conventional control algorithms will restore full required performance.

Since no attempt has been made to ensure representative relationships between the strengths of the classical applied fields, further interpretation of the data discussed above should be made with extreme caution.

4.4 Discussion

The performance of SPM systems is critically dependent on the precise magnetic properties of the core material, particularly the intrinsic polarization and useful coercivity (see Section 4.3).

There seems good reason to expect considerable improvements in
the values of these parameters exhibited by the best available
materials in the near future.   Fig. 4.20 shows how the highest
reported values of BH_{max}, the classical parameter of magnetic
performance, have risen consistently over the past decades, the
performance of ReCo materials still being well below the theoretical
limits at least in the respect of intrinsic coercivity (28, 34).
The torque capabilities calculated heretofore are thus expected to
rise as time passes within the limits of the assumptions made.
Further, it is widely accepted that as the temperature of ReCo
materials is lowered (below 300K, say) their magnetic properties
tend to improve steadily.   The parameters of interest here, that
is intrinsic polarization and coercive force, are typically found
to increase by a few per cent and many tens of per cent respec-
tively, during cooling from room temperature to around 80K (28, 30,35,
36, 37 and Fig. 4.21).   The force and torque capability of a ReCo
cored MSBS model would thus be significantly greater at the typical
lowest operating temperatures of a cryogenic wind tunnel than at
"normal" temperatures.

4.5   E/M configurations for SPM roll control

The E/M configuration chosen so far is a fully symmetric quadrupole
(Fig. 4.8).   There is no particular reason to regard this as being
in any way optimum.

From Fig. 4.11 it is seen that roll torque capability falls
rapidly with increasing roll displacement from the selected datum
orientation.   This would be a serious limitation in practice, being
due to the inability of the chosen array to develop $H_{yz'}$ along a
y' axis displaced by 45° in the roll sense.   This problem may be
completely overcome by including extra E/Ms in the roll array.
These may perhaps be shared with other force/torque generation duties
but will be regarded here as entirely specialised for simplicity.

The complete 8 E/M array used for the SIM calculations (the
SPM 4 E/M array being, of course, derived from this) provides roll
torque at any roll angle, the variation of torque capability with
angle being shown in Fig. 4.22.

If 360° roll angle capability is deemed unnecessary, then the 4
E/M array may be adapted to increase the angular capability, certain
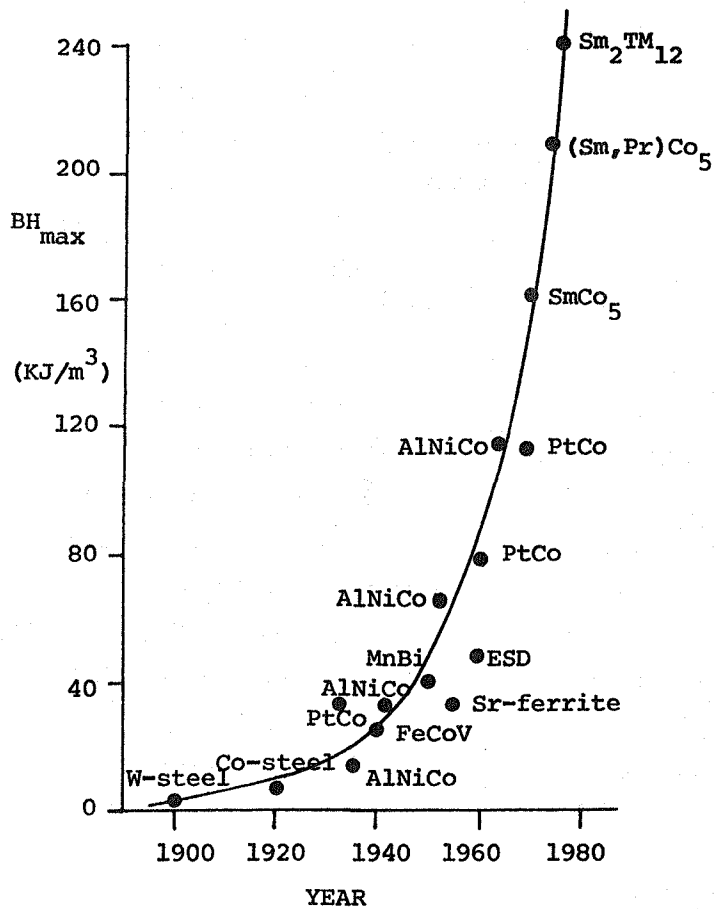
Fig. 4.20 Increase in highest reported values of energy product with time

After Ref. 35.
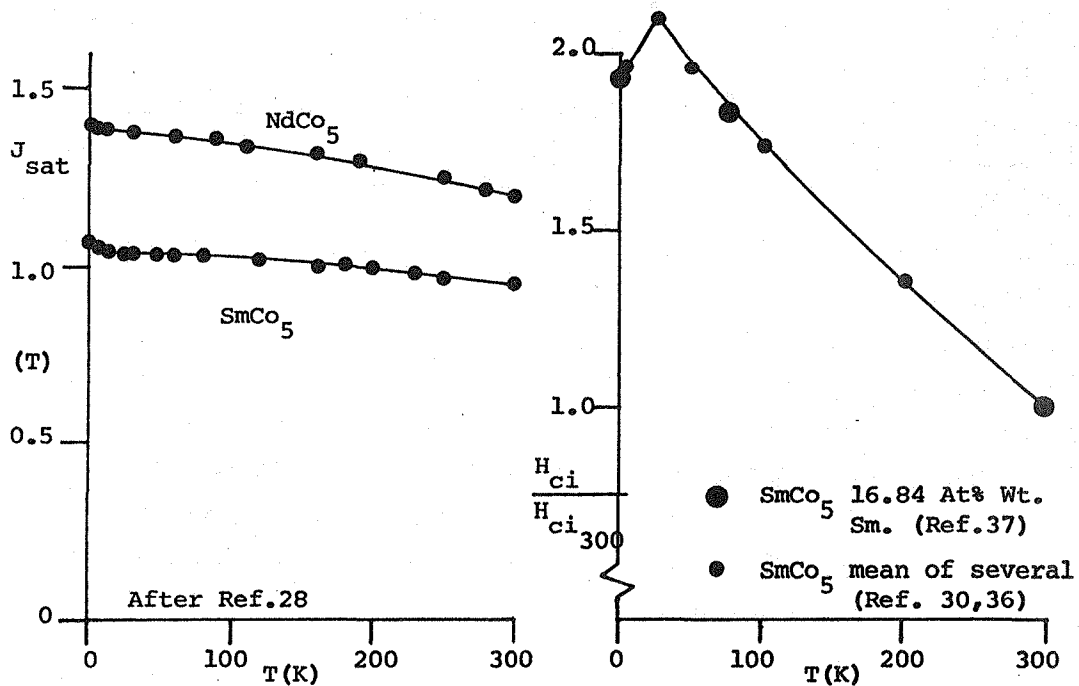
Fig. 4.21 Variations of intrinsic polarization and coercivity with temperature for Rare-Earth Cobalt materials
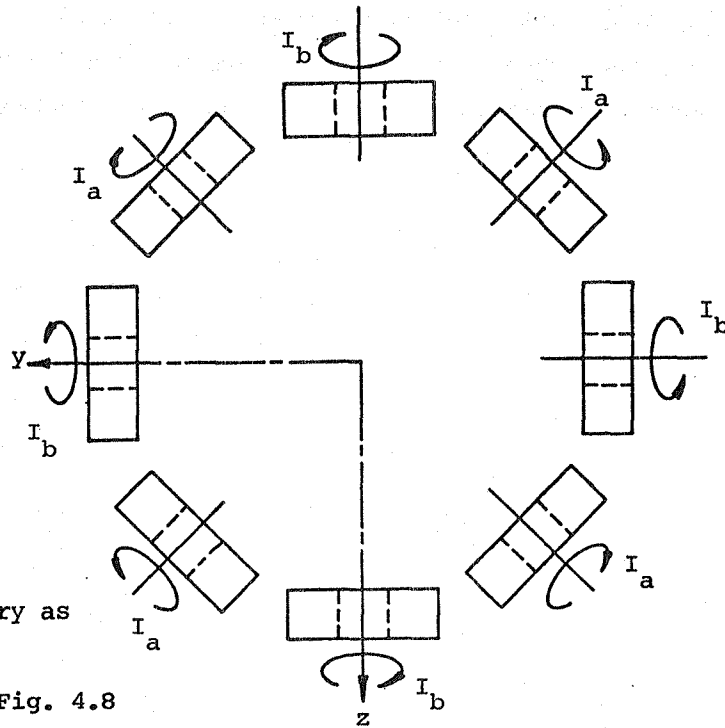
E/M geometry as
Fig. 5.4

E/Ms a as Fig. 4.8

All currents are 1,459,240 A
    (1000 A/cm^2)

Current directions chosen
to create positive torque
at all angles
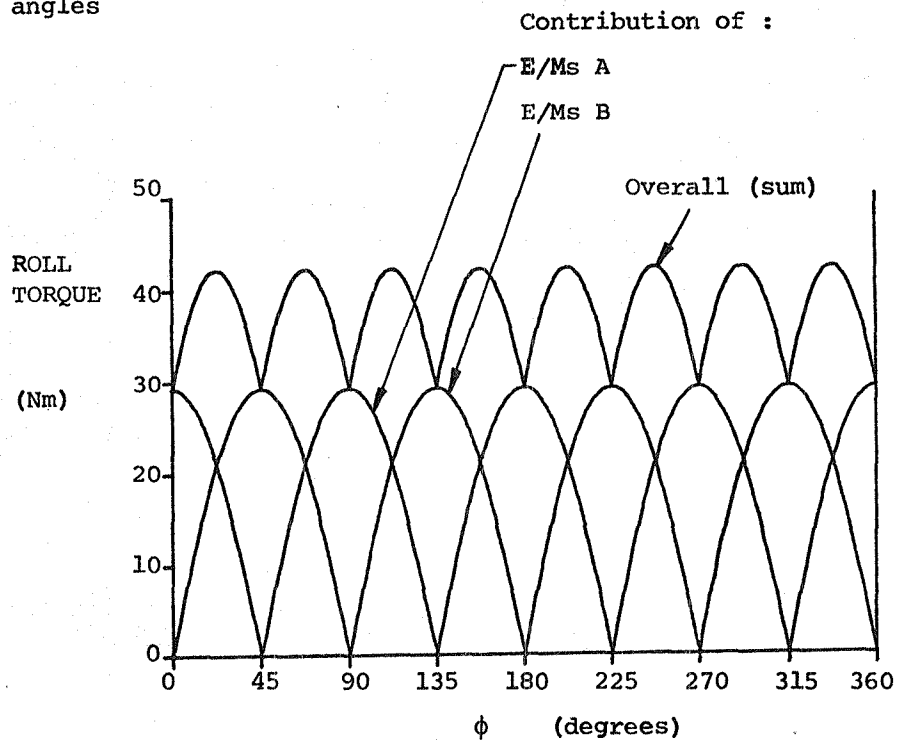
Fig. 4.22   Variation of roll torque with roll displacement for
            complete SIM E/M array (SPM cores) of Fig. 5.4

possible adaptions being illustrated in Fig. 4.23. Comprehen-
sive treatment cannot be attempted here but Figs. 4.24a-d illustrate
that some improvements are possible, using the techniques of Fig.
4.23.

d may be positive or negative

ξ may be greater or less than 45°

Cylinder of exclusion, radius = 2.245m

Individual E/Ms as Figs. 4.8 and 5.4
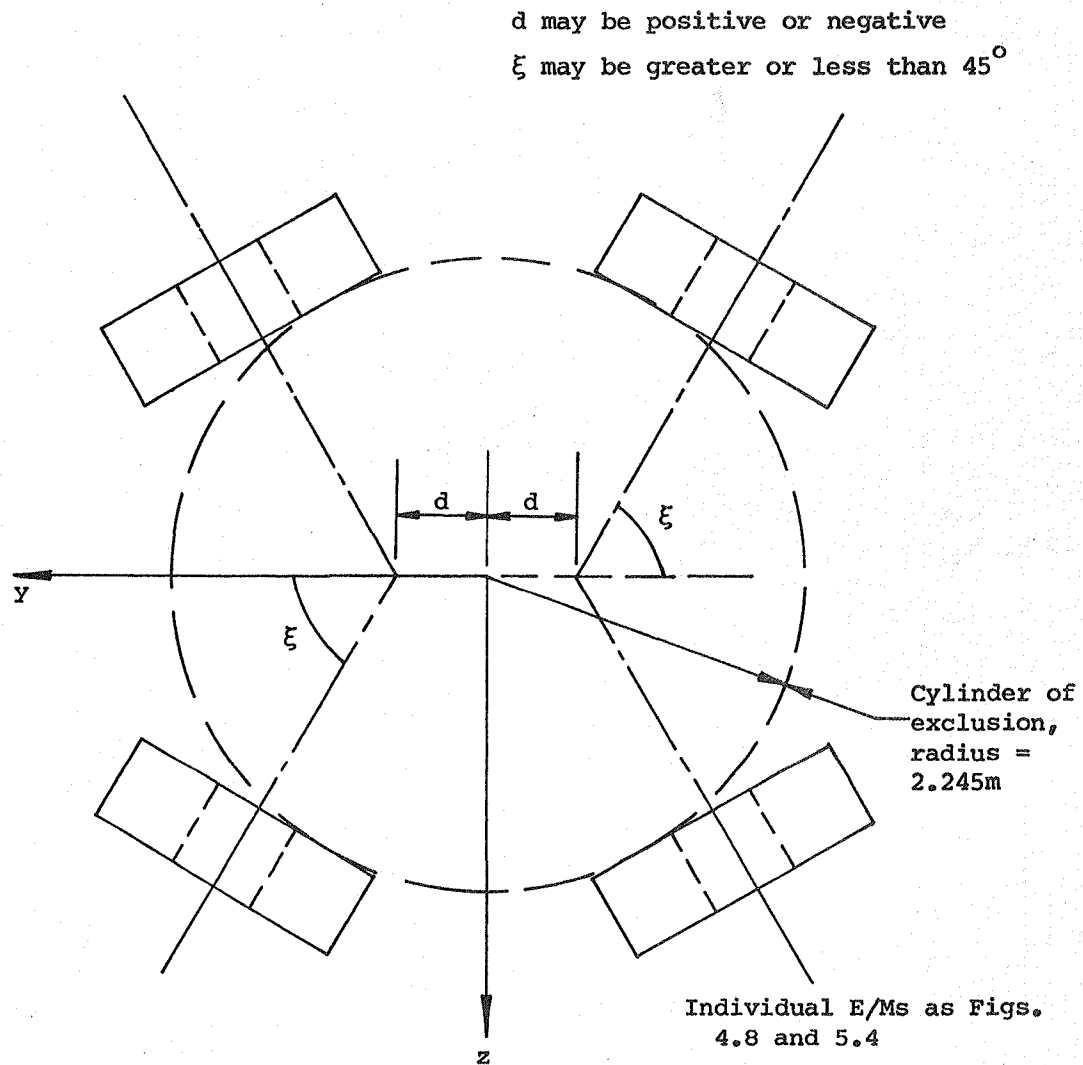
Fig. 4.23 Possible modifications of 4 E/M SPM roll
array to enhance angular capability

E/Ms as Fig. 4.23 Model as Fig. 4.7
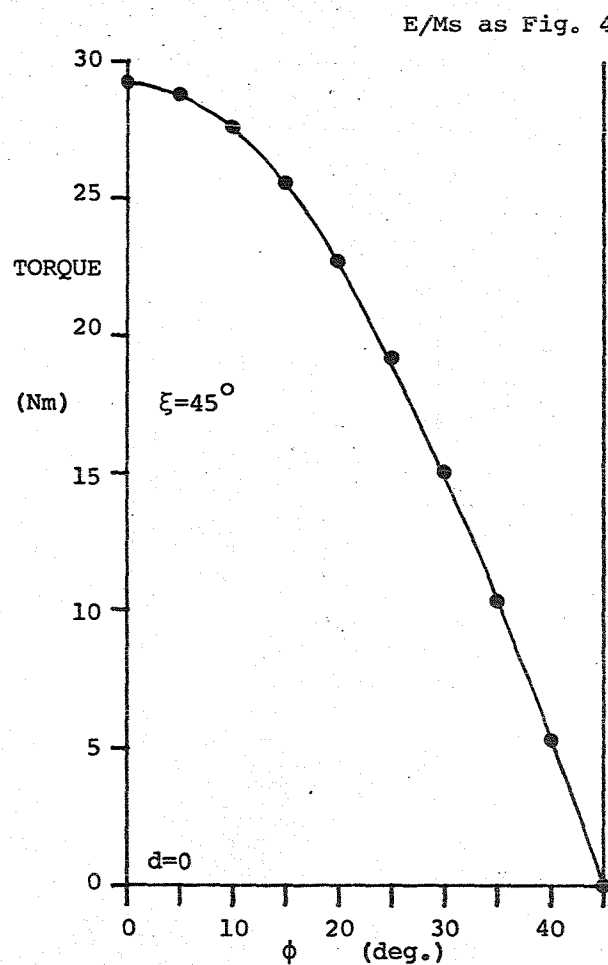
Fig. 4.24a(i) Unmodified geometry
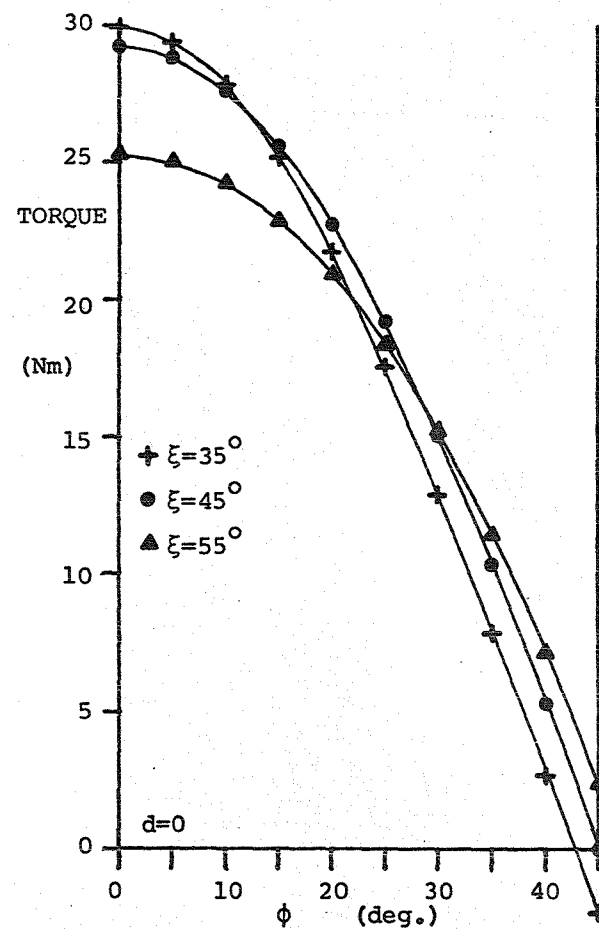
Fig. 4.24a(ii) Modified (d=0)

Fig. 4.24a Variation of roll torque capability with roll angle for modified quadruplet geometries.

E/Ms as Fig. 4.23   Model as Fig. 4.7
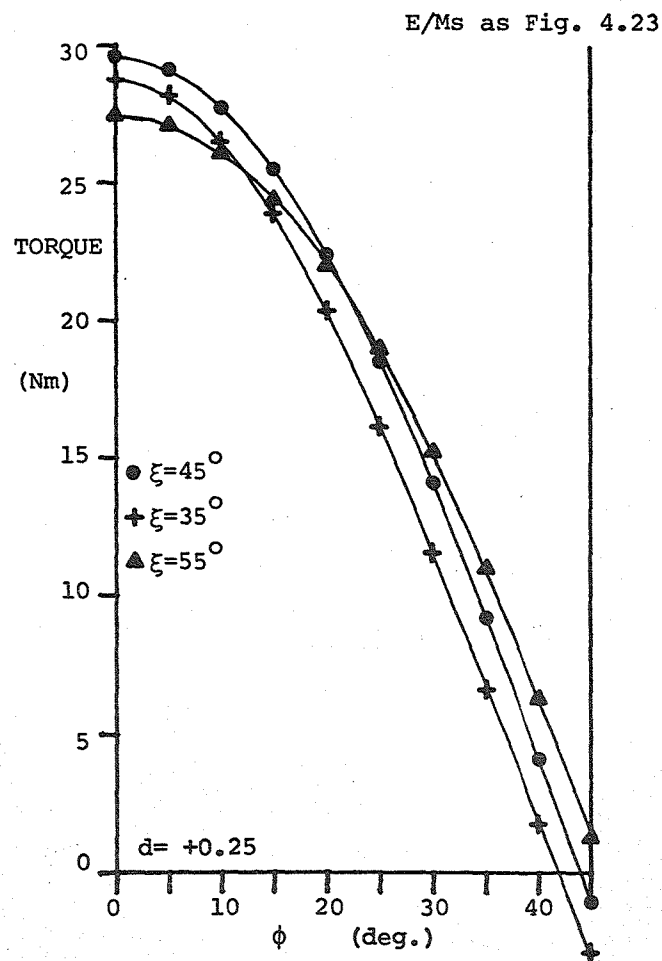
Fig. 4.24b (i) Modified (d= +0.25)
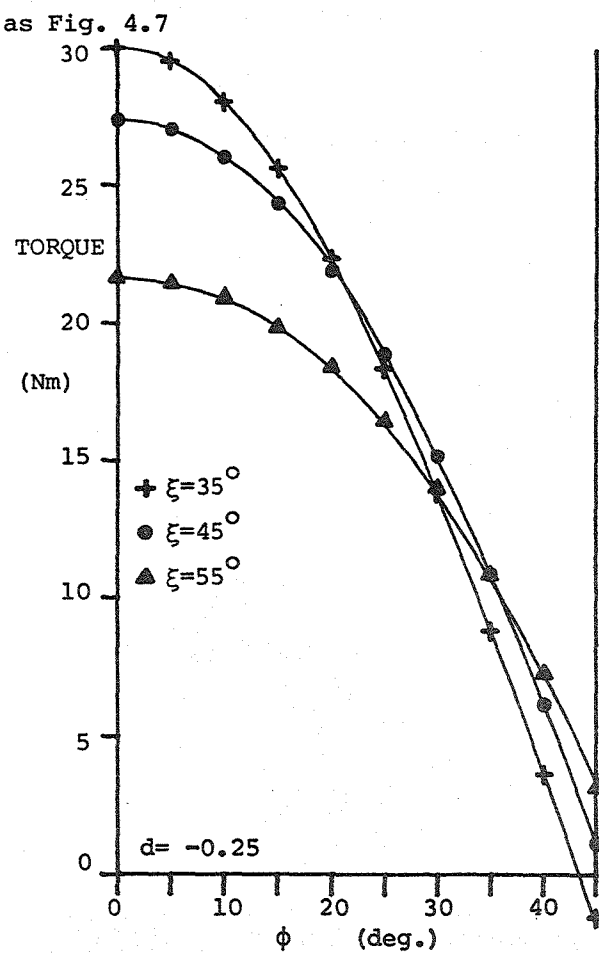
Fig. 4.24b (ii) Modified (d= -0.25)

Fig. 4.24b   Variation of roll torque capability with roll angle for modified quadruplet geometries.

- 64 -

5. SPANWISE IRON MAGNETS (SIMs)

5.1 Introduction

Symmetrically disposed transverse magnetization components can relatively easily be induced in a magnetically soft wing core by application of a symmetrical field as shown below:

Fig. 5.1 Spanwise iron magnet magnetizing field
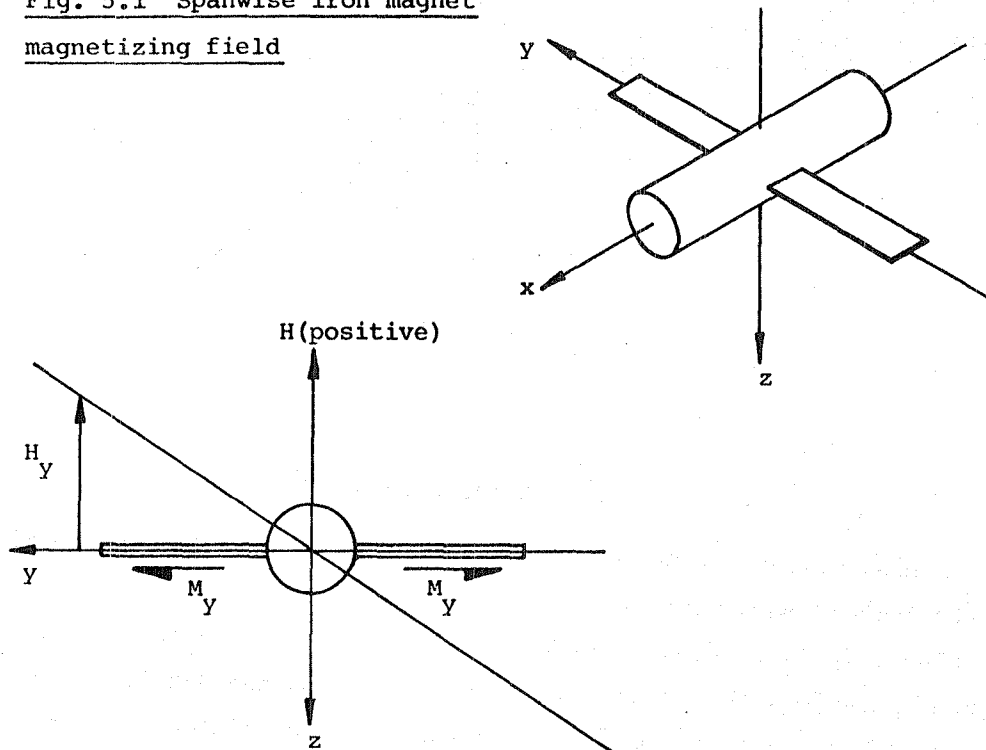
Rolling moment will be generated with application of through wing fields as in Fig 5.2., Section 3.2.2., and Section 4. Rotation of the induced spanwise magnetization vectors by the through wing fields will be inhibited by the high demagnetizing factors in the through wing direction. Calculation of the performance of SIM systems is not straightforward, the induced magnetizations not being directly analytic.
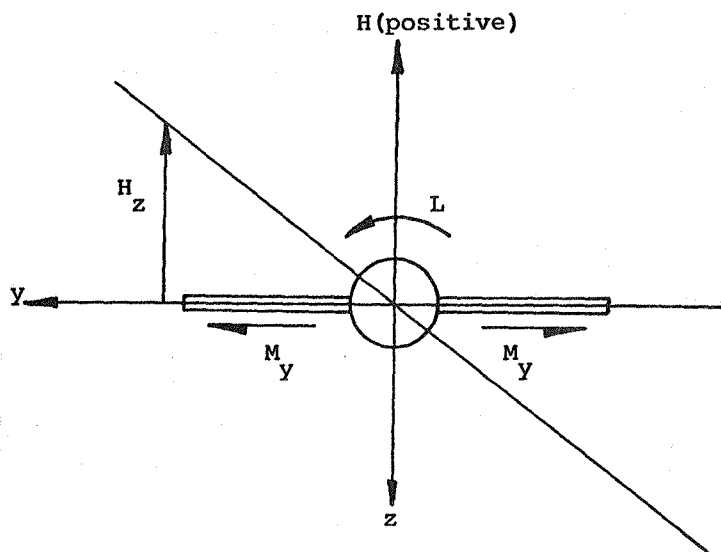
Fig. 5.2   SIM through wing field

Thus, whilst the SPM equations may be approximately applied if the induced magnetizations remain predominantly spanwise and the value of polarization is replaced by some mean value of induced magnetization, that value of magnetization and the detail performance of the SIM system cannot be adequately predicted without further analysis.

However, many magnetically soft materials exhibit saturation inductions of approximately 2 Tesla and high permeabilities to around that value.   Operation with higher levels of spanwise magnetization than those achievable with SPMs (approximately 1 Tesla) is thus possible, leading at least to higher torques per unit through wing field.   Further, it is assumed (Section 5.4) that magnetically soft materials with good mechanical properties are available, allowing the entire wing volume to be utilised if required, and since no irreversible demagnetization effects exist in the SIM case it is to be expected that the absolute maximum available torque for any configuration may be greater than with SPMs.

Since soft magnetic materials generally behave entirely isotropically, available material data is sufficient to permit, in principle,

calculation of the performance of the SIM system at all applied field levels.

5.2 Solution of iron-air-conductor magnetostatic systems

This class of problem has attracted considerable interest over recent years with the application of superconductors to various fields such as nuclear research and with the drive to improve performance and efficiency of electrical machines.

General magnetostatic problems involve the solution of Poisson's equation or, outside current carrying conductors, Laplace's equation. These equations may be solved in principle by a number of methods including (after 38)

1) Analogue   2) Graphical   3) Analytic   4) Numerical

Predictions of roll torque from SIMs require treatment of saturation effects, leading to non-linear solutions, and are inherently three dimensional.   In most practical cases methods 1) and 2) above are not able to handle the non- linear problem, indeed graphical methods are generally restricted to two dimensions.   Analytic methods are available for non-linear 3D problems but only for highly restricted geometries of conductor and iron.   Application to general problems is currently quite impractical.   Again following (38) existing numerical methods in this field may be divided into four principal categories:

1) Finite difference   2) Images
3) Integral equations   4) Variational formulations

although other classes of solution do exist, such as the Monte-Carlo method (39).

It would appear that image methods are inapplicable to non-linear problems within the bounds of the present formulations.   Method 4) above may be considered an energy method, somewhat analogous to virtual work methods in structural problems, whereas 1) above tackles Poisson's or Laplace's equation directly but both generally require that the complete volume of the problem is meshed with a computation grid. The characteristic geometry of the SIM roll system is very "open" (Fig. 5.3), that is a small iron region separated from the conductors by large air gaps.   Methods 1) and 4) above would thus require meshing of considerable volumes of air, at least enclosing all the conductors, leading to large computation times.   Integral equation methods
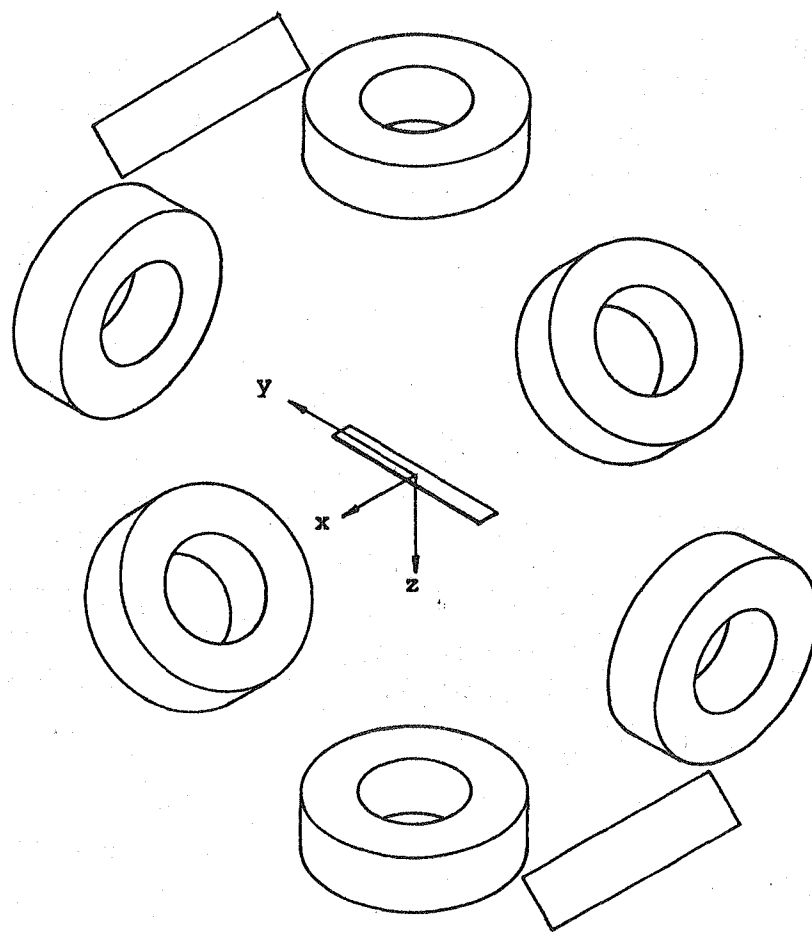
Fig. 5.3 Characteristic configuration of SIM rolling moment

generating system.   (8 symmetrically disposed E/Ms)

(3 above) need only require meshing of iron regions and thus appear
appropriate here.

5.3 Program GFUN

This program, developed at the Rutherford Laboratory, Didcot,
Oxon, U.K. since 1970 by Trowbridge et al, is an example of the use
of integral equation methods.   GFUN has been applied to a wide
range of problems over many years (38, 40, 41, 42, 43) and has
exhibited consistently good accuracy, consequently gaining a high
international reputation.   A disadvantage inherent to the solution
procedures employed is a somewhat awkward representation of field
within iron regions, as the vector sum of the fields from external
currents and induced magnetizations, expressed as constant within
suitably shaped elements (such as tetrahedra).   In high permeability
regions the two contributions to the field may be nearly equal and
opposite, leading to rather poor resolution of the internal field.
GFUN in fact handles the simultaneous integral equations as a single
matrix equation, solution of the latter generating eigen solutions for
the internal field.   Clearly, prediction of the detail geometry of
the internal field is affected by the choice of element distributions.
The lack of precise information concerning the internal field of the
SIM cores is not thought to be especially critical.   It must be noted
that the nature of the solution procedure implies that the foregoing
adverse comments do not apply outside the iron region, however para-
doxical that may seem, and need not apply to the resolution of forces
and torques provided methods of field integration over control volumes
external to the iron are chosen.

Access to GFUN was granted by the British Science Research Council*
under Grant No. GR/B/3691.5.   Modifications to the program were carried
out by Simkin to permit the full symmetry existing in many of the
required SIM cases to be exploited (reducing computation time) and to
provide a torque integration option.   The torque integration scheme
is conceptually similar to the well established methods for force cal-
culations but the fact that previous users have apparently not required
torque information must be seen to represent a major possible source
of systematic error in data included hereafter, indeed some diffi-
culties were experienced before a consistent integration scheme could

* Now the Science and Engineering Research Council.

be identified. To counter this uncertainty, various low field torque measurements have been made and limited cross checking under-taken (Section 5.7). Saturation of iron regions,which could not be achieved in corroborative experiments, should not directly influence the reliability of torque predictions due to the nature of the methods used.

5.4 Baseline GFUN geometry and configuration

A baseline geometry and configuration is required from which the effects of variations of various parameters, such as wing aspect ratio, may be examined. At the time of commencement of this study there existed no clear specific choice of geometry of either model or E/Ms, necessitating evolution of a baseline geometry on the following, somewhat arbitrary, basis.

The favoured scale for studies of LMSBSs has been a test section of approximately 8 ft x 8 ft cross section (such as NTF). Calculations are therefore made at this scale, but the scaling of results to different tunnel sizes is quite straightforward (Appendix 3). The test section is assumed square with no corner fillets. Clearance is allowed around the aerodynamic cross section for structure, plenum chamber etc., and is chosen to be one foot (5). A similar allowance is made for the thermal insulation and structure surrounding each E/M (5). The most uncertain characteristics of the E/Ms are the winding shape and maximum usable current density. It appears (5) that manu-facturers prefer circular windings where possible due to reduction of difficulties associated with conductor stressing. An idealized 8 E/M configuration has been chosen (Fig. 5.4). The problem of optimizing the E/M array must be dealt with separately, being heavily influenced by particular requirements for forces and moments in other degrees of freedom. Maximum usable overall current density (J) for super-conducting E/Ms varies from order 1500 A/cm^2 for cryostable conductors to order 15000 A/cm^2 for adiabatically stable conductors, within the limits of present technology. Doubts exist (5) as to whether adia-batically stable conductors could be applied to the 8 ft scale case so generous winding cross sections are allowed in the E/Ms, permitting partial saturation of the wing cores at suitably low values of J. High J data is included for the purpose of identifying trends at high field levels. The current levels in the E/Ms are represented by J_r and J_m as defined by Figure 5.4.

Part section
in yz plane

0.305

r=0.383

r=0.765

r=0.305

≈0.305

1.219

1.219

0.305

Approx 8x8 foot
test section

y

2.245

0.382

z

J_r

J_m

J_r

Section in yz plane

All J's positive in
senses shown.

J_m

J_r

45°

45°

J_m

J_r

J_r

J_m

z

Fig. 5.4   Baseline GFUN E/M geometry and configuration. Dimensions

in metres.

- 71 -
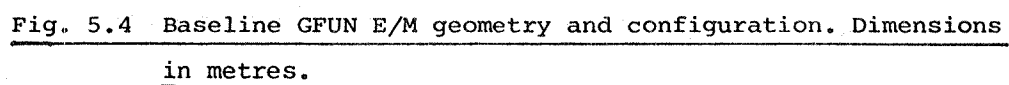
The geometry of the baseline SIM wing core is simply chosen as a 10% thick, 10:1 aspect ratio rectangular hexahedron (rectangular "slab" core) spanning slightly under one half (49.2%) of the test section width (Fig. 5.5).

The choice of core material (or its magnetic characteristics) presents some difficulty at this stage due to the necessity in a final design to achieve an optimum compromise between many magnetic, electrical and mechanical properties. The SIM wing cores are visualised as occupying nearly all the aerodynamic volume of the wings with only those detail fittings and features potentially subject to changes during test programs being added from non-magnetic material. It is recognised that this view may require qualification in the light of detailed results and experience in model design, but it is nonetheless clear that the core material requires good mechanical properties such as high yield point, low brittleness and high Young's Modulus, perhaps also at low temperatures. High electrical resistivity may be preferred in order to suppress eddy current flow in the cores but is not essential to fundamental operation of the system. Low coercive force is necessary to avoid torque calibration being dependent on the recent past magnetic history of the cores, although if cores are operated far into saturation this feature becomes of lesser importance. Ultra high permeability is not necessary since in any airgap dominated system, iron regions of medium and higher permeabilities tend to behave as if infinitely permeable. The key magnetic parameter is undoubtedly saturation induction. Studies of LMSBSs (5) have indicated that valuable economies can be made in E/M size, hence cost, by utilising fuselage core materials with the highest available saturation induction. It is logical that similar criteria should apply to the SIM case since operation of the core beyond the saturation point is anticipated.

One class of materials that appears promising is the cobalt iron alloys, classically represented by the 50:50 Iron-Cobalt alloy "Permendur". These materials have not found widespread industrial application due to their relatively high cost but this is unlikely to be a problem in LMSBS applications. Indeed the cost of a fuselage core for an 8 ft tunnel has been estimated at U.S. $ 5000 (1981 $), (5). This is small compared to a typical manufacturing cost of a large wind tunnel model.

Magnetic and mechanical properties of material of this type are dependent on the precise alloying constituents, heat treatment and

40

y

External control
volume for torque
integrations.
(half shown)

y

Section in yz plane

20

This quarter by reflection
in yz plane. Other half by
reflection in xz plane.

70

1.2

x

21

45

Each hexahedral element
composed of 5
tetrahedral
sub-elements as
shown.

2

6   1

3   z

5

7

4

12

60

8

Fig. 5.5 Baseline GFUN

wing core geometry.

Dimensions in cms.
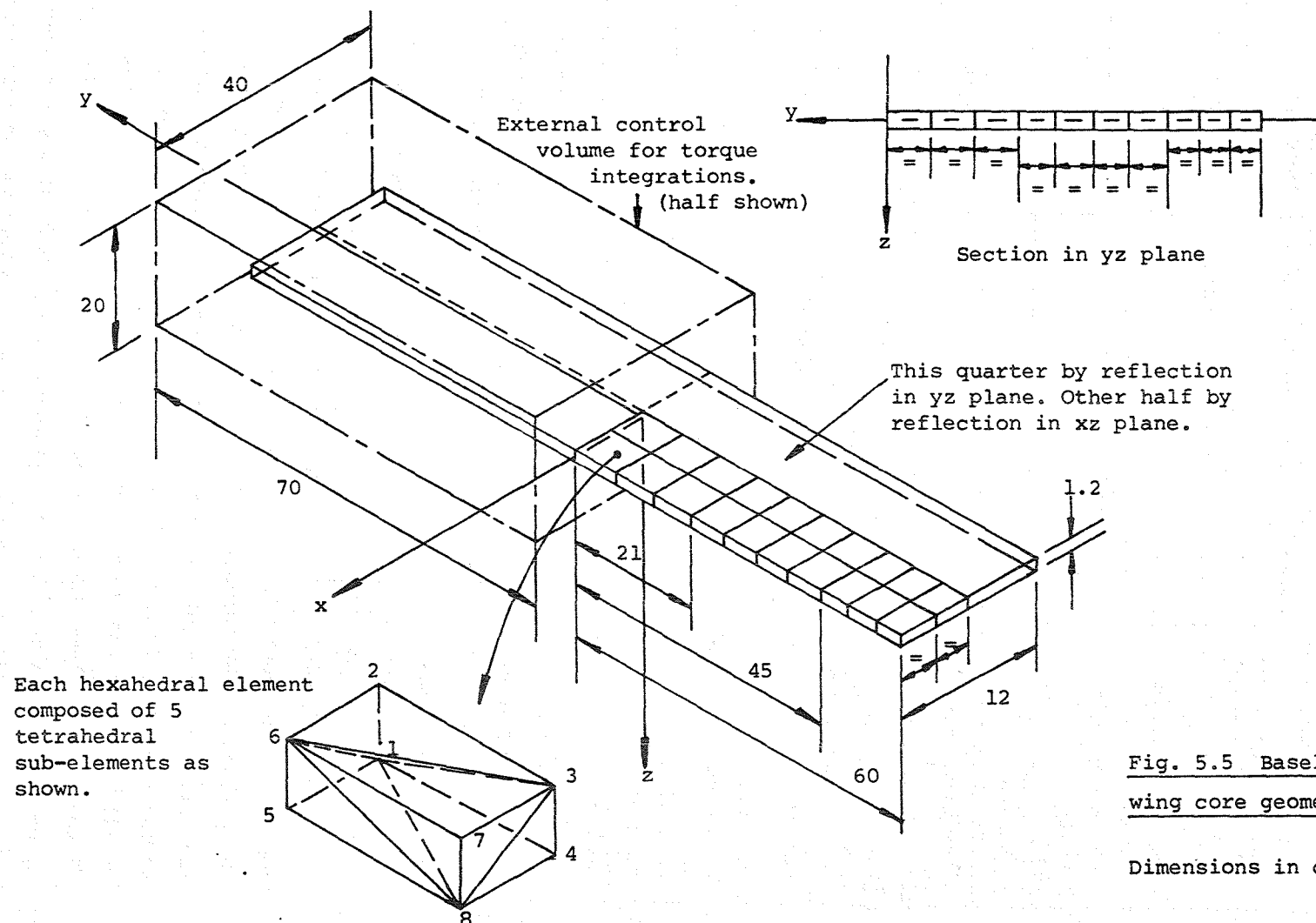
preparation of samples but typical properties for some commercially available materials are shown below.

Material (Trade Name)	Permendur	Vanadium Permendur	Vacoflux 50
Source	Western Electric Co. Ltd.		Vacuumschmelze GmbH
Reference	44	44	45
Density (kg/m^3)	8300	8300	8150
Initial μ	800	800	1000
Saturation Induction (T)	2.45	2.4	2.35
Static coercivity (A/m)	159	159	110
Resistivity Ωm	0.7×10^{-6}	0.26×10^{-6}	0.35×10^{-6}
Youngs Modulus GPa	-	-	230
Yield strength MPa	-	-	400

It should be noted that the saturation inductions, in the range 2.35 - 2.45T (exceeding 2.5T in laboratory specimens) are substantially higher than the corresponding value for high purity iron of some 2.158T (room temperature, Ref. 44).

The peaks in the permeability versus magnetizing field strength curves for the above materials (Fig. 5.6) present some problems to GFUN. The permeability of each iron element in GFUN is assumed constant throughout the element and is updated at each iteration. Sharp rises in the permeability of elements with relatively small increases in the magnetizing field acting on those elements (and vice versa) occurring from one iteration to the next may cause local oscillations of the iron's interior field and consequently slow convergence. These potential problems may be avoided in early work by choosing a permeability versus magnetizing field strength charac- teristic that falls monotonically. This has been done by arbitrarily fitting intermediate points between the initial constant permeability line and the terminal saturation boundary, thus establishing the base- line characteristic shown in Fig. 5.7. A slightly conservative value

Fig. 5.6 GFUN baseline and other permeability curves
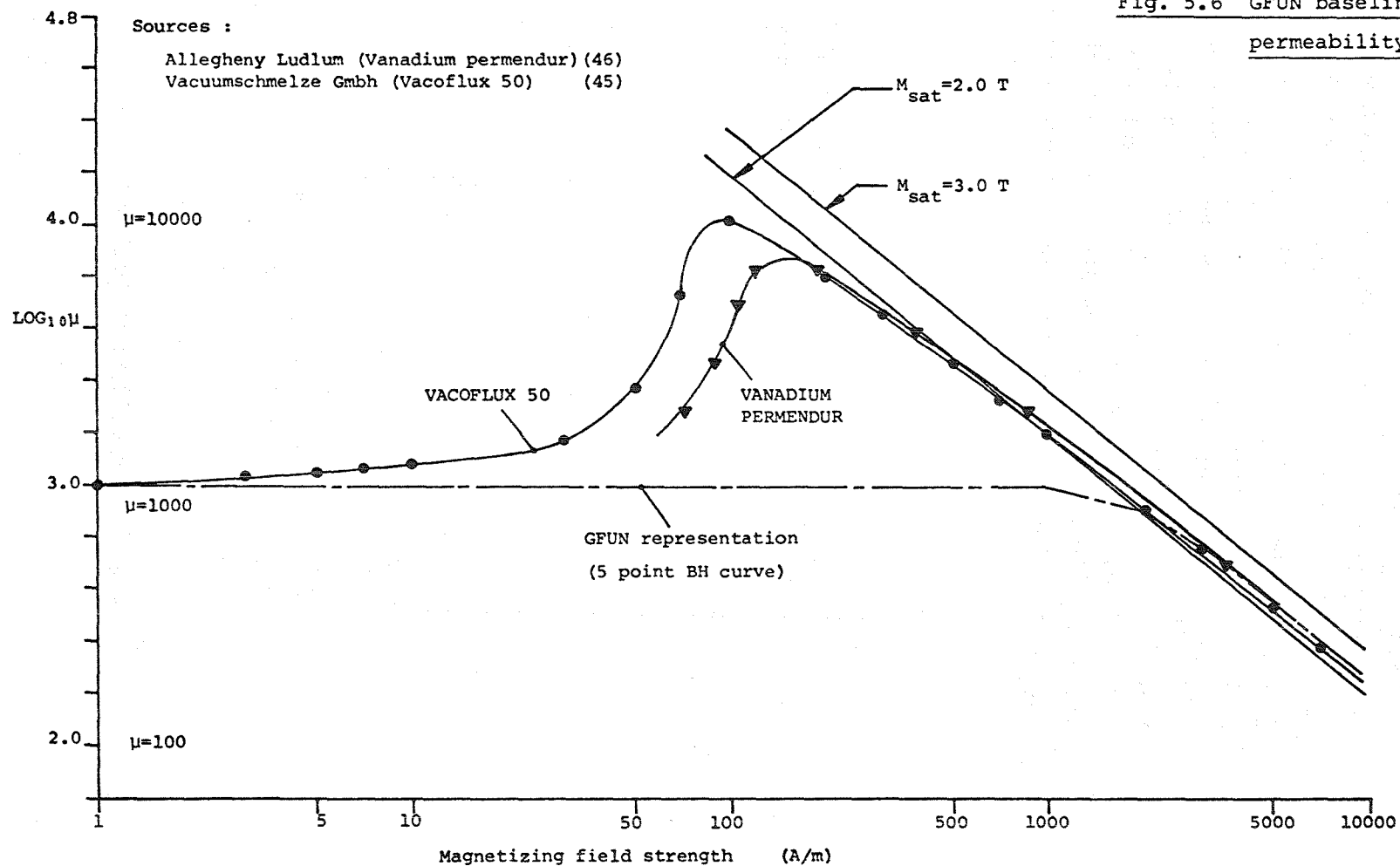
of 2.3T is chosen for M_{sat}. The effects of variations of some
material properties on the torque capability of the SIM system is
studied later.

The baseline wing element distribution is chosen along well
established principles.   Tetrahedral elements have proven to be the
most reliable choice for GFUN, the total number of elements is the
largest that can be handled by the convenient batch version of the
program and the spatial distribution of the elements is chosen such
that the elements are relatively numerous in the region of strongest
anticipated magnetization.   This non-uniform element distribution
also yields superior convergence.   The control volume for use with
the torque integration schemes is dimensioned such that its surfaces
lie close to the model core, thus yielding best accuracy.
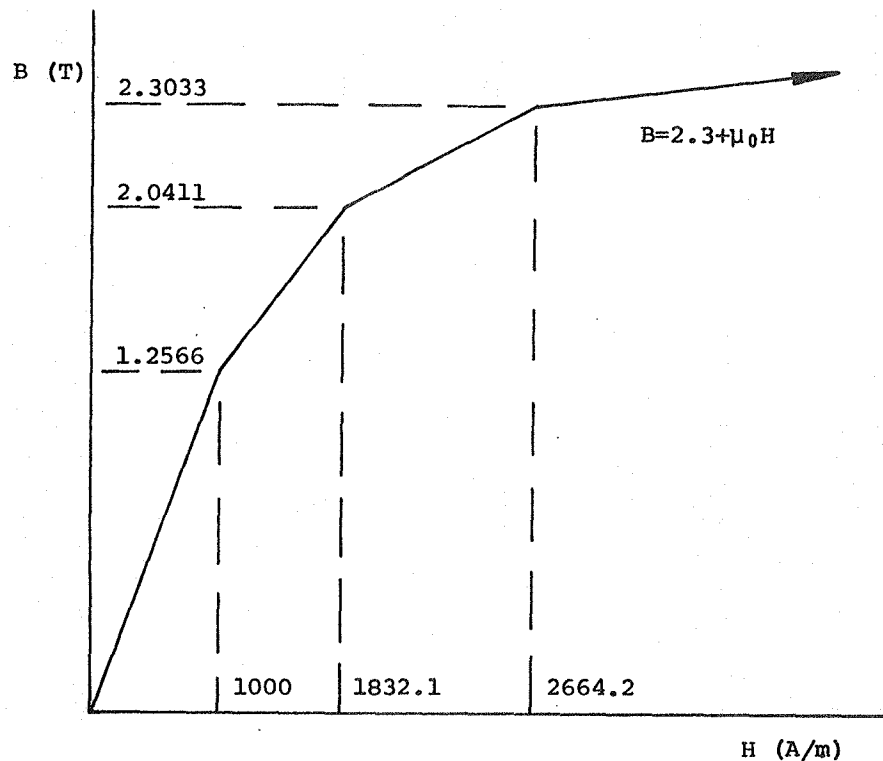
Fig. 5.7 GFUN baseline BH curve

- 76 -

5.5 Simple theoretical approximations

5.5.1 Torque on ellipsoids

Some insight into the behaviour of the SIM system may perhaps
be gained by study of some magnetostatic torque producing system
that is analytic.   Unfortunately, as previously mentioned, few such
systems exist and few of these yield to straightforward analysis.
One suitable example is torque on magnetically soft uniform ellipsoids
in uniform applied fields.   The general equations applying are as
follows:-
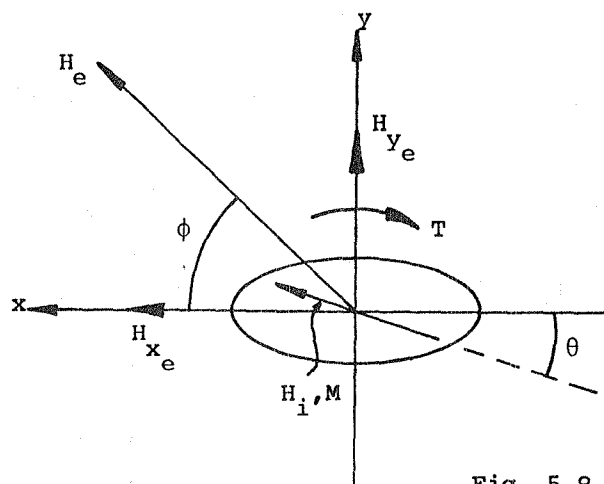
Fig. 5.8   Ellipsoid in uniform
applied field

$$H_{x_i} = H_{x_e} - \frac{N_x M_x}{\mu_o} \qquad - \quad (5.1a)$$

$$H_{y_i} = H_{y_e} - \frac{N_y M_y}{\mu_o} \qquad - \quad (5.1b)$$

$$B_{x_i} = (1-N_x) M_x + \mu_o H_{x_e} \qquad - \quad (5.2a)$$

$$B_{y_i} = (1-N_y) M_y + \mu_o H_{y_e} \qquad - \quad (5.2b)$$

$$\chi_m = \frac{|M|}{\mu_o |H_i|} \qquad - \quad (5.3)$$

Combining (5.1) and (5.3)

$$M_x = \mu_o H_{x_e} \left(\frac{\chi_m}{1 + \chi_m N_x} \right) \qquad - \text{(5.4a)}$$

$$M_y = \mu_o H_{y_e} \left(\frac{\chi_m}{1 + \chi_m N_y} \right) \qquad - \text{(5.4b)}$$

The torque on the ellipsoid is as follows:

$$T = (M_x H_{y_e} - M_y H_{x_e}) V \qquad - \text{(5.5)}$$

Following Fig. 5.8 we have from (5.1):

$$H_i \cos\theta = H_e \cos\phi - \frac{N_x M \cos\theta}{\mu_o} \qquad - \text{(5.6a)}$$

$$H_i \sin\theta = H_e \sin\phi - \frac{N_y M \sin\theta}{\mu_o} \qquad - \text{(5.6b)}$$

Combining (5.6a) and (5.6b):

$$1 = \left(\frac{H_e \cos\phi}{H_i + \frac{N_x M}{\mu_o}} \right)^2 + \left(\frac{H_e \sin\phi}{H_i + \frac{N_y M}{\mu_o}} \right)^2 \quad - \text{(5.7)}$$

This equation gives H_i from any given H_e, ϕ and M. Below saturation M, H and χ_m are functions of each other (Eqn. 5.3). Solution of (5.7) thus involves an iterative process using a material's particular BH curve. When H_i is found, χ_m is known from the BH curve and torque can be found from (5.4) and (5.5). This procedure is somewhat inconvenient. Where χ_m is large (permeable material below saturation) we have $H_i \simeq 0$ and Eqns. 5.1 collapse to:

$$M_x \simeq \frac{\mu_o H_e \cos\phi}{N_x} \qquad - \text{(5.8a)}$$

$$M_y \simeq \frac{\mu_o H_e \sin\phi}{N_y} \qquad - \text{(5.8b)}$$

and from (5.5):

$$T \simeq \left(\frac{1}{N_x} - \frac{1}{N_y} \right) \mu_o H_e^2 \cos\phi \sin\phi \, V \quad - \text{(5.9)}$$

Directly, for maximum torque at any given applied field strength $\phi = 45^o$ and:

$$T \, \alpha \, \text{applied field}^2 \quad \text{(at any given } \phi) \quad - \text{(5.10)}$$

Where the material is far into saturation $M = M_{sat} = $ constant, and $\chi_m \simeq \dfrac{M_{sat}}{\mu_o |H_i|}$

From (5.6):

$$\frac{H_e \, Cos\phi}{Cos\theta} - \frac{N_x M_{sat}}{\mu_o} = \frac{H_e \, Sin\phi}{Sin\theta} - \frac{N_y M_{sat}}{\mu_o}$$

Re-arranging:

$$H_e \, Sin \, (\phi - \theta) = \tfrac{1}{2}(N_y - N_x) \, \frac{M_{sat}}{\mu_o} \, Sin \, 2\theta \qquad - \quad (5.11)$$

Giving:

$$\phi = Sin^{-1} \left(\frac{(N_y - N_x) \, M_{sat} \, Sin \, 2\theta}{2 \, \mu_o \, H_e} \right) + \theta \qquad - \quad (5.12)$$

And from (5.5):

$$\frac{T}{V} = M_{sat} H_e \, Sin \, (\phi - \theta) \quad \text{and using (5.11):}$$

$$\frac{T}{V} = \frac{M_{sat}^{\;2} \, (N_y - N_x) \, Sin \, 2\theta}{2 \, \mu_o} \qquad - \quad (5.13)$$

(5.13) shows that $\left(\dfrac{T}{V} \right)_{Max}$ is independent of H_e and has the value:

$$\left(\frac{T}{V} \right)_{Max} = \frac{M_{sat}^{\;2} \, (N_y - N_x)}{2 \, \mu_o} \qquad - \quad (5.14)$$

where $\theta = 45^\circ$. Now $(N_y - N_x)$ can never exceed unity thus:

$$\left(\frac{T}{V} \right)_{Max_{Max}} = \frac{M_{sat}^{\;2}}{2 \, \mu_o} \qquad - \quad (5.15)$$

Equation (5.12) becomes:

$$\phi \left(\frac{T}{V} \right)_{Max} = Sin^{-1} \left(\frac{(N_y - N_x) \, M_{sat}}{2 \, \mu_o \, H_e} \right) + 45^\circ \qquad - \quad (5.16)$$

It should be noted that (5.16) and (5.12) break down where H_e is small. From (5.6) again:

$$\left(H_i + \frac{N_x M_{sat}}{\mu_o} \right) \frac{Cos\theta}{Cos\phi} = \left(H_i + \frac{N_y M_{sat}}{\mu_o} \right) \frac{Sin\theta}{Sin\phi} \quad - \quad (5.17)$$
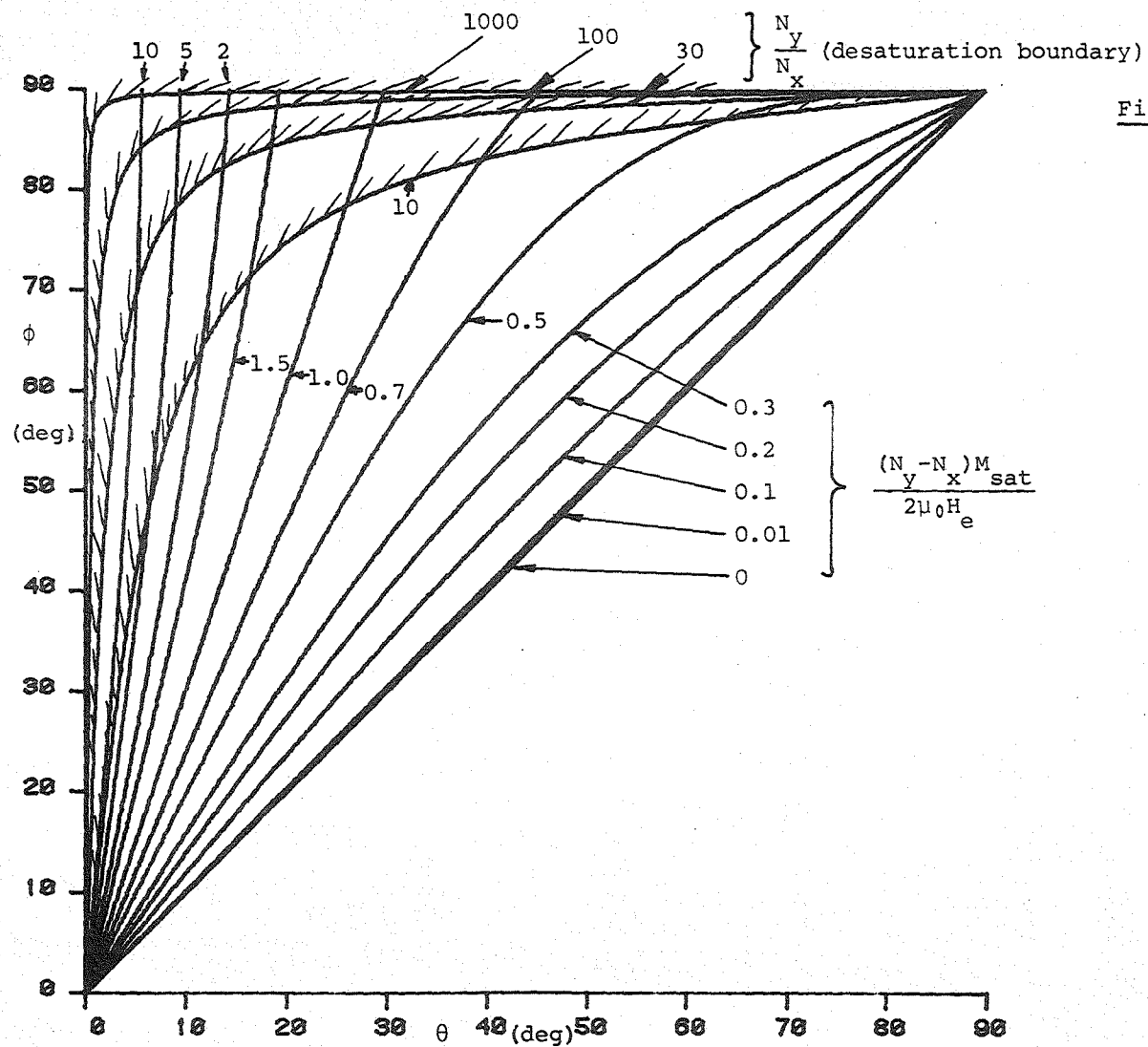
Fig. 5.9 Variation of the direction of induced magnetization.

From Eqns. 5.12 and 5.18
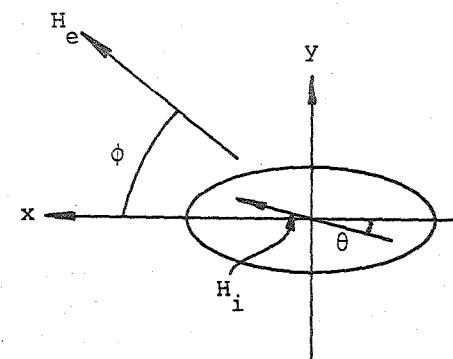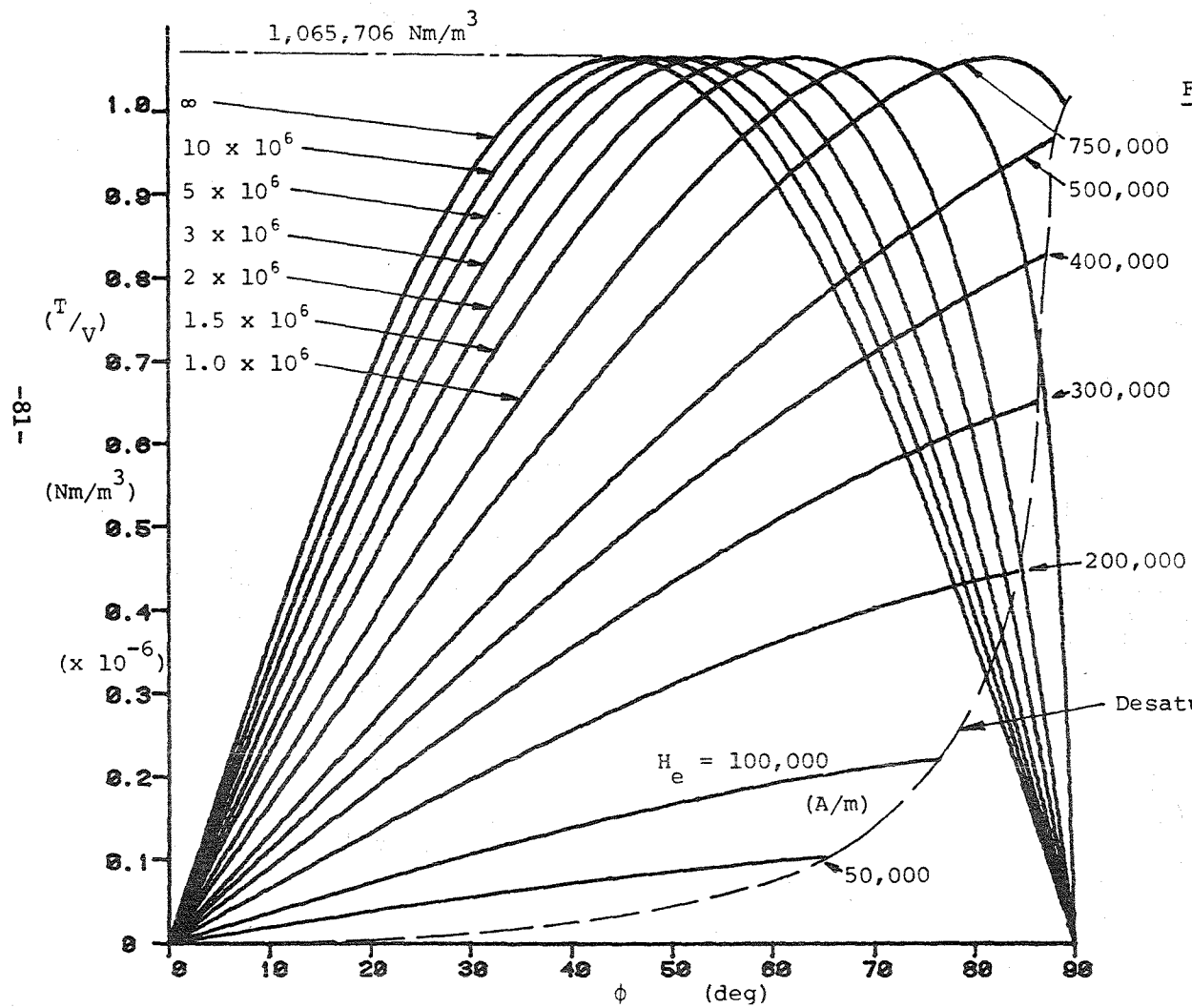
Fig. 5.10 Torque per unit volume for specific ellipsoidal core.

$M_{sat} = 2.35T$

$N_y = 0.495$ } prolate ellipsoid

$N_x = 0.01$
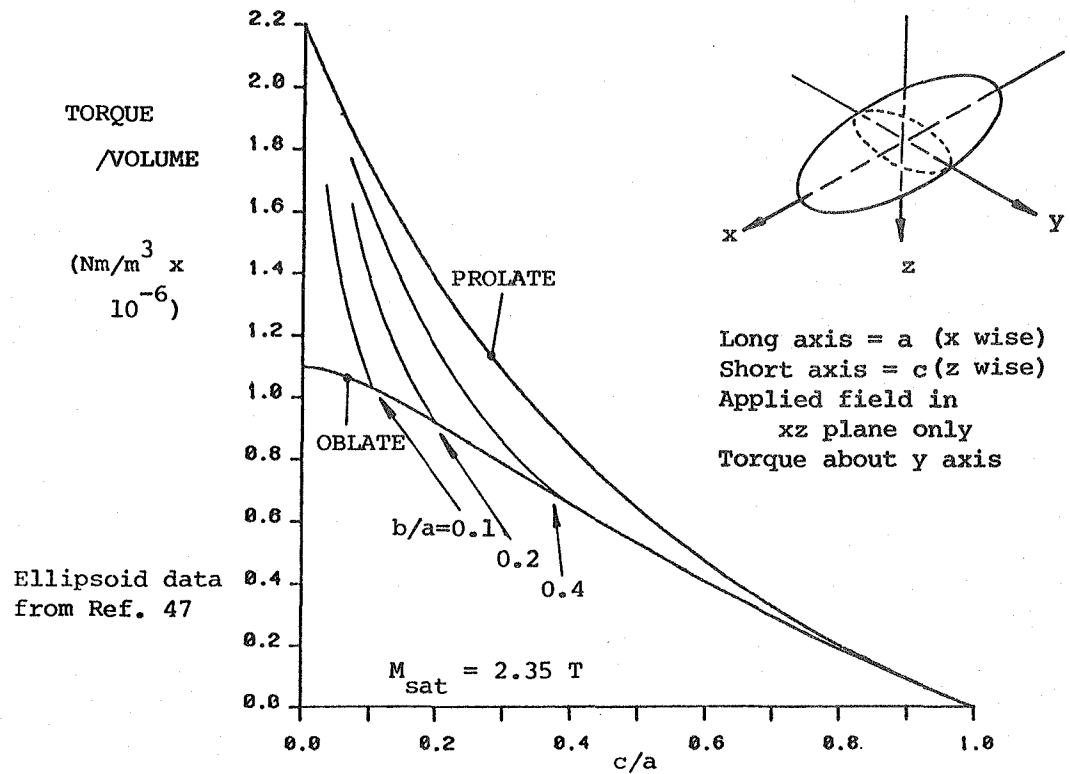
Fig. 5.11a Torque per unit volume (maximum) for ellipsoids.
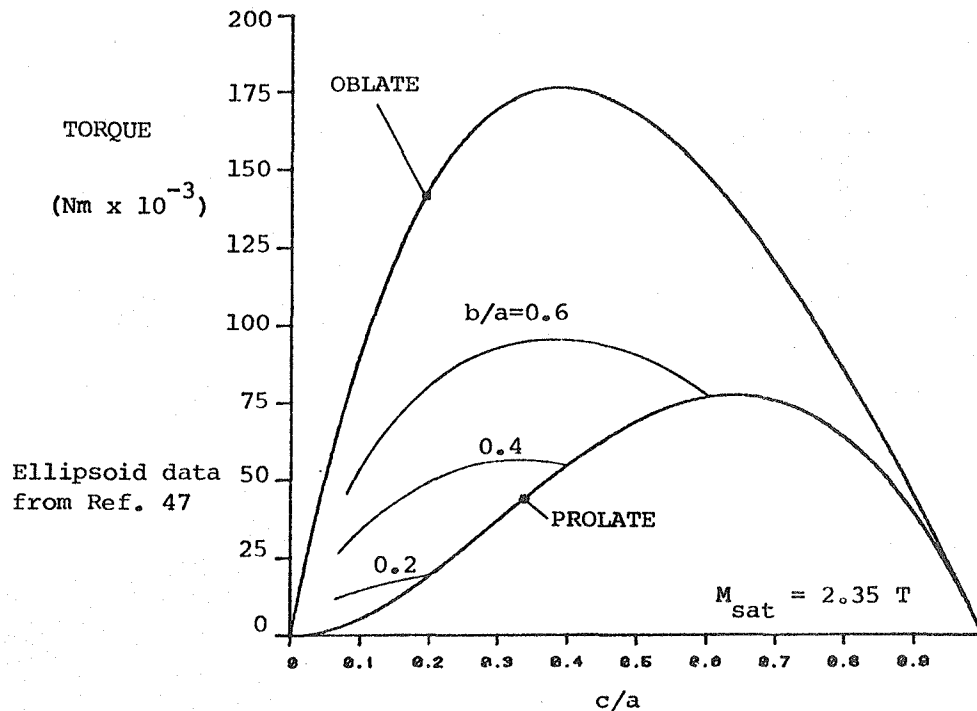
Fig. 5.11b Maximum torque for ellipsoids

- 82 -

The breakdown occurs where $H_i = 0$ ($\chi_m = \infty$). At this point, from (5.17):

$$\text{Tan}\,\phi = \text{Tan}\,\theta \left(\frac{N_y}{N_x}\right) \qquad - \quad (5.18)$$

Fig. 5.9 shows the variation of the direction of induced magnetization, after Eqn. 5.12, for a variety of cores. It is seen that with a powerful applied field the induced magnetization lies nearly parallel to that field.

Fig. 5.10 shows torque per unit volume for a particular core (Eqn. 5.13) and clearly illustrates the existence of a finite and approachable absolute maximum torque. For any given geometry and applied field direction it is seen that the torque per unit applied field is far from constant. In fact, at high values of ϕ with powerful applied fields, increases in applied field strength may apparently result in reductions in torque.

The variations of the maximum torque and torque per unit volume with ellipsoid geometry are of interest and are shown in Fig. 5.11, using data from Ref. 47. The significant feature here is that relatively slender ellipsoids are capable of generating high torques, perhaps implying that slender wing cores (SIMs) will remain relatively capable torque producers.

5.5.2 Linear SIM theory

The field at any point P, in the principal plane of a symmetric quadrupole may be written as follows:
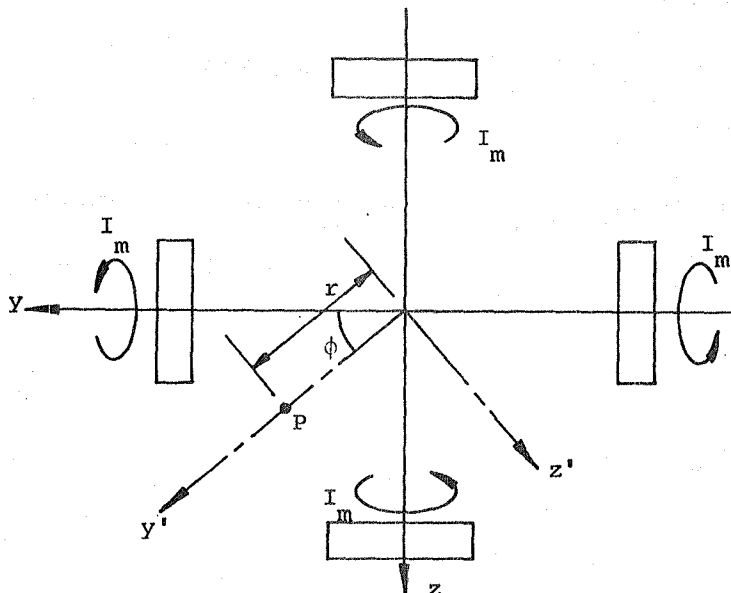
Fig. 5.12 SIM quadrupole magnetizing field

$$H_{y'_p} = I_m (k_{1_r} \, Cos2\phi + k_{2_r} \, Cos4\phi + \text{-----}) \qquad - \quad (5.19a)$$

$$H_{z'_p} = -I_m (l_{1_r} \, Sin2\phi + l_{2_r} \, Sin4\phi + \text{-----})$$

where k_{n_r} and l_{n_r} are functions of r. For an identical quadrupole displaced by 45° about the x axis (giving the through-wing field quadrupole):

$$H_{y'_p} = I_r (k_{1_r} \, Sin2\phi + k_{2_r} \, Sin4\phi + \text{-----}) \qquad - \quad (5.19b)$$

$$H_{z'_p} = I_r (l_{1_r} \, Cos2\phi + l_{2_r} \, Cos4\phi + \text{-----})$$

If a linear magnetization characteristic is assumed for the wing core (permeability constant or $\gg 1$) and a suitable radius chosen, we may write:

$$\bar{M}_{y'} \simeq \frac{\mu_o H_{y'_R}}{D_{y'}} \qquad\qquad \bar{M}_{z'} \simeq \frac{\mu_o H_{z'_R}}{D_{z'}} \qquad - \quad (5.20)$$

where $D_{y'}$ and $D_{z'}$ are effective demagnetizing factors in the y' and z' directions respectively. If $H_{yz'}$ is assumed to be fairly constant along any particular radial we have:

$$H_{z'_r} \simeq \overline{H_{yz'}} r \qquad\qquad - \quad (5.21)$$

Equation 4.4 becomes:

$$L \simeq \overline{4M_{y'}} \, \overline{H_{yz'}} \int_{b=o}^{s} A_o g(b) b \; db \quad + \quad M_{z'} \text{ term}$$

For constant geometry and neglecting the $M_{z'}$ term:

$$L \stackrel{.}{\propto} \overline{M_{y'}} \, \overline{H_{yz'}} \qquad\qquad - \quad (5.22)$$

Applying a magnetizing field and a through-wing field simultaneously:

$$L \stackrel{.}{\propto} \left[I_m(k_{1_R} Cos2\phi + \text{---}) + I_r(k_{1_R} Sin2\phi + \text{---}) \right] \times$$

$$\left[I_r(l_{1_R} Cos2\phi + \text{---}) - I_m(l_{1_R} Sin2\phi + \text{---}) \right]$$

Neglecting terms above 2ϕ:

$$L \stackrel{.}{\propto} \tfrac{1}{2}(I_r - I_m) Sin4\phi + I_r I_m Cos4\phi \qquad - \quad (5.23)$$
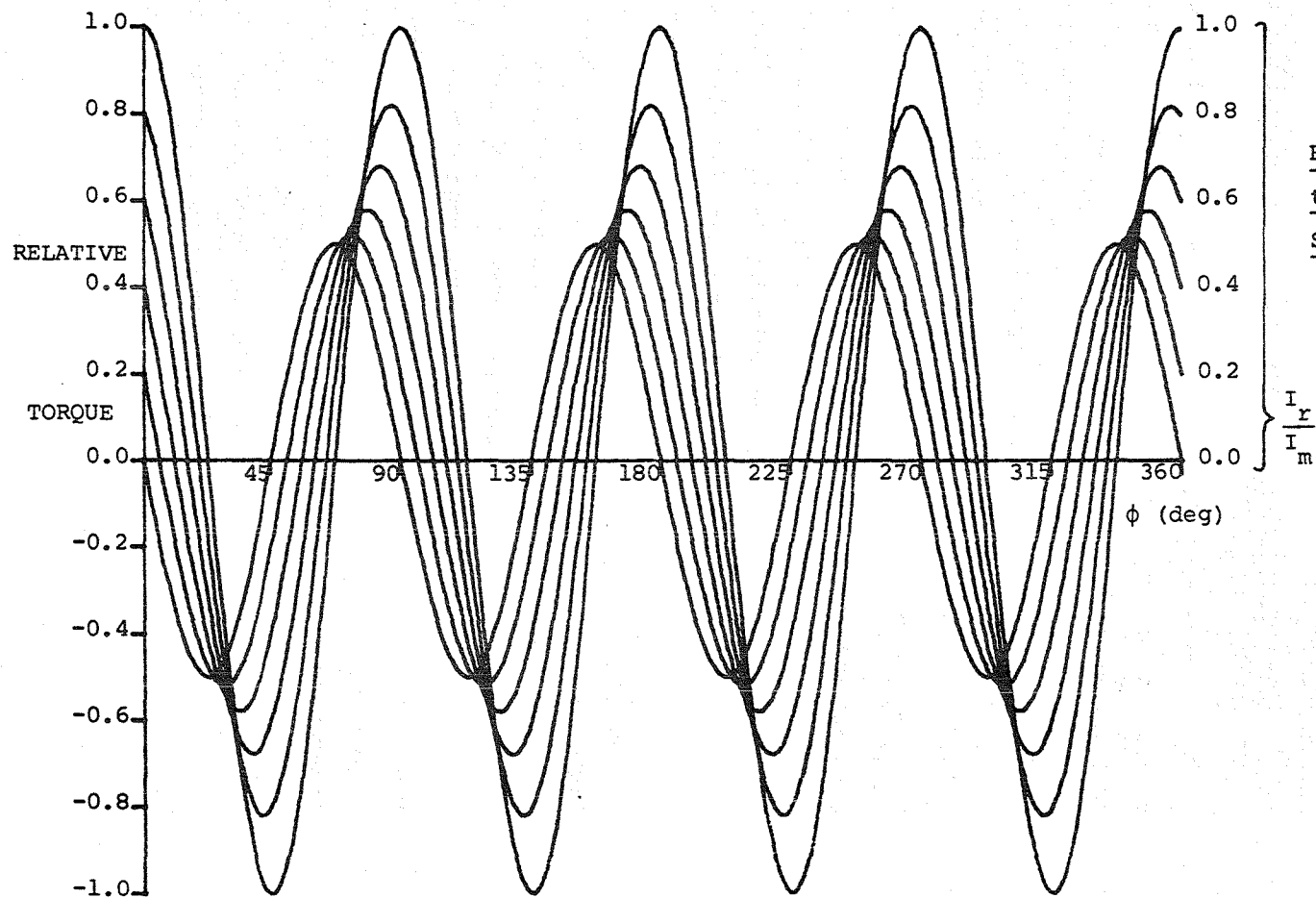
Fig.5.13 Variation of roll torque with ϕ, I_r, I_m. Simplified linear theory.

This equation is illustrated in Fig. 5.13. Where $\phi = 0$, it is seen from Eqn. 5.23 that:

$$L \overset{\propto}{.} I_r I_m \qquad - \quad (5.24)$$

Thus, in a fully symmetric configuration, the maximum torque for given total available ampere-turns will occur at:

$$I_m = I_r \qquad (\phi = 0)$$

5.6 GFUN results

5.6.1 Baseline geometry - Effect of variation in material properties, low and intermediate applied fields

Where the permeability of the core is constant (linear solution, typical of low applied field levels) the effects of the magnetizing (J_m) and through-wing (J_r) fields are independent. Since, under these conditions, the spanwise magnetization is everywhere proportional to J_m and the through-wing field proportional to J_r, the roll torque is expected to vary as the product $J_m J_r$. This is confirmed in Fig. 5.14 - 5.16, being as predicted by Eqns. 5.9 and 5.24.

The variation of torque with core permeability, permeability held constant within each solution, is of interest, Fig. 5.17 showing comparatively low sensitivity to permeability variations at high values of permeability, the core then behaving as if infinitely permeable.

Using the baseline BH curve it is clear that there exists some maximum level of applied field commensurate with the whole core lying in the initial constant permeability region of the BH curve. At higher applied field levels the permeability of certain strongly magnetized volumes of the core will progressively fall, eventually the bulk of the core settling onto the terminal (saturated) region of the BH curve. During this process the magnetization is no longer proportional to J_m, rather reaching some limiting value. It might therefore be expected that torque becomes proportional to J_r alone. However at high values of through-wing field the induced magnetizations may no longer be predominantly spanwise, rather turning to lie more nearly parallel with the direction of local (applied) field (see Fig. 5.9). Torque may therefore reach some limiting value, or continue to rise (or fall, see Fig. 5.10) with rising applied fields as some function of J_r and J_m (Fig. 5.18).

NOTE μ in this Section
strictly represents μ_r
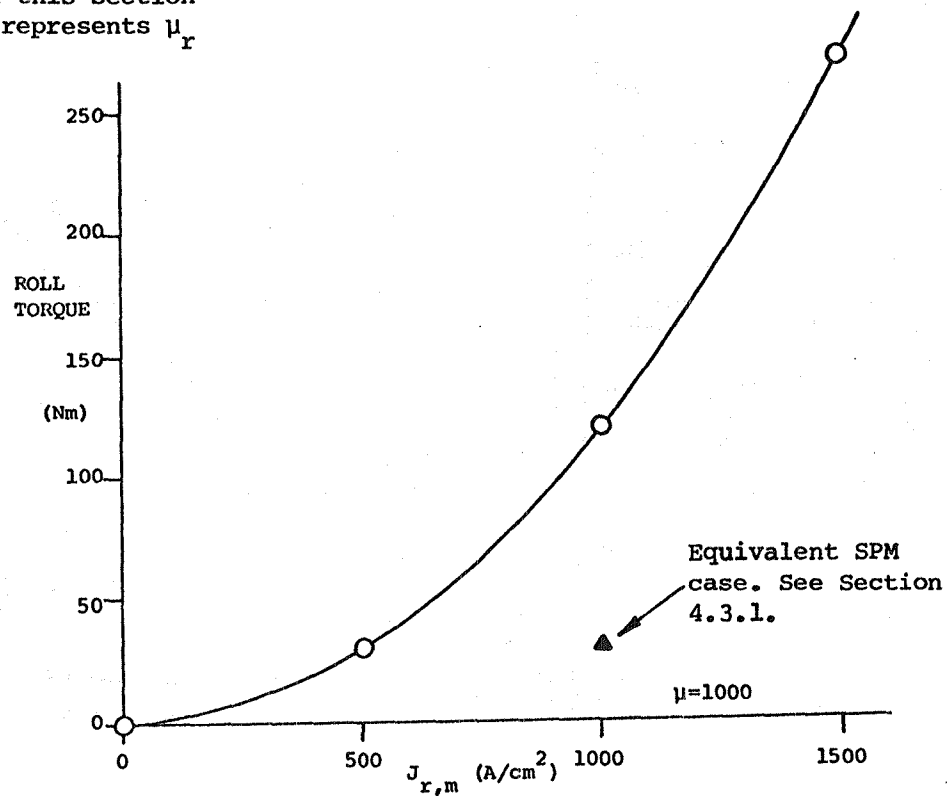
Fig. 5.14   Torque versus $J_{r,m}$. Baseline core and E/Ms. Linear solutions
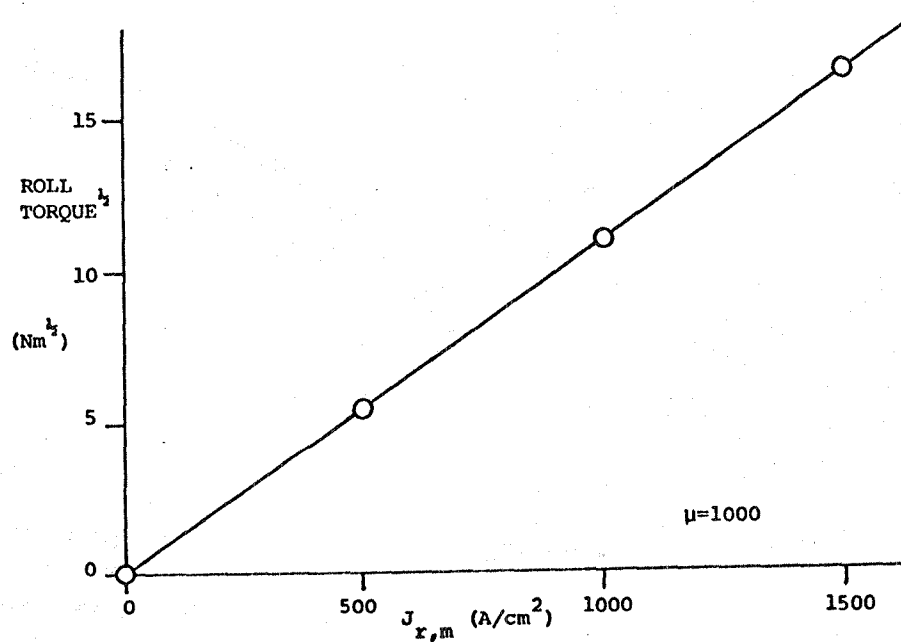
Fig. 5.15   Square-root torque versus $J_{r,m}$. As Fig. 5.14.
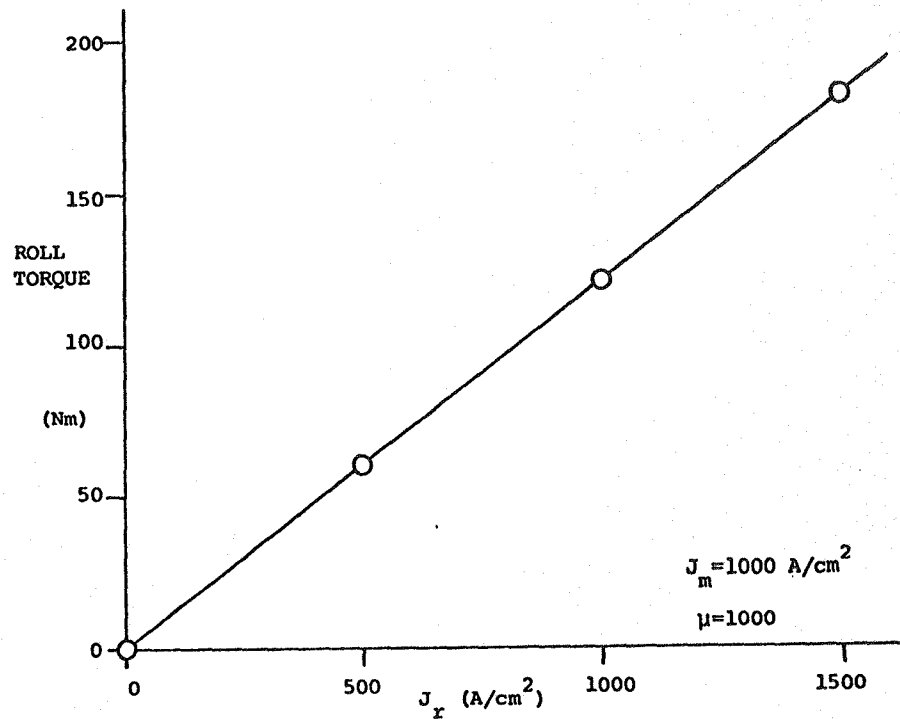
Fig. 5.16   Torque versus J_r, J_m constant. Baseline core and E/Ms.
Linear solutions.
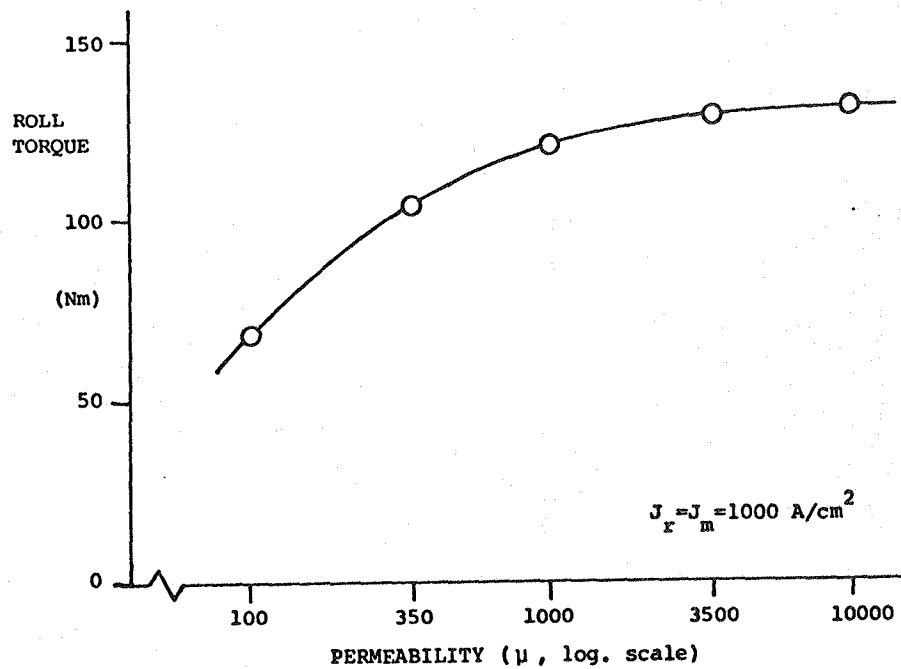
Fig. 5.17   Torque versus permeability. Baseline core and E/Ms.
Linear solutions.

Torque
(L)

Linear
$L \propto H^2$

Saturated core
$L \propto H$

Terminal
character-
istic

Applied field strength (H)
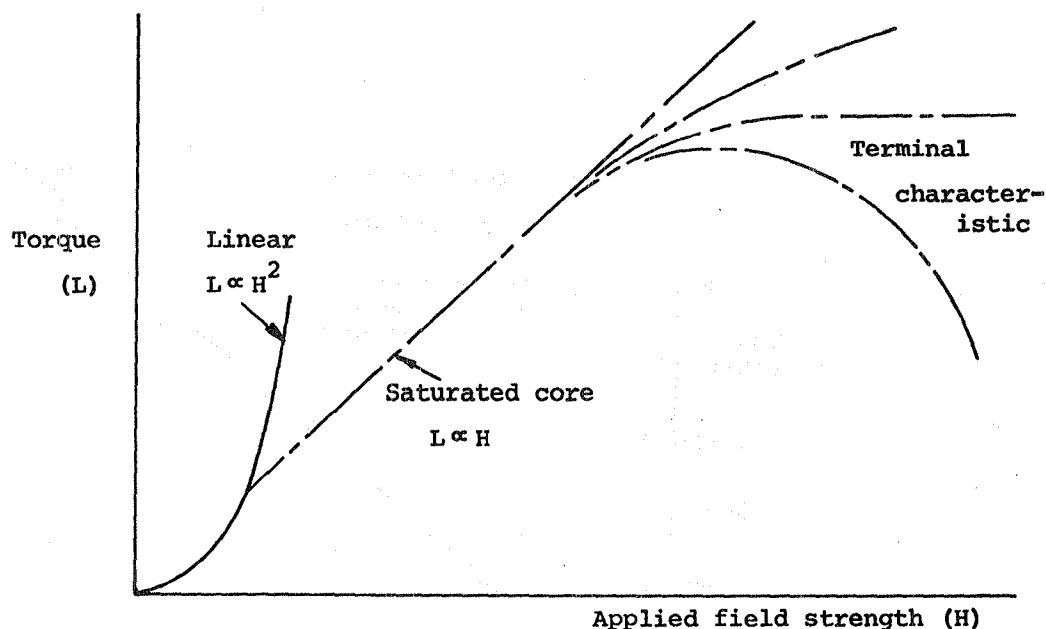
Fig. 5.18 Schematic diagram showing possible
terminal torque characteristics

Figs. 5.19, 5.20 show the breakaway from the linear permeability
curve onto a near straight line characteristic at moderate applied
field levels. Data is included for a close approximation to the
representative vanadium permendur BH curve in Fig. 5.6, showing a
very weak influence of precise core magnetic properties.

5.6.2 Variations of baseline geometry. Effect of wing AR,
        t/c and taper

GFUN solves linear (constant permeability) cases directly,
without recourse to iterative procedures, hence relatively economi-
cally. The variations of the initial (constant permeability)
torque capability of the system with various geometrical parameters
as defined in Fig. 5.21 are shown in Figs. 5.22 - 5.24, the solid
symbols representing the baseline core.

These figures require some explanation. It is clear that the
torque for a given applied field is far from being a constant per
unit core volume and in fact does not obey any simple relation to
geometry (such as first moment of volume about the x axis). It
is believed that this effect is due to the fact that the effective
spanwise demagnetizing factors are predominantly determined by the
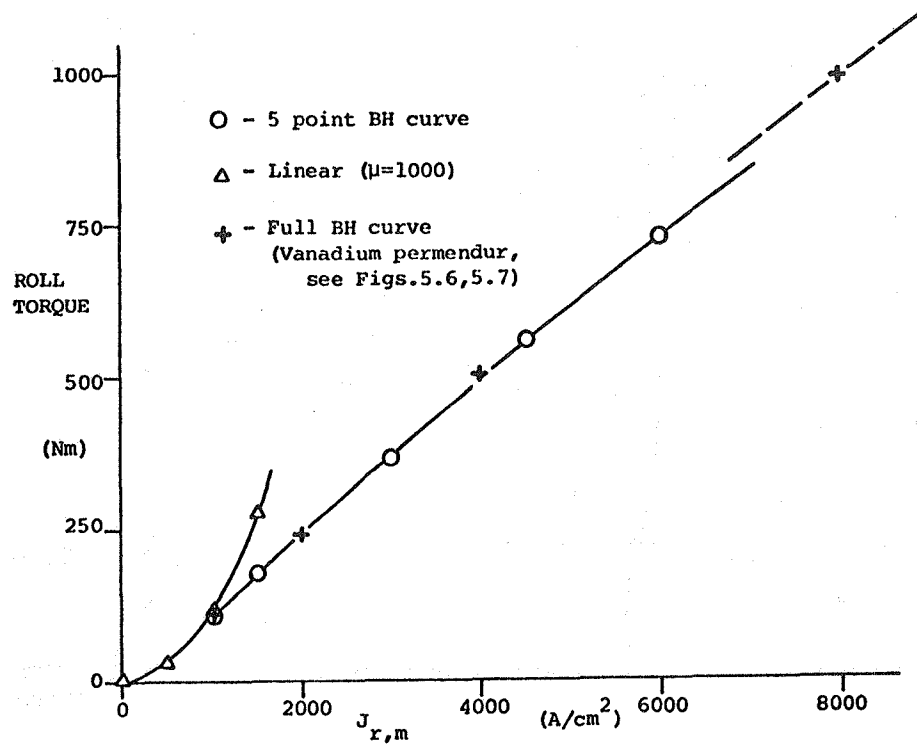
Fig. 5.19 Torque versus $J_{r,m}$. Baseline core geometry and E/Ms.
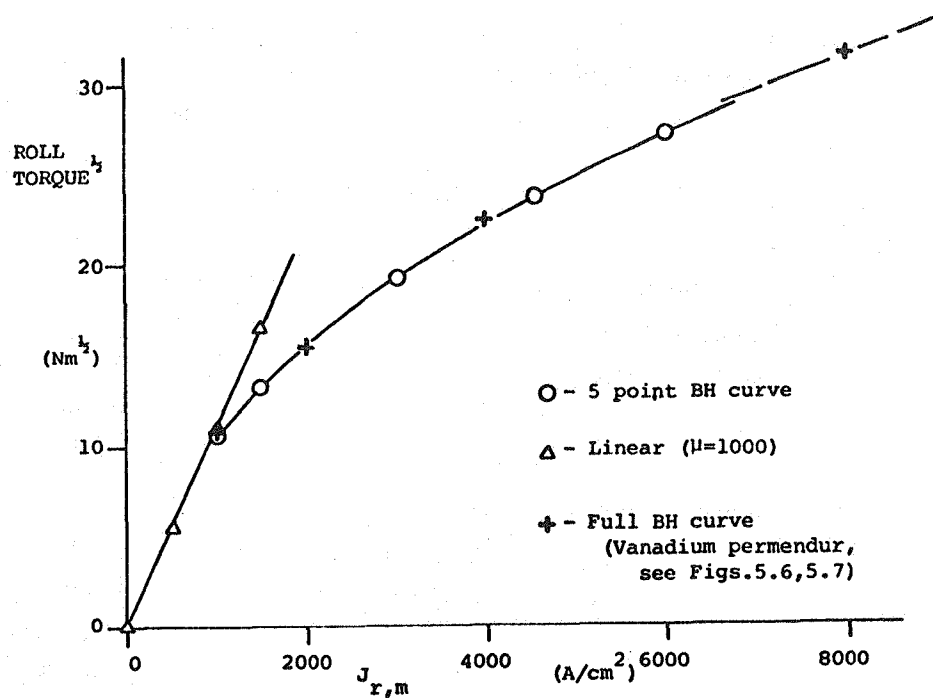
Fig. 5.20 Square-root torque versus $J_{r,m}$. As Fig.5.19
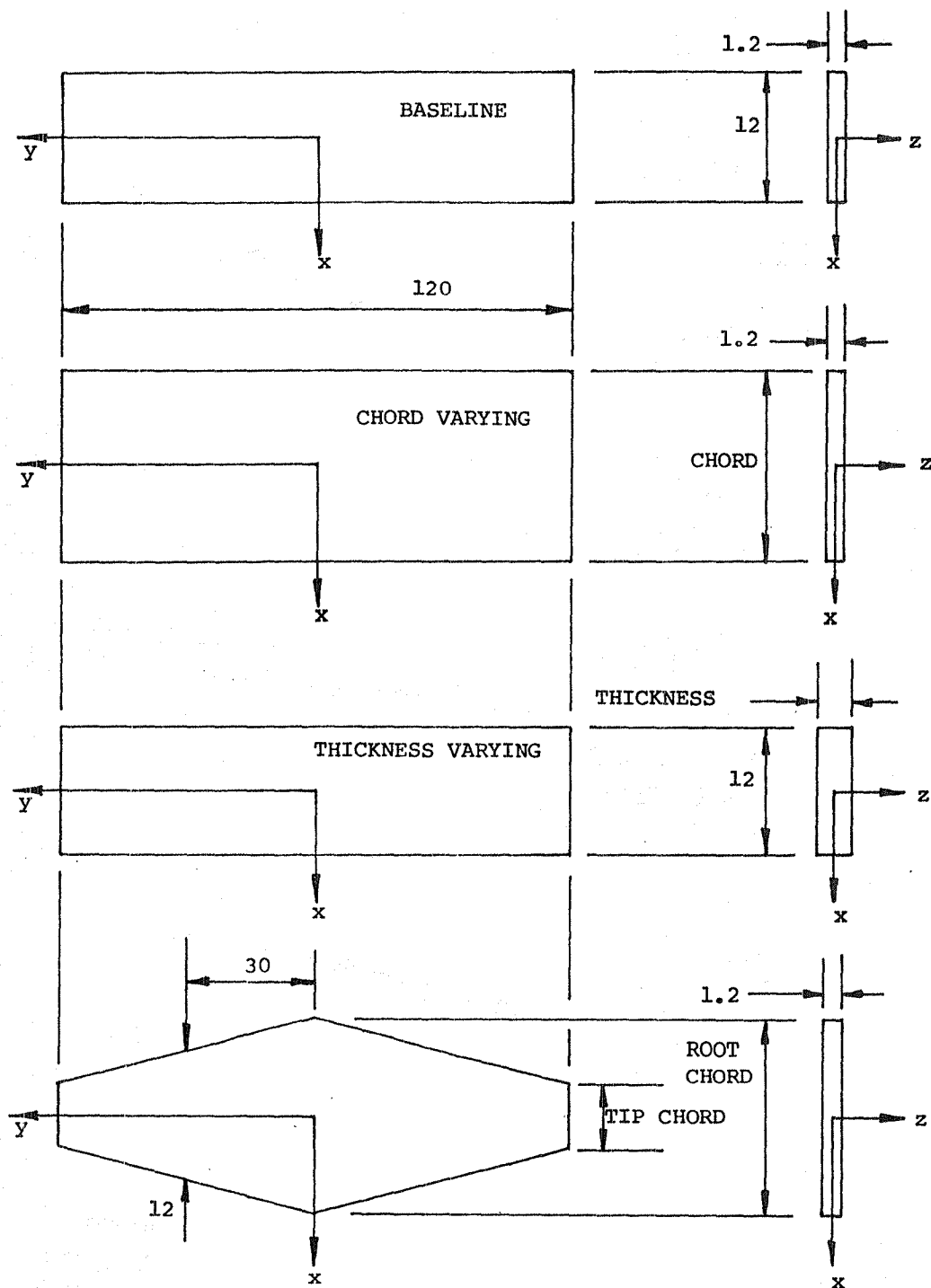
Fig. 5.21 Definitions of variations of baseline geometry.
All dimensions in cms.
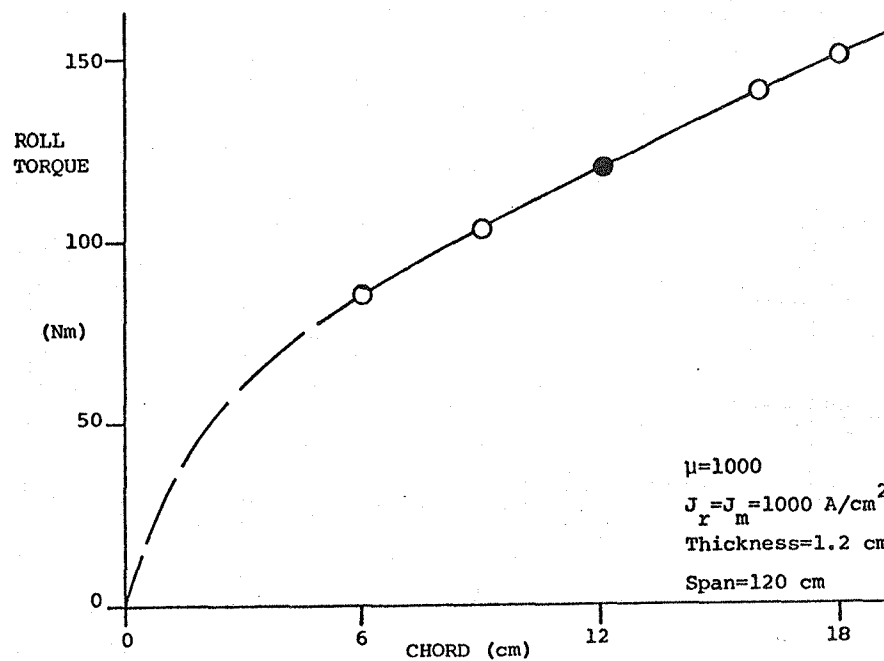
Fig. 5.22   Torque versus chord. Baseline E/Ms. Core as Fig.5.21.
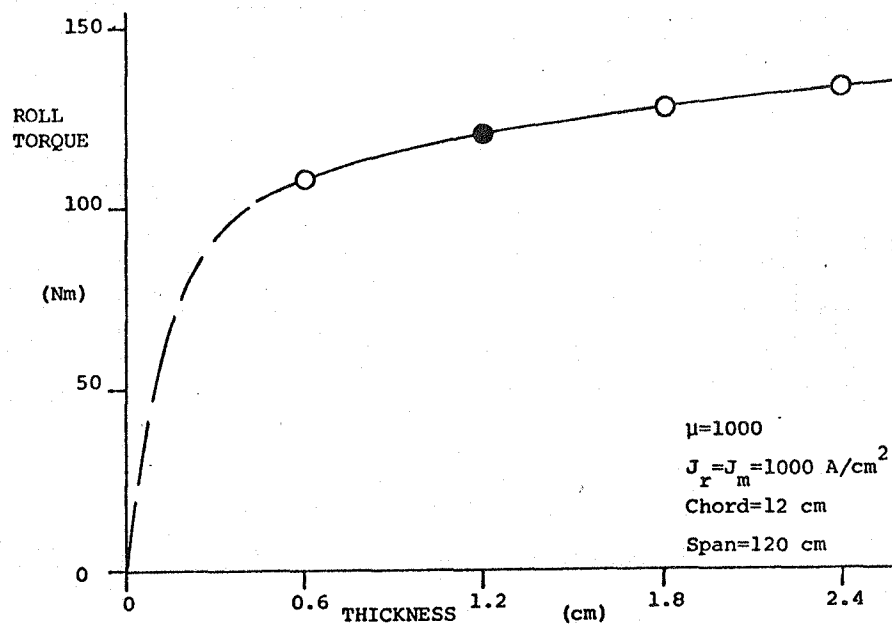
Linear solutions.

Fig. 5.23   Torque versus thickness. Baseline E/Ms. Core as Fig.5.21

Linear solutions.
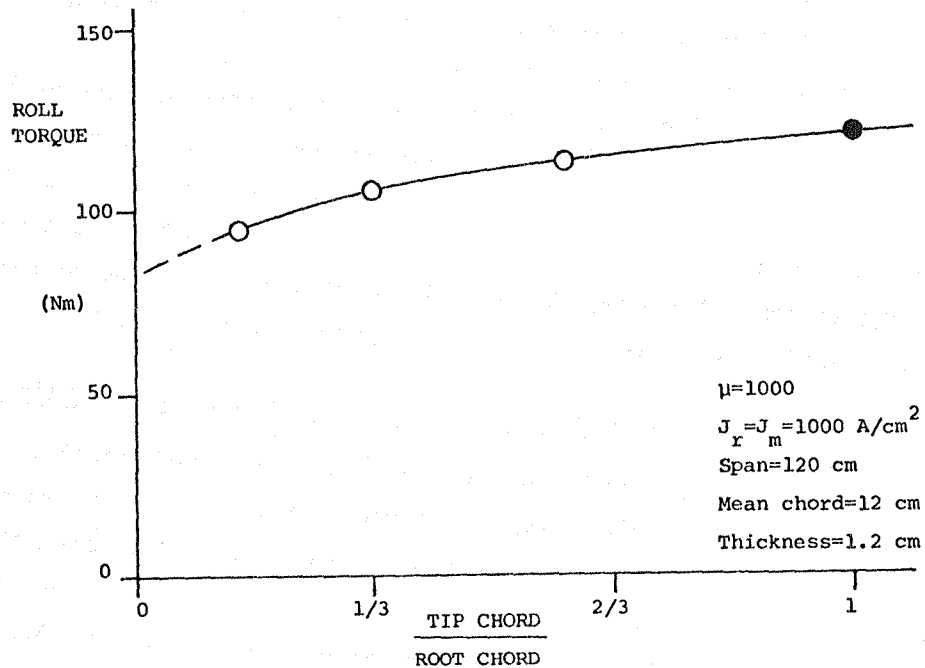
Fig. 5.24   Torque versus taper. Baseline E/Ms. Core as Fig.5.21.
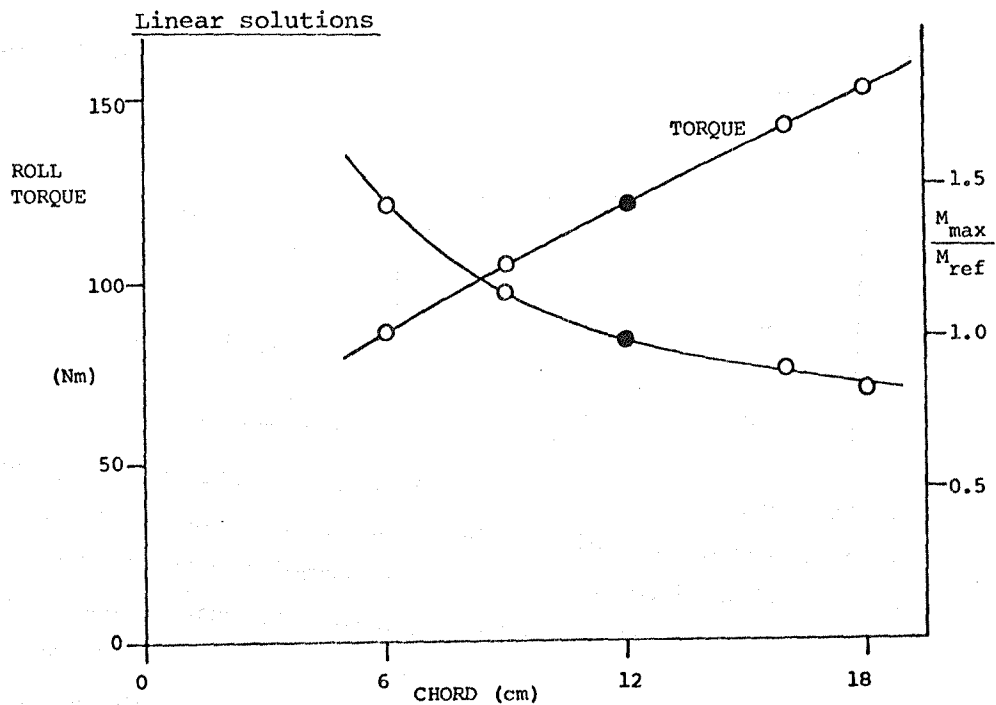
Fig. 5.25   Torque versus chord showing peak induced magnetizations

Otherwise as Fig. 5.22.

slenderness of the core, being lower for more slender cases. Thus
the removal of wing volume by reduction of chord or thickness lowers
the effective spanwise demagnetizing factor, hence increasing the
level of spanwise magnetization of the core for any given applied
field level. This may be partly justified by inspection of Figs.
5.25 – 5.26, showing the increase in the peak element spanwise
magnetization with increasing slenderness.

Tapering the core under the criteria chosen does not affect the
core volume but displaces volume from the most effective regions
near the tips to less effective regions near the roots. The slender-
ness of the tip portions of the core is increased and since these lie
in the regions of strongest applied fields the peak value of element
magnetization tends to be increased as shown in Fig. 5.27.

5.6.3 Effect of the presence of fuselage and axial magnetizing field

It is to be expected that the presence of an unsaturated iron
fuselage should act to increase the mean level of spanwise magneti-
zation in the wing cores since it provides an easy flux path at the
wing root (Fig. 5.28). A saturated fuselage may or may not act
similarly. With the fuselage geometry as defined in Fig. 5.29, the
wing core span remains unchanged, the root now being enveloped by the
fuselage core. The table below shows some results for this geometry,
confirming the expectation of augmentation of torque with fuselage
present. The effect appears weak.

Fuselage Dimensions (cms)	Torque (Nm)
Absent	109.78
50 x 5.2 x 5.2	110.22
50 x 7.4 x 7.4	113.53
100 x 7.4 x 7.4	114.40

If a soft iron fuselage core is used it will generally require an
axial magnetizing field. The effect of an axial field on the wing
cores will tend to be to rotate the spanwise magnetization vectors in
the plane of the wing, in the sense of sweepback or sweepforward.
Where the core permeability is constant, the magnitudes of the span-
wise components will be unaffected. A reduction in the spanwise
components, hence torque, will be expected where the wing core
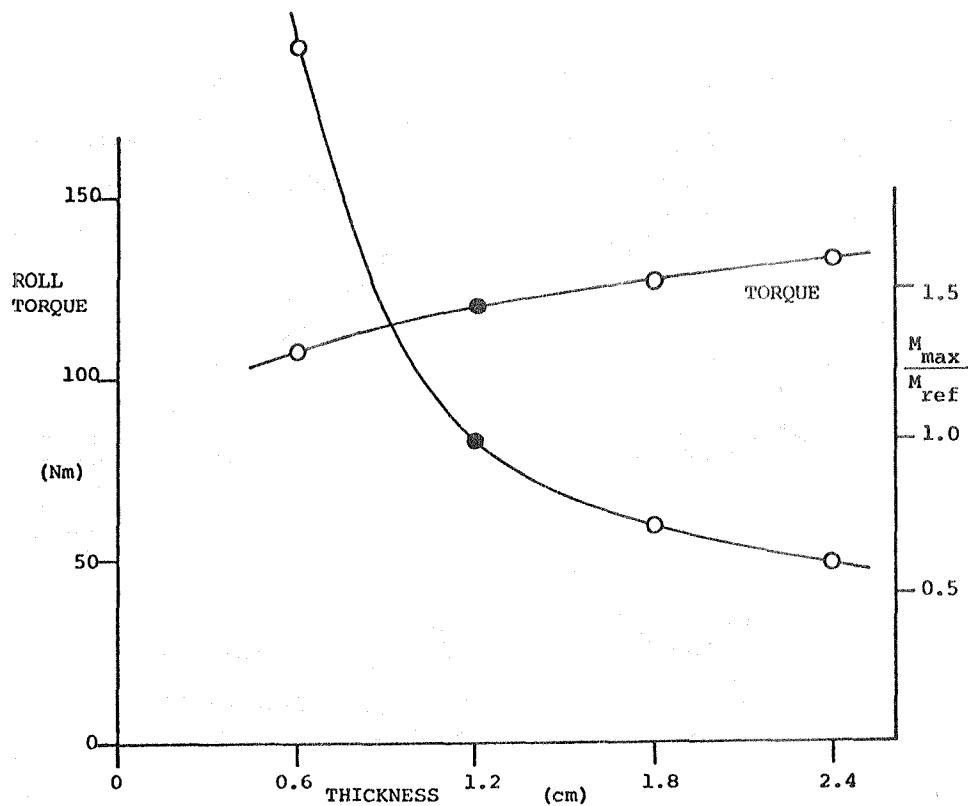
Fig. 5.26   Torque versus thickness showing peak induced magnetizations.

Otherwise as Fig. 5.23
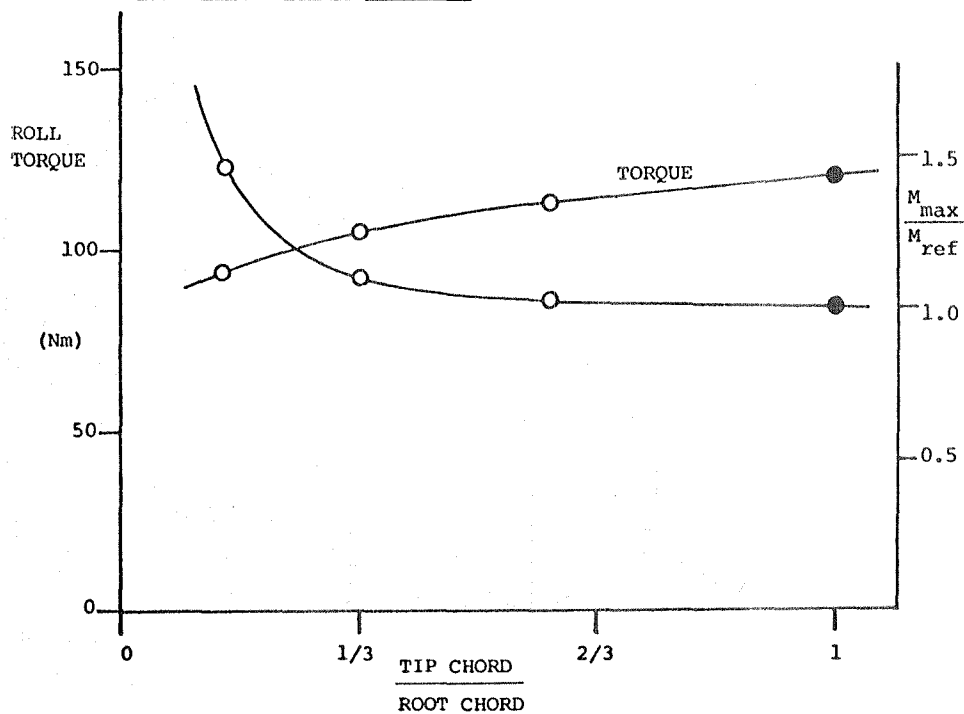
Fig. 5.27   Torque versus taper showing peak induced magnetizations.

Otherwise as Fig. 5.24.
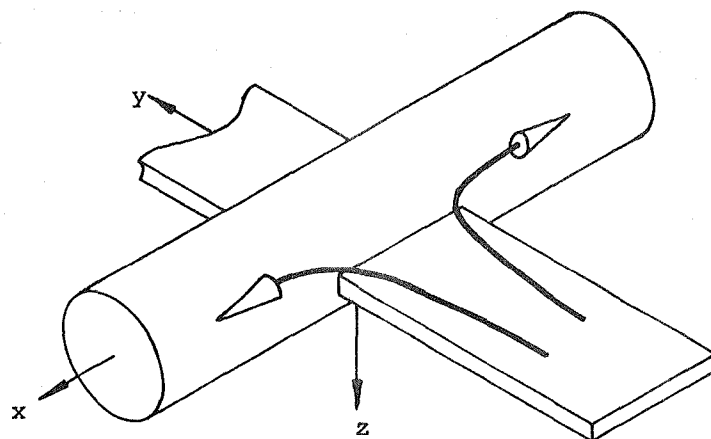
With fuselage.
Most flux carried
into fuselage core.

Fig. 5.28 Easy flux
path at wing root with
fuselage present.
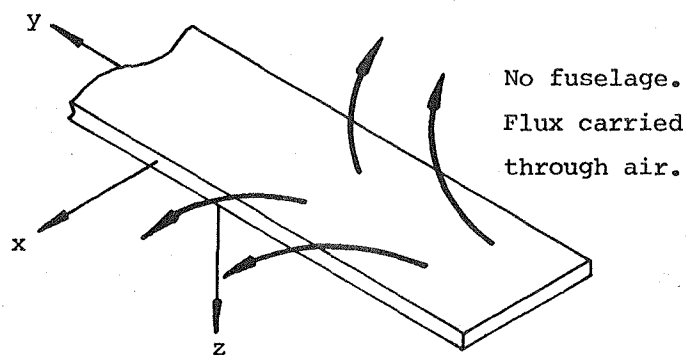
No fuselage.
Flux carried
through air.

B

C
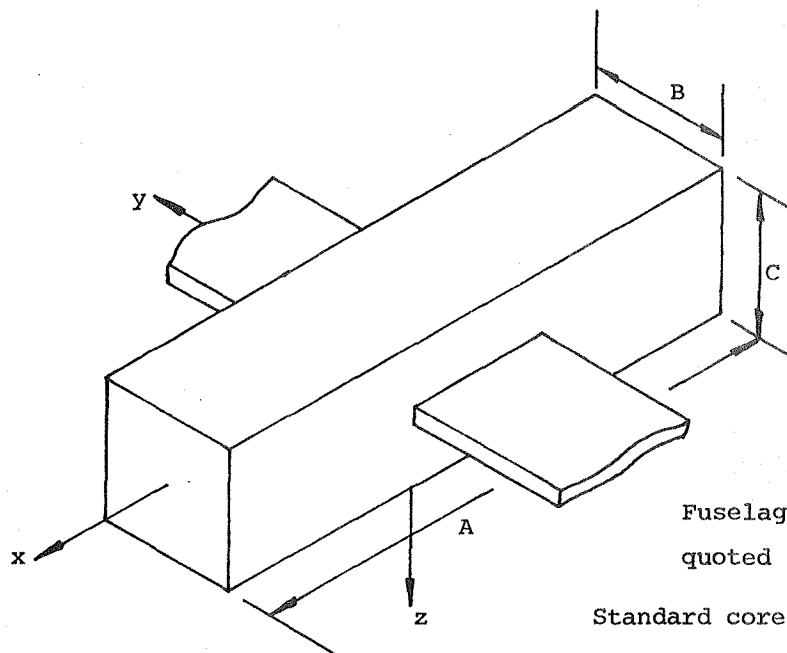
Fuselage dimensions
quoted as A*B*C (cms.)

Standard core 50*7.4*7.4

A

Fig. 5.29 Standard dimensions of fuselage core.

permeability is falling with rising magnetization. With the fuse-
lage dimensions fixed at 50 x 7.4 x 7.4 cms (Fig. 5.29) and a near
uniform axial field of representative strength applied by a large
Helmholtz E/M pair of otherwise arbitrary dimensions this expectation
is confirmed by the results shown in Fig. 5.30.

The magnitude of the axial magnetization components induced in the
wing core by the axial field will depend to a large extent on the
axial slenderness of the core, which will in turn be most strongly
affected by the core's thickness to chord ratio, relatively thick,
narrow chord cores being least powerfully affected. Very thin cores,
such as the F-16 case studied later, may thus be seriously affected
although no relevant data currently exists.

5.6.4 Effect of sweepback

Sweepback of the wing cores as defined in Fig. 5.31 rotates the
easy axis of wing core magnetization away from the spanwise direction,
but does not affect the core volume nor the position of the centroid
of volume. The induced magnetization vectors with a purely spanwise
magnetizing field are thus expected to themselves be sweptback, at
some angle probably less than the geometrical sweep angle. This
would, in general, lead to lower torque per unit applied field.
However, at low sweep angles it would appear that the increasing
slenderness of the core, caused by the chosen geometry, dominates,
leading to slightly augmented torques at modest sweep angles, as shown
in Fig. 5.32.

When an axial magnetizing field is applied, components of that field
act along the easy axis of magnetization of the sweptback core, in-
creasing or decreasing the spanwise magnetization components (hence
torque) depending on the field polarity. For a sweep angle of 30
degrees Figs. 5.33, 5.34 show the effect to be significant. At
relatively low spanwise fields it is seen that powerful axial fields
of either polarity reduce the torque for particular spanwise and
through-wing field levels.

5.6.5 Behaviour at high levels of roll torque generating field

At high applied roll field levels the core becomes saturated over
most of its volume. The induced magnetization components then behave
as vectors of constant strength but variable direction, as predicted
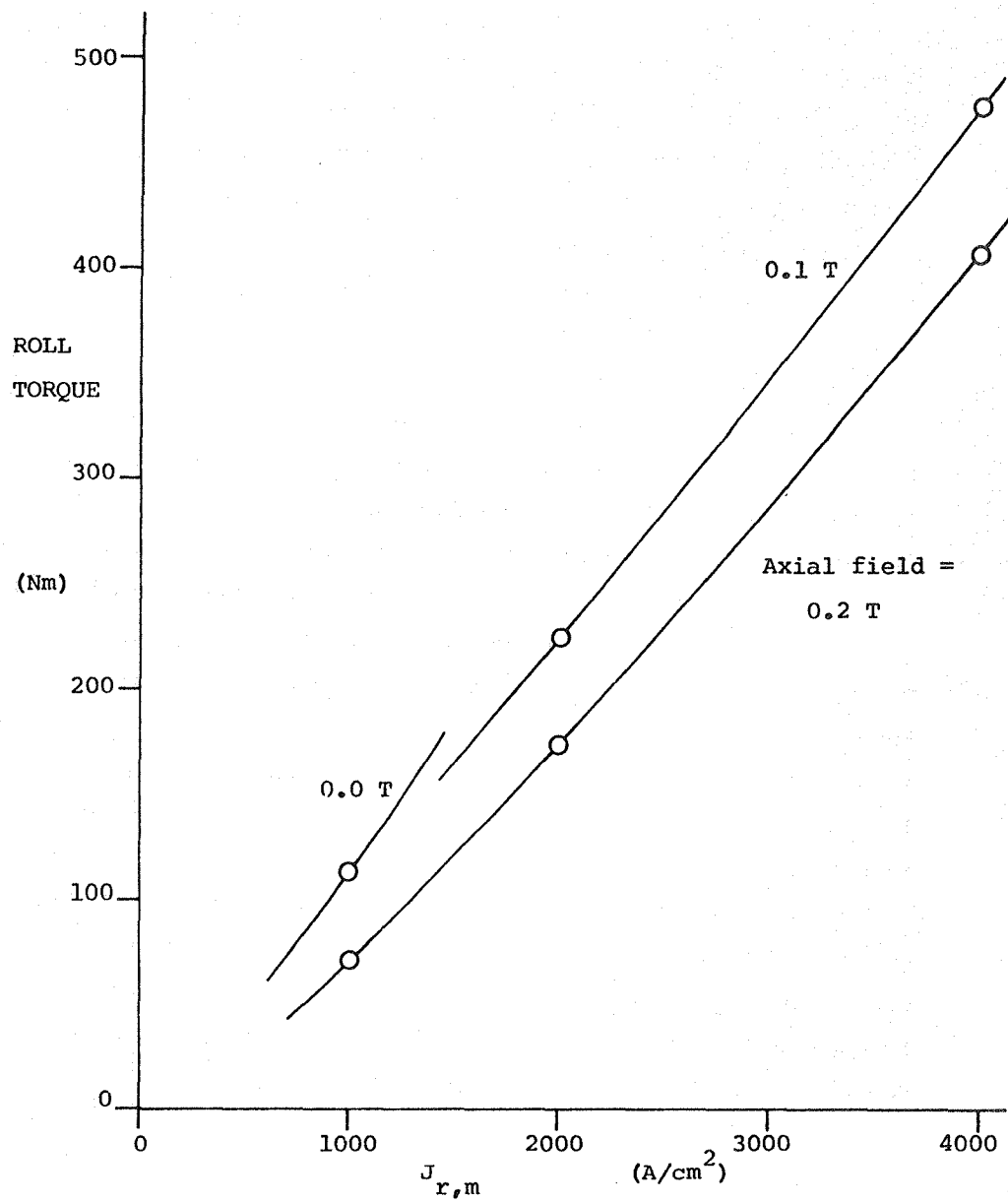
Fig. 5.30 Torque versus $J_{r,m}$. Baseline core with fuselage as Fig. 5.29 Baseline E/Ms. 5 point BH curve.
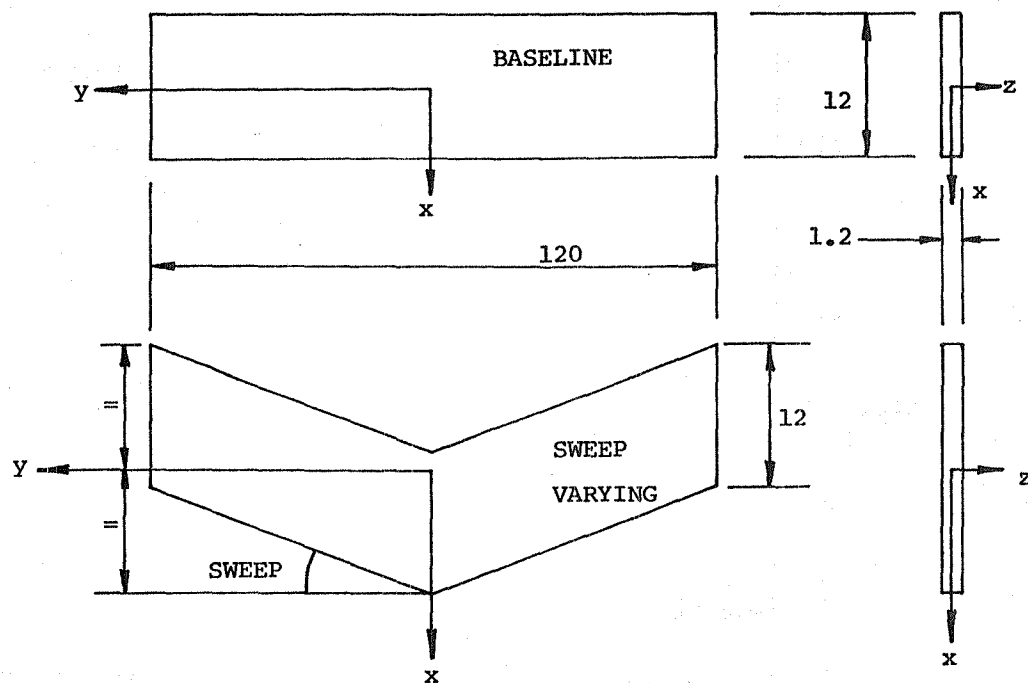
Fig. 5.31   Definition of sweepback. All dimensions cms.
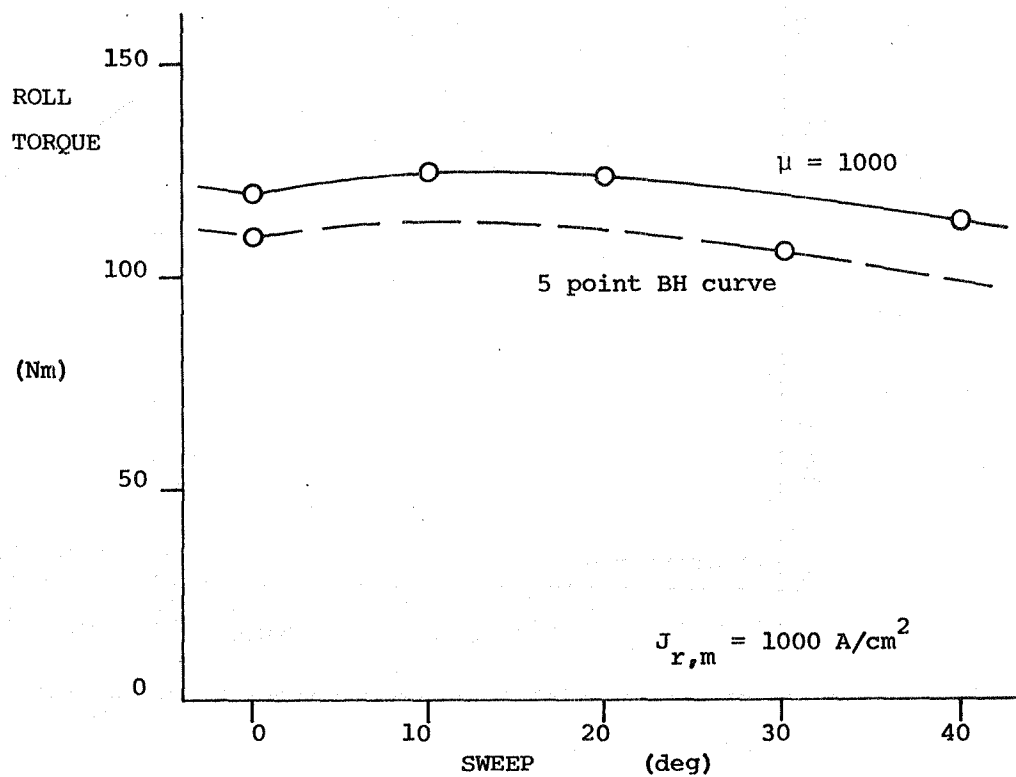
Fig. 5.32   Torque versus sweep angle. Baseline E/Ms. Core as Fig. 5.31.
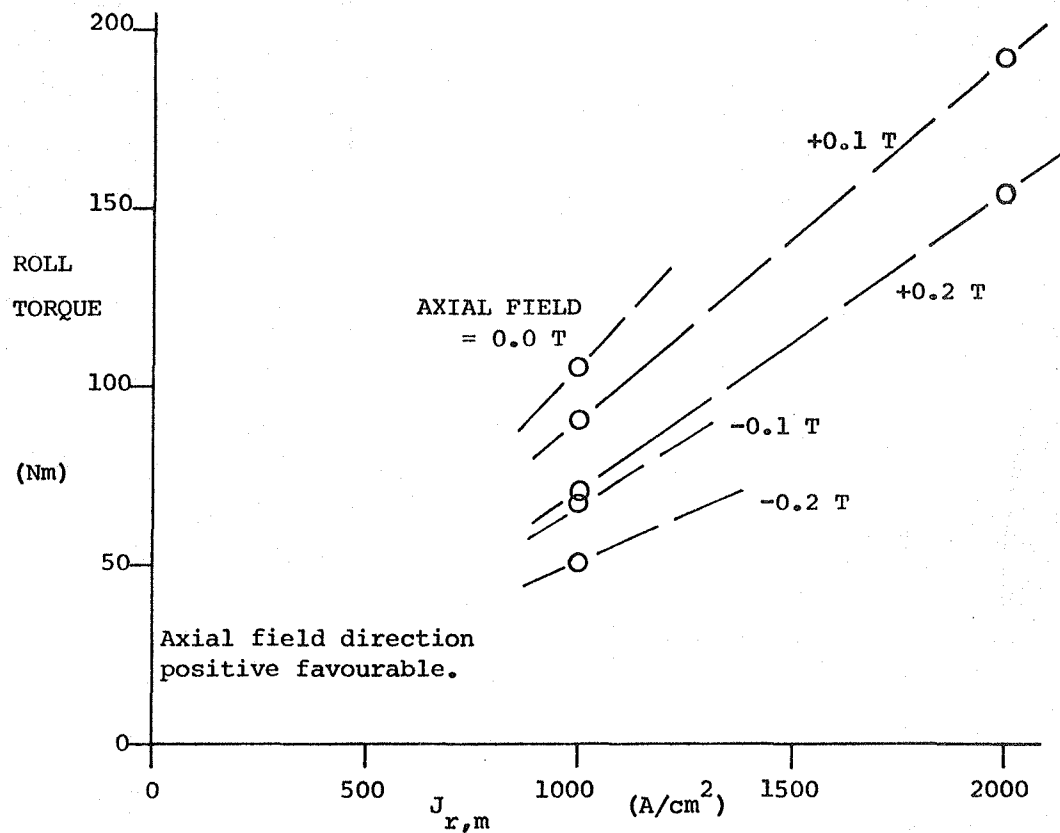
Fig. 5.33   Effect of axial field on sweptback core. Baseline E/Ms.
Core as Fig. 5.31. Sweep = 30°. 5 point BH curve.
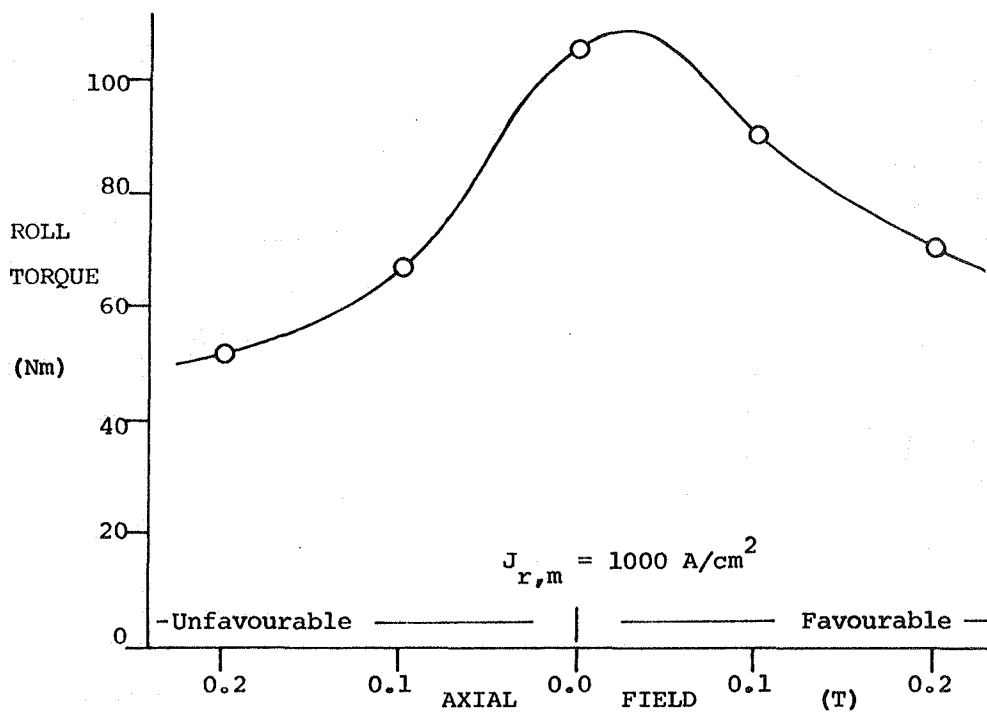
Fig. 5.34   Effect of axial field on sweptback core. Baseline E/Ms.
As Fig. 5.33.

for ellipsoids in Section 5.5.1.   It is not immediately obvious whether, under these conditions, increases in applied field should lead to increases in torque generated and, indeed, whether or not some absolute maximum torque capability will exist in this case for each particular core geometry.

The studies in Section 5.5.1 suggest that an absolute maximum should exist and that this maximum can be realised with finite applied fields of appropriate sense and direction.

Various high applied field cases have been computed with GFUN (Figs. 5.35, 5.36) with somewhat inconclusive results, a clear limit or limiting trend not being identified.   It should be noted here that the torque integration schemes in GFUN are expected to become progressively less reliable at increasing applied field levels. This is due to the difficulty of accurately resolving on the surface of the external control volumes (Section 5.3, Fig. 5.5 and (43)) the "model" field (due to the core's induced magnetization and now of essentially fixed magnitude) from the total field, which becomes mostly due to the applied field from the E/Ms.

The peak torque levels achieved in Figs.5.35, 5.36 are, however, at least one order of magnitude in excess of apparent existing LMSBS requirements (5).

5.6.6 Pseudo F-16 wing core performance

It is understood that a representative aircraft type for use in LMSBS design studies has previously been chosen to be the F-16 fighter. This type presents a considerable challenge to the SIM roll scheme since its wing thickness (hence volume) is very low, the blockage effects of the fuselage would necessitate choice of model wingspan considerably below the 50% of test section width used heretofore and the extreme taper both in chord and thickness leaves relatively little volume in the magnetically most effective regions of the wing (the tips).

Each wing panel has been crudely represented with GFUN as a hexa-hedral slab, uniformly tapered in both thickness and chord, with approximately the same span, total core volume and moment of volume about the chordwise centroids of volume as a typical F-16 model (Fig. 5.37).   The element distribution, particularly the element aspect ratio, within the core is at the limits of what is generally
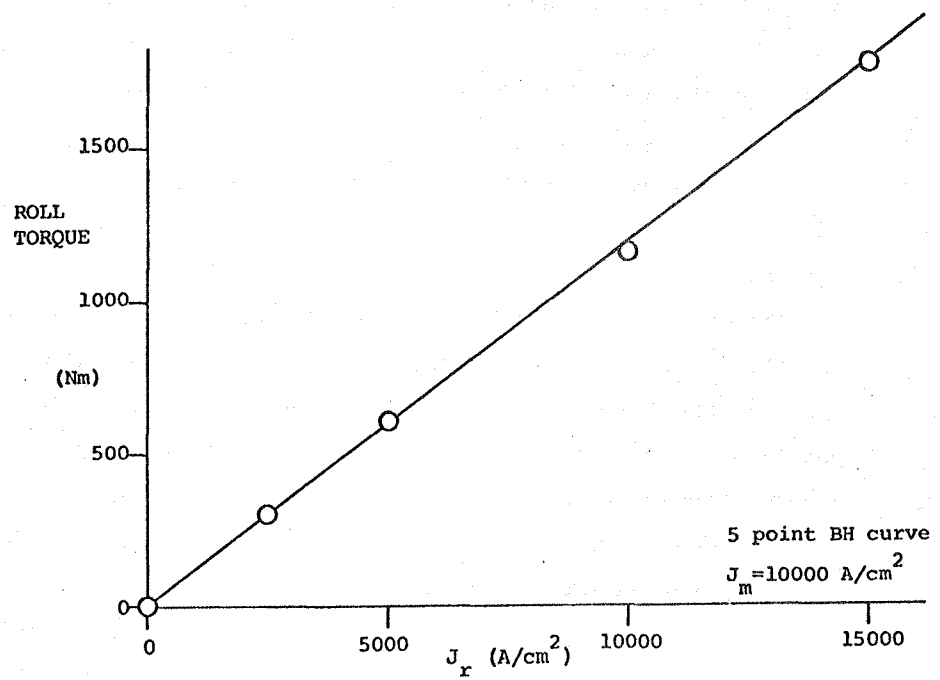
Fig. 5.35   Torque versus J_r, J_m constant. High applied field levels. Baseline E/Ms. Baseline core. 5 point BH curve.
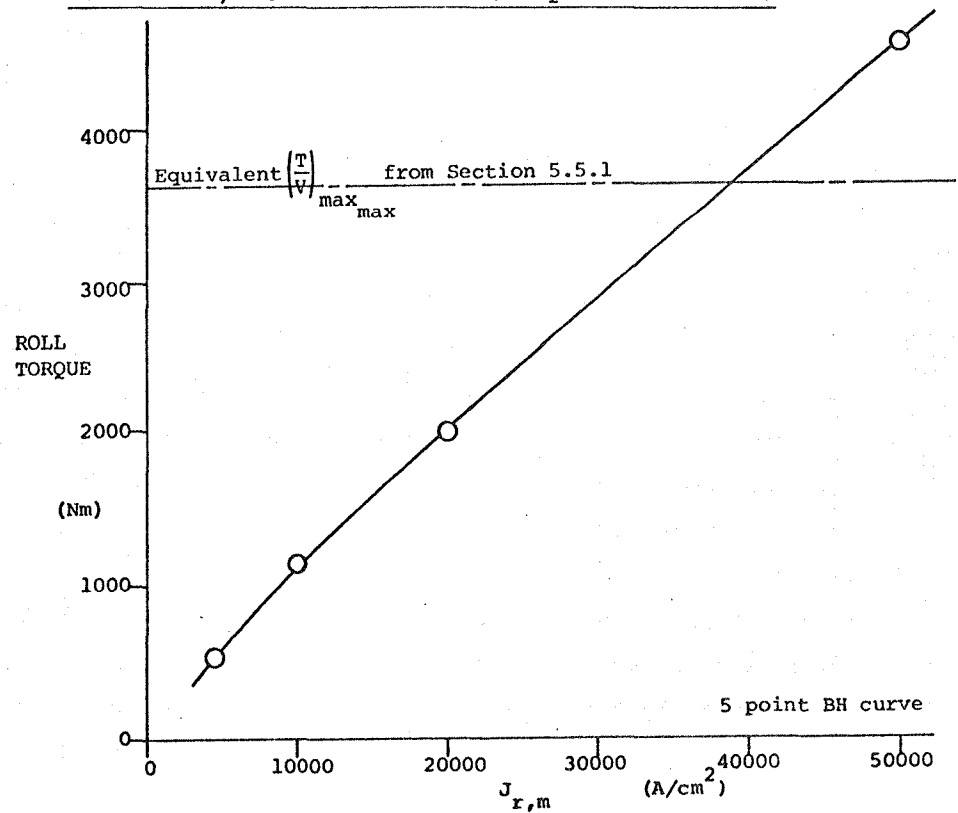
Fig. 5.36   Torque versus $J_{r,m}$. Baseline E/Ms and core. 5 point BH curve.

Uniform chordwise element
distribution

Uniform taper in chord and
thickness

Each hexahedral
element composed
of five tetrahedral
sub-elements as
Fig. 5.5

36

40

30

22

12

Same as
starboard panel

Y

X

z

Section on
centreline

31.4   4.6

1.55

(not to
  scale)

8.0

0.36

Section on
tip

X

z

X

z
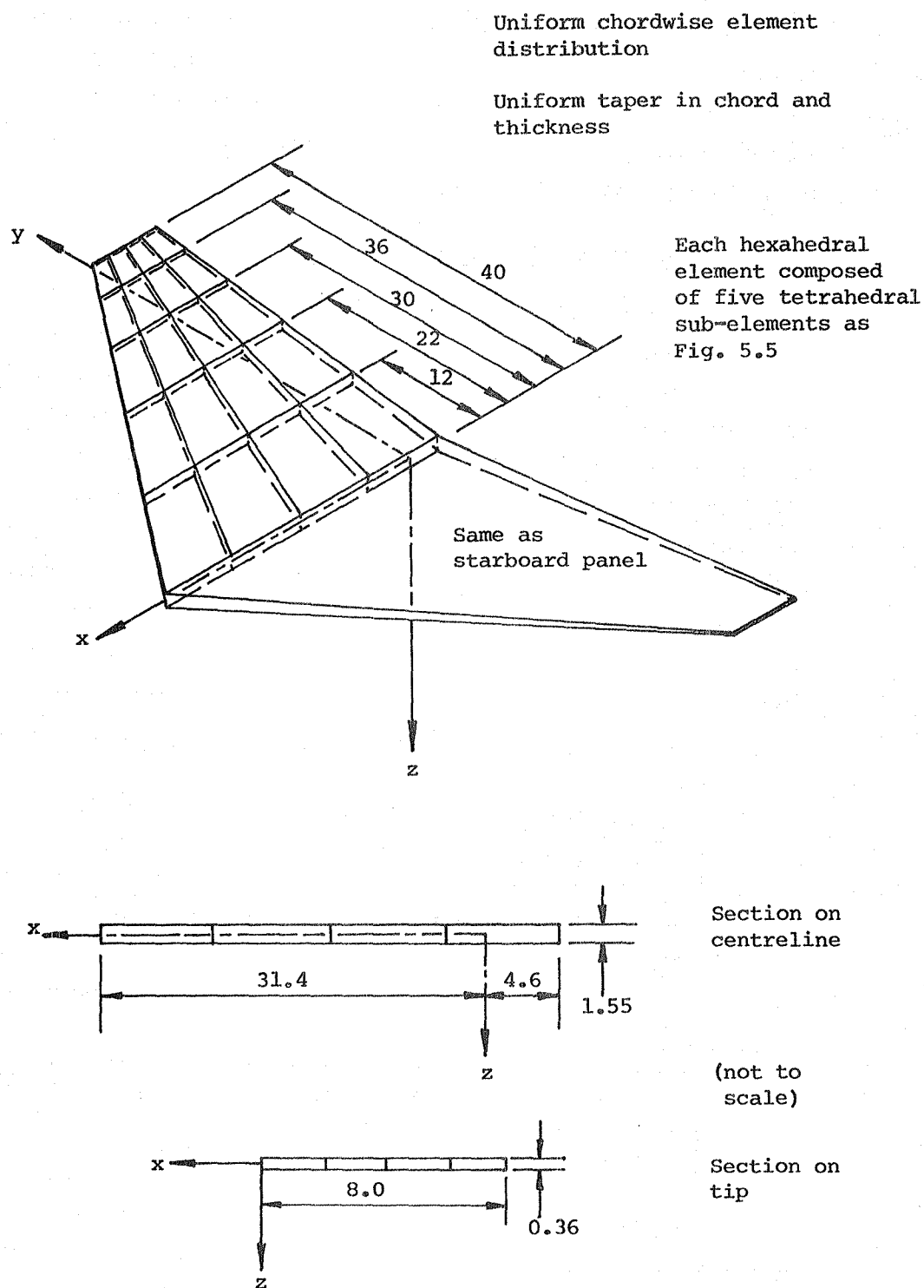
Fig. 5.37   "F-16" slab core geometry. All dimensions in cms.

acceptable with GFUN, hence the results must be regarded as subject to increased uncertainty (see Section 5.7) but again comfortably exceed apparent LMSBS requirements (5) at moderate applied field levels (Figs. 5.38 - 5.41). Ref. 5 was, in fact, based upon a requirement for 140 Nm roll torque at the scale computed herein, this in turn being based upon a requirement for testing at atmospheric stagnation pressure, Mach. 0.85.

5.6.7 Effect of variations of E/M geometry

Non-circular E/Ms, for instance those in Fig. 5.42, exhibit improved packing around the wind tunnel test section compared to the circular baseline E/Ms. The field distribution in the region of the model will be altered also, although the effect tends to be slight due to the relative remoteness of the E/Ms. The performance of different E/M configurations may be approximately normalized by an appropriate measure of the field in the region of the model, but calculated with the model absent. This has been done by computing the mean field level along the y axis, taken over the span of the model. It is seen in the tables below that the effect of E/M geometry on the generated torque under these conditions is small.

E/M geometry	Normalized $J_{r,m}$	Torque ($\mu = 1000$)
Fig. 5.4	1000.0	120.51
Fig. 5.42	894.97	119.78

For reasons other than production of rolling moments, the classical array of 8 E/Ms distributed in the yz plane may not be preferred. A 16 E/M system, shown in Fig. 5.43 has therefore been computed as an example with E/M performance normalized as above:

E/M geometry	Normalized $J_{r,m}$	Torque ($\mu = 1000$)
Fig. 5.43	869.65	112.82

It is clear that the performance of the SIM system is not strongly affected by the detail geometry of the E/Ms, hence permitting consideration of alternative E/M geometries and configurations with the existing GFUN results being approximately applicable provided E/M performance is normalized by the model's near field using Fig. 5.44.
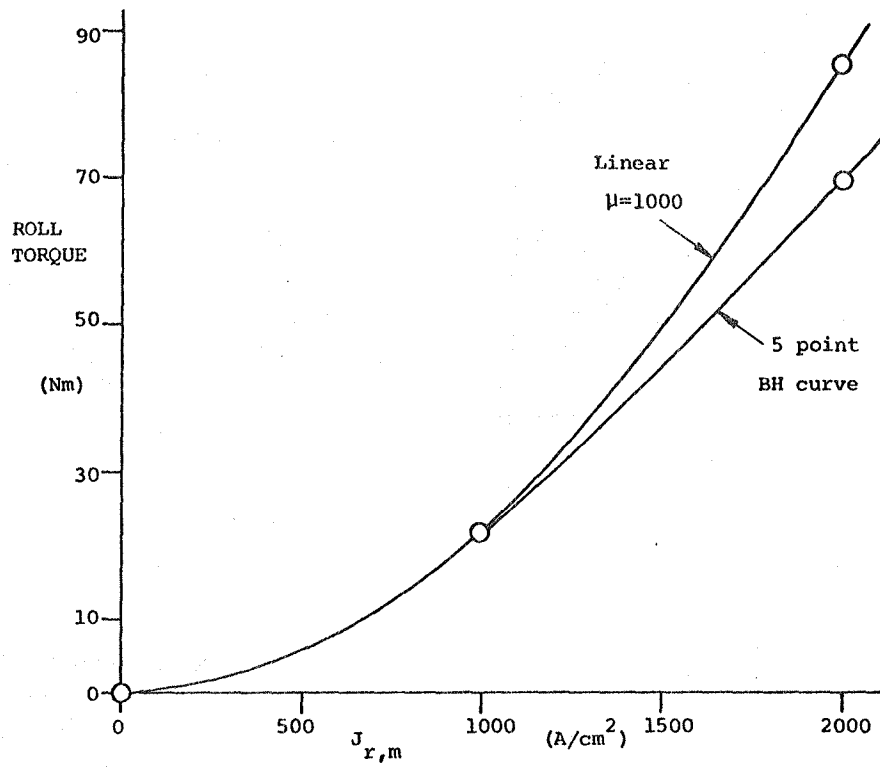
Fig. 5.38 Torque versus $J_{r,m}$. Baseline E/Ms. "F-16" core geometry.
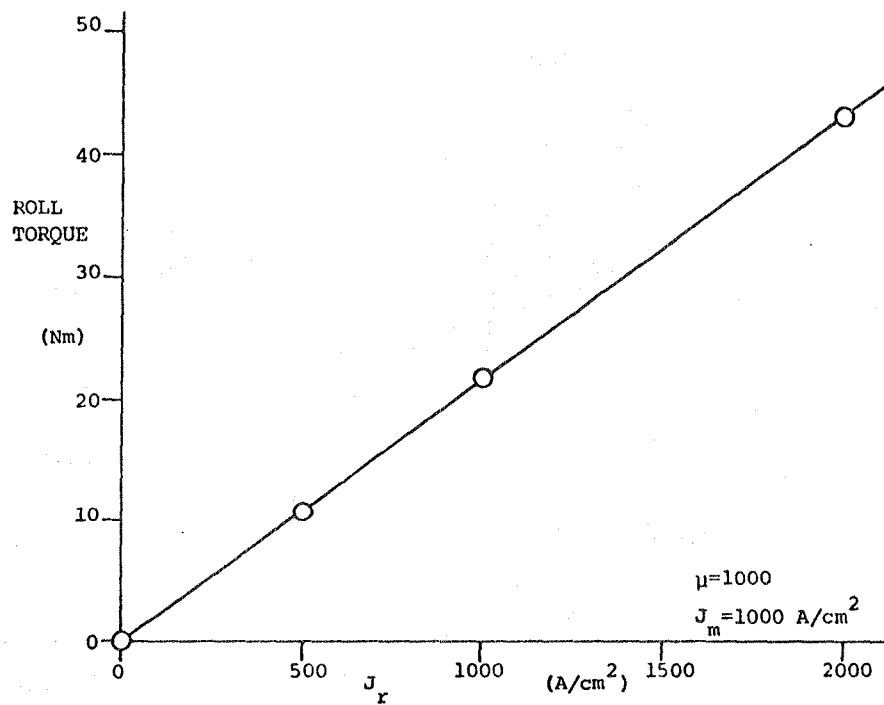
Fig. 5.39 Torque versus J_r, J_m constant. Baseline E/Ms. "F-16" core geometry.
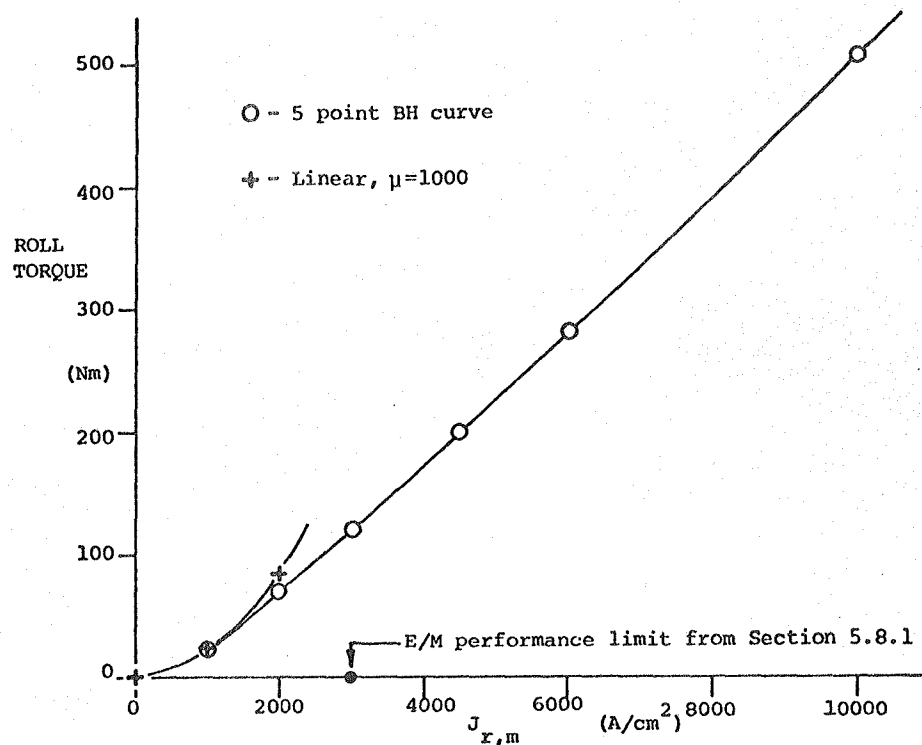
Fig. 5.40 Torque versus $J_{r,m}$. Baseline E/Ms. "F-16" core geometry.
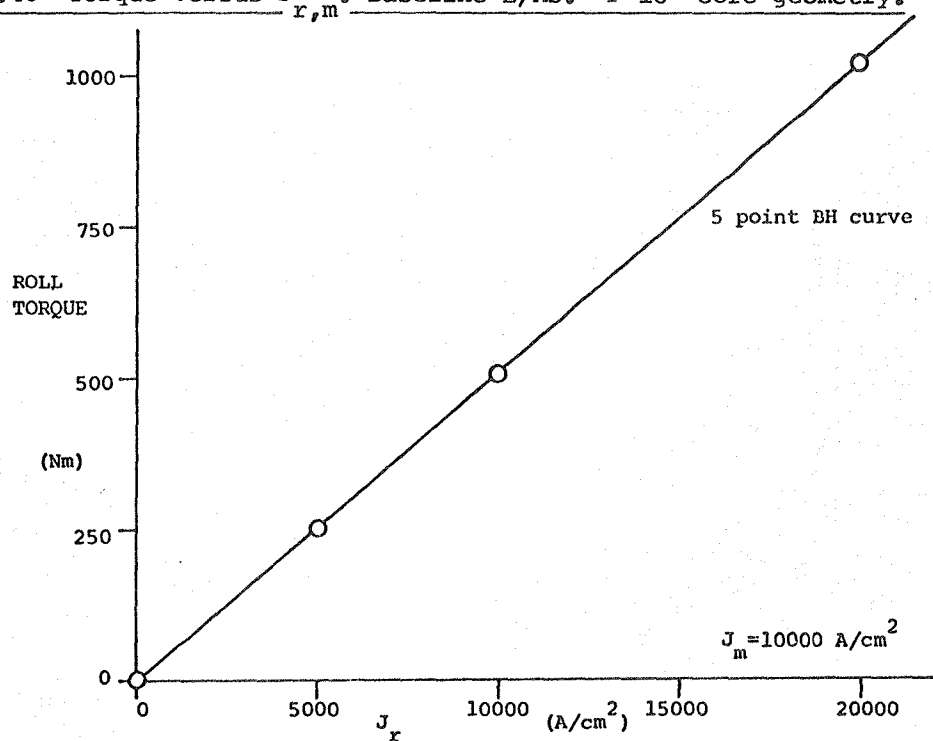
Fig. 5.41 Torque versus J_r, J_m constant. Baseline E/Ms. "F-16" core.

r=0.05

r=0.415

r=0.383

r=0.765

1.53

0.382

0.365

0.80

Section on AA

Section on BB

$J_{baseline} = 1000$ A/cm^2

$J_{equivalent} = 894.714$ A/cm^2
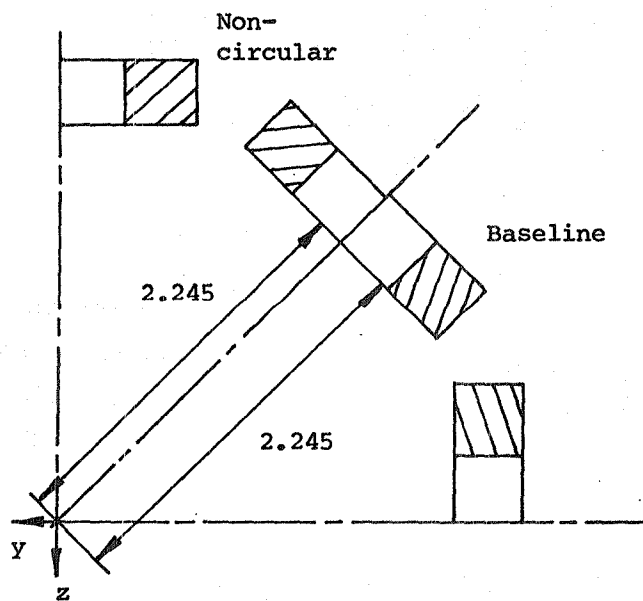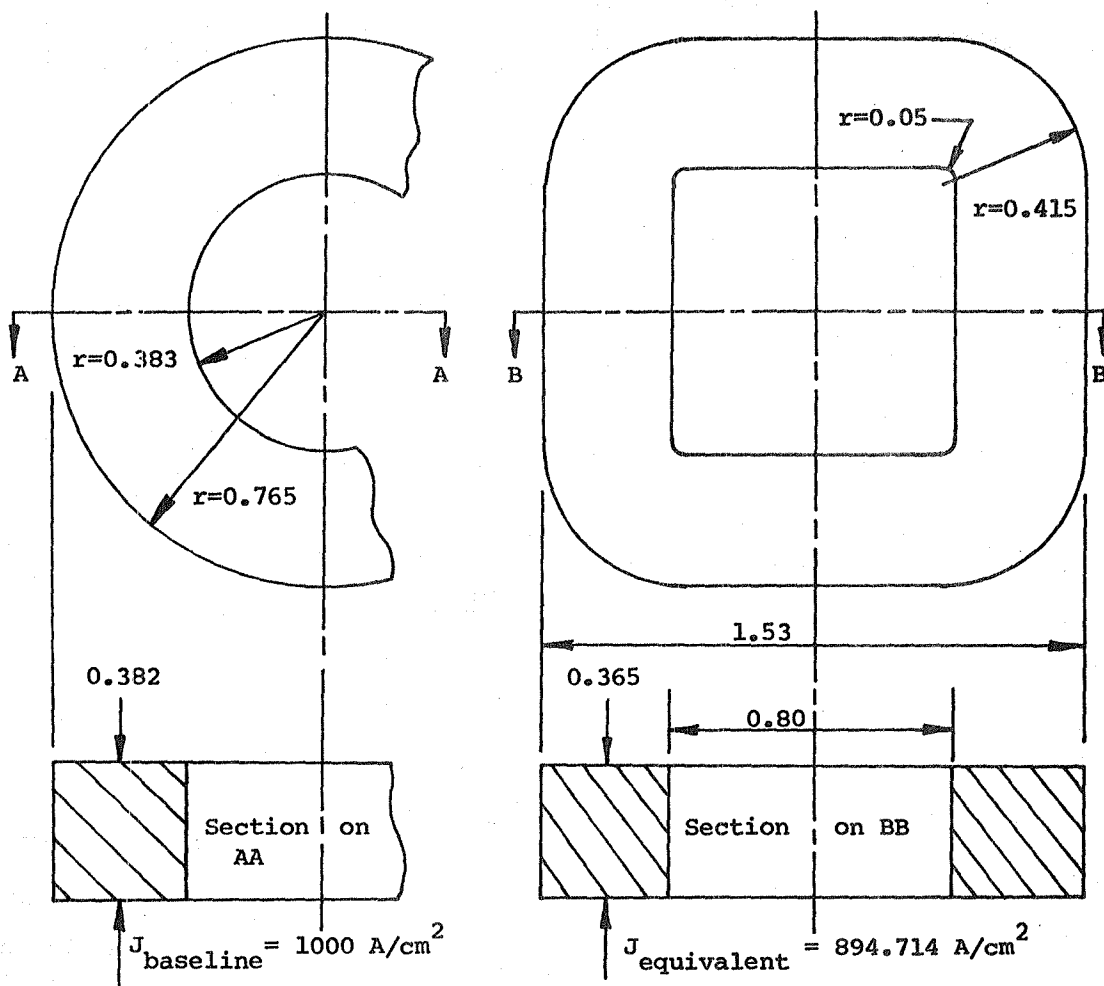
Non-circular

J in non-circular E/Ms corrected to approximate baseline field in region of model

2.245

Baseline

2.245

Fig. 5.42 Comparison of baseline and equivalent non-circular E/M geometry.

All dimensions in metres.

Part view on
y axis.

0.915   0.915

z

View on
x axis

$J_{equivalent} =$

869.65 A/cm^2

(matches base-
line field in
region of
model)

45°

45°

y

2.245

Individual E/M
geometry identical
to baseline E/Ms
(Fig. 5.4)

z
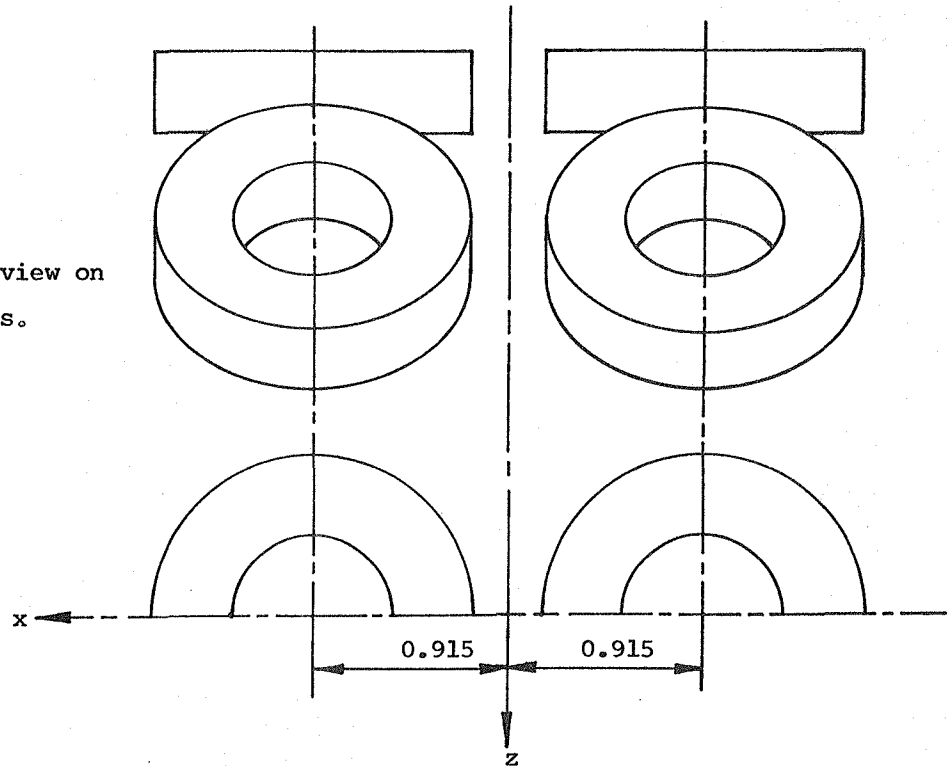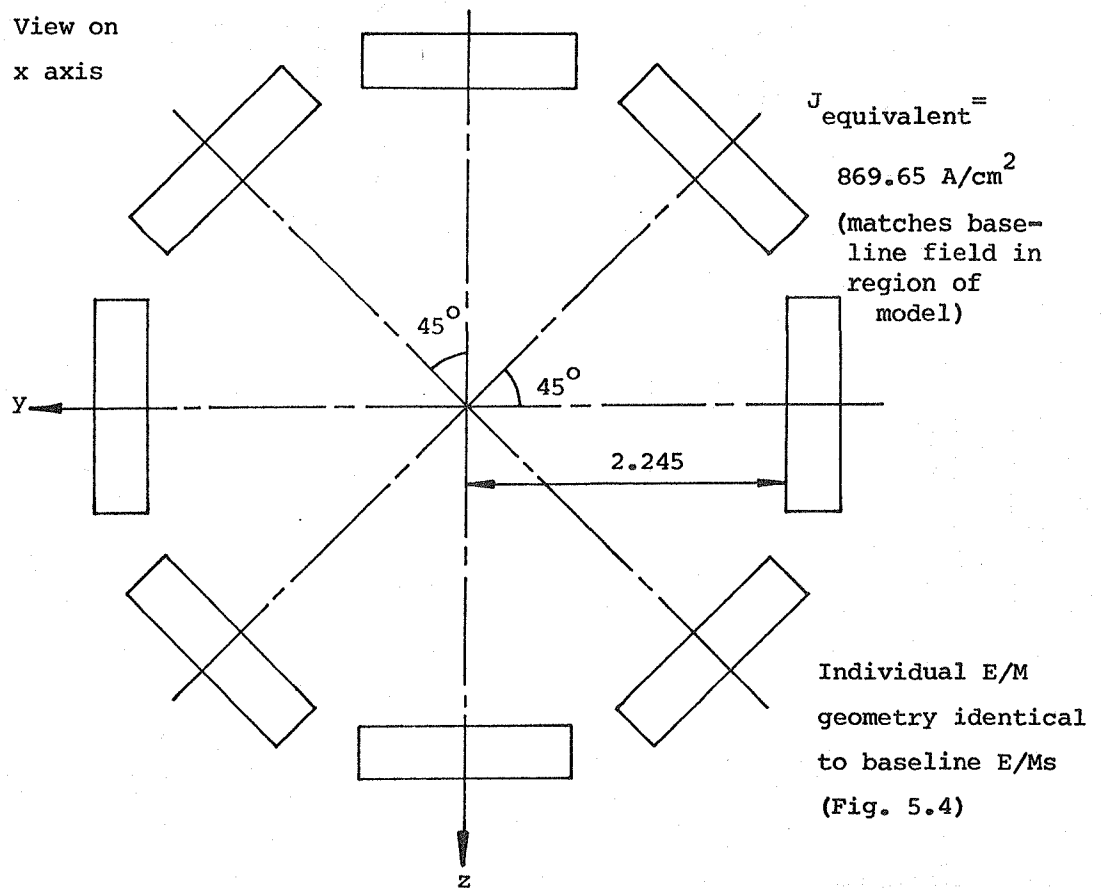
Fig. 5.43   16 E/M roll array geometry and configuration. All dimensions
            in metres.

Fig. 5.44a Near field of GFUN baseline magnetizing field

$J_m = 1000$ A/cm^2 $J_r = 0$

E/Ms as Fig. 5.4

Location			Field			Field gradients					
----metres-----			-----tesla------			--------------------tesla / metre----------------					
X	Y	Z	BX	BY	BZ	BXX	BXY	BXZ	BYY	BYZ	BZZ
0.0000	0.0000	0.0000	-0.0000	0.0000	-0.0000	-0.0000	-0.0000	0.0000	0.0691	-0.0000	-0.0691
0.0000	0.0000	0.1000	-0.0000	0.0000	-0.0069	0.0004	0.0000	0.0000	0.0691	-0.0000	-0.0695
0.0000	0.1000	0.0000	0.0000	0.0069	-0.0000	-0.0004	-0.0000	-0.0000	0.0695	-0.0000	-0.0691
0.0000	0.1000	0.1000	-0.0000	0.0069	-0.0069	-0.0000	-0.0000	0.0000	0.0695	-0.0000	-0.0695
0.0000	0.2000	0.0000	-0.0000	0.0139	0.0000	-0.0017	-0.0000	0.0000	0.0708	-0.0000	-0.0691
0.0000	0.2000	0.1000	0.0000	0.0139	-0.0069	-0.0013	-0.0000	0.0000	0.0707	-0.0001	-0.0695
0.0000	0.3000	0.0000	-0.0000	0.0211	-0.0000	-0.0039	-0.0000	0.0000	0.0732	-0.0000	-0.0693
0.0000	0.3000	0.1000	0.0000	0.0211	-0.0069	-0.0034	-0.0000	0.0000	0.0730	-0.0003	-0.0696
0.0000	0.4000	0.0000	-0.0000	0.0286	-0.0000	-0.0070	-0.0000	-0.0000	0.0768	-0.0000	-0.0698
0.0000	0.4000	0.1000	-0.0000	0.0286	-0.0070	-0.0066	-0.0000	0.0000	0.0765	-0.0007	-0.0699
0.0000	0.5000	0.0000	-0.0000	0.0365	-0.0000	-0.0113	-0.0000	-0.0000	0.0822	-0.0000	-0.0708
0.0000	0.5000	0.1000	-0.0000	0.0365	-0.0071	-0.0109	-0.0000	0.0000	0.0817	-0.0014	-0.0706
0.0000	0.6000	0.0000	-0.0000	0.0451	-0.0000	-0.0170	-0.0000	-0.0000	0.0897	-0.0000	-0.0728
0.0000	0.6000	0.1000	0.0000	0.0450	-0.0073	-0.0165	-0.0000	-0.0000	0.0891	-0.0024	-0.0725
0.0000	0.7000	0.0000	-0.0000	0.0546	-0.0000	-0.0243	-0.0000	0.0000	0.1003	-0.0000	-0.0740
0.0000	0.7000	0.1000	-0.0000	0.0544	-0.0076	-0.0238	-0.0000	-0.0000	0.0994	-0.0040	-0.0756
0.1000	0.0000	0.0000	-0.0000	0.0000	-0.0000	-0.0000	-0.0000	0.0000	0.0687	-0.0000	-0.0687
0.1000	0.0000	0.1000	0.0000	0.0000	-0.0069	0.0004	0.0000	0.0008	0.0687	-0.0000	-0.0691
0.1000	0.1000	0.0000	-0.0000	0.0069	-0.0000	-0.0004	-0.0008	0.0000	0.0691	-0.0000	-0.0687
0.1000	0.1000	0.1000	-0.0000	0.0069	-0.0069	-0.0000	-0.0008	0.0008	0.0691	-0.0000	-0.0691
0.1000	0.2000	0.0000	-0.0002	0.0138	-0.0000	-0.0017	-0.0017	-0.0000	0.0704	-0.0000	-0.0687
0.1000	0.2000	0.1000	-0.0001	0.0138	-0.0069	-0.0012	-0.0017	0.0008	0.0703	-0.0001	-0.0690
0.1000	0.3000	0.0000	-0.0004	0.0210	-0.0000	-0.0038	-0.0026	0.0000	0.0727	0.0000	-0.0689
0.1000	0.3000	0.1000	-0.0003	0.0210	-0.0069	-0.0034	-0.0026	0.0008	0.0725	-0.0003	-0.0691
0.1000	0.4000	0.0000	-0.0007	0.0284	-0.0000	-0.0069	-0.0037	0.0000	0.0762	-0.0000	-0.0694
0.1000	0.4000	0.1000	-0.0007	0.0284	-0.0069	-0.0065	-0.0037	0.0008	0.0760	-0.0007	-0.0695
0.1000	0.5000	0.0000	-0.0011	0.0363	-0.0000	-0.0111	-0.0049	0.0000	0.0815	-0.0000	-0.0704
0.1000	0.5000	0.1000	-0.0011	0.0362	-0.0070	-0.0107	-0.0049	0.0009	0.0811	-0.0013	-0.0704
0.1000	0.6000	0.0000	-0.0017	0.0448	-0.0000	-0.0166	-0.0064	0.0000	0.0889	-0.0000	-0.0723
0.1000	0.6000	0.1000	-0.0016	0.0447	-0.0072	-0.0162	-0.0064	0.0009	0.0883	-0.0024	-0.0721
0.1000	0.7000	0.0000	-0.0024	0.0542	-0.0000	-0.0238	-0.0082	0.0000	0.0993	-0.0000	-0.0755
0.1000	0.7000	0.1000	-0.0024	0.0540	-0.0075	-0.0233	-0.0082	0.0010	0.0984	-0.0039	-0.0751
0.2000	0.0000	0.0000	-0.0000	0.0000	-0.0000	0.0000	-0.0000	0.0000	0.0674	-0.0000	-0.0674
0.2000	0.0000	0.1000	0.0001	0.0000	-0.0068	0.0004	-0.0000	0.0016	0.0674	-0.0000	-0.0678
0.2000	0.1000	0.0000	-0.0001	0.0068	-0.0000	-0.0004	-0.0016	0.0000	0.0678	-0.0000	-0.0674
0.2000	0.1000	0.1000	0.0000	0.0048	-0.0068	-0.0000	-0.0016	0.0016	0.0678	-0.0000	-0.0678
0.2000	0.2000	0.0000	-0.0003	0.0136	-0.0000	-0.0016	-0.0033	0.0000	0.0690	-0.0000	-0.0675
0.2000	0.2000	0.1000	-0.0002	0.0136	-0.0068	-0.0012	-0.0033	0.0016	0.0690	-0.0001	-0.0678
0.2000	0.3000	0.0000	-0.0008	0.0206	0.0000	-0.0035	-0.0052	0.0000	0.0712	-0.0000	-0.0676
0.2000	0.3000	0.1000	-0.0007	0.0206	-0.0068	-0.0032	-0.0051	0.0016	0.0711	-0.0003	-0.0679
0.2000	0.4000	0.0000	-0.0014	0.0279	-0.0000	-0.0065	-0.0072	0.0000	0.0746	-0.0000	-0.0681
0.2000	0.4000	0.1000	-0.0013	0.0278	-0.0068	-0.0061	-0.0072	0.0017	0.0743	-0.0006	-0.0682
0.2000	0.5000	0.0000	-0.0022	0.0356	-0.0000	-0.0104	-0.0096	0.0000	0.0795	-0.0000	-0.0691
0.2000	0.5000	0.1000	-0.0021	0.0355	-0.0069	-0.0100	-0.0096	0.0017	0.0791	-0.0013	-0.0691
0.2000	0.6000	0.0000	-0.0033	0.0438	-0.0000	-0.0155	-0.0125	-0.0000	0.0865	-0.0000	-0.0710
0.2000	0.6000	0.1000	-0.0032	0.0437	-0.0071	-0.0151	-0.0124	0.0018	0.0859	-0.0023	-0.0708
0.2000	0.7000	0.0000	-0.0047	0.0530	-0.0000	-0.0222	-0.0160	0.0000	0.0962	-0.0000	-0.0741
0.2000	0.7000	0.1000	-0.0046	0.0528	-0.0074	-0.0217	-0.0159	0.0019	0.0953	-0.0038	-0.0736

Location   Field   Field gradients

X	Y	Z	BX	BY	BZ	BXX	BXY	BXZ	BYY	BYZ	BZZ
	-----metres-----			-----tesla-------				-------tesla / metre-------			
0.0000	0.0000	0.0000	-0.0000	0.0000	-0.0000	-0.0000	0.0000	-0.0000	0.0000	0.0000	-0.0000
0.0000	0.0000	0.1000	-0.0000	0.0069	0.0000	-0.0000	0.0000	0.0000	0.0000	0.0691	-0.0000
0.0000	0.1000	0.0000	-0.0000	0.0000	0.0069	0.0000	-0.0000	0.0000	0.0000	0.0693	-0.0000
0.0000	0.1000	0.1000	-0.0000	0.0069	0.0069	-0.0008	0.0000	-0.0000	0.0004	0.0695	0.0004
0.0000	0.2000	0.0000	0.0000	0.0000	0.0139	-0.0000	0.0000	-0.0000	0.0000	0.0699	0.0000
0.0000	0.2000	0.1000	0.0000	0.0070	0.0139	-0.0017	0.0000	-0.0000	0.0008	0.0701	0.0009
0.0000	0.3000	0.0000	-0.0000	0.0000	0.0209	-0.0000	-0.0000	0.0000	0.0000	0.0707	0.0000
0.0000	0.3000	0.1000	-0.0000	0.0071	0.0210	-0.0026	-0.0000	-0.0000	0.0010	0.0711	0.0016
0.0000	0.4000	0.0000	-0.0000	-0.0000	0.0280	-0.0000	-0.0000	-0.0000	0.0000	0.0718	0.0000
0.0000	0.4000	0.1000	0.0000	0.0072	0.0281	-0.0035	0.0000	-0.0000	0.0011	0.0723	0.0024
0.0000	0.5000	0.0000	-0.0000	0.0000	0.0352	-0.0000	0.0000	-0.0000	0.0000	0.0727	0.0000
0.0000	0.5000	0.1000	0.0000	0.0073	0.0354	-0.0045	0.0000	-0.0000	0.0009	0.0734	0.0036
0.0000	0.6000	0.0000	0.0000	0.0000	0.0426	-0.0000	0.0000	-0.0000	-0.0000	0.0733	0.0000
0.0000	0.6000	0.1000	0.0000	0.0074	0.0428	-0.0056	0.0000	-0.0000	0.0004	0.0742	0.0052
0.0000	0.7000	0.0000	-0.0000	0.0000	0.0499	-0.0000	0.0000	-0.0000	-0.0000	0.0733	0.0000
0.0000	0.7000	0.1000	0.0000	0.0074	0.0503	-0.0067	0.0000	0.0000	-0.0005	0.0744	0.0072
0.1000	0.0000	0.0000	-0.0000	0.0000	0.0000	-0.0000	-0.0000	-0.0000	0.0000	0.0687	-0.0000
0.1000	0.0000	0.1000	-0.0000	0.0069	-0.0000	-0.0000	-0.0008	-0.0000	0.0000	0.0689	-0.0000
0.1000	0.1000	0.0000	-0.0000	0.0000	0.0069	-0.0000	-0.0000	-0.0008	0.0000	0.0689	0.0000
0.1000	0.1000	0.1000	-0.0001	0.0069	0.0069	-0.0008	-0.0008	-0.0008	0.0004	0.0691	0.0004
0.1000	0.2000	0.0000	-0.0000	0.0000	0.0138	-0.0000	-0.0000	-0.0017	0.0000	0.0694	0.0000
0.1000	0.2000	0.1000	-0.0002	0.0070	0.0138	-0.0017	-0.0009	-0.0017	0.0008	0.0697	0.0009
0.1000	0.3000	0.0000	-0.0000	0.0000	0.0208	-0.0000	-0.0000	-0.0025	0.0000	0.0703	-0.0000
0.1000	0.3000	0.1000	-0.0003	0.0070	0.0208	-0.0025	-0.0009	-0.0026	0.0010	0.0707	0.0015
0.1000	0.4000	0.0000	0.0000	0.0000	0.0279	-0.0000	-0.0000	-0.0035	0.0000	0.0713	0.0000
0.1000	0.4000	0.1000	-0.0003	0.0071	0.0280	-0.0034	-0.0010	-0.0035	0.0011	0.0718	0.0024
0.1000	0.5000	0.0000	-0.0000	0.0000	0.0350	-0.0000	0.0000	-0.0044	0.0000	0.0722	0.0000
0.1000	0.5000	0.1000	-0.0004	0.0072	0.0352	-0.0044	-0.0010	-0.0045	0.0009	0.0729	0.0035
0.1000	0.6000	0.0000	-0.0000	0.0000	0.0423	-0.0000	0.0000	-0.0055	0.0000	0.0728	0.0000
0.1000	0.6000	0.1000	-0.0006	0.0073	0.0425	-0.0054	-0.0011	-0.0056	0.0004	0.0737	0.0051
0.1000	0.7000	0.0000	-0.0000	0.0000	0.0496	-0.0000	0.0000	-0.0066	-0.0000	0.0727	0.0000
0.1000	0.7000	0.1000	-0.0007	0.0073	0.0499	-0.0065	-0.0012	-0.0067	-0.0005	0.0738	0.0070
0.2000	0.0000	0.0000	-0.0000	0.0000	-0.0000	0.0000	-0.0000	-0.0000	0.0000	0.0674	0.0000
0.2000	0.0000	0.1000	-0.0000	0.0067	0.0000	-0.0000	-0.0016	-0.0000	0.0000	0.0676	-0.0000
0.2000	0.1000	0.0000	-0.0000	0.0000	0.0067	-0.0000	-0.0000	-0.0016	0.0000	0.0676	-0.0000
0.2000	0.1000	0.1000	-0.0002	0.0068	0.0068	-0.0008	-0.0016	-0.0016	0.0004	0.0678	0.0004
0.2000	0.2000	0.0000	-0.0000	0.0000	0.0135	-0.0000	-0.0000	-0.0033	0.0000	0.0682	0.0000
0.2000	0.2000	0.1000	-0.0003	0.0068	0.0136	-0.0016	-0.0017	-0.0033	0.0007	0.0684	0.0008
0.2000	0.3000	0.0000	-0.0000	0.0000	0.0204	0.0000	-0.0000	-0.0050	0.0000	0.0690	0.0000
0.2000	0.3000	0.1000	-0.0005	0.0069	0.0205	-0.0024	-0.0018	-0.0050	0.0009	0.0693	0.0014
0.2000	0.4000	0.0000	-0.0000	0.0000	0.0273	-0.0000	-0.0000	-0.0068	0.0000	0.0699	0.0000
0.2000	0.4000	0.1000	-0.0007	0.0070	0.0274	-0.0032	-0.0019	-0.0069	0.0010	0.0704	0.0023
0.2000	0.5000	0.0000	-0.0000	0.0000	0.0344	-0.0000	-0.0000	-0.0087	0.0000	0.0707	0.0000
0.2000	0.5000	0.1000	-0.0009	0.0071	0.0345	-0.0041	-0.0020	-0.0088	0.0008	0.0714	0.0034
0.2000	0.6000	0.0000	-0.0000	0.0000	0.0415	-0.0000	-0.0000	-0.0107	-0.0000	0.0712	0.0000
0.2000	0.6000	0.1000	-0.0011	0.0071	0.0417	-0.0051	-0.0021	-0.0109	0.0003	0.0720	0.0048
0.2000	0.7000	0.0000	-0.0000	0.0000	0.0486	-0.0000	-0.0000	-0.0129	-0.0000	0.0710	0.0000
0.2000	0.7000	0.1000	-0.0013	0.0071	0.0489	-0.0061	-0.0023	-0.0131	-0.0006	0.0721	0.0067

Fig. 5.44b Near field of GFUN baseline through-wing field

$$J_r = 1000 \text{ A/cm}^2 \qquad J_m = 0$$

E/Ms as Fig. 5.4

5.7 Verification of GFUN data

5.7.1 Alternative torque computations

No direct alternative computations of the performance of any representative SIM system have been attempted since this would necessarily require access to an alternative computer program of comparable power and sophistication to GFUN, preferably solving the magnetostatic system by an entirely different method. Such programs probably do exist.

However, as mentioned earlier, the reliability of GFUN's prediction of magnetization of iron regions has been considered good for many years and there seems no particular reason to regard the computed wing core magnetizations as being subject to any more than the usual levels of uncertainty (43). Were this the only source of uncertainty, the computed torques could be regarded as likely to be accurate, within the limits of geometrical and other assumptions, to plus or minus very few percentage points at all computed applied field levels for the baseline and similar geometries, with somewhat greater uncertainty in certain cases, such as the F-16 core, where the iron element distribution was sparser than desirable (see Section 5.7.3).

The main potential source of uncertainty must be regarded as the torque integration schemes themselves, since these have been specially developed for the SIM computations and hence not subjected to such extensive testing and verification as the rest of GFUN.

It is possible with GFUN to arbitrarily fix the induced magnetization in iron elements, thus effectively converting them to permanent magnet material. If this is done in such a way as to approximately preserve the typical spanwise magnetization in the SIM cores (Fig. 5.45) then direct and representative verification of the torque integration schemes is possible. Alternative calculations have been made using the computer program FORCE (Appendix 2) which calculates forces and torques by elementary numerical integration of the relevant vector products of applied field and core magnetization over the volume of the core. This method differs fundamentally from the methods used in GFUN. Results for the geometry of Fig. 5.45 are as follows:

y

This half by reflection
in xz plane

1.2

12

21

x

45

Dimensions in cms.

60

z

3 —

CORE

Approximated for
FORCE comparisons (2)

GFUN (original)

MAGNET-
IZATION

2 —

(1)

(3)

1 —

(T)

ROOT

TIP

0 —

0   21   Spanwise position   45   (cms)   60
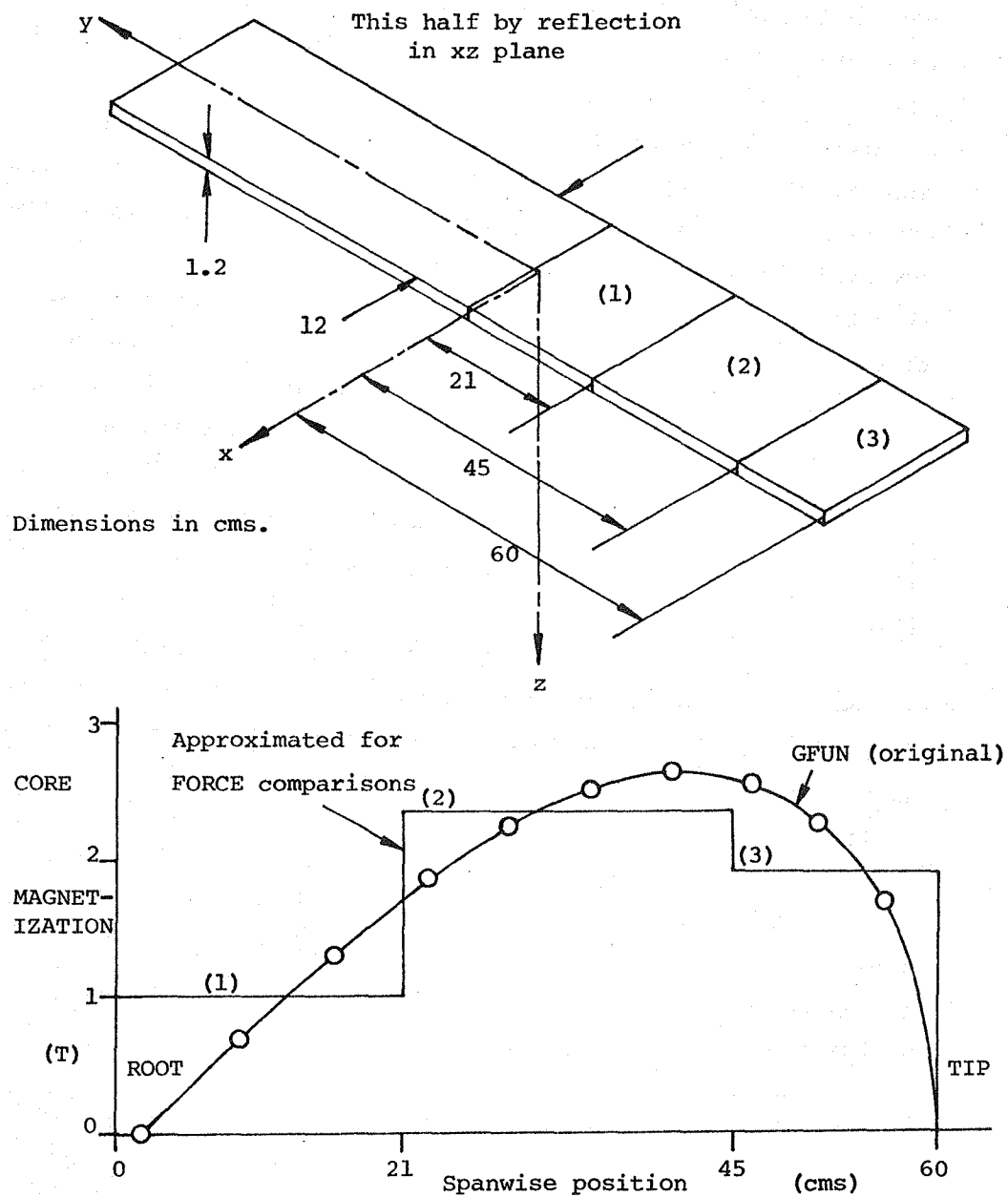
Fig. 5.45   Approximate spanwise magnetization distribution (along y
axis) for comparison of GFUN and FORCE torque integration
schemes.

Torque integration scheme	Predicted Roll Torque (Nm)
GFUN by Maxwell field stress integration over surfaces of external control volume. 140 x 40 x 20 cms. overall	113.94
FORCE by vector product integration over volume of core	116.82

The discrepancy of approximately 2.5% is considered acceptable though leaving scope for future improvement.

Certain comparisons have been made of predicted torques over differing GFUN control volumes with typical results as follows:

GFUN control volume overall dimensions (cm)	Relative torque to standard volume
140 x 40 x 20 (assuming symmetry in the yz plane)	1.0
140 x 40 x 20 (no symmetry)	0.999993
180 x 70 x 50 (yz symmetry)	0.9856

These results are similarly considered acceptable.

As mentioned in Section 5.6.5 it is thought that the accuracy of the GFUN torque integration schemes will fall with rising applied field level when the SIM cores are well into saturation. No direct high field computations were made with permanent magnet cores specified and this was a serious omission but has been partially rectified by more detailed analysis and computation using existing data. Specifically, since the publication of Ref.48, the induced magnetization distribution of two high field GFUN cases has been used as input data to FORCE, each GFUN element now representing a uniformly magnetized tetrahedra of permanent magnet material.

The vector product integration procedures carried out by FORCE are not likely to yield accurate estimates of the "true" torque produced in these particular cases, indeed such procedures would otherwise be used in GFUN, being relatively straightforward. The reasons for this cannot be fully explained herein, but are principally founded on the fact that GFUN's prediction of local external field

is markedly superior to that of local internal field, hence magneti-
zations.   In these cases the predicted internal magnetization dis-
tribution will be somewhat erroneous, but the field external to the
core should be well resolved (see (41, 42)).   Fig. 5.46 shows that
discrepancies do exist between GFUN's torque predictions and the
FORCE estimates from GFUN magnetization data, and that the magnitude
of these discrepancies rises with rising applied field level.   In
the principal region of interest ($J < 10,000$ A/cm^2) it is considered
that the agreement is sufficiently close, bearing in mind the comments
above, to manifest significant extra confidence in the GFUN torque
integration scheme, although further verification would clearly be
advantageous.

5.7.2 Experimental measurement of torque with low applied fields and correlation with GFUN predictions

Experimental verifications of the bulk of GFUN's predictions are
not possible without an array of powerful (high field) E/Ms.   Such
an array was not available.   However, the 8 main E/Ms from SUMSBS
became available during the reconstruction of that system, enabling
some representative low field (approximately constant permeability)
torque measurements to be made.   These E/Ms are not, unfortunately,
axisymmetric but it is believed that the SIM system is not particu-
larly sensitive to detail E/M geometry, rather to the mean applied
field levels in the region of the SIM cores (see Section 5.6.7).

The geometry and characteristics of the experimental SIM cores is
shown in Fig. 5.47, the E/M layout in Fig. 5.48 and the experimental
layout in Fig. 5.49.   Torque could be applied to the wing cores via
a fine thread, pulley, scale pan and weights (Fig. 5.49), the
experimental procedure being to measure the equilibrium angular
positions of the wing with known E/M currents and applied torque.
There are, as predicted by Eqn. 5.23, generally two such positions
in each octant, one stable, the other not.   Fig. 5.50 shows a
typical calibration curve for one octant, the general form of which
is repeated for all combinations of currents.   Taking the (measured)
reference angle for zero torque at zero roll current as 91.6°, Eqn.
5.23 may be used to generate a set of theoretical calibration curves
with insertion of an appropriate scaling factor.   This factor is
chosen so as to zeroise the cumulative torque error over all measured
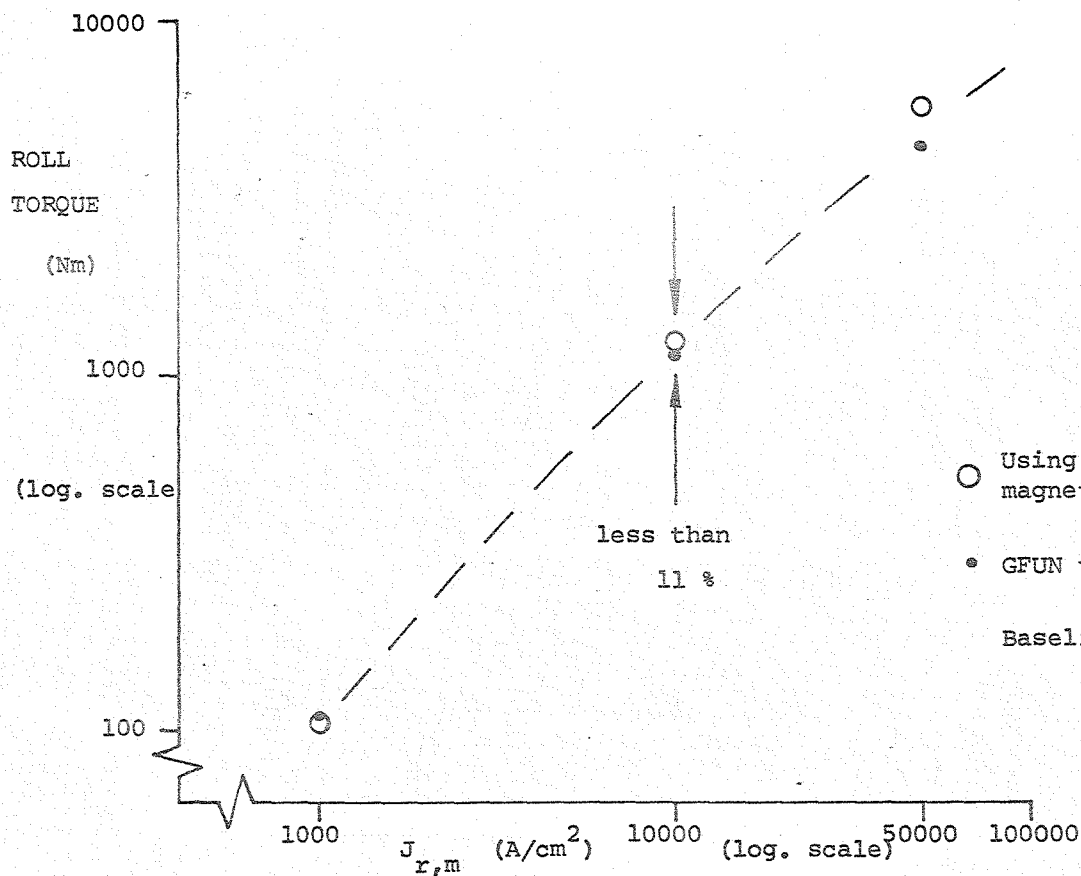
Fig. 5.46 Comparison of torque at high applied field levels, calculated directly from GFUN and via GFUN magnetization distribution, using FORCE.

ROLL TORQUE (Nm)

(log. scale)

less than 11 %

○ Using FORCE from GFUN magnetization distributions

● GFUN torque integration scheme

Baseline core and E/Ms. 5 point BH curve

$J_{r,m}$ (A/cm^2) (log. scale)

Wing cores from
Stalloy 74
laminations

9.0

0.54

1.0

z

Dimensions in inches

0.125

Assumed BH curve for Stalloy 74
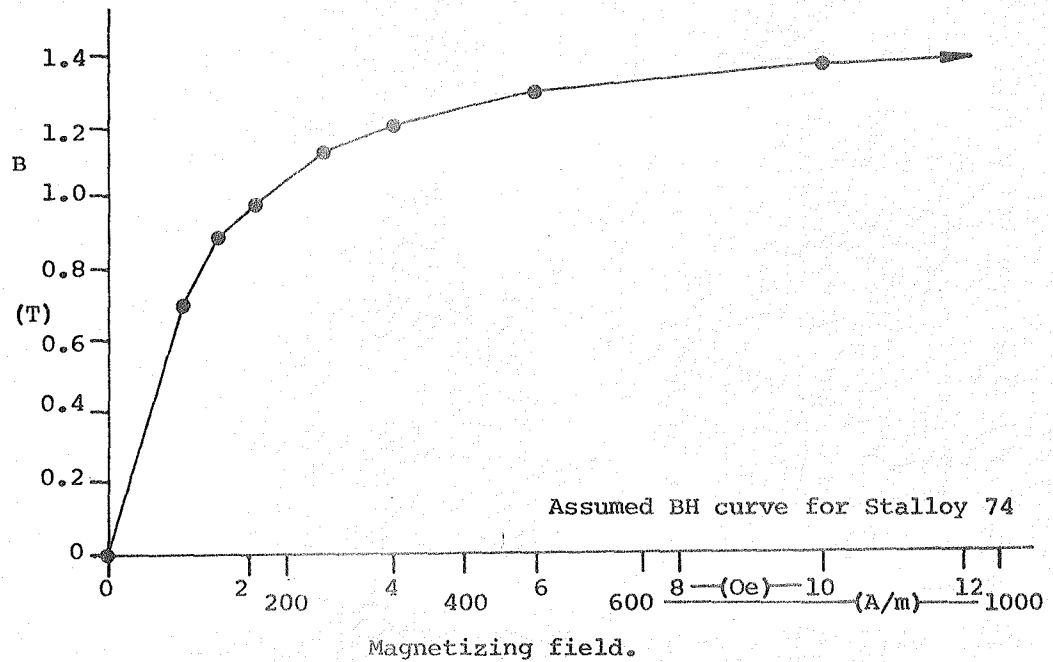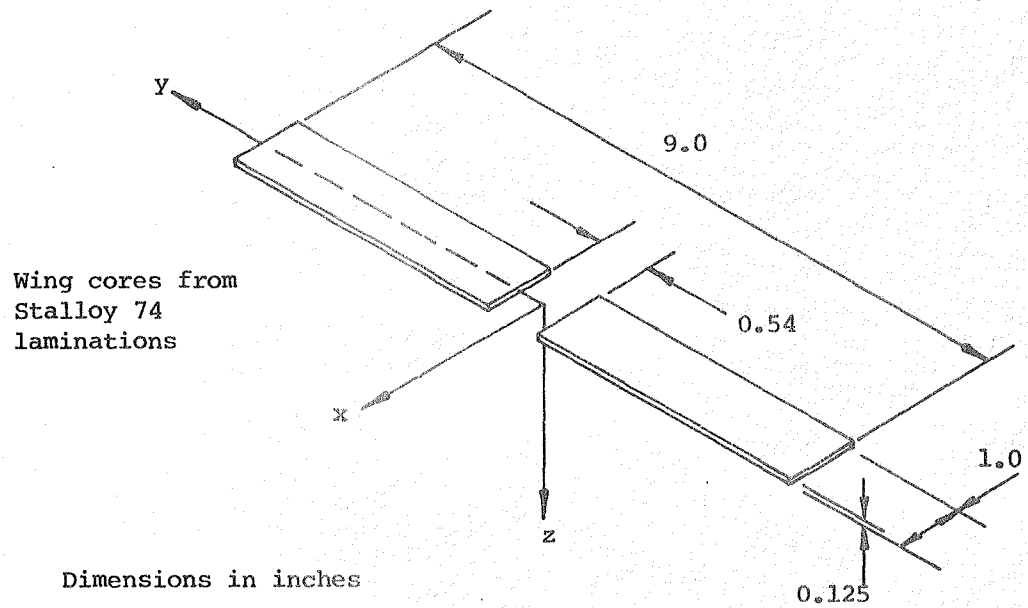
Magnetizing field.

Fig. 5.47 Geometry and characteristics of SIM cores for experimental
verification of GFUN predictions.

Section on BB

Section on AA

4.0
(10.16)

0.25
(0.63)

0.25
(0.63)

5.5
(13.97)

1.685
(4.28)

0.5
(1.27)

1.375
(3.49)

3.54
(8.99)

1.315
(3.34)

3.0
(7.62)

9.0
(22.86)

3.5
(8.89)

400 turns 12 gauge
enamelled copper wire
in 9 layers.

I_m

Conventional
current directions
shown

I_r

Fig. 5.48 Dimensions of
E/Ms and formers for
verification of GFUN
predictions.

10.5
(26.7)

Dimensions in inches
(centimetres)

45°

Y

z

I_m

One quadrant shown,
others by rotation.
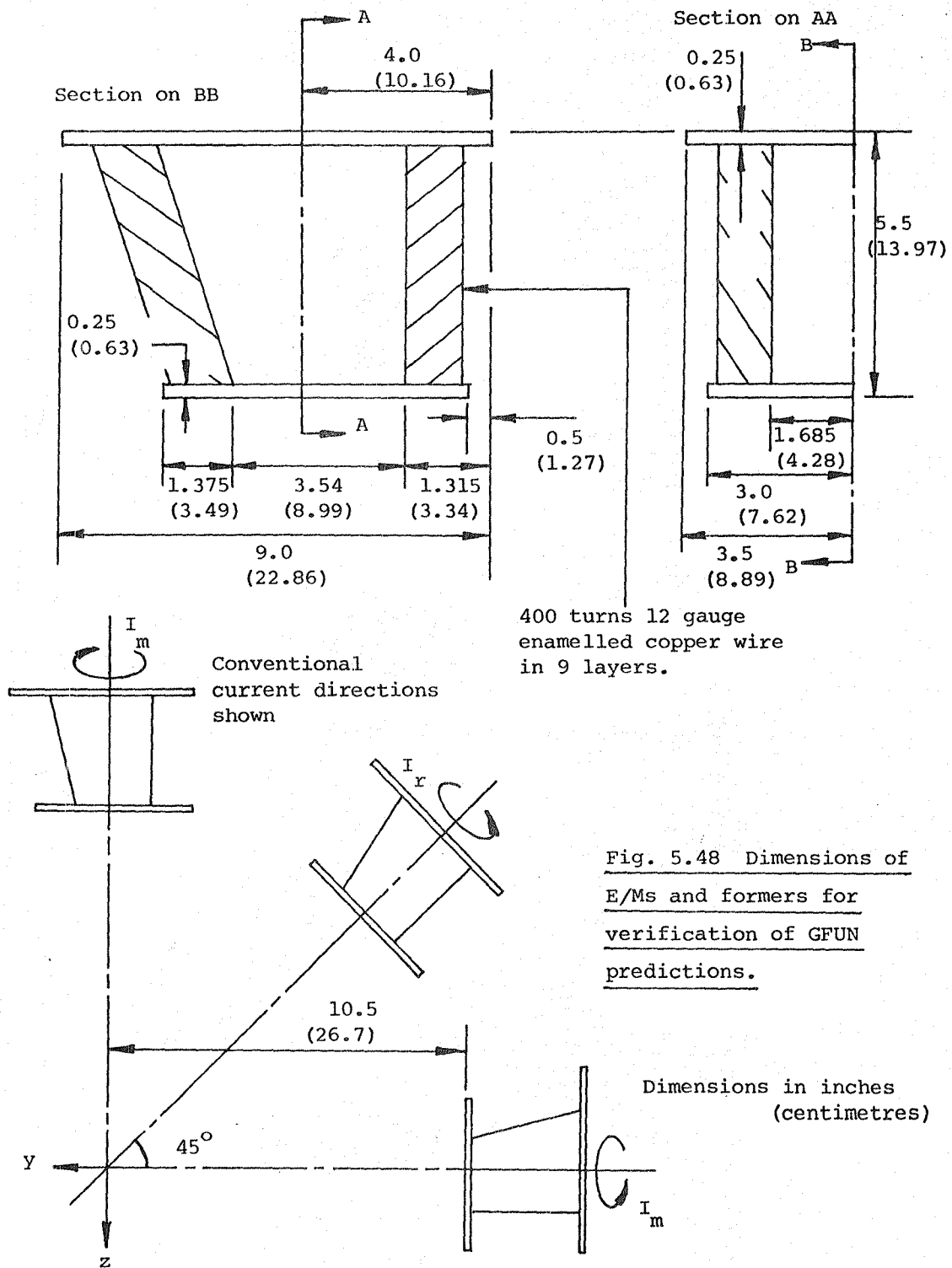
Fig. 5.49 Experimental measurement of roll torque (plate overleaf)

"Magnetizing" E/Ms marked A
"Through-wing" field E/Ms marked B

E/M functions reversed
at high roll
displacements

A

B

Field probe support

B

A

A

B

Wing support
and bearing

Wing
cores

B

A

Applied
torque

Wing
assy.

pulley

Applied
weight
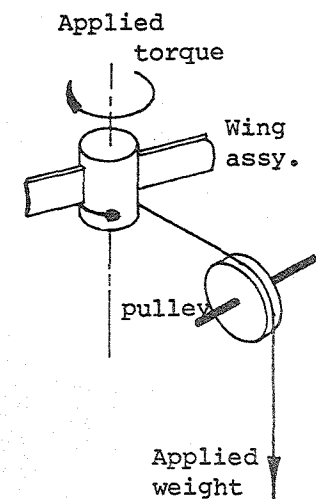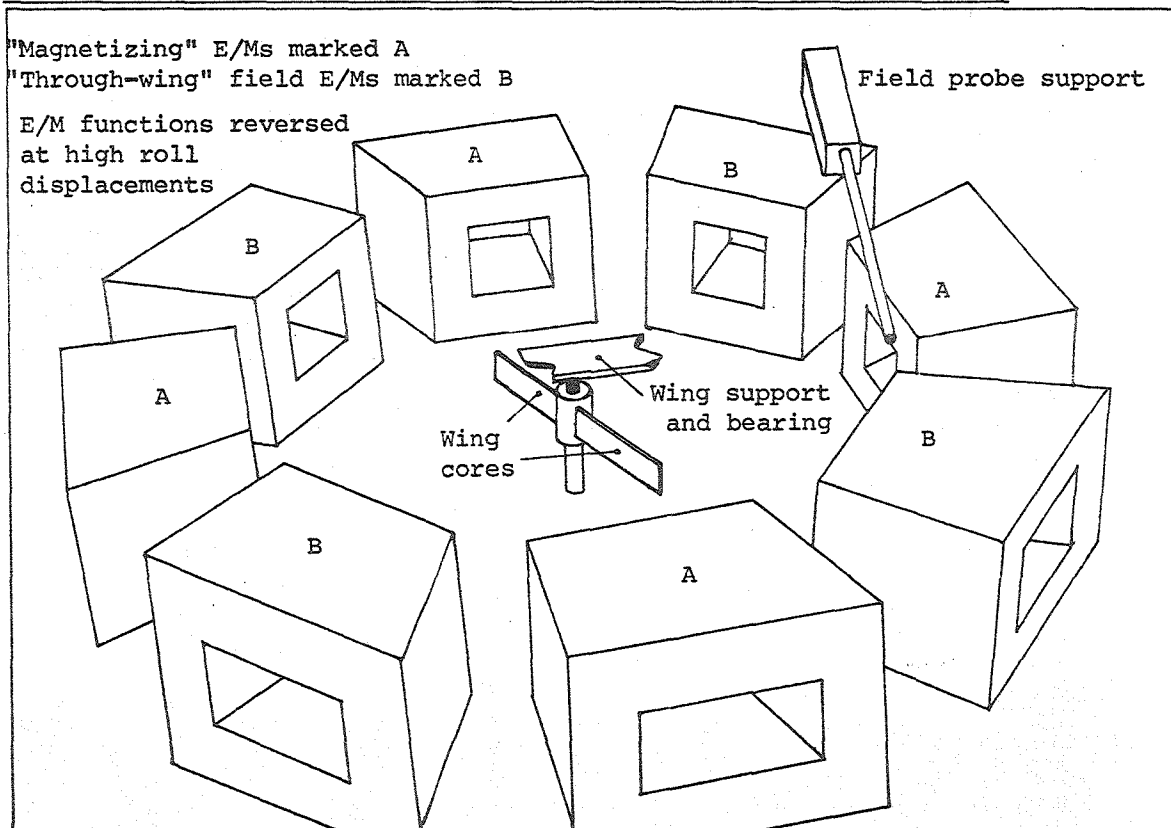
Application of roll
torque
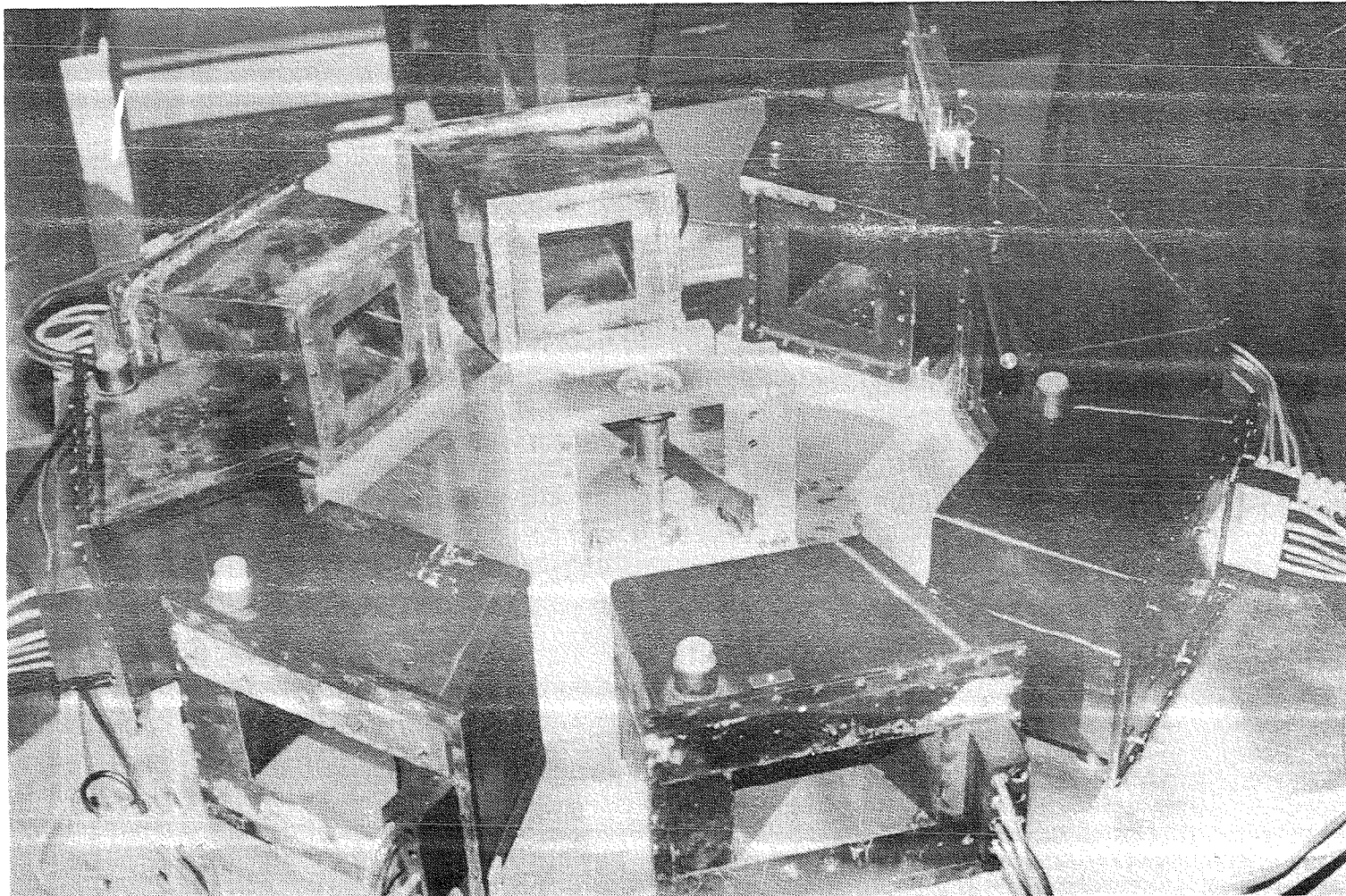
Fig. 5.49 Experimental measurement of roll torque (see diagram overleaf)
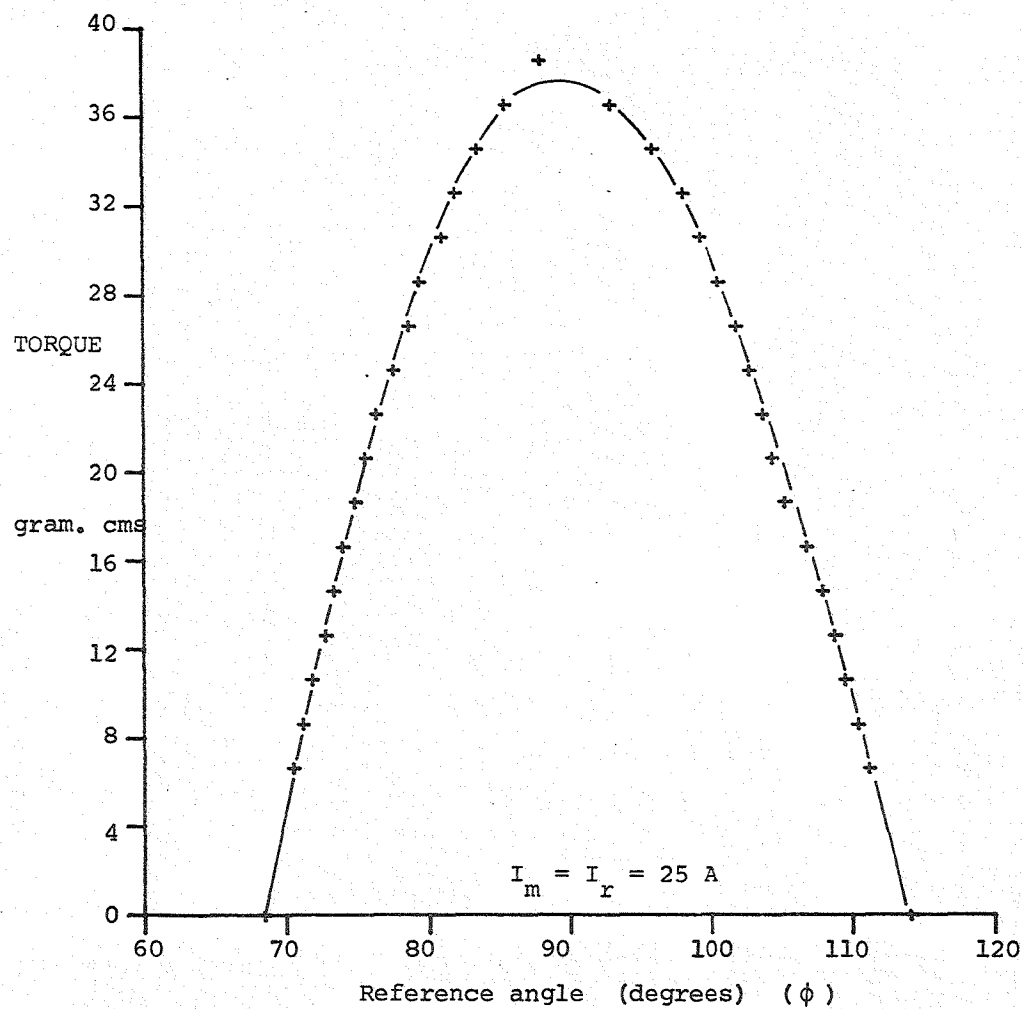
Fig. 5.50 Typical curve of roll torque versus angular position for 8 E/M experimental SIM system.

25 A cable current in E/Ms corresponds to 10,000 A-turns

data points, taking the measured angular positions as correct. Fig. 5.51 shows the comparison between these theoretical curves and all measured data.

Certain irregularities in the experimental data are inevitable. The non-axisymmetry of the E/Ms is expected to result in slight loss of left-right symmetry of the calibration curves, taken about their nominal peaks, in Fig. 5.51. Some evidence of this is apparent but the effect appears weak. Friction and irregularities in the wing assembly support bearings, together with the usual uncertainties in measurements, introduce significant random and systematic errors, which are considered to be of comparable magnitude to the observed residual discrepancies in Fig. 5.51. It is thus concluded that this Figure effectively verifies the simplified theory of Section 5.5.2.

The GFUN representation of the E/Ms was, of necessity, somewhat idealised (Fig. 5.52), and a small correction to E/M current density proved necessary to achieve correct predicted field strengths in the region of the model. Complete measurement of the field of the experimental E/M array and comparison with the GFUN representation proved to be too laborious, therefore the current density correction was calculated by measurement of the through-wing field components along a datum spanwise axis of the experimental SIM cores, with the cores absent. This axis corresponds to the reference axis of the E/Ms ($\phi = 90^{\circ}$, see Fig. 5.51) rather than the spanwise axis of the SIM cores with the cores in their zero roll torque, zero roll current orientation ($\phi = 91.6^{\circ}$). The comparison between experimental and predicted (corrected current density) fields is shown in Fig. 5.53. Since the magnetizing field E/Ms are nominally identical to those creating the through-wing field, the data shown effectively verifies the complete E/M array, although detail discrepancies in the field distribution are still possible. GFUN's predicted field distribution (corrected) is shown more fully in Fig. 5.54.

Comparison between selected performance curves from Fig. 5.51, two GFUN predictions and fitted linear theory (Section 5.5.2) is shown in Figs. 5.55 and 5.56. Only two GFUN points were computed due to the lengthening of the calculations caused by the complex E/M geometry. Taking into consideration the extensive computational idealisations and various possible sources of experimental error,
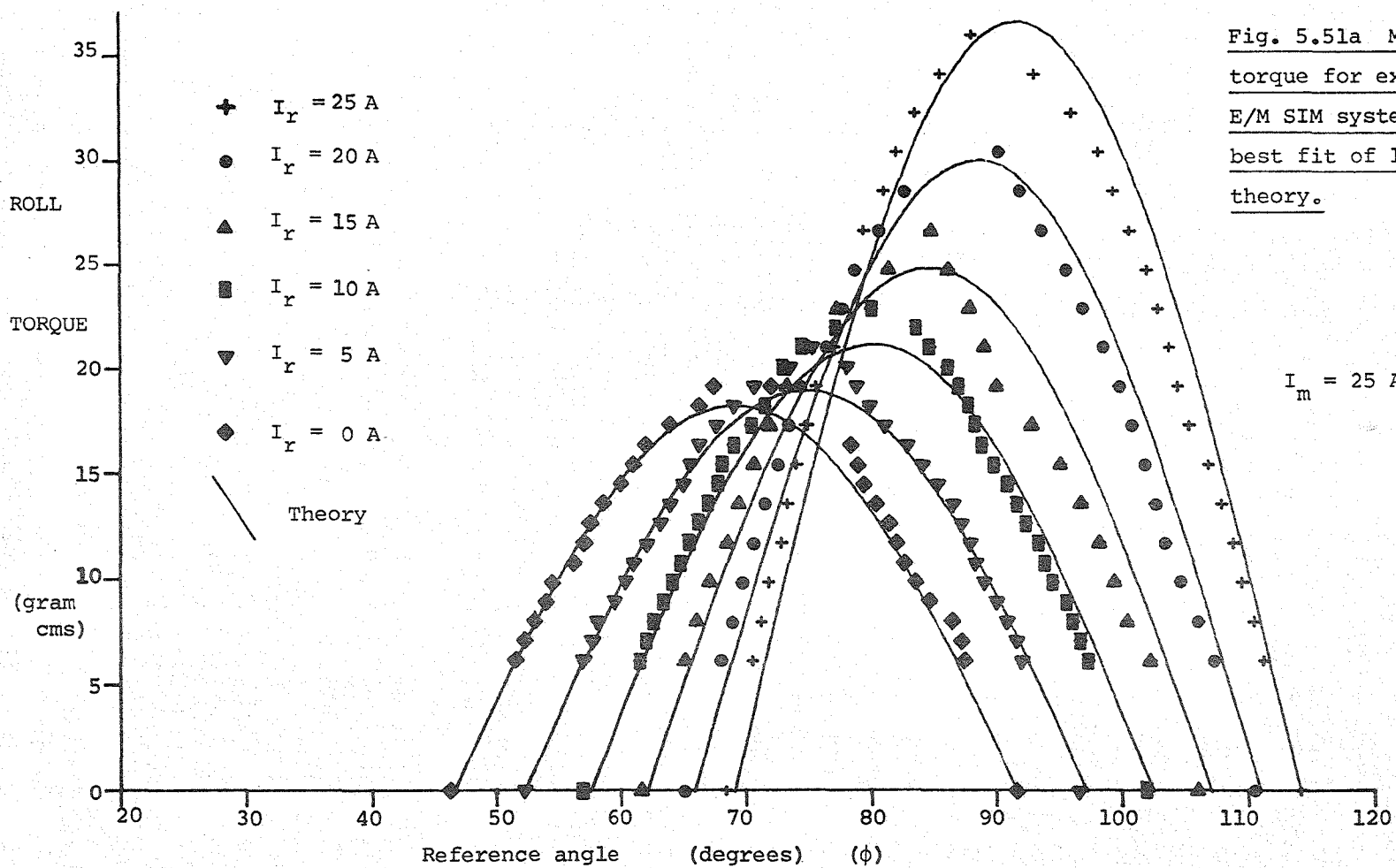
Fig. 5.51a Measured roll torque for experimental 8 E/M SIM system, showing best fit of linearized theory.

$I_m = 25$ A
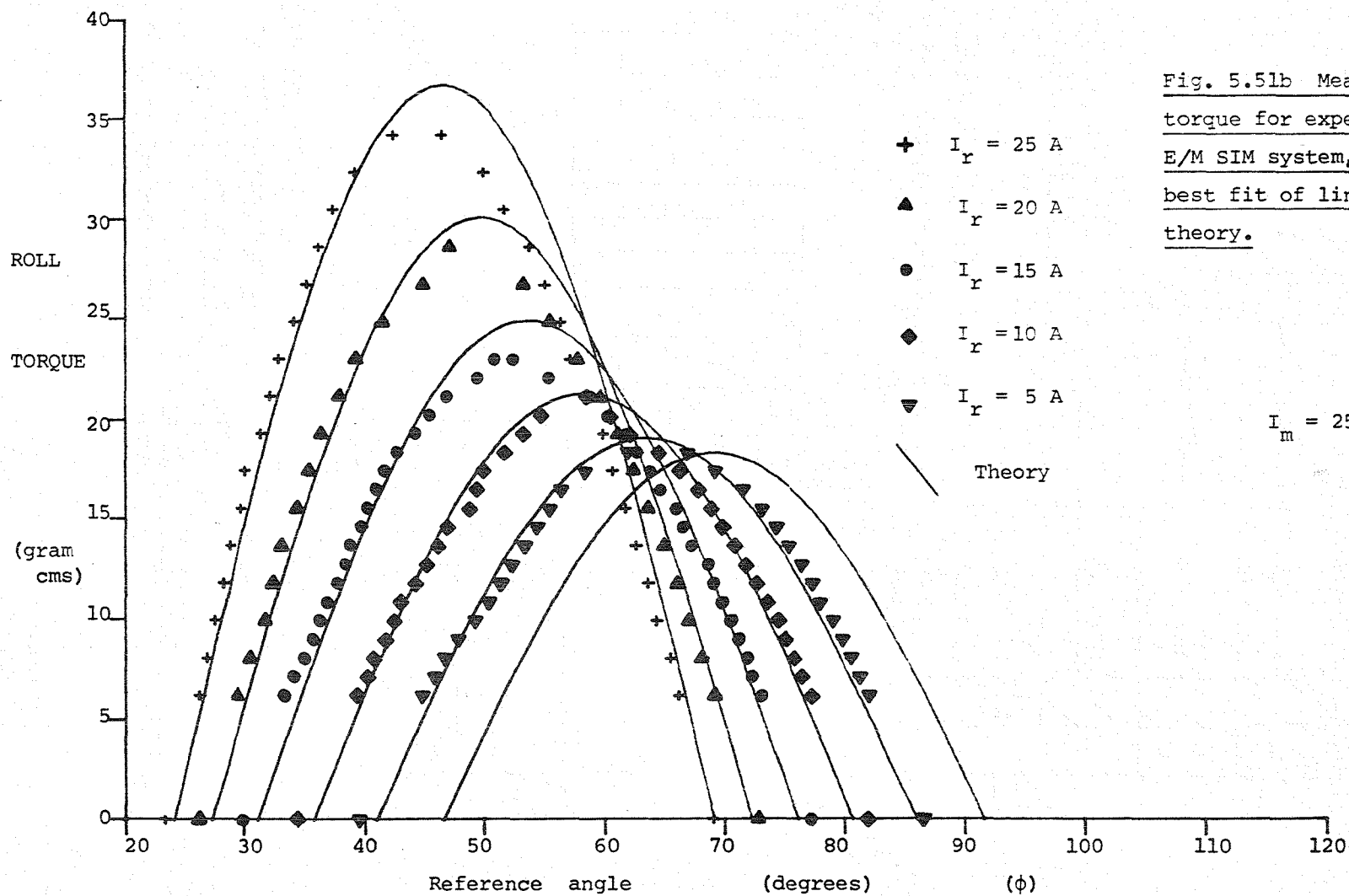
Fig. 5.51b Measured roll torque for experimental 8 E/M SIM system, showing best fit of linearized theory.

130.7

119.06

107.44

95.8

130.0

97.5

65.0

32.5

Section on AA

16.2

32.5

57.1

$J_{r,m} = 24.958$ A/cm^2, equivalent to 25 A cable current in experimental E/Ms.

A
A

All internal radii = 5

42.85

49.05

55.25

All external radii = 21.2

Part section in yz plane
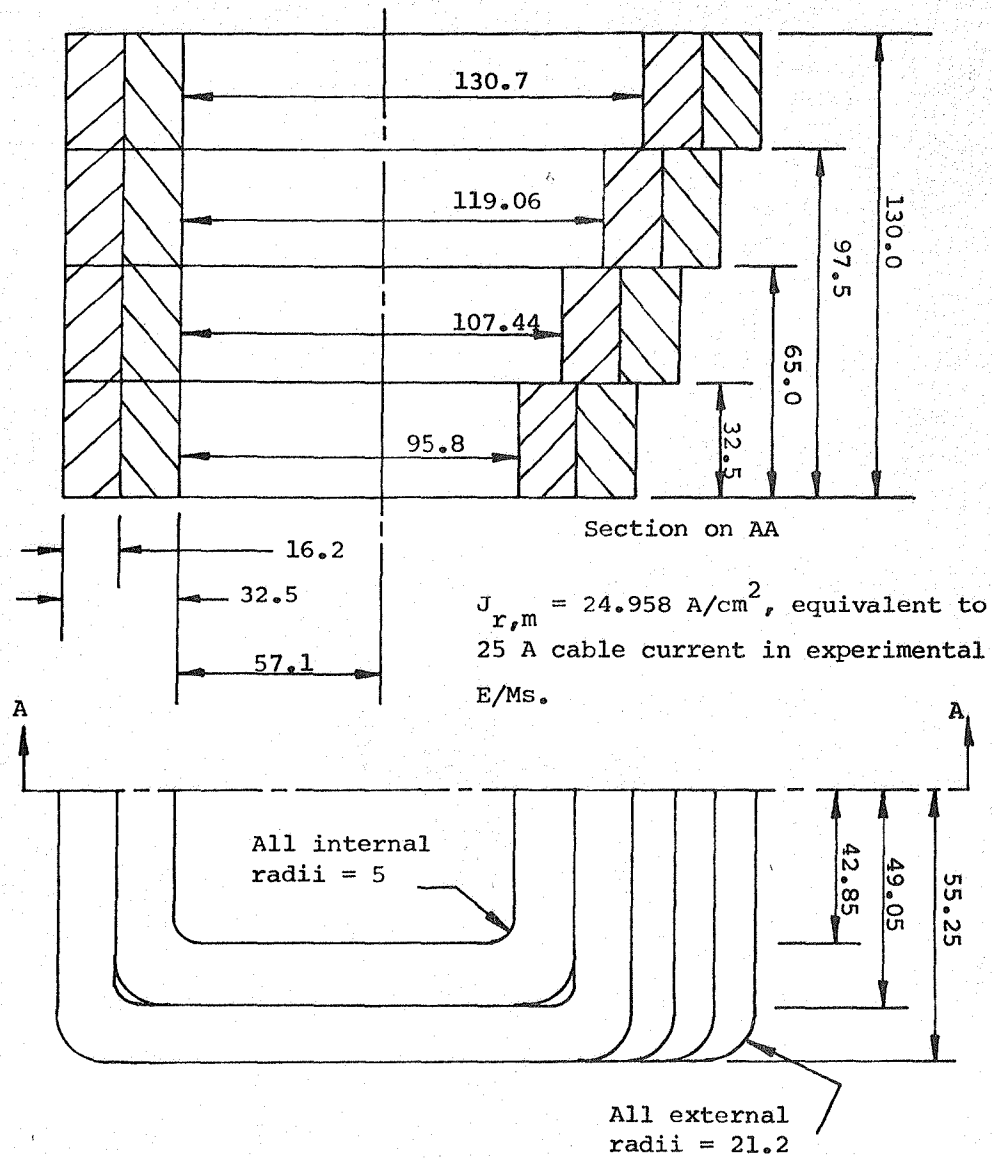
Dimensions in cms.
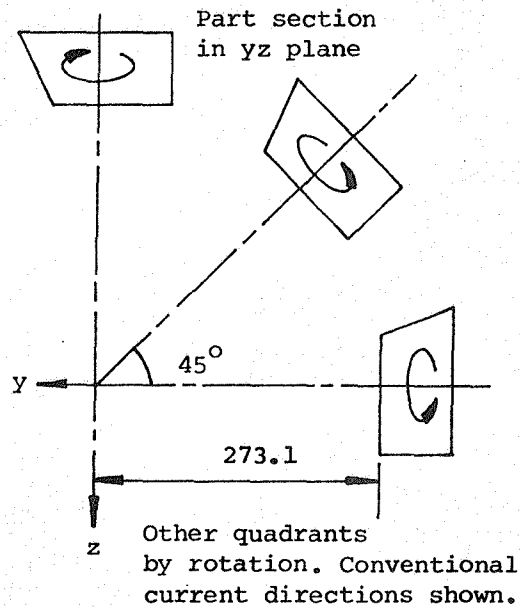
Fig. 5.52 GFUN representation of Southampton E/Ms for SIM computations.

45°

y

273.1

GFUN calculations at 10 times true scale for convenience.

Scaled using Appendix 3

z

Other quadrants by rotation. Conventional current directions shown.

Fig. 5.53 Comparison of measured field from experimental SIM array (through-wing field only, $I_r = 25$ A, $I_m = 0$) and GFUN predictions.

FIELD MAGNITUDE

(gauss, tesla x 10^4)

O - measured

- GFUN (scaled)

Location of wingtip

GFUN current densities corrected using this Figure to correctly approximate measured field.

y coordinate (cm)

Fig. 5.54 GFUN field distribution for SIM magnetizing field.

E/M configuration as Fig. 5.52
Field in other quadrants by symmetry

y	z	B_y	B_z	y	z	B_y	B_z
-----cms-----		--gauss (T*1000)-		-----cms----		--gauss (T*1000)-	
-200	-200	15.640	-17.204	-75	-100	17.817	-22.331
-175	-200	22.981	-17.701	-50	-100	12.532	-23.552
-150	-200	30.714	-20.492	-25	-100	6.765	-24.741
-125	-200	36.933	-27.400	0	-100	0.645	-25.376
-100	-200	46.512	-40.466	-200	-75	71.027	-50.635
-75	-200	49.927	-60.635	-175	-75	52.041	-32.442
-50	-200	44.129	-84.573	-150	-75	39.372	-23.214
-25	-200	27.648	-104.278	-125	-75	30.360	-18.727
0	-200	4.736	-113.284	-100	-75	23.357	-16.877
-200	-175	16.623	-25.027	-75	-75	17.344	-16.494
-175	-175	22.463	-23.552	-50	-75	11.686	-16.818
-150	-175	27.278	-24.292	-25	-75	6.034	-17.310
-125	-175	31.232	-28.230	0	-75	0.433	-17.638
-100	-175	33.637	-35.904	-200	-50	94.552	-39.414
-75	-175	32.913	-46.893	-175	-50	63.928	-24.551
-50	-175	27.363	-59.087	-150	-50	45.376	-16.956
-25	-175	16.702	-69.044	-125	-50	33.182	-13.166
0	-175	2.643	-73.743	-100	-50	24.414	-11.454
-200	-150	20.650	-33.832	-75	-50	17.458	-10.867
-175	-150	24.504	-28.753	-50	-50	11.411	-10.846
-150	-150	26.475	-26.570	-25	-50	5.772	-11.036
-125	-150	27.241	-27.426	0	-50	0.275	-11.221
-100	-150	26.649	-31.047	-200	-25	109.838	-19.213
-75	-150	24.054	-36.660	-175	-25	71.888	-12.056
-50	-150	18.859	-42.887	-150	-25	49.446	-8.293
-25	-150	11.078	-47.976	-125	-25	35.154	-6.406
0	-150	1.554	-50.403	-100	-25	25.228	-5.534
-200	-125	30.117	-43.241	-75	-25	17.659	-5.233
-175	-125	30.148	-32.966	-50	-25	11.327	-5.222
-150	-125	28.563	-27.495	-25	-25	5.608	-5.333
-125	-125	26.343	-25.651	0	-25	0.137	-5.470
-100	-125	23.494	-26.406	-200	0	113.284	4.736
-75	-125	19.673	-28.811	-175	0	73.743	2.643
-50	-125	14.567	-31.809	-150	0	50.403	1.554
-25	-125	8.193	-34.350	-125	0	35.598	0.973
0	-125	0.973	-35.598	-100	0	25.376	0.645
-200	-100	47.258	-50.625	-75	0	17.638	0.433
-175	-100	39.747	-34.858	-50	0	11.221	0.275
-150	-100	33.209	-26.618	-25	0	5.470	0.137
-125	-100	27.712	-22.839	0	0	0.000	0.000
-100	-100	22.754	-21.797				
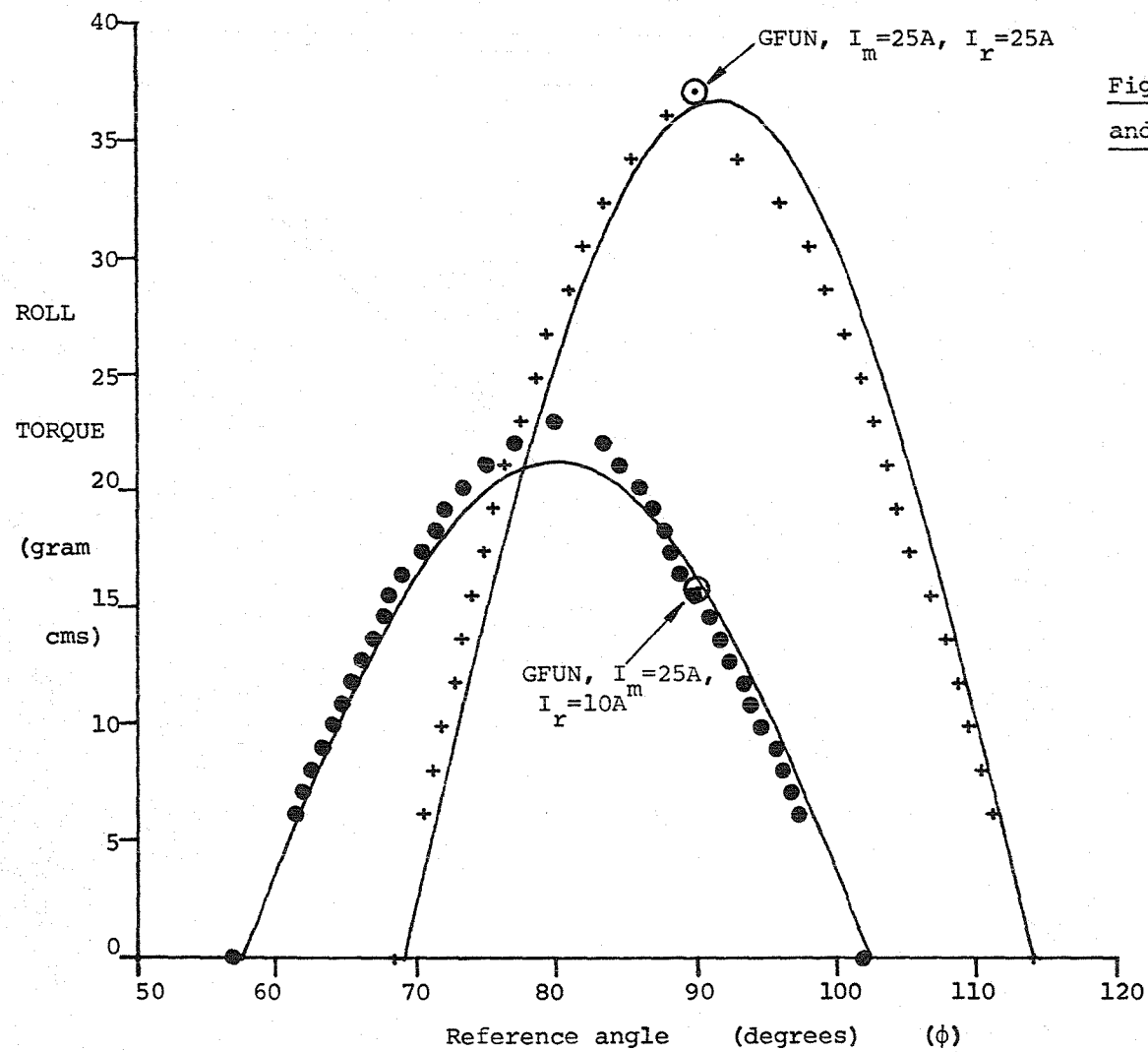
Fig. 5.55   Comparison between measured and predicted roll torque

$I_m = 25$ A

$+$ Measured, $I_r = 25$A

$\bullet$ Measured, $I_r = 10$A

$\odot$ GFUN

$\diagdown$ Linear theory
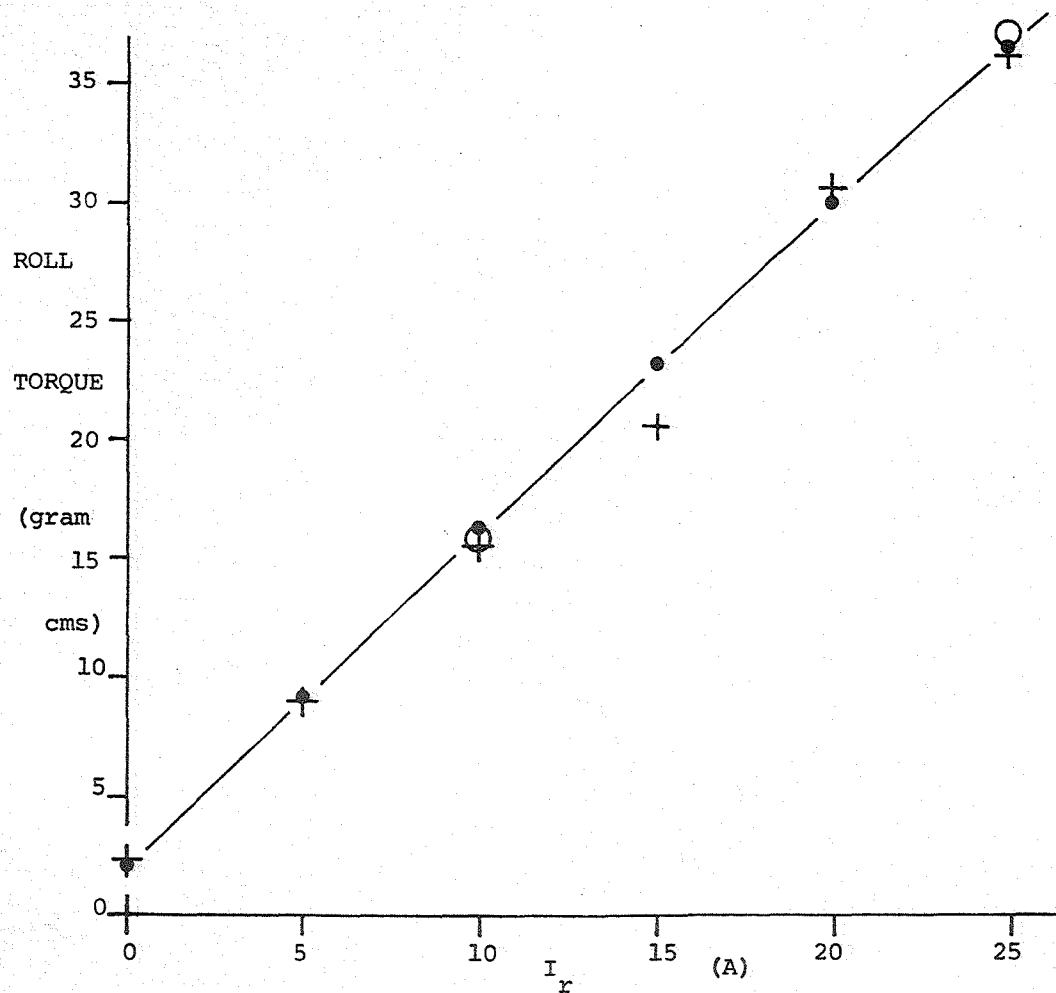
Fig. 5.56 Comparison between measured and predicted roll torque

$I_m = 25$ A

$+$ Interpolated from experimental data (Figs. 5.51)

$\bullet$ Linearized theory

$\bigcirc$ GFUN

the agreement is considered to be excellent. The apparent discrepancies may, in fact, be unrepresentatively small (see Section 5.7.3), being less than the estimated experimental error alone. It is concluded that major systematic errors in the predictions of GFUN at low or moderate field levels are unlikely.

5.7.3 An assessment of likely accuracies of GFUN results

Considering previous results with GFUN (40, 41, 42, 43) regarding prediction of magnetization levels, the agreement between the GFUN torque integration scheme and an alternative method applied to a representative low field case (Section 5.7.1.) and the performance of GFUN in predicting torque for the experimental system (Section 5.7.2.), it is thought that the error magnitude in any GFUN prediction for the baseline or similar geometries at low applied field levels should not exceed 10%. Typical error may be significantly less than this figure, perhaps 5%. The error will tend to be mostly systematic in nature, available data showing low random content. This implies that trends in performance should be reliably identified provided fairly consistent formulations of the problem (for instance element distributions) are used. This was in fact done. The effects of geometrical and other idealisations are not included in the above figures. It being anticipated that increased inaccuracy may occur with rising applied field levels and a predominantly saturated core, it would seem appropriate to increase the figure for peak anticipated error to perhaps 20% for intermediate applied field levels (arbitrarily $2000 < J_{r,m} < 10000 A/cm^2$). At still higher applied field levels the predictions become progressively less relevant to immediate requirements (5) since the torques predicted are high and the peak E/M fields required to achieve those torques are outside the limits of existing technology (Section 5.8.2.). The high applied field results ($J_{r,m} > 10000 A/cm^2$) should therefore, perhaps, be regarded for the time being as somewhat speculative and requiring further verification, such as more detailed testing of the GFUN torque integration scheme at high field levels.

Significant departures from the baseline core geometry (sweep, etc.) are achieved only by utilising iron element distributions that are undesirably sparse. A version of GFUN exists (using the subprogram GETM 400) that can deal with up to 400 independent iron elements, rather than the 100 in the standard batch program, which

could tackle most cases herein with nearly ideal element distributions. This facility did not become available during the period of this study and anyhow would require much greater CPU time for a solution, CPU time for solving the magnetizations being limited and varying approximately as the square of the number of iron elements. Thus, cases such as those involving core sweepback, the effect of axial fields and the F-16 cores, are subject to increased uncertainty.

Estimates of the likely peak error magnitudes in the above cases are principally based on judgement but realistic estimates are thought to be:

Case	Peak anticipated error.	Comments
Baseline		
low fields	10%	
high fields	20%	Rising with applied field
very high fields (J > 10000)	50%	Requires further verification. Ditto.
Sweepback < 20°		Standard integration volume.
low fields	20%	No usable symmetry.
Sweepback > 20°		
low fields	25%	Increased integration volume necessary
high fields (positive Axial)	30%	
high fields (negative Axial)	40%	Poor convergence of solutions.
Axial field with fuselage		
low fields	20%	Large integration volume.
high fields	30%	No usable symmetry.
F-16		
low fields	40%	Undesirably sparse element distribution.
high fields	60%	

The principal idealisation inherent in all cases herein is the representation of wing chordwise cross sections (airfoil sections) as rectangles, since it has not (Section 5.4) been thought that slab cores buried inside non-magnetic aerodynamic envelopes would be used in practice. In order that the existing GFUN predictions be applicable to MSBS cases with true airfoil sections some appraisal of the

effects of this idealisation is necessary. However, it is not obvious on what basis, apart from cross sectional area, GFUN data can be matched to true sections. In the computed F-16 cases the moment of volume about the centroid of area was chosen arbitrarily to generate a GFUN representation. The thickness to chord ratio, defined conventionally, could also be used, leading to generally similar results with classical streamline wing sections. Typical comparison between a GFUN section and a true section is shown in Fig. 5.57 :
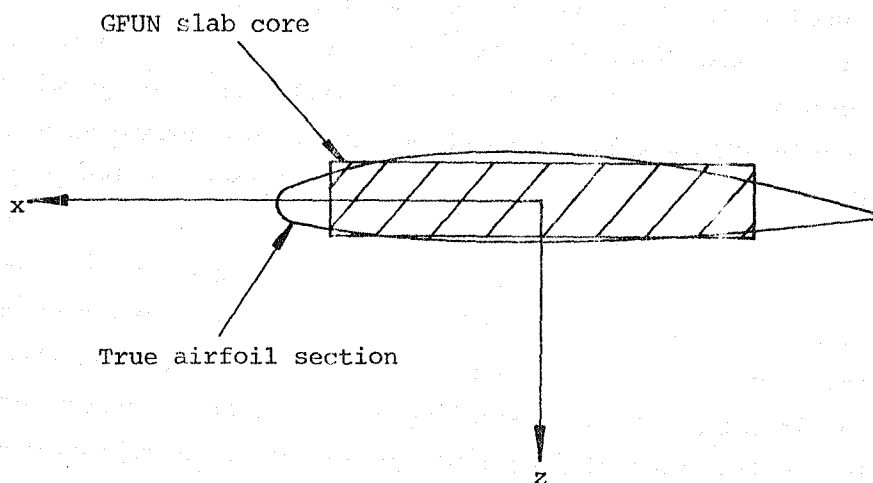
Fig. 5.57. Comparison of GFUN and true core cross sections

Since the spanwise slenderness is scarcely affected, it is expected that the mean spanwise magnetizations should be near identical in both cases, though the detail distributions must be different. The chordwise and through wing slenderness will be affected by the change of section, though the precise value of through wing slenderness is not thought to be critical at low or moderate fields. The (increased) chordwise slenderness with the true section will lead to somewhat greater sensitivity to axial fields, the amount by which the effects of the axial field are amplified being perhaps in the range 0 - 50%.

5.8 Discussion and conclusions

5.8.1 Further use of GFUN in SIM computations

GFUN's creators could not have envisaged that it would see use

in this type of problem. Because of this, several detail features
are inconvenient for SIM computations. Some of these, such as the
lack of a proven torque integration scheme, have been partially
rectified (by Simkin at Rutherford Laboratory) during the course of
this study, but some remain. Examples are the inability to exploit
all the symmetry existing in all problems, the lack of a torque
integration scheme with the high element number version of GFUN, and
the doubts concerning torque predictions at high applied field levels.
It is believed that these difficulties can be overcome relatively
easily by further improvements or expansions of the program code.
If this were done it seems likely that GFUN could provide torque (and
force) predictions to a much higher level of accuracy than those
estimated for the results herein. Definition of E/M and model core
requirements for specific performance demands (all degrees of freedom)
for specific LMSBSs should then be possible, to adequate accuracy for
preliminary and intermediate LMSBS design and cost studies. It is
difficult to imagine GFUN or similar programs becoming sufficiently
accurate for precise predictions of performance (say better than 1%
accuracy) in all cases of interest, due principally to the geometrical
idealisations required in the formulations of the problem, though this
level of accuracy should be attainable for certain simple cases.
Empirical calibration of practical systems would therefore appear
mandatory. Universally high accuracy may, however, be considered
unnecessary, for instance where significant over-capacity is incor-
porated in LMSBS E/Ms.

5.8.2 Application of the SIM system to LMSBSs

Even taking account of the relatively large errors considered
likely to exist in the computed results, it is clear that the apparent
torque capability of the SIM system considerably exceeds those pre-
dicted heretofore for other rolling moment generating systems. For
instance, with the baseline geometry (5 point BH curve), the value of
600,000 Nm/m^3 of (permanent magnet) core predicted in Section 4.3,
perhaps 300,000 Nm/m^3 of wing volume, is exceeded at approximately
4000 A/cm^2 in all E/Ms.

Subject to the provision of adequately powerful E/Ms the SIM scheme
must be considered a viable contender for LMSBS application. The
matter of E/M design requires further analysis, but data is included

(Fig. 5.58), showing the baseline magnetizing field at 1000 A/cm^2. The baseline through-wing field is similar but indexed by 45°. Examining this data it is difficult to imagine the specified E/Ms being operated above, perhaps, 3000 A/cm^2, with existing technology superconductors, whence the peak field within their bores becomes approximately 6.6 T.   That value of field may not be increased by geometrical adjustments, only by improvements in superconducting E/M technology.   Whilst certain optimisations of E/M geometry remains possible, it is seen that a fundamental limit to the available torque from a particular SIM system exists.

Where peak performance is required it is easily seen that the E/Ms should generally be located as close to the model as possible (Fig. 5.59).

The matter of cross couplings between roll and other degrees of freedom due to the presence of the spanwise magnetizations, or the (applied) wing core magnetizing or through wing fields, has not been directly addressed here.   It is felt that the analysis presented in Section 4 will remain approximately applicable though the presence of axial magnetizations and/or the lack of fore-and-aft symmetry in swept wing (such as the F-16) cases will result in relatively complex couplings, mostly second order in magnitude.

This study has indicated that at least with respect to available roll torque, the SIM system is viable for application to LMSBSs.

Calculated via FORCE
GFUN field closely
similar.

0.39   0.58   0.98
              1.19
0.51   0.79   1.37
              1.51
0.60   0.94   1.58   2.17   2.07
                      2.01   2.16   1.90   1.41   0.85
0.66   0.98   1.40   1.72   1.69   1.32   0.90

                                            0.15m

0.68   0.96   1.33   1.56   1.54   1.26   0.91
                                            0.075m
y

0.15m   0.075m

2.075m to origin
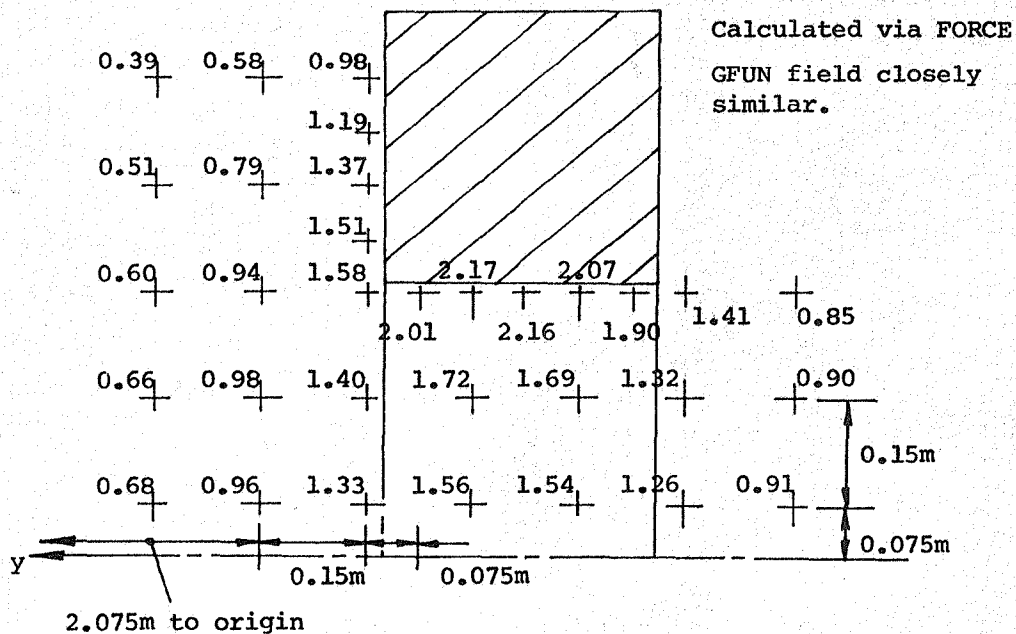
Fig. 5.58 Field intensity around baseline magnetizing field E/Ms.

$J_r = 0$, $J_m = 1000$ A/cm^2. Fields in tesla. Dims. in metres

Field

Local field fairly
independent of E/M
location

Field at model
increased with E/M
location (B) compared
to initial location (A)

Wing
core

y

(B)   (A)

Wind
tunnel
wall

z
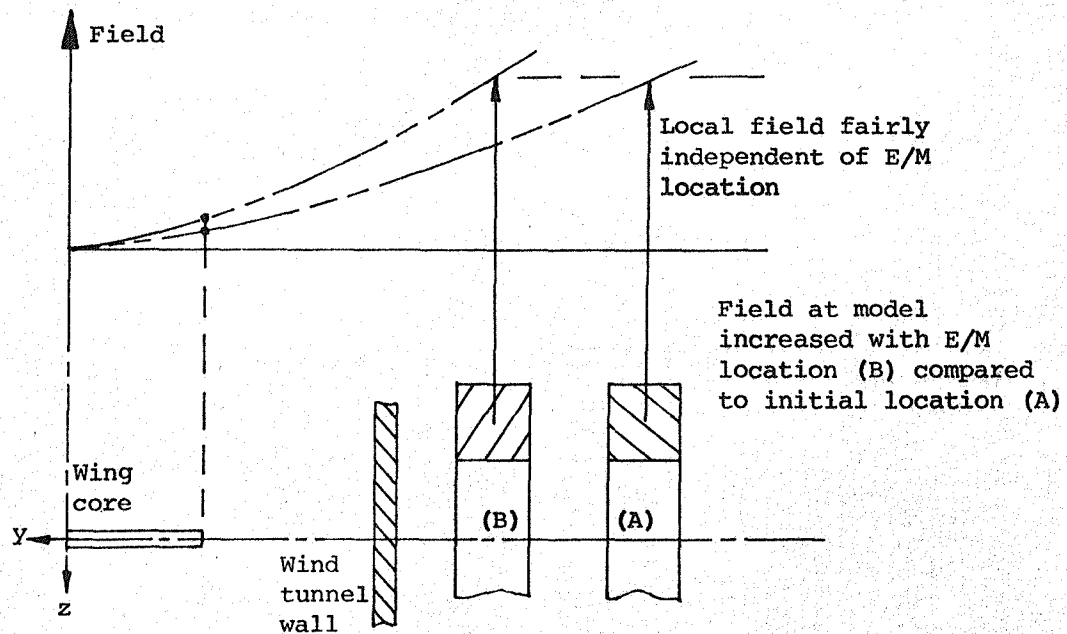
Fig. 5.59 Improvement in E/M effectiveness with closer packing

to wind tunnel wall.

- 134 -

6. SPANWISE PERMANENT MAGNET ROLL CONTROL WITH SUMSBS

6.1 Introduction

Since the Spanwise Permanent Magnet roll control technique was
viewed as potentially the most suitable method for use with SUMSBS
in the foreseeable future, preliminary suspension and minimum cali-
bration of a pilot model has been attempted in order that this view
might be verified.

6.2 Special features of SUMSBS for roll control

SPM roll control requires that SUMSBS be used in its X con-
figuration, achieved by rotating the model's datum axes by 45° in
the roll sense (Fig. 6.1). The E/M geometry thus generated does
not directly correspond to previously discussed SPM E/M arrays
(Section 4) due to the fore-and-aft separation of the two quadrupole
groups of main E/Ms, but the required through-wing fields are still
generated relatively effectively (Fig. 6.2).

The pilot SPM model merely consisted of a standard axisymmetric
model (Appendix 1), crudely adapted to carry vaguely representative
permanent magnet wing cores (Fig. 6.3 and Appendix 1). All magnetic
cores were Alnico V. The awkward appearance of this model must be
excused but it should be noted that the wing core cross sections and
volumes are in approximately representative proportion to the fuselage
core for an aircraft of relatively high wing volume, such as an A-10.
The measured torque capability may, of course, be satisfactorily
scaled to differing wing sizes (Section 6.4).

The roll attitude sensing system, described more fully in Appendix
1, consisted of a low power laser directed onto a model-mounted
mirror, the reflected beam falling onto a light spot position
detecting device. Some difficulties were experienced with stray
reflections of the laser beam, but the sensing system is not neces-
sarily seen as representing anything more than a short term solution.

All-digital control was employed (Appendix 1) with the roll
stabilisation loop incorporating, purely for convenience, only one
phase advance network (see 11, 59), instead of the two (in series)
used in all other degrees of freedom. This corresponds to previous
practice with SUMSBS.

The magnetic couplings occurring due to the presence of the span-
wise magnetizations were expected to require adjustments to the
control algorithms to alleviate their effects, but accurate estimates

B represents the
through-wing field
required for roll
torque generation
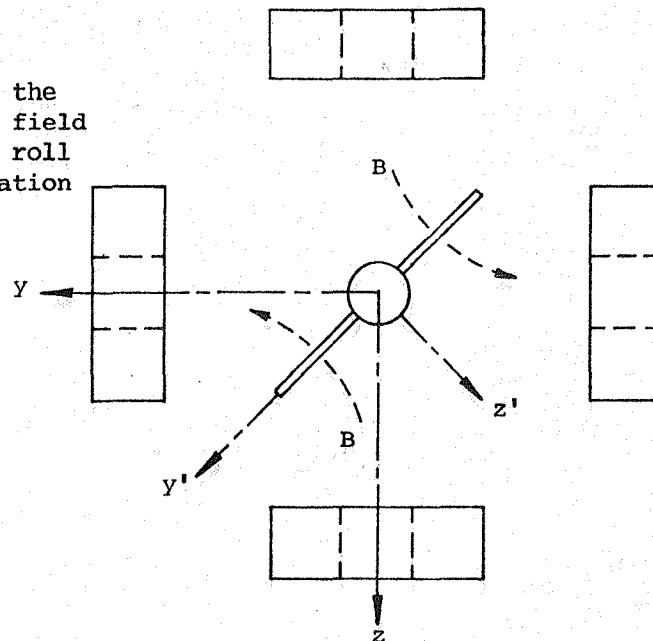
Fig. 6.1 Operation of SUMSBS in an X configuration (SPM roll control)

The E/Ms shown
represent E/Ms
1-8 from SUMSBS
(see Fig.2.1)
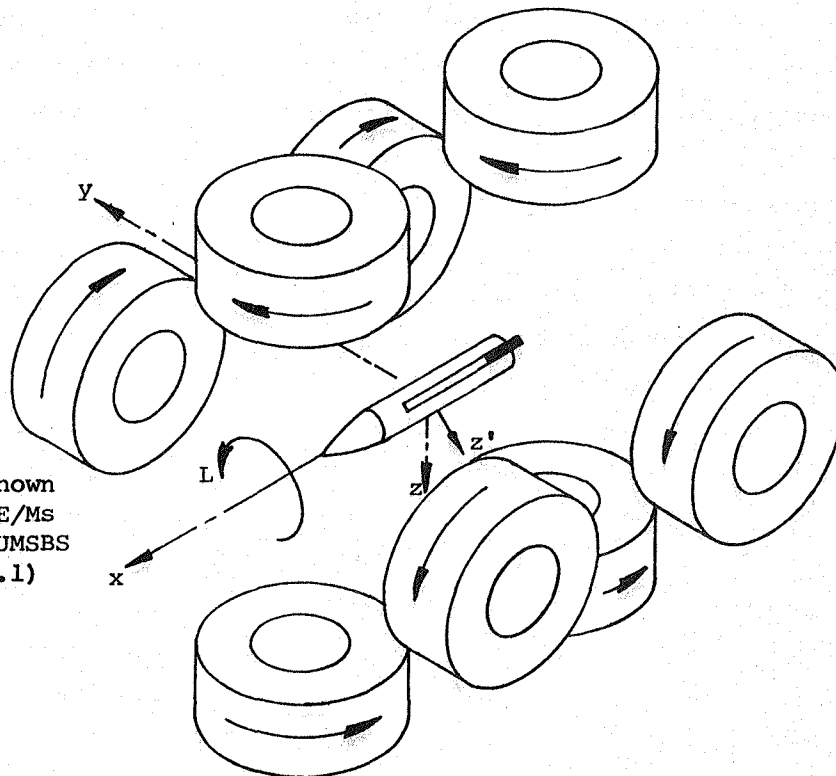
Fig. 6.2 Generation of through-wing fields with SUMSBS
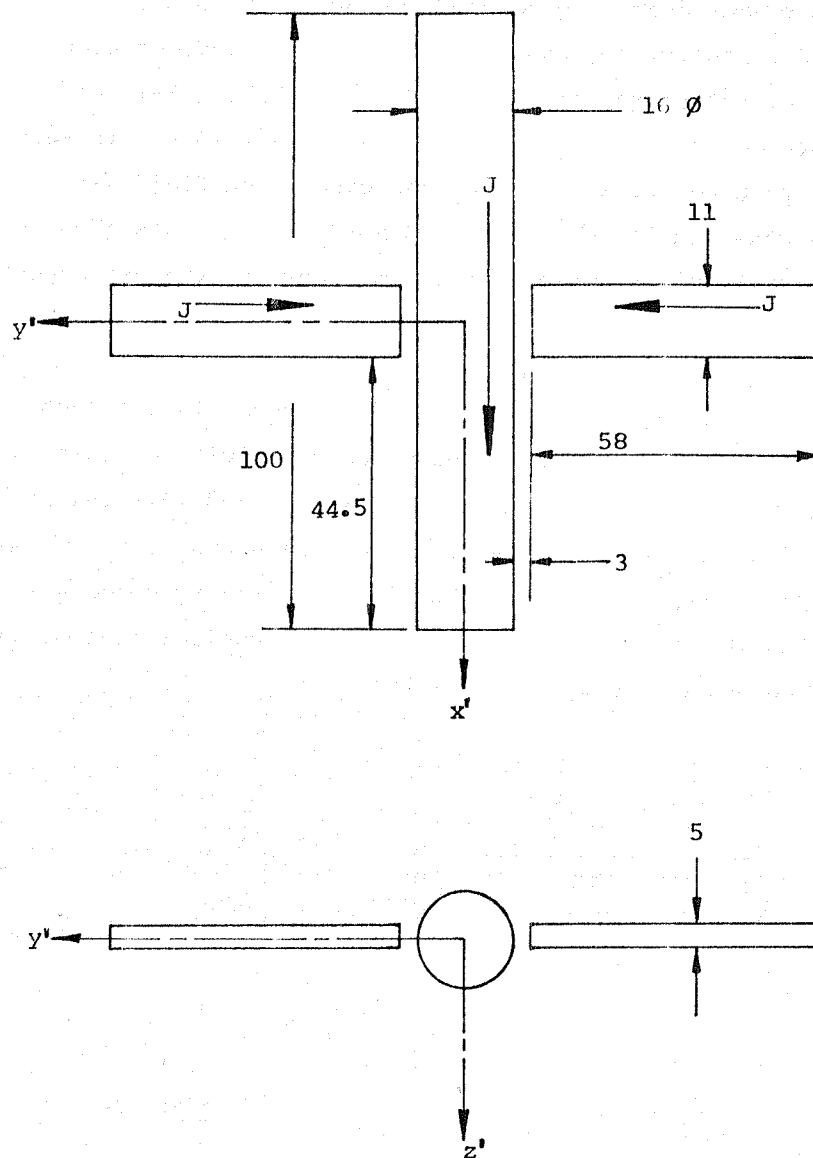
Fig. 6.3 Geometry of pilot SPM model. Dimensions in mm.s

All magnetic cores Alnico V
Polarization (J) assumed as 1.25T for FORCE calculations

Non-magnetic envelope not shown

of coupling effects were not possible for two principal reasons:

1) The iron cores of the main E/Ms preclude accurate
representation of these E/Ms with FORCE (Appendix 2)
and measurement of the actual field distributions in
SUMSBS was deemed to be too lengthy.   Therefore, the
line conductor approximation to SUMSBS' configuration
and geometry used in Section 7 (Figs. 7.5, 7.18) was
employed for this study, with the current levels in each
E/M adjusted so as to match the calculated field with
the measured field at the origin of balance axes (Fig. 6.5).
The field distributions around this origin are not expected
to be particularly well represented.

2) The polarization distribution of Alnico V cores will
not be constant and uniform, as is assumed in all FORCE
computations.   The relatively low coercivity of this
material typically results in weakening and splaying of
the polarization vectors, particularly around the extremities
of the core, partly due to self demagnetizing effects and
partly due to local demagnetization by applied fields, as
illustrated in Fig. 6.4.

Idealized   Practical
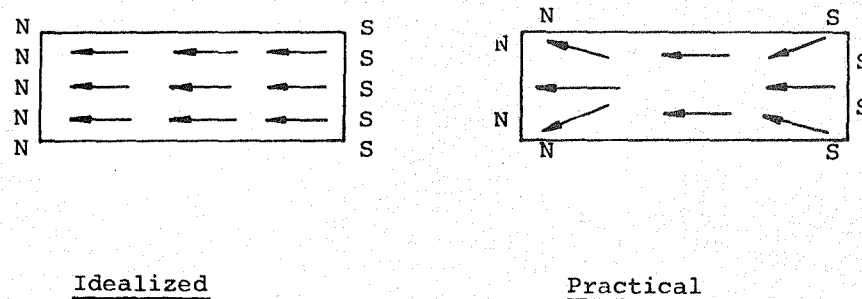
Fig. 6.4 Idealised and practical polarization
distributions for Alnico V cores.

For FORCE calculations the core polarization was assumed constant
and uniform at 1 Tesla.   This figure is below the saturation polar-
ization of Alnico V ($\simeq$1.25T, Ref. 25) but may represent an over-
estimate of the effective polarization level.   The forces and
torques generated due to various classical demands (calculated)

are shown in Tables 6.1 and 6.2, with the E/M geometry and current
directions clarified in Fig. 6.5.   Pure roll torque or drag force
components are generated by classical roll or drag demands respec-
tively and there exist no couplings into roll torque or drag
force from other demands (lift etc.).   It is concluded that de-
coupling of the controller is unnecessary for preliminary work
since no coupling terms are of the same order of magnitude as the
relevant primary terms (Table 6.2), with only one coupling
appearing as significant, that being the expected coupling into
Yaw from a Sideforce demand.   Further, generous stability margins
are available.

Table 6.1   Required current directions for generation of classical
demands with X configuration (SUMSBS)

E/Ms as Fig. 6.5.

Current directions shown as positive (+) or negative (-) as Fig. 6.5.

Demand (model axes)	I_1	I_2	I_3	I_4	I_5	I_6	I_7	I_8
Lift	+	+	-	-	-	-	+	+
Sideforce	+	-	-	+	-	+	+	-
Pitch	-	-	+	+	-	-	+	+
Yaw	+	-	-	+	+	-	-	+

Table 6.2   Coupling terms for SUMSBS classical applied fields
with SPM pilot model

Fields as Table 6.1.

Model as Fig. 6.3.

FORCE calculations

Demand (model axes)	$F_{z'}$	$F_{y'}$	M'	N'
Lift ($F_{z'}$)	<u>0.394</u>	0	10^{-5}	0
Sideforce ($F_{y'}$)	0	<u>0.394</u>	0	-0.01
Pitch (M')	-0.03	0	<u>0.03</u>	0
Yaw (N')	0	-0.08	0	<u>0.03</u>

Primary terms (e.g. lift force from lift demand) shown underlined.

Forces given as N per ampere (relevant E/Ms, in SUMSBS)

Torques given as Nm per ampere (similarly).

Currents shown
in E/Ms this side
only

View on AA

Currents shown in
E/Ms this end only
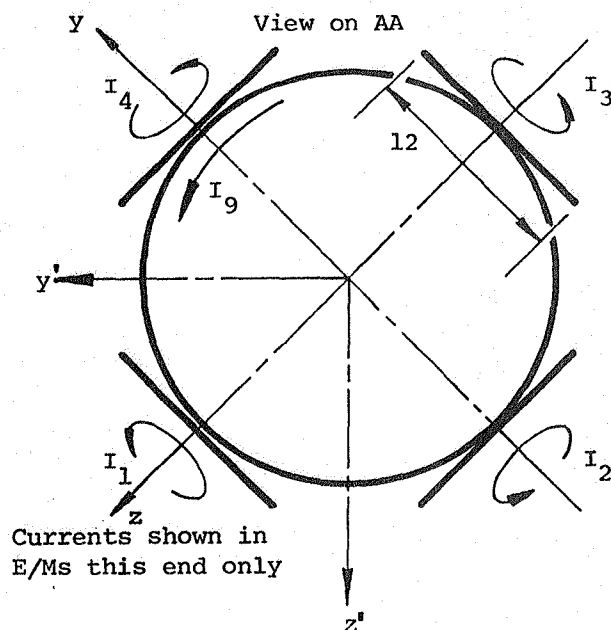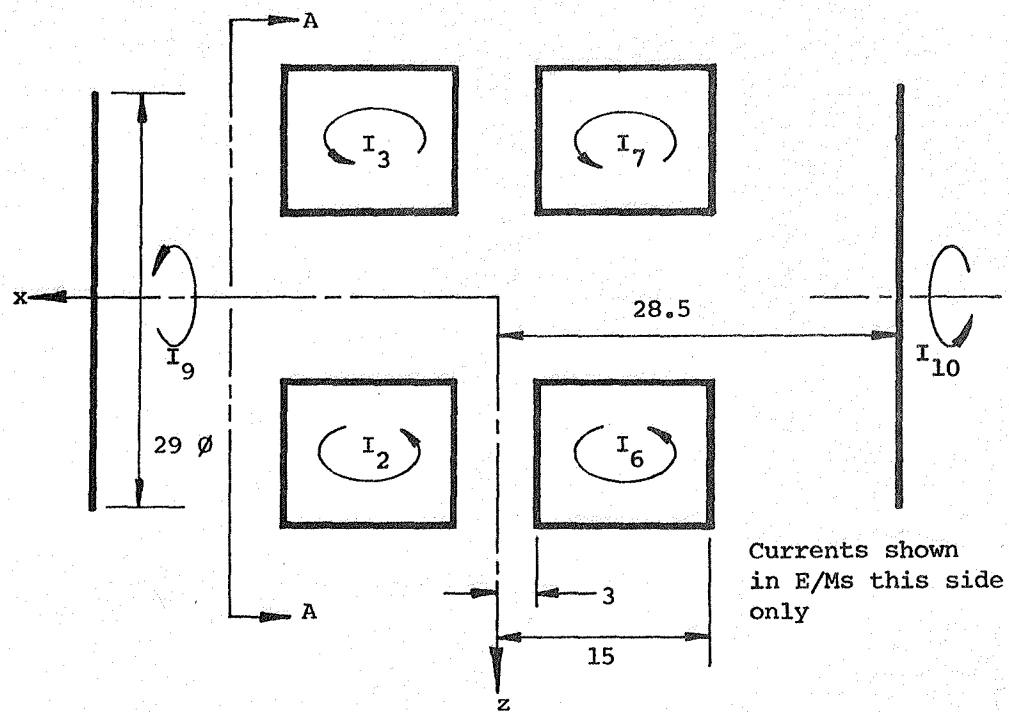
Fig. 6.5 Geometry of
X E/M configuration
for FORCE SPM
calculations.

$I_1 - I_8 = 19734.8$ A

$I_9 - I_{10} = 11809.3$ A

equivalent to 20 A cable
         current in SUMSBS
This geometry derived
by rotation of +
geometry of Fig. 7.5

Dimensions in cms.

6.3 Suspension and calibration

Stable suspension was achieved very easily, following trimming
of D.C. offsets within the controller (to provide standing currents
to support the model's weight) and adjustments to various loop
gains.   This latter requirement was due to the large increase in
the deadweight and moments of inertia of the model compared to the
unwinged case.   Suspension quality was good.

Time only permitted the absolute minimum calibration to be
attempted, that being measurements of roll torque versus E/M
currents for a model at one position and attitude (the usual datum).
For convenience, roll torque was applied via a lightweight torque
rod attached to the extreme nose of the model (Fig. 6.6).   This
technique has not been widely used in the past and has certain dis-
advantages, perhaps principally the likelihood of applying axial
forces to the model as well as roll torques.

Fig. 6.6 Application of
roll torque to suspended
model.
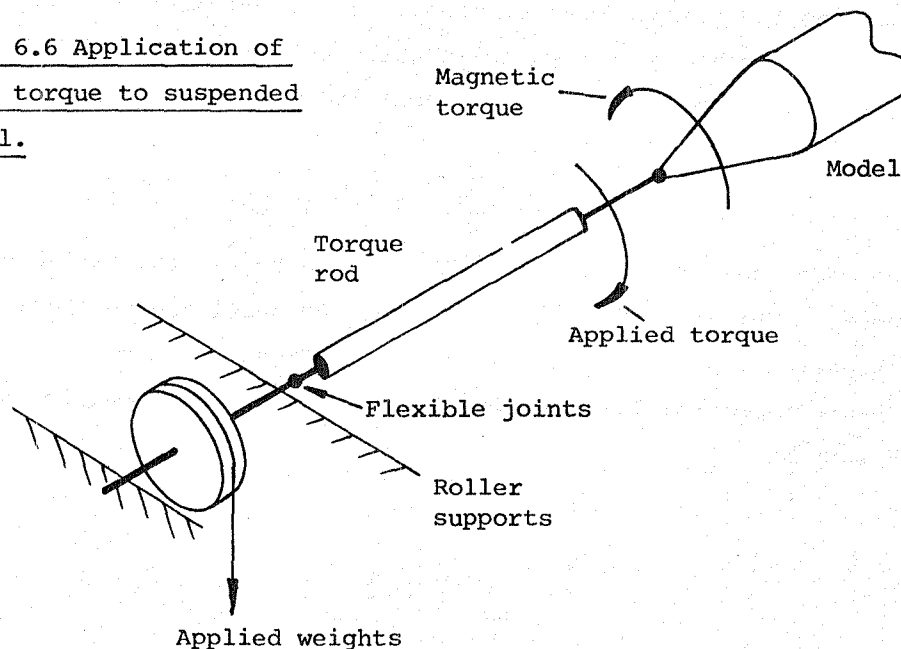
Only one E/M current could be accurately monitored with available
equipment, but it is assumed that the current increment in all E/Ms
due to the applied roll torque will be nearly equal.   The restriction
of the model to one fixed position and attitude (position/orientation
error integrators operating in all control loops) further validates
this approach.   The line conductor approximation to SUMSBS (Fig.6.5)
was again used to generate an estimate of the roll torque per ampere

(8 E/Ms) with the specified model.

Results are presented in Fig. 6.7 with Figs. 6.8 - 6.10 illustrating **certain** aspects of performance.

6.4 Discussion

The torque capability demonstrated is at least ten times higher than has been possible previously, under comparable conditions, with other SUMSBS roll control systems (11, 23).

The calibration curve of Fig. 6.7 exhibits slight nonlinearities and a slope approximately 50% less than the computed estimate shown. However, the shortcomings in the experimental technique, the gross simplification of E/M (hence field) geometry in the computed E/M configuration and the partly unknown model magnetization distributions are thought to be sufficient to account for these discrepancies and neither point is regarded as a matter for any concern at this stage.

Scaling the measured calibration curve, using Eqn. 4.4, to a realistic aircraft geometry, taken to be the Cessna Citation I (a convenient choice with zero sweepback) indicates a torque capability of the order of :

8.2 gm.cm./Ampere ; perhaps $\pm$ 80 gm.cms. normally usable:

- the model span being taken as $4\frac{1}{2}$ inches with representative core volumes.   This is lower than the pilot SPM model due to the lower thickness and span, also the taper of the Citation wing.

SPM roll control is concluded to be entirely practical for use with SUMSBS.
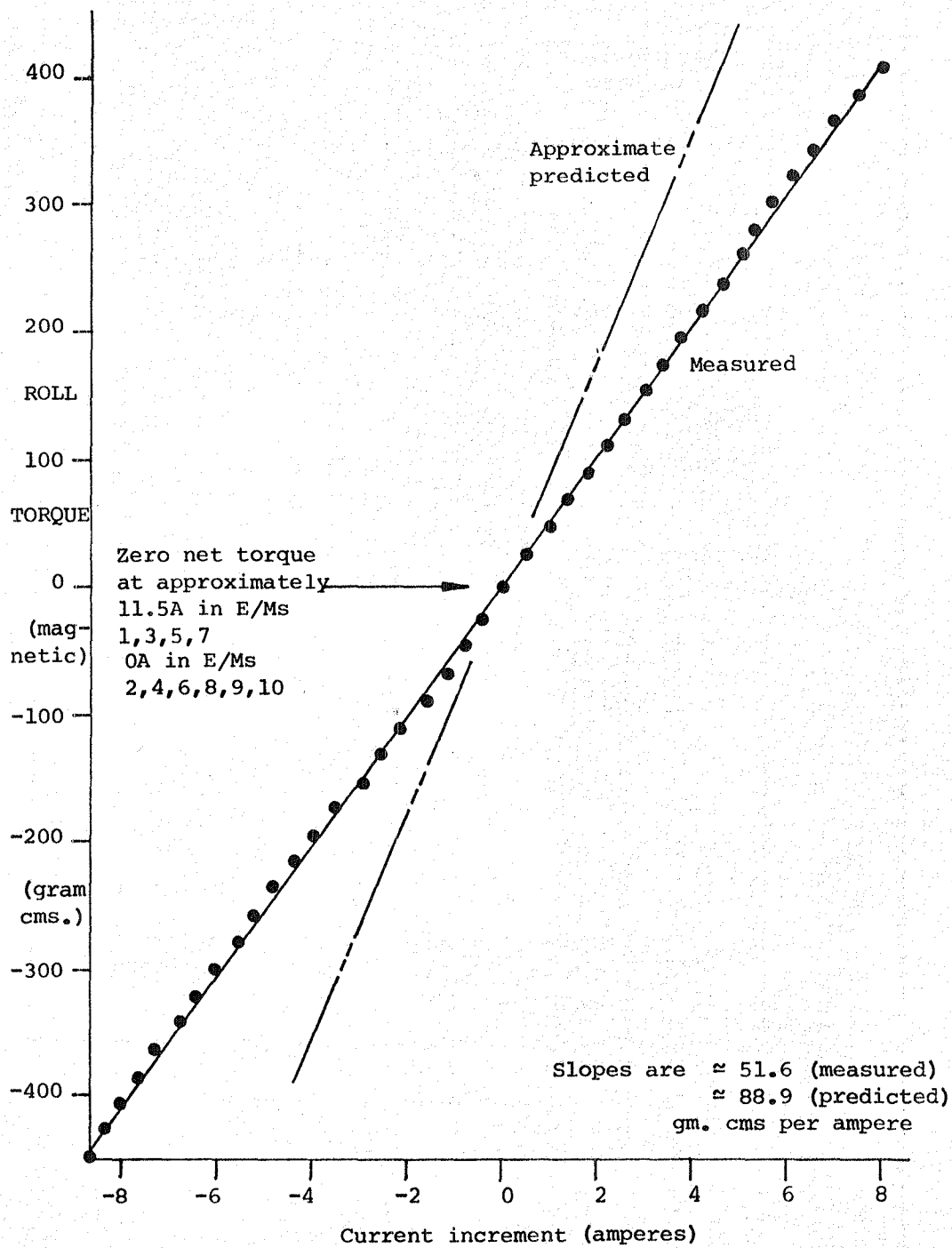
Fig. 6.7 Experimental measurements of roll torque versus E/M current increment for pilot SPM model.

path of
axial position
sensing beam

non-magnetic
supports

magnetic cores

path of roll
attitude sen-
sing beam

roll
attitude
sensor

Fig. 6.8 SPM
pilot model in
suspension
$\phi = 0^{\circ}$
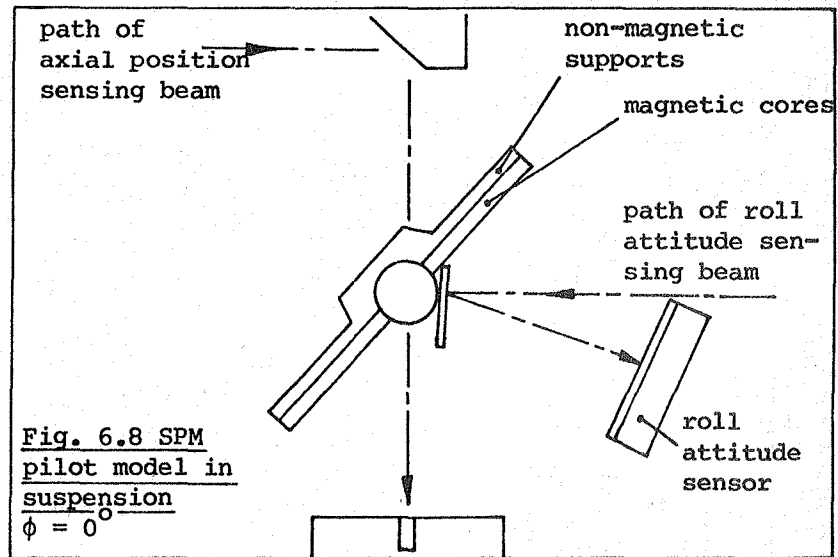
PLATES   OVERLEAF

Fig. 6.9 SPM model in suspension, model rolled from
datum orientation in sense of starboard
wing down.

Fig. 6.10 SPM model in suspension, model rolled from
datum orientation in sense of starboard
wing up.
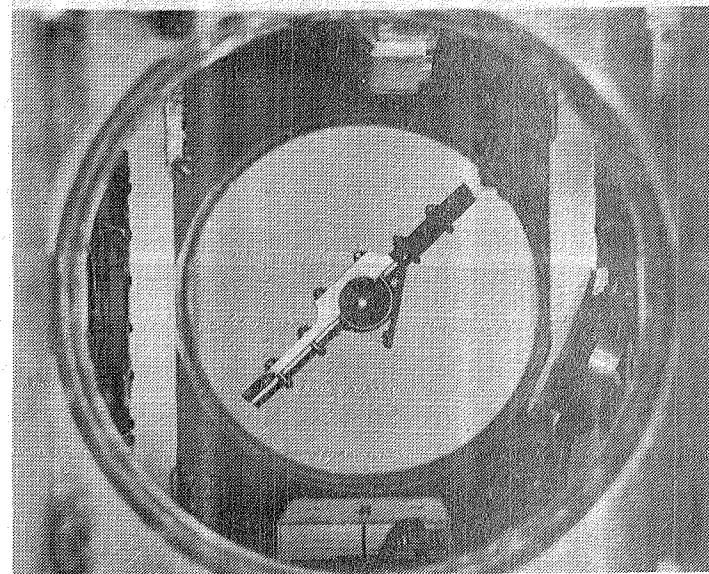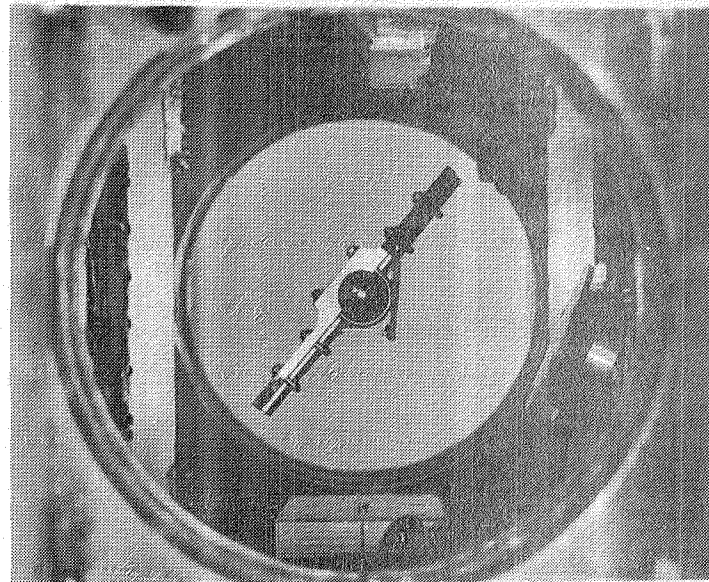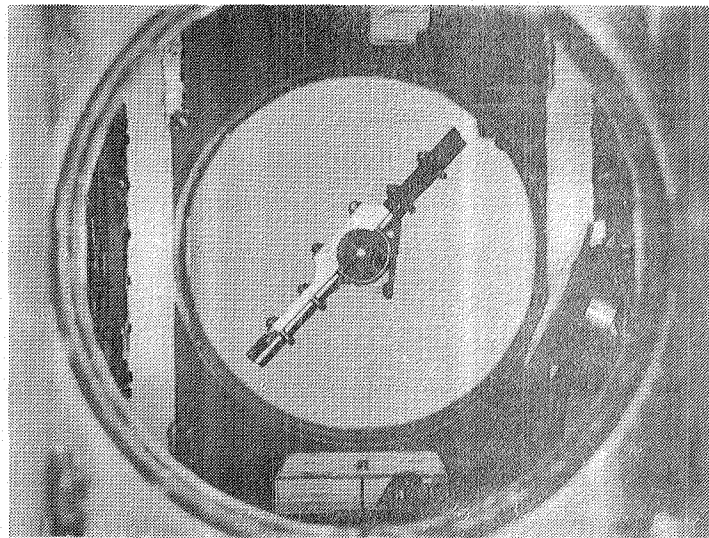
7. EXTREME ATTITUDE TESTING WITH MAGNETIC SUSPENSION AND BALANCE SYSTEMS

7.1 Introduction

Contemporary small MSBSs have not previously been capable of suspending models over a particularly wide range of attitudes, the axis of the model's fuselage typically being limited to approximately 30 degrees excursion from the major axis (wind axis) of the MSBS (MIT(B)) or less. Whilst restricted ranges of sensitivity of position sensing systems represents the primary limit to such excursions in most cases, it is undoubtedly true that none of the existing MSBSs (apart from the modified SUMSBS) have been configured with the intention of suspending models significantly outside this range, indeed in the majority of cases the MSBSs would be magnetically incapable of realistic operation over a substantially wider range.

It would be highly desirable for a LMSBS to be capable of supporting and restraining typical test models over a wide range of test attitudes under representative test conditions. This would enable rapid exploration of the aerodynamic characteristics of aircraft or missile models over their complete attitude envelope, including of course the regimes where the model may be thought of as being wholly or partially stalled. Such regimes are currently of great interest in military work and tend to be rather intractable analytically. Current test methods in this class generally require a range of model supports, each functional over a restricted range of attitudes. Support interference corrections can be virtually impossible since the supports often lie in regions of grossly turbulent wake.

In the context of this report "extreme" attitudes are classified as any attitude outside the model axis excursion limit (30 deg.) mentioned above. It is thought that extreme attitude capability for a MSBS should include model axis angular excursions up to and including 90 degrees in at least one plane, permitting, for instance, model testing over the range of angle of attack of -90 to +90 degrees. Yaw and roll excursions need not be over such wide ranges but ideally would be so. Since the model's magnetic characteristics are completely insensitive to the wind direction, combined pitch, yaw and roll excursions over a -90 to +90 degree range would encompass, with "reversal" of the model in the MSBS axes, the complete range of possible attitudes.

Several fundamental difficulties arise when considering model suspension at extreme attitudes.   These include :

1) Identification of E/M array geometries and configurations capable of generating, via field and field gradient components, forces and torques on the model in the required senses and magnitudes over the full range of model attitudes.

2) Synthesis of control algorithms capable of accommodating large changes in model aerodynamic characteristics and magnetic couplings to the E/Ms.

3) Design of position, attitude and other sensors to monitor wide ranges of model motion.

Part of 1) above is addressed here, that is, the inclusion of adequate versatility into the E/M array configuration.   Sizing the E/Ms thus specified to satisfy particular absolute force and torque requirements must be performed separately.

7.2 Theoretical background

7.2.1 Required field and field gradient components

Forces and torques with conventional slender, axially magnetized models are assumed to be predominantly created by the following field and field gradient components (Appendix 5) :

Table 7.1   Required field and field gradient components

Force/torque	Component	
F_x, (axial force)	H_{xx_o},	
F_y, (sideforce)	H_{xy_o},	
F_z, (normal force)	H_{xz_o},	
L' (rolling torque)	H_{yz_o},	(spanwise magnets)
M' (pitching torque)	H_{z_o},	
N' (yawing torque)	H_{y_o},	
— (magnetizing field)	H_{x_o},	(soft iron fuselage core)
— (magnetizing field)	H_{yy_o},	(soft iron spanwise magnets)

Axes as Fig 7.1

In "normal" suspension model and balance axes coincide and these components correspond, neglecting the cases of roll and magnetizing fields, to:

$$H_{xx_o} \ , \quad H_{xy_o} \ , \quad H_{xz_o} \ , \quad H_{z_o} \ , \quad H_{y_o}$$

Fig. 7.1 Model and tunnel axis
systems
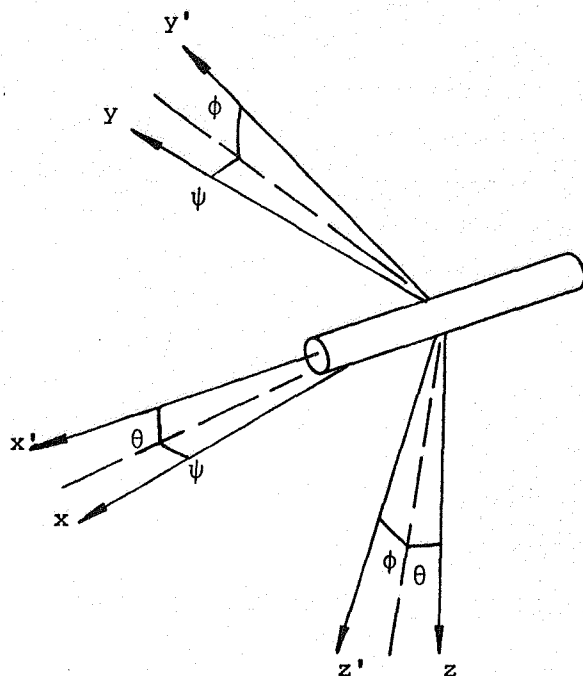
Tunnel axes --
    x, y, z

Model axes --
    x', y', z'

Sequence of rotations -
    Yaw, pitch, roll

o subscripts indicate
the origin of axes.

Pitching or yawing the model through 90 degrees translates these components into:

$$H_{zz_o}, \quad -H_{yz_o} \ , \quad -H_{xz_o}, \quad H_{x_o} \ , \quad H_{y_o} \qquad \text{and}$$

$$H_{yy_o}, \quad -H_{xy_o}, \quad H_{yz_o}, \quad H_{z_o}, \quad -H_{x_o} \qquad \text{respectively.}$$

It may be immediately noticed that all nine primary field components :

$$H_x \ , \ H_y \ , \ H_z \ , \ H_{xx} \ , \ H_{xy} \ , \ H_{xz} \ , \ H_{yy} \ , \ H_{yz} \ , \ H_{zz}$$

are required independently at the origin for the full range of model attitudes to be usable

The generalized couplings between field and field gradient components in tunnel and model axes may be calculated as follows:

The transformation matrices for Yaw (Ψ), Pitch (Θ) and Roll (Φ), in tunnel axes are as follows:

$$
\begin{vmatrix} \text{Cos}\psi & -\text{Sin}\psi & 0 \\ \text{Sin}\psi & \text{Cos}\psi & 0 \\ 0 & 0 & 1 \end{vmatrix}
\quad
\begin{vmatrix} \text{Cos}\theta & 0 & \text{Sin}\theta \\ 0 & 1 & 0 \\ -\text{Sin}\theta & 0 & \text{Cos}\theta \end{vmatrix}
\quad
\begin{vmatrix} 1 & 0 & 0 \\ 0 & \text{Cos}\phi & -\text{Sin}\phi \\ 0 & \text{Sin}\phi & \text{Cos}\phi \end{vmatrix}
$$

The couplings for a vector in model axes are given by the product of the reverse coupling matrices :

$$
\begin{vmatrix} V_{x'} \\ V_{y'} \\ V_{z'} \end{vmatrix}
=
\begin{vmatrix}
\text{Cos}\theta\text{Cos}\psi & \text{Cos}\theta\text{Sin}\psi & -\text{Sin}\theta \\
\begin{matrix} \text{Sin}\theta\text{Sin}\phi\text{Cos}\psi \\ -\text{Cos}\phi\text{Sin}\psi \end{matrix} & \begin{matrix} \text{Cos}\phi\text{Cos}\psi \\ +\text{Sin}\phi\text{Sin}\theta\text{Sin}\psi \end{matrix} & \text{Cos}\theta\text{Sin}\phi \\
\begin{matrix} \text{Sin}\phi\text{Sin}\psi \\ +\text{Cos}\phi\text{Sin}\theta\text{Cos}\psi \end{matrix} & \begin{matrix} \text{Cos}\phi\text{Sin}\theta\text{Sin}\psi \\ -\text{Sin}\phi\text{Cos}\psi \end{matrix} & \text{Cos}\phi\text{Cos}\theta
\end{vmatrix}
\begin{vmatrix} V_x \\ V_y \\ V_z \end{vmatrix}
\quad (7.1)
$$

Which may be written as: $\quad \underline{V}' = A\underline{V}$

The couplings for field components are given straightforwardly by:

$$\underline{H}' = A\underline{H} \qquad\qquad - (7.2)$$

Whereas for field gradient components :

$$\nabla' = A\nabla \qquad\qquad \text{and using (7.2)}$$

$$\nabla'.\underline{H}' = A\nabla.A\underline{H} = B\nabla\underline{H} \qquad\qquad - (7.3)$$

where the reduced form of B is given by :

$$
\begin{vmatrix} H_{xx'} \\ H_{xy'} \\ H_{xz'} \\ H_{yy'} \\ H_{yz'} \\ H_{zz'} \end{vmatrix}
=
\begin{vmatrix}
a_1^2 & 2a_1a_2 & 2a_1a_3 & a_2^2 & 2a_2a_3 & a_3^2 \\
a_1b_1 & a_1b_2+a_2b_1 & a_1b_3+a_3b_1 & a_2b_2 & a_2b_3+a_3b_2 & a_3b_3 \\
a_1c_1 & a_1c_2+a_2c_1 & a_1c_3+a_3c_1 & a_2c_2 & a_2c_3+a_3c_2 & a_3c_3 \\
b_1^2 & 2b_1b_2 & 2b_1b_3 & b_2^2 & 2b_2b_3 & b_3^2 \\
b_1c_1 & b_1c_2+b_2c_1 & b_1c_3+b_3c_1 & b_2c_2 & b_2c_3+b_3c_2 & b_3c_3 \\
c_1^2 & 2c_1c_2 & 2c_1c_3 & c_2^2 & 2c_2c_3 & c_3^2
\end{vmatrix}
\begin{vmatrix} H_{xx} \\ H_{xy} \\ H_{xz} \\ H_{yy} \\ H_{yz} \\ H_{zz} \end{vmatrix}
\quad -(7.3a)
$$

The matrix A being written as :

$$A = \begin{vmatrix} a_1 & a_2 & a_3 \\ b_1 & b_2 & b_3 \\ c_1 & c_2 & c_3 \end{vmatrix}$$

It is seen that field components behave as vectors during axis rotations whereas field gradient components do not and that the couplings from applied field gradients to field gradients in model axes are extremely complex. Certain simplifications are possible where rotation is restricted to one plane, say pitch, where :

$$\psi \, , \, \phi \; = 0 : \qquad \begin{vmatrix} H_{x'} \\ H_{y'} \\ H_{z'} \end{vmatrix} = \begin{vmatrix} \text{Cos}\theta & 0 & -\text{Sin}\theta \\ 0 & 1 & 0 \\ \text{Sin}\theta & 0 & \text{Cos}\theta \end{vmatrix} \begin{vmatrix} H_x \\ H_y \\ H_z \end{vmatrix} \qquad - (7.2a)$$

and:

$$\begin{vmatrix} H_{xx'} \\ H_{xy'} \\ H_{xz'} \\ H_{yy'} \\ H_{yz'} \\ H_{zz'} \end{vmatrix} = \begin{vmatrix} \text{Cos}^2\theta & 0 & -2\text{Cos}\theta\text{Sin}\theta & 0 & 0 & \text{Sin}^2\theta \\ 0 & \text{Cos}\theta & 0 & 0 & -\text{Sin}\theta & 0 \\ \text{Cos}\theta\text{Sin}\theta & 0 & \text{Cos}^2\theta-\text{Sin}^2\theta & 0 & 0 & -\text{Sin}\theta\text{Cos}\theta \\ 0 & 0 & 0 & 1 & 0 & 0 \\ 0 & \text{Sin}\theta & 0 & 0 & \text{Cos}\theta & 0 \\ \text{Sin}^2\theta & 0 & 2\text{Sin}\theta\text{Cos}\theta & 0 & 0 & \text{Cos}^2\theta \end{vmatrix} \begin{vmatrix} H_{xx} \\ H_{xy} \\ H_{xz} \\ H_{yy} \\ H_{yz} \\ H_{zz} \end{vmatrix}$$

$$- (7.3b)$$

Model forces and torques can be given by any of the above using :

$$\underline{F} = {}_v\!\!\int \underline{M}.\nabla\underline{H} \; dV \qquad \text{and} \qquad \underline{T} = {}_v\!\!\int \underline{M} \times \underline{H} + \underline{r} \times (\underline{M}.\nabla\underline{H}) \; dv$$

$$- \text{ following Eqns. 3.1}$$

The force and torque couplings will differ from 7.2, 7.3 etc., due to the effects of the spatial variations of the applied fields over the volume of the model's core. Where the applied fields are relatively uniform over the core these effects will be of second order and the force and torque couplings will be approximated by 7.2, 7.3 etc.

It is considerably more convenient in many cases to represent the couplings by transforming model magnetizations into tunnel axes

rather than field and field gradient components into model axes :

$$
\begin{vmatrix} F_x \\ F_y \\ F_z \end{vmatrix} \simeq V \begin{vmatrix} H_{xx} & H_{xy} & H_{xz} \\ H_{xy} & H_{yy} & H_{yz} \\ H_{xz} & H_{yz} & H_{zz} \end{vmatrix} \begin{vmatrix} M_x \\ M_y \\ M_z \end{vmatrix}
$$

$$
\begin{vmatrix} L \\ M \\ N \end{vmatrix} \simeq V \begin{vmatrix} 0 & H_z & -H_y \\ -H_z & 0 & H_x \\ H_y & -H_x & 0 \end{vmatrix} \begin{vmatrix} M_x \\ M_y \\ M_z \end{vmatrix} + \int_V \underline{r} \times \delta\underline{F} \text{ term}
$$

$$ - (7.4) $$

model magnetizations being given by :

$$ \underline{M} = \Phi \; \Theta \; \Psi \; \underline{M}' $$

7.2.2   E/M configurations for multiple independent field and field gradient component generation.

The requirement to generate 9 field or field gradient components independently necessitates at least 9 independent E/Ms. The desire for symmetry in the E/M array (Section 1.2.1) acts to increase this figure.

A symmetric quadruplet of E/Ms as shown in Fig. 7.2 can generate four field gradient components at the origin; H_{xz_0} (I_1, $I_4 = -I_2$, I_3),

H_{xx_0} (I_1, I_2, $I_3 = I_4$), H_{yy_0} (I_1, I_2, $I_3 = I_4$), and

H_{zz_0} (I_1, I_2, $I_3 = I_4$), but it is immediately seen that H_{xx_0}, H_{yy_0}

and H_{zz_0} are not independent.   Two field components at the origin;

H_{x_0} (I_1, $I_2 = -I_3$, I_4) and H_{z_0} (I_1, $I_3 = -I_2$, I_4), may also be

generated.   Modified geometries (Fig 7.3), in fact corresponding to the "vertical" or "lateral" E/Ms in SUMSBS, are found to be relatively weak in H_{xx_0} as shown.   If H_{zz_0} (or H_{yy_0}) were regarded as a prime component of field for this sub-configuration and the 'stray' components H_{xx_0} and H_{yy_0} (H_{zz_0}) were countered by some other means, the modified quadruplet would be a useful generator of four independent field or field gradient components; H_{x_0}, H_{z_0}, H_{xz_0}, H_{zz_0}, (H_{yy_0}).

A symmetric pair of E/Ms can generate one field and one field gradient component independently at the origin H_{x_0}, and H_{xx_0} as shown in Fig. 7.4, with stray components H_{yy_0} and H_{zz_0}.

Fig. 7.2 Symmetric quadruplet
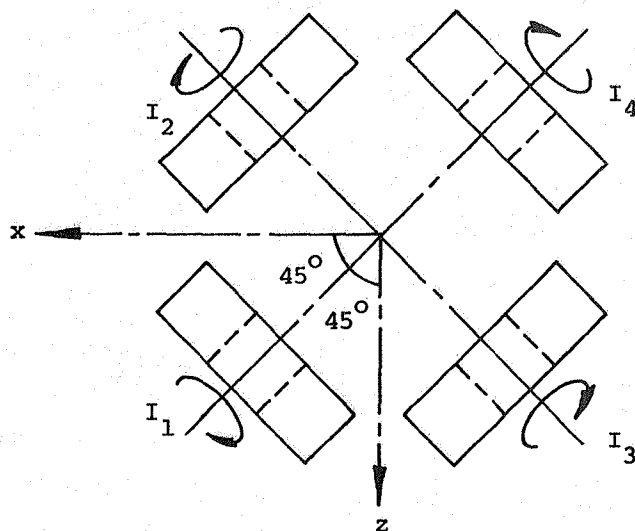
of E/Ms

Fig. 7.3 Modified

quadruplet of E/Ms
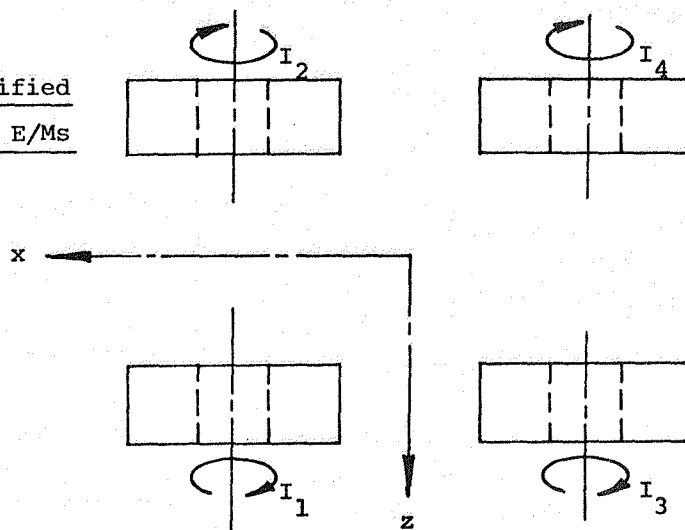
Fig. 7.4 Symmetric

pair of E/Ms
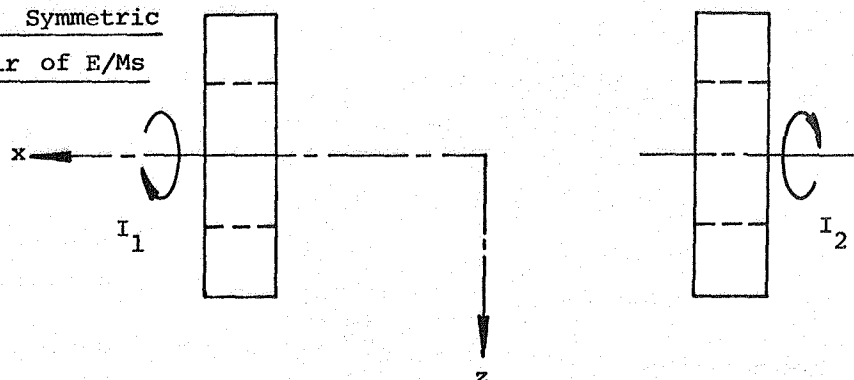
Conventional E/M configurations can be considered as an assembly of quadruplets and pairs as defined above and it is straightforward to arrange for all required field and field gradient components to be somehow provided.

In fact, current MSBS configurations (eg. MIT(B), SUMSBS) are frequently capable of generating 8 field or field gradient components $(H_{x_o}, H_{y_o}, H_{z_o}, H_{xx_o}, H_{xy_o}, H_{xz_o}, H_{yy_o}, H_{zz_o})$, effectively though not completely independently and typically lack capability only in H_{yz_o}. It may thus be expected that conventional configurations are capable of sensible operation over a wider range of attitudes than has been exploited previously.

7.3 Identification of maximum force and torque capabilities of a MSBS

Any extreme attitude capable MSBS will incorporate a number of independent E/Ms, perhaps between 10 and 20. Each E/M tends to create all nine independent field and field gradient components at general points. Thus, with a suspended model at a general attitude and position, each E/M creates force and torque components along or about each axis (x, y, z). It is clear that there will seldom exist a unique solution for E/M currents with any particular force and torque requirement. The absolute maximum force and torque capability of a particular system may not, therefore, be directly analytic.

With 6 independent E/Ms however, there is no serious difficulty since, neglecting demagnetization or saturation effects (see Section 7.7), the required senses for force and torque specify variables $k_1 - k_5$ such that :

$$k_1 F_y = k_2 F_z = k_3 L = k_4 M = k_5 N = F_x \qquad - (7.5)$$

The effects of the 6 E/Ms may be written :

$$
\begin{pmatrix} F_x \\ F_y \\ F_z \\ L \\ M \\ N \end{pmatrix}
=
\begin{pmatrix}
a_1 & a_2 & a_3 & a_4 & a_5 & a_6 \\
b_1 & b_2 & b_3 & b_4 & b_5 & b_6 \\
c_1 & c_2 & c_3 & c_4 & c_5 & c_6 \\
d_1 & d_2 & d_3 & d_4 & d_5 & d_6 \\
e_1 & e_2 & e_3 & e_4 & e_5 & e_6 \\
f_1 & f_2 & f_3 & f_4 & f_5 & f_6
\end{pmatrix}
\begin{pmatrix} I_1 \\ I_2 \\ I_3 \\ I_4 \\ I_5 \\ I_6 \end{pmatrix}
\qquad - (7.6)
$$

where $a_1 - f_6$ are dependent on the system's geometry and magnetic characteristics and are functions of model position and attitude; $I_1 - I_6$ representing the current levels in each E/M. It is immediately

seen that where a_1-f_6 are mostly non-zero, I_2-I_6 (say) are dependent variables with only I_1 unspecified. Since all E/M currents are now fixed relative to each other, the absolute maximum capability is found by increasing all currents until one reaches its limiting value, that value being determined by the E/M design.

Useful results may be obtained for the case of 7 E/Ms, starting with the equations for a 6 E/M system operating with one current (say I_1) at its limiting value ($I_1{}^p$), as above :

$$
\begin{vmatrix} F_x \\ F_y \\ F_z \\ L \\ M \\ N \end{vmatrix}
=
\begin{vmatrix}
a_1 & a_2 & a_3 & a_4 & a_5 & a_6 \\
b_1 & b_2 & b_3 & b_4 & b_5 & b_6 \\
c_1 & c_2 & c_3 & c_4 & c_5 & c_6 \\
d_1 & d_2 & d_3 & d_4 & d_5 & d_6 \\
e_1 & e_2 & e_3 & e_4 & e_5 & e_6 \\
f_1 & f_2 & f_3 & f_4 & f_5 & f_6
\end{vmatrix}
\begin{vmatrix} I_1{}^p \\ I_2 \\ I_3 \\ I_4 \\ I_5 \\ I_6 \end{vmatrix}
\qquad - (7.7)
$$

I_2-I_6 being determined using Eqns. 7.7 and 7.5. Introducing another E/M (I_7), the equations may be reformed :

$$
\begin{vmatrix} F_x \\ F_y \\ F_z \\ L \\ M \\ N \end{vmatrix}
- I_1{}^p
\begin{vmatrix} a_1 \\ b_1 \\ c_1 \\ d_1 \\ e_1 \\ f_1 \end{vmatrix}
=
\begin{vmatrix}
a_2 & a_3 & a_4 & a_5 & a_6 & a_7 \\
b_2 & b_3 & b_4 & b_5 & b_6 & b_7 \\
c_2 & c_3 & c_4 & c_5 & c_6 & c_7 \\
d_2 & d_3 & d_4 & d_5 & d_6 & d_7 \\
e_2 & e_3 & e_4 & e_5 & e_6 & e_7 \\
f_2 & f_3 & f_4 & f_5 & f_6 & f_7
\end{vmatrix}
\begin{vmatrix} I_2 \\ I_3 \\ I_4 \\ I_5 \\ I_6 \\ I_7 \end{vmatrix}
\qquad - (7.8)
$$

Since the coefficients a_1-f_1 and $I_1{}^p$ are constants for any particular model attitude and position, resolution of 7.8 follows a similar procedure to 7.6. This leads to a second current reaching its limiting value, say $I_2{}^p$.

If the number of E/Ms is represented by n, then the cases above yield the criteria that where $n=6$ or $n=7$, $n-5$ E/Ms should be operated at their peak design currents to achieve a particular maximum force and torque capability. It is now argued that this criteria holds for all $n \geqslant 6$. It is not, however, obvious which $n-5$ E/Ms should be chosen to be at their respective peak currents, but this can be resolved by computing all permutations.

Cases where the matrix in 7.6 etc. is sparse may be dealt with by reduced forms of the analysis above.

7.4 "+" E/M configuration study

7.4.1 Geometry

The revised configuration for SUMSBS can fall into this category (see Sections 1.2.1 and 2.2.1). The performance of this system cannot be explicitly computed by FORCE (Appendix 2) since the main E/Ms are iron cored, however a system having similar proportions but arbitrary exact dimensions has been computed to yield an indication of the usable attitude range of SUMSBS (Fig. 7.5).

This representative system is chosen to be at ten times the scale of SUMSBS for convenience. Single loop E/Ms are used to simplify calculations but are expected to provide adequate approximations of the performance of SUMSBS' E/Ms, the current levels being adjusted where appropriate to approximate the relative field capabilities of the E/Ms in SUMSBS.

7.4.2 Performance

As might be expected from Eqns. 7.3 etc., the generalized couplings between E/Ms and model core are likely to be extremely complex. Since the inherent limitations of the optical position sensing system used in SUMSBS would, at least initially, restrict large angular displacements to one plane, specifically the xz (pitch) plane, all computations presented here are made with the model restricted to this plane, with its centroid fixed at the origin of balance axes. Thus $x=y=z=\psi=\phi=0$.

With or without the above restriction, the magnetic couplings between representative E/Ms (Fig. 7.5) and a typical model (Fig. 7.6) are easily found for given model attitudes and positions using FORCE.

It is not, however, clear in what form the couplings should be presented; as couplings from individual E/Ms (Fig. 7.7a-d) or as couplings from conventional groupings of E/Ms (Fig. 7.8a-j). In this case, the latter approach fully separates the creation of magnetic forces and torques but is less general, partly because the groups of E/Ms are not mutually exclusive.

The effects of the spatial variations of the applied fields around the origin of axes may be found by recomputing Figs. 7.8 with model polarization concentrated into a single dipole at the origin (Figs. 7.9a-j). It is found that these results are identical to direct computation from Eqns. 7.3 etc. with the field capabilities of the E/M groupings (calculated) as:

All E/Ms are line conductors

All currents are positive as shown

All E/M current
limits are 10^6 amps.

2.90
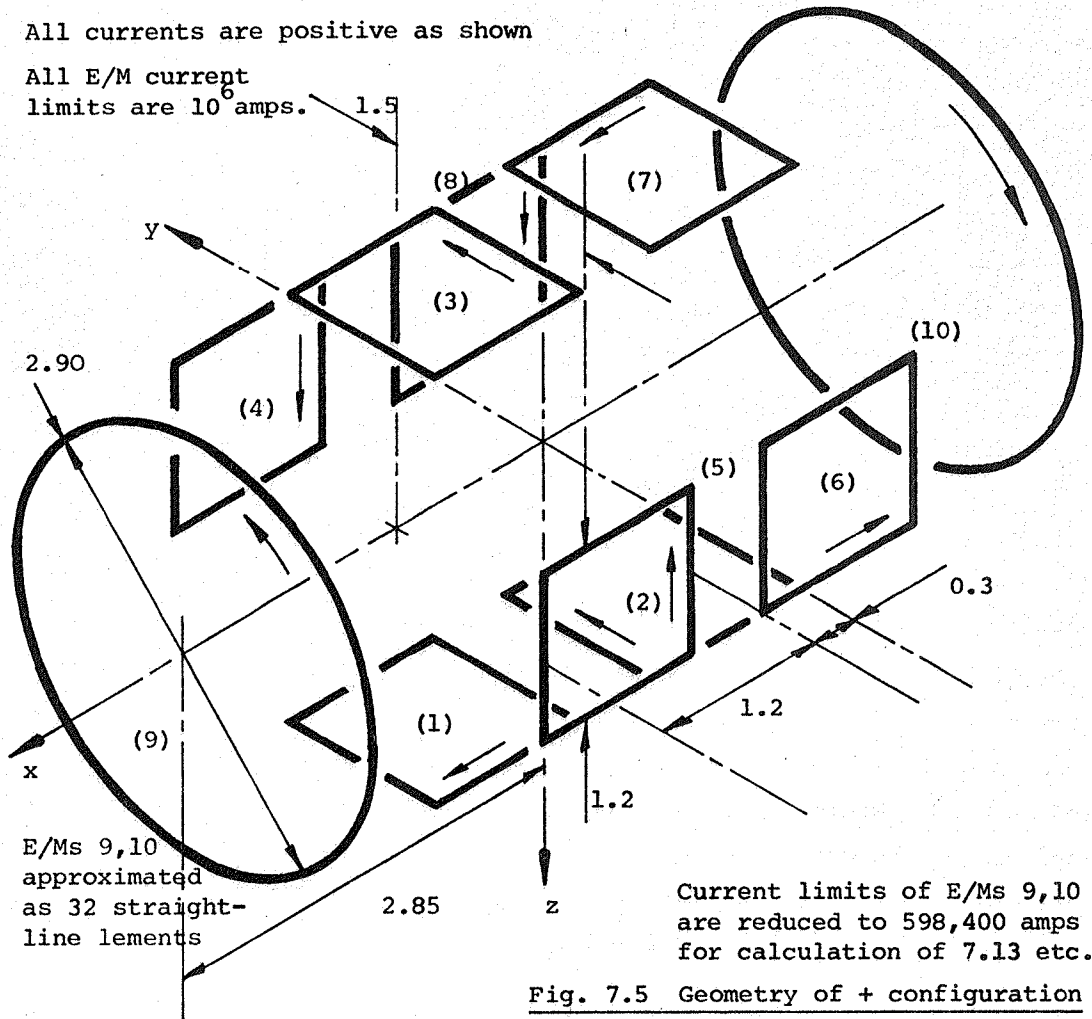
E/Ms 9,10
approximated
as 32 straight-
line lements

2.85

1.5

(8)   (7)

(3)

(4)

y

(10)

(5)   (6)

(2)

(1)

(9)

x

z

0.3

1.2

1.2

Current limits of E/Ms 9,10
are reduced to 598,400 amps
for calculation of 7.13 etc.

Fig. 7.5   Geometry of + configuration

Dimensions in metres. This config-
uration represents an enlarged
representation of SUMSBS

0.16∅

1.0

y'

x'

z'

J

Angle
of   (θ)
attack

x

z'
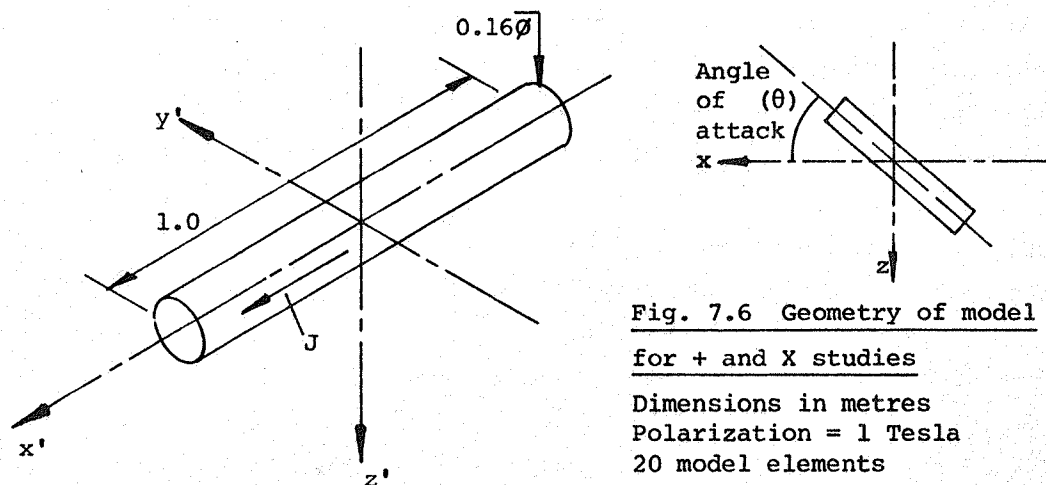
Fig. 7.6   Geometry of model

for + and X studies

Dimensions in metres
Polarization = 1 Tesla
20 model elements

Fig. 7.7 Couplings from + configuration individual E/Ms

E/Ms as Fig. 7.5

Model as Fig. 7.6

Data is shown specifically for only 4 E/Ms. Remaining E/Ms may be deduced from this data by symmetry, resulting in the sign table below:

Signs of force/torque components in:

Fig.7.7a

E/M	F_X	F_Z	M
1 (shown)	−	+	−
7	−	+	+

Fig. 7.7b

E/M	F_X	F_Z	M
3 (shown)	+	−	+
5	+	−	−

Fig.7.7c

E/M	F_X	F_Y	F_Z	L	M	N
2 (shown)	−	−	+	−	−	−
4	−	+	+	+	−	+
6	−	+	+	−	+	−
8	−	−	+	+	+	+

Fig.7.7d

E/M	F_X	F_Z	M
9 (shown)	+	+	−
10	+	+	+

Fig. 7.7a

+ Configuration
E/M 1 (7)

- 157 -
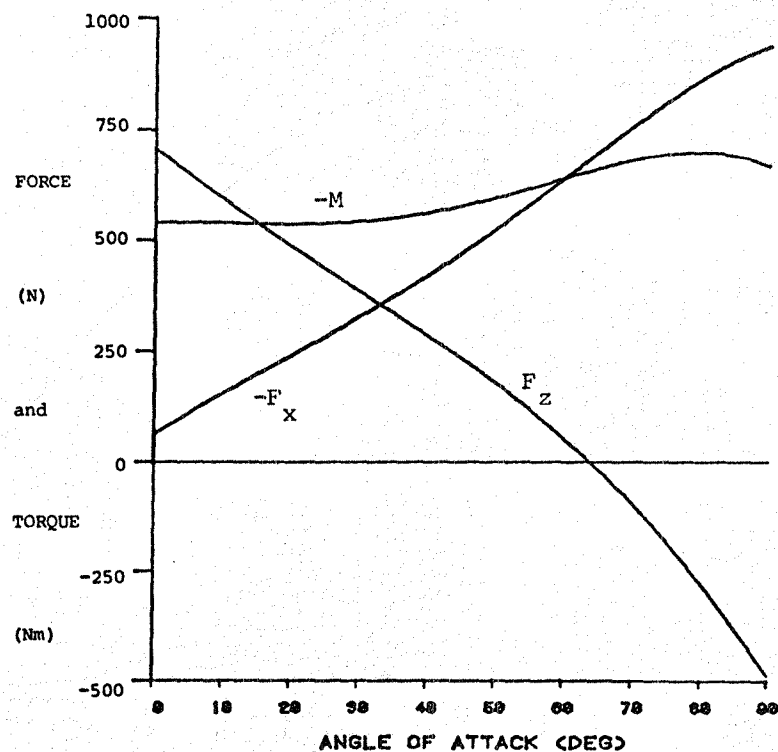
Fig. 7.7b

+ Configuration
E/M 3 (5)
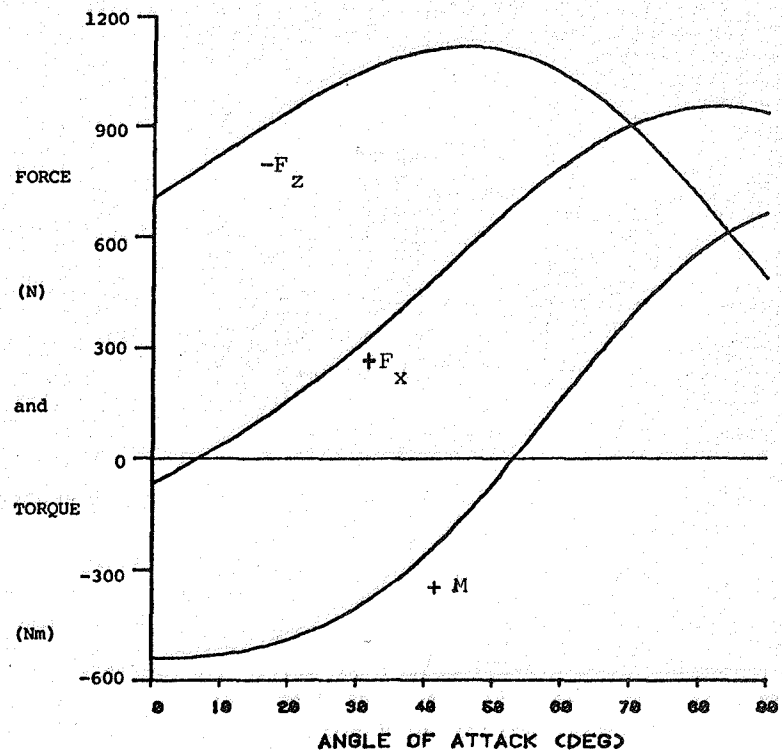
Fig. 7.7c(i)

+ configuration
E/M 2 (4,6,8)

Forces
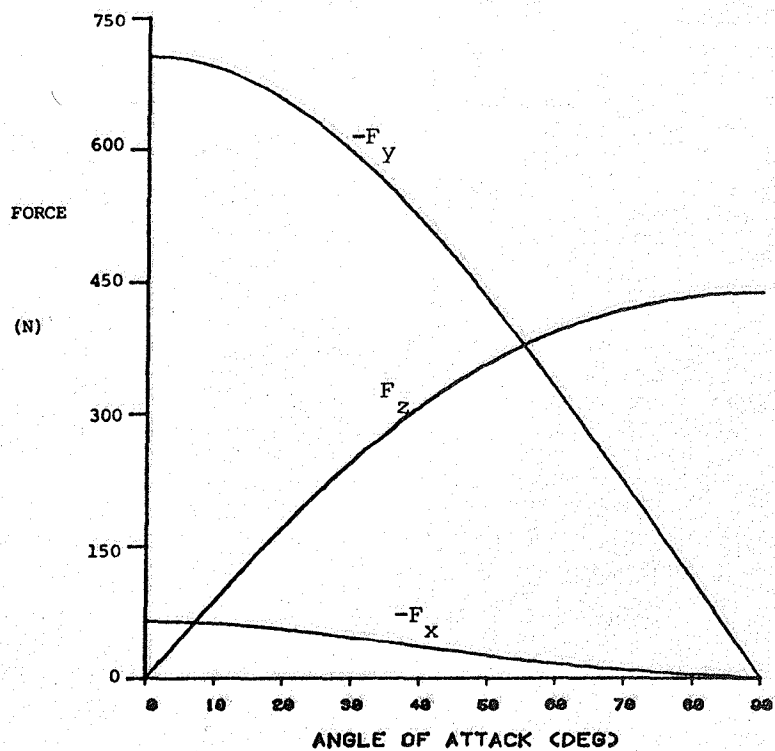
Fig. 7.7c(ii)

+ configuration
E/M 2 (4,6,8)

Torques
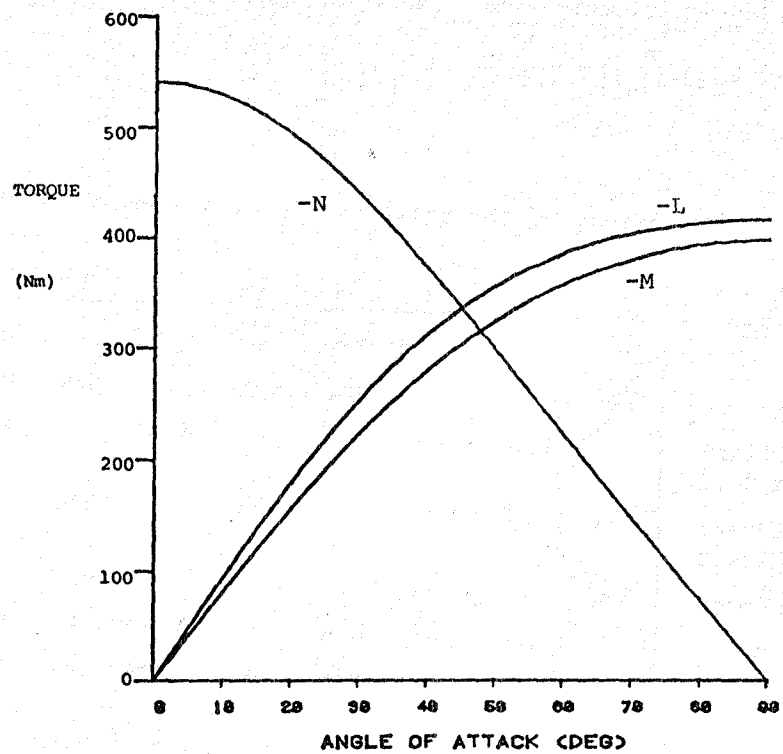
Fig. 7.7d

+ configuration
E/M 9 (10)
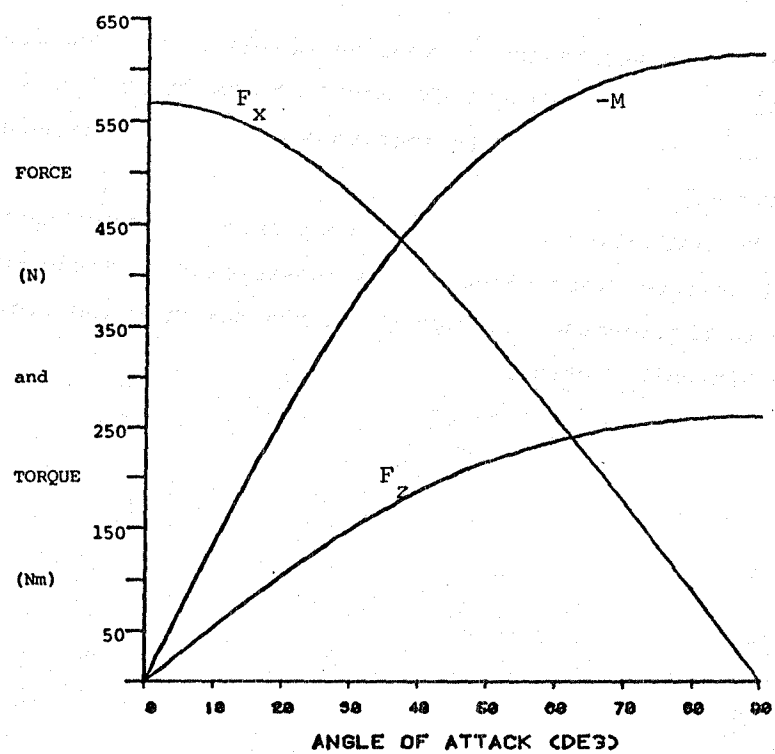
Fig. 7.8 Couplings from + configuration classical applied fields

E/Ms as Fig. 7.5

Model as Fig. 7.6

Fields are defined by the relationship of E/M currents as shown below:

Field	I_1	I_2	I_3	I_4	I_5	I_6	I_7	I_8	I_9	I_{10}
Lift	+	N/A	−	N/A	−	N/A	+	N/A	N/A	N/A
Drag	N/A	N/A	N/A	N/A	N/A	N/A	N/A	N/A	+	+
Auxiliary drag No.1	−	N/A	−	N/A	−	N/A	−	N/A	N/A	N/A
Auxiliary drag No.2	N/A	−	N/A	−	N/A	−	N/A	−	N/A	N/A
Sideforce	N/A	−	N/A	+	N/A	+	N/A	−	N/A	N/A
Pitch	−	N/A	+	N/A	−	N/A	+	N/A	N/A	N/A
Auxiliary pitch No.1	−	N/A	−	N/A	+	N/A	+	N/A	N/A	N/A
Auxiliary pitch No.2	N/A	−	N/A	−	N/A	+	N/A	+	N/A	N/A
Axial	N/A	N/A	N/A	N/A	N/A	N/A	N/A	N/A	−	+
Yaw	N/A	−	N/A	+	N/A	−	N/A	+	N/A	N/A

− following Fig. 7.5

This representation of applied fields is derived from the fields classically applied with the model at its datum position (lift, pitch etc.), augmented so as to encompass all possible combinations of currents.

The separation of Auxiliary Drag into two constituents (Figs.7.8c & d) is done since simultaneous application of these two fields with one in the reverse sense produces the through-wing field used in SUMSBS for SPM roll control.

Fig. 7.8a

Lift field
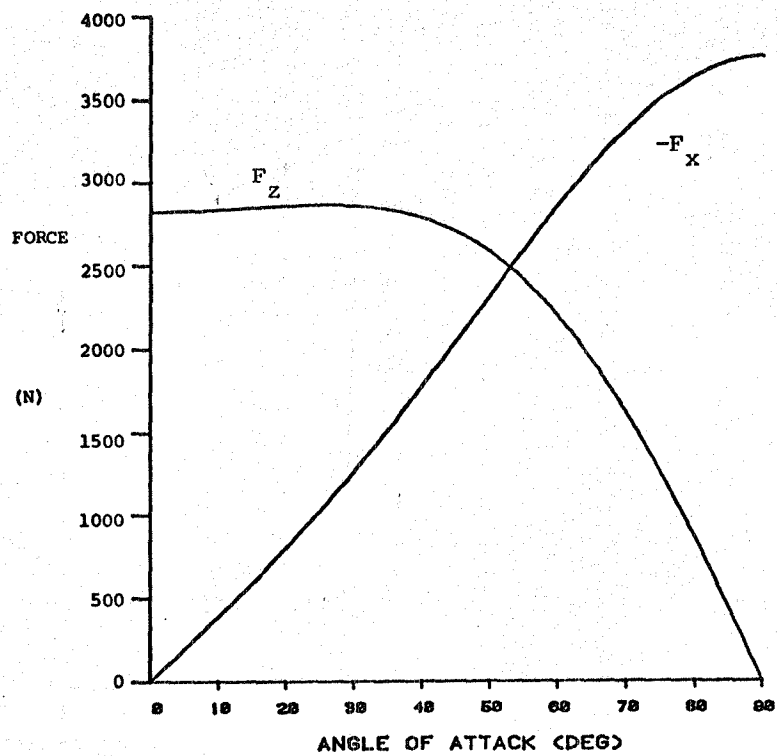
Fig. 7.8b

Drag field
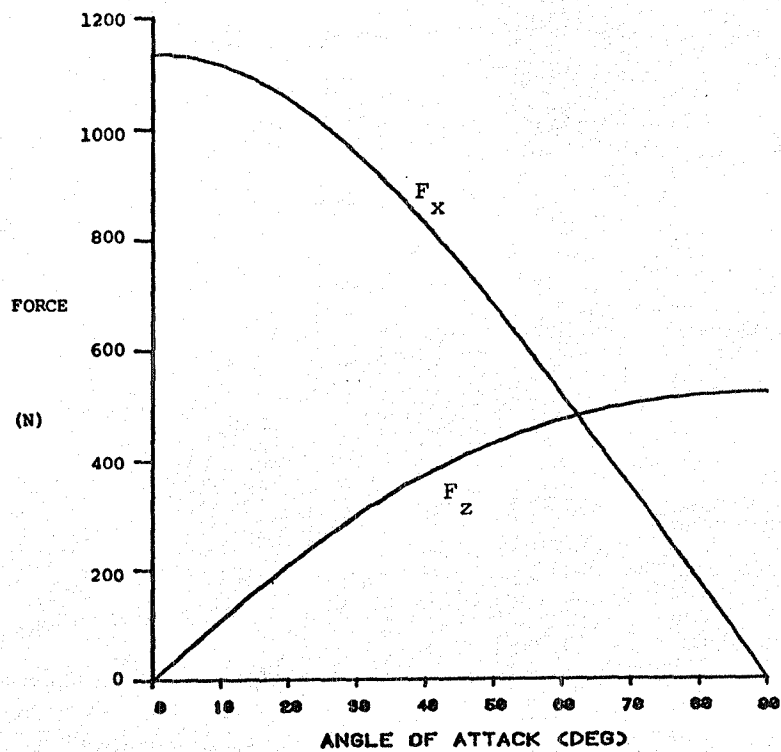
Fig. 7.8c

Auxiliary drag
No.1 field
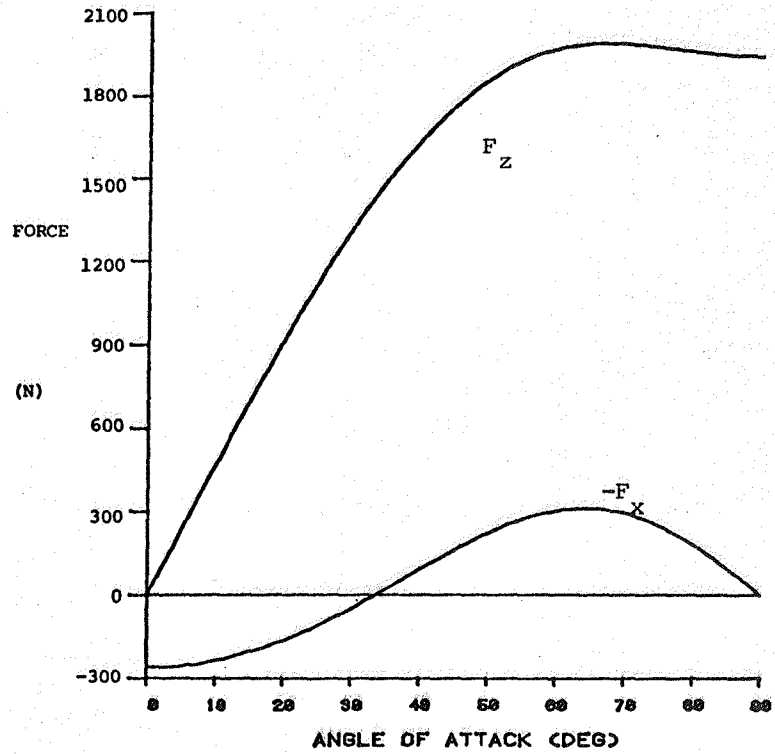
Fig. 7.8d

Auxiliary drag
No.2 field
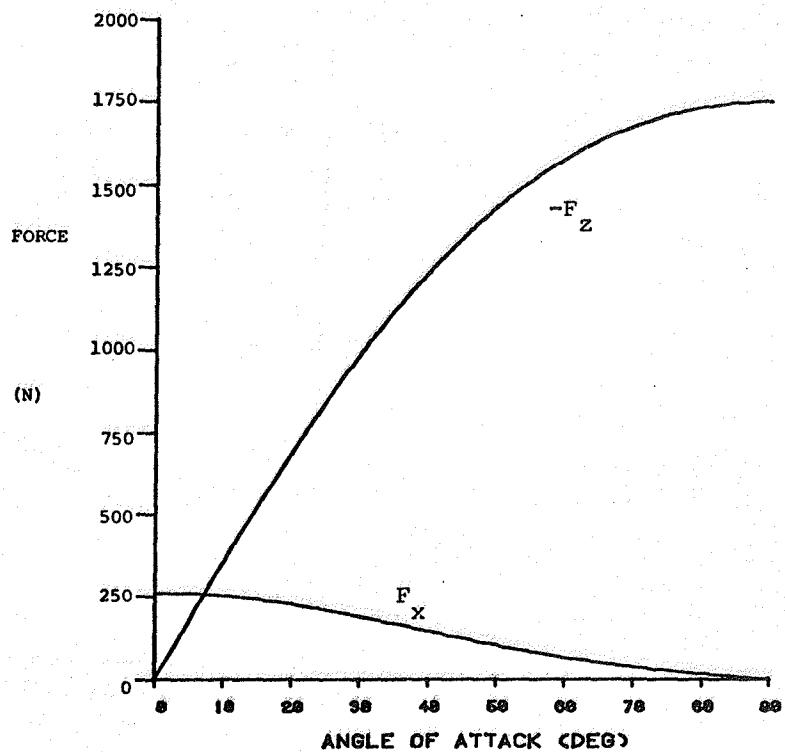
Fig. 7.8e

Fig. 7.8e

Sideforce field

FORCE

(N)

F_y

ANGLE OF ATTACK (DEG)

Fig. 7.8f

Pitch field

TORQUE

(Nm)

M

ANGLE OF ATTACK (DEG)
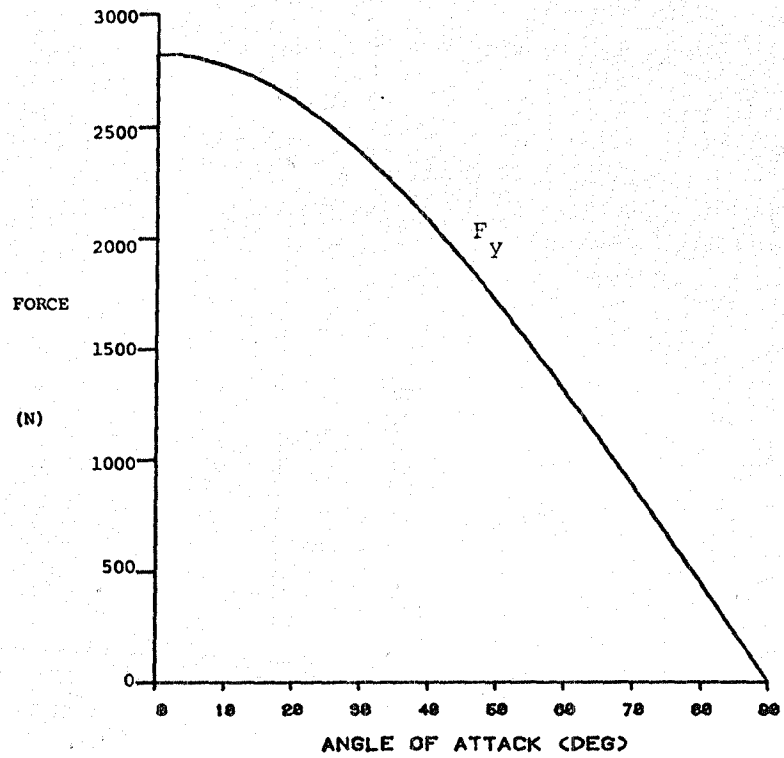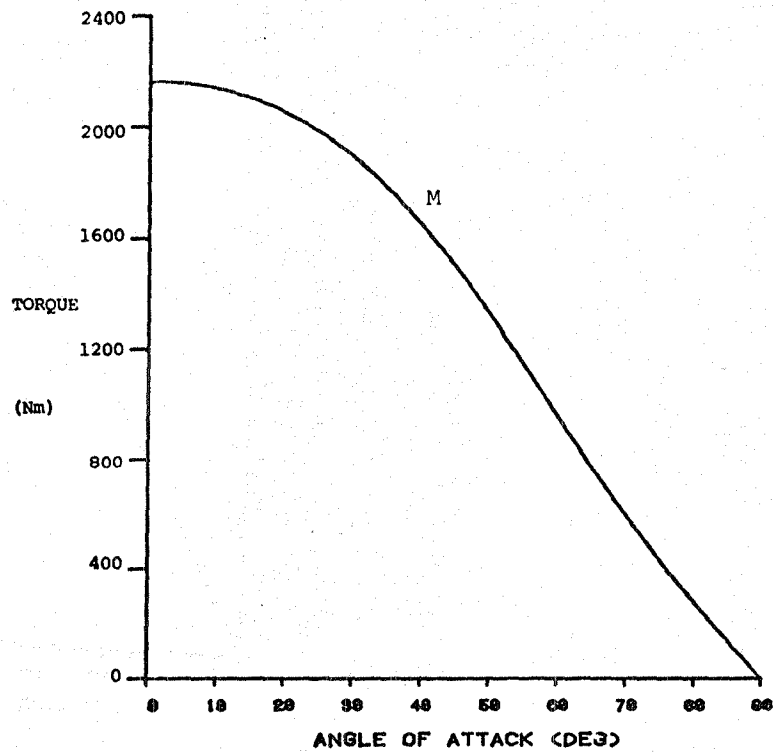
Fig. 7.8g

Auxiliary pitch
No.1 field

TORQUE

(Nm)

M

ANGLE OF ATTACK (DEG)
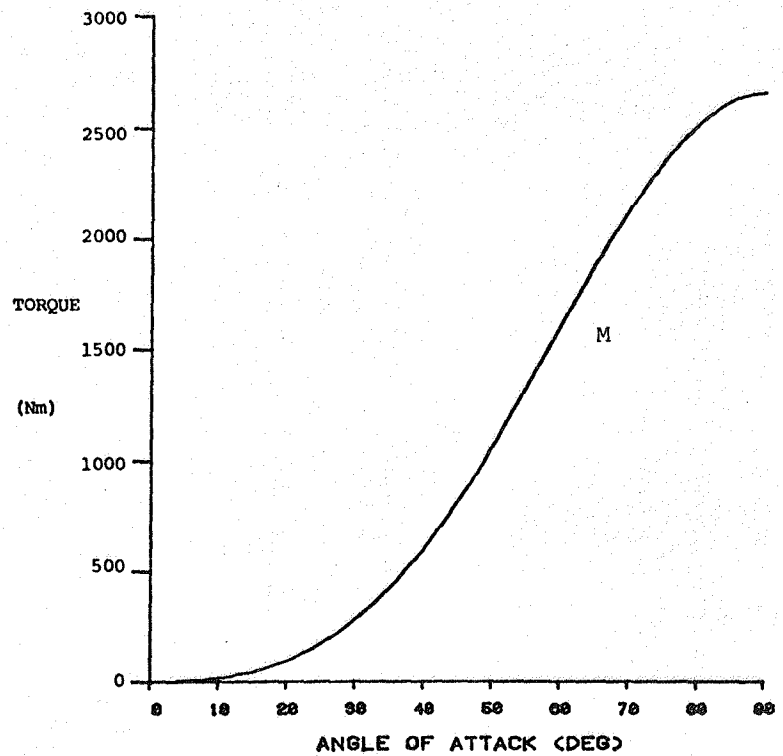
Fig. 7.8h

Auxiliary pitch
No.2 field

TORQUE

(Nm)

M

ANGLE OF ATTACK (DEG)
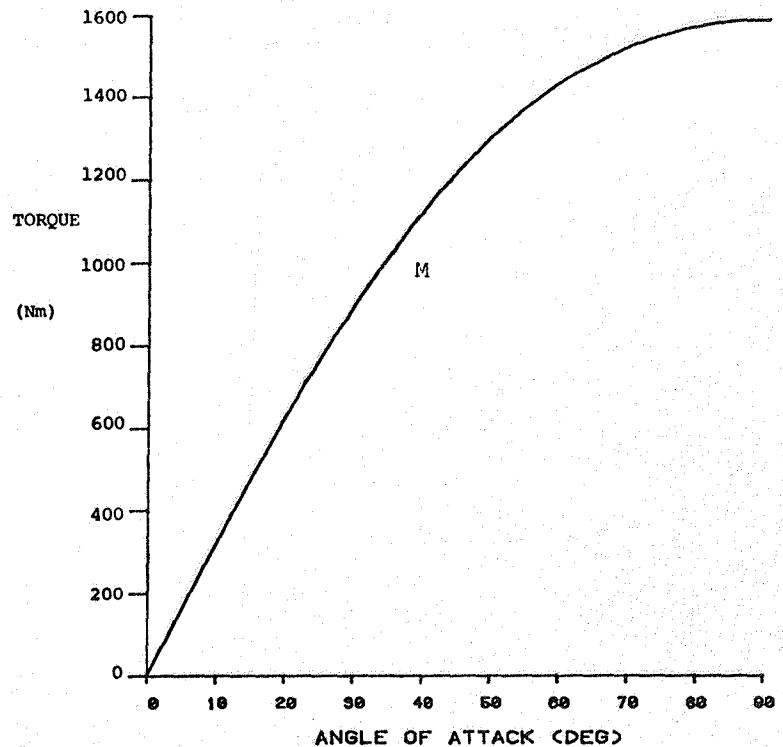
Fig. 7.8i
Axial field

Fig. 7.8j
Yaw field
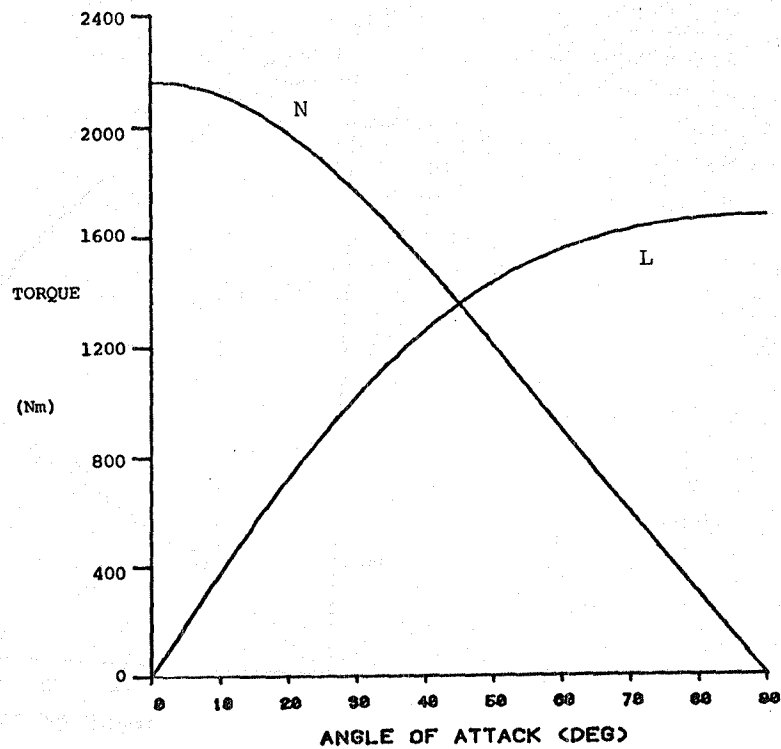
Fig. 7.9a

+ configuration

Lift field
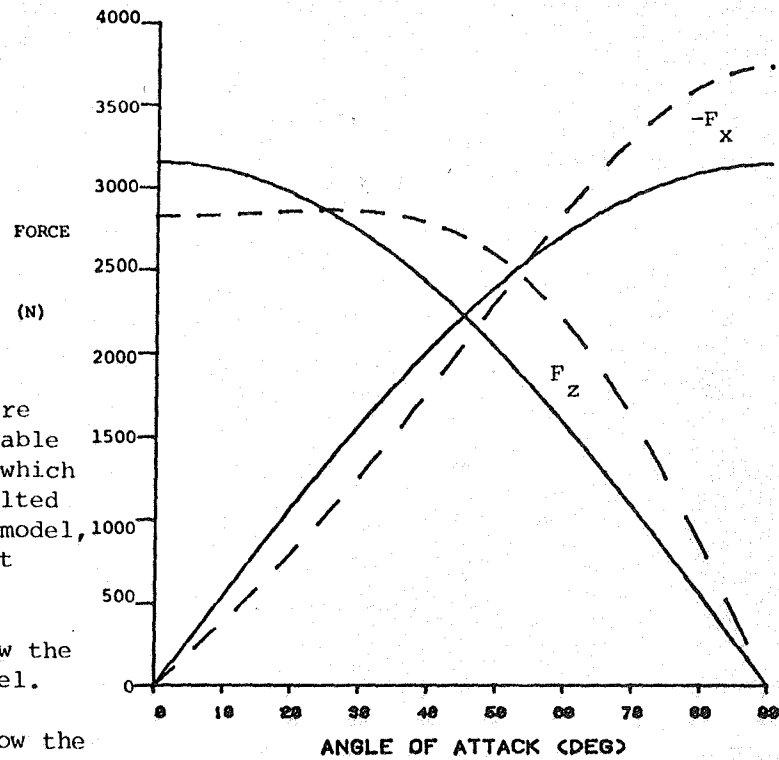
These Figures are directly comparable with Figs.7.8, which should be consulted for details of model, E/Ms and current relationships.

SOLID lines show the zero volume model.

BROKEN lines show the standard model, and **are** identical to the corresponding Figs.7.8

Fig. 7.9b

+ configuration
Drag field
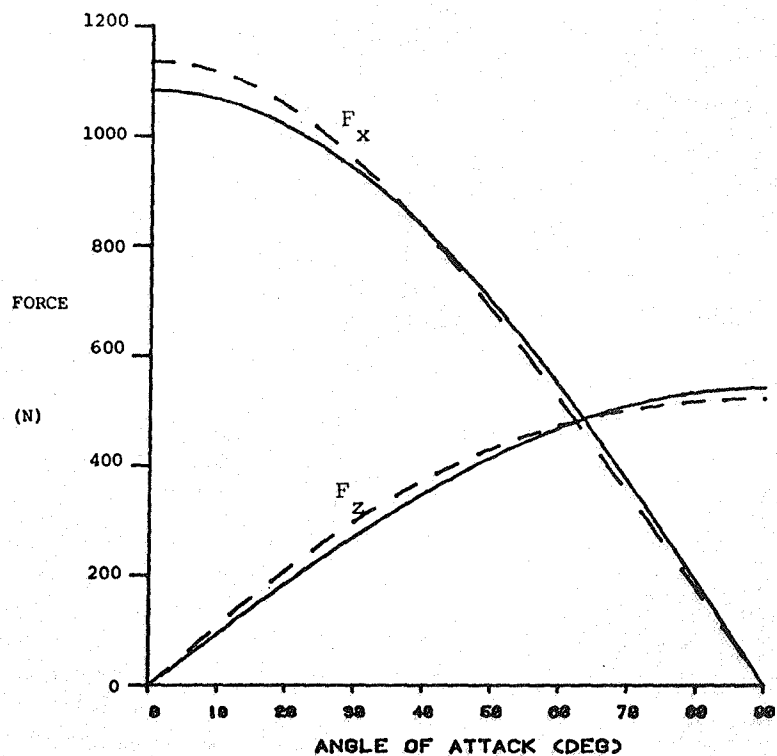
Fig. 7.9c

+ configuration
Auxiliary drag
No.1 field
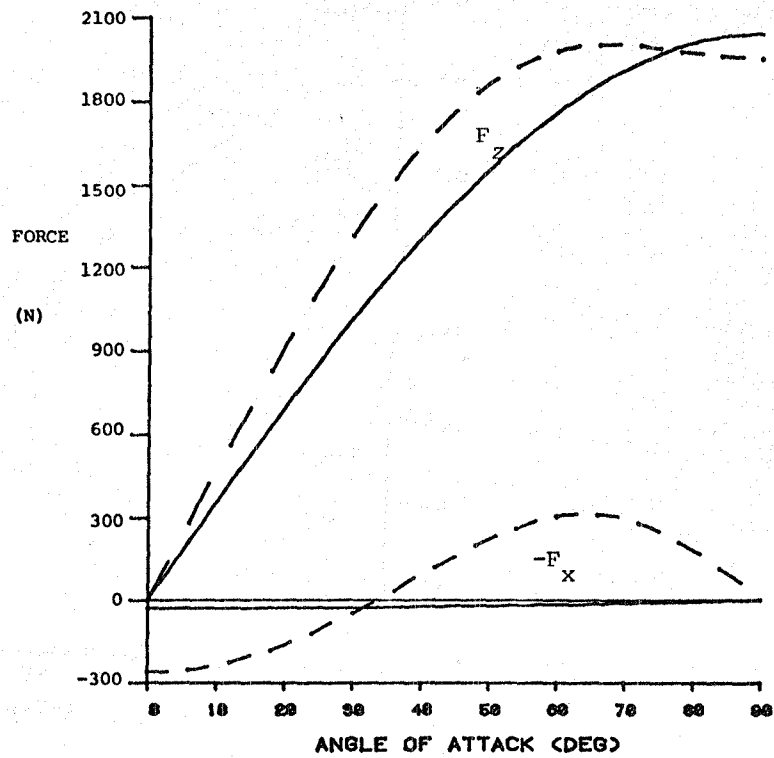
Fig. 7.9d

+ configuration
Auxiliary drag
No.2 field
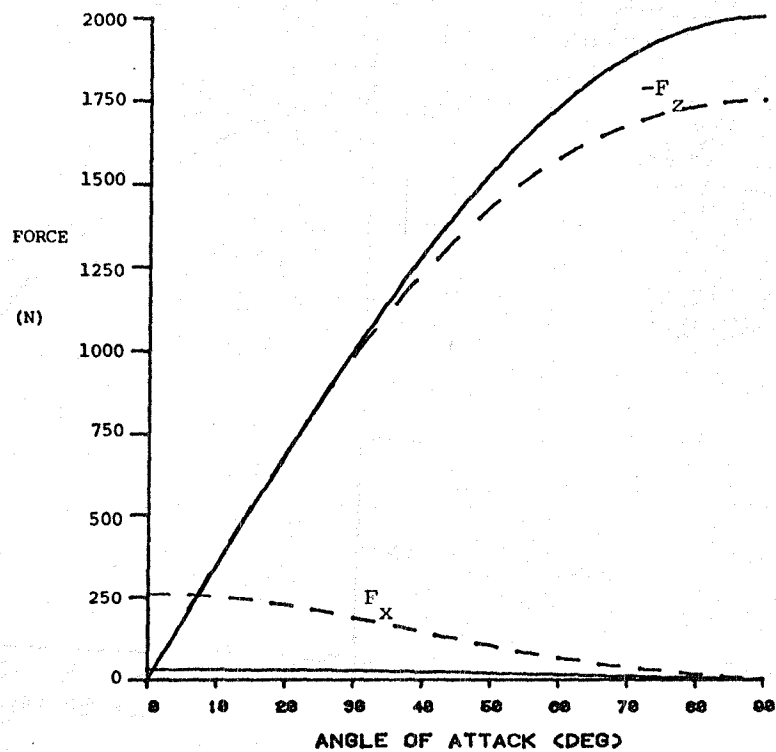
Fig. 7.9e
+ configuration
Sideforce field

FORCE

(N)

F_y

ANGLE OF ATTACK (DEG)
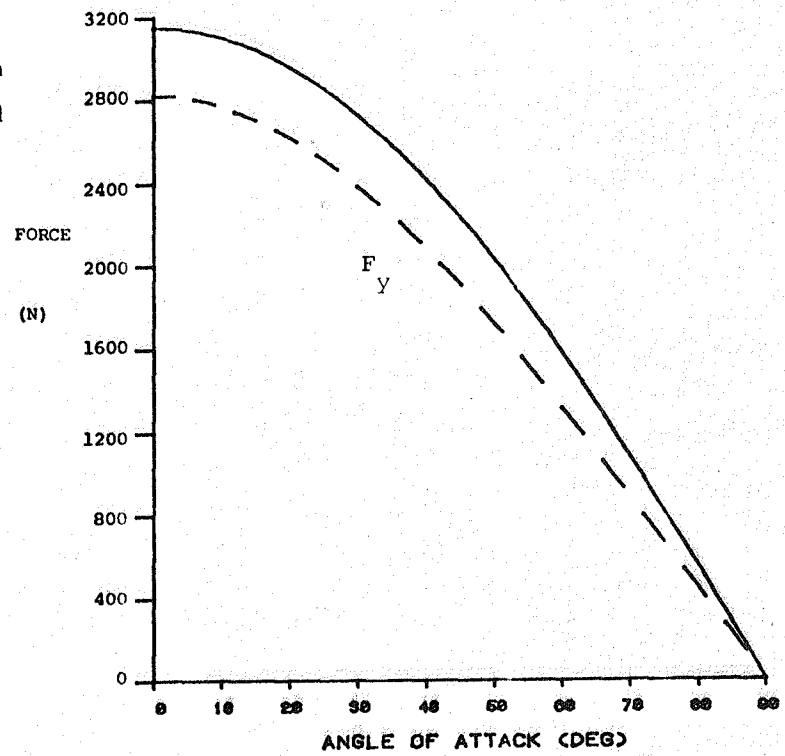
Fig. 7.9f
+ configuration
Pitch field

TORQUE

(Nm)

M

ANGLE OF ATTACK (DEG)
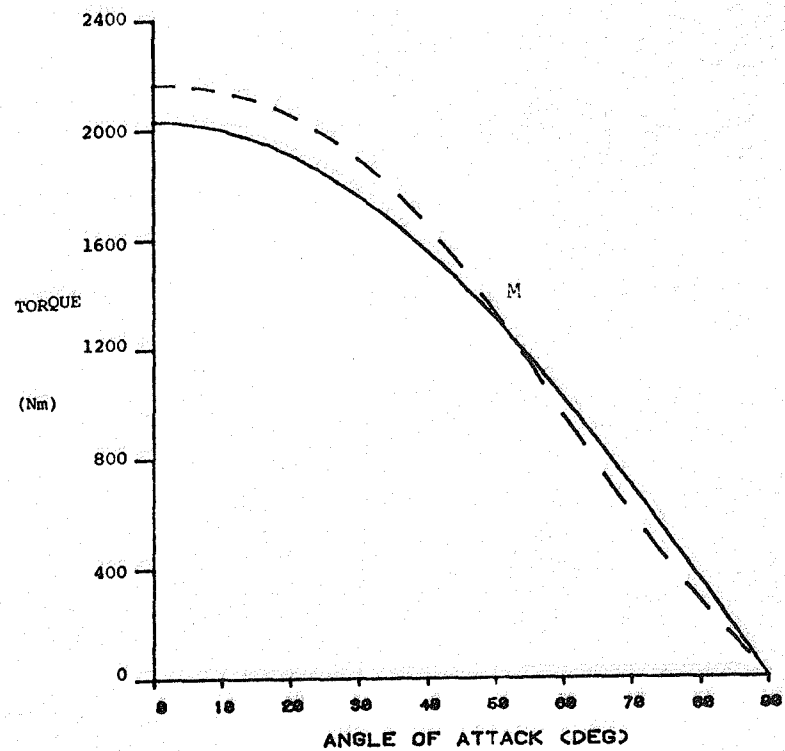
Fig. 7.9g

+ configuration
Auxiliary pitch
No.1 field
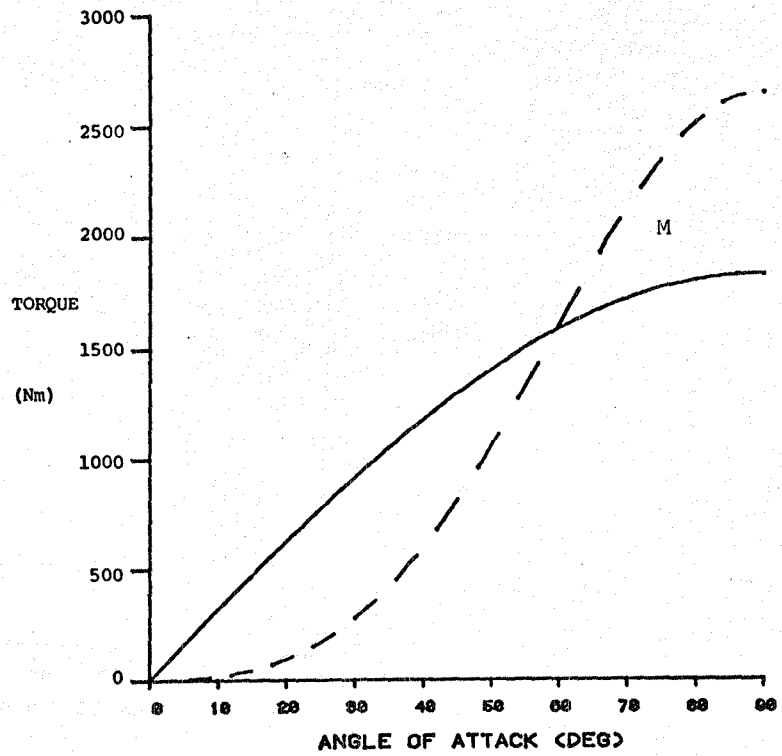
Fig. 7.9h

+ configuration
Auxiliary pitch
No.2 field
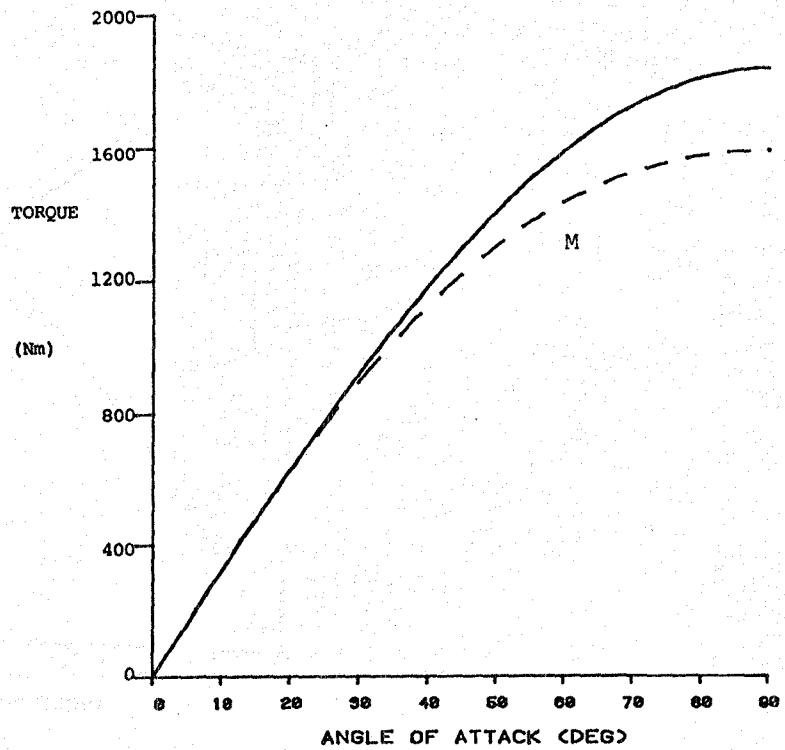
Fig. 7.9i

+ configuration
Axial field

TORQUE

(Nm)

ANGLE OF ATTACK (DEG)
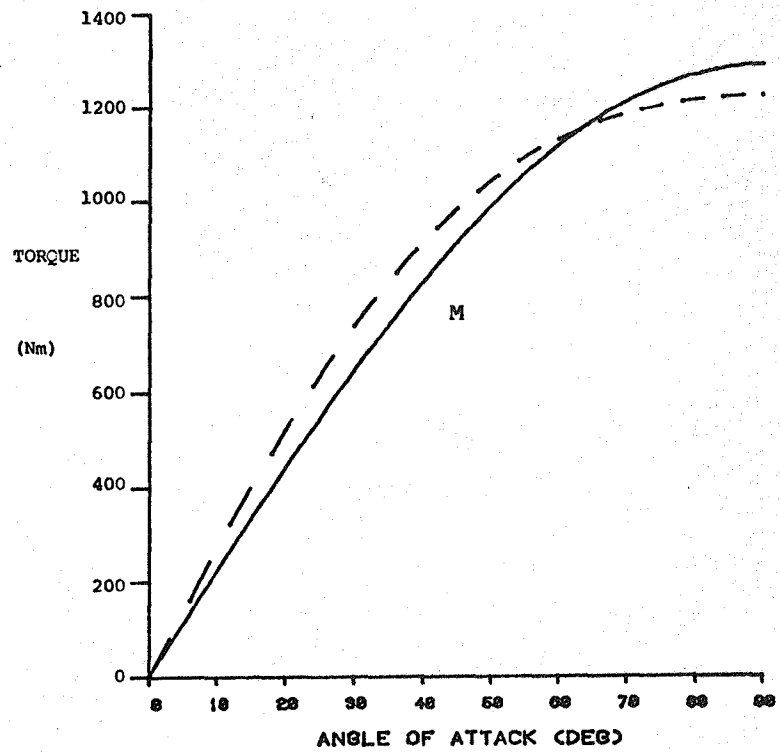
Fig. 7.9j

+ configuration
Yaw field

TORQUE

(Nm)

ANGLE OF ATTACK (DEG)

- 170 -
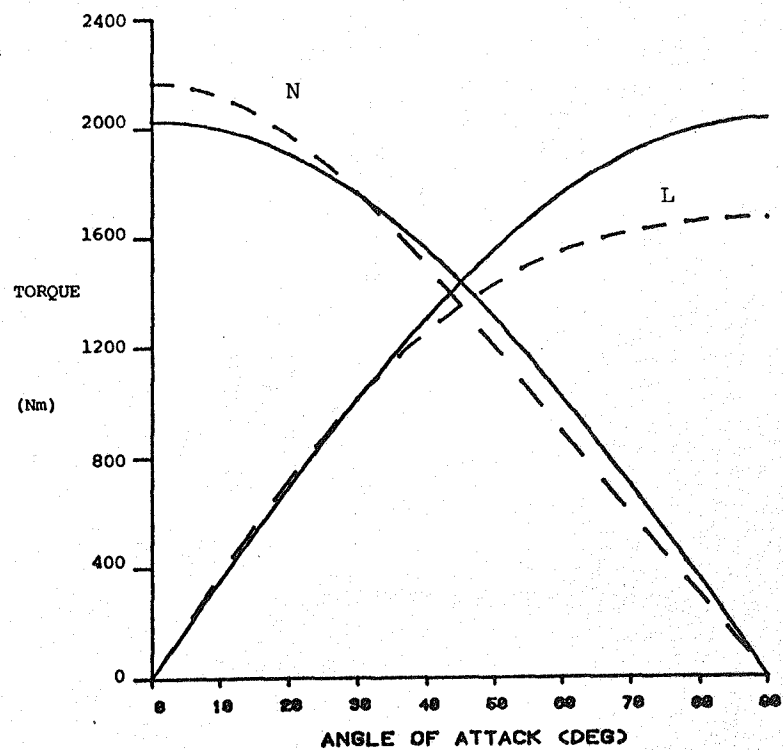
Table 7.2 Field capabilities for + configuration

Field components (T) / 10^6AT /E/M

E/M grouping	B_{xx_o}	B_{xy_o}	B_{xz_o}	B_{yy_o}	B_{yz_o}	B_{zz_o}	B_{x,y,z_o}
Lift	0	0	0.1969	0	0	0	0
Drag	0.0676	0	0	-0.0338	0	-0.0338	0
Auxiliary drag 1	0.002	0	0	0.1252	0	-0.1272	0
Auxiliary drag 2	0.002	0	0	-0.1272	0	0.1252	0
Sideforce	0	0.1969	0	0	0	0	0

	B_{x_o}	B_{y_o}	B_{z_o}	All gradients
Pitch	0	0	-0.1267	0
Auxiliary pitch 1	-0.1147	0	0	0
Auxiliary pitch 2	-0.1147	0	0	0
Axial	-0.0808	0	0	0
Yaw	0	0.1267	0	0

The correlation between the couplings for the representative model and the zero volume model, the latter being essentially theoretical results, is generally fair, the cases where the E/Ms are relatively remote from the model (Figs. 7.9b, 7.9h) exhibiting the best agreement. The "theoretical" curves may thus be adequate for synthesis of experimental control algorithms, provided generous stability margins are available and such algorithms would not then require updating following minor model changes. Peak performance of the system is, however, unlikely to be approached unless the computed couplings of Fig. 7.8 or similar are used directly.

The variations of the maximum force and torque capability can be found from the data in Fig 7.7 using the methods of Section 7.3. Again there is difficulty due to the range of possible combinations of model forces and torques. However magnetic torque capability, apart from roll torque, is seldom a critical factor in MSBSs and with model excursions restricted to the pitch plane, sideforce capability may be largely neglected. Figs. 7.10(a-b) thus illustrate the maximum force capability for the representative + system with the force vector constrained to lie in the plane of pitching and with all torques zero. The sense of the force vector is clarified in Fig.7.11.

Fig. 7.10 Maximum performance of the + configuration

FORCE (N)

ANGLE OF ATTACK (DEG)

β=90°

80°

70°

60°

50°

40°
30°
20°
10°
β=0°

FORCE (N)

ANGLE OF ATTACK (DEG)

-70°

-80°

-90°

-60°

-50°

-40°

-30°

β=0°

-10°

-20°

F_y =L=M=N=0

E/Ms as Fig.7.5
Model as Fig.7.6
Force vectors as Fig.7.11
Current limits for E/Ms
  9,10 reduced to 598,400A
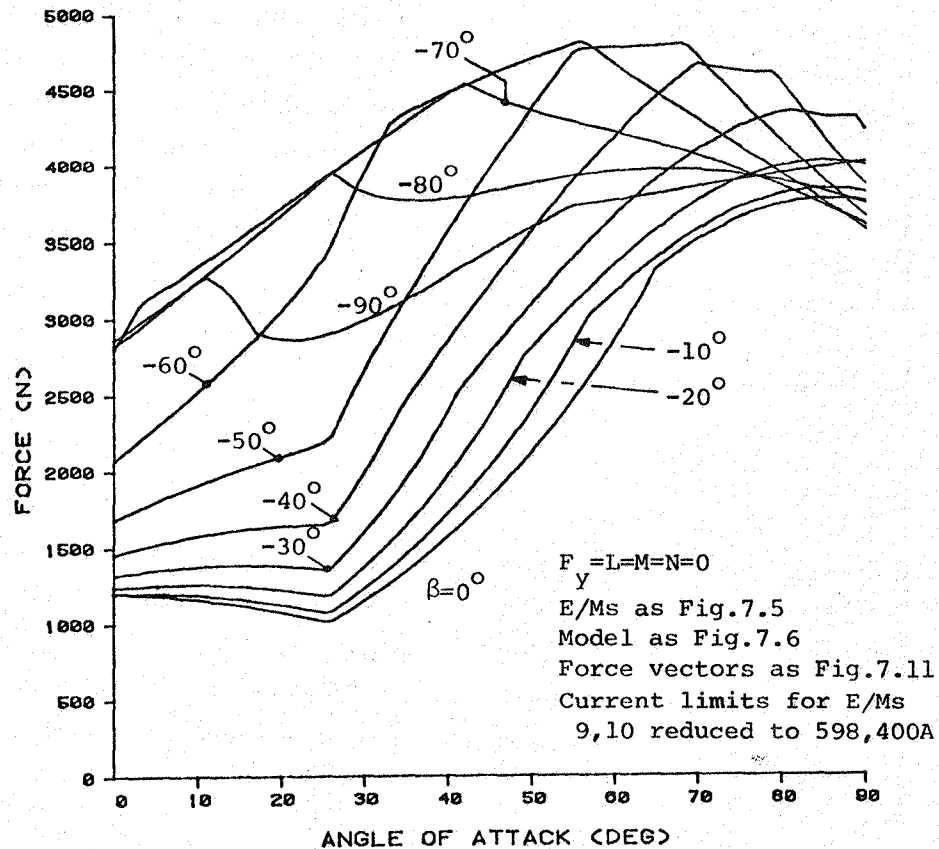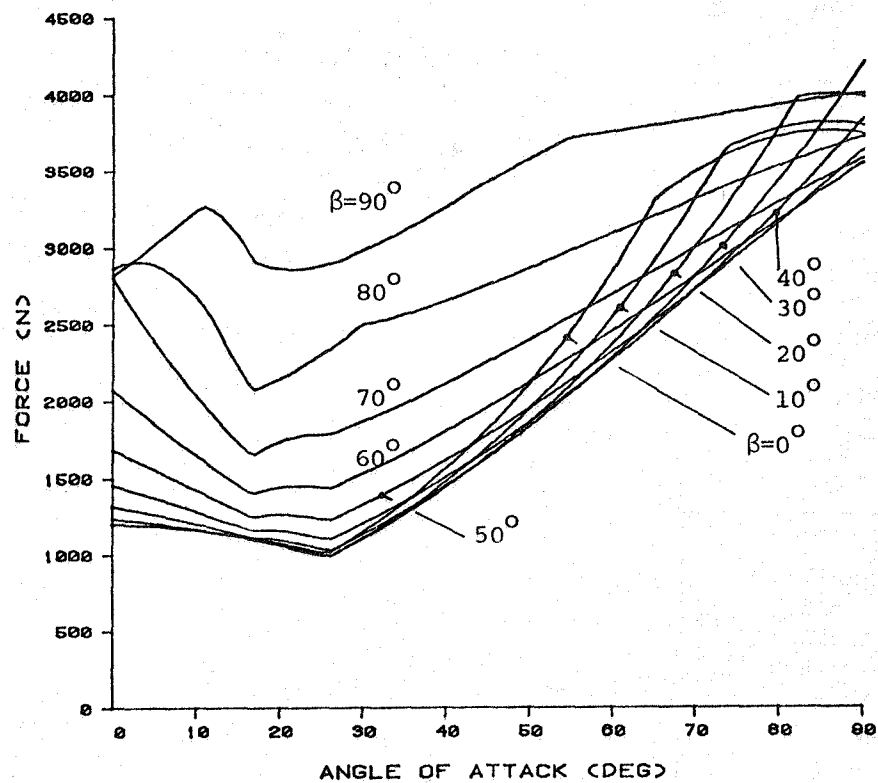
The direction of the magnetic force vector required to oppose the net aerodynamic force would normally be expected to lie in the quadrant defined by $0 \leqslant \beta \leqslant 90^\circ$. Transient forces may be outside this range, as may be the model's weight vector. However, for the purpose of identifying the absolute maximum force capabilities of a MSBS, and since the curves of Fig. 7.10 are repeated for $\beta \rightarrow \beta \pm 180^\circ$ the $0 \leqslant \beta \leqslant 90^\circ$ quadrant is seen to be of principal interest. Some of the content of Fig. 7.10 may now be simplified by choosing three components of aerodynamic significance, namely pure lift force, pure drag force and normal force, all defined in Fig. 7.12, and adding the envelopes within which all curves for $0 \leqslant \beta \leqslant 90^\circ$ must lie (Fig. 7.13). The axial E/M current limits (E/Ms 9 and 10) have been factored by 0.5984 to approximate the measured relative performance of the main and axial E/Ms in SUMSBS. Computation for the zero volume model is illustrated in Fig. 7.14 and exhibits significant differences in certain areas, such as drag forces at low angles of attack. Effects of variations in the E/M array geometry are well illustrated with this form of presentation. For instance, doubling the current limit applied to the axial E/Ms (E/Ms 9 and 10) increases, as would be expected, the drag force capability at small angles of attack but also attenuates the otherwise rapid fall off in normal force capability with angle of attack increasing from small angles (Fig. 7.15).

The discontinuities in slope of the curves in Figs. 7.13 - 7.15 are caused by changes in the distribution of E/M current limiting, for example at some particular angle of attack E/Ms 1 and 7 (say) may be operating below their current limits, with all other E/Ms at their respective limits (see Section 7.3). Small increases in angle of attack may result in the currents in E/Ms 1 and 7 increasing, other currents remaining fixed, and at some angle all E/Ms will be at their limiting currents. Further increases in angle of attack will generally require E/Ms other than E/Ms 1 and 7 to be reduced in current, overall performance then being delineated effectively by a different performance curve. This may be illustrated for one case, chosen to be the normal force curve from Fig. 7.13, Fig. 7.17 clearly showing the changing E/M current distributions.

7.4.3 Discussion

Reserving treatment of the significance of the absolute magnitudes

Fig. 7.11 Sense of general
magnetic force vector
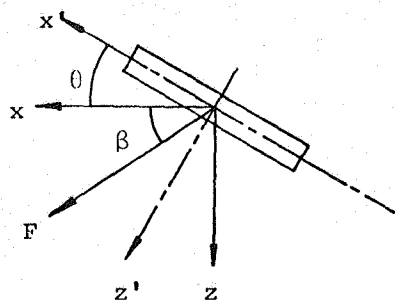
Fig. 7.12 Sense of drag, lift
and normal force vectors

$(0 \leq \beta \leq 90^{\circ})$
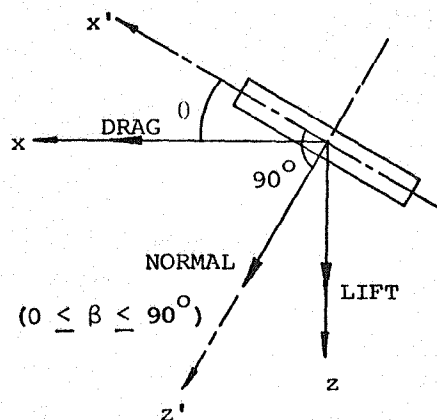
Fig. 7.13 Maximum performance of the + configuration
E/Ms as Fig. 7.5   Model as Fig. 7.6   Force vectors as Fig. 7.12

Pure
lift

Best case
β's

Pure
drag

Normal
force

Worst case β's

$(0 \leq \beta \leq 90^{\circ})$

FORCE (N)

ANGLE OF ATTACK (DEG)

- 174 -

Fig. 7.14   Maximum performance of the + configuration with zero
volume model. Otherwise as Fig. 7.13

Fig. 7.15   Maximum performance of the + configuration with E/Ms
9,10 doubled in strength.   Otherwise as Fig.7.13
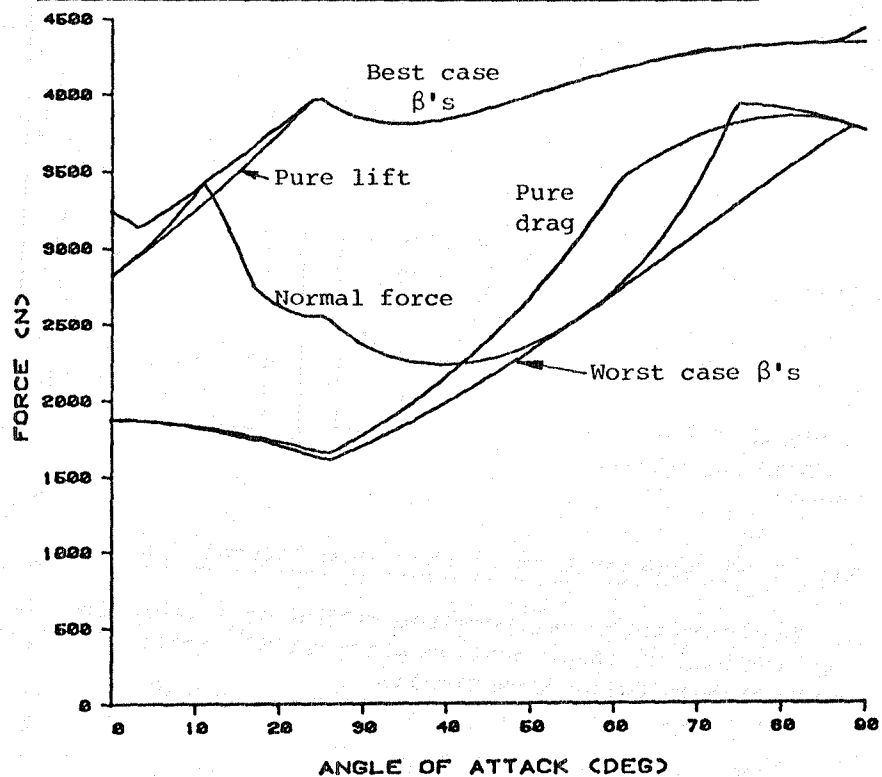
Diagrams are schematic only

Both sides skewed
in the same sense

Opposite sides
skewed in opposite
senses
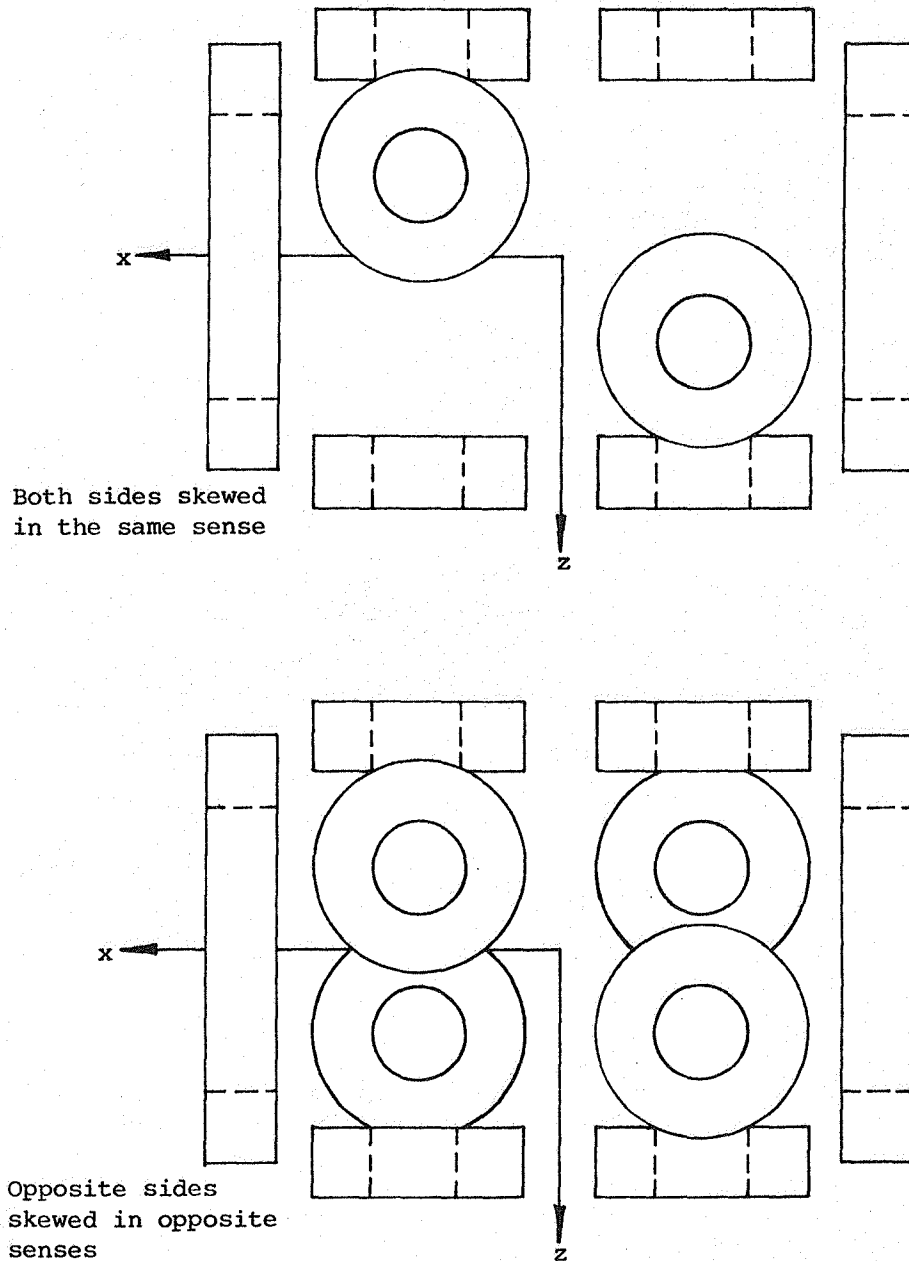
Fig. 7.16 Incorporation of skew into lateral E/Ms

This represents one possible method of alleviating the poor performance of the + configuration at 90° angle of attack, but has not been fully investigated.

Skewed lateral E/Ms produce sideforce at 90°
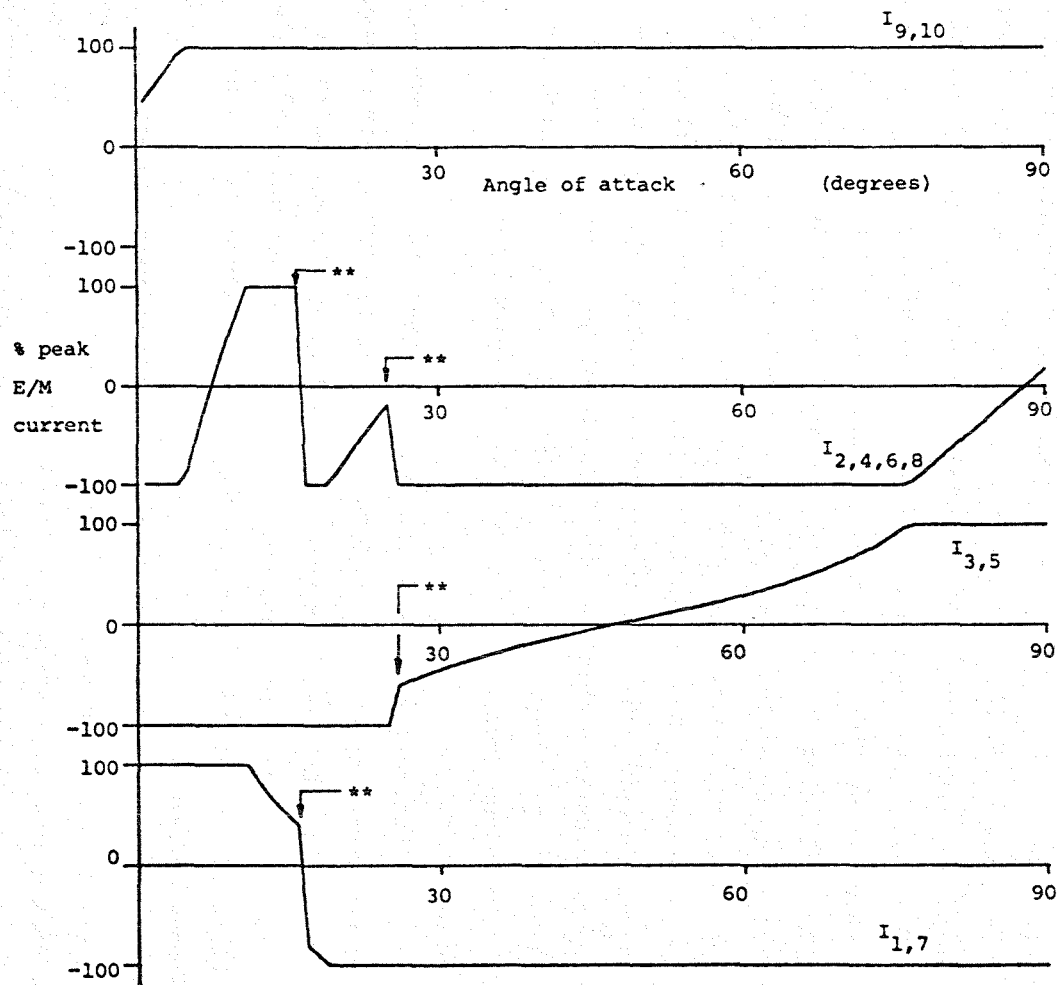
Fig. 7.17   E/M current requirements for maximum normal force generation

As Fig.7.13

** Points marked thus correspond to instantaneous changes of current but appear as having finite slope due to the discretization of the calculations.

of forces and moments in Figs. 7.7 - 7.10 and 7.13 - 7.15 for

Section 7.7, the computed couplings do nevertheless indicate the

practicality of the particular + configuration geometry studied

for high angle of attack testing.

Figs. 7.10 and 7.13 clearly illustrate that the principal aero-

dynamic forces (appearing in the plane of pitching) can be

countered relatively effectively at most angles of attack with

only the normal and drag force minima around 30° angle of attack

presenting any serious difficulty. Augmentation of the main

drag field partially alleviates this problem, the severity of which

is heavily dependent on the precise geometry (see (49)). Without

indulging in further analysis it is concluded from Figs. 7.8f-j

that sufficient capability for the purposes of generating pitch and

yaw torques (roll not being treated here) exists at all angles of

attack, leaving only one fundamental flaw in the E/M configuration,

that is the inability to generate sideforce at 90° angle of attack

(Fig. 7.8e). This is due to the lack of capability in H_{yz}, which

was shown in Section 7.2.1 to be required for this purpose.

The particular geometry studied appears to be practical for

operation up to at least 60° angle of attack, then being limited

principally by falling sideforce capability. It is thought that

this view remains broadly valid for all + configurations of con-

ventional proportions (49), though detail optimisation of perfor-

mance is clearly possible. One example of this might be the in-

corporation of "skew" into the lateral E/Ms (Fig. 7.16), although

this technique does partially destroy the symmetry of the

configuration.

It is important to recall at this stage that the field component

required for generation of roll torque using the SPM or SIM schemes

is H_{yz}. If the E/M array were augmented in such a way so as to

include capability for this component, then operation to 90° angle

of attack and, in fact, through 360° pitch attitude range would

appear possible.

The somewhat bizarre fluctuations in E/M currents apparently

required to achieve maximum force capability with rising angles of

attack (Fig. 7.17) are almost certainly impractical due to the low

E/M current slewing rates available in realistic MSBSs. However,

the complete reversals of current occurring with small increases in

angle of attack at certain points in Fig. 7.17 generally indicate
that the E/M in question is relatively ineffective in generating
force in the required sense at that particular attitude. Approxi-
mation to the absolute maximum performance with appropriate
restrictions on current fluctuations are thus expected to be possible
with relatively small performance degradation, though no analysis
has yet been attempted.

7.5 "X" E/M configuration study
7.5.1 Geometry

The lack of capability in H_{yz} of the + configuration can be
rectified by simply rotating the model's axis system (in the roll
sense) so as to convert the + configuration to an X configuration.
A representation of this version of SUMSBS has been computed, using
identical E/M and model geometry and characteristics as the represen-
tative + system of Section 7.4 (Fig. 7.18).

7.5.2 Performance

Following identical analytic procedures to those employed for the
+ system, Figs. 7.19a-b show the main E/M couplings, those from the
axial E/Ms (E/Ms 9 and 10) remaining as shown in Fig. 7.7d. Figs.
7.20a-g show the couplings from classical E/M groupings, with
couplings to the zero volume model presented in Figs. 7.21a-g.
Immediately it can be seen that sideforce capability exists at 90°
angle of attack (Figs. 7.20/7.21d).

Computing the maximum force capabilities in the plane of pitching
yields a disappointing result (Fig. 7.22). Although the lift force
capability at zero angle of attack is augmented, compared to the +
configuration, as would be expected since all 8 main E/Ms now contri-
bute to lift force, the performance around 45° angle of attack is
disastrous. The zero volume model exhibits similar results
(Fig. 7.23), whilst doubling the axial E/M strength effects a
significant but probably inadequate improvement (Fig. 7.24).

Eqns. 7.3 etc. may be used to illustrate the reason for the
poor performance around 45°, using the (calculated) field
capabilities of the E/M groupings :

+ geometry as shown
in Fig. 7.5

E/Ms (3) & 7

E/Ms (4)
& 8

E/Ms (2)
& 6

y

Rotation of entire
array by 45° about
the x axis

E/Ms (1) & 5

z

X geometry

E/Ms (4)
& 8

E/Ms (3) & 7

y

E/Ms (1)
& 5

E/Ms (2) & 6

z
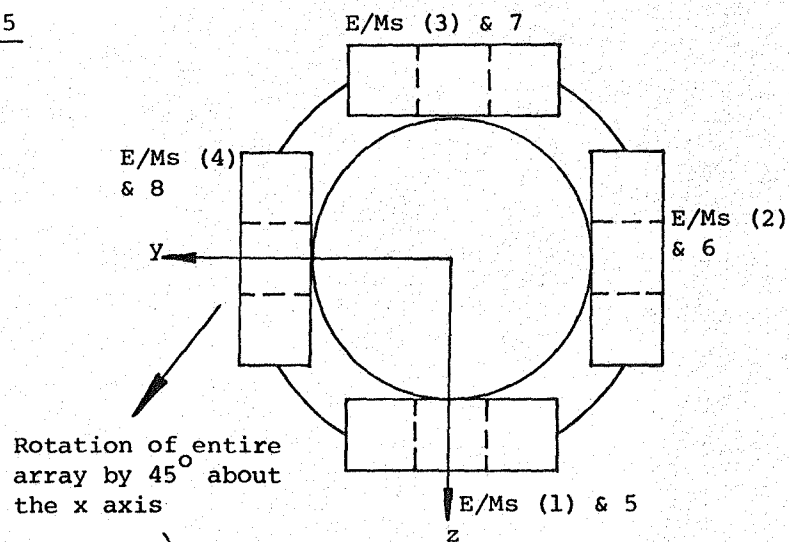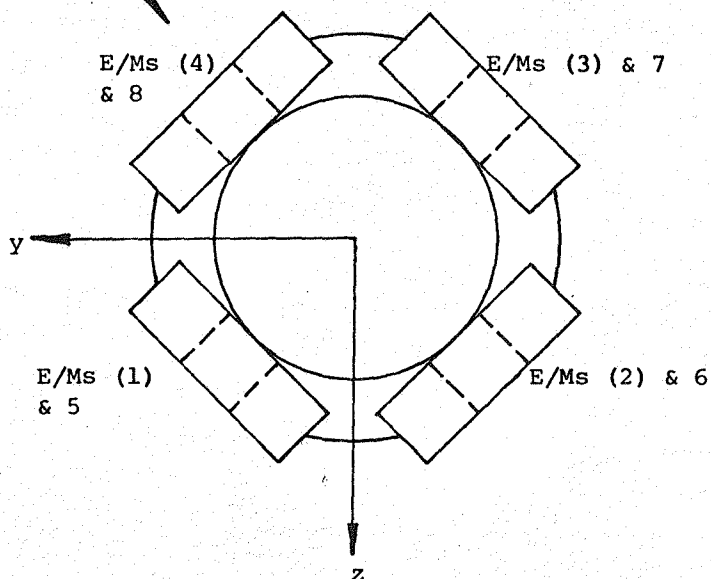
Fig. 7.18 Derivation of X configuration geometry

Both geometries shown schematically and in Section through the

yz plane

Fig. 7.19 Couplings from X configuration individual E/Ms

E/Ms as Fig. 7.18
Model as Fig. 7.6

Data is shown specifically for only 2 E/Ms. E/Ms 9 and 10 remain
as shown in Fig. 7.7d. Remaining E/Ms may be deduced from the data
shown by symmetry, resulting in the sign table below:

Signs of force/torque components in Fig. 7.19a

E/M	F_x	F_y	F_z	L	M	N	
1	−	+	+	+	−	+	(shown)
2	−	−	+	−	−	−	
7	−	+	+	−	+	−	
8	−	−	+	+	+	+	

Signs of force/torque components in Fig. 7.19b

E/M	F_x	F_y	F_z	L	M	N	
3	+	−	−	−	−	−	(shown)
4	+	+	−	+	−	+	
5	+	−	−	+	+	+	
6	+	+	−	−	+	−	

Fig. 7.19a(i)

X configuration
E/M 1 (2,7,8)
Forces
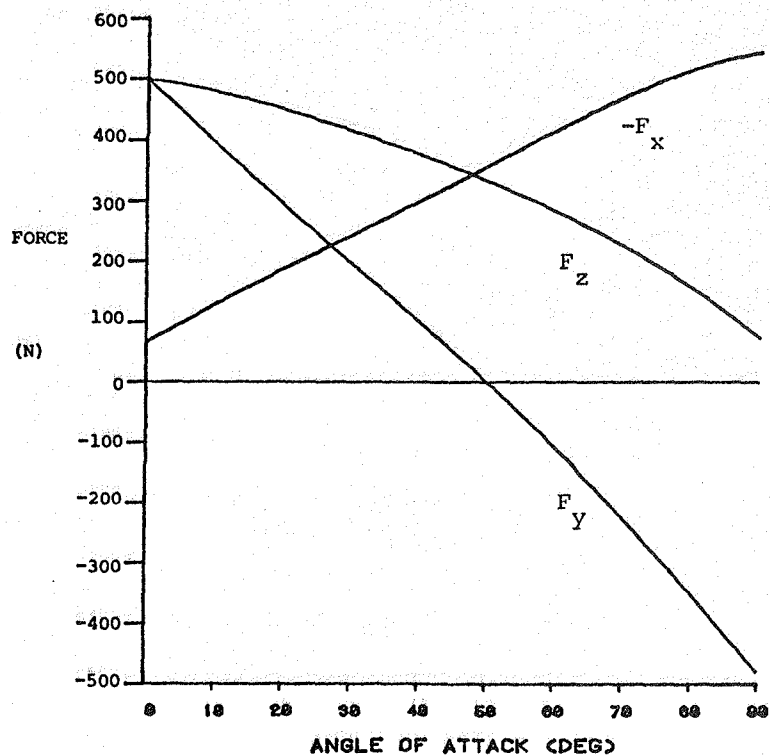
Fig. 7.19a(ii)

X configuration
E/M 1 (2,7,8)
Torques
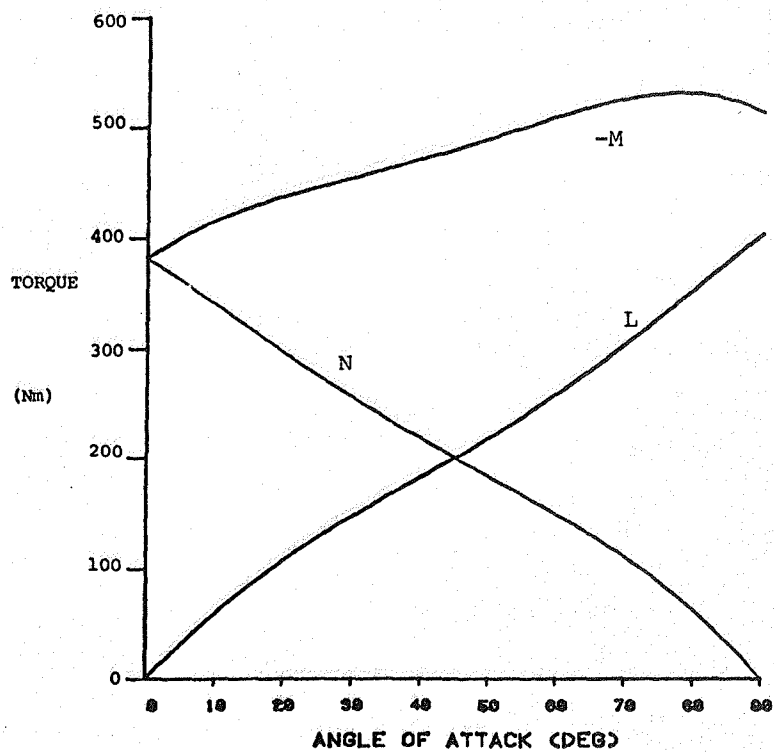
Fig. 7.19b(i)

X configuration

E/M 3 (4,5,6)

Forces
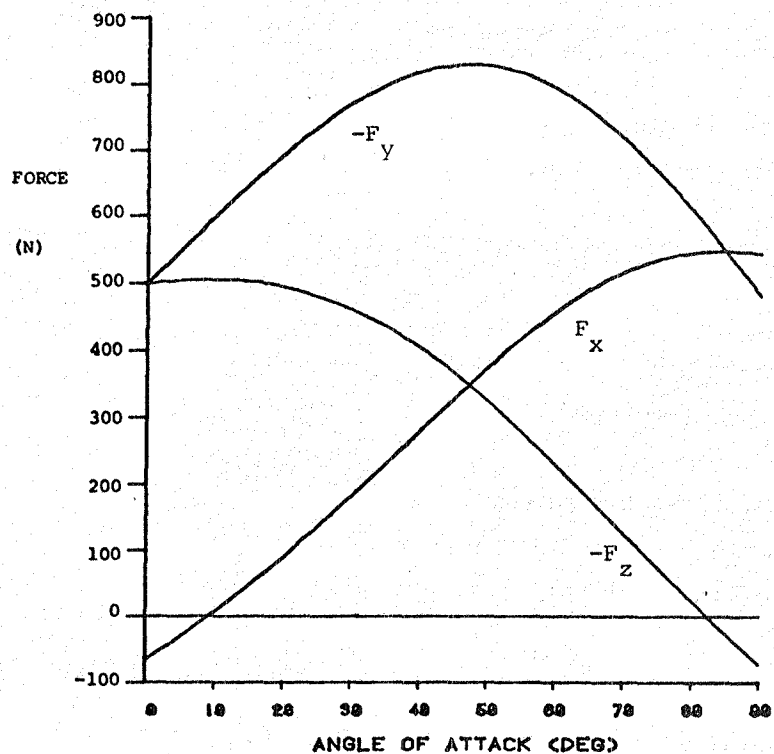
Fig. 7.19b(ii)

X configuration
E/M 3 (4,5,6)
Torques
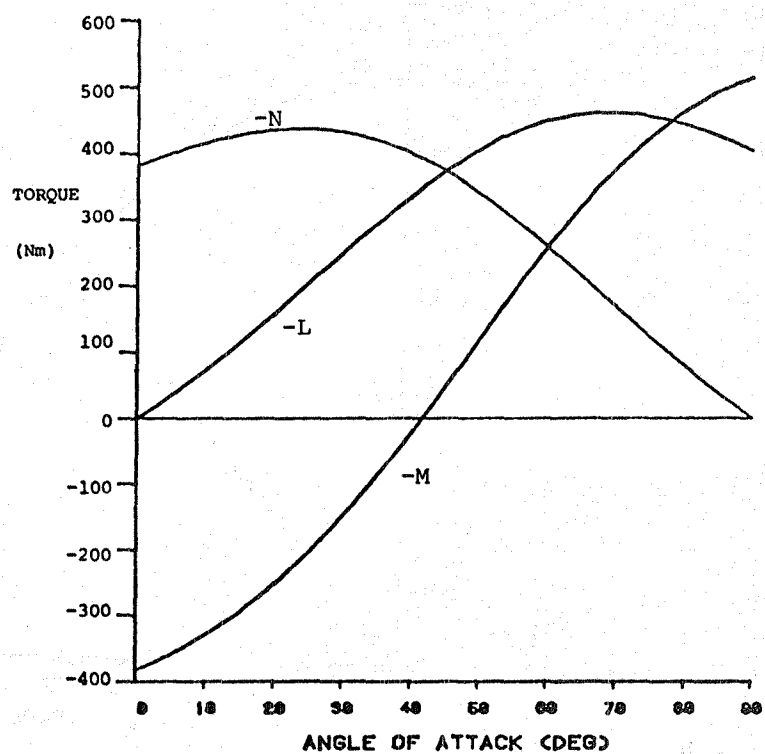
Fig. 7.20 Couplings from X configuration classical applied fields

E/Ms as Fig. 7.18
Model as Fig. 7.6

Fields defined by relationships of currents as below:

	I_1	I_2	I_3	I_4	I_5	I_6	I_7	I_8	I_9	I_{10}
Lift	+	+	-	-	-	-	+	+	N/A	N/A
Auxiliary drag	-	-	-	-	+	+	+	+	N/A	N/A
Sideforce	+	-	-	+	-	+	+	-	N/A	N/A
Auxiliary sideforce	+	-	+	-	+	-	+	-	N/A	N/A
Pitch	+	+	-	-	-	-	+	+	N/A	N/A
Auxiliary pitch	+	+	+	+	-	-	-	-	N/A	N/A
Yaw	+	-	-	+	+	-	-	+	N/A	N/A

- following Figs. 7.5, 7.18

Axial fields (E/Ms 9 & 10) are as Figs. 7.8 b & i

Fig. 7.20a

Lift field

FORCE

(N)

ANGLE OF ATTACK (DEG)

F_z

$-F_x$

Fig. 7.20b
Auxiliary drag field
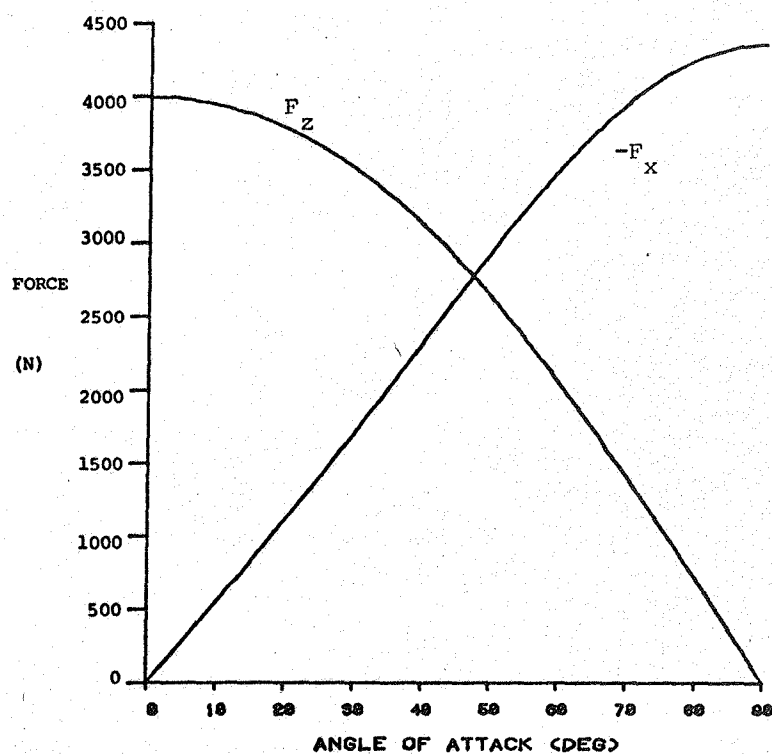
Fig. 7.20b
Auxiliary drag field
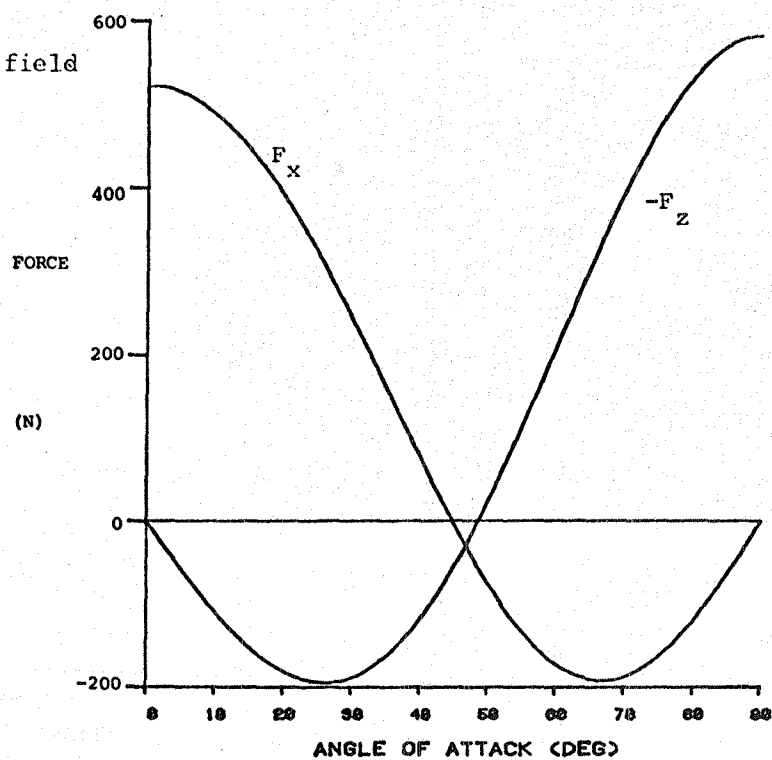
Fig. 7.20c
Sideforce field
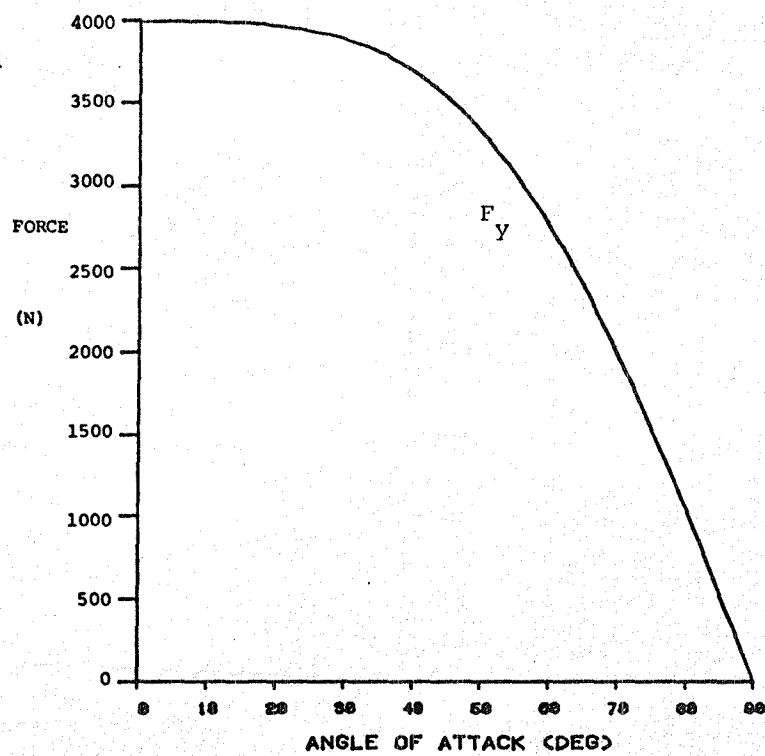
Fig. 7.20d

Auxiliary sideforce field
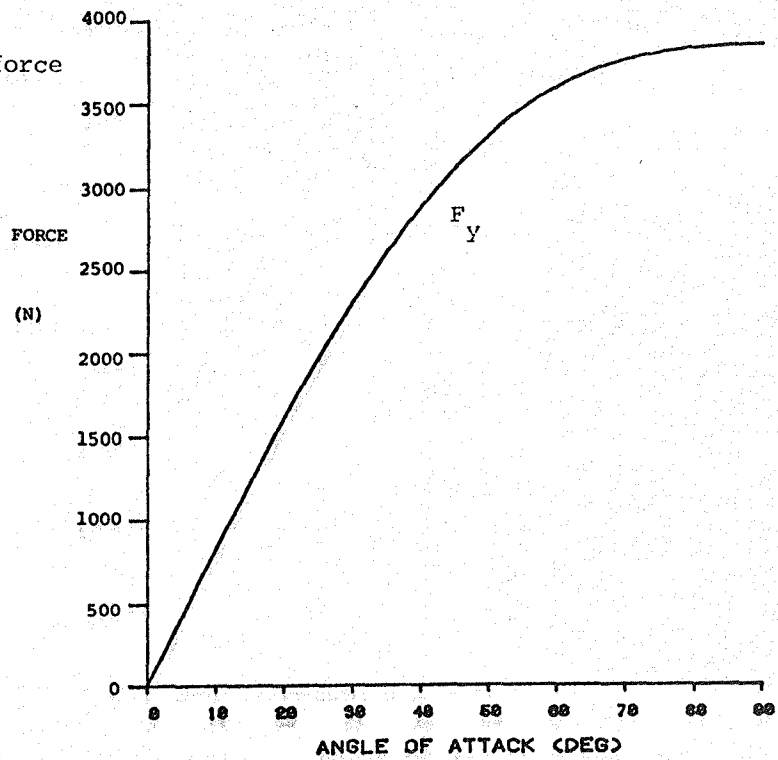
Fig. 7.20e

Pitch field
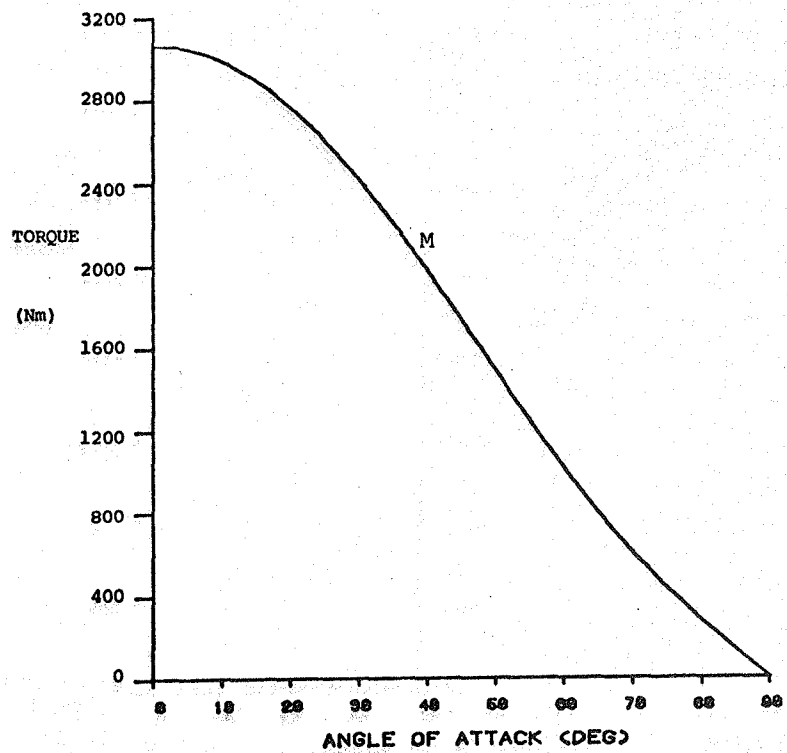
Fig. 7.20f

Auxiliary pitch field
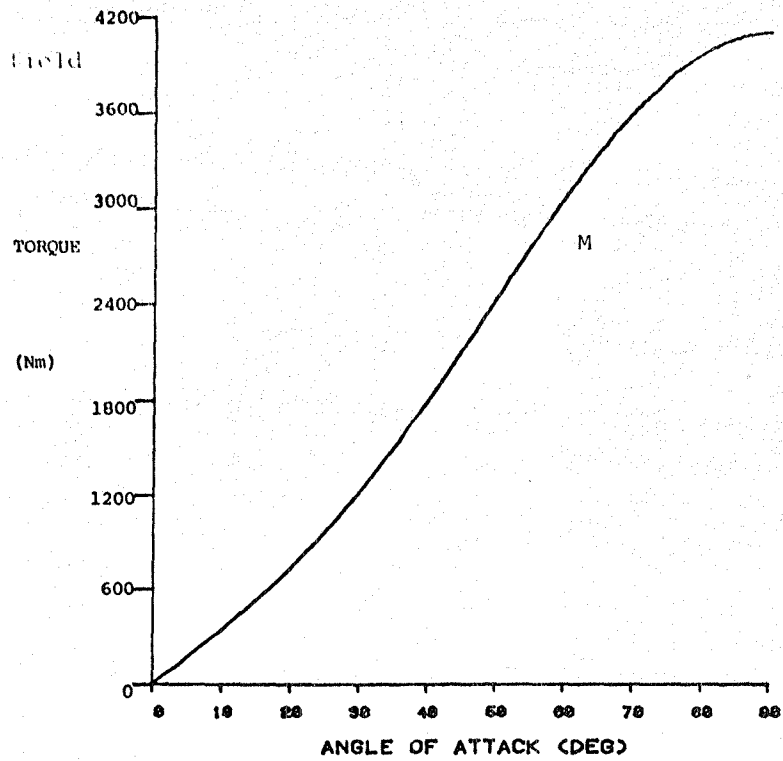
Fig. 7.20g

Yaw field
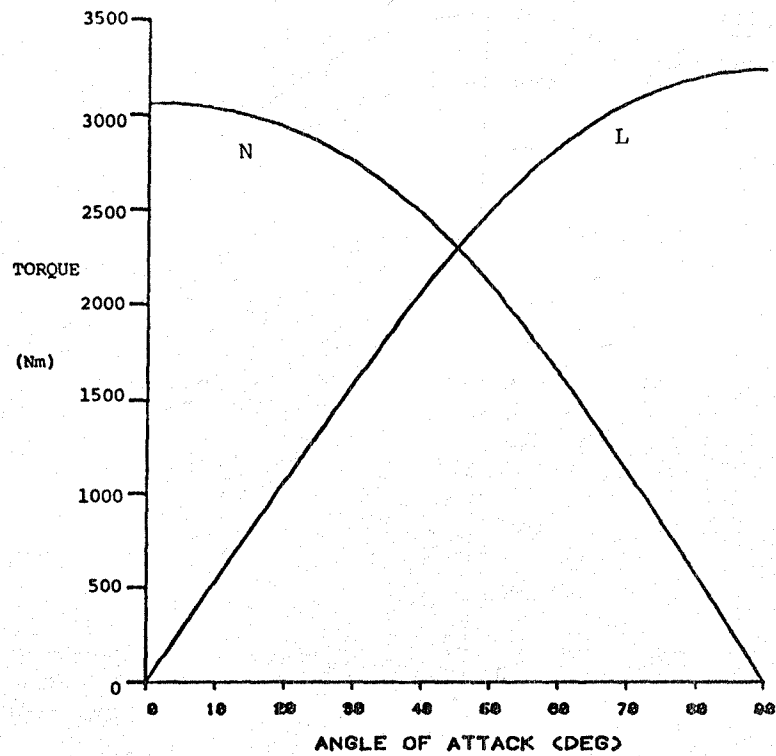
Fig. 7.21 Couplings from X configuration classical applied fields

- showing zero volume model

These Figures are directly comparable with Figs. 7.20, which
should be consulted for details of model, E/Ms and current relation-
ships.

SOLID lines represent the zero volume model.

BROKEN lines show the standard model and are identical to the
corresponding Figs.7.20.

Fig. 7.21a

X configuration
Lift field

FORCE

(N)

ANGLE OF ATTACK (DEG)
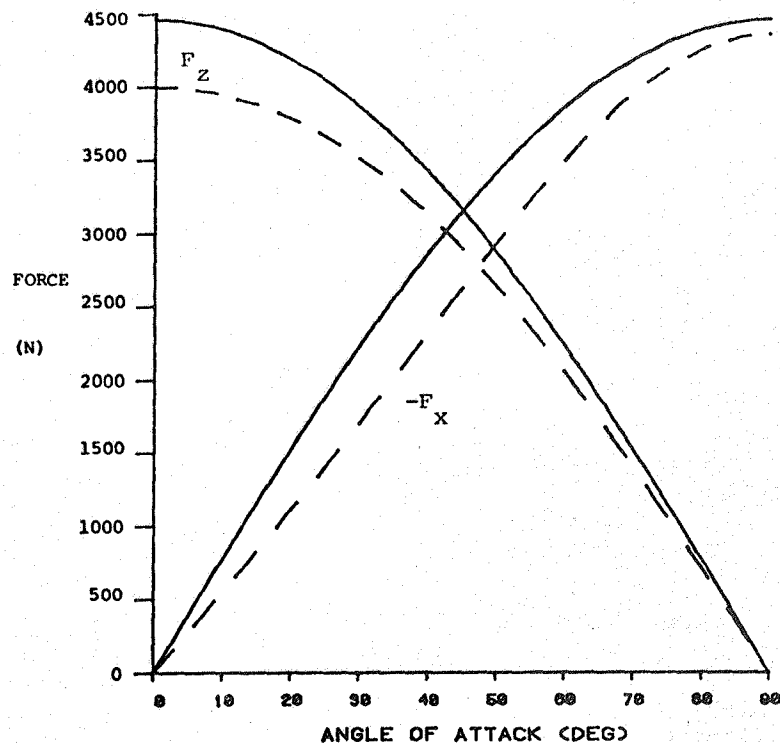
Fig. 7.21b

X configuration
Auxiliary drag field
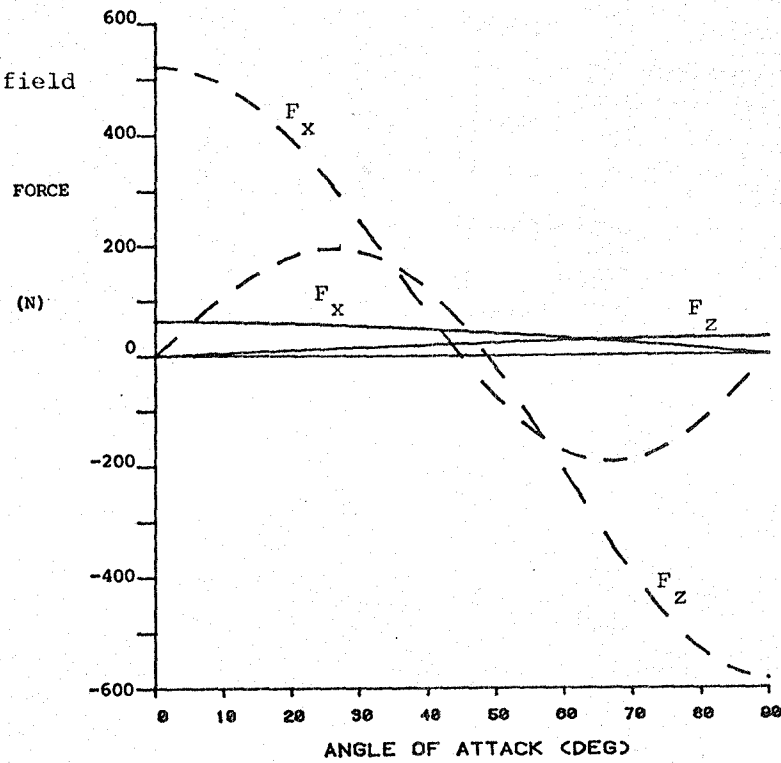
Fig. 7.21c

X configuration
Sideforce field
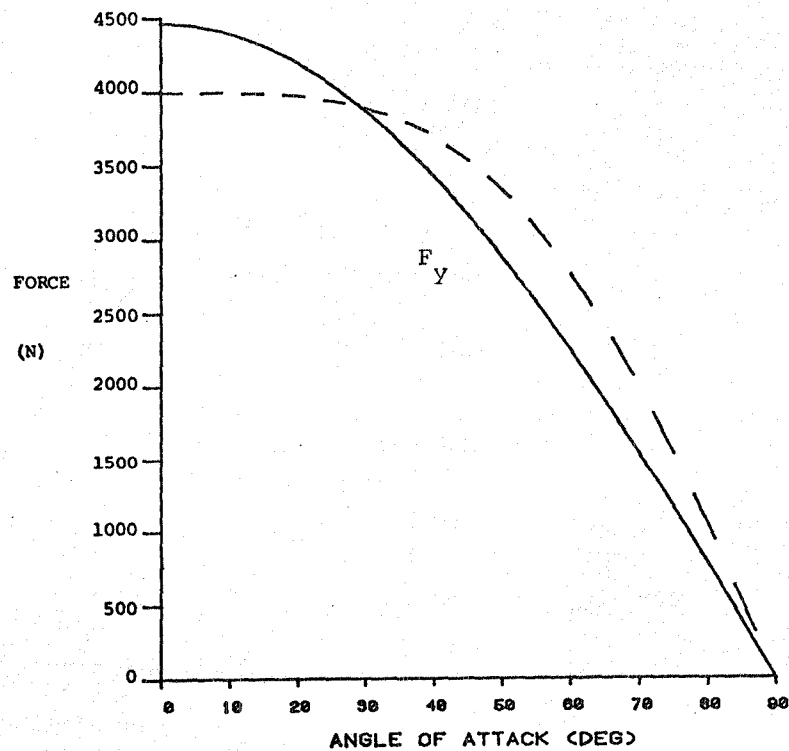
Fig. 7.21d

X configuration
Auxiliary sideforce
field
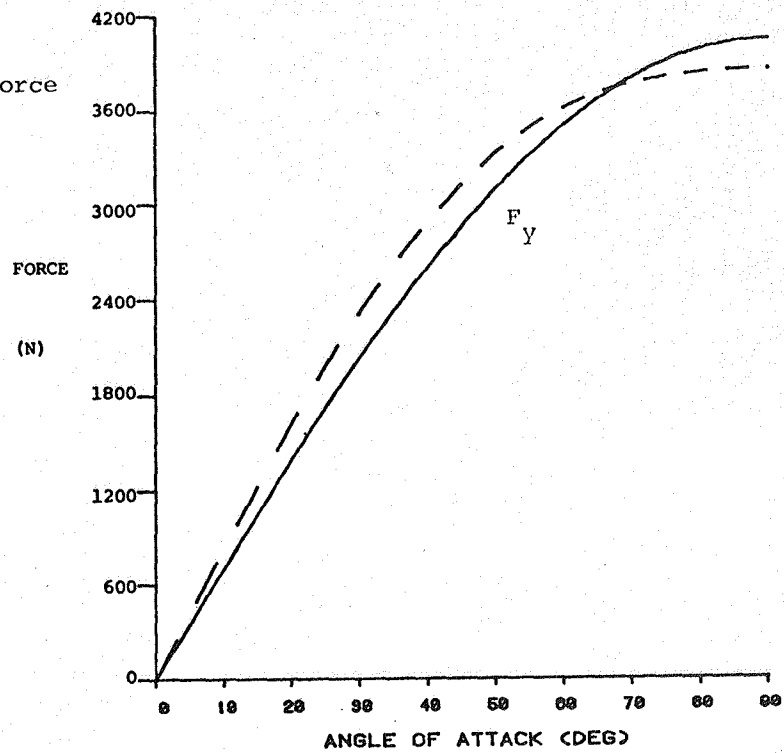
Fig. 7.21e

X configuration
Pitch field
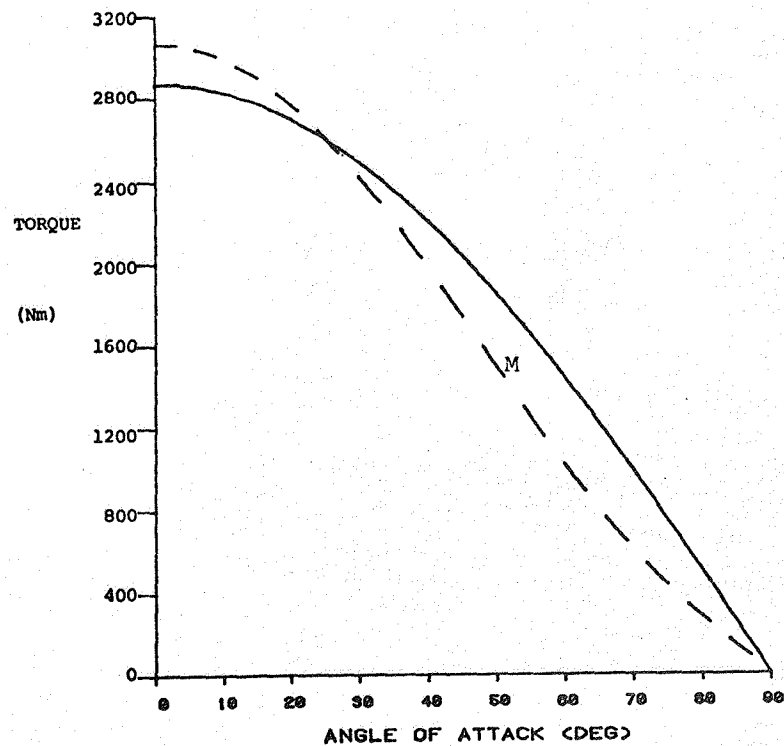
Fig. 7.21f

X configuration
Auxiliary pitch field
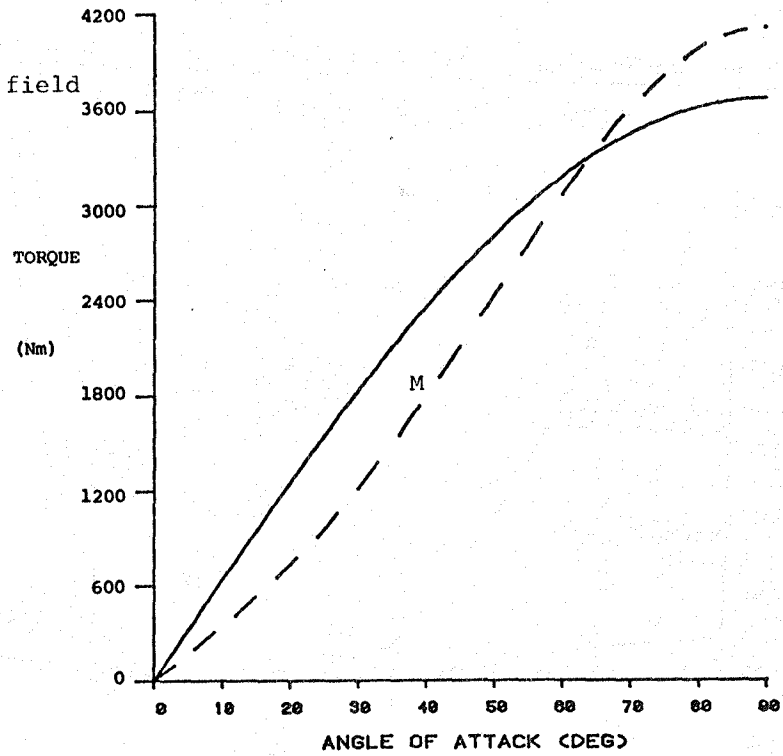
Fig. 7.21g

X configuration
Yaw field
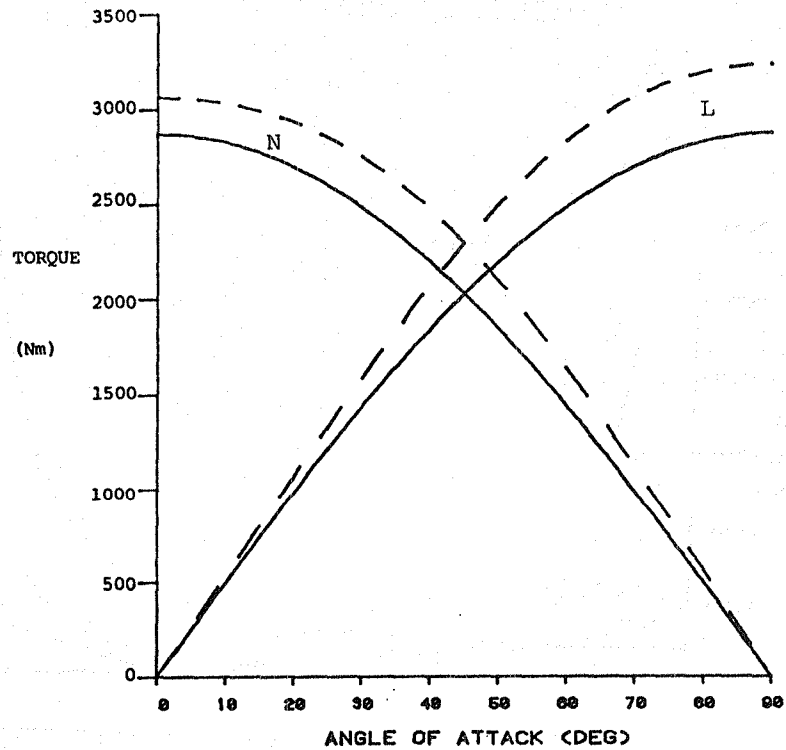
Fig. 7.22 Maximum performance of the X configuration   E/Ms as Fig.7.18

Model as Fig.7.6. Forces as Fig.7.12
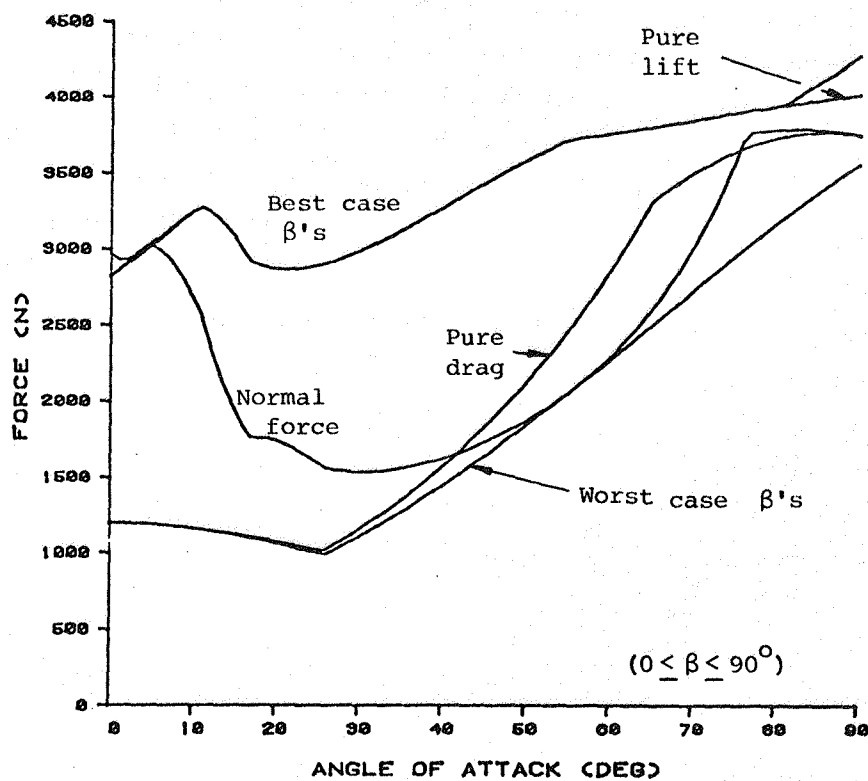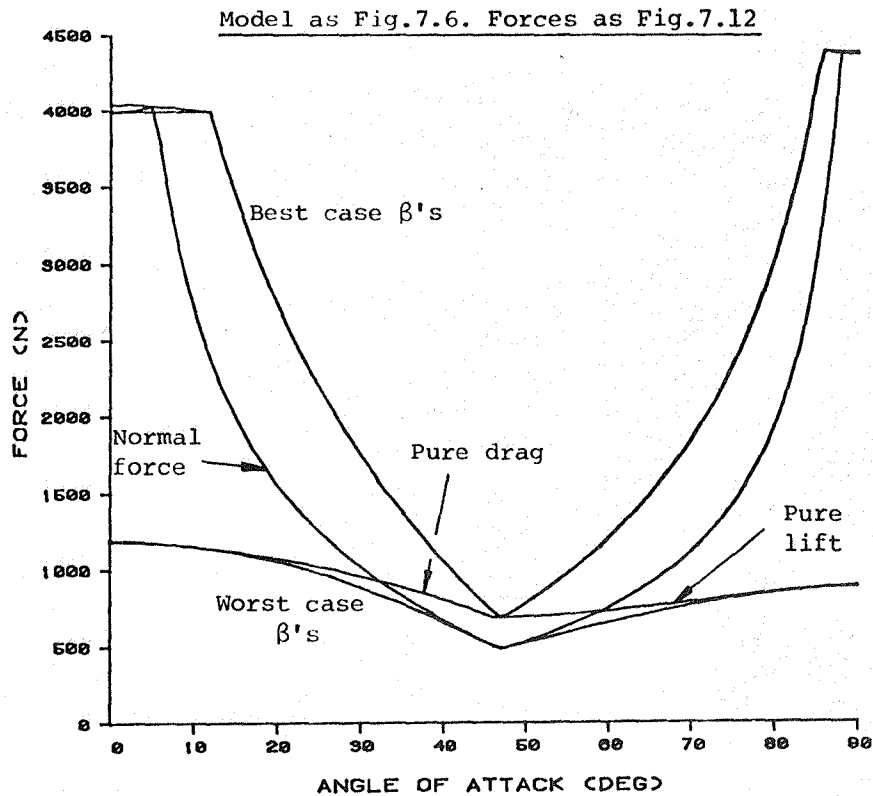

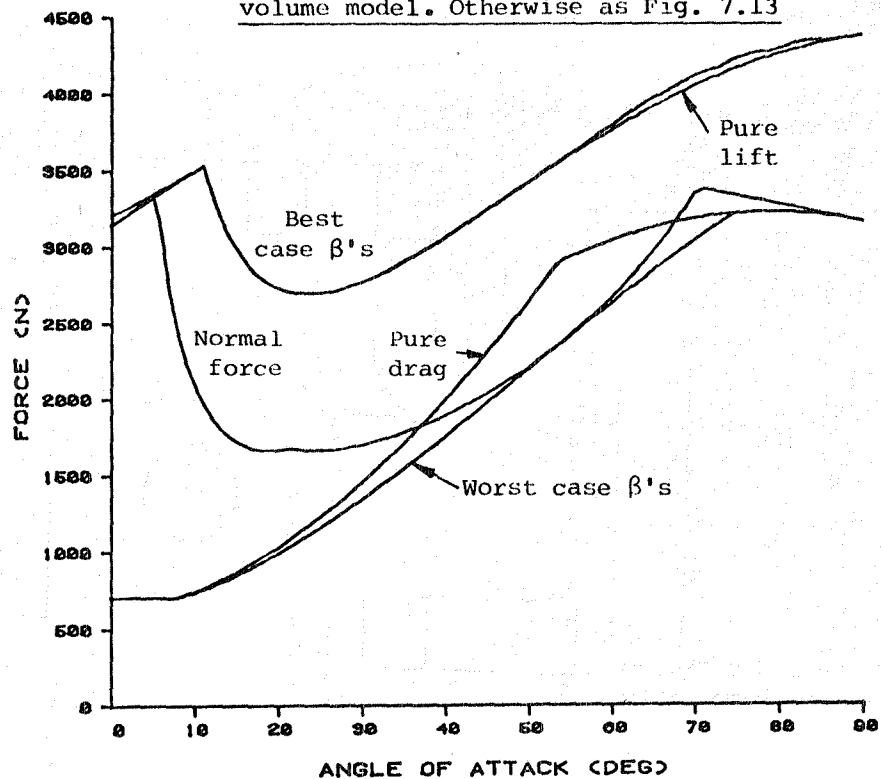Fig.7.23 Maximum performance of X configuration with zero volume model

Otherwise as Fig. 7.22
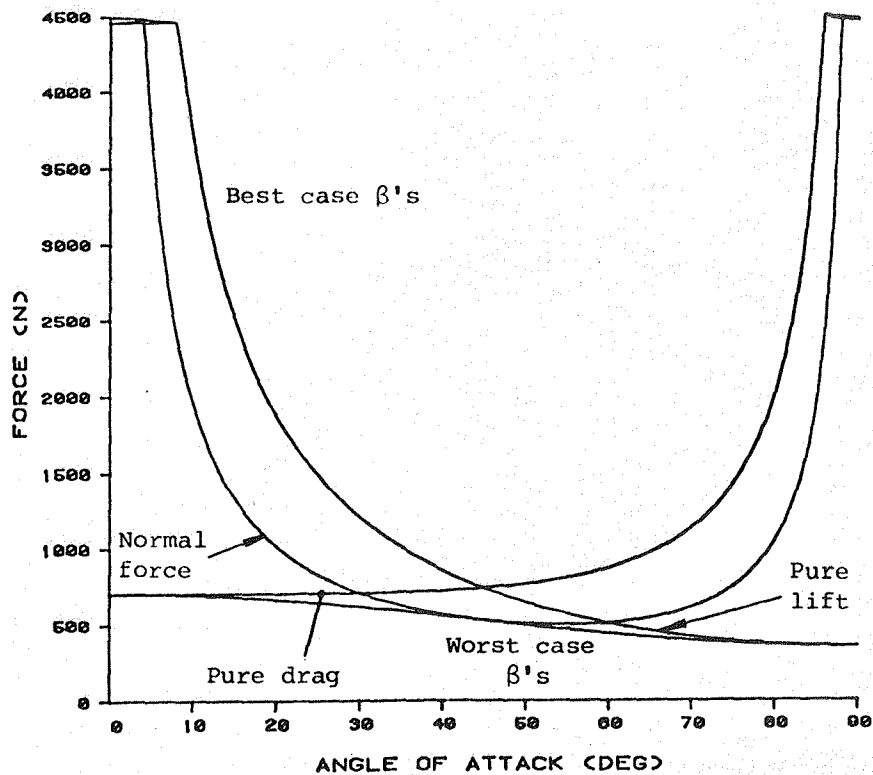
Fig. 7.24 Maximum performance of the X configuration. Axial E/Ms
doubled in strength. Otherwise as Fig.7.22
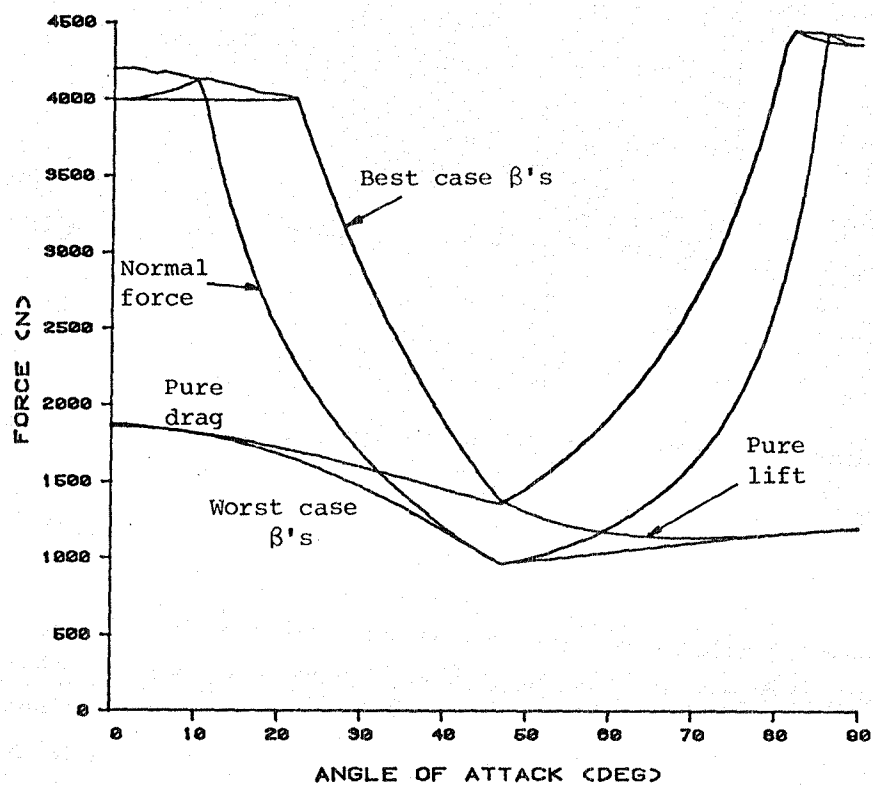
Table 7.3   Field capabilities for X configuration

Field components (T) / 10^6 AT / E/M

E/M grouping	B_{xx_o}	B_{xy_o}	B_{xz_o}	B_{yy_o}	B_{yz_o}	B_{zz_o}	B_{x,y,z_o}
Lift	0	0	0.2786	0	0	0	0
Drag	0.0676	0	0	−0.0338	0	−0.0338	0
Auxiliary drag	0.0039	0	0	−0.0019	0	−0.0019	0
Sideforce	0	0.2786	0	0	0	0	0
Auxiliary sideforce	0	0	0	0	−0.2525	0	0

	B_{x_o}	B_{y_o}	B_{z_o}	All gradients
Pitch	0	0	−0.1793	0
Auxiliary pitch	−0.2296	0	0	0
Axial	−0.0808	0	0	0
Yaw	0	0.1793	0	0

Eqn. 7.4 gives, for the x and z components of force in this case:

$$F_x = V (H_{xx} M_x + H_{xz} M_z)$$

$$F_z = V (H_{xz} M_x + H_{zz} M_z)$$

and since $M_x = M \cos\theta$ and $M_z = -M\sin\theta$ we have, at $45°$ angle of attack:

$$F_x = k (H_{xx} - H_{xz})$$

$$F_z = k (H_{xz} - H_{zz}) \qquad (k = MV/\sqrt{2}) \qquad - (7.9)$$

These equations are heavily coupled, directly via the H_{xz} term and via the lack of independent capability in H_{xx} or H_{zz}, shown in the table above.   The requirement is generally to develop positive F_x and positive F_z simultaneously in some proportion and it is seen that since H_{xz} contributes to F_x and F_z in opposite senses and that the (coupled) H_{xx} and H_{zz} components are relatively small in the chosen configuration the available magnitudes of forces will tend to be low.

7.5.3.   Discussion

Referring to Tables 7.2 and 7.3 it is seen that where H_{xx}, H_{yy} and H_{zz} components only are developed at the origin, the sum of these components is always zero.   This corresponds to Maxwell's equations for a conservative field with no free poles :

$$V \cdot B = B_{xx} + B_{yy} + B_{zz} = 0 \qquad - (7.10)$$

applied in free space.   By symmetry it can be seen, using Eqn. 7.10, that in the case of symmetric axial E/Ms or the complete symmetric X array (E/Ms 9 and 10 or X E/Ms 1-8) :

$$B_{yy} = B_{zz} = -\tfrac{1}{2}B_{xx} \qquad - (7.11)$$

Decoupling of Eqn. 7.9 using 7.11 is thus not attractive.   In the case of the vertical or lateral E/M quadruplets from the + array (+E/Ms 1-10) however :

$$B_{yy} = -B_{zz} \gg B_{xx} \qquad - (7.12)$$

Modifications to the geometry of the X array, such as realignment of the E/Ms as shown below, may prove to affect Eqn. 7.11 sufficiently powerfully to partially restore the viability of the X configuration but no investigations have yet been attempted.

d may be positive or negative

ξ may be greater than or less than 90°
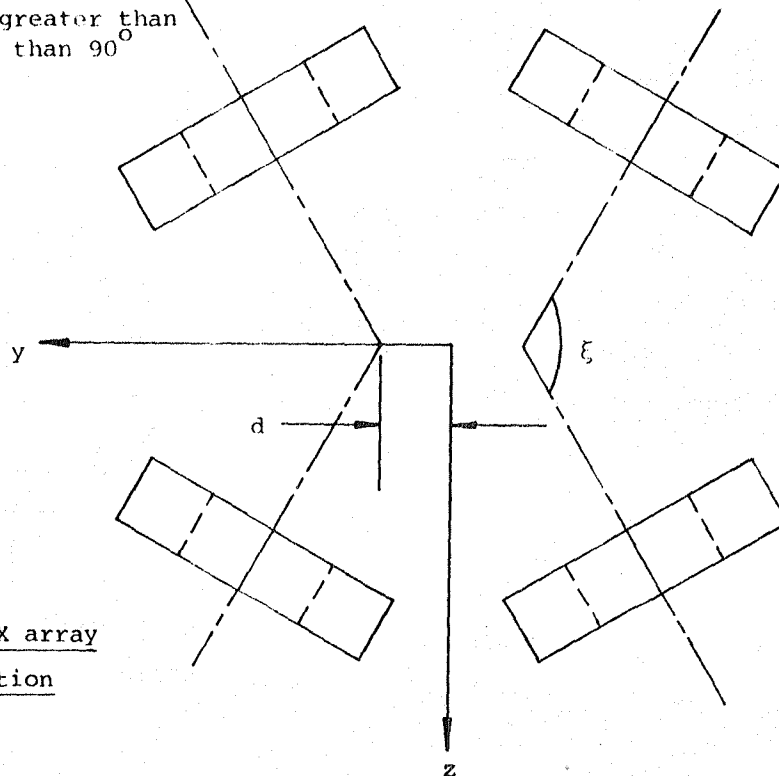
Fig. 7.25

Modified X array

configuration

7.6 E/M configurations for LMSBSs

The examples of + and X configurations studied herein cannot be assumed to be fully representative of the general classes of such configurations, since large variations in overall proportions and relative E/M capabilities are possible.   However, the inability to generate H_{yz}, hence sideforce at 90° angle of attack with the + configuration, and the difficulties around 45° angle of attack with the symmetric X configuration are thought to be fundamental.

There is no objection in principle to combining the two configurations in an attempt to combine their advantages and negate their disadvantages, indeed this was envisaged (but never carried out) in Ref. 49.   Numerous detail variations are possible, such as :

a) Symmetric "star"

b) Non-symmetric "star"

c) Symmetric 6 E/M array
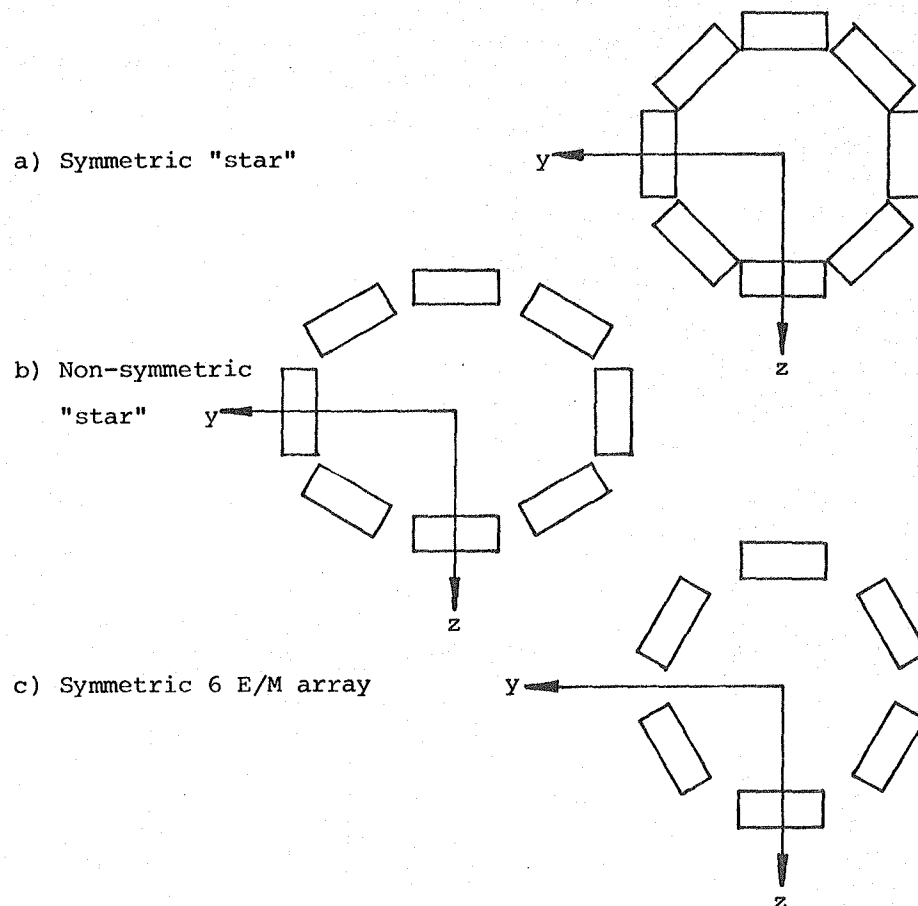
(Fore and aft spacing of E/Ms is not shown and may itself be subject to considerable variation)

Configurations a) and b) above correspond closely to proposed SIM roll arrays (Section 5.8). Indeed, although roll control has generally not been treated in this Section it is the case that the X array as specified can effectively generate the required through wing fields ($H_{yz'_o}$) for all model angles of attack. Large roll displacements from datum would not be permissible with the X array, however, since $H_{yz'_o}$ cannot be generated at $\phi=45^o$ (Section 4.3.1). The hybridised arrays above (a-c) do not suffer this limitation.

The employment of model core geometries other than the conventional slender, axially magnetized configuration is possible, particularly with permanent magnet core material, but would generally lead to other complications, including increases in the complexity and/or severity of cross couplings between model degrees of freedom.

7.7 Discussion

The absolute magnitudes of forces (or torques) shown in the various Figures in this chapter are of somewhat limited significance. They do not represent the maximum attainable forces for the chosen configuration, merely the forces attainable within the constraints of given E/M current limits and model characteristics. The absolute maximum attainable forces with a permanent magnet core are principally set by the magnetic behaviour of the core (demagnetization and usable polarization) but these limits could not be identified at the time of writing due to the lack of data concerning high coercivity permanent magnet materials (see Section 4.3). The corresponding limits for a soft iron core will be set by the behaviour of the induced magnetizations as the core material enters its saturation region, presenting a challenging computational problem (see Section 5).

The studies made herein are principally intended to indicate the general practicality of the + and X configurations, partly by identification of any magnetic shortcomings in these configurations, and the magnitude of the control difficulties caused by the changing couplings between model and E/Ms. Further investigation of the latter area appears appropriate but cannot be undertaken here.

In the design of an extreme attitude capable MSBS it is probably more appropriate to consider the E/M array simply as a generator of field and field gradient components in the test section, rather than an assembly of "lift", "drag", etc., E/Ms, as has been common

previously. Usable model attitudes are unlimited if all components
can be generated effectively and independently. It would be to
advantage if the applied fields were relatively pure and uniform
in the region of the model in order to minimise cross coupling
effects and this requirement may perhaps be met by the use of
Helmholtz pairs and corresponding optimised quadruplet geometries.

7.8 Experimental demonstration of suspension with SUMSBS at high angles of attack

7.8.1 Introduction

Section 7.4 concluded that SUMSBS should be usable, in its +
configuration, to around 60° angle of attack with conventional models.
Preliminary attempts at suspending models up to this angle of attack
have been made and are reported briefly here.

7.8.2 Special features of SUMSBS for high angle of attack operation

The position sensing system, fully described in Appendix 1,
represents only an expedient and very short term solution to the
difficult problem of accurately monitoring model position and
attitude over wide ranges of attitude. The system devised achieves
high angle of attack capability only by mechanical rotation and
realignment of the four main sensors, axial position being monitored
by a single fixed sensor (Appendix 1, Fig. 7.26).

Without modification, SUMSBS was capable of suspending conventional
axisymmetric models to around 30° angle of attack.

It was decided to attempt initial high angle of attack suspension
at around 50°, requiring suitable relocation of position sensors of
course, and decoupling of the now grossly coupled and quite inoperable
controller. Decoupling proceeded using the computed couplings of
Section 7.4, and was performed in model axes, since the position
sensing system operates essentially in this axis system. The
precise methods used are described below, but it should be carefully
noted that they represent a considerable simplification from the
ideal, made entirely for convenience, it being believed that
successful stable suspension would be sufficient to verify the
fundamental theory of this Section, even if achieved on a less than
wholly representative basis.

Fig. 7.8j shows that yaw torque (model axes of course) is only weakly affected by pitch rotation, with Fig. 7.8e furthur indicating that sideforce is only affected by falling gain, easily restored by appropriate increase in controller loop gain. Consulting Fig. 7.7a it is seen that if E/Ms 1 and 7 are operated in conjunction, but with opposite signs of currents, then only pitch torque is generated and relatively effectively. The full pitch torque capability previously enjoyed is restored by supplementing the effect of E/Ms 1 and 7 by the use of E/Ms 2,4,6 and 8 via the Auxiliary Pitch No.2 field, as Fig. 7.8h.

The residual difficulty lies in the generation of forces in the required senses and magnitudes in the xz plane. Now Fig. 7.7d indicates that the use of E/Ms 9 and 10 (the axial E/Ms) in conjunction produces a net force approximately perpendicular to the x' axis of the model, with the model at 50° angle of attack (Fig. 7.27). Forces approximately parallel to the model's x' axis are conveniently provided by E/Ms 3 and 5, with these E/Ms operated in conjunction, as Fig. 7.7b and Fig. 7.27. It was found that the currents required in E/Ms 9 and 10 required to oppose the relevant component of the model's weight proved to be very close to the available current limits (20 A). A standing current was thus demanded in E/Ms 2,4,6 and 8 corresponding to the Auxiliary Drag No.2 field (Fig.7.8d), effectively reducing the residual model weight required to be supported otherwise.

Careful adjustment of controller loop gains was necessary before stable suspension could be achieved, but the "50°" controller subsequently proved capable of suspension over the range of angle of attack of 40° to 60°. No calibration or detail examination or optimisation of performance was attempted but the Figs. 7.28a-g illustrate the full range of angle of attack explored.

Suspension quality at the higher angles of attack was poor, perhaps not surprisingly in view of the highly simplified experimental approach, and considerable further study is thought appropriate, some aspects of which are discussed in Section 9.2.2.

However Figs. 7.28 are thought to validate the fundamental and key conclusion of this Section, that is that the use of MSBSs for high angle of attack or extreme attitude wind tunnel testing is absolutely viable.

Upper E/Ms

Model

y

Path of main
position sensor
beams.(Config.A)

z

A

View on A
Configuration C
$\approx 50^{\circ}$ angle of
attack

x

30°

z

x

Location of
position sensor
beams (schematic)

View on A
Configuration
A (Normal)

z

View on A. Configuration
B. $\approx 30^{\circ}$ angle of
attack

x

z
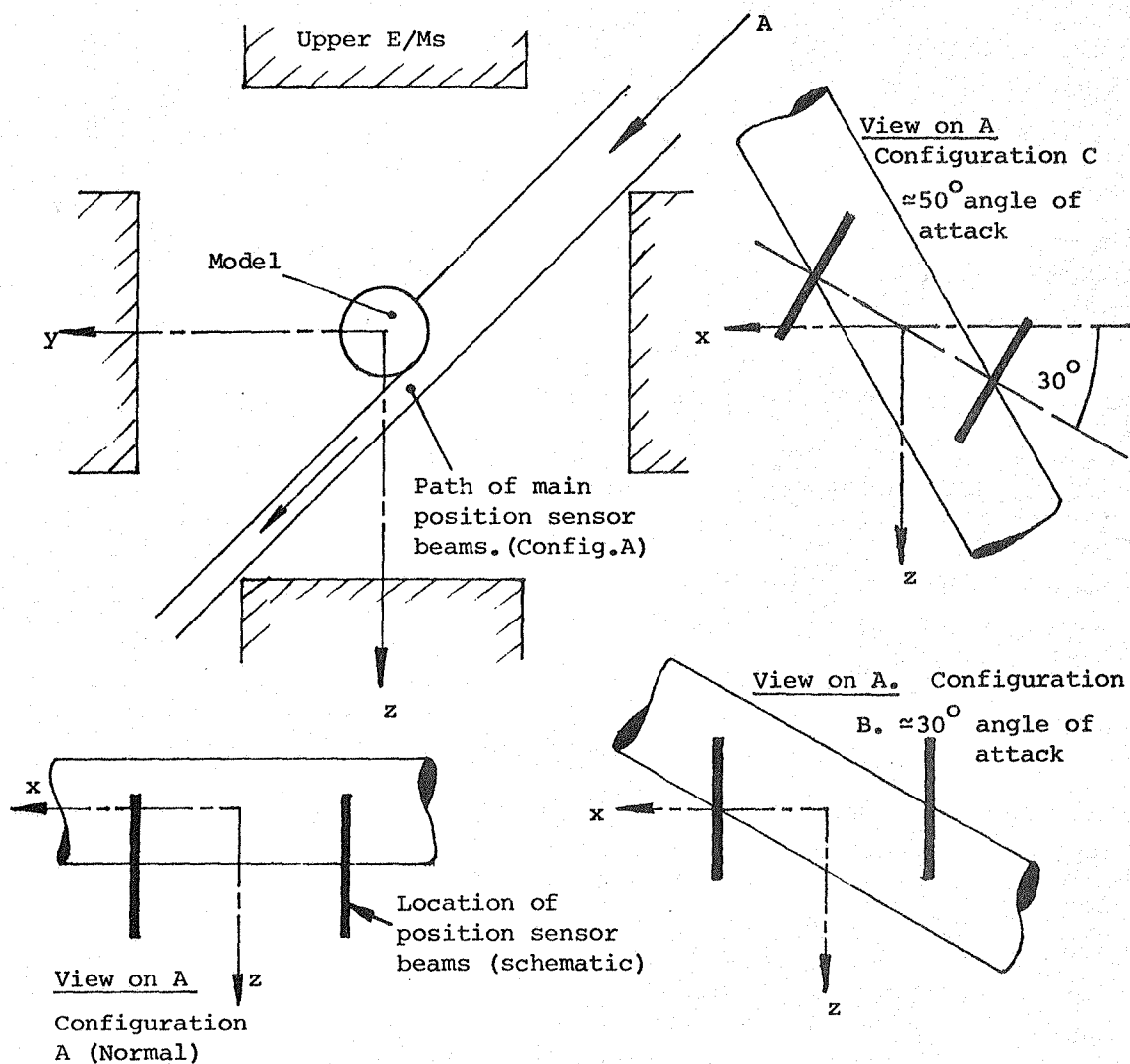
Fig. 7.26   Schematic diagram of main position sensors showing adaption

for high angle of attack operation

x'

F_1

10.2°

50°

x

F_2

7.6°

z'

z

FORCE calculations

F_1 created by E/Ms
3 and 5

F_2 created by E/Ms
9 and 10

E/M array as Fig.7.5

Model as Fig. 7.6
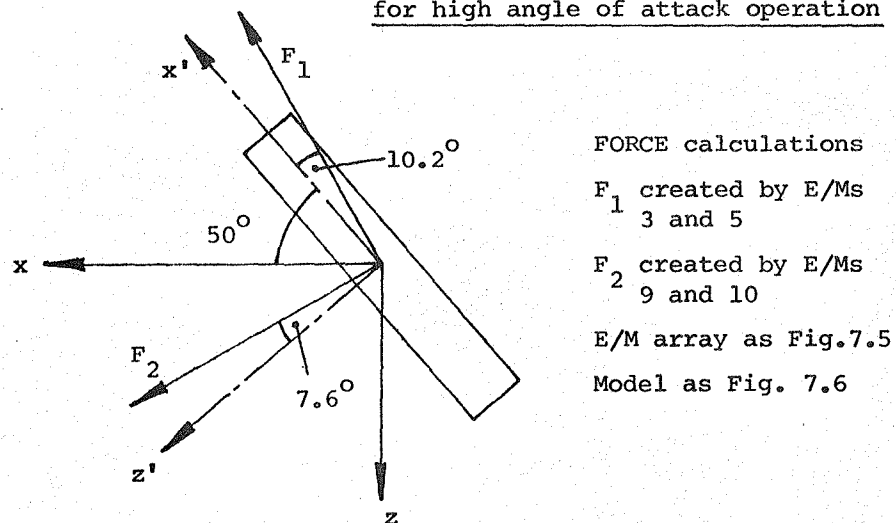
Fig. 7.27   Schematic diagram showing creation of forces in the xz
plane at 50° angle of attack

-200-

Plates

overleaf

Fig. 7.28a

-5° angle of attack

Normal controller and position
   sensors (configuration A)

See Fig. 7.26 for details of
   position sensor configur-
   ations

Fig. 7.28b

0° angle of attack, as 7.28a
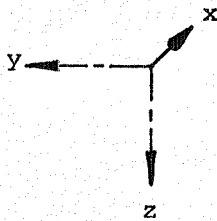
Fig. 7.28c

15° angle of attack

Normal controller

Position sensors in B configur-
   ation.

Fig. 7.28d

30° angle of attack

Normal controller

Position sensors in B configur-
   ation.

Fig. 7.28e

40° angle of attack

"50°" controller

Position sensors in C configur-
   ation.

Fig. 7.28f

50° angle of attack

"50°" controller

Position sensors in C configur-
   ation.

Fig. 7.28g

60° angle of attack

"50°" controller

Position sensors in C configur-
   ation.
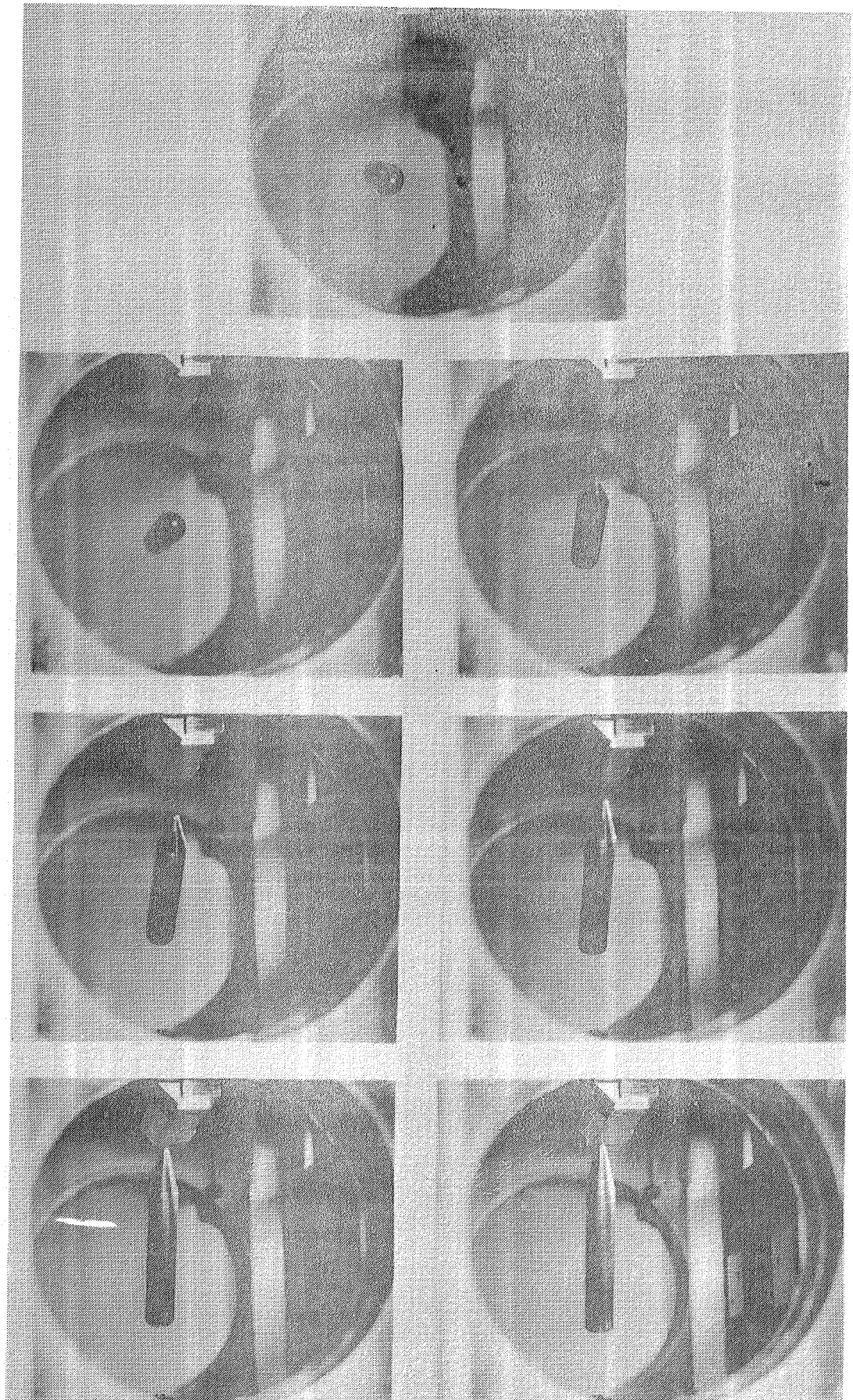
8.   RELIABILITY OF LARGE MAGNETIC SUSPENSION AND BALANCE SYSTEMS

8.1 Introduction, the need for reliability

MSBSs are inherently complex systems, incorporating a wide
variety of sub-systems such as E/Ms, perhaps with associated
cryogenic plant, power supplies, at least one set of model position
sensors, analogue or digital closed-loop control systems and, of
course, a wind tunnel and its ancillaries.   Due largely to this
complexity, all existing MSBSs are rather "unreliable" in the sense
that control over model position is lost relatively frequently,
perhaps after every few hours of operation.   Model "flyaway"
inevitably follows, since MSBSs of the types considered to date are
open-loop unstable in at least one model degree of freedom (Earnshaw's
Theorem).   Flyaway is seldom more than inconvenient with small
systems since models tend to be small, relatively simple and
inexpensive and operated with low tunnel dynamic pressures.

In the case of a LMSBS, however, high dynamic pressures may be
required to satisfy demands for Reynolds number and Mach number,
and winged models are likely to be operated in high lift configura-
tions at these dynamic pressures, leading to large net forces.
Despite the fact that models will be relatively massive, since it is
essential to occupy a high proportion of model volume with magnetic
material, the typical maximum aerodynamic force will exceed the
model's weight by a large factor (approximately 10 in Ref. 5).
Model accelerations following a worst-case control loss may thus be
high and it is clear that enormous impact loads would be generated
if a breakaway model struck a tunnel wall.   Whilst it would be
mandatory to ensure that the tunnel itself could withstand such
impact, extensive damage to the model would seem inevitable.   Con-
ventional large wind tunnel models represent considerable financial
and temporal investment and it is thus certain that model control
loss in a LMSBS cannot be permitted to be anything other than a very
rare event.

The prime reason for building a LMSBS is to acquire aerodynamic
data concerning the test model.   Precisely the same goal motivates
the construction of most large wind tunnels of any type.   Test
programs in existing large tunnels tend to be interrupted relatively
frequently by equipment malfunctions affecting data acquisition.
This situation is tolerated since aerodynamic test programs can

usually accommodate delays or slippages without serious consequence and testing is frequently modified and new tests devised on the basis of early results. There seems no particular reason to assume that testing in a LMSBS should be any different in this respect.

It would seem appropriate, therefore, to conceive of the "control" segments of a LMSBS being highly reliable, with data acquisition and ancillary functions remaining relatively unreliable.

At this juncture the usage of the word "reliable" must be clarified. "Failures" of general systems are often classified into two types, these being "unreliability" where hardware mechanically fractures or electrically shorts etc; or "lack of integrity" where no identifiable physical failure occurs but nevertheless the system fails to perform its design task due to some other factor, perhaps adverse environmental conditions, such as electrical interference. Often the use of these two terms overlaps considerably and precise classification of particular failures is not always possible. The uncertainty over the terms seems especially severe in the case of MSBSs where the causes of loss of model control frequently do not involve simple mechanical or electrical failure. Herein, therefore, the reader should be aware of the use of the terms "reliability" and "integrity" somewhat interchangeably, the former usually encompassing the latter, though not vice versa, and implying the probabilistic likelihood of continuous control of the model being maintained within predetermined operational constraints.

The inherent reliability of key hardware in contemporary MSBSs is not especially high and the large number of subsystems required leads to low overall reliability unless special measures are taken. Development of a LMSBS will involve high technical risk since at least the first LMSBS will be unique in overall architecture and most of its subsystems can be expected to incorporate significant technical innovations and exhibit considerable differences from any contemporary hardware in design, duty and environment. It is thus expected that considerable design effort is both essential and worthwhile, and that the total system configuration must be especially formulated, in order to ensure that a LMSBS be capable of reliable operation.

This Section seeks to explore the impact on overall MSBS architecture of a requirement for highly reliable operation. Detailed

definition of hardware features or performance is not attempted.

8.2   Reliability engineering in LMSBSs
8.2.1   Modular design in LMSBSs

The simplified architecture of a MSBS shown below suggests a
natural division of the overall system into five major subsystems.
There may be certain overlap in function between these subsystems,
for instance, the system controller may include processing of model
sensor outputs, but the division is valid insofar as the interfaces
between subsystems are principally unidirectional and either
fundamentally fixed or entirely optional.
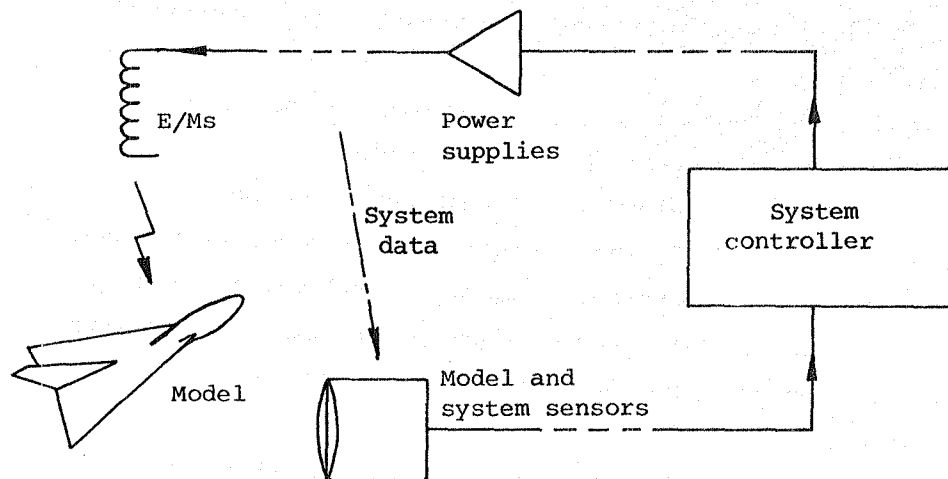
Module	Primary interface to next subsystem	Comments
Model	Fixed: Dynamics	−
Model and system sensors	Optional: probably electronic	May be sensitive to environment
System controller	Optional: probably electronic	May include sensor processing
Power supplies	Fixed: Current, Voltage	Closely coupled to E/Ms
E/Ms	Fixed: Magnetic fields	Mutual coupling between E/Ms

Fig. 8.1   Inherent modularity of MSBSs

A highly modular design approach is thought to be particularly applicable in LMSBS development where the complete system will be novel, highly complex and composed of devices and systems from widely differing branches of engineering. Modularisation can be advantageously applied at the subsystem as well as the system level and the potential benefits of this approach include:-

(1) Simplified system development. Devices or subsystems from several different working groups may be brought together in an agreed and considered overall architecture with minimum difficulty.

(2) Easy upgrading of subsystems. A major advantage in LMSBS design since very few will be built and hence each will tend to be rather experimental in nature. As operational experience is gained and design or construction techniques improve, enhancements to overall performance may be made most economically by subsystem upgrading.

(3) Simplified development and maintenance of subsystems. LMSBSs will certainly include many similar components within many modules or subsystems (such as several power supplies). Considerable benefits accrue if groups of similar components can be arranged to be fundamentally identical and the number of different groups of components reduced.

(4) Reduced overall cost. If (1) and (3) can be successfully implemented the overall manufacturing costs will be reduced due to elimination of the duplication of component or subsystem development.

8.2.2. Operational task classification and general reliability considerations

It has already been noted that the tasks undertaken by a MSBS may be divided into two major classes, that is "Suspension" and "Balance". These tasks are of quite different criticality to the system and merit different approaches to their reliability.

The suspension task is critical and failure to prevent model flyaway will be regarded as catastrophic failure of the system. No particular constraint need be placed on the quality of model suspension for fulfilment of this task.

The balance task is of lesser criticality and may in principle be unconditionally aborted at any time and with any frequency

without triggering catastrophic failure.   The quality of suspension should be high but useful fulfilment of this task merely requires that the overall system's mean time between any event causing unacceptable degradation of suspension quality be reasonably long, with a correspondingly short mean downtime.   These criteria should be satisfactorily met by a well-designed system without recourse to special measures.

The suspension task requires that the mean time between flyaway be very long indeed, perhaps in the order of thousands of hours. Taking into account the fact that each LMSBS will be of complex and largely novel design there seems no possibility of realising this objective without recourse to special design features.   Further, if component failure rates in a LMSBS follow the classical "bath-tub" curve[*] then comparatively large numbers of failures would be expected in the early life of that system.   Unless massive and lengthy test programs, such as those carried out for manned space missions, are contemplated, it would be unreasonable to expect that all latent design or manufacturing errors or "infant mortality" failures could be detected.   This assertion leads directly to consideration of a design strategy where the system may somehow survive at least one random single point failure - a "fault tolerant" design strategy.

Fault tolerant systems may be conveniently subdivided into two classes:

    (1) Fail operational

    (2) Fail soft

The fail operational strategy implies that sufficient spare capacity is somehow incorporated so that the system may continue operation following a failure, usually at undiminished performance. Hardware redundancy is essential if this strategy is to be successful in surviving any single point failure.   The fail soft strategy abandons the requirement for continued operation of the system at full performance but seeks to ensure that the consequences of any

---

[*]
<u>Classical</u>
<u>bathtub</u>
<u>curve for</u>
<u>component</u>
<u>failure rates</u>

Failure Rate. "Infant mortality". Constant fail.rate. "Wear-out". Time.
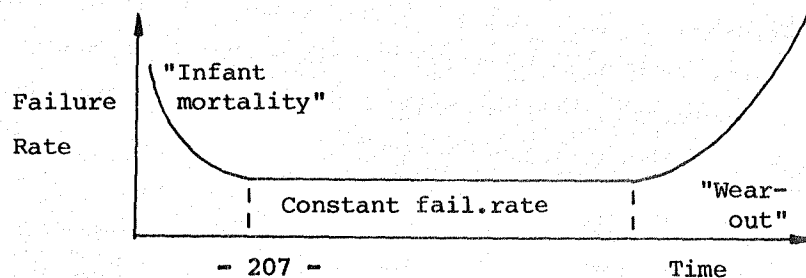
failure are sufficiently attenuated so as to permit planned and graceful degradation of system performance. The requirements placed on LMSBSs suggest something of a hybridisation of these two philosophies. Critical suspension modules must fail operational although certain degradation of performance may be permissible. Balance hardware need not fail operational but must fail soft insofar as disruption of the suspension task must be prevented. Both fail operational and fail soft strategies generally require that propagation of failures through the system ("cascade" failures) be prevented. Graceful degradation of overall system performance following a failure is quite acceptable, perhaps desirable, and could be manifested as an operational strategy where the suspension task is rapidly aborted, such as by initiation of a rapid shut-down sequence (RSS), on detection of any failure in key hardware. It is interesting to note that this option is not open to, for instance, the designer of an advanced flight control system. In order to achieve good mean time between RSSs either the agglomerated mean time between failure of all key components and systems must be long or sufficient redundancy must be incorporated to permit continued operation at low risk following one or more component failures.

Good serviceability requires that the fraction:

$$\frac{\text{Mean downtime following RSSs}}{\text{Mean time between RSSs}}$$

be small. It is frequently proposed in other contexts that this criterion be met in complex systems by holding spare components or subsystems in reserve, rapidly to replace failed units. Since it has been anticipated that a substantial proportion of the causes of RSS initiation might not involve classical hardware failure, imposition of requirements for extensive spares holdings is inappropriate here.

It happens that even following loss of model control there will exist an identifiable optimum strategy, involving suspension E/Ms and perhaps wind tunnel controls, which would "guide" the resultant flyaway, so as to cause minimum damage to the model and/or tunnel.

One type of failure more serious than that described above as catastrophic may be contemplated, that is, a sequence of events triggering cascade mechanical failures of the suspension E/Ms.

This type of failure is technically credible, such as through helium supply disruption to an array of certain types of superconducting E/Ms, but can and should be rendered virtually inconceivable by careful design of relevant systems. Such a gross failure could otherwise be justifiably regarded as cataclysmic.

8.3 Configuration of reliable LMSBSs by incorporation of hardware redundancy and some other techniques

8.3.1 Incorporation of hardware redundancy into the E/Ms and some further considerations

Introduction of some form of redundancy into the E/M array is necessary if sufficient force/moment capability to maintain the model under control is to remain following an E/M failure. However, overheads are incurred on several counts, including :

(a) Provision of surplus redundant ampere-turns. An E/M could incorporate redundancy by being composed of several independent windings, each winding creating substantially the same useful field, configured such that the E/M is capable of supplying its maximum design field with one winding failed. The redundant E/M must incorporate more ampere-turns that the equivalent non-redundant E/M and the factor :

$$\frac{\text{Total ampere-turns in redundant E/M}}{\text{Ampere-turns in equivalent non-redundant E/M}}$$

represents an E/M cost factor which depends on the number of independent windings per E/M.

(b) Increased complexity in the design of the E/M array. This is particularly important since provision of multiple separate dewars (superconducting E/Ms) may seriously compromise close packing of E/Ms around the working section. Some segmentation of dewars is likely to be required to prevent certain serious failures, such as LHe supply loss, cascading through more than one winding. Failure to pack E/Ms closely causes larger E/Ms to be required since the operational effectiveness of each is depleted.

(c) Lower thermal efficiency of superconducting E/Ms. A major path for heat leakage into the LHe environment is along the current supply leads to each winding where they enter the inner dewar. Further, since the leads cannot be superconducting, resistive power is dissipated along their length. Proliferation of supply leads will be expected to increase power losses on both

of the above counts.

The effect of (a) is to decrease the E/M cost factor with increasing number of windings per E/M whereas (b) increases the cost factor with increasing number of windings per E/M. It is thus seen that there may be an optimum number of windings per E/M (Fig. 8.2). (c) demands that the number be low.

It is thought that the E/M cost factor will be relatively small with the optimum number of windings per E/M and that that optimum number will be small due principally to three factors :

(1) Use of Automatic Power Off (APO). Without APO one worst case failure is a power supply runaway. In this event effectively two windings of a particular E/M are lost after one failure since the equivalent of one winding must simply be used to neutralise the runaway winding. The reduction in the idealised cost factor with APO varies with the number of windings per E/M as shown in Fig. 8.3. The system must be designed to cope with the current transient in the chosen APO procedure .

(2) "Passive" Redundancy (PR). For reasons other than provision of redundancy it seems certain that a major architectural feature of any LMSBS will be the positioning of E/Ms all around the tunnel working section with extensive symmetry. Generally, at least the mirror image of any E/M suffering failure may take all or part of the load previously taken by that E/M. If this fact is exploited the complexity of each E/M may be reduced (Fig. 8.4).

(3) State of the art of E/M dewar design. Continuous progress in this area is being made by many teams engaged in the design and construction of cryogenic systems for a wide variety of applications. It appears that the overall thickness of dewar and thermal insulation required to achieve satisfactorily low heat leakage into the LHe environment can be quite small, of the order of 1.5 inches (50, 51, 52). Provision of separate dewars on this basis would not seriously compromise the packing of E/Ms with the largest contemplated LMSBSs (perhaps 8 feet test sections). Smaller systems would be more seriously affected, the thickness of insulation required not being a function of physical scale. However, full insulation is not necessarily required between the closest packed E/Ms (Fig. 8.5).

In order to raise the fundamental reliability of each E/M winding
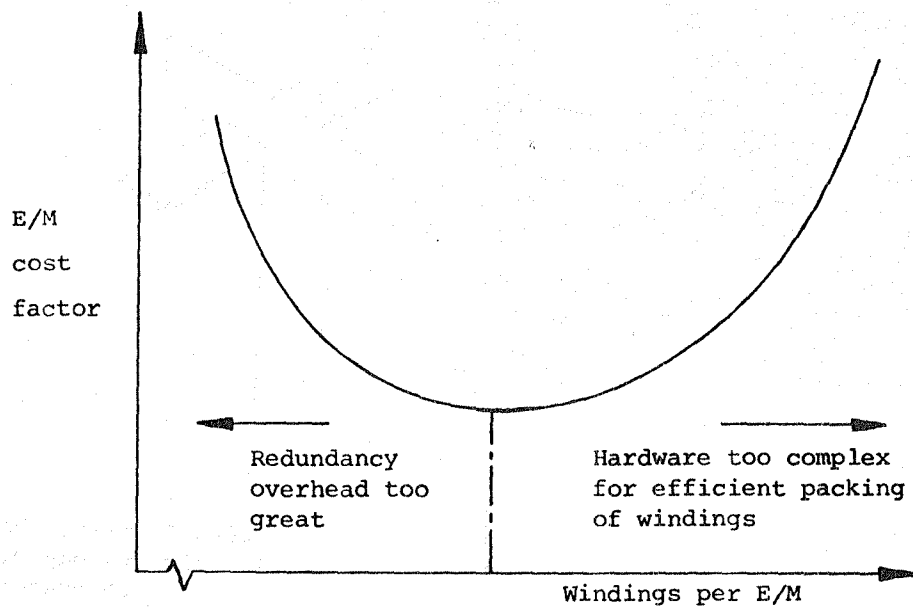
Fig. 8.2   The optimum number of windings per E/M
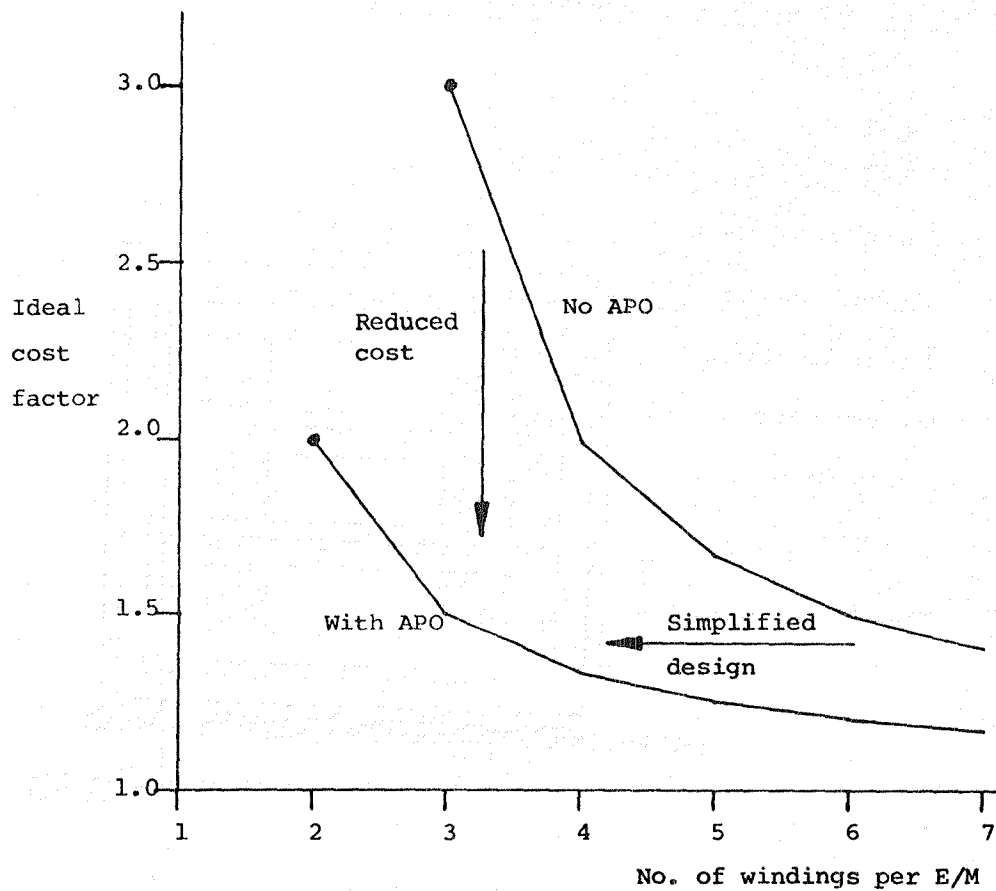
Fig. 8.3   The effect of APO on E/M cost factors (No passive
redundancy)

If, say, winding A fails, then windings B-F inclusive may all contribute usefully to creating the, say, lift force previously created by winding A.
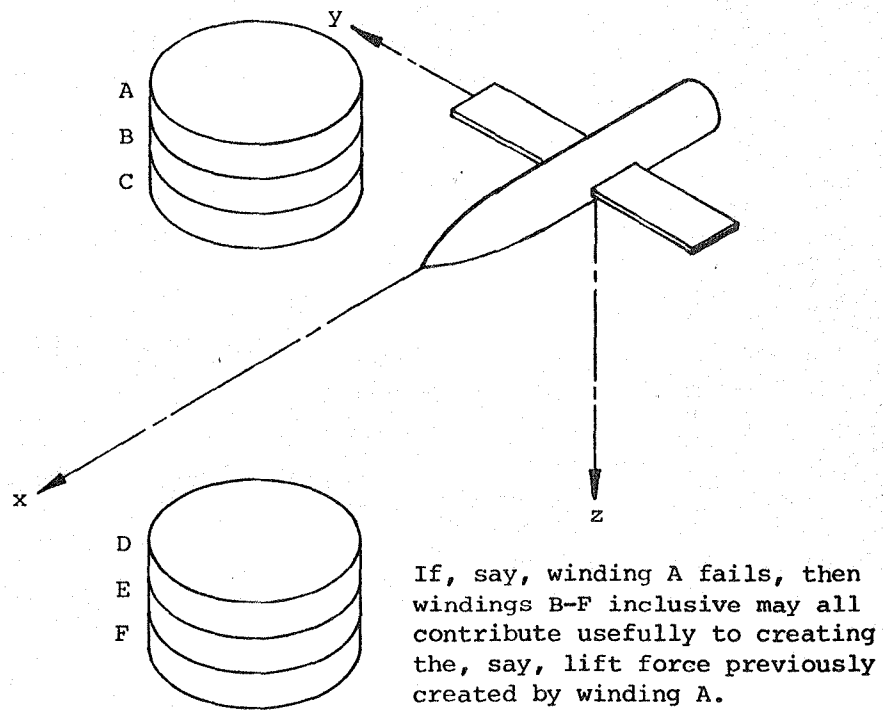
Fig. 8.4   The concept of passive redundancy
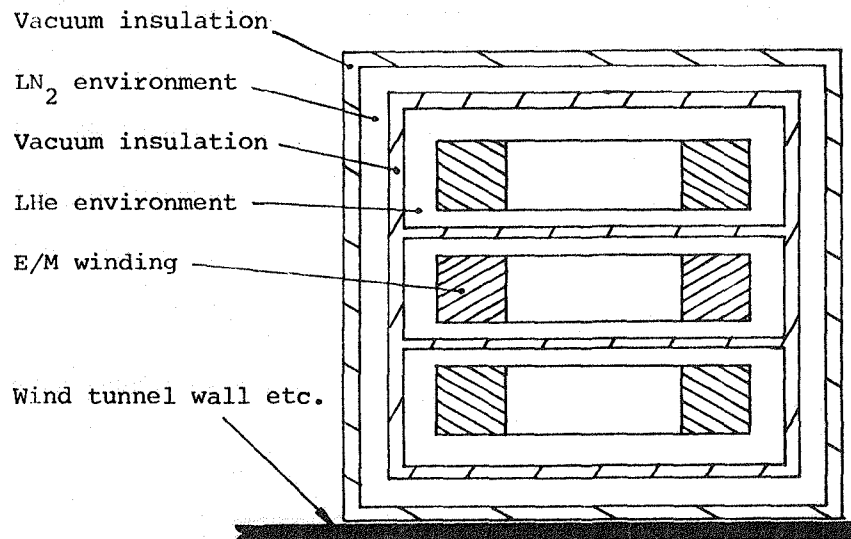
Fig. 8.5   Suggested insulation requirements for close-packed E/M windings

it may be decided to incorporate redundancy into the associated ancillary systems. These are particularly numerous in the case of superconducting E/Ms, typically including cryogenic plant, external dump resistors for discharging a winding following failure, and instrumentation such as helium level detectors.

It is relatively straightforward to incorporate redundant plant, sensors, etc., into the E/Ms but this would only be beneficial where the probability of an E/M quench being initiated by means external to the E/M (perhaps mechanical shock) was low compared to the probability due to the ancillaries themselves.

8.3.2. Incorporation of hardware redundancy into the E/M power supplies

Each winding of each E/M requires some form of power supply. The majority, perhaps all, of the E/Ms in a LMSBS would require current to be controlled with large amplitude frequency response to a few Hz. Terminal voltages of either sign are essential and it is likely that various factors would necessitate bipolar current capability, forcing choice of a four quadrant supply. Precise current and voltage requirements would depend critically on a system's detail design and specification but there seems no possibility at present of operation of a LMSBS without individual power supply capabilities of the order of several hundred amps and volts respectively. No supply is currently known to exist which simultaneously approaches the above requirements.

The difficulties associated with switching powerful electrical supplies are severe, particularly where large quantities of energy (millions of Joules in Ref. 5) can be stored in each E/M. Large current and voltage transients might be expected during switching processes in this case. Therefore, whereas it is technically feasible to incorporate redundancy in power supplies by straightforward duplication of supplies to each winding, with appropriate means to switch to backup units following primary supply failure, it may be thought an unattractive possibility on practical grounds. The financial penalty associated with duplication of power supplies is, of course, a significant further consideration.

If each E/M winding is operated with a single non-redundant power supply, failure of that supply necessitates immediate withdrawal of the winding from suspension duties since the winding current is

no longer controllable. With superconducting E/Ms, it is not necessary to power down a winding following supply failure, since the winding's time constant is effectively infinite. However, as previously mentioned, the possibility of supply runaway suggests immediate application of an APO procedure. The conventional means of achieving rapid power down with existing superconducting E/Ms is simply to short circuit the E/M terminals with an external dump resistor of suitable value. The hardware necessary for this type of procedure is easily duplicated, where required, to achieve highly reliable operation.

It may be possible to exploit the inductive coupling that exists between windings, particularly between windings of the same E/M, which will, following Lenz's Law, tend to maintain the net magnetic field of any E/M as constant. Controlled shutdown of one E/M winding might thus tend to induce a natural increase of current in the other windings of that E/M, with little external intervention. This, of course, broadly corresponds to the required system response following winding failure.

Interruptions of the power utility are not out of the question and some buffering would seem to be essential. Conventional means of buffering supply interruptions include :

> Emergency generators.
>
> Motor-generator sets in main power feeds.
>
> Batteries with static inverters.

Considering the high transient powers involved, the use of any of the above techniques would place a considerable cost overhead on a LMSBS. However, since the power dissipation in the load E/Ms will be nominally zero, the power supplies may be regarded as operating by supplying energy to the E/Ms where current increase is required and retrieving it where decrease is required. It then becomes highly attractive from the point of view of energy efficiency to arrange for a quantity of energy to be somehow stored, perhaps within each supply, at least equal to the magnetostatic energy stored in the associated E/M windings at peak design currents. Energy is then simply transferred between the energy store and E/Ms with the utility demand being devoted merely to losses and ancillaries. As previously discussed, the supplies used with the UVa superconducting E/M MSBS featured energy storage (on internal

capacitors) in precisely the fashion described above (7), as do
the supplies now used with SUMSBS (Appendix 1). It is immediately
seen that supplies of this type could be made capable of executing
a controlled RSS following loss of utility power, with only
ancillaries such as control systems requiring supply buffering.

8.3.3 Reliability and hardware redundancy in the system controller

The system controller is seen as the key module of any advanced
LMSBS, since it must encompass a wide variety of functions, which
together directly influence the configuration and operation of all
other parts of the total system. These functions include :

a) Model stabilisation and control. The principal traditional
feature of MSBS control systems. LMSBSs are certain to be operated
with test models covering a wide range of variations in aerodynamic
and/or magnetic configurations and characteristics. The control
algorithms must, therefore, exhibit considerable versatility and
robustness if they are to operate successfully, even over short time
scales, since the aerodynamic characteristics of the test models
will not be known in detail or to any accuracy before a test program
commences.

b) Prevention of model demagnetization. Permanent magnet cores
and, to a lesser extent, magnetically soft cores, would need to be
protected from exposure to combinations of applied fields that would
result in partial (loss of calibration) or extensive (loss of model
control) demagnetization of these cores. Demagnetization of
permanent magnet cores will be possible in all realistic LMSBS
designs and loss of magnetization of magnetically soft cores is
credible in all MSBSs.

c) System monitoring. The controller must incorporate
extensive subsystem health monitoring if it is to respond intelli-
gently to significant failures, such as by initiation of a RSS.
It is obvious that the monitoring processes themselves should be
carried out reliably.

Very highly reliable system control hardware, implementing
very dependable algorithms is seen as the foundation of a successful
LMSBS design.

Since it seems certain that the major part of the control system
of a LMSBS will be realised with digital computers, there would be
no particular difficulty in the incorporation of hardware redundancy.

- 215 -

Several options are available to achieve this, including :

(1)   Overall redundancy (Fig. 8.6)

A small number, perhaps three, mainframe or mini-
computers could relatively easily be configured as parallel
independent channels such that the complete control (suspension)
task is implemented simultaneously on each channel. Failure
of one channel could presumably be detected by some form of
majority voting procedure, with the failed channel being
switched out by command signals from serviceable channels.

This approach permits relatively straightforward execution
in hardware, though at the cost of a considerable surplus of
computing power (200% in a triplicated system).

(2)   Localised parallel redundancy (Fig. 8.7)

Series connection of several stages configured as (1) above,
produces a configuration exhibiting improved tolerance of
multiple failures but at the expense of increased hardware com-
plexity and no reduction in the required surplus of computing
power.

(3)   Multiprocessing (Fig. 8.8)

A relatively large number of versatile processing units can
be connected by multiple independent data buses as shown, to
effectively form a single processing system.   This system can
exhibit high tolerance to multiple failures where the task
previously performed by failed units is rapidly re-allocated,
either by software or hardware actions, amongst surviving units.
This architectural approach appears to be favoured currently
for ultra-reliable flight control systems, and is consequently
under intensive development for this application (53, 54).

The hardware and software complexity can be extreme however,
although typically only a modest surplus of computing power
(perhaps 50%) is required.

The MSBS control task is broadly comparable to that of a compre-
hensive flight control system in respect of the nature, complexity
and frequency of the calculations required.   However, the possi-
bility of rapidly aborting the control task, such as by use of some
form of RSS (Section 8.2.2), following detection of subsystem
failure, limits the number of independent failures that need be
tolerated.   The development of a specialised multi-processing

Model,
tunnel &
E/M sensors

Input
isolation
buffers

Mainframe, mini-
or dedicated
processors

Output
data
bus

Output
voters

Channel A

Channel B

Channel C

to power
supplies

Input data bus

Output
isolation
buffers

Interprocessor data
transfer buses
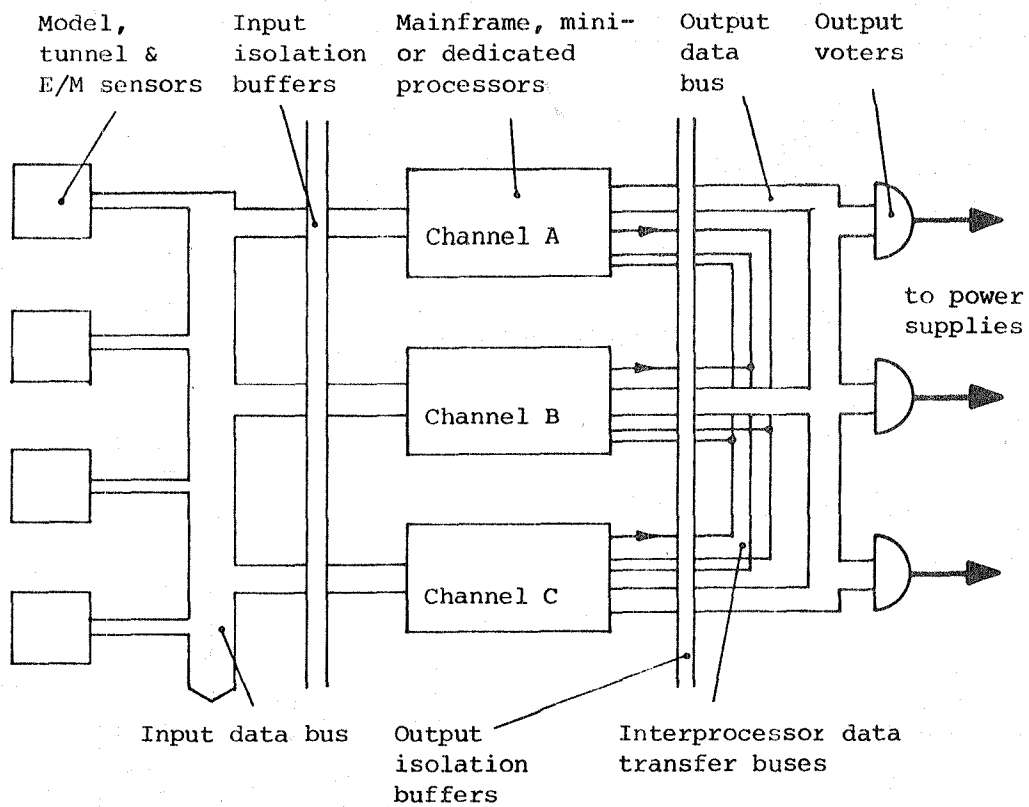
Fig. 8.6   Overall redundancy in the model control system (schematic)

Input isolation
buffers

Mini-, micro- or
dedicated processors

Majority
voters

Output isolation
buffers

as Fig.
8.6

as Fig.
8.6
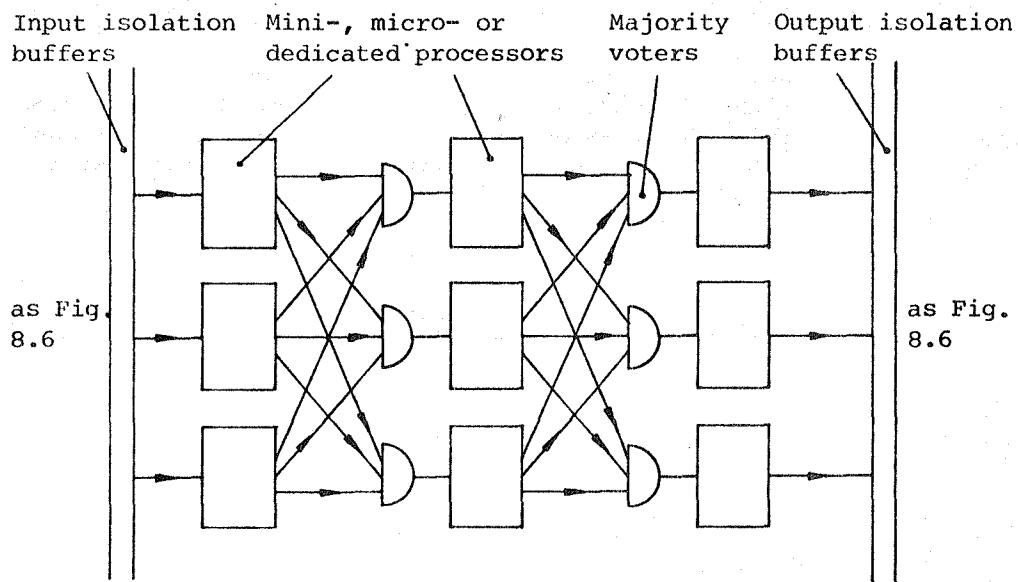
Fig. 8.7   Localised parallel redundancy in the model control system
(schematic)

Multiple parallel independent
internal data buses

as
Fig.
8.6

as Fig.
8.6

Multiple versatile processors (B), communicate
with multiple internal data buses via bus protection
units (A). Failed processors switched out by command
signals from surviving units (C). Task reallocated
automatically amongst serviceable units.
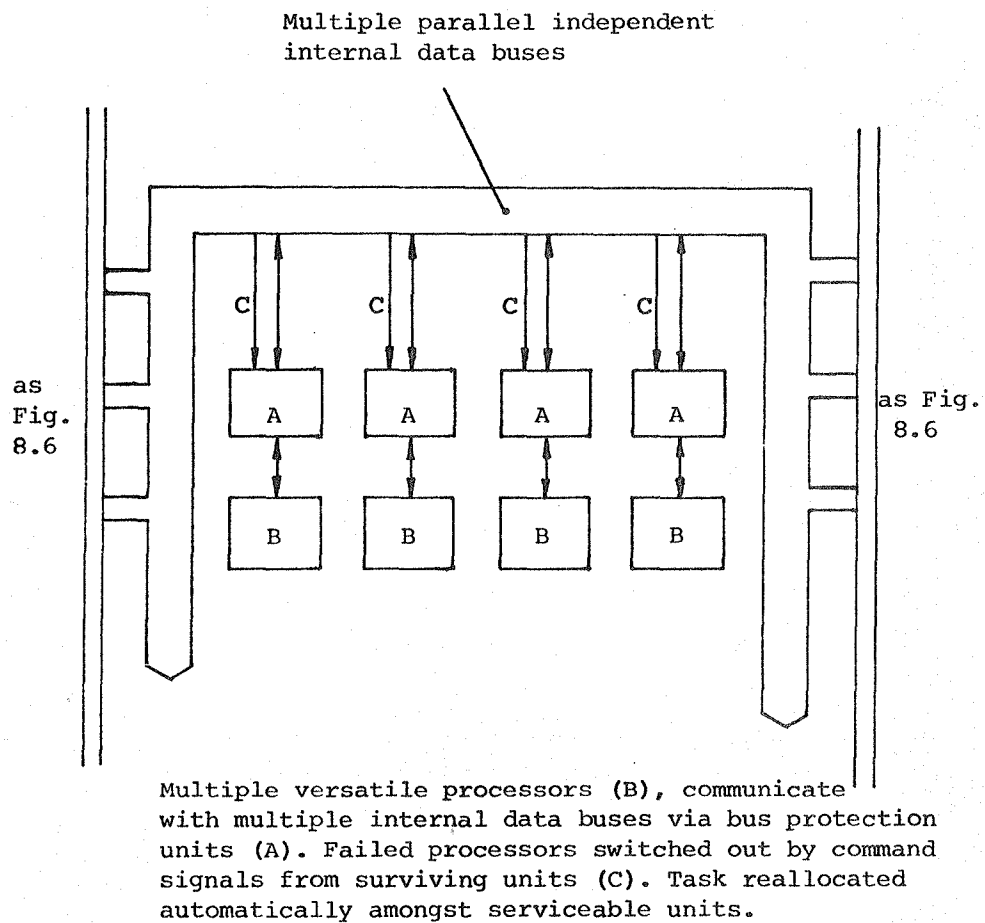
Fig. 8.8   Multiprocessing in the model control system (schematic)

controller specifically for this application may not, therefore, be justified.

Further, whilst certain series segmentation of the control task appears possible, for instance :

  (a) Model state estimation, including sensor processing.

  (b) Control response calculation.

  (c) Translation to required power supply demands.

the extent to which this segmentation is possible may be too limited to favour implementation of (2) above.

The fact that the control computers are unlikely to represent the dominant cost in a LMSBS and since frequent upgrades or revisions of software are likely, particularly in the early stages of LMSBS development, appears to mitigate towards (1) above.

Considerable attention will need to be paid to the software used in the control computers in order to ensure its own reliability, particularly since parallel operation of identical software is envisaged (parallel redundancy). This is, however, a very difficult area, the science of software testing and reliability being very much in its infancy, and cannot be further addressed herein.

8.3.4 Hardware and other redundancy in the model position sensors

All model position (also velocity etc.) sensing systems so far considered for use with LMSBSs suffer a serious lack of integrity, even where the hardware used is reliable. Specifically :

1) Optical systems.   The type of system used to date with SUMSBS ((11) and Appendix 1) is inoperable where rapid variations of the transmittivity of the optical paths are encountered. Such variations must be expected to occur relatively frequently in a cryogenic wind tunnel, for instance with free stream condensation, and in all tunnels when flow visualization is undertaken.

Methods which measure in either an analogue (e.g. T.V. or laser scanning) or in a pseudo-digital fashion (solid state arrays) the absolute position of either a target affixed to, or of a suitable part of, the model, may be designed to tolerate the conditions mentioned above (24), but all optical systems must fail in conditions of severe degradation of the optical path.

2) Electromagnetic position sensor (EPS). Any high intensity burst of electromagnetic radiation with suitable frequency content

will "white-out" an EPS. Such a burst might occur, for instance,
during electrical storms or catastrophic failure of E/M windings
or power supplies.   At present, considering the problems experienced
by the known users of EPS systems in filtering E/M power supply noise
(10, 55) it seems unreasonable to assume that the problem of white-
out may be easily overcome.

It is seen that a powerful argument exists, quite separately from
consideration of the reliability of position sensing hardware,
favouring the simultaneous use of at least two fundamentally
different position sensing techniques.   As an example, this may
perhaps be achieved by use of some form of optical system together
with an EPS, since there is no particular reason to expect simul-
taneous obscuration of the optical paths across the test section and
electromagnetic disturbance.   Without such provision a LMSBS would
be unprotected against the common-mode loss of all position sensing
systems arising from the adverse environmental conditions mentioned
above.

Subsystem redundancy may still be attractive in cases where hard-
ware reliability tends to be low (eg. light sources) but the inclusion
of totally redundant sensing systems of similar type may not be
fruitful in the context of the previous discussion, a particular case
in point being the EPS.

The only method by which sensible overall redundancy could be
incorporated into the EPS is by use of systems operating at different
frequencies since, for instance, duplicated sets of sensing coils
would otherwise pick up the same (possibly erroneous) signals.   It
is not, however, clear whether wide spacing of frequencies is tech-
nically feasible, the available frequency band being limited at low
frequencies by the inherent electromagnetic noise spectra of the MSBS
and by EPS coil and other system inductances at high frequencies.
Now, the EPS hardware physically located within the E/M array of a
MSBS is limited, merely an assembly of excitation and sensing coils.
These can be made very reliable indeed.   The driving, sensing and
signal processing electronics will typically be located remotely to
the MSBS and may relatively easily be duplicated, perhaps with fast
switching out of failed units.   There may, therefore, be no require-
ment for overall redundancy within the EPS.

It would seem reasonable to consider the application of special

analytic techniques to position sensor outputs in order that
spurious information be rejected. The considerable redundancy
of information that will exist, even with limited sensor redun-
dancy, recommends the techniques of analytic redundancy, that is
the detection of false sensor outputs by comparison of all
available data with predictions derived from a real-time mathe-
matical model. Such techniques are under intensive development
for other purposes (56, 57).

8.4 The impact of redundancy requirements on the sizing of the E/M array for a representative + configuration

8.4.1 Theoretical background

If each E/M is divided into a number of windings, say three,
with the intention of tolerating the failure of one winding, then
the E/M does not necessarily require 50% (in this case, assuming
APO) surplus ampere-turns. The effect of passive redundancy
(Section 8.3.1) is to reduce the requirement for surplus E/M
capacity by distributing the load previously taken by the failed
winding over a number of E/Ms, including, but not exclusively, the
remaining windings of the partially failed E/M.

It happens that the methods derived in Section 7.3 may be used
to examine the effects of E/M failures on the maximum force and
torque capability of specific MSBSs simply by adjusting (downwards)
the current limit applied to a specific E/M, in order to simulate
failure of a winding within that E/M. These methods seek to find
the absolute optimum distributions of currents in all available (in
this case, remaining) E/Ms so as to manifest the maximum capability
for a particular combination of forces and torques. Here, this
will tend to yield estimates of the minimum conceivable effect of the
failure in question. Shortcomings in the re-distribution and
manipulation of E/M currents will result in further performance
degradation.

Since there exists an infinite number of combinations of model
attitude, position and force and torque requirements it is clearly
impractical to attempt to present a comprehensive study of the
effects of E/M failure, even within a single specific geometry.
The approach taken here, therefore, is to examine the effects of E/M
failure on some of the data from Section 7, specifically the maximum
force capabilities of the + configuration, with the model simply
pitching, the resultant force vector constrained to lie in the plane

of pitching, and with zero magnetic torques. To recap, this system is of essentially similar overall configuration as SUMSBS, albeit geometrically and physically simplified to enable FORCE to be used to calculate the system's performance, and at ten times the true scale of SUMSBS for convenience. The absolute magnitudes of forces emerging from this analysis are not relevant here, but the relative effects of various failures, shown later, will be closely representative of the effects of the corresponding failures in SUMSBS. These studies are of limited significance insofar as they may convey somewhat optimistic or pessimistic assessments of the overall influences of the relevant failures, sideforce and torque generation not being studied, but serve to illustrate the powerful effect of passive redundancy.

Certain simplifications have proved to be necessary in order to prevent the computation of each set of performance curves becoming excessively laborious. In fact the envelopes within which relevant overall performance curves in Section 7 must lie (see Figs. 7.13 - 7.15 and accompanying text) are omitted.

8.4.2   Results

The configuration here is identical to that used in Section 7, and is specified in Figs. 7.5 and 7.6. Fig. 8.9 defines a numbering sequence for the E/Ms. With the sense of the three force vectors of interest defined in Fig. 8.10, Fig. 8.11 shows the system performance with all E/Ms fully operational. This Figure is identical to the relevant parts of Fig. 7.13. Figs. 8.12 to 8.19 contrast this performance to that with one-third or two-thirds of each E/M failed. One-third failure corresponds to a failure, with APO, of single windings of the main E/Ms of SUMSBS; two-thirds to failure, with APO, of two windings in the same E/M, or to worst-case failure of single windings without APO. SUMSBS' axial E/Ms have only dual windings, but one-third and two-thirds failures are computed here for consistency.

8.5   Discussion

The content of Figs. 8.12 - 8.19 has great significance to the cost of a LMSBS. With one-third of an arbitrary E/M failed, the reduction in force capability for the cases computed is nowhere
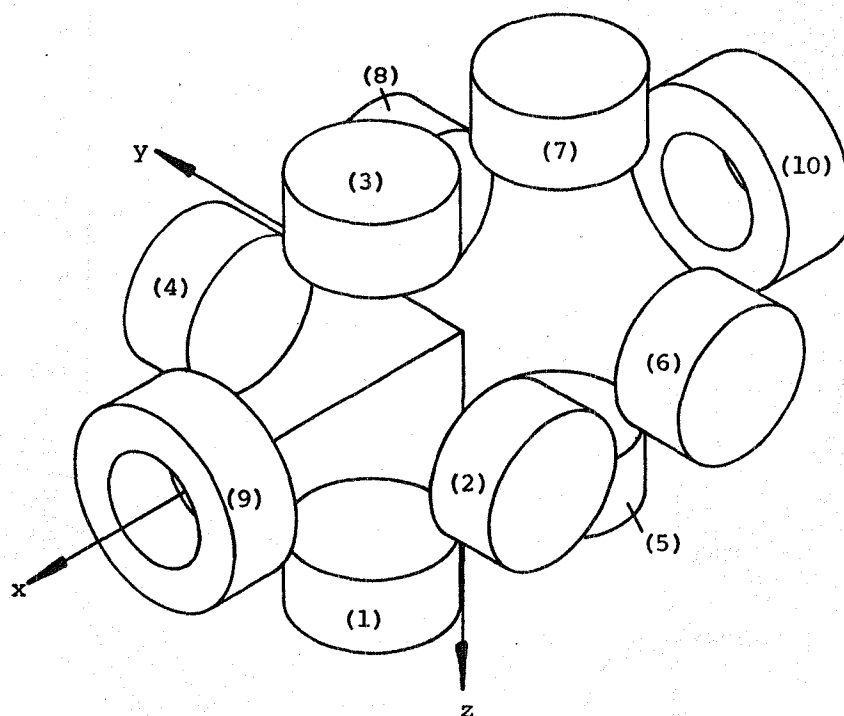
Fig. 8.9 Numbering sequence for E/Ms of + geometry, as Figs. 7.5, 7.6

The magnetic forces shown act to oppose the net aerodynamic forces.

ANGLE OF ATTACK

(θ)

x

DRAG

WIND DIRECTION

NORMAL (perpendicular to fuselage axis)

LIFT

z
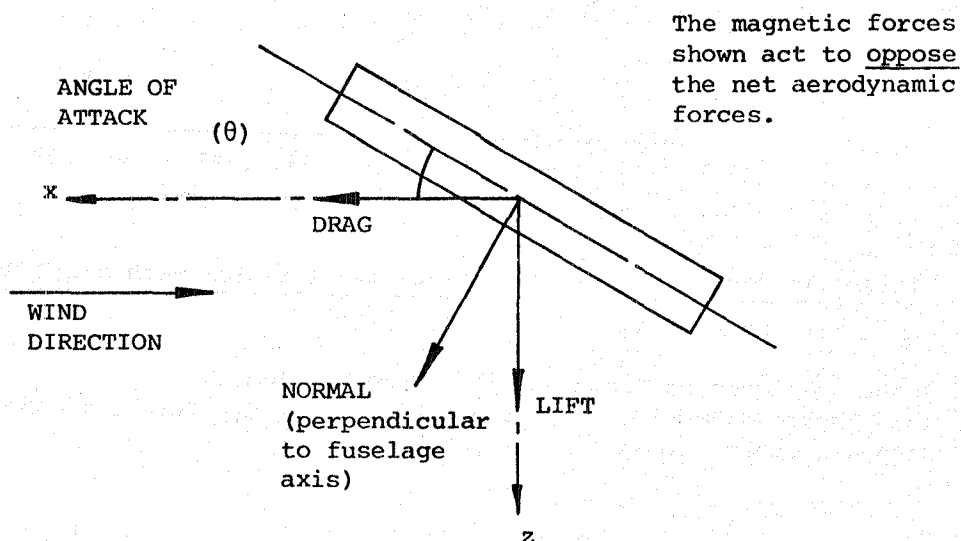
Fig. 8.10 Sense of force vectors for Figs. 8.11 - 8.19
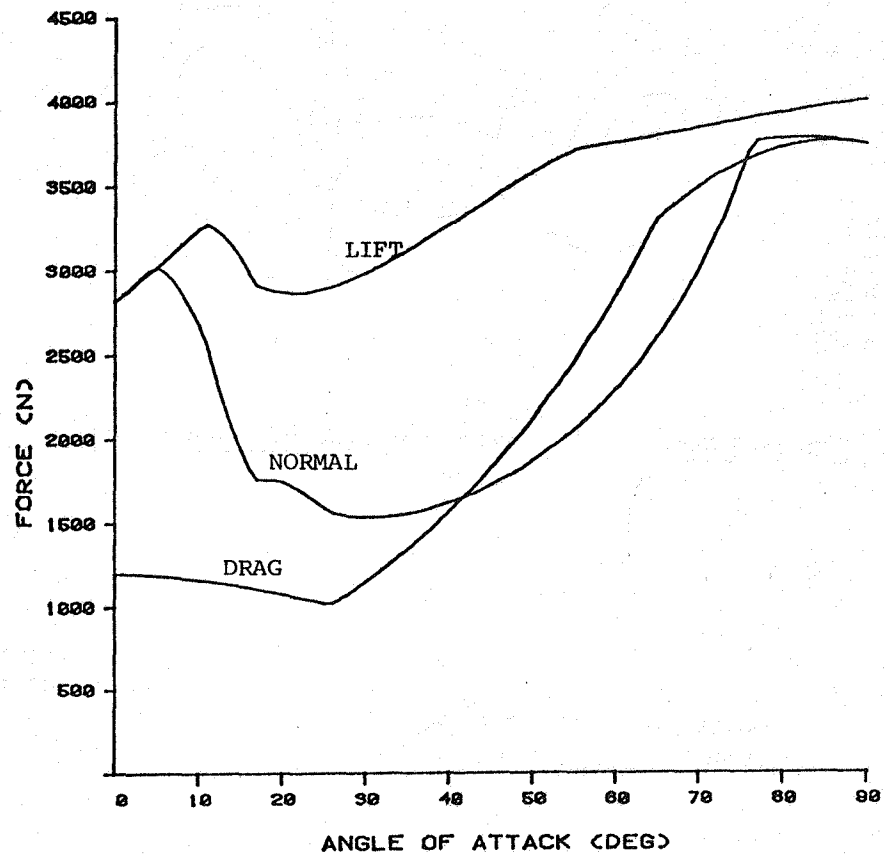
Fig. 8.11 Performance of representative + system with all E/Ms

operational

Sense of forces as Fig.8.10. Geometry as Figs. 7.5,7.6.
This Figure shows the MAXIMUM capability for the forces as shown,
with all other forces and torques zero.
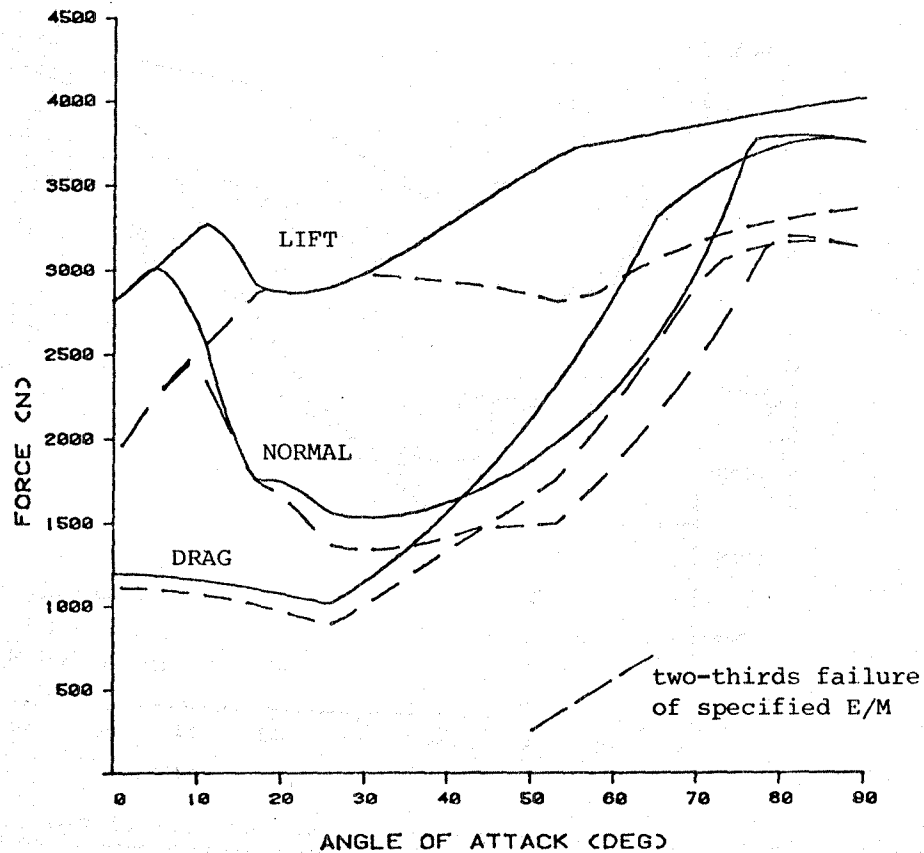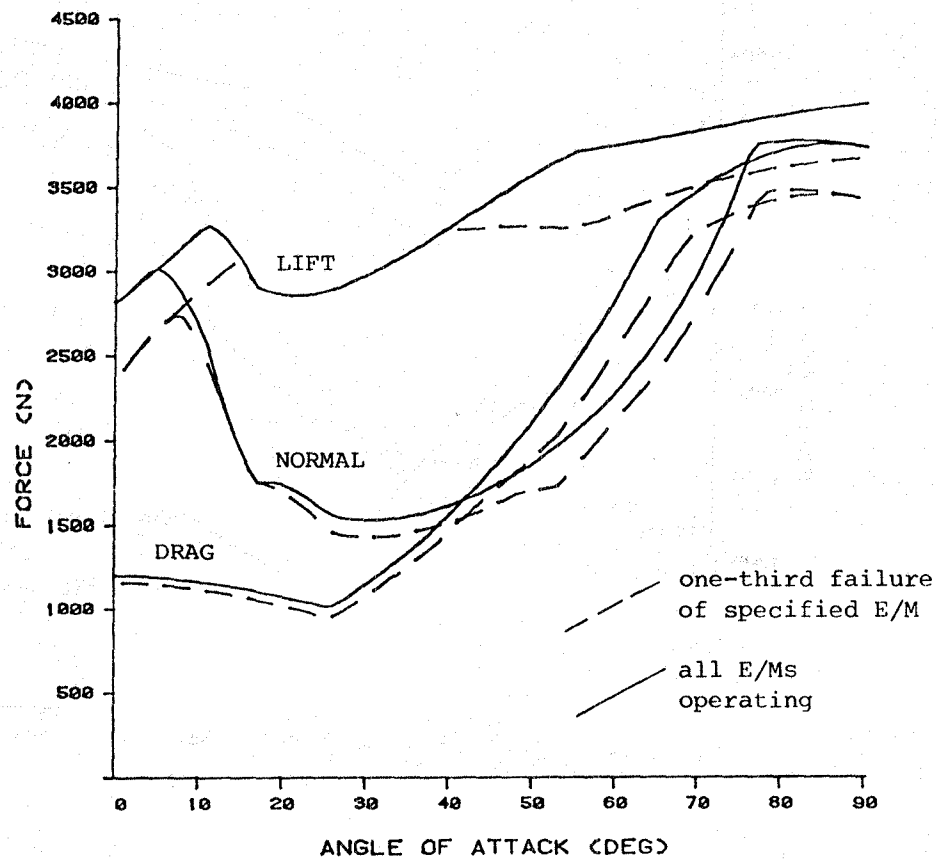
Fig. 8.12/8.13 Performance of + system with failure of E/M 1 (or 7)
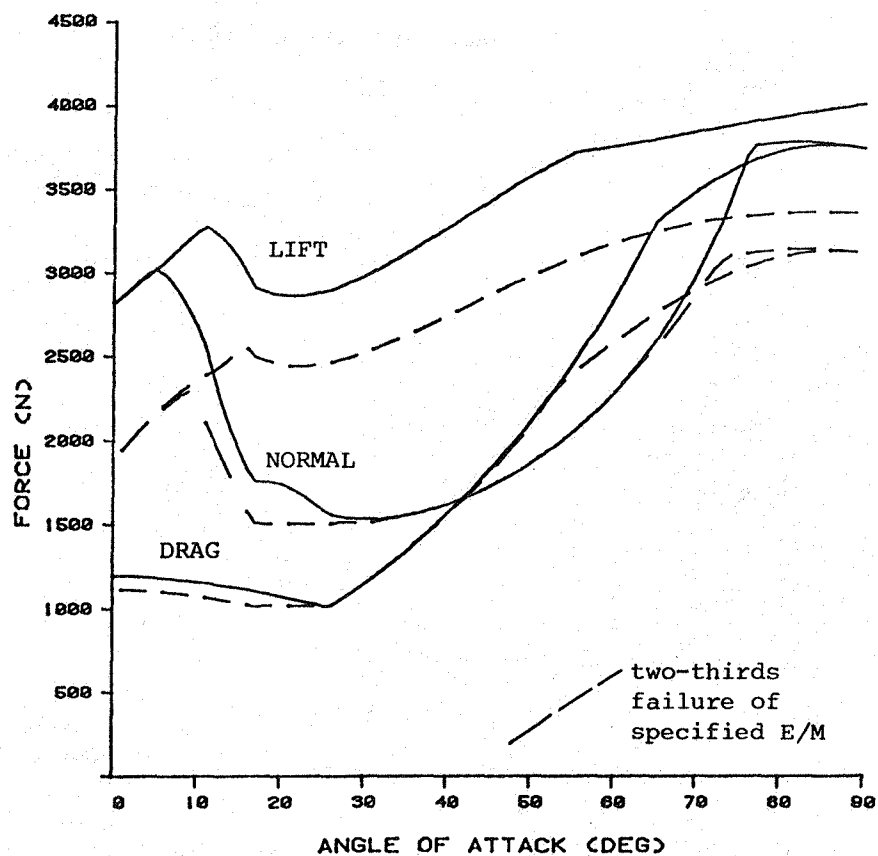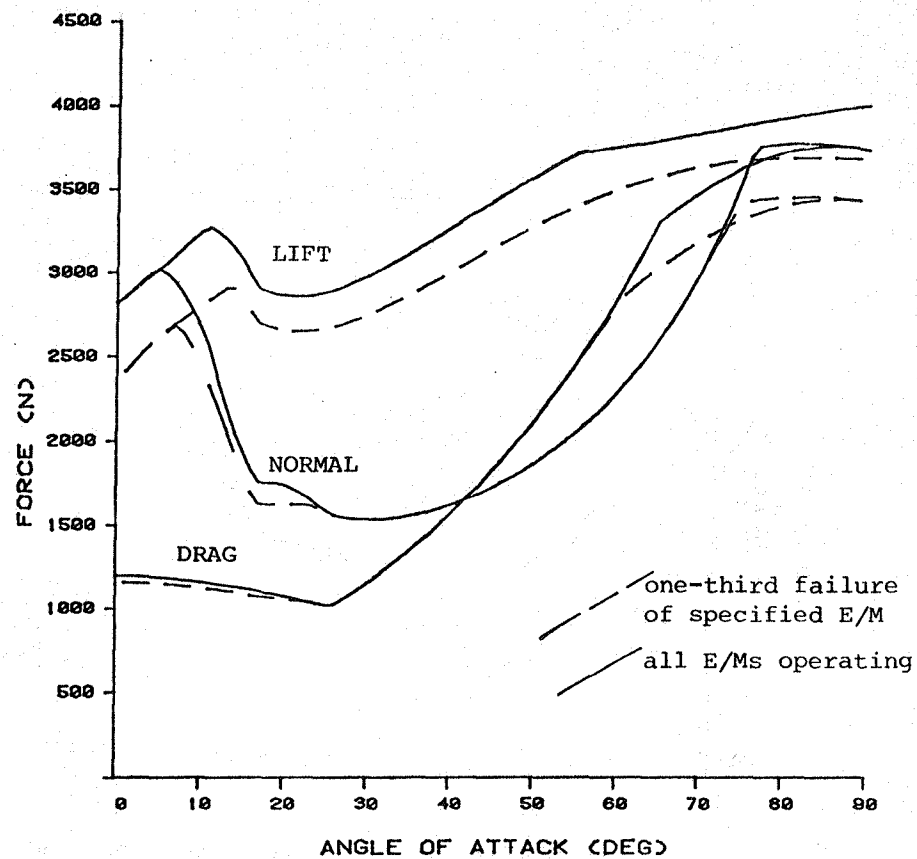
Fig. 8.14/15 Performance of + system with failure of E/M 3 (or 5)
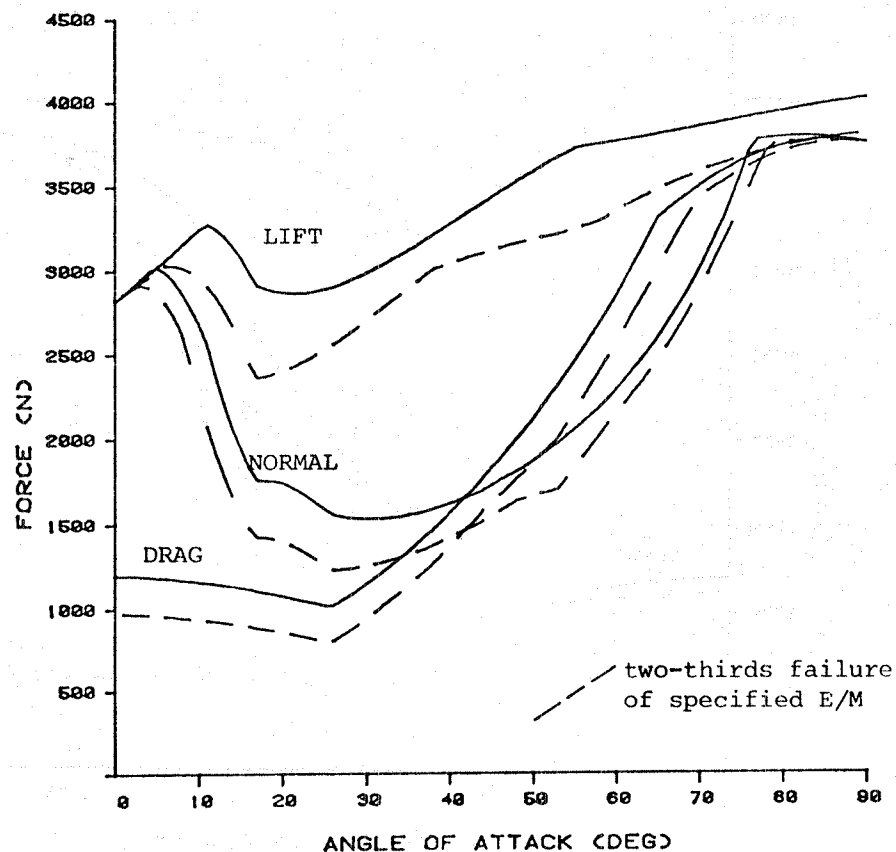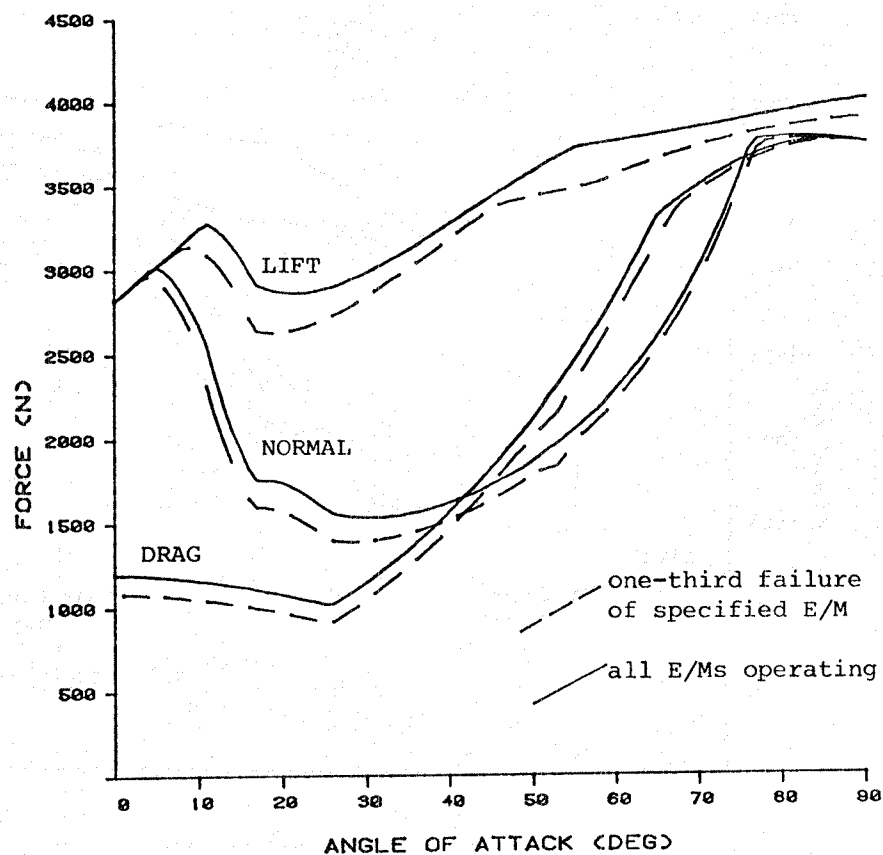
Fig. 8.16/8.17 Performance of + system with failure of E/M 9 (or 10)
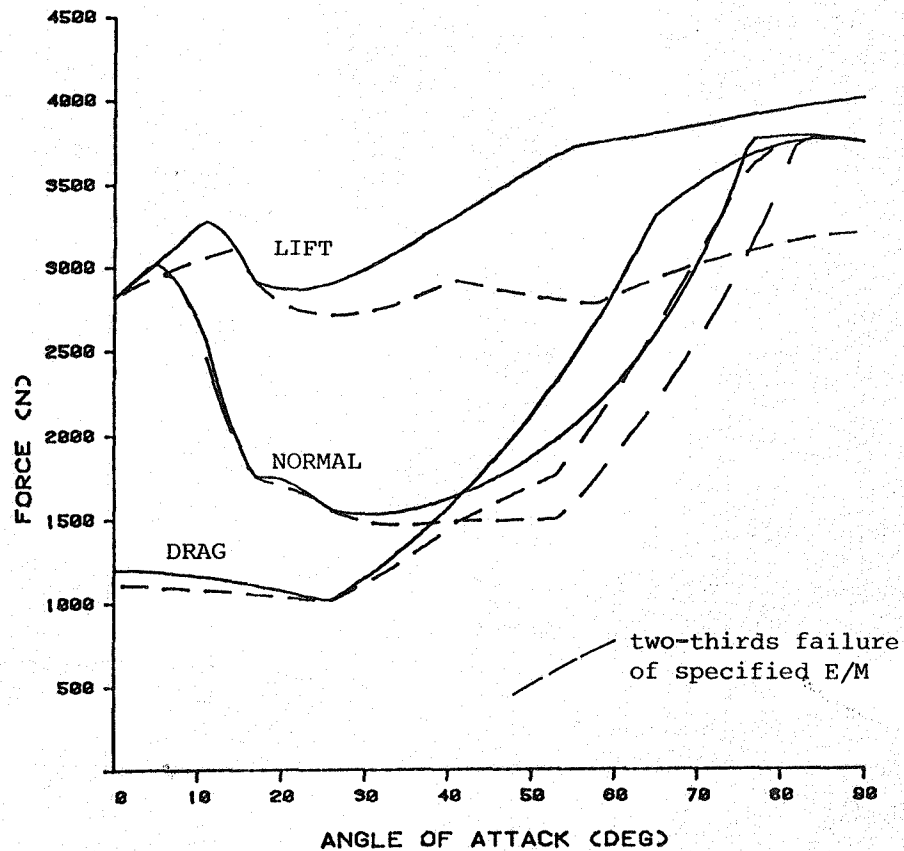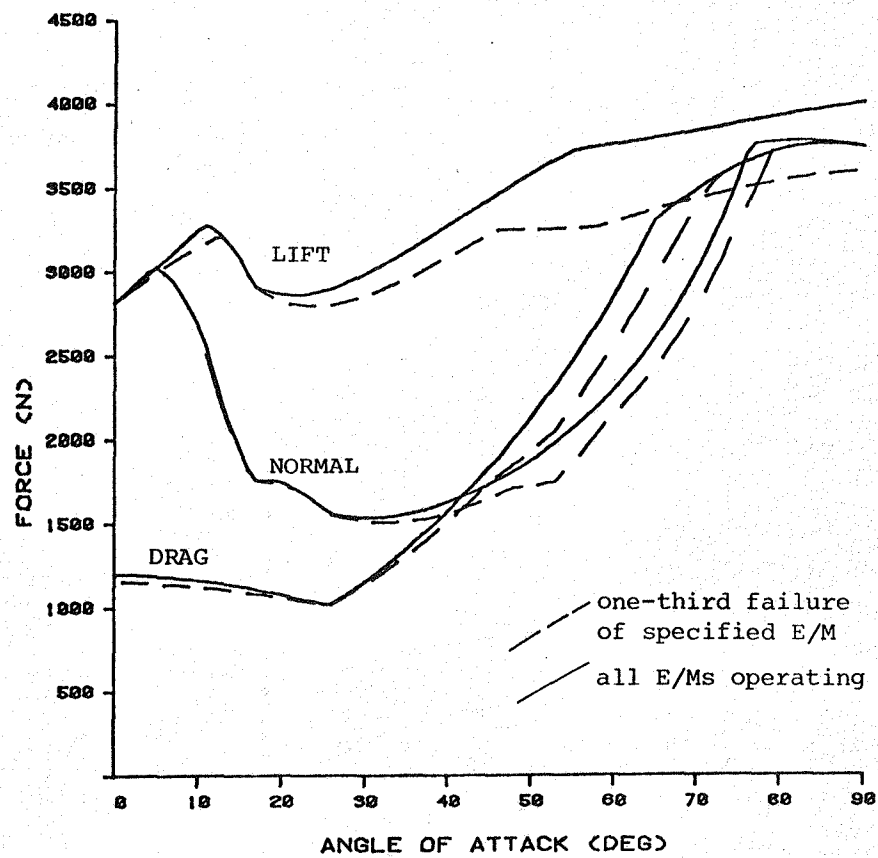
Fig. 8.18/8.19 Performance of + system with failure of E/M 2 (or 4,6,8)

greater than one-sixth and is typically around half that value.
Should this data prove to be representative of all cases, it would
follow that the surplus E/M capacity required to permit tolerance
of single arbitrary winding failures with triple E/M windings is
not greater than 20%.   This should be contrasted to the value of
50% shown in Fig. 8.3, where passive redundancy was not considered.
Dependent upon which parts of the performance curves, such as Fig.
8.11, prove to be critical, the requirement for surplus capacity
may be even less than stated above.

It is currently thought that the further cost overheads incurred
due to the extra complexity of, say, triple windings, as compared
to single windings of similar total ampere-turns, will prove to be
modest and acceptable.   Further, it is seen that dual windings may
be viable, incurring a basic cost factor increment of not more than
33%, and that large numbers of windings per E/M are unlikely to be
worthwhile (see Fig. 8.20).

Whilst no corroborative computed data is available, it is easily
seen that increases in the number of individual E/Ms in a MSBS will
tend to increase the effect of passive redundancy, thus decreasing
the cost factors for given numbers of windings per E/M, since there
would then exist greater opportunity for redistribution of the load
of a failed winding.   The number of E/Ms in SUMSBS is 10 and is
thought to represent a minimum conceivable number for LMSBS designs.
LMSBS cost factors are thus likely to be lower than those quoted
above for comparable cases.

Briefly to summarise this Section, it has been shown that the
increase in cost, complexity and sophistication of LMSBS hardware
caused by a requirement for highly reliable operation need not be
outrageous.   E/M cost factors can be kept satisfactorily low with
apparently modest hardware complexity, appropriate use of existing
types of position sensor should provide adequate redundancy and
independence of information, comparatively straightforward control
system hardware may be used and the overall power consumption of the
complete system need not be materially affected.
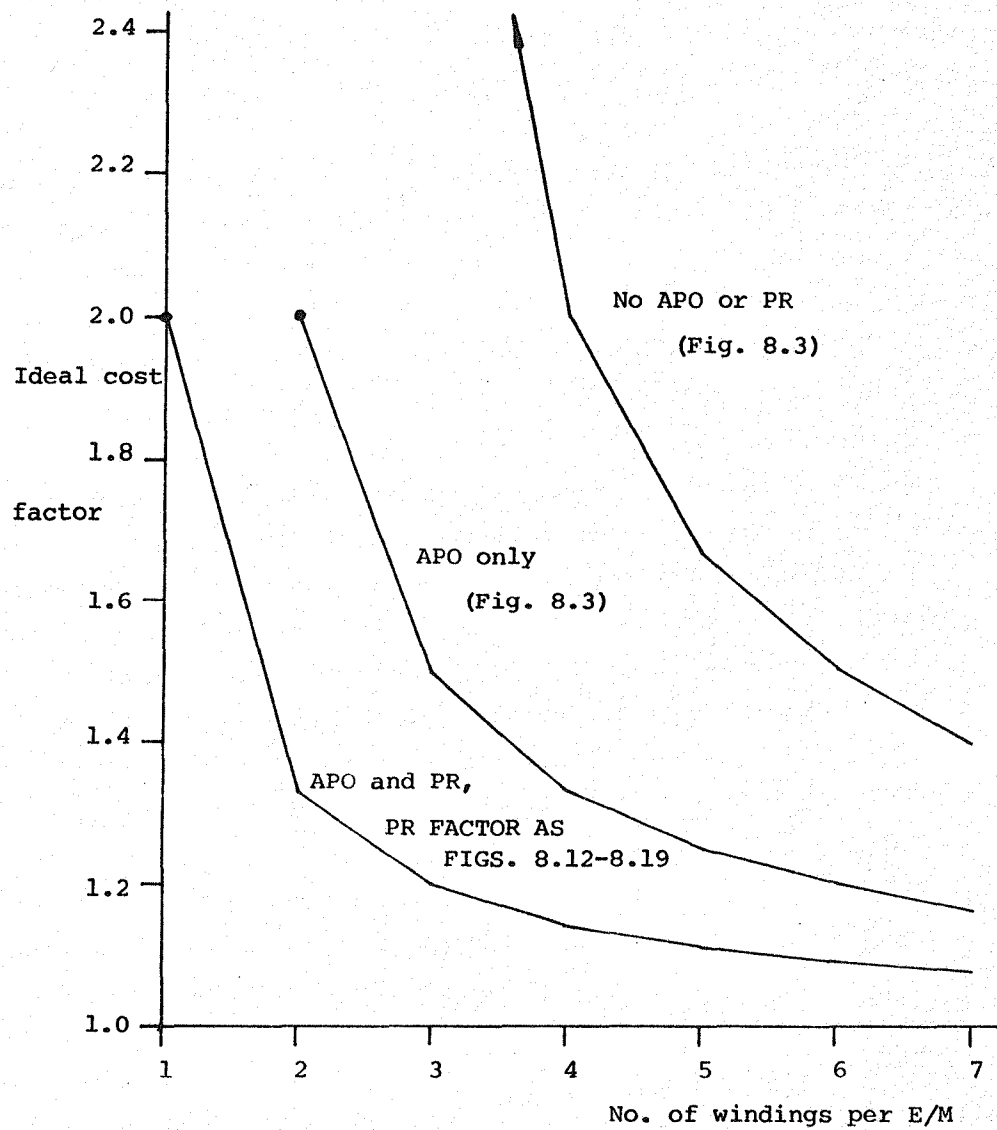
Fig. 8.20 The effect of passive redundancy (PR) and APO on E/M

cost factors, PR factor as Figs. 8.12-8.19

9. DISCUSSION AND CONCLUSIONS

Since the content of this thesis divides into three principal subject areas (roll control, extreme attitude testing and reliability), the first part of this Section is divided likewise.   These sub-sections will commence with a brief summary of material from the main text, followed by specific discussion and conclusions.

9.1 Roll control

9.1.1 Summary

A new method of roll control has been proposed, based on the magnetization, in the spanwise sense and with port-starboard symmetry, of the wings of winged aircraft models.   The system exhibits two principal variations, since the spanwise magnetizations may be permanent (SPMs) or induced (SIMs).

The roll torque generated by SPMs in a suitable uniform applied field gradient is shown to be proportional, at low applied field levels, to the first moment of core volume about the model's plane of symmetry, also, of course, to the applied field strength and the intensity of the spanwise magnetizations.   The maximum torque capability of SPMs is of major interest and is expected to depend principally on the magnetic properties of the core material (almost certainly ReCo) but, due to the lack of available data, has proved impossible to identify at this stage.   However a crude estimate indicates that substantial torques may be available.

The existence of cross couplings between model degrees of freedom is recognized but it is shown that with unswept wings there exists only one primary coupling and relatively few other couplings of significance.

A pilot model with SPM wings has been suspended in full 6-component control (with an all-digital control system, in fact) with no difficulty.   The demonstrated roll torque capability and the achieved levels of stiffness and damping of rolling motion were adequate to recommend the system as a first choice for future use in SUMSBS.

Subject to the provision of adequate E/M power, the SIM system will provide greater roll torque capability than SPMs, due partly to the higher levels of spanwise magnetization that are attainable.   No full demonstrations of the system were possible (that is, with 6-component model suspension) due to the unsuitability of the available E/M configuration.   However, comprehensive numerical computations (GFUN)

- 231 -

clearly indicate that high torques will be available, restricted
principally by current E/M technology.   Limited experimental
torque measurements at low applied field levels exhibit excellent
agreement with corresponding calculations.

9.1.2 Discussion and conclusions

It is thought that development of a powerful method of active
roll control is absolutely essential before construction of a LMSBS
could be attempted.

The variant of the Spanwise Magnet scheme that could be fully
demonstrated (SPMs) may be practical for LMSBS application, subject
to accurate identification of adequate maximum torque capabilities.
Some complication of model design is necessary to incorporate
permanent magnet cores into load bearing wing structure and, princi-
pally for this reason, the system is regarded with less favour than
the alternative variant of the Spanwise Magnet scheme, that is, SIMs.

The limited practical experience so far gained with SPMs indicates
that the system is an excellent choice for SUMSBS and demonstrates
the general practicality of Spanwise Magnet roll control (SPMs or
SIMs).   Cross couplings between model degrees of freedom due to
the presence of the spanwise magnetizations are easily handled by
suitable control algorithms and present no serious difficulty.
Suspension quality with the SPM winged model was good.   The spanwise
magnetizations and the applied "roll" and other fields do alter
(mostly adversely) the natural magnetic stiffness in several degrees
of freedom but modest adjustments to the controller will be sufficient
to restore the full stiffness and high stability currently achieved
with unwinged models.   Further computations of these effects would
be appropriate, though the data presented in Section 4.3.1 contains
the essential elements for a preliminary examination.

The SIM system is currently viewed as the most promising system
for LMSBS application.   Model design is very straightforward, since
wings may be machined from the solid with suitably chosen materials
and the predicted torque capabilities are very high, limited princi-
pally by current E/M technology.

The level of confidence placed on the available calculations, of
crucial importance of course, is currently high.   However, extensive
further and alternative calculations and a comprehensive demonstration
at small scale are seen as essential before a LMSBS is committed to

the system.   Such verification would necessarily include treatment
of cross coupling effects, which are expected to be somewhat more
pronounced than with SPMs.

Subject to such computation and verification being satisfactory
it is believed that careful study and optimisation of the roll E/M
array will prove fruitful.   The configurations used herein were
chosen to be representative of likely LMSBS E/M arrays but were
dimensioned entirely arbitrarily and are clearly deficient in many
respects.   If the ratio of useful field at, say, the model wing tip
to the peak field level within or around the individual E/Ms is taken
as a measure of performance, then the performance of the chosen SIM
arrays is low.   Adjustments to the E/M sizes, locations and winding
cross-sections are expected to yield significant improvements.

9.2   Extreme attitude testing

9.2.1   Summary

The largely intuitive realisation that the suspended model is
influenced merely by the local applied magnetic fields and is other-
wise unaffected, apart from the direction of the gravity vector, by
its location or orientation within the suspension system, is easily
illustrated by analysis.

This realisation leads directly to the inherent ability of MSBSs
to suspend and control models at any attitude and location, provided
that fields and field gradients in the required senses and magnitudes
local to the model can be somehow developed.

It happens that the transformations between applied fields in
balance axes and those seen in model axes are straightforward, but
corresponding couplings for field gradients are relatively complex.
Further difficulties are presented by the effects of the spatial
variations of the applied fields and field gradients about the model's
centroid.   These are quite pronounced in systems such as SUMSBS
where the E/M faces are in relatively close proximity to the model,
but will tend to be of lesser magnitude in LMSBSs.   Such effects
render the adequate separation of model degrees of freedom, essential
for the operation of contemporary control algorithms, quite complex.

The prediction that SUMSBS would be usable, in the + configuration,
from nominally 0° to 60° angle of attack (5-component control) was
verified by achieving suspension of an axisymmetric model over this
range.   The inability of SUMSBS to operate around 90° angle of attack

in the + configuration and the difficulties apparent with the X
configuration were traced to straightforward deficiencies in the
E/M array.

9.2.2 Discussion and conclusions

It has long been claimed that one major advantage of wind tunnel
MSBSs was the possibility of rapidly selecting near-arbitrary model
attitudes.   However, it is believed that no analytic or practical
verification had previously been attempted.

The problems presented by the gross changes in magnetic coupling
between E/Ms and model, occurring during large changes of model
attitude, are difficult but surmountable, the couplings being, of
course, analytic or near-analytic and repeatable.

Digital control is essential for sensible operation over wide ranges
of angle of attack in order to permit adaption of the control loops
to the changes in magnetic couplings and full digital control was, in
fact, used for all demonstrations.

Suspension quality with SUMSBS at the higher angles of attack was
poor due to three major factors:

(i)   The decoupling of the axial position sensor was
inadequate, resulting in coupling between pitch, heave
and axial motions.

(ii)   The already approximate computed magnetic couplings
(using FORCE), essential for adequate decoupling of model
degrees of freedom in the controller, were further simplified
before incorporation into that controller, for convenience.

(iii)   The natural magnetic stiffness of certain model
degrees of freedom in the quasi-steady applied fields
supporting the model's deadweight apparently became strongly
negative at the higher angles of attack.   Analysis and com-
putation of this effect should be undertaken before further
attempts at high angle of attack suspension are made.

The inability of SUMSBS to operate above about 60° angle of attack
in the + configuration and the poor performance predicted for the X
configuration indicate that this simple fully symmetric 10 E/M array
is unlikely to represent a good choice for a LMSBS.   However, the
shortcomings of the configuration, identified theoretically, are
easily rectified by augmentation of the E/M array, indeed such

augmentation would be likely if SIM or SPM roll control was employed, and it is strongly believed that unlimited model attitudes, with full 6-component control, will be easily achievable in realistic LMSBS configurations. The most difficult problem in such a system may, indeed, prove to be the provision of model position and other sensors capable of satisfactorily monitoring wide ranges of model attitudes and motion.

9.3 Reliability

9.3.1 Summary

The widespread concern that the capital cost overhead incurred by a requirement for highly reliable operation would drive already expensive LMSBSs out of reach, has been partly dispelled. The two areas of greatest expenditure, that is the E/Ms (with associated plant) and the E/M power supplies, need only carry modest levels of redundancy and the complication of design, such as segmentation of E/Ms into several separate windings, is not severe. Indeed, segmentation of E/Ms and corresponding duplication of power supplies was featured in the only comprehensive LMSBS design study made to date (5), for reasons apparently unconnected with reliability.

It is shown that the reliability of the remaining MSBS subsystems such as model position sensors and control systems may be adequately raised, albeit at the expense of some design complication, such as by the incorporation of at least two fundamentally different position sensing systems.

9.3.2 Discussion and conclusions

An unreliable LMSBS would be an expensive burden rather than a benefit. Any attempts to argue that a relatively high attrition rate of models in a "cheap" LMSBS could be justified is undermined by simple application of Murphy's Law, which indicates that the most expensive and intricate models would be destroyed before any useful aerodynamic data had been obtained.

Though full technical presentation would be inappropriate here, preliminary demonstrations of hardware (E/M and E/M power supply) redundancy have already been made with SUMSBS. Specifically, with an axisymmetric model in steady suspension (wind-off and low angles of attack), ANY power supply, including those contributing towards the support of the model's weight, may be switched off with impunity.

The transient motion following the switch-off (or switch-on) is naturally controlled by the existing control algorithms, the model's weight, for instance, simply being redistributed amongst remaining operational E/Ms, and motion could be virtually eliminated if the controller was able to detect the "failure" of the power supply in real time, such as by monitoring the E/M currents. These demonstrations clearly confirm the existence and the powerful effect of Passive Redundancy, in this case not depending in any way on special configuration or adaption of a relatively simple MSBS.

The key to reliable and economical LMSBSs is the EXPLOITATION rather than the SUPPRESSION of the many unique features of such systems.

9.4 SUMSBS

The commissioning of the new features, hardware or otherwise, of SUMSBS, has proved remarkably trouble free.

Incorporation of digital control hardware and digitized control algorithms has been straightforward, with no particular difficulty in interfacing with the rest of the system. This success owes much to the care taken in the hardware design phase to create a system of high integrity, such as by the incorporation of complete electrical isolation between the control computer and the MSBS rig itself and the incorporation of sensible analogue filtering in position sensor preamplifiers and power supplies. The general performance of the controller is now as good as had ever been achieved previously with analogue systems. Changes or adjustments of control parameters may be made with precision and repeatability in seconds, rather than minutes or hours, and there now seems no reason to consider anything other than full digital control for a LMSBS or, indeed, any new MSBS.

Considerable scope for improvements to the performance of the controller certainly remains, including the quality of suspension achievable with wind-on, the adaption of the controller to changing test conditions and the performance at extreme model attitudes.

The new transistor switching power supplies, radically different from anything known to have been used previously in this application, are steadily amassing many hours of operation, to date completely faultlessly. The E/M loads (high inductance, low resistance) appear to be well suited to this type of supply. The level of radiated electrical noise, due to the high frequency switching, is much less

than had been feared, and has presented no serious difficulty.
Accurate monitoring of E/M currents is not straightforward, but
can be achieved with appropriate techniques. The independent
and bipolar operation of each E/M has considerably enhanced the
performance and versatility of the system, with no significant
disadvantage yet apparent.

The principal weakness in SUMSBS remains the position sensors.
Significant changes in model geometry or gross changes of model
attitude are only possible with mechanical realignment of the
sensors. This is a serious inconvenience but in no way indicates
a fundamental difficulty. Superior position sensing systems,
optical or otherwise, are available and may be gradually incor-
porated into SUMSBS in future years.

THE SOUTHAMPTON UNIVERSITY MAGNETIC SUSPENSION AND BALANCE SYSTEM

Contents		Page

A1.1 Introduction

The present status of SUMSBS hardware represents only an interim phase in a more or less continuous program of development.   This Appendix seeks merely to acquaint the reader with the current major features of SUMSBS, particularly those relatively recently introduced or updated.   Fuller descriptions of certain hardware may be found in some earlier material, such as Refs. 11, 15.

A1.2 E/M geometry and configuration

The approximate dimensions of the main E/Ms and associated iron cores are shown in Figs. A1.1/2. All 8 E/Ms are nominally identical, 6 in fact being carried over from earlier versions of SUMSBS. Previously, the iron cores had been configured rather as yokes (Fig. A1.2) with one "upstream" and one "downstream" E/M per assembly. The cores have been modified by removal of the centre portions (shaded in Fig. A1.2) in order to reduce the fore-and-aft inductive couplings between associated E/Ms.   This coupling had not previously been unduly troublesome, in fact the presence of the link augmented, for instance, the conventional "lift" field by some 30% due to the provision of return flux paths, but was considered undesirable for suspension at high angles of attack, or with spanwise magnet roll control, where more or less independent control of individual E/Ms is mandatory. Each E/M is wound with approximately 400 turns of 12 gauge enamelled copper wire, uncooled, and split into three sections normally connected in series.

Section on BB

4.0

Iron cores
not shown

400 turns
enamelled
copper
wire in 9
layers

0.25

0.5

1.375   3.54   1.315

9.0

Section
on AA

0.25

5.5

1.685

3.0

3.5

Part
View on BB

4.0675

A

x

z

Part
View on A

4.5

y

z
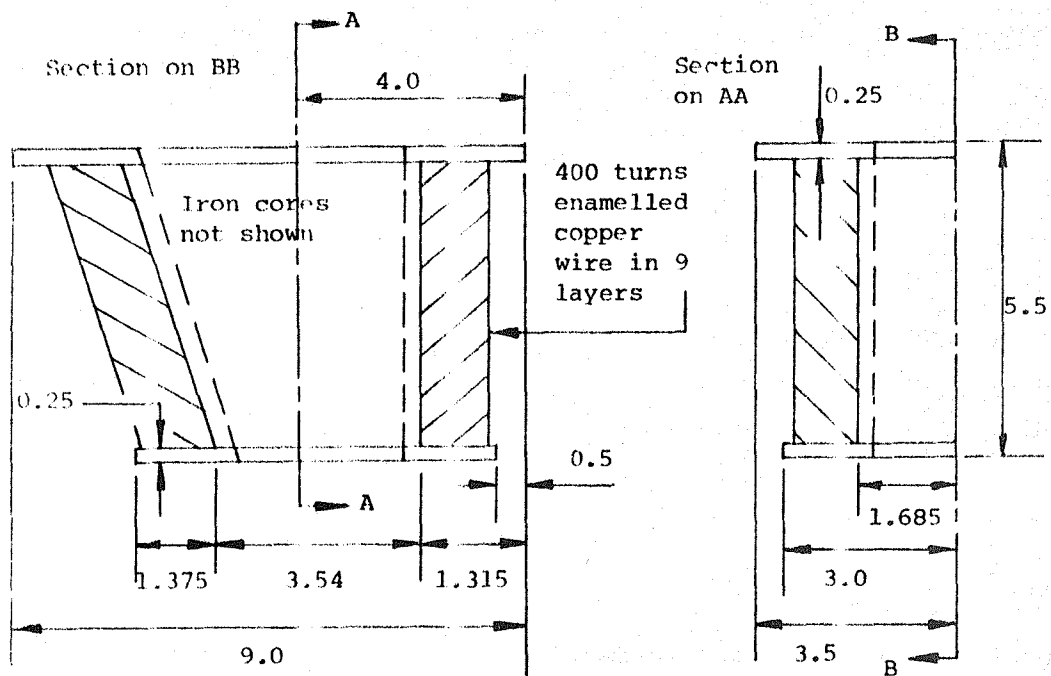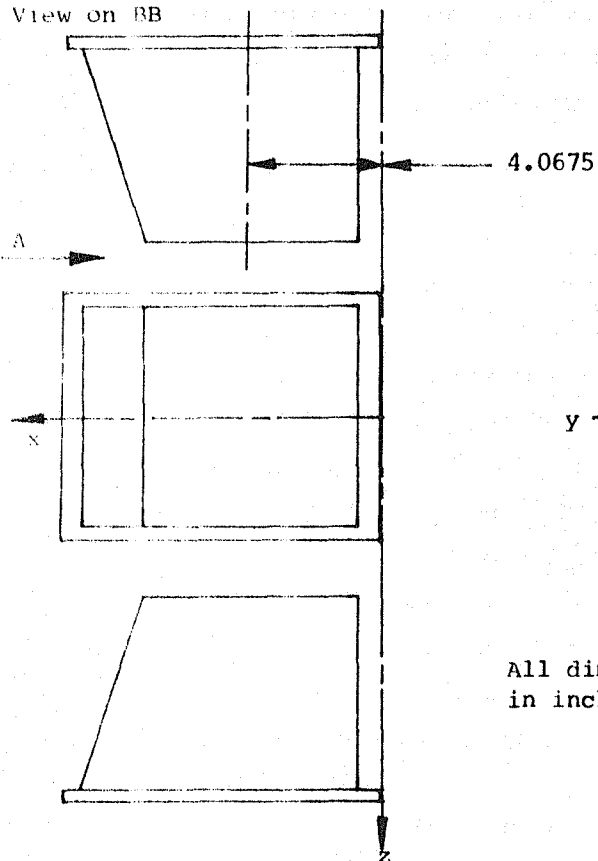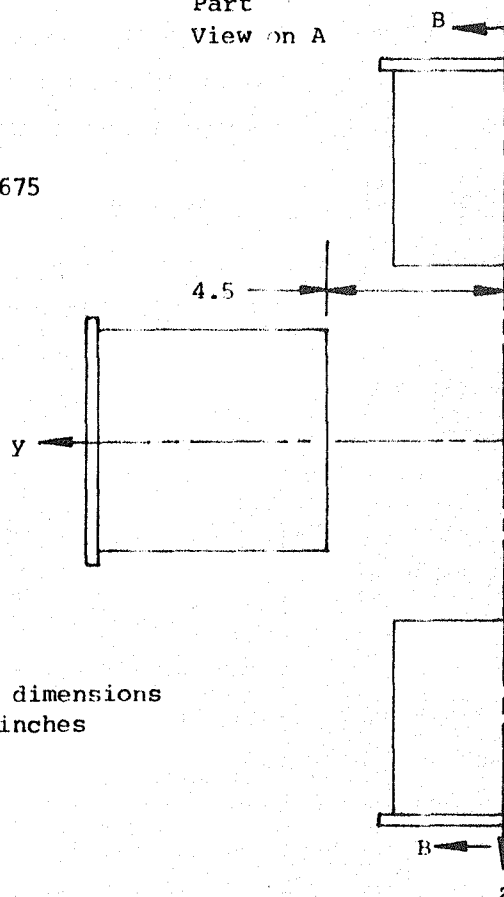
All dimensions
in inches

Fig. A1.1 Dimensions of main E/Ms of SUMSBS, showing configuration.
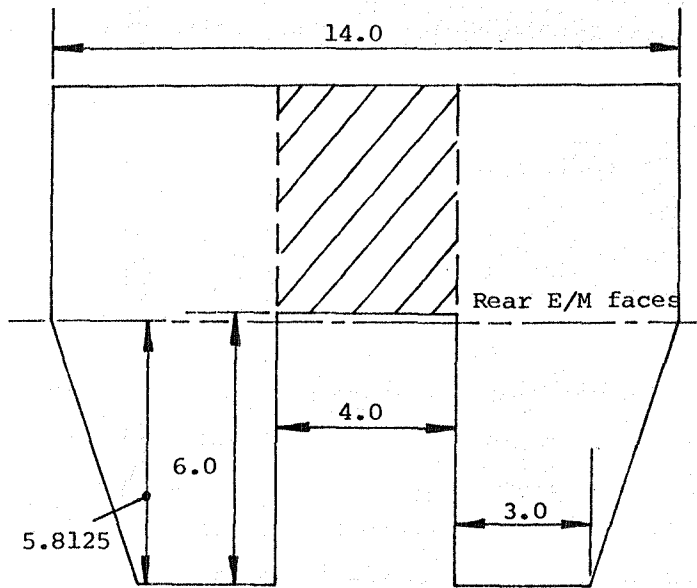
Cores are approx.
200 Stalloy laminations
between 0.125 gauge
plate facings.

Overall thickness of
cores is approx.
2.9375

Shaded portions
now removed

Fig. Al.2 Dimensions of main E/M iron cores. Dimensions in inches
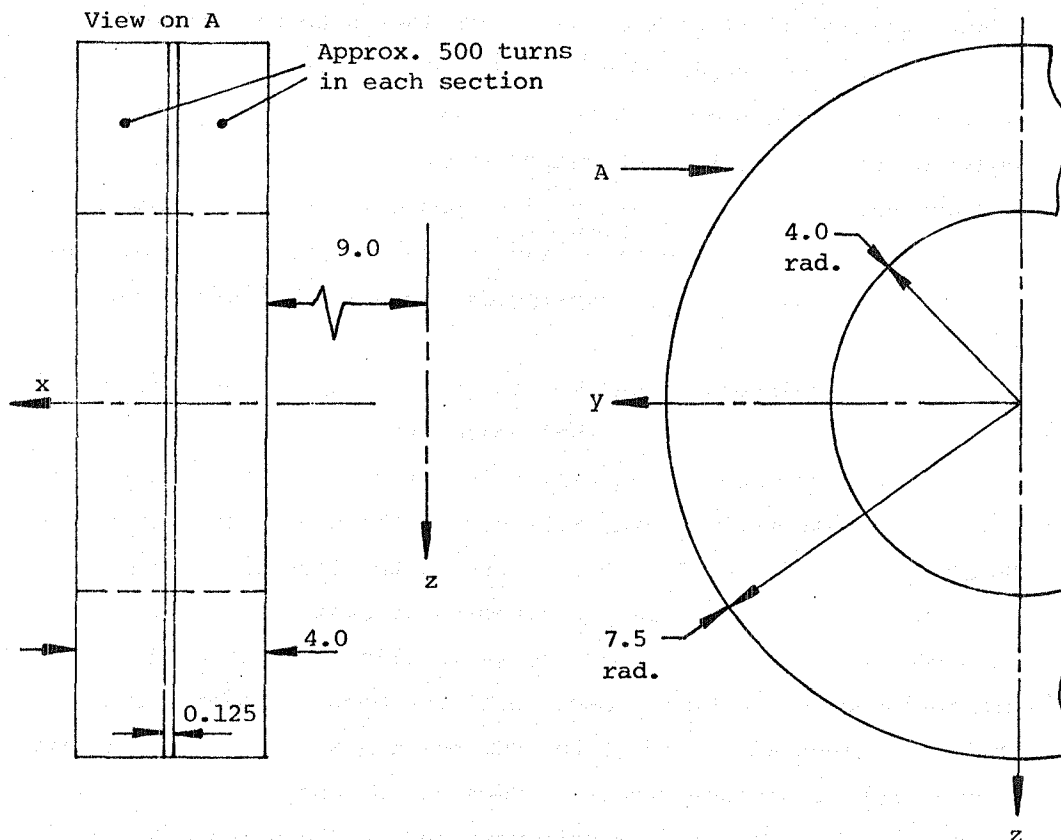
Fig. Al.3 Dimensions of axial E/Ms of SUMSBS, showing configuration

The twin axial E/Ms (Fig. A1.3) are somewhat similar in construction but are wound with thinner wire (14 gauge) split into two sections of approximately 500 turns each, normally connected in parallel.

The E/M configuration is fully symmetric and is illustrated in Figs. A1.4 - A1.8.

A1.3 Power Supplies

All 10 E/Ms are currently independently controlled by CSR Contraves NC 421 servo controllers (Ref. 58 and Figs. A1.9 - A1.10). These controllers, rated at 21A continuous, 45A peak and 100V for four quadrant operation, were, in fact, designed for industrial D.C. servomotor drives but are well suited to this application. The fundamental mode of operation is pulse width modulation, with the ability to be driven unconditionally to 0% or 100% modulation. Since the switching frequency is nominally 5kHz the forward path voltage gain, neglecting the effects of current feedback, can be set flat to around 1kHz, representing a considerable advance over previous SUMSBS supplies (11). Fixed internal current feedback is in fact provided (Fig. A1.11) and is considered to be extremely advantageous. Synthesis of model control algorithms is eased, countering the lengthening of the E/M time constants caused by removal of the series ballast resistors previously used (Section 2.2.2 and Ref.11), the linearity of response is improved, output drift with temperature and time reduced and the effects of voltages induced in E/Ms by magnetic coupling from others is significantly attenuated.

The power regulators which feed the controllers (Figs. A1.12, A1.13) themselves feature internal energy storage (on capacitors) totalling some 280 Joules overall, this being slightly greater than the total magnetostatic energy retained in the E/M array with all E/Ms at peak continuous current. Despite the fact that only some 20% of this capacity is normally dynamically available, it is seen that since regeneration of load energy is allowed (four quadrant operation) the net power consumption of the complete system under normal conditions will tend to be low, being mostly due to resistive losses in E/Ms and power stages. Some 25 kW (continuous rating) of power is available from transformers and has been found to be more than adequate for all requirements.

Fig. Al.4 E/M array with axial E/Ms not installed.

Upper E/Ms
(2)

Port E/Ms
(2)

View
upstream

Stb. E/Ms
(2)

Lower E/Ms
(2)

Some
position
sensors
just visible

PLATES OVERLEAF

Fig. Al.5 E/M array from port side.

Upper E/M iron
cores

Light
sources

Roll
attitude
sensor laser
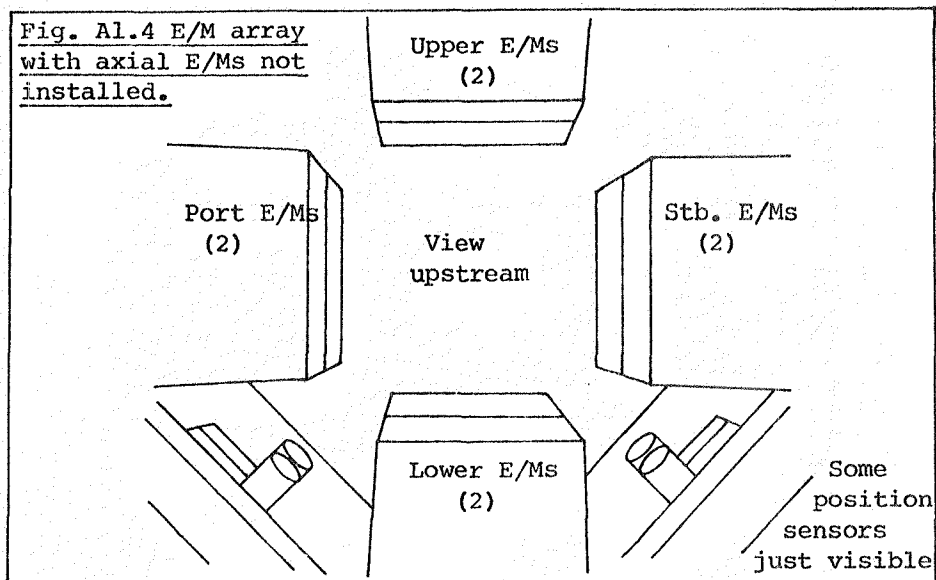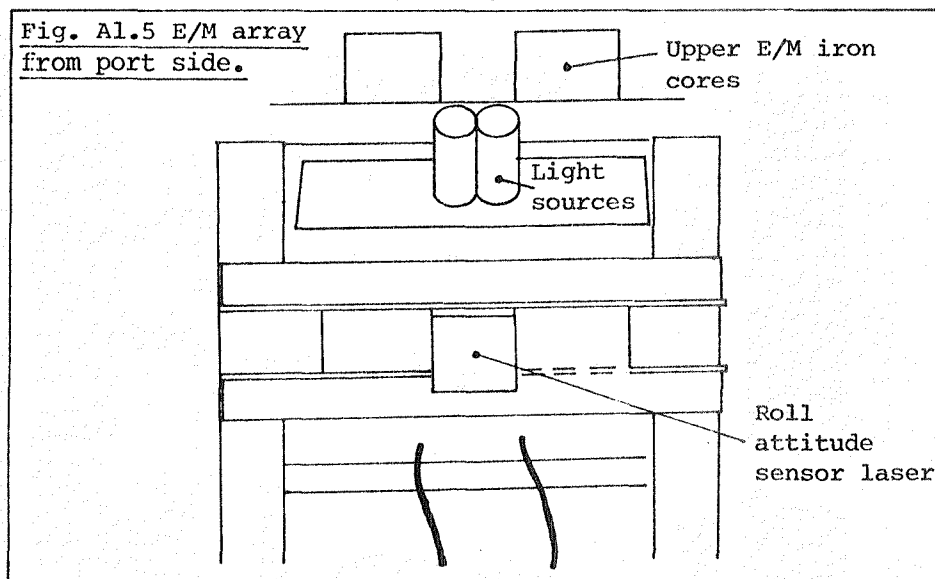
PLATES OVERLEAF

Fig. Al.6 E/M array. Front threequarter view.

Light sources

Roll laser

Axial
E/M
(No.9)

Some position
sensor pickups
just visible

- 243 -
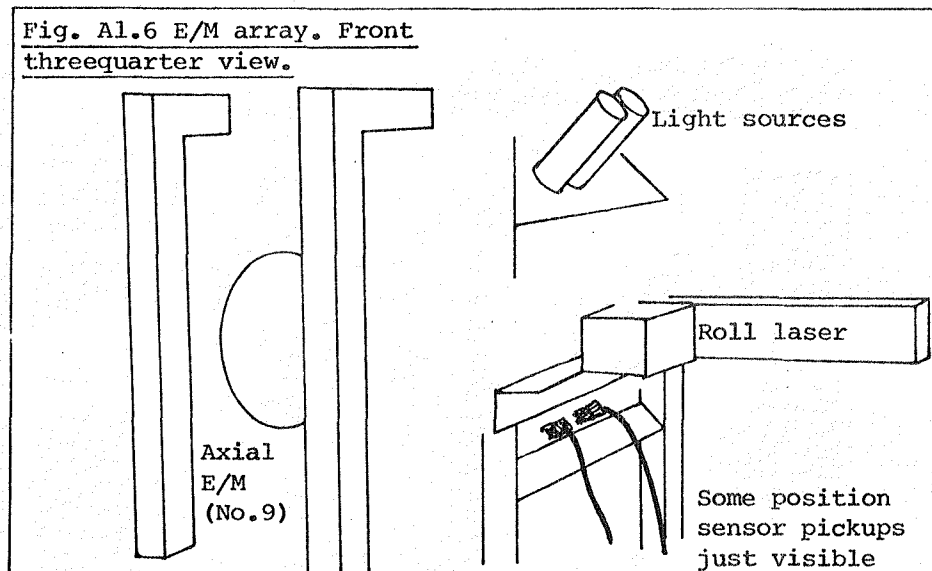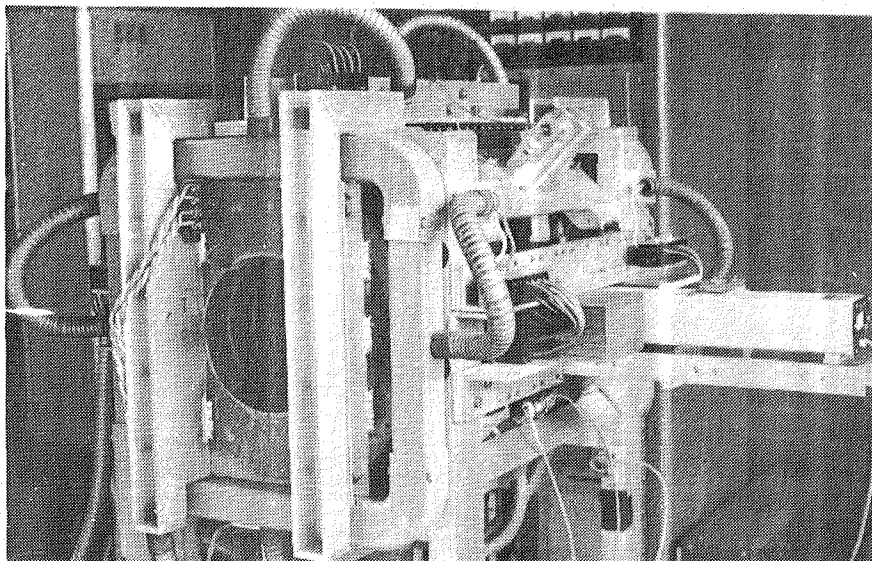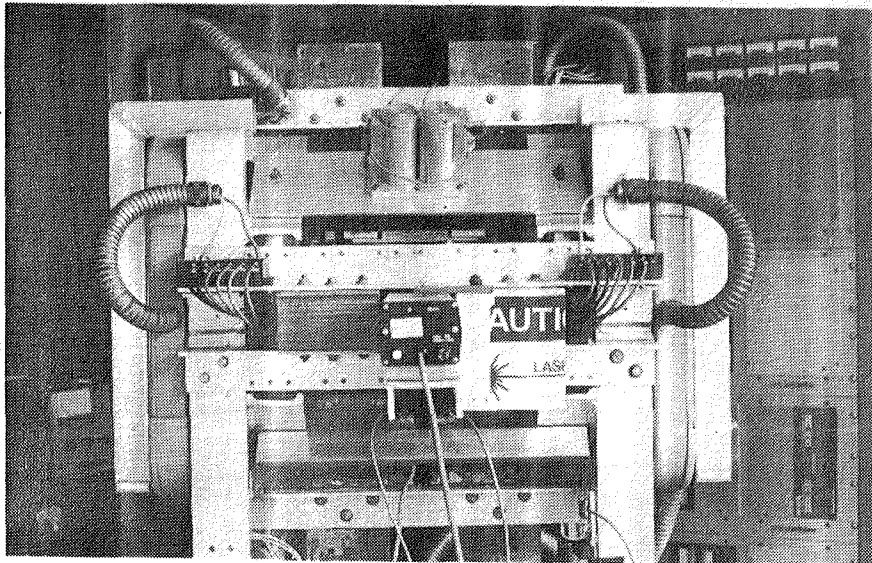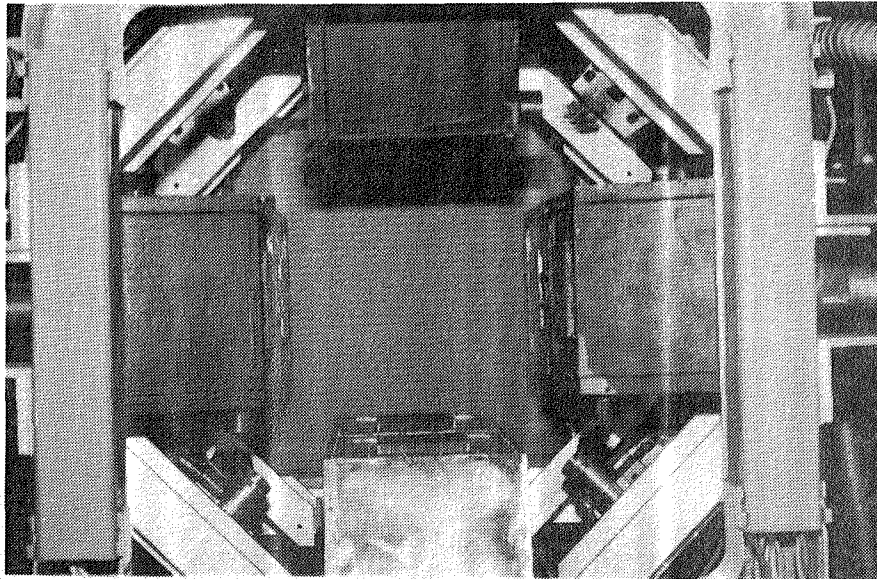
Fig. A1.7 Schematic diagram of

SUMSBS' E/M array.

Upper main E/Ms

Aft axial E/M

Starboard
main E/Ms

Port main E/Ms

Forward
axial E/M

Lower main E/Ms

x

y

z

Fig. Al.8 E/M array. Front view

Axial E/M

Main E/M iron cores

Standard model

PLATES OVERLEAF

1 regulator per full blank panel

10 idependent controllers fed as two triples and two pairs.
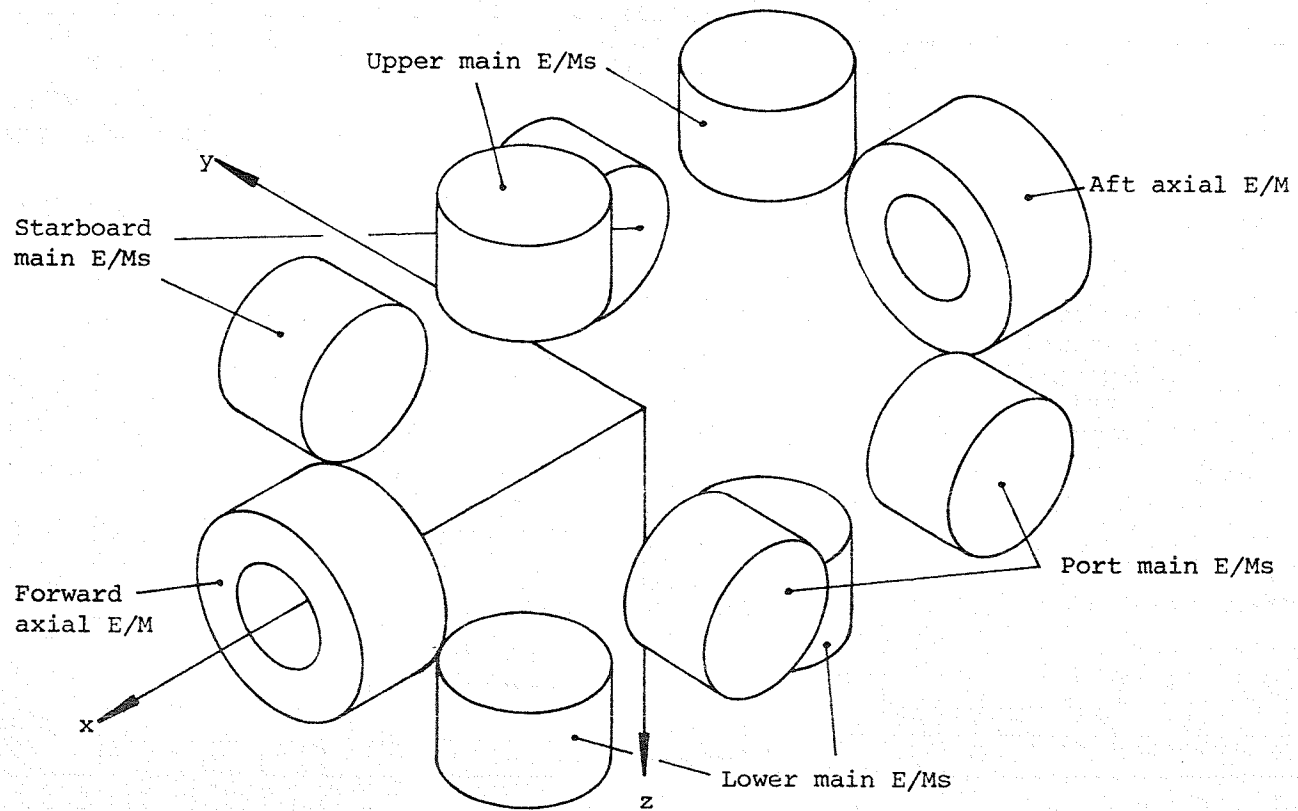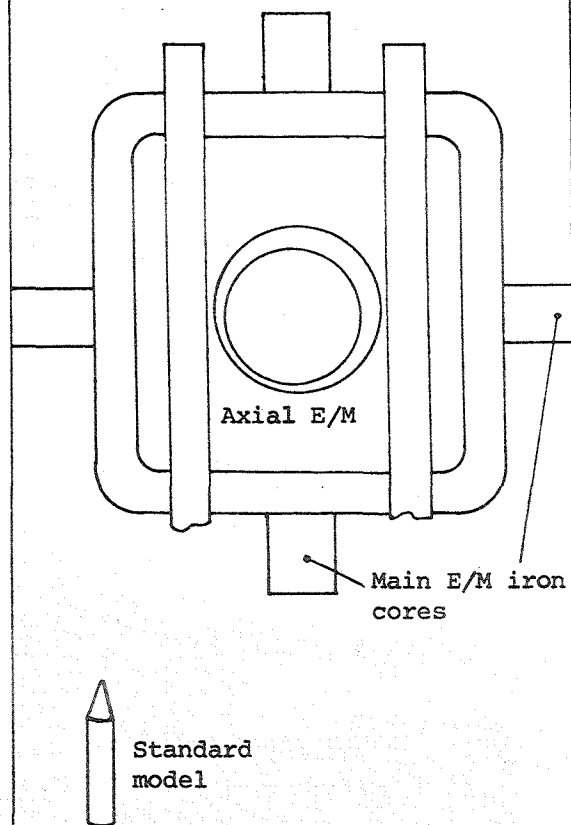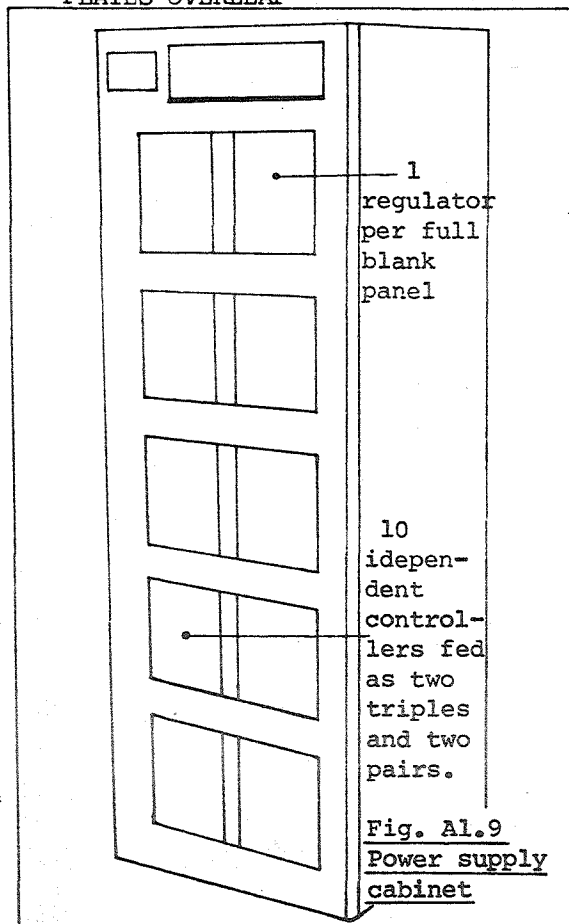
Fig. Al.9 Power supply cabinet

Fig. Al.10 CSR Contraves NC400 servo controller card

Power output stages

Control and switching electronics this side
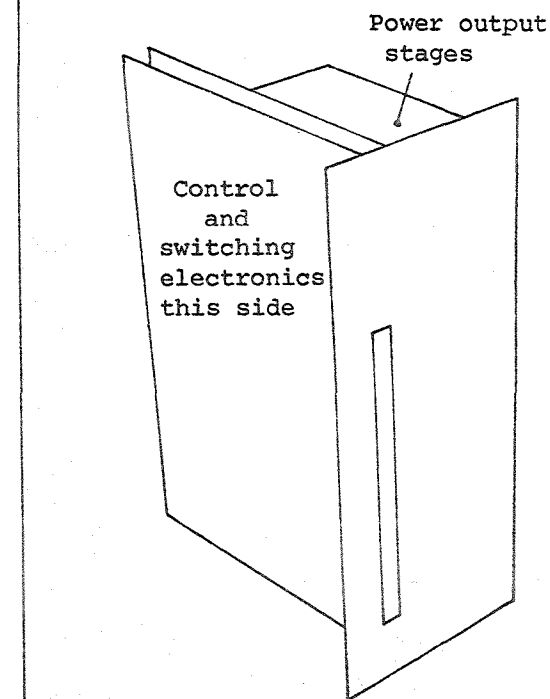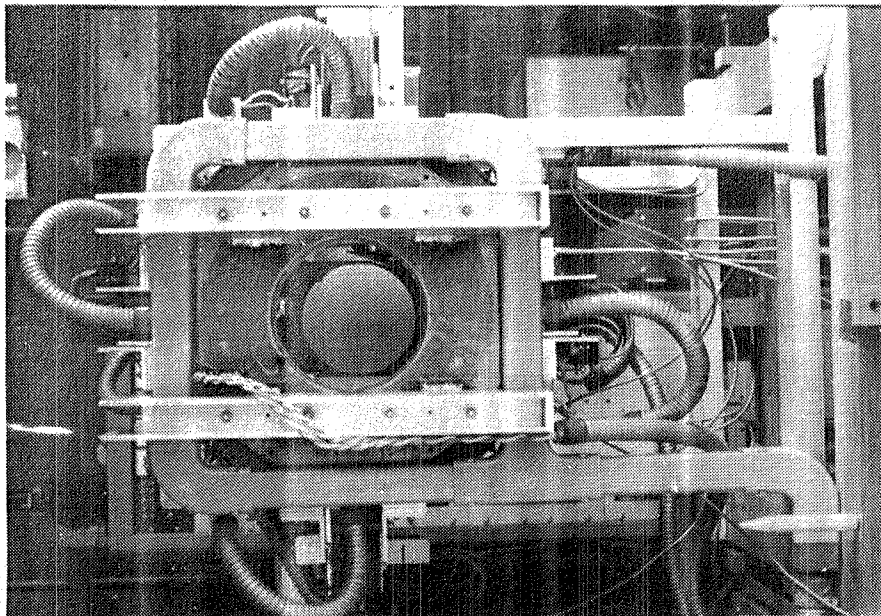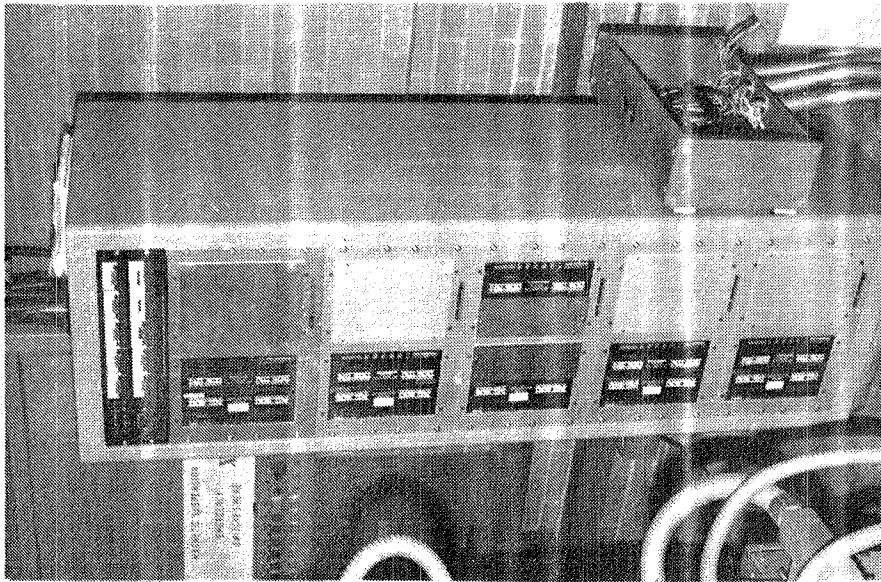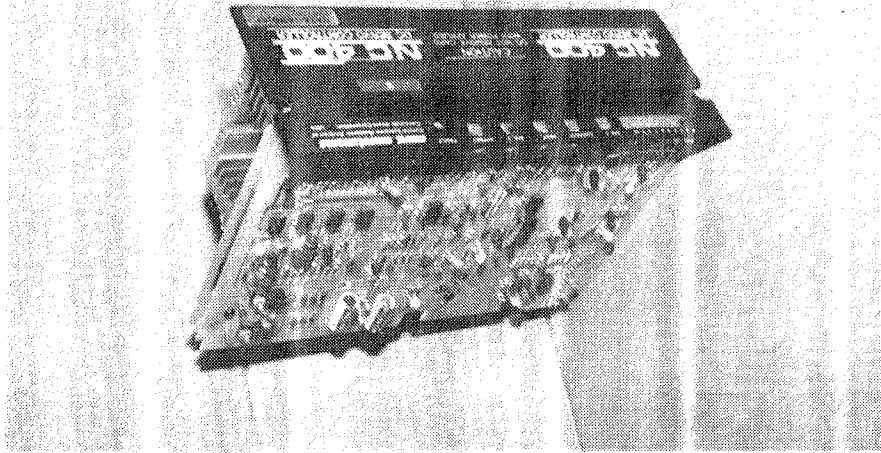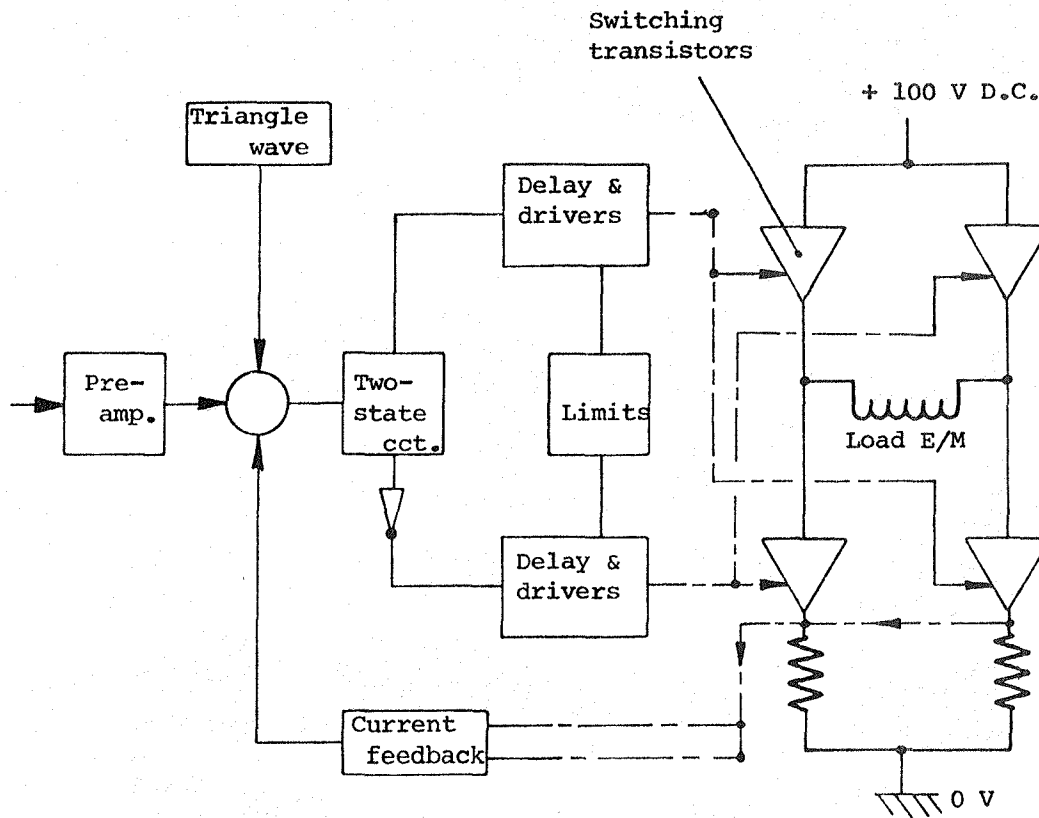
Fig. A1.11   Schematic diagram of operation of NC400 controllers

(after Ref.58)
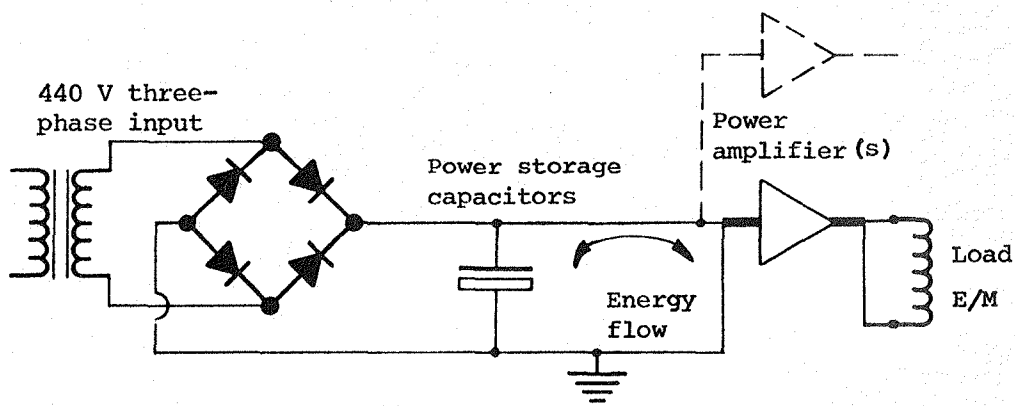
Fig. A1.12   Schematic diagram of D.C. power supply to power amplifiers

A1.4 Position sensors

The basis of the position sensing system used currently is an array of four analogue detectors of traditional form (Ref. 11 and Figs. A1.14 - A1.21). Certain detail improvements have been made, most significantly to the light pickup assemblies where the first stage of amplification and filtering is now incorporated directly behind the sensor (Fig. A1.18). This is done in order to reduce the pickup of airborne electrical noise along the cabling between the MSBS rig and the main control system, this cabling now carrying relatively high level signals.

High angle of attack capability is effected simply by appropriately rotating the aforementioned sensors broadly in the pitch sense (Figs. A1.21, A1.22). The range of sensitivity is such that sensing of a range of angle of attack from 0 to 60 degrees is practicable (see Section 7.8).

Two sensors differ significantly from those described above, namely the axial position and roll attitude sensors. The axial position sensor was required to be capable of monitoring relatively large apparent axial motions, these being induced during large pitch rotations in the chosen configuration (Figs. A1.20, A1.21). A long, slender photodiode provides the necessary pickup range but would tend to be unduly sensitive to ambient light unless further measures are taken. Utilisation of a laser light source (1mW He - Ne) enables a narrow band optical filter of suitable wavelength to be installed in front of the photodiode, reducing the ambient light pickup by a factor of approximately 50 (measured).

The roll attitude sensor comprises a laser (again 1mW He - Ne), directed onto a mirror suitably located on the model, the reflected beam falling onto a UDT PIN-SC/50 two axis position sensing detector (Refs. 60, 61, and Figs. A1.20, A1.21). This device is essentially analogue in nature, providing four output signals which, when suitably processed, yield information as to the location of the centroid of the total incident light on the device's surface. The output can be made relatively insensitive to ambient light, partly by use of optical filters, and to variations in the intensity of the signal beam. The two axis capability of the device may be more fully exploited if 6-component high angle of attack suspension is attempted.

Fig. A1.13
Power supply assembly

Controller A B

Rectifiers

Storage

capacitors
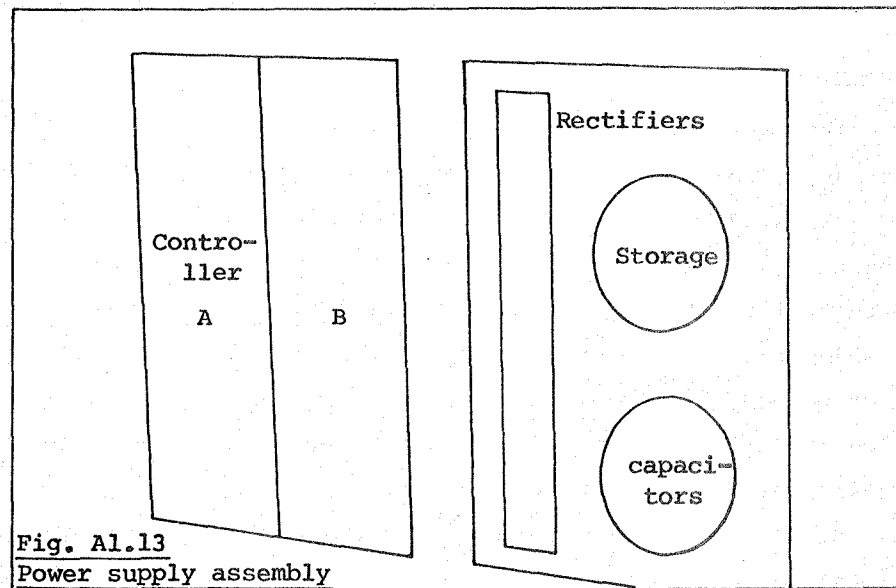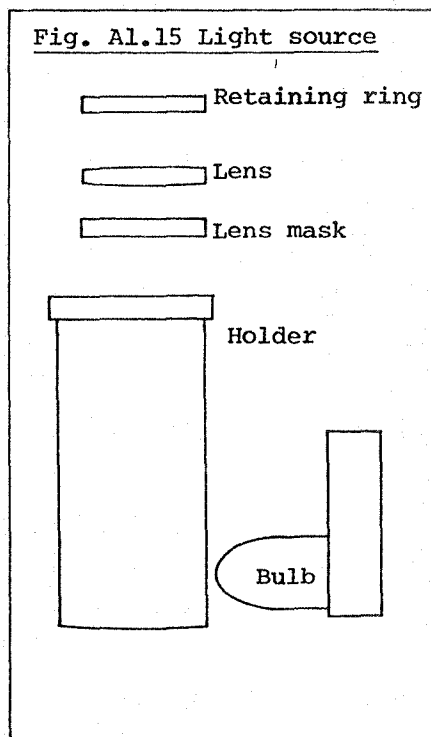
PLATES OVERLEAF

Fig. A1.14 Twin light source assembly

Fig. A1.15 Light source

Retaining ring

Lens

Lens mask

Holder

Bulb
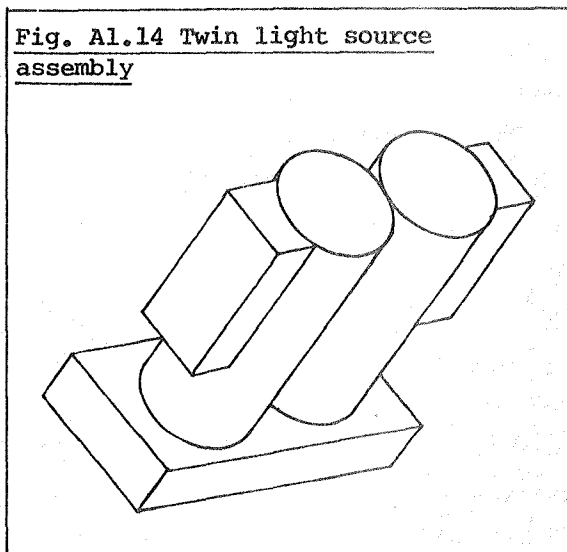
Fig. A1.16 Twin light source assembly

Lens masks visible

Fig. A1.17 Light pickup

Mask   Lens   Sleeve   Sleeve with photo-diode inside   Amplifier assembly
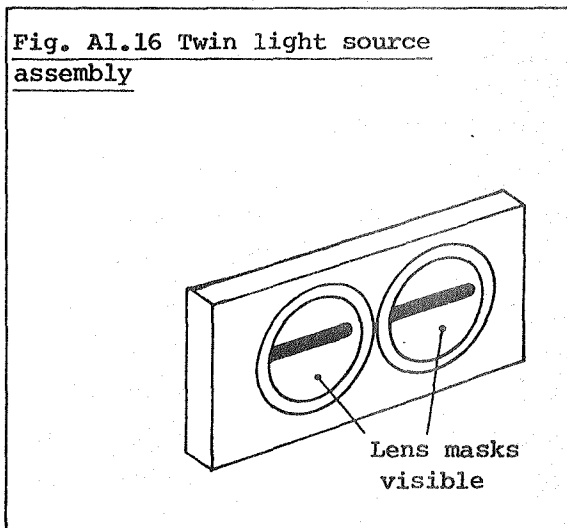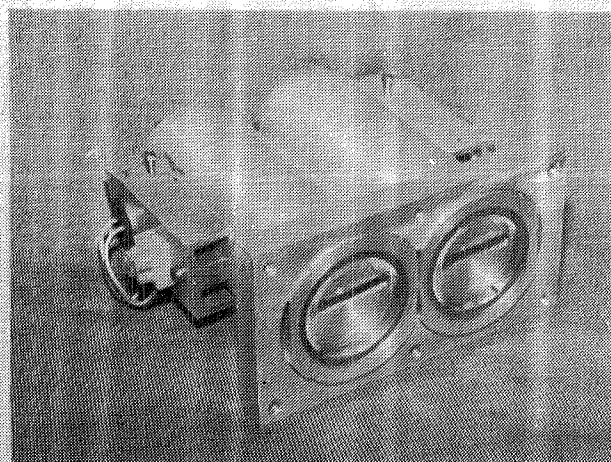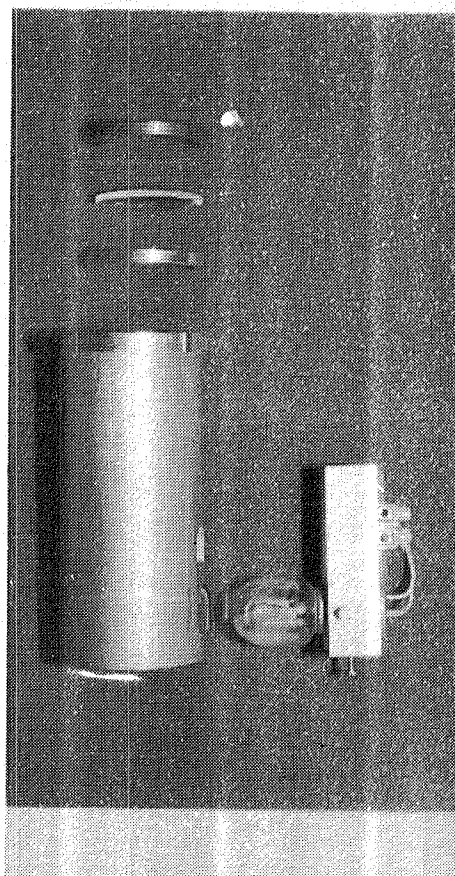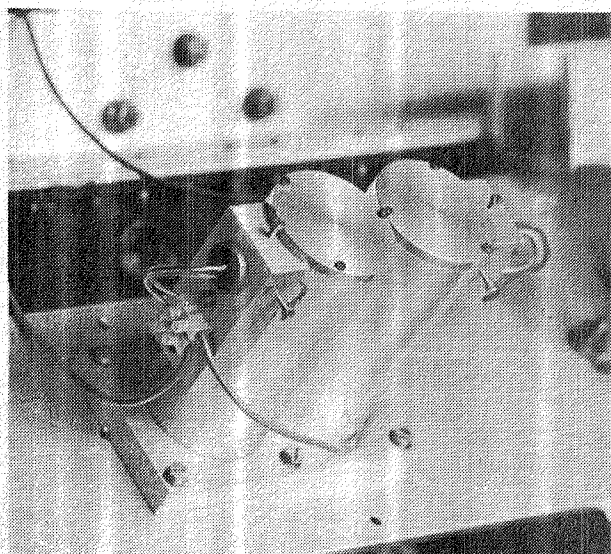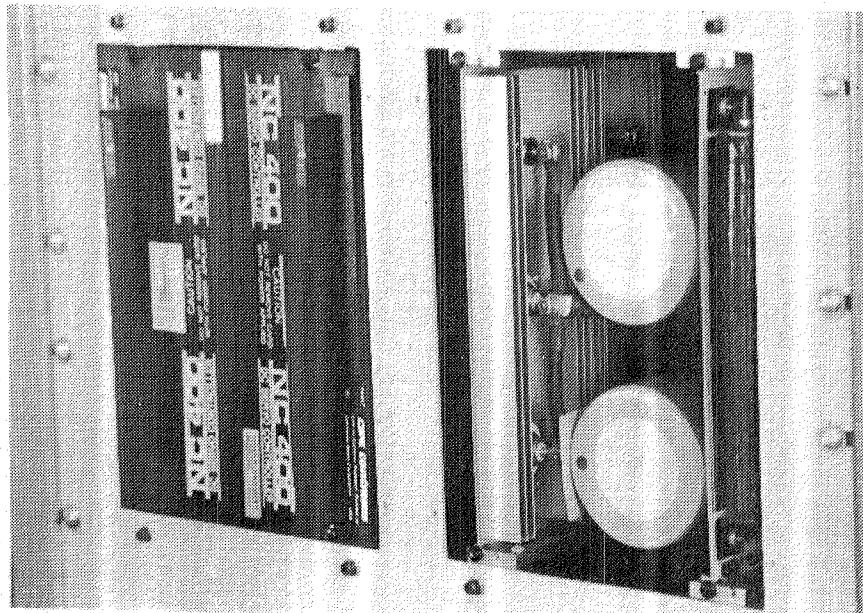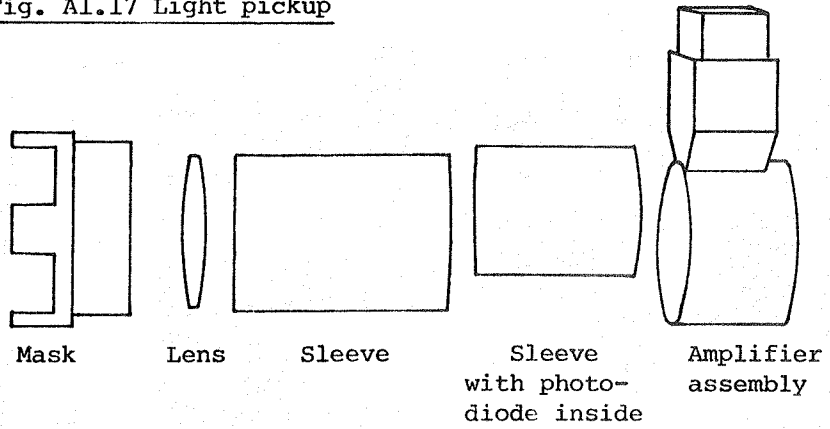
Fig. A1.18 Photodiode amplifier
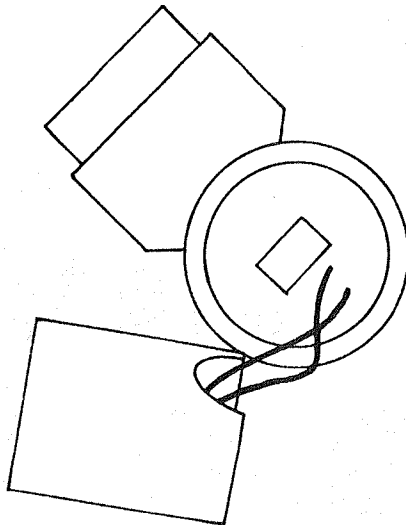
Fig. A1.19 Light pickup assembly

Mask
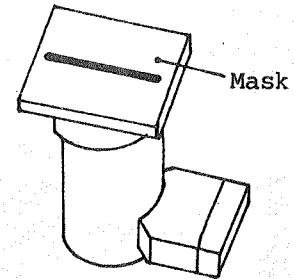
PLATES OVERLEAF

Fig. A1.20 View downstream with model in suspension

Axial beam mirror

Roll sensor

Laser filter

Axial sensor with laser filter

Beam-
spreader

"Drag"
laser
beam

45° mirror

Light
source

Light
source

A

B

y

C

"Roll"
laser

Laser
spot
position
detector

Pick-
up

Pick-
up

Long
photo-
diode

z

Detail A

"Drag"
laser

Glass
rod

Detail C

Model

x

Detail B

x

D

z

Location of
main position
sensing beams.
Main sensors
rotated in sense D
for high angle of
attack operation.
(see Fig. 7.26)

Long photodiode with
optical filter

z

z

Fig. A1.21 Schematic diagram of SUMSBS' position sensors

Fig. A1.22 Main position sensors in high angle of attack configuration

30°

This axis parallel to x axis

Axial position sensor laser

PLATES OVERLEAF

Fig. A1.23, A1.24 Models

Standard axisymmetric model

SPM roll adapted model

Mirror

Wing cores
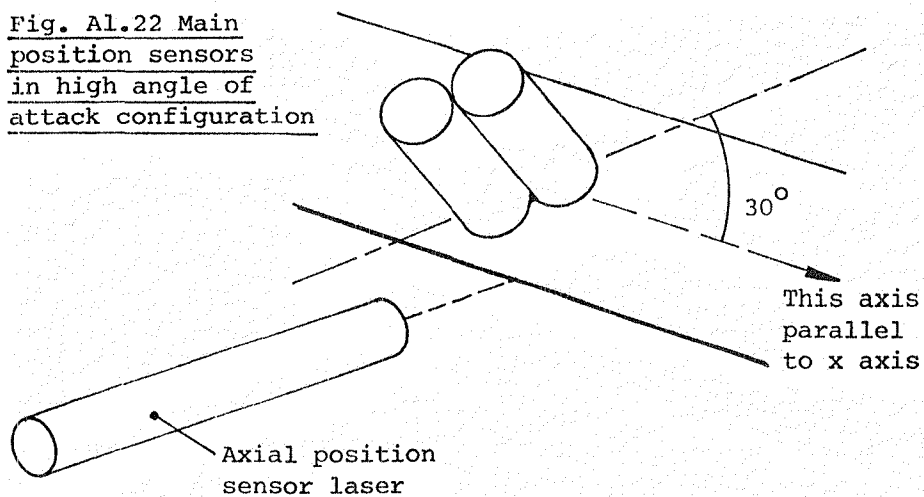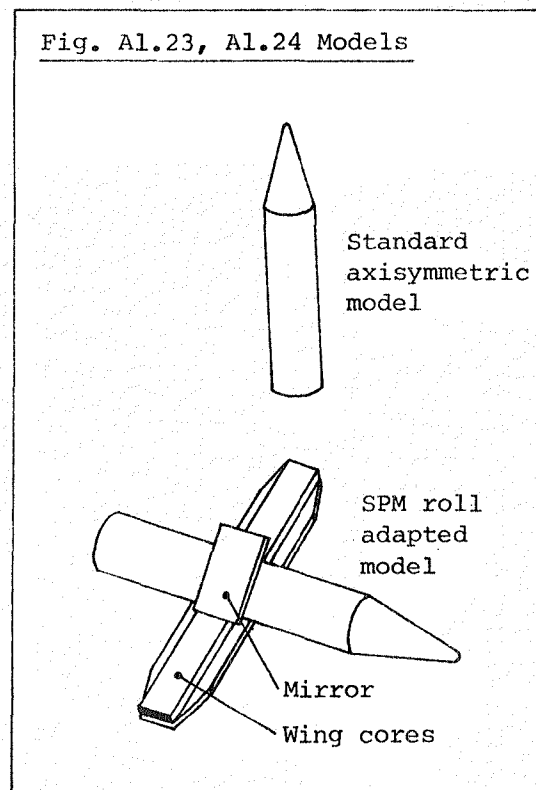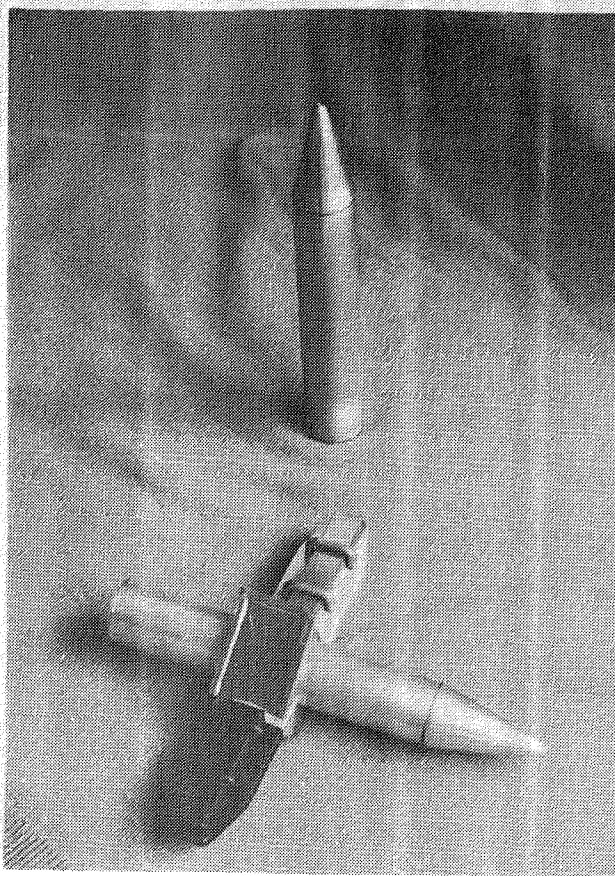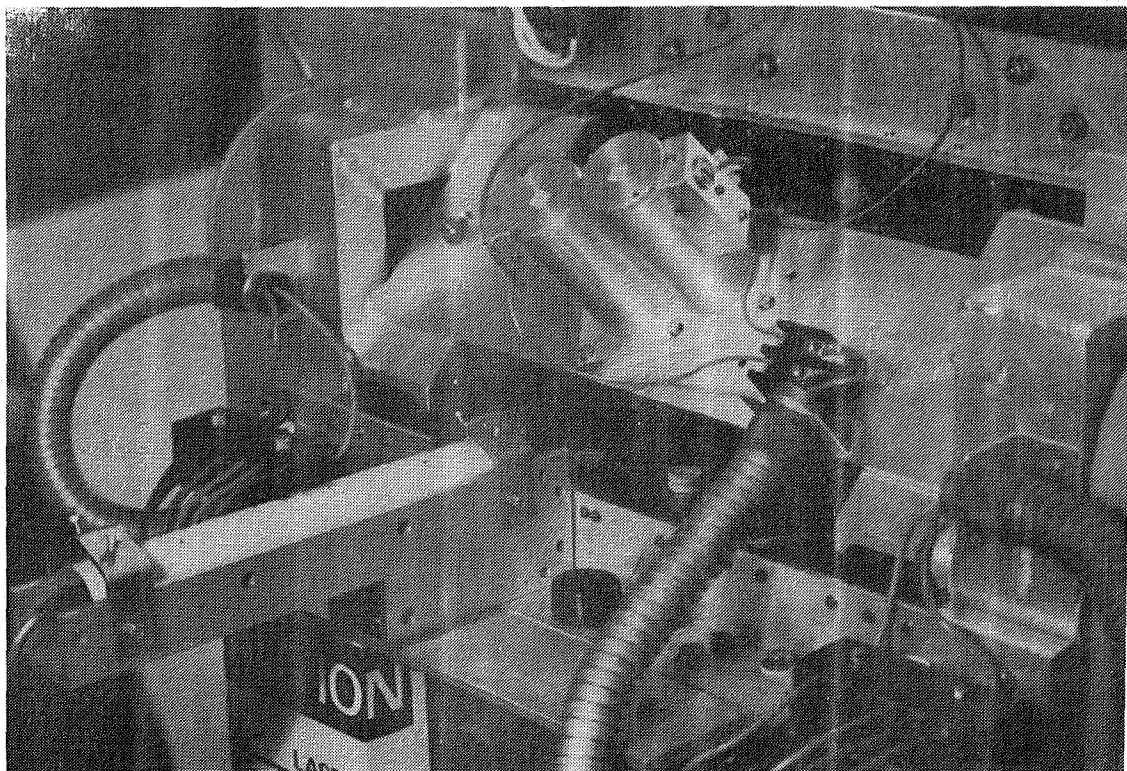
A1.5 Models

Recent recommissioning of SUMSBS has been performed almost entirely with simple cylindrical models of arbitrary aerodynamic shape (Fig. A1.23) fitted with existing cylindrical Alnico V magnetic cores. It has been found that these cores can now be demagnetized following model flyaway by certain combinations of applied fields, necessitating automatic shut-off of all E/Ms whenever position sensor signals indicate that the model is departing from their range. Even with this protection, the long term calibration of such a core must be regarded as dubious, recommending future changes in the core material.

Exploratory 6-component suspension with spanwise magnet roll control has been achieved with a model basically as described above, but crudely adapted to carry arbitrarily dimensioned Alnico V wing cores (Fig. A1.24). The initial configuration of the roll angle sensor (Figs. A1.20, A1.21) necessitated a somewhat awkward location of the model-mounted mirror but this is, of course, not a fundamental shortcoming of this general technique.

A1.6 E/M current sensing

Since the output voltage from the CSR power supplies appears as a pulse width modulated, 5kHz, 100 V peak-to-peak square wave, with neither output terminal near ground potential (Fig. A1.25), special measures are necessary to acquire accurate signals from conventional shunts in the E/M supply leads. A shunt signal typically consists, under these conditions, of a small ($\simeq$ 1V) differential component representing load current, together with a common-mode AC signal of approximately 100 V peak-to-peak (Fig. A1.25). Fully isolated signal amplifiers are necessary to permit safe handling of the peak common-mode voltages and high rejection of this signal component is essential for accurate resolution of load current.

Configuring dual series shunts as signal sources for a linear isolation amplifier (Burr-Brown 3650 HG, Ref. 62), as shown in Fig. A1.26, causes the "common-mode" signal to appear, in fact, as an "isolation" signal, that is, wholly between the input common and true ground. Adequate rejection capability of this signal is available from the chosen class of device, specifically some 140 dB at D.C. falling to approximately 90 dB at 5kHz, all figures given for a device

Power
supply
output

(NC 400)

Shunt

Load
E/M

Switching frequency is
nominal 5kHz.

Volts

100

0

Time

Shunt
common-
mode signal

Shunt
differ-
ential
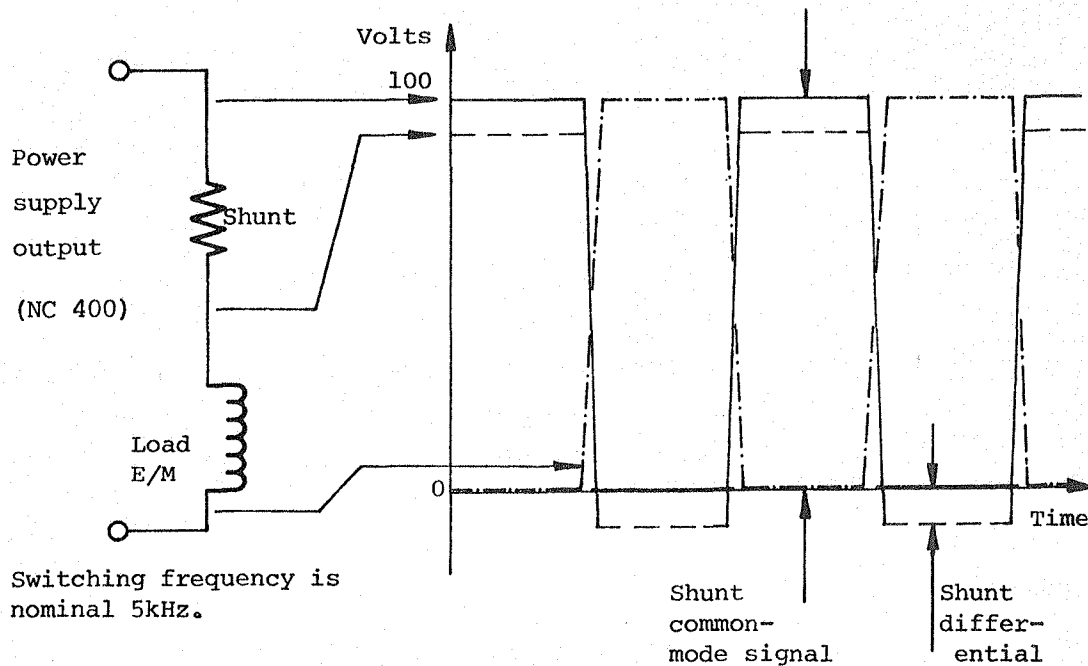
Fig. Al.25 Shunt common-mode and differential signal components

DC / DC converter

(Burr-Brown
model 710)

± 15 V D.C.

Isolated
power

Power
supply
output

(NC 400)

Shunt A

B

Load E/M

Isolation
amplifier

Input
common

Output signal
conditioning

100 V peak-to-peak
isolation signal

Isolation
amplifier is
Burr-Brown model
3650.
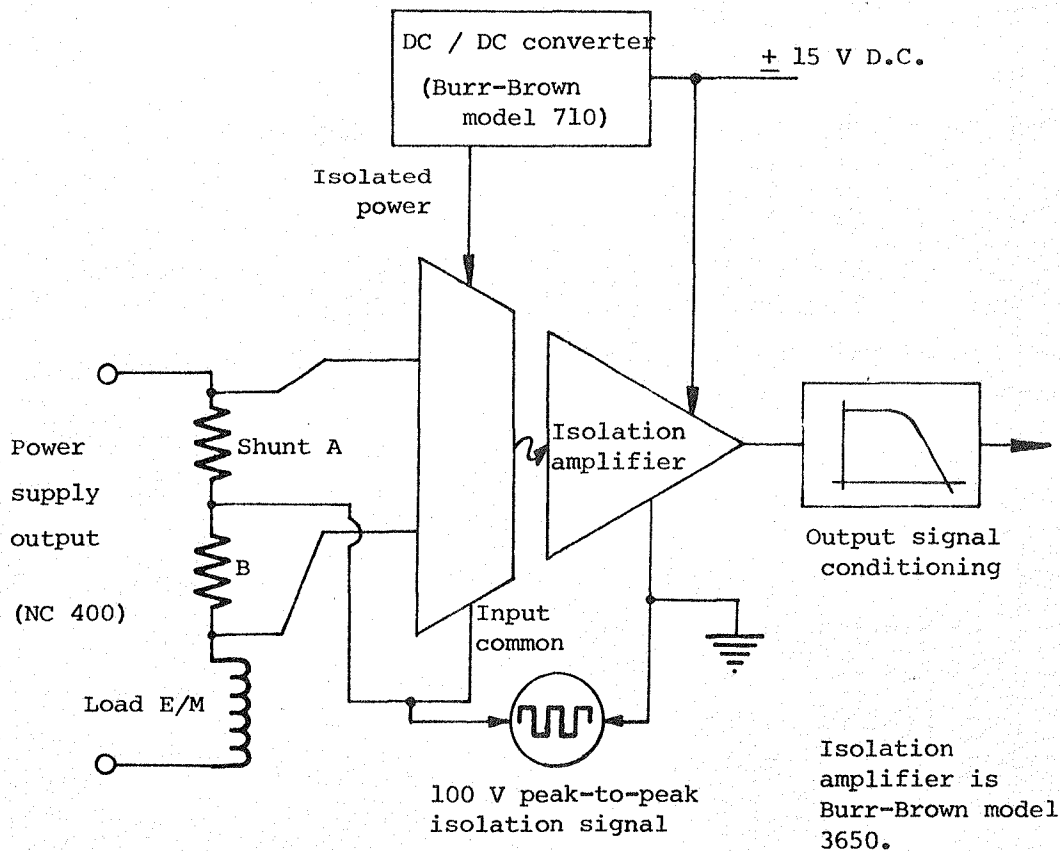
Fig. Al.26 Isolated shunt signal acquisition

voltage gain of 10, from Ref. 62. In fact, the electrically noisy environment in which the devices are operated causes some degradation of this performance, mostly with regard to output noise, but modest filtering of the output provides a satisfactorily clean and effectively real-time signal for data acquisition purposes.

A1.7 Control systems

The control loop is implemented wholly on a digital computer (PDP - 11/34) with only limited signal conditioning performed externally. Local 12 bit A/D and D/A converters communicate with the host computer via two fully isolated, high speed, uni-directional 16 (+ control) bit data buses, the computer in fact being located some 90 feet from SUMSBS itself (Figs. A1.27 - A1.28). Treatment of the control algorithms used is outside the scope of this report but all suspension necessary for the work reported herein has been accomplished with relatively simple digital versions (59) of traditional analogue algorithms (11), absolute performance of such controllers thus being comparable to that achieved by the previous analogue systems.

16+control

16 bit digital
output

Host

computer

(PDP 11/34)

16 bit digital
input

Line
drivers

Double screened
twisted pair
cables

90 feet

Receiver
and opto-
isolator

D/A
subsystem

14
analogue
+
1 x12
bit
digital

out

Address and
control

Receiver
and opto-
isolator

16+control

Line
drivers

A/D
subsystem

16
true
diff-
erential

in
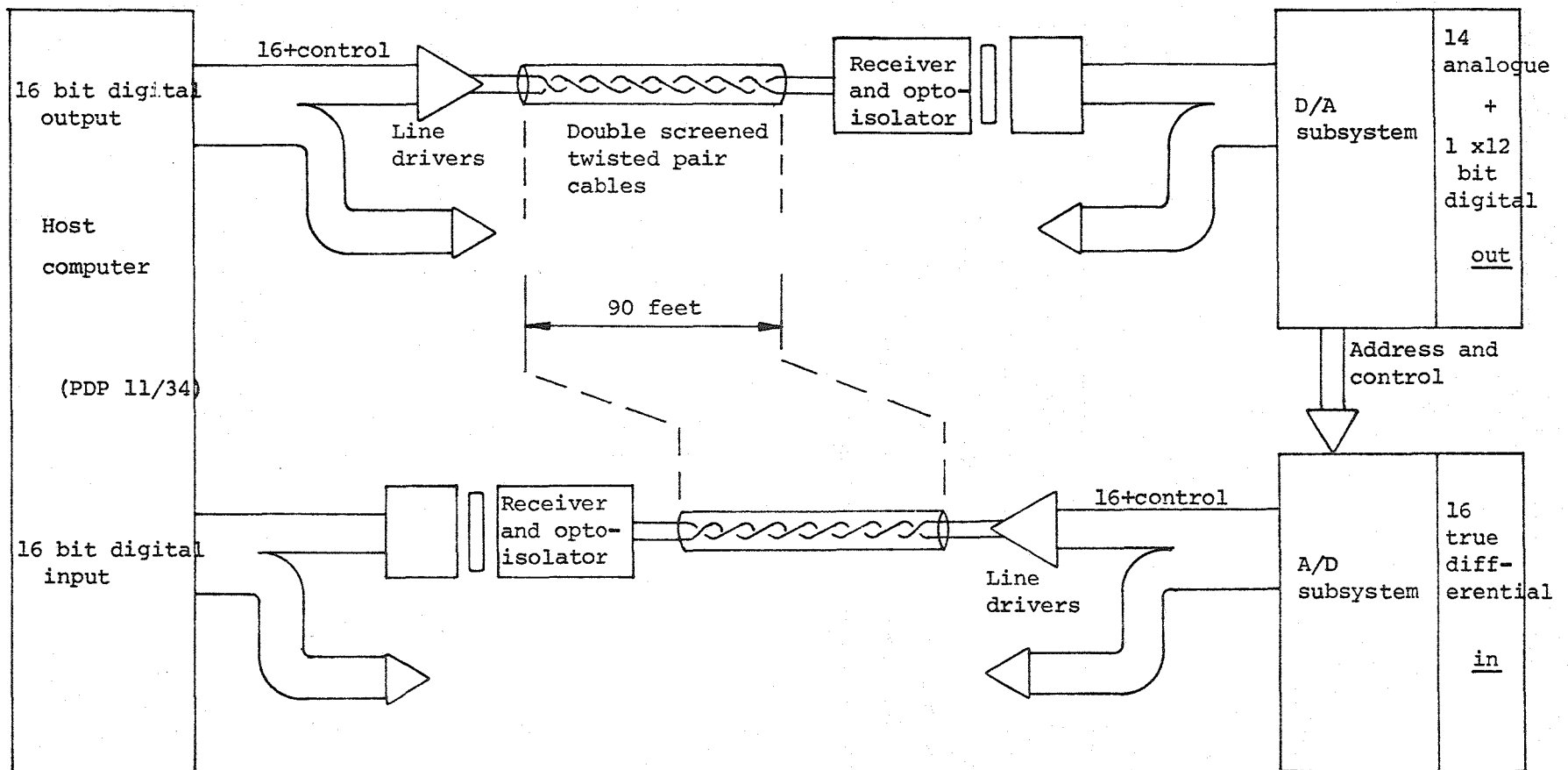
Fig. A1.27   Schematic diagram of digital control system hardware

D/As are Burr-Brown
model DAC 85

Bus
control

Latch

D/A

Analogue
to power
supplies

D/A subsystem

Latch

12 bit output

Latch

12 bit

To
A/D
sub-
system

From D/A subsystem

Control logic

Bus
driver

Latch

A/D

Sample-
and
hold

Analogue multiplexer

Input
signal
conditi-
oning

Burr-Brown SDM 853
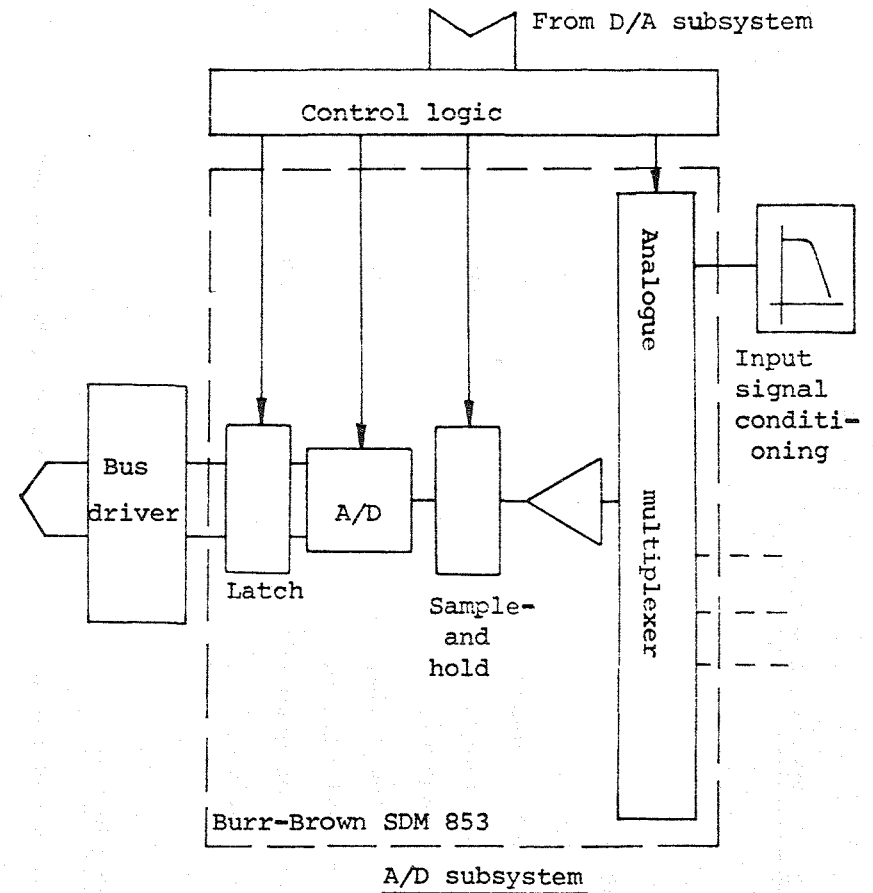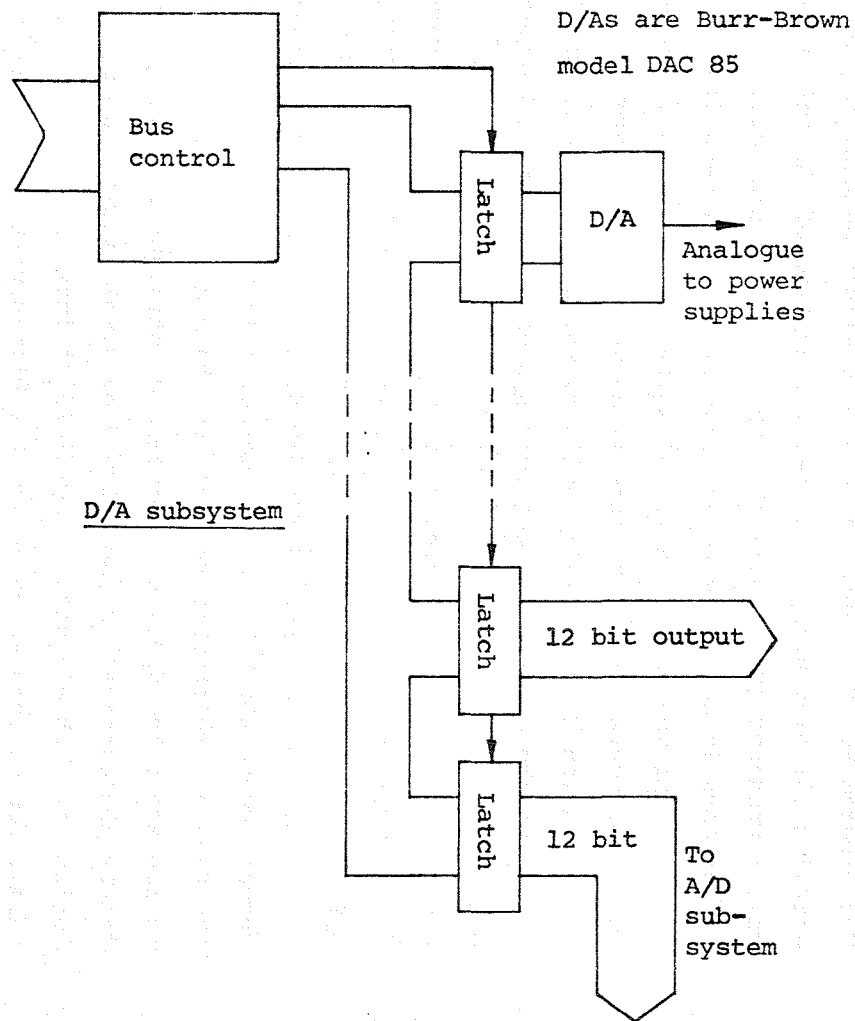
A/D subsystem

Fig. A1.28 Schematic diagrams of A/D and D/A
converter subsystems.

APPENDIX 2   THE PROGRAM "FORCE"

Contents   Page

A2.1   Introduction

   The forces and torques acting on isolated bodies whose
magnetization distribution is known, are amenable to approximate
numerical calculation where the applied field can be somehow found.
The program FORCE is an example of one simple method, in fact
carrying out elementary numerical integration of the relevant
vector products (Eqns. 3.1) over the volume of the core.

   The core is converted to an array of dipoles, each dipole
representing the magnetization of suitably chosen model elements.
Such representation of the core is only straightforward if the core
magnetization is essentially uniform, whence each dipole can be
placed at the centroid of the corresponding element.   Uniform
magnetization is frequently assumed in the case of ReCo materials,
where the material's high coercive force precludes self-demagnet-
ization effects.   However, computations may be approximately
applied to other cases, such as slender axially magnetized iron cores.

   Computation of applied E/M fields is generally only straight-
forward where the E/Ms are air-cored.   In the case of MSBSs where
the E/Ms are relatively remote from the model it is usually adequate
to represent the E/Ms as assemblies of straight line wire elements,
whence the external field is found by simple summation of the contri-
bution of each element.   The field of individual elements is
easily found, such as by use of the Biot-Savart law (63 and various).
A program segment that had been shown to reliably compute the field
from straight line wire elements was extracted from the program

TABLE, courtesy Massachusetts Institute of Technology (64, 65), and is used in FORCE essentially unmodified.

A2.2 Program structure

The fundamental program structure is shown in Fig. A2.1. The program is heavily modularised to permit implementation on a minicomputer (PDP 11-34) with relatively limited available memory. Main model and E/M data storage is in virtual arrays. Memory requirements are comfortably below the available 28K words (main code) and 32K words (virtual arrays) with 1000 model and 1000 E/M elements (see Fig. A2.2).

The main (root) segment of the program simply performs the function of calling the operational subroutines in sequence, this approach allowing these subroutines to be overlaid in memory, as Fig. A2.2.

A2.3 Subroutine descriptions

MODIN controls the filling of the model core dipole array via calls to user named datafiles or the subroutines FUSIN or WING. Model core data can be output to the console device or to user named datafiles. The model can be located arbitrarily in space and looping can be called whereby one locating parameter, say pitch attitude, is stepped by chosen increments over a chosen range, with force and torque calculations repeated at each step.

The fundamental equations controlling the creation of the dipole array are as follows:

$$\underline{M}^* = \int_V \underline{M} \; \delta V \qquad \text{where the integration is over volume of a single element.}$$

leading to modified forms of Eqns. 3.1 :

$$\underline{F} \simeq \sum_i (\underline{M}_i^* \cdot \nabla) \; \underline{H}_i$$

$$\underline{T} \simeq \sum_i \underline{M}_i^* \times \underline{H}_i \qquad \qquad - \; (A2.1)$$

FUSIN permits representation of simple axisymmetric fuselage geometries as shown in Fig A2.3 Where FORCE is used simply to calculate fields due to particular E/M arrays, FUSIN fills the CORE array with dummy model elements of zero magnetization (Fig. A2.4).
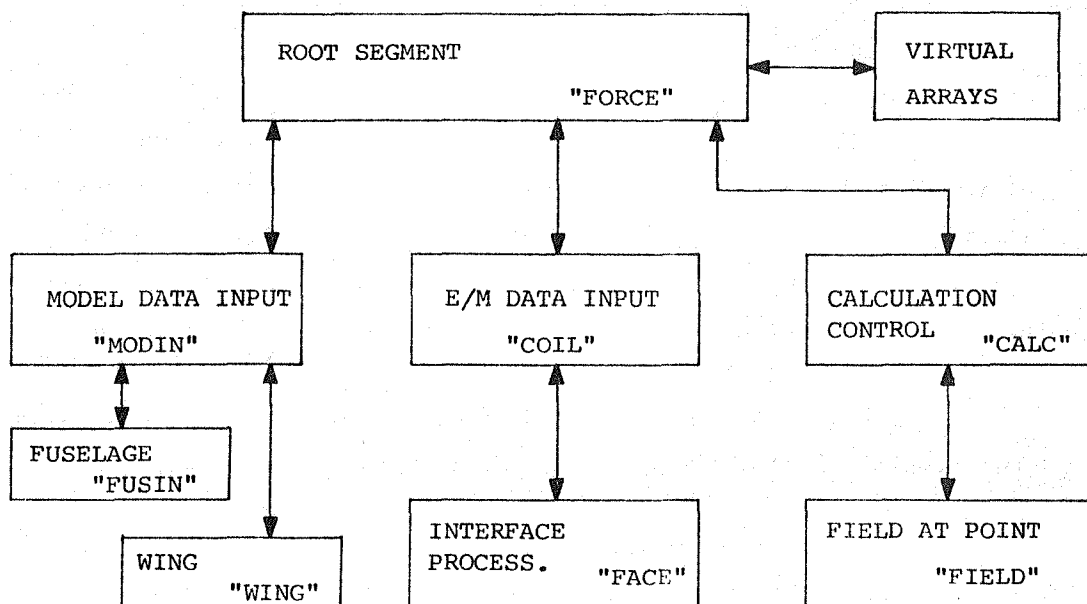
Fig. A2.1 Fundamental block structure of program FORCE
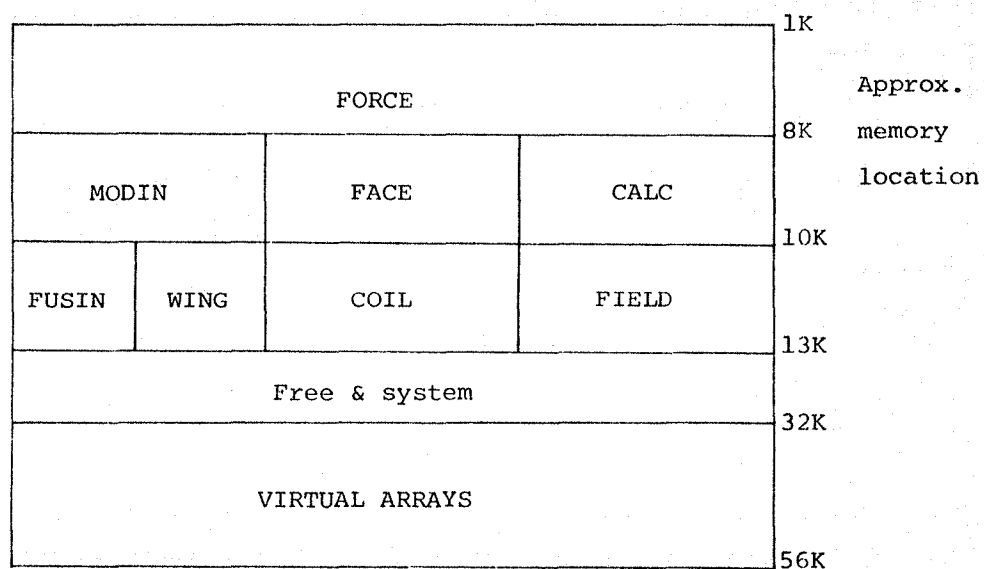
Fig. A2.2 Memory overlay structure of program FORCE
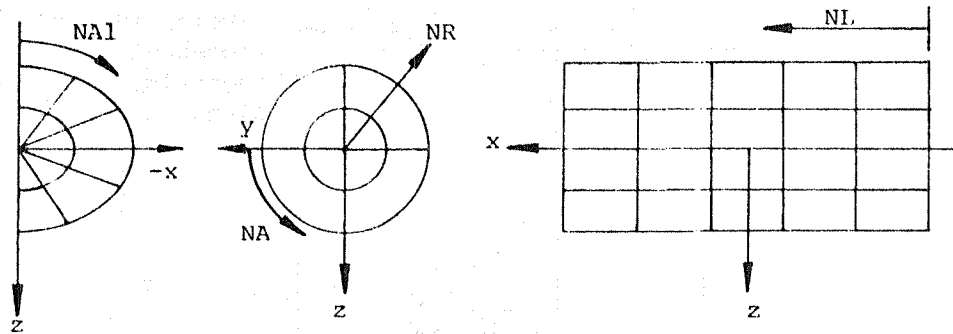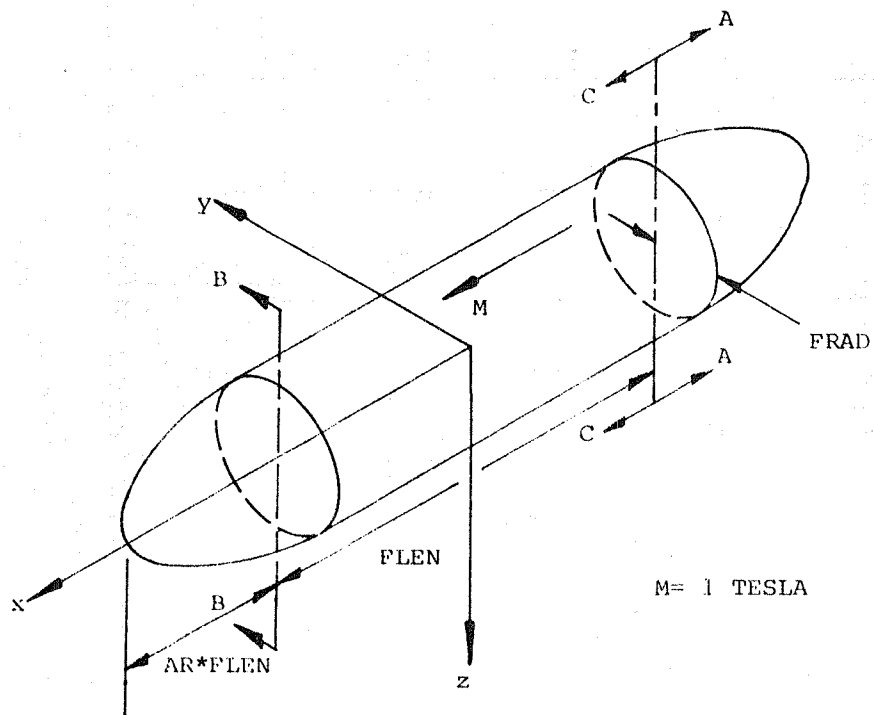
Section on AA   Section on BB   Section on CC

-- showing element distributions

As shown, NL = 5,   NA = 4,   NR = 2,   NA1 = 3

Fig. A2.3 Axisymmetric fuselage geometry. Fuselage input option = 1,3
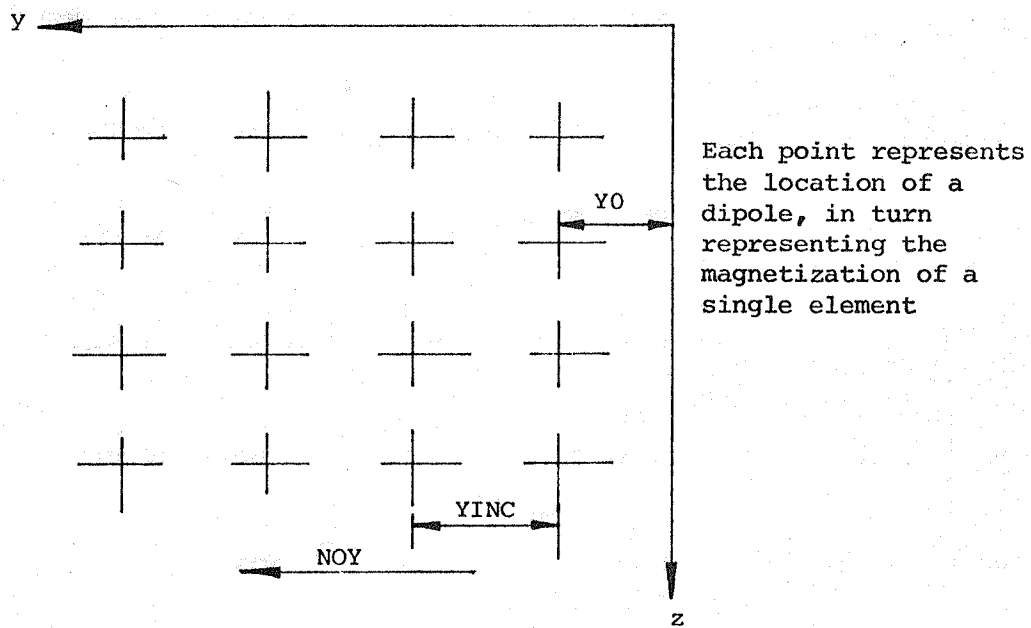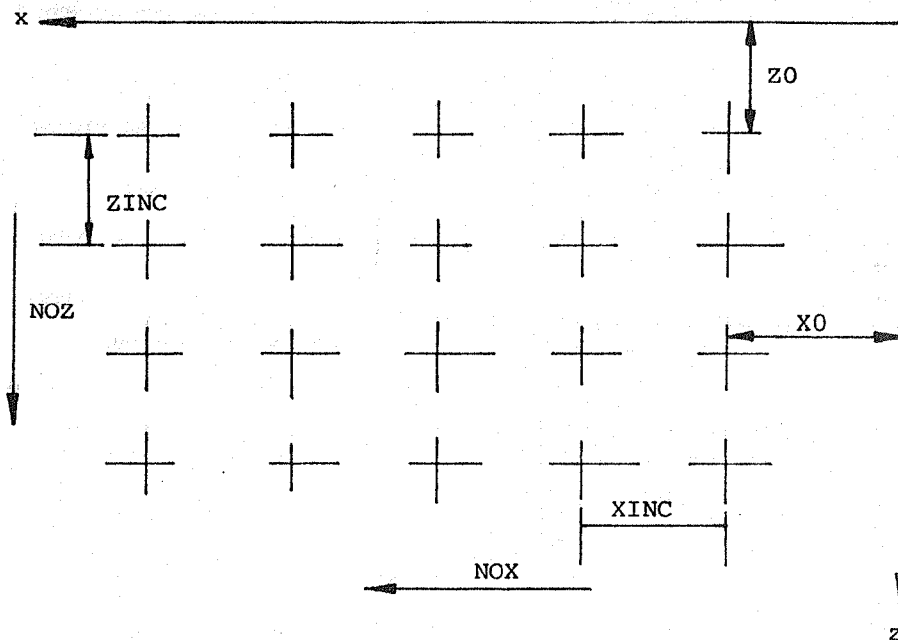
As shown, NOX = 5, NOY = 4, NOZ = 4

Fig. A2.4 Field grid. Fuselage input option = 2. Zero magnetization

in all elements

WING permits representation of simple slab wings, magnetized symmetrically (SPMs, see Section 4), as shown in Fig. A2.5

COIL creates an array of straight line wire elements representing the assembly of E/Ms. Symmetry is used extensively to reduce the quantity of user input per program run and the program's main memory requirement. Data is input for a single "master" E/M, which can later be reflected and/or rotated in certain ways to generate other E/Ms in that particular "set" (Fig. A2.6). Up to five E/M sets may be input sequentially, permitting analysis of relatively complex MSBS configurations. Four types of E/M may be specified, single wire loops (Fig. A2.7), E/Ms effectively composed of straight blocks of conductor of quadrilateral cross section (Fig. A2.8) and "lateral" or "axial" pseudo-circular E/Ms (Figs. A2.9, A2.10). Pseudo-circular E/Ms are reduced to assemblies of circumferential straight line elements, positioned at suitable radii so as to create a field at the centre of each loop identical to that created by the equivalent circular loop carrying the same current. E/M data may be output to user named datafiles or to the console device. Data for a complete array (several E/M sets where required) may be input from a user named datafile.

E/M ampere-turn products are input individually at the console device in a standard sequence (Fig. A2.11).

FACE generates the co-ordinates of straight line wire elements distributed over the cross section of a block of conductor, permitting E/Ms to be input as a series of co-ordinates representing the interfaces where blocks of conductor join as Fig. A2.8.

FACE is derived from the TABLE subroutine COORS (MIT, (65)), but differs in two important respects. Firstly, since COORS only generated wire element distributions that correctly simulated uniform current density over the winding cross section when the interfaces were quadrilateral, FACE generates the fourth corner of each interface internally. Secondly, COORS used the input interface co-ordinates to define directly the location of the outermost wire elements. FACE uses the interface co-ordinates to describe an outer envelope, inside which all elements are distributed. Thus, identical input data to COORS and FACE will result in different wire element distributions.
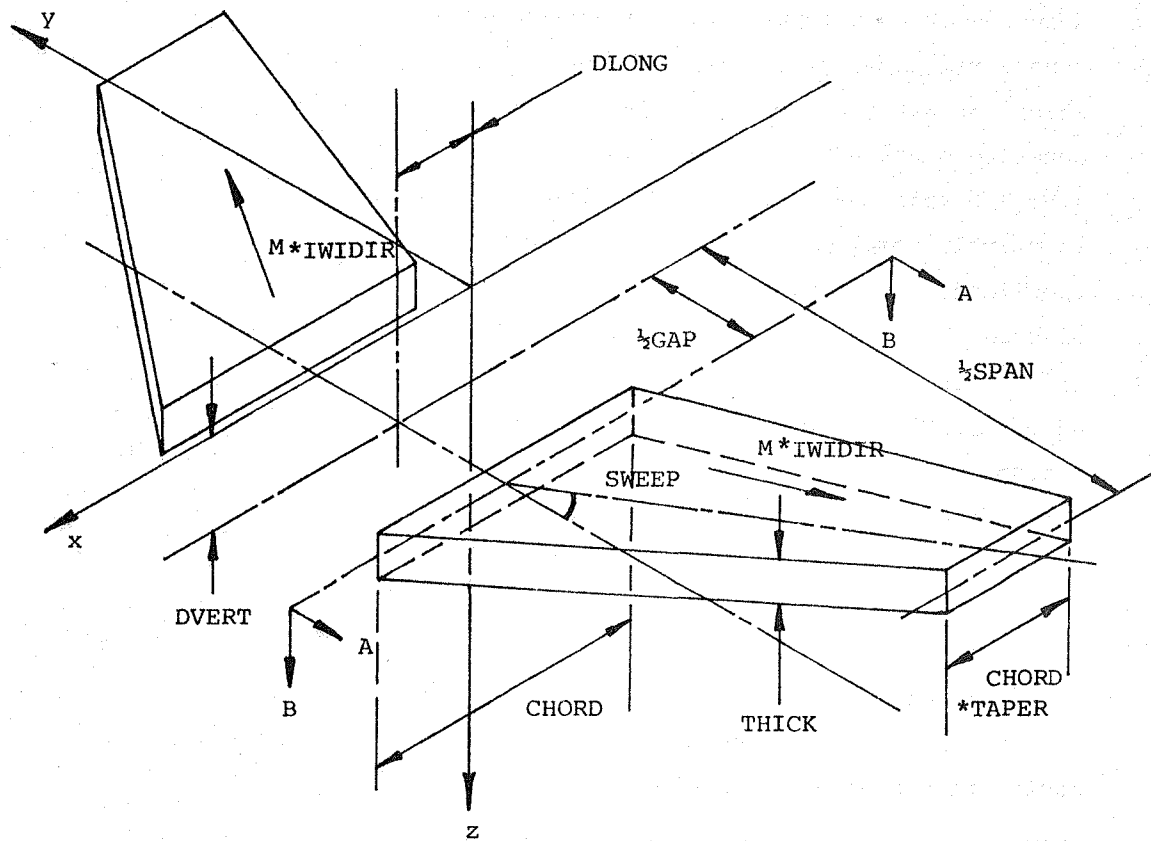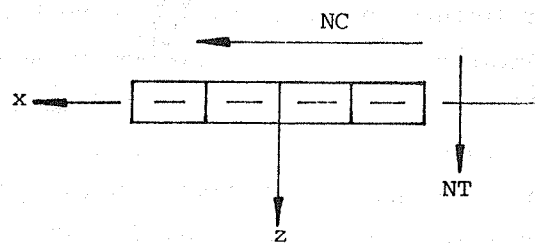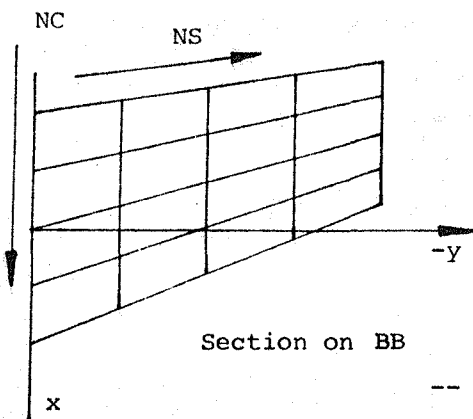
Fig. A2.5 Slab wing geometry. Wing input option = 1

ISYMM = 1 No reflections
or rotations

Y

MASTER
E/M

Z

E/M current directions

shown by : ● ○

Y

ISYMM = 2 Reflection
in x,y and x,z planes

Z

MASTER
E/M

ISYMM = 3, 1 rotation $\gamma=180^{\circ}$

4, 3 rotations $\gamma=90^{\circ}$

5, 6 rotations $\gamma=60^{\circ}$

6, 8 rotations $\gamma=45^{\circ}$

(ISYMM=4 shown)

Y

γ

Z

MASTER
E/M

ISYMM = 7,8,9,10,11,12 derived
from 1,2,3,4,5,6 with reflection
of entire array in y,z plane
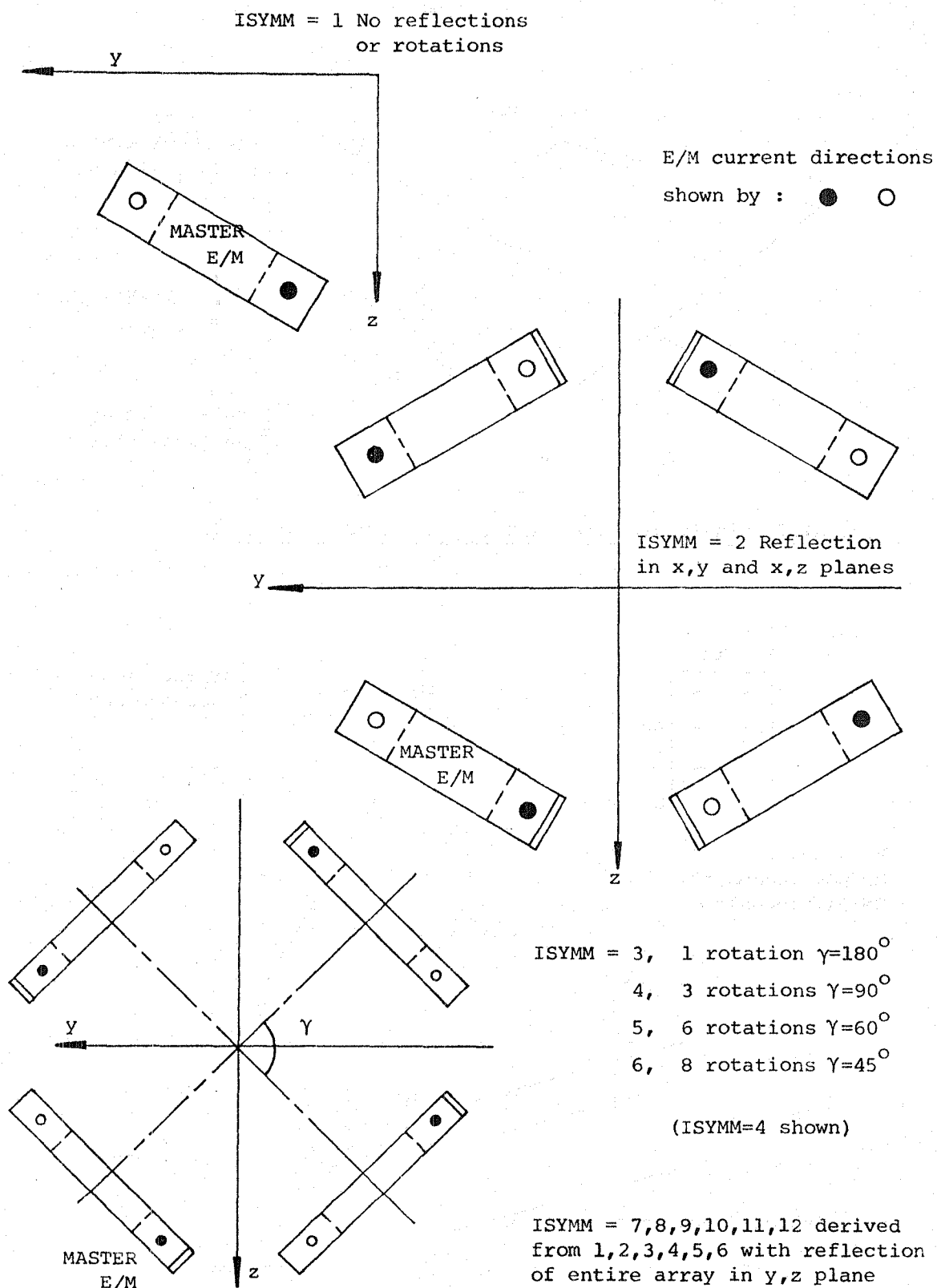
Fig. A2.6 Symmetry options for E/M sets

As shown NINT=4
(no. elements)

Endpoints input
in sequence thus:

$x_1, y_1, z_1, x_2,$ ---

--- y_4, z_4

Current flows
in sense shown

x_4, y_4, z_4

x_3, y_3, z_3

x_1, y_1, z_1

x_2, y_2, z_2
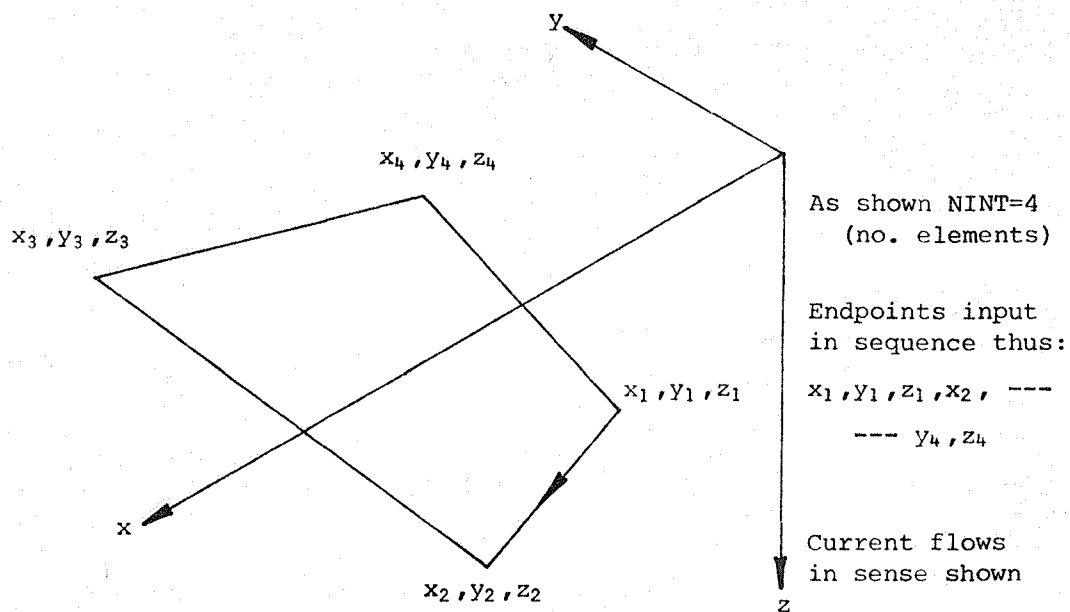
Fig. A2.7 Single wire loop E/Ms. E/M input option = 1

Detail of interface 1

B   MM   A

NN

C   D
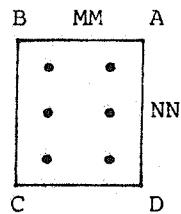
As shown, NINT=4,
MM(no. layers)=2,
NN(no. loops)=3

Current flows
in sense shown

(4)

A

B

C

B   A

B   C   D   (1)

A   B

(3)

D

Reference edge

A

Coordinates input in sequence
thus:

$X_{A_1}, Y_{A_1}, Z_{A_1}, X_{B_1}$ ---

--- Y_{C_4}, Z_{C_4}

(2)   D

Coordinates of
D edge generated
internally
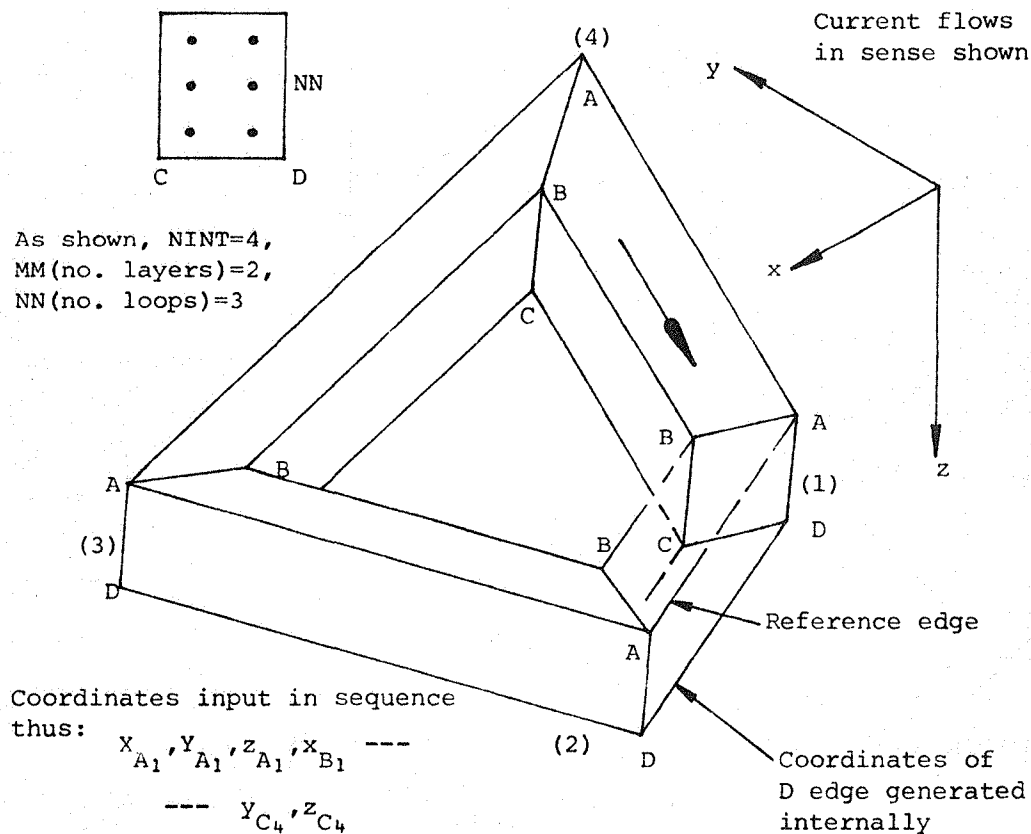
Fig. A2.8   Interface array E/M input. E/M input option = 2

AXIAL

LATERAL

AXIAL and LATERAL

Section on AA showing
wire loop distribution

As shown:

NDIVR=1, NSEG=12

NDIVY(lateral) =2

NDIVX(axial) =2
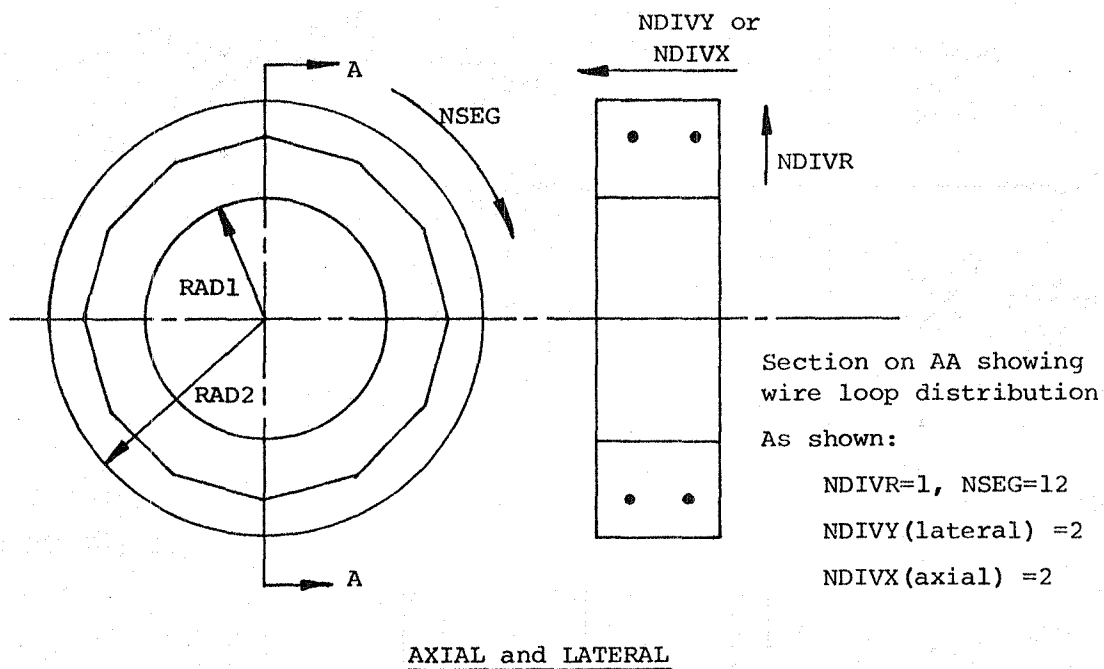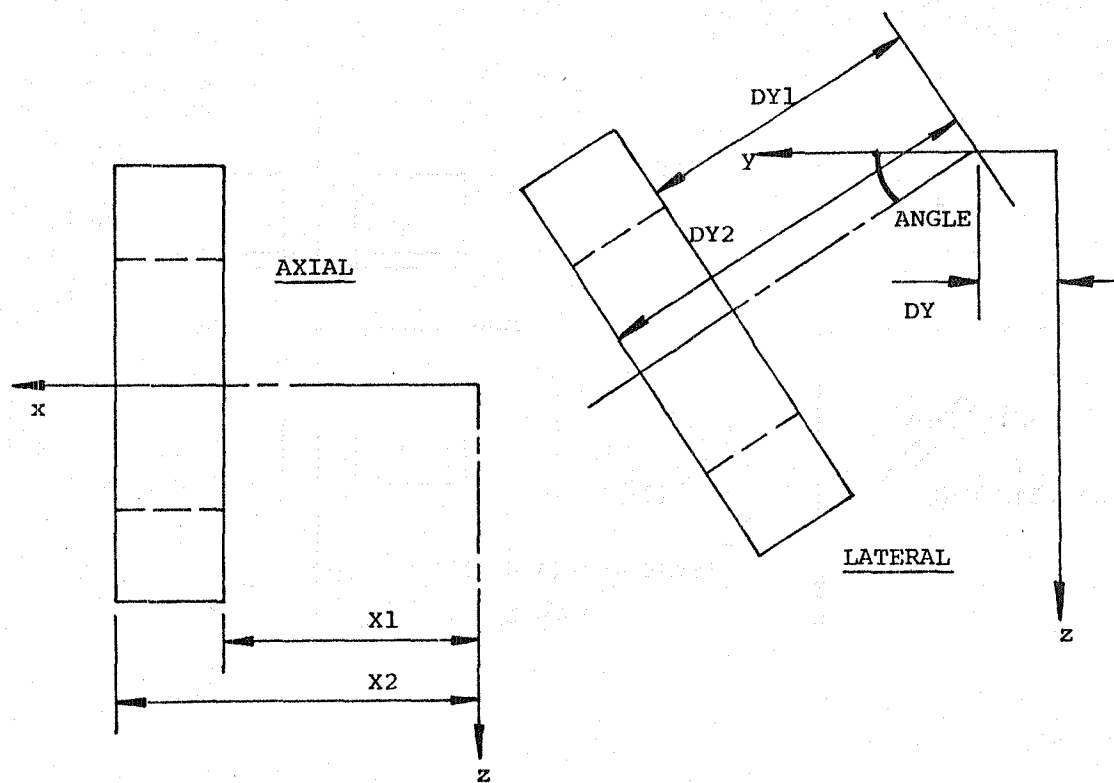
Fig. A2.9 and A2.10   Lateral and Axial Pseudo-circular E/Ms. E/M input

option = 3,4.
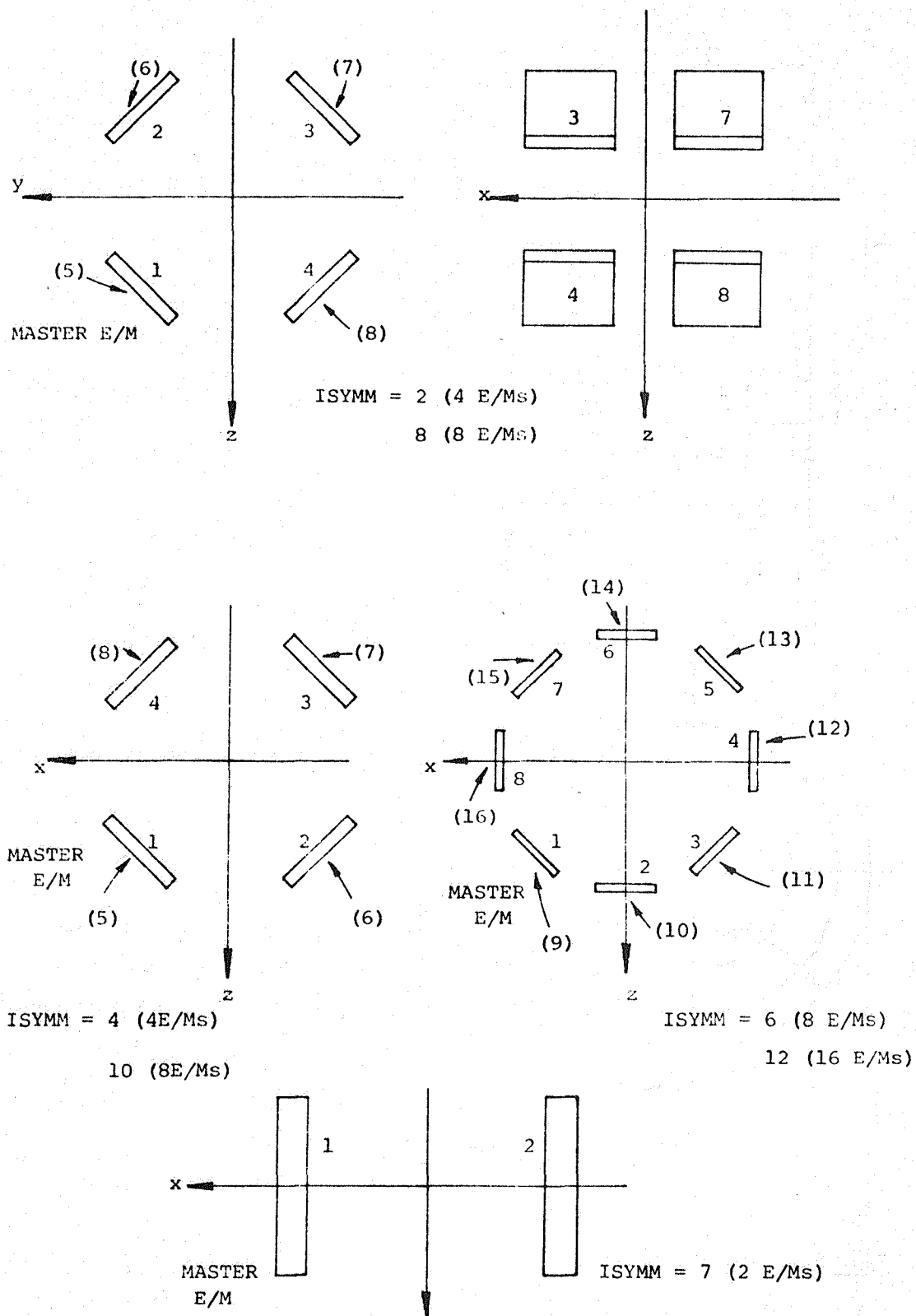
Fig. A2.11 Standard sequence of E/M ampere-turn input

CALC controls the calculation of E/M fields, via calls to the subroutine FIELD, summation of model forces and torques and the routing of calculated data. The position and orientation of model elements is updated using previously input data (Fig. A2.12). FIELD then provides the field and field gradient components at each model element in turn, the relevant vector products of field and magnetization being calculated and summed. Model forces and torques are expressed about the model's own co-ordinate origin, in translated but unrotated axes (Fig. A2.13). The calculated field at each model element may be output to datafile or the console device. Force and torque data may be routed likewise. Calculations are repeated if stepping of the model position or orientation had been previously selected.

FIELD calculates the field and field gradient components at the single points required, due to the specified E/M array. Individual E/M set calculations are made first for the master E/M, then for E/Ms generated by the chosen reflection/rotation symmetries. Set calculations are repeated for all specified sets with the final field data being the sum over all E/Ms of all sets.

MSBS fixed axes :

 x,y,z

Model translated
axes :
x',y',z'

Model final axes :
x" ,y" ,z"

Fig. A2.12   Translation of
model coordinate system
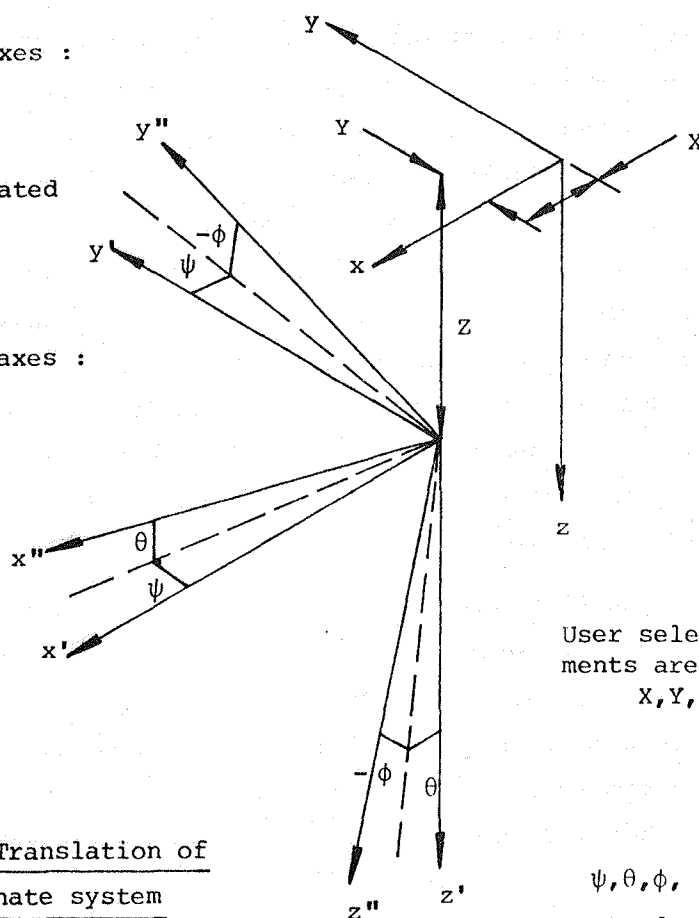
User selected displac-
ments are :
 X,Y,Z,ψ,θ,ϕ
      as shown

ψ,θ,ϕ, correspond to
standard Euler angles

Fig. A2.13   Definition of
sense of calculated torques

Torques resolved in
translated but UNROTATED
axes.
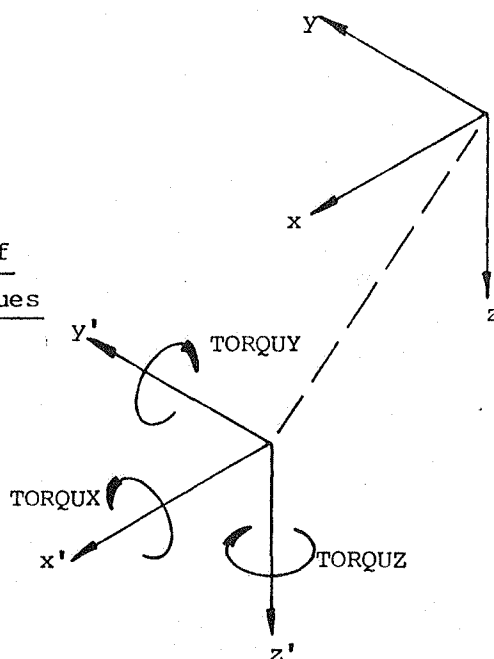
GENERAL INSTRUCTIONS FOR USERS OF PROGRAM FORCE   ************************

THE MAXIMUM NUMBER OF MODEL ELEMENTS CURRENTLY PERMITTED IS 1000
THE NUMBER OF ELEMENTS REQUIRED FOR A PARTICULAR MODEL MAY BE CALCULATED
AS FOLLOWS:

$$N = (NOX+1)*(NOY+1)*(NOZ+1) \qquad --- \text{ FIELD GRID}$$
$$= NL*NA*NR \qquad\qquad\qquad --- \text{ CYL. FUSE.}$$
$$+NA*NR*NA1*2 \qquad\qquad --- \text{ ELLIP. ENDCAPS}$$
$$+NS*NC*NT*2 \qquad\qquad\;\; --- \text{ SLAB WINGS}$$

THE MAXIMUM NUMBER OF E/M WIRE ELEMENTS CURRENTLY PERMITTED IS 1000
THE NUMBER OF ELEMENTS IN A PARTICULAR E/M ARRAY MAY BE CALCULATED
AS FOLLOWS:

M=SUM OVER ALL SETS OF:

NINT	--- SINGLE LOOP
NINT*MM*NN	--- INTERFACE ARRAY
NDIVR*NDIVY*NSEG	--- LATERAL CIRCULAR
NDIVR*NDIVX*NSEG	--- AXIAL CIRCULAR

ONLY THE MASTER E/M IN EACH SET AFFECTS THE VALUE OF M.   E/MS GENERATED
BY SYMMETRY OPTIONS DO NOT REQUIRE FURTHUR STORAGE ALLOCATION.

THE NUMBER OF MODEL AND E/M ELEMENTS SHOULD ALWAYS BE CHOSEN TO BE AS
SMALL AS WILL YIELD ACCEPTABLE RESULTS. CHOICE OF UNNECESSARILY LARGE
NUMBERS OF ELEMENTS WILL RESULT IN INCONVENIENTLY LONG EXECUTION TIMES
AND PERHAPS IN THE ACCUMULATION OF ROUNDING ERRORS.
        COMPUTAION TIME, TAKEN FROM THE COMPLETION OF THE LAST USER
INPUT TO FINAL PROGRAM COMPLETION, NEGLECTING HARDCOPY PRINT TIMES,
HAS BEEN FOUND TO BE APPROXIMATELY:

$$T = N*MM*(STEPS+1)*0.01$$

WHERE MM=TOTAL NUMBER OF E/M ELEMENTS SUMMED OVER ALL
E/MS OF ALL SETS.
            PDP 11-34 WITH HARDWARE FLOATING POINT OPTION,
            RT-11 OPERATING SYSTEM, GIVEN IN SECONDS.

THE STANDARD FORMAT FOR THE TITLES OF USER NAMED DATAFILES UNDER RT-11
IS AS FOLLOWS:

                ******.DAT

WHERE ****** IS AN ARBITRARY 6 CHARACTER ALPHANUMERIC NAME

ALL INPUT/OUTPUT IS IN SI UNITS, SPECIFICALLY:
        DIMENSIONS IN METRES
        FIELDS IN TESLA
        FIELD GRADIENTS IN TESLA/METRE
        ANGLES IN DEGREES (CONVERTED INTERNALLY TO RADIANS)

USER INPUT VARIABLES FOR PROGRAM FORCE   ************************************

REFER TO FIGS.A2.1 TO A2.13 FOR DEFINITION OF VARIABLES
NOT CITED BELOW

MODEL GEOMETRY OPTION (MOPT)
```
        AB          WHERE:
                    A=WING INPUT OPTION
                            0       NO WING
                            1       SLAB WING
                    B=FUSELAGE INPUT OPTION
                            0 FROM DATAFILE (WHOLE MODEL)
                            1 CYLINDRICAL FUSELAGE
                            2 FIELD GRID
                            3 AS 1+ELLIPSOID ENDCAPS
                    EG. MOPT=11 SPECIFIES CYLINDRICAL FUSE. WITH SLAB WINGS
                        MOPT=1  SPECIFIES CYLINDRICAL FUSE. ONLY
```

MODEL OUTPUT OPTION (IOUTOP)
```
        0           NONE
        1           TO CONSOLE
        2           TO DATAFILE
```

MODEL DISPLACEMENT OPTION (MDISPO)
```
        0           NONE
        1           SINGLE SPECIFIED DISPLACEMENT
        2           LOOPING OF CHOSEN PARAMETER FROM SPECIFIED INITIAL
                    DISPLACEMENT
       -2           AS 2 BUT FROM NULL INITIAL DISPLACEMENT
WHERE MDISPO=2,-2
        STEPS       NO. OF INCREMENTS IN CHOSEN PARAMETER NOT INCLUDING
                    START POSITION
        PARM        1-6 SELECTING X,Y,Z,YAW,PITCH,ROLL DISPL. RESPECTIVELY
        SIZE        SIZE OF STEPS (METRES OR DEGREES)
```

NO. OF E/M SETS (NSET)
```
                    NO. OF INDEPENDANTLY SPECIFIED SETS OF E/MS
        0           INPUT COMPLETE ARRAY FROM DATAFILE
```

(E/M) INPUT OPTION (INPOPT)
```
        1           SINGLE LOOP
        2           INTERFACE ARRAY
        3           LATERAL PSEUDO-CIRCULAR
        4           AXIAL PSEUDO-CIRCULAR
```

(E/M) SYMMETRY (ISYMM(I,J))
```
        1           NONE (MASTER E/M ONLY)
        2           REFLECTION IN Y,Z AND X,Z PLANES
        3           1 ROTATION ABOUT X AXIS - BY 180 DEGREES
        4           3 ROTATIONS                 90
        5           5                           60
        6           7                           45
        7           REFLECT IN Y,Z PLANE
        8           REFLECT IN X,Y X,Z AND Y,Z PLANES
        9           AS 3 WITH REFLECTION IN Y,Z PLANE
        10          AS 4                   Y,Z
        11          AS 5                   Y,Z
        12          AS 6                   Y,Z
```

E/M OUTPUT (IOUTOP)
```
        0           NONE
```

```
     1          INTERFACE ARRAY COORDINATES ONLY
     2          AS 1+WIRE ELEMENT COORDS.
     3          WIRE ELEMENTS TO DATAFILE

E/M AMPERE TURNS
        TOTAL AMPERE-TURN PRODUCT FOR EACH E/M, INPUT IN STANDARD SEQ.
                (WIRE ELEMENT CURRENTS DERIVED APPROPRIATELY)
        THE SIGN FOR CURRENT IN SYMMETRY-DERIVED E/MS IS SUCH THAT
        THE COMPONENT OF FIELD RADIALLY IN TOWARDS THE ORIGIN IS
        MAINTAINED CONSTANT (IN MAGNITUDE, NOT DIRECTION) WITH
        CONSTANT E/M CURRENTS

(DATA) OUTPUT OPTION (IOUT)
        =AB       WHERE:
                  A=FIELD LISTING OPTION
                        0          NONE
                        1          TO CONSOLE
                        2          TO DATAFILE (2FIELD.DAT)
                  B=FORCE/TORQUE OUTPUT OPTION
                        0          TO CONSOLE
                        1          TO DATAFILE (2FORCE.DAT)
                  EG.21 ROUTES FIELD AND FORCE/TORQUE DATA TO FILES
                  0 ROUTES FORCE/TORQUE DATA TO CONSOLE, FIELD DATA LOST
```

Refer to subroutine principal variable lists for description of

detail input variables.

```
      C ROOT SEGMENT OF PROGRAM FORCE   **********************************
      C NO VARIABLES FUNCTIONAL IN THIS SEGMENT
      C
0001        VIRTUAL CX(1000,2),CY(1000,2),CZ(1000,2),CORE(1000,6)
0002        DIMENSION DISP(7),FORCE(9),ISYMM(5,3),CURR(16,5),IDISP(3)
      C
      C MODEL DATA INPUT
      C
0003        CALL MODIN(CORE,DISP,IDISP)
      C
      C COIL DATA INPUT
      C
0004        CALL COIL(CX,CY,CZ,ISYMM,CURR)
      C
      C FORCE,TORQUE AND FIELD CALCULATION
      C
0005        CALL CALC(CX,CY,CZ,CORE,DISP,ISYMM,CURR,IDISP)
0006        STOP ' HAVE A NICE DAY'
0007        END
```

```
0001          SUBROUTINE MODIN(CORE,DISP,IDISP)
0002          VIRTUAL CORE(1000,6)
0003          DIMENSION DISP(7),IDISP(3)
0004          PI=3.141592654
       C
       C ZEROISE CORE AND DISPL. ARRAYS
       C
0005          DO 10 J=1,3
0006   10     IDISP(J)=0
0007          DO 20 I=1,6
0008          DO 20 J=1,1000
0009   20     CORE(J,I)=0.
0010          NE=0
       C
       C MODEL INPUT SECTION
       C
0011   30     TYPE 40
0012   40     FORMAT(' MODEL GEOMETRY OPTION?')
0013          READ(5,*,ERR=30) MOPT
0014          IF(MOPT.EQ.0) GO TO 60
0016          MOPT2=MOPT/10
0017          MOPT1=MOPT-MOPT2*10
0018          CALL FUSIN(MOPT1,NE,CORE)
0019          CALL WING(MOPT2,NE,CORE)
0020          IDISP(3)=NE
0021          GO TO 50
       C
       C MODEL INPUT FROM DATAFILE
       C
0022   60     TYPE 70
0023   70     FORMAT(' FILENAME?'/)
0024          CALL ASSIGN(1,,-1,'OLD',,)
0025          DEFINE FILE 1 (1001,12,U,NREC)
0026          DO 80 I=1,1000
0027   80     READ(1'I)(CORE(I,J),J=1,6)
0028          READ(1'1001) IDISP(3)
0029          CLOSE(UNIT=1)
       C
       C MODEL OUTPUT OPTION
       C
0030   50     TYPE 90
0031   90     FORMAT(' MODEL OUTPUT?')
0032          READ(5,*,ERR=50) IOUTOP
       C
       C MODEL OUTPUT
       C
0033          GO TO(100,110,120),(IOUTOP+1)
0034   110    TYPE 130
0035          TYPE 140
0036   130    FORMAT(' MODEL CORE COORDS. AND MAG.')
0037   140    FORMAT(4X,1HX,7X,1HY,7X,1HZ,8X,6H(J*V)X,8X,6H(J*V)Y
              1,8X,6H(J*V)Z)
0038          DO 150 I=1,IDISP(3)
0039   150    TYPE 160,(CORE(I,J),J=1,6)
```

```
0040   160    FORMAT(3F8.4,3E14.4)
0041          GO TO 100
       C
       C MODEL OUTPUT TO DATAFILE
       C
0042   120    TYPE 70
0043          CALL ASSIGN(2,,-1,'NEW',,,)
0044          DEFINE FILE 2 (1001,12,U,NREC)
0045          DO 170 I=1,1000
0046   170    WRITE(2'I)(CORE(I,J),J=1,6)
0047          WRITE(2'1001)IDISP(3)
0048          CLOSE(UNIT=2)
       C
       C GET MODEL POSN. AND ATTITUDE
       C
0049   100    TYPE 180
0050   180    FORMAT(' MODEL DISP. OPTION?')
0051          READ(5,*,ERR=100) MDISPO
0052          IF(MDISPO.GT.0) GO TO 190
       C
       C MDISPO=0,-2
       C
0054          DO 200 J=1,7
0055   200    DISP(J)=0.
0056          IF(MDISPO.EQ.-2) GO TO 220
0058          GO TO 210
       C
       C MDISPO=1
       C
0059   190    TYPE 230
0060   230    FORMAT(' MODEL DISP.(X,Y,Z), ORI(YAW,PITCH,ROLL)?')
0061          READ(5,*,ERR=190)(DISP(J),J=1,6)
0062          DISP(7)=0.
0063          DO 240 J=4,6
0064   240    DISP(J)=DISP(J)*PI/180.
0065          IF(MDISPO.EQ.1) GO TO 210
       C
       C MDISPO=2,-2
       C
0067   220    TYPE 250
0068   250    FORMAT(' STEPS,PARAMETER,SIZE?')
0069          READ(5,*,ERR=220) IDISP(1),IDISP(2),DISP(7)
0070          IF(IDISP(2).LT.4) GO TO 210
0072          DISP(7)=DISP(7)*PI/180.
0073   210    RETURN
0074          END
```

```
0001          SUBROUTINE FUSIN(MOPT1,NE,CORE)
0002          VIRTUAL CORE(1000,6)
0003          PI=3.141592654
0004          GO TO (30,20,10,20),(MOPT1+1)
       C
       C FIELD GRID SECTION
       C
0005   10     TYPE 40
0006   40     FORMAT(' X0,Y0,Z0, XINC,YINC,ZINC, NOX,NOY,NOZ?')
0007          READ(5,*) X0,Y0,Z0,XINC,YINC,ZINC,NOX,NOY,NOZ
0008          DO 50 IX=1,NOX
0009          DO 50 IY=1,NOY
0010          DO 50 IZ=1,NOZ
0011          NE=NE+1
0012          CORE(NE,1)=X0+(IX-1)*XINC
0013          CORE(NE,2)=Y0+(IY-1)*YINC
0014   50     CORE(NE,3)=Z0+(IZ-1)*ZINC
0015          GO TO 30
       C
       C CYLINDRICAL SECTION
       C
0016   20     TYPE 60
0017   60     FORMAT(' CYLIND.FUSE.:FLEN,FRAD,NA,NR?')
0018          READ(5,*) FLEN,FRAD,NL,NA,NR
0019          IF(NL.EQ.0) GO TO 80
0021          ANGL=PI*2./NA
       C
       C LOOP FOR RADIUS
       C
0022          DO 70 IRAD=0,NR-1
0023          R2=(IRAD+1)*FRAD/NR
0024          R1=IRAD*FRAD/NR
0025          XAREA=ANGL*(R2*R2-R1*R1)/2.
0026          D=4.*(R2**3-R1**3)*SIN(ANGL/2.)/(3.*(R2*R2-R1*R1)*ANGL)
       C
       C LOOP FOR ANGLE
       C
0027          DO 70 IANG=0,NA-1
0028          ANG=IANG*ANGL
       C
       C LOOP FOR AXIAL POS.
       C
0029          DO 70 ILEN=0,NL-1
0030          NE=NE+1
0031          CORE(NE,1)=-FLEN/2.+(ILEN+0.5)*FLEN/NL
0032          CORE(NE,2)=D*COS(ANG)
0033          CORE(NE,3)=D*SIN(ANG)
0034          CORE(NE,4)=XAREA*FLEN/NL
0035   70     CONTINUE
       C
       C END OF CYLINDRICAL SECTION
       C ELLIPSOID ENDCAPS SECTION
       C
0036   80     IF(MOPT1.NE.3) GO TO 30
```

```
0038            TYPE 90
0039    90      FORMAT(' ELLIP.ENDCAPS:AR,NA1?')
0040            READ(5,*) AR,NA1
0041            THETA=PI/(NA1*2)
        C
        C LOOP FOR ANGLE FROM AXIS
        C
0042            DO 100 ITHETA=0,NA1-1
0043            THETA1=THETA*ITHETA
0044            THETA2=THETA*(ITHETA+1)
0045            D=COS(THETA1)-COS(THETA2)
0046            T=COS(THETA1*2.)-COS(THETA2*2.)
        C
        C LOOP FOR ANGLE AROUND AXIS
        C
0047            DO 100 IANG=0,NA-1
0048            ANG=IANG*ANGL
        C
        C LOOP FOR FRONT/BACK AND PSEUDO RADIUS
        C
0049            DO 100 IFRBAK=-1,1,2
0050            DO 100 IRAD=0,NR-1
0051            R1=IRAD*FRAD/NR
0052            R2=(IRAD+1)*FRAD/NR
0053            R=(R2**4-R1**4)/(R2**3-R1**3)
0054            NE=NE+1
0055            C=3.*SIN(ANGL/2.)*R*(THETA+T)/(4.*ANGL*D)
0056            CORE(NE,1)=IFRBAK*(-FLEN/2.-AR*R*T*3./(D*16.))
0057            CORE(NE,2)=C*COS(ANG)
0058            CORE(NE,3)=C*SIN(ANG)
0059            CORE(NE,4)=(R2**3-R1**3)*ANGL*AR*D/3.
0060    100     CONTINUE
        C
        C END OF ELLIP. ENDCAPS
        C
0061    30      RETURN
0062            END
```

```
0001          SUBROUTINE WING(MOPT2,NE,CORE)
0002          VIRTUAL CORE(1000,6)
0003          PI=3.141592654
0004          IF(MOPT2.EQ.0) GO TO 60
       C
       C SLAB WING INPUT
       C
0006   10     TYPE 20
0007   20     FORMAT(' SLAB WING:1/2SPAN,1/2GAP,CHORD,THICK,TAPER,SWEEP?')
0008          READ(5,*,ERR=10) SPAN,FRAD,CHORD,THICK,TAPER,SWEEP
0009   30     TYPE 40
0010   40     FORMAT(' DLONG,DVERT,NS,NC,NT,IWIDIR?')
0011          READ(5,*,ERR=30) DLONG,DVERT,NS,NC,NT,IWIDIR
0012          SWEEP=SWEEP*PI/180.
0013          SINSWE=SIN(SWEEP)
0014          COSWE=COS(SWEEP)
0015          SPAN2=SPAN-FRAD
       C
       C LOOP FOR PORT AND STB. WINGS
       C
0016          DO 50 IWING=-1,1,2
       C
       C LOOP FOR SPAN AND THICKNESS
       C
0017          DO 50 ISPAN=0,NS-1
0018          DO 50 ITHICK=0,NT-1
       C
       C CALCULATE CORE DIPOLES
       C
0019          DO 50 ICHORD=0,NC-1
0020          NE=NE+1
0021          T=((1.-TAPER)*(ISPAN+1)-NS)/((1.-TAPER)*ISPAN-NS)
0022          TYPO=FLOAT(ISPAN)/NS+(1.-2.*(1-T)/3.)/((1.+T)*NS)
0023          CHORDL=CHORD*(1.-(1.-TAPER)*TYPO)
0024          VOL=CHORD*THICK*SPAN2*(1.+T)/(2.*NC*NT*NS)
0025          CORE(NE,1)=DLONG-CHORDL*(0.5-(0.5+ICHORD)/NC)-SPAN2*TYPO
              1*SINSWE/COSWE
0026          CORE(NE,2)=(SPAN2*TYPO+FRAD)*IWING
0027          CORE(NE,3)=DVERT-THICK*(0.5-(0.5+ITHICK)/NT)
0028          CORE(NE,4)=VOL*SINSWE*IWIDIR
0029          CORE(NE,5)=VOL*COSWE*IWIDIR*IWING
0030   50     CONTINUE
0031   60     RETURN
0032          END
```

```
0001          SUBROUTINE COIL(CX,CY,CZ,ISYMM,CURR)
0002          VIRTUAL CX(1000,2),CY(1000,2),CZ(1000,2)
0003          DIMENSION XX(4,10),YY(4,10),ZZ(4,10),ISYMM(5,3),CURR(16,5)
0004          DIMENSION INOCO(12)
0005          DATA INOCO/1,4,2,4,6,8,2,8,4,8,12,16/
0006          NSET=0
0007          IWIRE=1
0008          IOUTOP=0
0009          PI=3.141592654
0010          DO 10 J=1,5
0011          ISYMM(J,1)=0
0012          DO 10 I=1,16
0013    10    CURR(I,J)=1.
0014    20    TYPE 30
0015    30    FORMAT(' NO. E/M SETS?')
0016          READ(5,*,ERR=20) NSET
0017          IF(NSET.GT.0) GO TO 40
        C
        C COMPLETE SYSTEM DATAFILE INPUT
        C
0019          TYPE 50
0020    50    FORMAT(' FILENAME?'/)
0021          CALL ASSIGN(1,,-1,'OLD',,)
0022          DEFINE FILE 1 (1003,12,U,M)
0023          DO 60 I=1,3
0024    60    READ(1'I)(ISYMM(J,I),J=1,5)
0025          DO 70 K=1,1000
0026    70    READ(1'K+3)(CX(K,J),CY(K,J),CZ(K,J),J=1,2)
0027          CLOSE(UNIT=1)
0028          DO 80 I=1,5
0029          IF(ISYMM(I,1).EQ.0) GO TO 80
0031          NSET=NSET+1
0032    80    CONTINUE
0033          GO TO 90
        C
        C E/M SET LOOP START
        C
0034    40    DO 100 ISETI=1,NSET
        C
        C GET MASTER E/M GEOMETRY FOR THIS SET
        C
0035          TYPE 110,ISETI
0036    110   FORMAT(' E/M SET',I5)
0037    120   TYPE 130
0038    130   FORMAT(' INPUT OPTION,SYMMETRY OPTION?')
0039          READ(5,*,ERR=120) INOPT,ISYMM(ISETI,1)
0040          GO TO (140,150,160,170) INOPT
        C
        C SINGLE LOOP INPUT SECTION
        C
0041    140   TYPE 180
0042    180   FORMAT(' NO. ELEMENTS?')
0043          READ(5,*,ERR=140) NINT
0044    190   TYPE 200
```

```
0045   200     FORMAT(' ELEMENT END POINTS?')
0046           READ(5,*,ERR=190) (CX(I,1),CY(I,1),CZ(I,1),I=1,NINT)
0047           NEND=NINT+IWIRE-1
0048           DO 210 J=IWIRE,(NEND-1)
0049           CX(J,2)=CX(J+1,1)
0050           CY(J,2)=CY(J+1,1)
0051   210     CZ(J,2)=CZ(J+1,1)
0052           CX(NEND,2)=CX(IWIRE,1)
0053           CY(NEND,2)=CY(IWIRE,1)
0054           CZ(NEND,2)=CZ(IWIRE,1)
0055           ISYMM(ISETI,3)=1
0056           GO TO 220
       C
       C INTERFACE ARRAY INPUT SECTION
       C
0057   150     TYPE 230
0058   230     FORMAT(' NUMBER OF LAYERS, LOOPS/LAYER, INTERFACES?')
0059           READ(5,*,ERR=150) MM,NN,NINT
0060   240     TYPE 250
0061   250     FORMAT(' INTERFACE COORDINATES?')
0062           DO 260 J=1,NINT
0063   260     READ(5,*,ERR=240) (XX(I,J),YY(I,J),ZZ(I,J),I=1,3)
0064           NEND=MM*NN*NINT+IWIRE-1
0065           CALL FACE(NINT,MM,NN,XX,CX,IWIRE)
0066           CALL FACE(NINT,MM,NN,YY,CY,IWIRE)
0067           CALL FACE(NINT,MM,NN,ZZ,CZ,IWIRE)
0068           ISYMM(ISETI,3)=MM*NN
0069           GO TO 220
       C
       C END OF INTERFACE ARRAY
       C LATERAL CIRCULAR E/M SECTION
       C
0070   160     TYPE 280
0071   280     FORMAT(' DX,DY,RAD1,RAD2,DY1,DY2,NDIVR,NDIVY,NSEG,ANGLE?')
0072           READ(5,*,ERR=160) DX,DY,RAD1,RAD2,DY1,DY2,NDIVR,NDIVY,NSEG,ANGLE
0073           COSANG=COS(ANGLE*PI/180.)
0074           SINANG=SIN(ANGLE*PI/180.)
       C
       C LOOP FOR AXIAL DEPTH
       C
0075           DO 290 I=1,NDIVY
0076           Y=DY1+(I-0.5)*(DY2-DY1)/NDIVY
       C
       C LOOP FOR RADIAL THICKNESS
       C
0077           DO 290 M=1,NDIVR
0078           R=RAD1+(M-0.5)*(RAD2-RAD1)/NDIVR
0079           R=R*NSEG*SIN(PI/NSEG)/(PI*COS(PI/NSEG))
       C
       C LOOP AROUND CIRCUMFERENCE
       C
0080           DO 290 J=1,NSEG
0081           K=((I-1)*NDIVR+M-1)*NSEG+J+IWIRE-1
0082           ANG=PI*2./NSEG
```

```
0083          ZT1=SIN(ANG*(J-1))*R
0084          ZT2=SIN(ANG*J)*R
0085          CX(K,1)=DX+COS(ANG*(J-1))*R
0086          CX(K,2)=DX+COS(ANG*J)*R
0087          CY(K,1)=Y*COSANG-ZT1*SINANG+DY
0088          CY(K,2)=Y*COSANG-ZT2*SINANG+DY
0089          CZ(K,1)=Y*SINANG+ZT1*COSANG
0090          CZ(K,2)=Y*SINANG+ZT2*COSANG
0091   290    CONTINUE
0092          NEND=NSEG*NDIVR*NDIVY+IWIRE-1
0093          ISYMM(ISETI,3)=NDIVR*NDIVY
0094          GO TO 220
       C
       C END OF LATERAL CIRCULAR E/M
       C AXIAL CIRCULAR E/M SECTION
       C
0095   170    TYPE 310
0096   310    FORMAT(' X1,X2,RAD1,RAD2,NDIVR,NDIVX,NSEG?')
0097          READ(5,*,ERR=170) X1,X2,RAD1,RAD2,NDIVR,NDIVX,NSEG
       C
       C LOOP FOR AXIAL DEPTH
       C
0098          DO 320 I=1,NDIVX
0099          X=X1+(I-0.5)*(X2-X1)/NDIVX
       C
       C LOOP FOR RADIAL THICKNESS
       C
0100          DO 320 M=1,NDIVR
0101          R=RAD1+(M-0.5)*(RAD2-RAD1)/NDIVR
0102          R=R*NSEG*SIN(PI/NSEG)/(PI*COS(PI/NSEG))
       C
       C LOOP AROUND CIRCUMFERENCE
       C
0103          DO 320 J=1,NSEG
0104          K=((I-1)*NDIVR+M-1)*NSEG+J+IWIRE-1
0105          ANG=PI*2./NSEG
0106          CX(K,1)=X
0107          CX(K,2)=X
0108          CY(K,1)=COS(ANG*(J-1))*R
0109          CY(K,2)=COS(ANG*J)*R
0110          CZ(K,1)=SIN(ANG*(J-1))*R
0111          CZ(K,2)=SIN(ANG*J)*R
0112   320    CONTINUE
0113          NEND=NSEG*NDIVX*NDIVR+IWIRE-1
0114          ISYMM(ISETI,3)=NDIVX*NDIVR
       C
       C END OF AXIAL CIRCULAR E/M
       C STORE E/M ELEMENT NO.
       C
0115   220    ISYMM(ISETI,2)=NEND-IWIRE+1
       C
       C   OUTPUT SECTION
       C
0116          IF(IOUTOP.EQ.3) GO TO 435
```

```
0118   340      TYPE 350
0119   350      FORMAT(' E/M OUTPUT?')
0120            READ(5,*,ERR=340) IOUTOP
0121            GO TO (435,360,370,435) (IOUTOP+1)
0122   370      TYPE 380
0123            TYPE 381
0124   380      FORMAT(' WIRE COORDINATES')
0125   381      FORMAT(5X,2HX1,8X,2HY1,8X,2HZ1,8X,2HX2,8X,2HY2,8X,2HZ2)
0126            DO 390 I=IWIRE,NEND
0127   390      TYPE 400,(CX(I,J),CY(I,J),CZ(I,J),J=1,2)
0128   400      FORMAT(6F10.5)
0129   360      IF(INPOPT.NE.2) GO TO 435
0131            TYPE 410
0132            TYPE 411
0133   410      FORMAT(' INTERFACE NO. AND COORDS')
0134   411      FORMAT(3X,4HINT.,9X,1HX,14X,1HY,14X,1HZ)
0135            DO 420 J=1,NINT
0136   420      TYPE 430,(J,XX(I,J),YY(I,J),ZZ(I,J),I=1,4)
0137   430      FORMAT(I5,3F15.5)
       C
       C INCREMENT WIRE ELEMENT COUNTER
       C
0138   435      IWIRE=NEND+1
0139   100      CONTINUE
       C
       C END OF E/M SET LOOP
       C COMPLETE SYSTEM DATAFILE OUTPUT
       C
0140   440      IF(IOUTOP.NE.3) GO TO 90
0142            TYPE 50
0143            CALL ASSIGN(2,,-1,'NEW',,)
0144            DEFINE FILE 2 (1003,12,U,M)
0145            DO 450 I=1,3
0146   450      WRITE(2'I)(ISYMM(J,I),J=1,5)
0147            DO 460 K=1,1000
0148   460      WRITE(2'K+3)(CX(K,J),CY(K,J),CZ(K,J),J=1,2)
0149            CLOSE(UNIT=2)
       C
       C READ AHEAD E/M CURRENTS
       C
0150   90       DO 470 ISETI=1,NSET
0151            NOC=INOCO(ISYMM(ISETI,1))
0152            TYPE 110,ISETI
0153   490      TYPE 500,NOC
0154   500      FORMAT(' E/M AMP.TURNS/1000?   (',I2,')')
0155            READ(5,*,ERR=490)(CURR(I,ISETI),I=1,NOC)
0156            DO 470 I=1,NOC
0157            CURR(I,ISETI)=CURR(I,ISETI)*1000.
0158   470      CONTINUE
0159            RETURN
0160            END
```

```
0001            SUBROUTINE CALC(CX,CY,CZ,CORE,DISP,ISYMM,CURR,IDISP)
0002            VIRTUAL CX(1000,2),CY(1000,2),CZ(1000,2),CORE(1000,6)
0003            DIMENSION POS(6),BB(3),GB(9),COSR(3),SINR(3),T(3),DPOS(3)
0004            DIMENSION DISP(7),FORCE(6),ISYMM(5,3),CURR(16,5),IDISP(3)
0005            PI=3.141592654
0006            XMU=0.00000125664
0007            LUNOUT=5
0008            LUNFLD=5
        C
        C OUTPUT ROUTING
        C OPEN DATAFILES IF REQUIRED
        C
0009   10       TYPE 20
0010   20       FORMAT(' OUTPUT OPTION?')
0011            READ(5,*,ERR=10) IOUT
0012            IFLIST=IOUT/10
0013            IOFILE=IOUT-IFLIST*10
0014            IF(IOFILE.NE.1) GO TO 30
0016            LUNOUT=1
0017            OPEN(UNIT=1,NAME='2FORCE.DAT',TYPE='NEW',FORM='FORMATTED'
               1,RECORDSIZE=78)
0018   30       IF(IFLIST.NE.2) GO TO 40
0020            LUNFLD=2
0021            OPEN(UNIT=2,NAME='2FIELD.DAT',TYPE='NEW',FORM='FORMATTED'
               1,RECORDSIZE=120)
0022   40       IF(IFLIST.EQ.0.OR.LUNFLD.EQ.2) GO TO 50
0024            WRITE(LUNFLD,60)
0025   60       FORMAT(1H0,5X,1HX,9X,1HY,9X,1HZ,8X,2HBX,8X,2HBY,8X,2HBZ,8X
               1,3HBXX,7X,3HBXY,7X,3HBXZ,7X,3HBYY,7X,3HBYZ,7X,3HBZZ)
        C
        C POSITION/ORIENTATION LOOP START
        C
0026   50       DO 70 K=0,IDISP(1)
0027            DO 80 N=1,6
0028   80       FORCE(N)=0.
        C
        C CONVERT MODEL ORIENTATION
        C
0029            DO 90 J=1,3
0030            COSR(J)=COS(DISP(J+3))
0031   90       SINR(J)=SIN(DISP(J+3))
        C
        C MODEL ELEMENT LOOP START
        C
0032   100      DO 110 N=1,IDISP(3)
        C
        C ROTATE ELEMENT
        C
0033            DO 120 JJ=1,2
0034            J=JJ*JJ
0035            POS(J)=CORE(N,J)*COSR(1)*COSR(2)-CORE(N,J+1)*SINR(1)
               1*COSR(2)+CORE(N,J+2)*SINR(2)
0036            POS(J+1)=CORE(N,J)*(SINR(1)*COSR(3)+COSR(1)*SINR(2)*
               1SINR(3))+CORE(N,J+1)*(COSR(1)*COSR(3)-SINR(1)*SINR(2)*SINR(3))
```

```
            2+CORE(N,J+2)*COSR(2)*SINR(3)
0037   120   POS(J+2)=CORE(N,J)*(SINR(1)*SINR(3)-COSR(1)*SINR(2)*COSR(3))
            1+CORE(N,J+1)*(COSR(1)*SINR(3)+SINR(1)*SINR(2)*COSR(3))
            2+CORE(N,J+2)*COSR(2)*COSR(3)
      C
      C GET MODEL ELEMENT ABSOLUTE POSITION
      C
0038         DO 130 J=1,3
0039   130   DPOS(J)=POS(J)+DISP(J)
      C
      C GET FIELD FOR THIS ELEMENT
      C
0040         CALL FIELD(BB,GB,CX,CY,CZ,ISYMM,CURR,DPOS)
      C
      C COMPUTE ELEMENT FORCES
      C
0041         DO 140 J=1,3
0042         JJ=(J-1)*3+1
0043         T(J)=(POS(4)*GB(JJ)+POS(5)*GB(JJ+1)+POS(6)*GB(JJ+2))
0044   140   FORCE(J)=FORCE(J)+T(J)/XMU
      C
      C AND ELEMENT TORQUES AND MOMENTS OF FORCES
      C
0045         FORCE(4)=FORCE(4)+((POS(2)*T(3)-POS(3)*T(2))+
            1(POS(5)*BB(3)-POS(6)*BB(2)))/XMU
0046         FORCE(5)=FORCE(5)+((POS(3)*T(1)-POS(1)*T(3))+
            1(POS(6)*BB(1)-POS(4)*BB(3)))/XMU
0047         FORCE(6)=FORCE(6)+((POS(1)*T(2)-POS(2)*T(1))+
            1(POS(4)*BB(2)-POS(5)*BB(1)))/XMU
      C
      C FIELD OUTPUTS?
      C
0048         IF(IFLIST.EQ.0) GO TO 110
0050         WRITE(LUNFLD,150) POS(1),POS(2),POS(3),BB(1),BB(2),BB(3)
            1,GB(1),GB(2),GB(3),GB(5),GB(6),GB(9)
0051   150   FORMAT(12F10.4)
0052   110   CONTINUE
      C
      C END OF ELEMENT LOOP
      C FINAL OUTPUTS
      C
0053         IF(K.GT.0.OR.IOFILE.EQ.1) GO TO 160
0055         WRITE(LUNOUT,170)
0056   170   FORMAT(7X,6HFORCEX,7X,6HFORCEY,7X,6HFORCEZ,7X,6HTORQUX,7X
            1,6HTORQUY,7X,6HTORQUZ)
0057   160   WRITE(LUNOUT,180)(FORCE(I),I=1,6)
0058   180   FORMAT(6F13.2)
      C
      C INCREMENT DISPLACEMENT
      C
0059         DISP(IDISP(2))=DISP(IDISP(2))+DISP(7)
0060   70    CONTINUE
      C
      C END OF DISPLACEMENT LOOP
```

```
      C
0061        IF(LUNOUT.NE.1) GO TO 190
0063        CLOSE(UNIT=1)
0064  190   IF(LUNFLD.NE.2) GO TO 200
0066        CLOSE(UNIT=2)
0067  200   RETURN
0068        END
```

```
0001        SUBROUTINE FACE(NINT,M,N,WW,W,IWIRE)
      C
      C THIS SUBROUTINE DERIVED FROM MIT PROGRAM 'TABLE', BUT WITH TWO
      C SIGNIFICANT ALTERATIONS IN FUNCTION. REFER TO PROGRAM DESCRIPTION
      C
0002        VIRTUAL W(1000,2)
0003        DIMENSION WW(4,10)
0004        IND=IWIRE-1
      C
      C GENERATE FOURTH CORNERS OF INTERFACES
      C
0005        DO 10 I=1,NINT
0006  10    WW(4,I)=WW(3,I)-WW(2,I)+WW(1,I)
      C
      C GENERATE INTERMEDIATE COORDINATES FOR EACH INTERFACE
      C
0007        DO 20 I=1,M
0008        DO 20 J=1,N
0009        DO 20 K=1,NINT
0010        IND=IND+1
0011        W(IND,1)=(WW(1,K)*(2*(N-J)+1)*(2*(M-I)+1)+WW(4,K)*(2*J-1)
           1*(2*(M-I)+1)+WW(2,K)*(2*I-1)*(2*(N-J)+1)+WW(3,K)*(2*I-1)
           2*(2*J-1))/(4*M*N)
0012  20    CONTINUE
      C
      C GENERATE W2 FROM W1 SO THAT ENDPOINTS OF WIRES ARE TOGETHER
      C
0013        DO 30 I=1,M*N
0014        J=(I-1)*NINT
0015        W(I*NINT,2)=W(J+1,1)
0016        DO 30 K=1,NINT-1
0017        W(J+K,2)=W(J+K+1,1)
0018  30    CONTINUE
0019        RETURN
0020        END
```

```
0001          SUBROUTINE FIELD(BB,GB,CX,CY,CZ,ISYMM,CURR,DPOS)
0002          VIRTUAL CX(1000,2),CY(1000,2),CZ(1000,2)
0003          DIMENSION S(3),T(3),DC(3),DD(3),DG(3),DP(3),DS(3)
0004          DIMENSION BB(3),GB(6),CURR(16,5),ISYMM(5,3),DPOS(3)
0005          IWIRE=1
0006          PI=3.141592654
0007          DO 10 N=1,9
0008   10     GB(N)=0.
0009          DO 20 N=1,3
0010   20     BB(N)=0.
       C
       C COIL SET LOOP START
       C
0011          DO 30 ISET=1,5
0012          INCOIL=0
0013          IF(ISYMM(ISET,1).EQ.0) GO TO 30
0015          IREFL=1
0016          IF(ISYMM(ISET,1).LT.7) GO TO 40
0018          IREFL=-1
       C
       C CALCULATION VECTORING AND CONTROL SECTION
       C
0019   40     DO 50 IX=1,IREFL,-2
       C
       C MASTER COIL
       C
0020          DY=1.
0021          DZ=1.
0022          DYZ=0.
0023          INCOIL=INCOIL+1
0024          ICURR=IX
0025          ASSIGN 60 TO IPOINT
0026          GO TO 1000
0027   60     IF(ISYMM(ISET,1).EQ.1.OR.ISYMM(ISET,1).EQ.7) GO TO 50
0029          IF(ISYMM(ISET,1).EQ.2.OR.ISYMM(ISET,1).EQ.8) GO TO 70
       C
       C ROTATIONAL SYMMETRIES
       C
0031          IF(ISYMM(ISET,1).GT.6) GO TO 80
0033          IROT=(ISYMM(ISET,1)-2)*2
0034          GO TO 90
0035   80     IROT=(ISYMM(ISET,1)-8)*2
0036   90     DO 100 N=1,IROT-1
0037          ANGL=2.*PI*N/IROT
0038          DY=COS(ANGL)
0039          DZ=DY
0040          DYZ=SIN(ANGL)
0041          INCOIL=INCOIL+1
0042          ICURR=IX
0043          ASSIGN 100 TO IPOINT
0044          GO TO 1000
0045   100    CONTINUE
0046          GO TO 50
       C
```

```
      C REFLECTION SYMMETRIES
      C
0047  70      DZ=-1.
0048          DY=1.
0049          DYZ=0.
0050          INCOIL=INCOIL+1
0051          ICURR=-IX
0052          ASSIGN 110 TO IPOINT
0053          GO TO 1000
0054  110     DY=-1.
0055          DZ=1.
0056          INCOIL=INCOIL+1
0057          ICURR=-IX
0058          ASSIGN 120 TO IPOINT
0059          GO TO 1000
0060  120     DY=-1.
0061          DZ=-1.
0062          INCOIL=INCOIL+1
0063          ICURR=IX
0064          ASSIGN 105 TO IPOINT
0065          GO TO 1000
0066  105     CONTINUE
0067  50      CONTINUE
      C
      C INCREMENT WIRE COUNTER
      C
0068          IWIRE=IWIRE+ISYMM(ISET,2)
0069  30      CONTINUE
      C
      C END OF COIL SET LOOP
      C COMPLETE DUMMY VARIABLES
      C
0070          GB(4)=GB(2)
0071          GB(7)=GB(3)
0072          GB(8)=GB(6)
0073          RETURN
      C******************************************************************
      C
      C FIELD AT POINT SECTION
      C
      C CORRECT WIRE CURRENTS
      C
0074  1000    CURREN=ICURR*CURR(INCOIL,ISET)/ISYMM(ISET,3)
      C
      C ****************************************************************
      C THE REMAINDER OF THIS SUBROUTINE IS TAKEN WITH NO SIGNIFICANT
      C ALTERATION FROM THE PROGRAM "TABLE" , COURTESY MASSACHUSETTS
      C INSTITUTE OF TECHNOLOGY.
      C ****************************************************************
      C
      C WIRE ELEMENT LOOP START
      C
0075          DO 2000 L=IWIRE,IWIRE+ISYMM(ISET,2)-1
      C
```

```
       C CALCULATE A,B,C,D,E,F
       C
0076          A=(IX*CX(L,1)-DPOS(1))
0077          B=(IX*CX(L,2)-DPOS(1))
0078          C=(DY*CY(L,1)-DYZ*CZ(L,1)-DPOS(2))
0079          D=(DY*CY(L,2)-DYZ*CZ(L,2)-DPOS(2))
0080          E=(DZ*CZ(L,1)+DYZ*CY(L,1)-DPOS(3))
0081          F=(DZ*CZ(L,2)+DYZ*CY(L,2)-DPOS(3))
       C
       C SUBSCRIPT A,B,C,D,E,F FOR LATER USE
       C
0082          S(1)=A
0083          S(2)=C
0084          S(3)=E
0085          T(1)=B
0086          T(2)=D
0087          T(3)=F
       C
       C CALCULATE U,V,W
       C
0088          U=C*F-D*E
0089          V=E*B-F*A
0090          W=A*D-B*C
       C
       C CALCULATE RHO1, RHO2 AND THEIR DOT, CROSS PRODUCTS
       C
0091          R1=(A*A+C*C+E*E)**0.5
0092          R2=(B*B+D*D+F*F)**0.5
0093          RS=R1+R2
0094          RM=R1*R2
0095          RDR=A*B+C*D+E*F
0096          RXR=U+V+W
       C
       C CALCULATE THE DERIVATIVES OF THE SUM, ETC. OF RHO1 AND RHO2
       C
0097          DO 1010 M=1,3
0098          DP(M)=-(S(M)*R2/R1+T(M)*R1/R2)
0099          DS(M)=-(S(M)/R1+T(M)/R2)
0100          DD(M)=-(S(M)+T(M))
0101   1010   CONTINUE
0102          DC(1)=F-E+C-D
0103          DC(2)=E-F+B-A
0104          DC(3)=D-C+A-B
       C
       C CALCULATE AND TEST H TO DETERMINE EQN. FOR G TO BE USED
       C
0105          H=(RM+RDR)/RM
0106          IF(H.LT.0.01) GO TO 1020
0108          G=RS/(RM*(RM+RDR))
       C
       C CALCULATE G AND ITS X,Y,Z DERIVATIVES
       C
0109          DO 1030 M=1,3
0110          DGA=RM*(RM+RDR)*DS(M)
```

```
0111          DGB=RS*(RM*(DP(M)+DD(M))+DP(M)*(RM+RDR))
0112   1030   DG(M)=(DGA-DGB)/(RM*(RM+RDR))**2
0113          GO TO 1040
0114   1020   G=((RS)*(RM-RDR))/(RM*RXR*RXR)
0115          DO 1050 M=1,3
0116          DGA=(RS*(DP(M)-DD(M))+DS(M)*(RM-RDR))*RM*RXR**2
0117          DGB=RS*(RM-RDR)*(RM*2.*RXR*DC(M)+DP(M)*RXR**2)
0118   1050   DG(M)=(DGA-DGB)/(RM*RXR**2)**2
       C
       C CALCULATE THE FIELD AND GRADIENT CONTRIBUTIONS OF EACH
       C CURRENT ELEMENT
       C
0119   1040   DGX=DG(1)
0120          DGY=DG(2)
0121          DGZ=DG(3)
0122          CURP=CURREN/10000000.
0123          CURM=CURP*G
       C
       C SUM THE INDIVIDUAL CONTRIBUTIONS TO THE FIELD AND GRADIENT TO
       C GET THE TOTAL FIELD AND GRADIENT
       C
0124          BB(1)=BB(1)+CURM*U
0125          BB(2)=BB(2)+CURM*V
0126          BB(3)=BB(3)+CURM*W
0127          GB(1)=GB(1)+CURP*U*DGX
0128          GB(2)=GB(2)+CURP*(G*(E-F)+U*DGY)
0129          GB(3)=GB(3)+CURP*(G*(D-C)+U*DGZ)
0130          GB(5)=GB(5)+CURP*V*DGY
0131          GB(6)=GB(6)+CURP*(G*(A-B)+V*DGZ)
0132          GB(9)=GB(9)+CURP*DGZ*W
0133   2000   CONTINUE
       C
       C END OF WIRE ELEMENT LOOP
       C
0134          GO TO IPOINT
0135          END
```

- 294 -

PRINCIPAL VARIABLE LIST FOR SUBROUTINE MODIN ***********************

VARIABLES PASSED INTO MODIN
    NONE

VARIABLES PASSED OUT OF MODIN
    CORE,DISP,IDISP   LOADED WITH MODEL CHARACTERISTICS

CORE   MODEL ELEMENT POSITION AND MAGNETIZATIONS
    (N,1)   X POSITION
    (N,2)   Y
    (N,3)   Z
    (N,4)   X WISE MAGNETIZATION*ELEMENT VOLUME
    (N,5)   Y
    (N,6)   Z
DISP   REQUIRED MODEL DISPLACEMENT FROM ZERO POSITION
    (1)   X DISPLACEMENT
    (2)   Y
    (3)   Z
    (4)   YAW DISPLACEMENT
    (5)   PITCH
    (6)   ROLL
    (7)   STEP SIZE FOR DISPLACEMENT LOOP WHERE REQUIRED
IDISP   LOOP CONTROL PARAMETERS
    (1)   NO. OF REQUIRED STEPS IN POSITION/ORIENTATION LOOP
    (2)   PARAMETER (IN ARRAY DISP) TO BE INCREMENTED
    (3)   TOTAL NO. OF MODEL ELEMENTS
MOPT   MODEL INPUT OPTION
    DECODED INTO
    MOPT1   FUSELAGE INPUT OPTION
    MOPT2   WING INPUT OPTION
NE   NUMBER OF MODEL ELEMENTS (PASSED TO IDISP(3))
IOUTOP   MODEL OUTPUT OPTION
    0   NONE
    1   LISTING ON CONSOLE DEVICE
    2   TO DATAFILE
MDISPO   MODEL DISPLACEMENT OPTION
    0   NONE
    1   SINGLE SELECTED POSITION/ORIENTATION
    2   SELECTED INITIAL DISPLACEMENT WITH STEPPING OF ONE
             SELECTED PARAMETER
    -2   AS 2 BUT NULL INITIAL DISPLACEMENT

PRINCIPAL VARIABLE LIST FOR SUBROUTINE FUSIN ***************************

VARIABLES PASSED INTO FUSIN
    MOPT1
    NE   =0

VARIABLES PASSED OUT OF FUSIN
    CORE   PARTLY LOADED WHERE MOPT1.NE.0
    NE   UPDATED WHERE APPROPRIATE

MOPT1   FUSELAGE INPUT OPTION
    0   NONE
    1   CYLINDRICAL
    2   FIELD GRID
    3   AS 1+ELLIPSOID ENDCAPS
NE   VECTOR TO LAST VALID ENTRY IN CORE
CORE   AS MODIN

FLEN   LENGTH OF CYLINDRICAL PORTION OF FUSELAGE
FRAD   RADIUS OF CYLINDRICAL PORTION OF FUSELAGE
NL,NA,NR   NO. OF LONGITUDINAL,CIRCUMFERENTIAL AND RADIAL
              ELEMENTS IN CYL. FUSELAGE

SOME VARIABLES ACTIVE IN THE FIELD GRID SECTION
    XO,YO,ZO   X,Y,Z COORDINATES OF START OF FIELD GRID
    XINC,YINC,ZINC   X,Y,Z INCREMENTS OF FIELD GRID
    NOX,NOY,NOZ   NO. OF X,Y,Z INCREMENTS

SOME VARIABLES ACTIVE IN THE CYLINDRICAL FUSELAGE SECTION
    R1,R2,XAREA   INNER,OUTER RADIUS AND CROSS SECTIONAL
                      AREA OF FUSELAGE ELEMENT
    D,ANG   RADIUS AND ANGULAR LOCATION OF CENTROID
                      OF ELEMENT

SOME VARIABLES ACTIVE IN THE ELLIPSOID ENDCAPS SECTION
    AR   LENGTH OF ELLIP. ENDCAP/FUSELAGE RADIUS
                      AR=1 FOR HEMISPHERICAL ENDCAPS
    NA1   NO. "LONGITUDINAL" ELEMENTS IN ENDCAP
    R1,R2   INNER,OUTER RADII OF ELEMENTAL SHELL
                      AT BASE OF ENDCAP
    C   RADIUS TO CENTROID OF ELEMENT

PRINCIPAL VARIABLE LIST FOR SUBROUTINE WING ****************************

VARIABLES PASSED INTO WING
          MOPT2   FROM MODIN
          NE   SET POINTING AT LAST ENTRY IN CORE ARRAY
          CORE   MAY BE PARTIALLY LOADED

VARIABLES PASSED OUT OF WING
          NE   UPDATED WHERE APPROPRIATE
          CORE   DITTO

SPAN   HALF WING SPAN
FRAD   HALF WING CENTRE GAP (FUSELAGE RADIUS?)
CHORD   WING ROOT CHORD
THICK   WING THICKNESS
TAPER   TIP CHORD/ROOT CHORD
SWEEP   WING SWEEPBACK
DLONG   X WISE DISPLACEMENT OF WING FROM MODEL DATUM
DVERT   Z WISE DISPLACEMENT OF WING FROM MODEL DATUM
          .   (DLONG,DVERT ONLY USEFUL WHERE FUSELAGE PRESENT)
NS   NO. OF ELEMENTS ALONG SINGLE WING PANEL
NC   NO. OF ELEMENTS ALONG WING CHORD
NT   NO. OF ELEMENTS THROUGH WING THICKNESS
IWIDIR   WING MAGNETIZATION DIRECTION
SINSWE   SINE OF SWEEP ANGLE
COSWE   COSINE OF SWEEP ANGLE
SPAN2   WING PANEL LENGTH
CHORDL   LOCAL CHORD
TYPD   DISTANCE OF CENTROID OF ELEMENT FROM WING ROOT
VOL   ELEMENT VOLUME
T   EQUIVALENT VALUE OF TAPER FOR SINGLE ELEMENT

PRINCIPAL VARIABLE LIST FOR SUBROUTINE FACE ****************************

VARIABLES PASSED INTO FACE
          NINT,M,N,WW,IWIRE

VARIABLES PASSED OUT OF FACE
          W   FILLED WITH WIRE COORDINATES

NINT   NO. INTERFACES
M   NO. LAYERS OF WIRE
N   NO. WIRES/LAYER
WW   INTERFACE COORDINATES (X,Y OR Z)
          (1,N)   CORNER 1
          (2,N)   2
          (3,N)   3
          (4,N)   4 (PROGRAM GENERATED)
IWIRE   POINTER TO FIRST FREE ENTRY IN W
W   GENERATED WIRE COORDINATES (X,Y OR Z)
          (N,1)   WIRE START
          (N,2)   WIRE END

PRINCIPAL VARIABLE LIST FOR SUBROUTINE COIL ****************************

VARIABLES PASSED INTO COIL
        NONE

VARIABLES PASSED OUT OF COIL
        CX,CY,CZ,ISYMM,CURR   E/M ARRAY DATA

CX,CY,CZ   X,Y,Z COORDINATES OF WIRE ELEMENTS
        (N,1)   WIRE ELEMENT START
        (N,2)   WIRE ELEMENT END
ISYMM   E/M SYMMETRY CODES AND SET DATA
        (N,1)   SYMMETRY OPTION FOR THIS SET
        (N,2)   NO. OF WIRE ELEMENTS PER E/M IN THIS SET
        (N,3)   NO. OF LOOPS OF ELEMENTS IN THIS SET
CURR   E/M TOTAL AMPERE-TURNS
        (1,N)   IN FIRST E/M OF SET
        (2,N)   SECOND
        ETC.   ETC.
XX,YY,ZZ   COORDINATES OF E/M INTERFACES (WHERE USED)
        (1,N)   FIRST CORNER
        (2,N)   SECOND
        (3,N)   THIRD
        (4,N)   FOURTH (PROGRAM GENERATED)
INOCO   NO. OF E/MS PER SET
        (N)   NO. IN SET WITH SYMMETRY OPTION N
NSET   NO. OF E/M SETS
ISETI   POINTER TO E/M SET DATA
IWIRE   POINTER TO FIRST WIRE ELEMENT OF E/M
NEND   POINTER TO LAST WIRE ELEMENT OF E/M
IOUTOP   E/M OUTPUT OPTION
INPOPT   E/M INPUT OPTION
NOC   NO. OF E/MS IN THIS SET

SOME VARIABLES ACTIVE IN THE SINGLE LOOP INPUT SECTION
        NINT   NO. OF ELEMENTS

SOME VARIABLES ACTIVE IN THE INTERFACE ARRAY INPUT SECTION
        MM,NN   NO. OF LAYERS,LOOPS/LAYER OF WIRE ELEMENTS
        NINT   NO. OF INTERFACES

SOME VARIABLES ACTIVE IN THE LATERAL CIRCULAR E/M INPUT SECTION
        DX,DY   X,Y WISE DISPLACEMENT OF ORIGIN OF E/M AXIS
        RAD1,RAD2   INNER,OUTER RADII OF E/M
        DY1,DY2   NORMAL DIST. FROM X AXIS TO E/M FRONT,REAR FACE
        NDIVR,NDIVY   NO. OF RADIAL,AXIAL LOOPS
        NSEG   NO. OF WIRE ELEMENTS/LOOP (CIRCUMFERENTIALLY)
        ANGLE   ANGLE FROM Y AXIS (IN YZ PLANE) TO E/M AXIS
        K   COUNTER OF WIRE ELEMENTS IN THIS E/M
        R   RADIUS FROM E/M AXIS TO END OF WIRE ELEMENT

SOME VARIABLES ACTIVE IN THE AXIAL CIRCULAR E/M INPUT SECTION
        X1,X2   AXIAL DISTANCE TO E/M INNER,OUTER FACE
        NDIVR,NDIVX   NO. OF RADIAL,AXIAL LOOPS
        NSEG,RAD1,
        RAD2,R,K   AS LATERAL CIRCULAR E/M SECTION

PRINCIPAL VARIABLE LIST FOR SUBROUTINE CALC ******************************

VARIABLES PASSED INTO CALC
         CX,CY,CZ,ISYMM,CURR   FROM COIL
         DISP,IDISP,CORE   FROM MODIN

VARIABLES PASSED OUT OF CALC
         NONE

XMU   PERMEABILITY OF FREE SPACE(SI)
LUNOUT   FORTRAN LOGICAL UNIT NUMBER FOR MAIN OUTPUTS
LUNFLD   FORTRAN LOGICAL UNIT NUMBER FOR FIELD LISTINGS
IOUT   OUTPUT OPTION
         DECODED INTO
         IFLIST =2   FIELD LISTING TO DATAFILE
                 =1   FIELD LISTING ON CONSOLE DEVICE
                 =0   NONE
         IOFILE =1   MAIN OUTPUTS TO DATAFILE
                 =0   MAIN OUTPUTS TO CONSOLE DEVICE
K   DUMMY VARIABLE CONTROLLING POSITION/ORIENTATION LOOP
FORCE   MAIN RESULTS ARRAY
         (1)   FORCE IN X DIRECTION
         (2)   Y
         (3)   Z
         (4)   TORQUE ABOUT X AXIS
         (5)   Y
         (6)   Z
COSR   COSINES OF MODEL ROTATIONS
         (1)   YAW
         (2)   PITCH
         (3)   ROLL
SINR   SINES OF MODEL ROTATIONS
         (1)   YAW
         (2)   PITCH
         (3)   ROLL
N   MODEL ELEMENT NUMBER
POS   POSITION AND MAGNETIZATION COMPONENTS OF MODEL ELEMENT
         (1)   X POSITION
         (2)   Y
         (3)   Z
         (4)   X WISE MAGNETIZATION
         (5)   Y
         (6)   Z
DPOS   ABSOLUTE POSITION OF TRANSLATED MODEL ELEMENT
         (1)   X
         (2)   Y
         (3)   Z

PRINCIPAL VARIABLE LIST FOR SUBROUTINE FIELD ******************************

VARIABLES PASSED INTO FIELD
        CX,CY,CZ,ISYMM,CURR   FROM COIL
        DPOS   FROM CALC

VARIABLES PASSED OUT OF FIELD
        BB,GB   FIELD AT REQUIRED POINT

BB		TOTAL FIELD AT POINT (TESLA)	
	(1)	X COMPONENT	
	(2)	Y	
	(3)	Z	
GB		FIELD GRADIENTS AT POINT (TESLA/METRE)	
	(1)	GRADIENT OF X FIELD IN X DIRECTION	
	(2)	X	Y
	(3)	X	Z
	(4)	Y	X
	(5)	Y	Y
	(6)	Y	Z
	(7)	Z	X
	(8)	Z	Y
	(9)	Z	Z

                    BY FREE SPACE FIELD EQUATIONS:
                           (4)=(2) , (7)=(3) , (8)=(6)

ISET	VECTOR FOR E/M SET DATA IN ISYMM, ETC.
INCOIL	VECTOR FOR E/M DATA IN CURR
IWIRE	VECTOR FOR WIRE ELEMENT DATA IN CX, ETC.
IREFL	AUXILIARY SYMMETRY CODE
1	NO REFLECTION IN YZ PLANE
-1	REFLECTION IN YZ PLANE
DX,DY,DYZ,IX	CONTROL PARAMETERS FOR REFLECTIONS AND ROTATIONS
IROT	NO. OF E/M ROTATIONS ABOUT X AXIS
ICURR	CURRENT DIRECTION CORRECTION
CURREN	CURRENT IN WIRE ELEMENT
IPOINT	RETURN VECTOR FROM MIT DERIVED SUBPROGRAM

                    VARIABLES SPECIFIC TO MIT DERIVED SUBPROGRAM
                    NOT CLASSIFIED

```
.RUN 2FORCE
MODEL GEOMETRY OPTION?
11
CYLIND.FUSE.:FLEN,FRAD,NA,NR?
1.0,0.1,3,4,1
SLAB WING:1/2SPAN,1/2GAP,CHORD,THICK,TAPER,SWEEP?
0.6,0.1,0.1,0.01,1.0,0.
DLONG,DVERT,NS,NC,NT,IWIDIR?
0.,0.,3,2,1,1
MODEL OUTPUT?
1
MODEL CORE COORDS. AND MAG.
```

X	Y	Z	(J*V)X	(J*V)Y	(J*V)Z
-0.3333	0.0600	0.0000	0.2618E-02	0.0000E+00	0.0000E+00
0.0000	0.0600	0.0000	0.2618E-02	0.0000E+00	0.0000E+00
0.3333	0.0600	0.0000	0.2618E-02	0.0000E+00	0.0000E+00
-0.3333	0.0000	0.0600	0.2618E-02	0.0000E+00	0.0000E+00
0.0000	0.0000	0.0600	0.2618E-02	0.0000E+00	0.0000E+00
0.3333	0.0000	0.0600	0.2618E-02	0.0000E+00	0.0000E+00
-0.3333	-0.0600	0.0000	0.2618E-02	0.0000E+00	0.0000E+00
0.0000	-0.0600	0.0000	0.2618E-02	0.0000E+00	0.0000E+00
0.3333	-0.0600	0.0000	0.2618E-02	0.0000E+00	0.0000E+00
-0.3333	0.0000	-0.0600	0.2618E-02	0.0000E+00	0.0000E+00
0.0000	0.0000	-0.0600	0.2618E-02	0.0000E+00	0.0000E+00
0.3333	0.0000	-0.0600	0.2618E-02	0.0000E+00	0.0000E+00
-0.0250	-0.1833	0.0000	0.0000E+00	-0.8333E-04	0.0000E+00
0.0250	-0.1833	0.0000	0.0000E+00	-0.8333E-04	0.0000E+00
-0.0250	-0.3500	0.0000	0.0000E+00	-0.8333E-04	0.0000E+00
0.0250	-0.3500	0.0000	0.0000E+00	-0.8333E-04	0.0000E+00
-0.0250	-0.5167	0.0000	0.0000E+00	-0.8333E-04	0.0000E+00
0.0250	-0.5167	0.0000	0.0000E+00	-0.8333E-04	0.0000E+00
-0.0250	0.1833	0.0000	0.0000E+00	0.8333E-04	0.0000E+00
0.0250	0.1833	0.0000	0.0000E+00	0.8333E-04	0.0000E+00
-0.0250	0.3500	0.0000	0.0000E+00	0.8333E-04	0.0000E+00
0.0250	0.3500	0.0000	0.0000E+00	0.8333E-04	0.0000E+00
-0.0250	0.5167	0.0000	0.0000E+00	0.8333E-04	0.0000E+00
0.0250	0.5167	0.0000	0.0000E+00	0.8333E-04	0.0000E+00

```
MODEL DISP. OPTION?
1
MODEL DISP.(X,Y,Z), ORI(YAW,PITCH,ROLL)?
0.,0.,0.,0.,45.,0
NO. E/M SETS?
1
E/M SET    1
INPUT OPTION,SYMMETRY OPTION?
3,10
DX,DY,RAD1,RAD2,DY1,DY2,NDIVR,NDIVY,NSEG,ANGLE?
2.0,0.,1.0,1.5,1.5,2.0,2,2,8,45.
E/M OUTPUT?
2
```

WIRE COORDINATES

X1	Y1	Z1	X2	Y2	Z2
3.18663	1.14905	1.14905	2.83908	0.55573	1.74237
2.83908	0.55573	1.74237	2.00000	0.30997	1.98813
2.00000	0.30997	1.98813	1.16092	0.55573	1.74237
1.16092	0.55573	1.74237	0.81337	1.14905	1.14905
0.81337	1.14905	1.14905	1.16092	1.74237	0.55573
1.16092	1.74237	0.55573	2.00000	1.98813	0.30997
2.00000	1.98813	0.30997	2.83908	1.74237	0.55573
2.83908	1.74237	0.55573	3.18663	1.14905	1.14905
3.45033	1.14905	1.14905	3.02554	0.42388	1.87421
3.02554	0.42388	1.87421	2.00000	0.12351	2.17459
2.00000	0.12351	2.17459	0.97446	0.42388	1.87421
0.97446	0.42388	1.87421	0.54967	1.14905	1.14905
0.54967	1.14905	1.14905	0.97446	1.87421	0.42388
0.97446	1.87421	0.42388	2.00000	2.17459	0.12351
2.00000	2.17459	0.12351	3.02554	1.87421	0.42388
3.02554	1.87421	0.42388	3.45033	1.14905	1.14905
3.18663	1.32583	1.32583	2.83908	0.73251	1.91914
2.83908	0.73251	1.91914	2.00000	0.48675	2.16490
2.00000	0.48675	2.16490	1.16092	0.73251	1.91914
1.16092	0.73251	1.91914	0.81337	1.32583	1.32583
0.81337	1.32583	1.32583	1.16092	1.91914	0.73251
1.16092	1.91914	0.73251	2.00000	2.16490	0.48675
2.00000	2.16490	0.48675	2.83908	1.91914	0.73251
2.83908	1.91914	0.73251	3.18663	1.32583	1.32583
3.45033	1.32583	1.32583	3.02554	0.60066	2.05099
3.02554	0.60066	2.05099	2.00000	0.30029	2.35136
2.00000	0.30029	2.35136	0.97446	0.60066	2.05099
0.97446	0.60066	2.05099	0.54967	1.32583	1.32583
0.54967	1.32583	1.32583	0.97446	2.05099	0.60066
0.97446	2.05099	0.60066	2.00000	2.35136	0.30029
2.00000	2.35136	0.30029	3.02554	2.05099	0.60066
3.02554	2.05099	0.60066	3.45033	1.32583	1.32583

```
E/M SET    1
E/M AMP.TURNS/1000?  ( 8)
1000.,1000.,-1000.,-1000.,-1000.,-1000.,1000.,1000.
OUTPUT OPTION?
10
```

			B_x	B_y etc.		B_{xx}	B_{xy} etc.				
X	Y	Z	BX	BY	BZ	BXX	BXY	BXZ	BYY	BYZ	BZZ
-0.2357	0.0600	0.2357	-0.0443	0.0004	0.0429	0.0050	-0.0021	-0.1844	0.0072	0.0018	-0.0122
0.0000	0.0600	0.0000	-0.0000	0.0000	-0.0000	-0.0000	-0.0000	-0.1873	-0.0000	0.0000	-0.0000
0.2357	0.0600	-0.2357	0.0443	0.0004	-0.0429	0.0050	0.0021	-0.1844	0.0072	-0.0018	-0.0122
-0.1933	0.0000	0.2781	-0.0518	0.0000	0.0346	0.0053	-0.0000	-0.1808	0.0069	0.0000	-0.0122
0.0424	0.0000	0.0424	-0.0079	0.0000	-0.0079	-0.0002	-0.0000	-0.1870	-0.0002	-0.0000	0.0004
0.2781	0.0000	-0.1933	0.0366	0.0000	-0.0513	0.0042	-0.0000	-0.1369	0.0072	-0.0000	-0.0115
-0.2357	-0.0600	0.2357	-0.0443	-0.0004	0.0429	0.0050	0.0021	-0.1844	0.0072	-0.0018	-0.0122
0.0000	-0.0600	0.0000	-0.0000	-0.0000	-0.0000	-0.0000	-0.0000	-0.1873	0.0000	-0.0000	-0.0000
0.2357	-0.0600	-0.2357	0.0443	-0.0004	-0.0429	0.0050	-0.0021	-0.1844	0.0072	0.0018	-0.0122
-0.2781	0.0000	0.1933	-0.0366	-0.0000	0.0513	0.0042	-0.0000	-0.1869	0.0072	0.0000	-0.0115
-0.0424	0.0000	-0.0424	0.0079	-0.0000	0.0079	-0.0002	-0.0000	-0.1870	-0.0002	0.0000	0.0004
0.1933	0.0000	-0.2781	0.0518	-0.0000	-0.0346	0.0053	0.0000	-0.1808	0.0069	-0.0000	-0.0122
-0.0177	-0.1833	0.0177	-0.0033	-0.0000	0.0033	0.0000	0.0004	-0.1891	0.0000	-0.0004	-0.0001
0.0177	-0.1833	-0.0177	0.0033	-0.0000	-0.0033	0.0000	-0.0004	-0.1891	0.0000	0.0004	-0.0001
-0.0177	-0.3500	0.0177	-0.0034	-0.0000	0.0034	0.0001	0.0006	-0.1939	0.0000	-0.0006	-0.0001
0.0177	-0.3500	-0.0177	0.0034	-0.0000	-0.0034	0.0001	-0.0006	-0.1939	0.0000	0.0006	-0.0001
-0.0177	-0.5167	0.0177	-0.0035	-0.0000	0.0035	0.0001	0.0007	-0.2003	-0.0000	-0.0007	-0.0001
0.0177	-0.5167	-0.0177	0.0035	-0.0000	-0.0035	0.0001	-0.0007	-0.2003	-0.0000	0.0007	-0.0001
-0.0177	0.1833	0.0177	-0.0033	0.0000	0.0033	0.0000	-0.0004	-0.1891	0.0000	0.0004	-0.0001
0.0177	0.1833	-0.0177	0.0033	0.0000	-0.0033	0.0000	0.0004	-0.1891	0.0000	-0.0004	-0.0001
-0.0177	0.3500	0.0177	-0.0034	0.0000	0.0034	0.0001	-0.0006	-0.1939	0.0000	0.0006	-0.0001
0.0177	0.3500	-0.0177	0.0034	0.0000	-0.0034	0.0001	0.0006	-0.1939	0.0000	-0.0006	-0.0001
-0.0177	0.5167	0.0177	-0.0035	0.0000	0.0035	0.0001	-0.0007	-0.2003	-0.0000	0.0007	-0.0001
0.0177	0.5167	-0.0177	0.0035	0.0000	-0.0035	0.0001	0.0007	-0.2003	-0.0000	-0.0007	-0.0001

FORCEX	FORCEY	FORCEZ	TORQUX	TORQUY	TORQUZ
3329.85	-0.00	-3131.94	0.00	0.00	0.00

STOP -- HAVE A NICE DAY

A2.9 Diagnostics

RT-11 FORTRAN generates WARNING diagnostics for the program segments MODIN, COIL and FIELD.   These may be ignored

Diagnostics for program unit MODIN

Warning in line 0026   Possible modification of index "I"
Warning in line 0045   Possible modification of index "I"

Diagnostics for program unit COIL

Warning in line 0023   Possible modification of index "I"
Warning in line 0144   Possible modification of index "I"

Diagnostics for program unit FIELD

Warning in line 0012   DO loop entry at label "60"
Warning in line 0019   DO loop entry at label "60"
Warning in line 0036   DO loop entry at label "100"

APPENDIX 3

Scaling of results to other physical sizes

The majority of the theoretical analysis presented herein is
unspecific as to the choice of physical scale. However, numerical
computations have generally been made at particular fixed scales
for convenience. Scaling of computed performance is thus of interest
and is relatively straightforward provided some care is taken.

Maximum force and torque capabilities

Exact magnetostatic equivalence of the model (any core material)
will only be obtained if the model's magnetic characteristics and the
applied field remain equal at all corresponding points during scaling.
The former condition may be taken for granted, the latter generally
requires adjustment of E/M characteristics. With consistent E/M
geometry and characteristics (notably current density) the field
strength at geometrically similar points varies as:

$$H \; \alpha \; \text{Scale}$$

Thus to preserve field equivalence, the E/M current density, for
instance, could be varied as:

$$J \; \alpha \; {}^{1}\!\big/\!_{\text{Scale}}$$

With such a condition it is clear that for fixed magnetic
configurations:

Model forces α Scale ^{2} (Vol.* Field gradient)

Model torques α Scale ^{3} (Vol.* Field)

This conflicts with the commonly quoted "Square-Cube" law (66
and numerous others), which implied that magnetic force capability
varied as core volume (Scale^3) whereas aerodynamic force varied as wing
area (Scale^2). With regard to the maximum force and torque capability
of MSBSs, the relations presented above (the "Square-Square" law?)
are undoubtedly valid where permanent magnet cores are used, since here
the performance of the core is limited by demagnetization, which in
turn depends only on the total local field strengths and is not other-
wise scale dependent. The relevance for soft iron cores is less
obvious, since there is no particular restriction to operation of the
core beyond saturation. However, when the core is far into saturation
there is some evidence to support the validity of the Square-Square law

as a measure of maximum capability, for instance Section 5.5.1, where torque capability was found to vary as $Scale^3$, implying of course that force capability may vary as $Scale^2$.

The absolute maximum capability for iron cores may prove to be unrealisable with existing technology E/Ms, as appears to be the case for the SIM computations in Section 5, thence the practical scaling law may lie between the Square-Cube and the Square-Square laws, inclusive.

General

Where maximum capabilities, core demagnetization etc. are not critical factors, the following conditions are easily identified (15, 49).

For consistent balance geometry, model magnetizations, E/M current densities, etc.:

$$\text{Model forces } \alpha \text{ Scale}^3$$
$$\text{Model torques } \alpha \text{ Scale}^4$$

Technological limitations on E/M performance are functions of scale, in particular the usable current density falls with increasing scale, but the trends are not continuous, apparently involving enforced abandonment of particular conductor technologies at specific limiting scales. Further treatment of these effects cannot be attempted here.

APPENDIX 4

Magnetic units and definitions

All equations are given in SI units, whence:

$$\underline{B} = \mu_o \underline{H} \text{ in free space} \quad (\mu_o = 4 \times 10^{-7} Hm^{-1}: \text{ B in Tesla;}$$
$$\text{H in A/m})$$

However, two alternative subsystems exist, the Kennelley and Sommerfeld systems. The Kennelley system is used in this report, in the belief that it is somewhat more convenient where permanent magnetic material is present. The key definitions of this system are:

$$\underline{B} = \mu_o \underline{H} + \underline{J} \qquad \text{(flux through permanent magnet material)}$$

$$\underline{\delta F} = \underline{J} \cdot \nabla \underline{H} \delta V \qquad \text{(force on a dipole)}$$

$$\underline{\delta T} = \underline{J} \times \underline{H} \, \delta V \qquad \text{(torque on a dipole)}$$

Both formulations lead acceptably to the classical:

$$\underline{B} = \mu_o \mu_r \underline{H} \qquad \underline{J} = \mu_o \chi_m \underline{H} \qquad \mu_r = 1 + \chi_m$$

In this report J is replaced by M where the equations are relatively unspecific regarding choice of material (permanent magnet or iron core). This is a non-standard symbology since the Sommerfeld system leads to (introducing primes to distinguish M' (traditional, in A/m) from M (Tesla)):

$$\underline{B} = \mu_o \, (\underline{H} + \underline{M}')$$

It is clear that $\underline{M}$ in fact equals $\mu_o \underline{M}'$. The use of M partially avoids the unfortunate clash between the standard symbology for polarization (J) and current density (J). There should be no contextual difficulty in distinguishing the two otherwise.

The first subscript to any field property describes the component under consideration, the second (where present) describes the gradient direction, e.g:

$$H_a \equiv \text{ field strength in direction a}$$

$$H_{ab} \equiv \text{ gradient of } H_a \text{ in the b direction}$$

$$\text{In free space } H_{ab} = H_{ba}$$

Occasionally a gradient of a gradient is required, this being given thus:

$$(H_{ab})_c \equiv \text{ the rate of change (gradient) of the } H_{ab}$$

$$\text{component taken in the c direction.}$$

APPENDIX 5

Characteristic symmetry of classical applied fields

It happens that classical applied fields in MSBSs with high levels
of E/M symmetry may be identified and classified by the character-
istic symmetry of those fields taken about the origin of axes and,
strictly, in balance axes. This method of representing fields has
been used extensively in Section 4 to derive relatively generalised
expressions for the magnetic couplings occuring with simple SPM wing
cores.

When a model is displaced or rotated away from the usual datum
position and orientation, the strict conditions of applied field
symmetry break down. However, the adjustments to E/M currents that
would be required to maintain the principal components of applied
field, hence the generated force and torque vectors, as fixed in
model axes, will tend to approximately preserve the symmetry
conditions cited herein, also in model axes. Analysis based on
applied field symmetry thus at least holds good for small displacements
and rotations of the model.

The E/M configuration employed in this Appendix is identical to
that used in Section 4 for the SPM roll coupling study, and readers
should refer to this Section (Figs. 4.8 - 4.10) for precise
definition of this geometry. However, the fundamental results remain
valid for any configuration of vaguely conventional form and all
geometries thereof, provided the E/M array incorporates the required
E/M symmetry. Fig. A5.1 thus illustrates the general E/M configura-
tion with Table A5.1 showing the definition of the applied fields for
this configuration.

Using FORCE, the field and field gradient components around
the origin of axes (at ± 0.1m in x,y and z directions in fact) are
easily found (Fig. A5.2). The respective signs of the field and
field gradient components are of principal interest, the magnitudes
being included here for information only.

The applied field symmetry matrices may be deduced directly from
Fig. A5.2 and represented as matrices of Odd (O) or Even (E)
functions of x,y and z, following Section 4, and Equations 4.8 and
4.9. The full derived matrices are presented in Fig. A5.3.
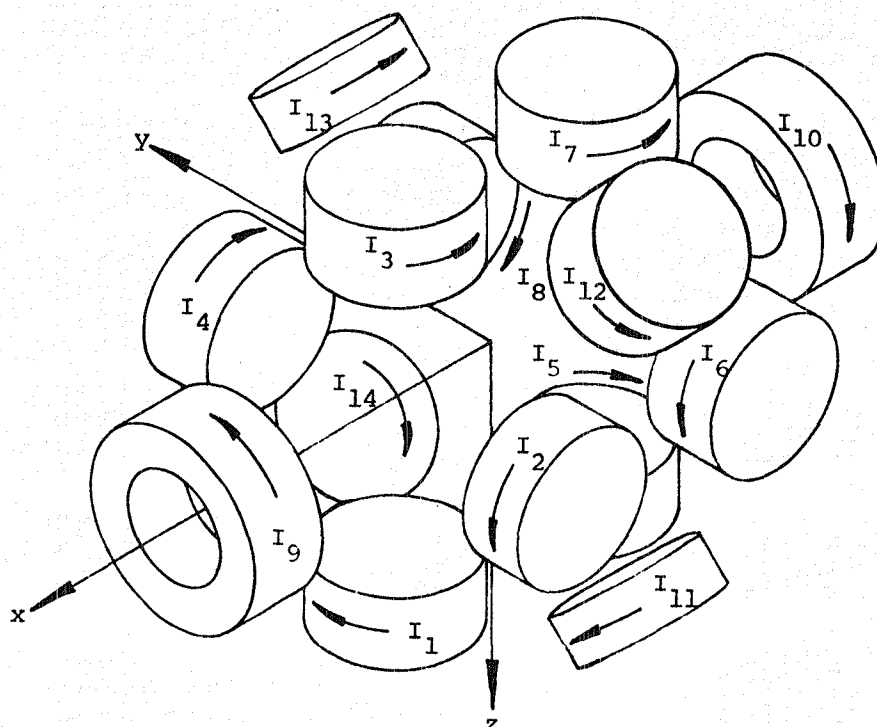
Fig. A5.1 Schematic diagram showing E/M configuration for field
symmetry analysis. Refer to Figs. 4.8 – 4.10 for precise
array geometry.

Table A5.1 Definition of E/M current directions for classical
applied fields. After Fig. A5.1

Classical field	Primary component	I_1	I_2	I_3	I_4	I_5	I_6	I_7	I_8	I_9	I_{10}
Lift	B_{xz}	+			−		−	+			
Drag	B_{xx}									+	+
Sideforce	B_{xy}		−		+		+		−		
Pitch	B_z	+		−		+		−			
Yaw	B_y		−		+		−		+		
Magnetizing (axial)	B_x									+	−

		I_{11}	I_{12}	I_{13}	I_{14}
Roll	B_{yz}	−	+	−	+

Current directions are chosen to make the classical primary field
component for each applied field positive.

	Position (m)			Field component (T)			Field gradient component (T/m)					
	X	Y	Z	BX	BY	BZ	BXX	BXY	BXZ	BYY	BYZ	BZZ
LIFT FIELD (B_{xz})	-0.1000	-0.1000	-0.1000	-0.0242	0.0002	-0.0244	-0.0022	-0.0016	0.2434	-0.0016	-0.0016	0.0037
	-0.1000	-0.1000	0.1000	0.0242	-0.0002	-0.0244	0.0022	0.0016	0.2434	0.0016	-0.0016	-0.0037
	-0.1000	0.1000	-0.1000	-0.0242	-0.0002	-0.0244	-0.0022	0.0016	0.2434	-0.0016	0.0016	0.0037
	-0.1000	0.1000	0.1000	0.0242	0.0002	-0.0244	0.0022	-0.0016	0.2434	0.0016	0.0016	-0.0037
	0.1000	-0.1000	-0.1000	-0.0242	-0.0002	0.0244	0.0022	-0.0016	0.2434	0.0016	0.0016	-0.0037
	0.1000	-0.1000	0.1000	0.0242	0.0002	0.0244	-0.0022	0.0016	0.2434	-0.0016	0.0016	0.0037
	0.1000	0.1000	-0.1000	-0.0242	0.0002	0.0244	0.0022	0.0016	0.2434	0.0016	-0.0016	-0.0037
	0.1000	0.1000	0.1000	0.0242	-0.0002	0.0244	-0.0022	-0.0016	0.2434	-0.0016	-0.0016	0.0037
DRAG FIELD (B_{xx})	-0.1000	-0.1000	-0.1000	-0.0226	0.0113	0.0113	0.2265	-0.0007	-0.0007	-0.1133	0.0002	-0.1133
	-0.1000	-0.1000	0.1000	-0.0226	0.0113	-0.0113	0.2265	-0.0007	0.0007	-0.1133	-0.0002	-0.1133
	-0.1000	0.1000	-0.1000	-0.0226	-0.0113	0.0113	0.2265	0.0007	-0.0007	-0.1133	-0.0002	-0.1133
	-0.1000	0.1000	0.1000	-0.0226	-0.0113	-0.0113	0.2265	0.0007	0.0007	-0.1133	0.0002	-0.1133
	0.1000	-0.1000	-0.1000	0.0226	0.0113	0.0113	0.2265	0.0007	0.0007	-0.1133	0.0002	-0.1133
	0.1000	-0.1000	0.1000	0.0226	0.0113	-0.0113	0.2265	0.0007	-0.0007	-0.1133	-0.0002	-0.1133
	0.1000	0.1000	-0.1000	0.0226	-0.0113	0.0113	0.2265	-0.0007	0.0007	-0.1133	-0.0002	-0.1133
	0.1000	0.1000	0.1000	0.0226	-0.0113	-0.0113	0.2265	-0.0007	-0.0007	-0.1133	0.0002	-0.1133
SIDEFORCE FIELD (B_{xy})	-0.1000	-0.1000	-0.1000	-0.0242	-0.0244	0.0002	-0.0022	0.2434	-0.0016	0.0037	-0.0016	-0.0016
	-0.1000	-0.1000	0.1000	-0.0242	-0.0244	-0.0002	-0.0022	0.2434	0.0016	0.0037	0.0016	-0.0016
	-0.1000	0.1000	-0.1000	0.0242	-0.0244	-0.0002	0.0022	0.2434	0.0016	-0.0037	-0.0016	0.0016
	-0.1000	0.1000	0.1000	0.0242	-0.0244	0.0002	0.0022	0.2434	-0.0016	-0.0037	-0.0016	0.0016
	0.1000	-0.1000	-0.1000	-0.0242	0.0244	-0.0002	0.0022	0.2434	-0.0016	-0.0037	0.0016	0.0016
	0.1000	-0.1000	0.1000	-0.0242	0.0244	0.0002	0.0022	0.2434	0.0016	-0.0037	0.0016	0.0016
	0.1000	0.1000	-0.1000	0.0242	0.0244	0.0002	-0.0022	0.2434	0.0016	0.0037	0.0016	-0.0016
	0.1000	0.1000	0.1000	0.0242	0.0244	-0.0002	-0.0022	0.2434	-0.0016	0.0037	-0.0016	-0.0016

PITCH FIELD (B_z)

X	Y	Z	BX	BY	BZ	BXX	BXY	BXZ	BYY	BYZ	BZZ
-0.1000	-0.1000	-0.1000	0.0014	-0.0014	0.1865	-0.0141	0.0001	-0.0146	0.0137	0.0139	0.0004
-0.1000	-0.1000	0.1000	-0.0014	0.0014	0.1865	0.0141	-0.0001	-0.0146	-0.0137	0.0139	-0.0004
-0.1000	0.1000	-0.1000	0.0014	0.0014	0.1865	-0.0141	-0.0001	-0.0146	0.0137	-0.0139	0.0004
-0.1000	0.1000	0.1000	-0.0014	-0.0014	0.1865	0.0141	0.0001	-0.0146	-0.0137	-0.0139	-0.0004
0.1000	-0.1000	-0.1000	-0.0014	-0.0014	0.1865	-0.0141	-0.0001	0.0146	0.0137	0.0139	0.0004
0.1000	-0.1000	0.1000	0.0014	0.0014	0.1865	0.0141	0.0001	0.0146	-0.0137	0.0139	-0.0004
0.1000	0.1000	-0.1000	-0.0014	0.0014	0.1865	-0.0141	0.0001	0.0146	0.0137	-0.0139	0.0004
0.1000	0.1000	0.1000	0.0014	-0.0014	0.1865	0.0141	-0.0001	0.0146	-0.0137	-0.0139	-0.0004

YAW FIELD (B_y)

X	Y	Z	BX	BY	BZ	BXX	BXY	BXZ	BYY	BYZ	BZZ
-0.1000	-0.1000	-0.1000	0.0014	0.1865	-0.0014	-0.0141	-0.0146	0.0001	0.0004	0.0139	0.0137
-0.1000	-0.1000	0.1000	0.0014	0.1865	0.0014	-0.0141	-0.0146	-0.0001	0.0004	-0.0139	0.0137
-0.1000	0.1000	-0.1000	-0.0014	0.1865	0.0014	0.0141	-0.0146	-0.0001	-0.0004	0.0139	-0.0137
-0.1000	0.1000	0.1000	-0.0014	0.1865	-0.0014	0.0141	-0.0146	0.0001	-0.0004	-0.0139	-0.0137
0.1000	-0.1000	-0.1000	-0.0014	0.1865	-0.0014	-0.0141	0.0146	-0.0001	0.0004	0.0139	0.0137
0.1000	-0.1000	0.1000	-0.0014	0.1865	0.0014	-0.0141	0.0146	0.0001	0.0004	-0.0139	0.0137
0.1000	0.1000	-0.1000	0.0014	0.1865	0.0014	0.0141	0.0146	0.0001	-0.0004	0.0139	-0.0137
0.1000	0.1000	0.1000	0.0014	0.1865	-0.0014	0.0141	0.0146	-0.0001	-0.0004	0.0139	-0.0137

ROLL FIELD (B_{yz})

X	Y	Z	BX	BY	BZ	BXX	BXY	BXZ	BYY	BYZ	BZZ
-0.1000	-0.1000	-0.1000	0.0001	-0.0069	-0.0069	-0.0008	-0.0008	-0.0008	0.0004	0.0691	0.0004
-0.1000	-0.1000	0.1000	-0.0001	0.0069	-0.0069	0.0008	0.0008	-0.0008	-0.0004	0.0691	-0.0004
-0.1000	0.1000	-0.1000	-0.0001	-0.0069	0.0069	0.0008	-0.0008	0.0008	-0.0004	0.0691	-0.0004
-0.1000	0.1000	0.1000	0.0001	0.0069	0.0069	-0.0008	0.0008	0.0008	0.0004	0.0691	0.0004
0.1000	-0.1000	-0.1000	-0.0001	-0.0069	-0.0069	-0.0008	0.0008	0.0008	0.0004	0.0691	0.0004
0.1000	-0.1000	0.1000	0.0001	0.0069	-0.0069	0.0008	-0.0008	0.0008	-0.0004	0.0691	-0.0004
0.1000	0.1000	-0.1000	0.0001	-0.0069	0.0069	0.0008	0.0008	-0.0008	-0.0004	0.0691	-0.0004
0.1000	0.1000	0.1000	-0.0001	0.0069	0.0069	-0.0008	-0.0008	-0.0008	0.0004	0.0691	0.0004

	X	Y	Z	BX	BY	BZ	BXX	BXY	BXZ	BYY	BYZ	BZZ
AXIAL	-0.1000	-0.1000	-0.1000	0.3274	-0.0009	-0.0009	-0.0179	0.0090	0.0090	0.0090	-0.0000	0.0090
	-0.1000	-0.1000	0.1000	0.3274	-0.0009	0.0009	-0.0179	0.0090	-0.0090	0.0090	0.0000	0.0090
FIELD	-0.1000	0.1000	-0.1000	0.3274	0.0009	-0.0009	-0.0179	-0.0090	0.0090	0.0090	0.0000	0.0090
	-0.1000	0.1000	0.1000	0.3274	0.0009	0.0009	-0.0179	-0.0090	-0.0090	0.0090	-0.0000	0.0090
(magnetizing)	0.1000	-0.1000	-0.1000	0.3274	0.0009	0.0009	0.0179	0.0090	0.0090	-0.0090	0.0000	-0.0090
	0.1000	-0.1000	0.1000	0.3274	0.0009	-0.0009	0.0179	0.0090	-0.0090	-0.0090	-0.0000	-0.0090
(B_x)	0.1000	0.1000	-0.1000	0.3274	-0.0009	0.0009	0.0179	-0.0090	0.0090	-0.0090	-0.0000	-0.0090
	0.1000	0.1000	0.1000	0.3274	-0.0009	-0.0009	0.0179	-0.0090	-0.0090	-0.0090	0.0000	-0.0090

Following Figs. A5.1, A5.2

The field symmetry is presented as in Eqns. 4.8, 4.9

LIFT

$$
\begin{vmatrix} H_x \\ H_y \\ H_z \\ H_{xx} \\ H_{xy} \\ H_{xz} \\ H_{yy} \\ H_{yz} \\ H_{zz} \end{vmatrix}
=
\begin{vmatrix} E & E & O \\ O & O & O \\ O & E & E \\ O & E & O \\ E & O & O \\ E & E & E \\ O & E & O \\ O & O & E \\ O & E & O \end{vmatrix}
\begin{vmatrix} x \\ y \\ z \end{vmatrix}
$$

For the remaining fields the matrix alone is presented.

DRAG

$$
\begin{vmatrix} O & E & E \\ E & O & E \\ E & E & O \\ E & E & E \\ O & O & E \\ O & E & O \\ E & E & E \\ E & O & O \\ E & E & E \end{vmatrix}
$$

SIDEFORCE

$$
\begin{vmatrix} E & O & E \\ O & E & E \\ O & O & O \\ O & O & E \\ E & E & E \\ E & O & O \\ O & O & E \\ O & E & O \\ O & O & E \end{vmatrix}
$$

PITCH

$$\begin{pmatrix} O & E & O \\ E & O & O \\ E & E & E \\ E & E & O \\ O & O & O \\ O & E & E \\ E & E & O \\ E & O & E \\ E & E & O \end{pmatrix}$$

YAW

$$\begin{pmatrix} O & O & E \\ E & E & E \\ E & O & O \\ E & O & E \\ O & E & E \\ O & O & O \\ E & O & E \\ E & E & O \\ E & O & E \end{pmatrix}$$

ROLL

$$\begin{pmatrix} O & O & O \\ E & E & O \\ E & O & E \\ E & O & O \\ O & E & O \\ O & O & E \\ E & O & O \\ E & E & E \\ E & O & O \end{pmatrix}$$

MAGNETIZING

(Axial)

$$\begin{pmatrix} E & E & E \\ O & O & E \\ O & E & O \\ O & E & E \\ E & O & E \\ E & E & O \\ O & E & E \\ O & O & O \\ O & E & E \end{pmatrix}$$

REFERENCES

1. Tournier, Marcel; Laurenceau, P.: Suspension Magnetique d'une maquette en soufflerie. La Recherche Aeronautique, No. 59, July-Aug. 1957, pp. 21-27.

2. Proceedings of ARL Symposium on magnetic wind tunnel model suspension and balance systems. ARL-66-0135, July 1966. Wright-Patterson AFB, Ohio, 13-14 April, 1966.

3. Tuttle, M.H.; Kilgore, R.A.; Boyden, R.P.: Magnetic suspension and balance systems - a selective annotated bibliography. NASA TM 80225, April 1980.

4. Proceedings of 2nd International Symposium on electro-magnetic suspension. University of Southampton, Southampton, England, 12-14 July, 1971.

5. General Electric Company: Design concepts and cost studies for magnetic suspension and balance systems. Final Report. Document No. 81LSP47251, March 1981.

6. Covert, E.E.; Finston, M.; Vlajinac, M.; Stevens, T.: Magnetic balance and suspension systems for use with wind tunnels. Progress in Aerospace Sciences, Vol. 14, 1973. pp. 27-107.

7. Jayasinghani, N.D.: Power supply for a magnetic suspension system. In (4) , pp. L1-L16.

8. Moreau, R.; Besson, J.; Horeau, R.: Electro-optical detectors for magnetic suspension and the study of the free motion of models. In (4) , pp. H1-H14.

9. Altmann, H.: An optical scanning detection system and its use with a magnetic suspension system for low density sphere drag measurements. In (4) , pp. I1-I15.

10. Stephens, T.: Design, construction and evaluation of a magnetic suspension and balance system for wind tunnels. MIT TR-136, NASA CR-66903, Nov. 1969.

11. Goodyer, M.J.: The magnetic suspension of wind tunnel models for dynamic testing. University of Southampton PhD Thesis, Dept. of Aeronautics and Astronautics, April 1968.

12. Goodyer, M.J.; Henderson, R.I.; Judd, M.: The measurement of Magnus force and moment using a magnetically suspended wind tunnel model. IEEE Trans. MAG-11, Sept. 1975, pp. 1514-1516.

13. Diab, T.A.G.: Improved wind tunnel testing and data reduction methods using a magnetic suspension system. University of Southampton PhD Thesis, Dept. of Aeronautics and Astronautics, July 1976.

14. Judd, M.: The effect of wind tunnel size on the power and voltage requirements of magnetic suspension systems. Southampton University A.A.S.U. Report No. 269, May 1967.

15. Britcher, C.P.: The magnetic suspension and balance system in the cryogenic wind tunnel. Southampton University BSc Honours project report, April 1978.

16. Britcher, C.P.; Goodyer M.J.: The Southampton University magnetic suspension/cryogenic wind tunnel facility. 1st International Symposium on cryogenic wind tunnels, Southampton University, Southampton, England, 3-5 April, 1979.

17. Burke, H.K. et al.: Design, fabrication and delivery of a charge injection device as a stellar tracking device. NASA CR-161226, April, 1979.

18. Goodyer, M.J.: The roll control of magnetically suspended wind tunnel models by transverse magnets. Southampton University A.A.S.U. Report No. 291, 1969.

19. Haldeman, C.W.; Kramer, R.A.; Way, P.: Developments at MIT related to magnetic model suspension and balance systems for large scale facilities. 1st International Symposium on cryogenic wind tunnels, Southampton, England, 3-5 April, 1979.

20. Blakelock, J.H.: Automatic control of aircraft and missiles. Wiley, 1965.

21. Babister, A.W.: Aircraft dynamic stability and response. Pergamon, 1980.

22. Stephens, T.: Methods of controlling the roll degree of freedom in a wind tunnel magnetic balance. Part 1 - the production of rolling moments. MIT TR-78, July, 1965.

23. Goodyer, M.J.: Roll control techniques on magnetic suspension systems. Aeronautical Quarterly, Vol. 18, Feb. 1967, pp. 22-42.

24. Britcher, C.P.; Fortescue, P.W.; Allcock, G.A.; Goodyer, M.J.: Investigations of design philosophies and features applicable to large magnetic suspension and balance systems. NASA CR-162433, Nov. 1979.

25. McCaig, M.: Permanent magnets in theory and practice. Pentech, 1977.

26. Nagel, H.; Klein, H.P.; Menth, A.: Magnetic properties of Nd-rich $ReCo_5$ magnets. IEEE Trans. MAG-11 No. 5, Sept. 1975.

27. Ermolenko, A.S.; Rozhda, A.F.: Magnetocrystalline anisotropy of $Sm_{1-x}Nd_xCo_5$ alloys. IEEE Trans. MAG-14 No. 5, Sept. 1978.

28. Nesbitt, E.A.; Wernick, J.H.: Rare earth permanent magnets. Academic press. 1973.

29. Martin, D.L.; Benz, M.G.: Review of cobalt-rare earth permanent magnet alloys. AIP Conference on magnetism and magnetic materials. 1971. pp. 970-990.

30. Livingston, J.D.: Present understanding of coercivity in cobalt-rare earths. AIP Conference proceedings No. 10, Part 1. 1973.

31. Zijlstra, H.: Permanent magnets in magnetic field calculations. Proceedings of Compumag conference, Oxford, U.K. April 1976. pp. 164-167.

32. Iden, D.J.; Ehrenfried, C.E.; Garrett, H.J.: Present and future applications of high coercive force magnets. AIP Conference proceedings No. 8, 1971. pp. 1026-1046.

33. Bachmann, K.: Rare earth cobalt permanent magnets. IEEE Conference publication No. 142. Sept. 1976. pp. 135-139.

34. Brailsford, F.: Magnetic Materials. Methuen 1960.

35. Schlenk, K.W.: Properties, applications and manufacture of cobalt-samarium base permanent magnets. From Magnetic Field No. 4. July 1981.

36. Martin, D.L.; Benz, M.G.: Temperature dependence of coercivity for Co-Sm permanent magnet alloys. IEEE Trans. MAG-8. Sept. 1972. pp. 562-563.

37. Trout, S.R.; Graham, C.D. Jr.: High field magnetic measurements on sintered $SmCo_5$ permanent magnets. AIP Conference proceedings No. 12, 1975. pp. 608-609.

38. Chari, M.V.K.; Silvester, P.P. (Eds).: Finite elements in electrical and magnetic field problems. Wiley 1980.

39. Binns, K.J.; Lawrenson, P.J.: Analysis and computation of electrical and magnetic fields. Pergamon 1963.

40. Newman, M.J.; Trowbridge, C.W.; Turner, L.R. GFUN: An interactive program as an aid to magnet design. 4th International Conference on Magnet Technology. Brookhaven, Sept. 1972.

41. Armstrong, A.G.A.M.; Collie, C.J.; Diserens, N.J.; Newman, M.J.; Simkin, J.; Trowbridge, C.W.: New developments in the magnet design program GFUN. 5th International Conference on Magnet Technology. Frascati, Rome, 1975. Also Rutherford Laboratory RL-75-066, March 1975.

42 Trowbridge, C.W.: Applications of integral equation methods for the numerical solution of magnetostatic and eddy current problems. Rutherford Laboratory RL-76-071, June 1976.

43. Armstrong, A.G.A.M.; Collie, C.J.; Diserens, N.J.; Newman, M.J.; Simkin, J.; Trowbridge, C.W.: GFUN 3D users guide. Rutherford Laboratory RL-76-029, November 1976, revised August 1979.

44. Bozorth, R.M. Ferromagnetism. Van Nostrand 1951.

45. Boll, R. (Ed): Soft magnetic materials (the Vacuumschmelze Handbook) Vacuumschmelze GmbH. Hanau. Heyden 1979.

46. Allegheny Ludlum Blue Sheets - Vanadium permendur. Reproduced in part in (5).

47. Osborn, J.A.: Demagnetizing factors of the general ellipsoid. Physical Review. Vol. 67 No. 11/12 June 1945. pp 351-357.

48. Britcher, C.P.: An assessment of the performance of the spanwise iron magnet rolling moment generating system for magnetic suspension and balance systems, using the finite element computer program "GFUN". NASA CR-165888 April 1982.

49. Britcher, C.P.: E/M configurations for extreme attitude testing in magnetic suspension and balance systems. NASA CR-163862 May 1981.

50. Kuchnir, M.; Sanger, P.: Thermal conductance measurements of mechanical supports for superconducting magnets. IEEE Trans. NS-22, June 1975, pp. 1183-1184.

51. Livdahl, P.V.: Status of the Fermilab energy doubler/saver project. IEEE Trans. NS-24, June 1977, pp. 1218-1221.

52. Biallas, G. et al.: The support and cryostat system for doubler magnets. IEEE Trans. MAG-15, Jan. 1979, pp. 131-133.

53. Wensley, J.H. et al.: Design study of a Software-Implemented Fault-Tolerance (SIFT) computer. SRI Int. report No. 4026, Interim technical report No. 1, June 1978.

54. Smith, T.B. et al.: A fault-tolerant multiprocessor architecture for aircraft. Vol. 1, NASA CR-3010, July 1978.

55. Towler, W.R.: Electromagnetic position sensor for a magne-
     tically supported model in a wind tunnel. In (4), pp. Q1-Q7.

56. Deckert, J.C.; Desai, M.N.; Deyst, J.J.; Willsky, A.S.:
     F-8 DFBW sensor failure identification using analytic
     redundancy.   IEEE Trans. AC-22, Oct. 1977, pp. 795-803.

57. Deckert, J.C. et al.: Reliable dual-redundant sensor failure
     detection and identification for the NASA F-8 DFBW A/C.
     Charles Stark Draper Lab. report R-1077, May 1977.

58. CSR Contraves, Contraves Goertz Corporation: Operating and
     service manual, NC400 Series servo controllers.

59. Fortescue, P.W.; Bouchalis, C.: Digital controllers for the
     vertical channels of a magnetic suspension system. NASA
     CR-165684 May 1981.

60. United Detector Technology: Position sensing detectors
     PIN-SC/10, PIN-SC/25, PIN-SC/50 Information sheet.

61. United Detector Technology: Application notes, photodetectors-
     continuous position sensing series. Part 1.

62. Burr-Brown Research Corporation: 1981 General catalogue.

63. Ferrari, R.L.: An introduction to electromagnetic fields.
     Van Nostrand 1975.

64. Stephens, T.; Adams, R.: Wind tunnel simulation of store
     jettison with the aid of magnetic artificial gravity.
     MIT TR-174, March 1971. also NASA CR-1955.

65. Way, P.: Memo to Professor E.E. Covert. Table program
     modifications. November 1977.

66. Bobbitt, P.J.: Modern fluid dynamics of subsonic and transonic
     flight. AIAA Paper 80-0861. From "Global technology 2000"
     Baltimore, Maryland 1980.

ACKNOWLEDGEMENTS

Throughout the period of this research, considerable support, guidance and assistance has been forthcoming from numerous sources and I wish to express my sincere thanks to at least all those mentioned below.

NASA Langley Research Center for generous financial and material support under Grant NSG-7523, and particularly the NASA Technical Monitor, Richmond P. Boyden and Dr. Robert A. Kilgore and William T. Shinn for their technical guidance and hospitality during two visits to that institution.

The British Science Research Council (now the Science and Engineeering Research Council) for personal financial support via Research Studentship No. 78305547. Also for permitting access to the computer program GFUN, with essential ancillary support services, under Grant GR/B/3691.5 and especially John Simkin of Rutherford Laboratory who spent long hours, partly beyond the call of duty, adapting GFUN to my specific requirements.

The Southampton University Research Fund for financial support through Grant Codes 78/AQ and 81/N which, particularly during the early phase of this work, was an essential prerequisite to the award of the NASA Grant.

The Aerophysics Laboratory, Massachusetts Institute of Technology and particularly Dr. Charles W. Haldeman for the use of the computer program TABLE and for hospitality and many valuable discussions during a visit to MIT.

The Aeronautics Department's mechanical workshops and allied technicians for supplying countless components and assemblies, notably Tim, Bill, Jan, Doug, Merlin, Dave, Colin, Roy, Tom and Denis.

The Aeronautics Department's electronic workshops for providing many vital pieces of equipment, particularly Geoff (analogue control hardware), Bob (superb digital communications and data conversion and many useful technical ideas), John, Keith and Terry.

Chris Bouchalis for providing all the digital control software and Peter W. Fortescue for assistance in that area and for many useful discussions over the period of this research.

Dr. M. Judd, formerly of the Aeronautics Department and associated for many years with MSBS matters at Southampton and elsewhere, for acting as external examiner.

Dr. M.J. Goodyer, my research supervisor and Principal Investigator for the NASA Grant, for almost limitless advice, encouragement and practical assistance proffered over my four and a half years involvement with MSBS activities. Without his presence and influence this work could never have commenced and the current prospects for construction of a Large MSBS would be bleak indeed.

End of Document